Petrologic, Geochemical and Isotopic Evolution of Rhyolite Lavas from the Okataina, Rotorua and Kapenga Volcanic Centres, Taupo Volcanic Zone, New Zealand.

A thesis submitted in fulfilment
of the requirements for the degree of
Doctor of Philosophy
in
Earth Sciences
at the
University of Waikato

by

Deborah Ann Bowyer

The
University
of Waikato
Te Whare Wānanga
o Waikato

University of Waikato
2001

Abstract

The Okataina Volcanic Centre (OVC) is a highly active modern silicic magmatic system at the northeastern end of the central Taupo Volcanic Zone, North Island, New Zealand. This study presents a set of petrographic, mineralogical, geochemical and isotopic data that focuses on the rhyolite lavas erupted from the OVC. These data have been combined with existing geochronological data and knowledge of vent positions to identify magma types, and hence provide a model for the spatial and temporal evolution of the silicic magmatic system. Representative samples of OVC rhyolite lavas were analysed for whole rock major and trace elements by XRF (90 samples), trace and rare earth elements by LA-ICPMS (32), and Sr (25), Nd (8) and Pb (4) isotopes by TIMS. Major element compositions of phenocrysts in 24 representative lavas were determined by EPMA. Rhyolite lavas of the OVC contain phenocrysts (5 - 35 %) of plagioclase, quartz, Fe-Ti oxides ± orthopyroxene ± calcic amphibole ± cummingtonite ± biotite. Apatite and zircon are accessory. Temperatures determined from Fe-Ti oxide geothermometry range from ~ 650 - 830°C. The lavas are dominantly peraluminous, medium-K, calc-alkaline rhyolites, with $SiO_2 \approx 72.5$ - 77.5 wt. %, $^{87}Sr/^{86}Sr \approx 0.70516$ - 0.70583, $\varepsilon_{Nd} \approx 0.02$ - 1.70, $^{206}Pb/^{204}Pb \approx 18.75$ - 18.84, $^{207}Pb/^{204}Pb \approx 15.55$ - 15.64 and $^{208}Pb/^{204}Pb \approx 38.42$ - 38.74. The volcanic history of the OVC can be subdivided into three periods, (i) > 220 ± 10 ka, (ii) 220 ± 10 - c. 65 ka, and (iii) < c. 65 ka. The two earlier periods involved eruption of caldera-forming ignimbrites and rhyolite lavas. The most recent period of activity involved eruption of the caldera-modifying Mangaone Pyroclastics Subgroup (c. 43 000 - 31 400 years B.P.), and the caldera-infilling rhyolite lavas and pyroclastics comprising the Haroharo, Okareka and Tarawera volcanic complexes (c. 25 000 years B.P. - present). In each period, a number of rhyolitic magma types or batches have been identified and distinguished based on their mineralogical, geochemical and isotopic characteristics. At least nine magma batches may have been erupted in the last 25 000 years, with estimated maximum generation times from c. 3 800 - 15 500 years, minimum generation rates from 3.1×10^{-4} - 3.2×10^{-3} km^3/year, residence times from c. 4 000 - 31 000 years and erupted volumes generally < 15 km^3. The Haroharo Volcanic Complex was built up in four rhyolitic eruptive episodes beginning c. 25 000 years B.P. The lavas and pyroclastics erupted in the Te Rere episode were derived from a single, genetically discrete, relatively volumetrically small magma batch. The lavas and pyroclastics erupted in the Rotoma, Mamaku and Whakatane episodes record the evolution of a relatively larger single magma batch over c. 4 000 years by closed-system fractional crystallisation processes. The Okareka Volcanic Complex was built up in two rhyolitic eruptive episodes at c. 25 000 and 15 800 years B.P., and a genetic relationship is suggested between the magma erupted in these episodes. The Tarawera Volcanic Complex was built up in four rhyolitic eruptive episodes beginning c. 22 500 years B.P. Multiple magma batches were erupted during the Okareka and Rerewhakaaitu episodes. The lavas and pyroclastics erupted in each of the two youngest episodes (Waiohau and Kaharoa) were derived from single, genetically discrete magma batches. The eruption of multiple, relatively small volume, genetically discrete magmas in the last c. 25 000 years precludes the coalescence of a large magma body beneath the OVC, and has implications for volcanic hazard assessment and eruption prediction. Future eruptions may involve either residual silicic magmas revived by basaltic intrusion, or basaltic magmas that have reached the surface without interacting with residual silicic magmas because they have crystallised, or new genetically discrete silicic magma. Mineralogical, geochemical and isotopic data obtained for rhyolite lavas erupted from the adjacent Rotorua and Kapenga volcanic centres reveal that their evolution has also involved eruption of multiple magma batches, but lack of geochemical, isotopic and age data preclude the development of any spatial and temporal models for these centres.

Acknowledgments

Firstly, a big thank you to my supervisory team - chief supervisor Roger Briggs for being encouraging and supportive, and for editing chapter drafts, Richard Smith for encouraging me that there is life out there after a PhD, and Richard Price for international negotiations and for taking me along to the Chateau for fine food and conversation.

Thanks to other staff of the Earth Sciences Department who provided assistance or just a friendly chat - David Lowe, Cam Nelson, Peter Hodder, Richard Chapman and Xu. Thanks to Sydney and Elaine for being eternally helpful with all those administrative matters. I would like to say a special thank you to all of the technical staff of the department for their assistance and advice over the last four years, especially Steve Bergin, Annette Rodgers, Renat Radosinsky and Laurence Gaylor (the best darn field technician ever !).

Fellow PhD students in the department are thanked for advice and discussions on various aspects of this thesis and for general comradeship - particularly Craig Cook, Blair Lynch-Blosse, Steve Krippner, Jo Horrocks, Andreas Fuchs, Penny Cooke, Avon McIntyre, Jeanette Gillespie and Rochelle Hansen.

Thanks to Steve Eggins, Charlotte Allen and Sally Stowe at ANU for assistance with the LA-ICPMS and CL-SEM, Roland Maas at La Trobe University for instruction on the TIMS and isotope sample preparation, Stephen Brown at Canterbury University for XRF analyses, and John Patterson at Victoria University for help with electron microprobe analyses.

Dave Dravitzki - thanks for letting me use your data from the Ngongotaha and Pukehangi volcanic complexes and for being silly enough to want to proof read chapters. Thanks to Ian Nairn for helpful advice and answers to my questions, and Will Esler for always having a thought-provoking question up your sleeve.

Fletcher Challenge Forests, Carter Holt Harvey, the Department of Conservation and private landowners are thanked for allowing me access to their property. Fletcher Challenge Forests provided absolutely luscious forest maps, which made fieldwork much easier. Thanks to Boofhead and Phil-the-Dil, as well as other characters we met in the field, for making the job more challenging and more fun!

On a financial note I am grateful to the University of Waikato for the post-graduate scholarship that allowed me to undertake this research. The New Zealand Vice Chancellors Committee (Claude McCarthy Fellowship), the New Zealand Federation of University Women (Harriette Jenkins Award), and the Department of Earth Sciences also provided financial support.

Last but not least, I would like to thank my parents and grandparents who have always been encouraging and interested in what I was doing. Ryan, I am grateful to you for supporting me through the highs and lows.

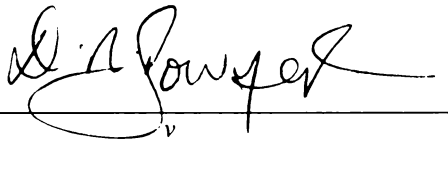

Table of Contents

Chapter Five: Mineralogy and Intensive Parameters

List of Figures

List of Plates

List of Tables

Chapter One:
Introduction and Literature Review

Chapter One: Introduction and Literature Review

1.1 INTRODUCTION

Large silicic magmatic systems, such as those found in the central Taupo Volcanic Zone (TVZ), North Island, New Zealand, are sources of the most violent and voluminous volcanic eruptions known. However, the evolution of these magmatic systems is poorly understood. Of interest, is (i) whether eruptions record the evolution of a single magma chamber, or of multiple magma bodies or 'batches', (ii) the length of time silicic magmas reside in the upper crust, and (iii) the nature and time-frame of magma chamber replenishment.

Models range from those in which rhyolites are derived from a single, relatively large, long-lived (> 100 000 years) magma chamber (eg. Halliday et al., 1989; Christensen and De Paolo, 1993) which underlies the volcano during repose periods, to those in which multiple relatively smaller silicic magma 'batches' are produced rapidly by crustal melting. These 'batches' then rise to the surface with only temporary development of small, short-lived (< 1 000 years) magma chambers just prior to the eruption (eg. Huppert and Sparks, 1988; Sparks et al., 1990, Sutton et al., 1995, 2000).

The central TVZ contains two highly active modern silicic magmatic systems, the Taupo and Okataina volcanic centres (Figure 1.1). Sutton et al. (1995, 2000) presented an outline geochemistry of the Taupo Volcanic Centre. Using rhyolite petrography, mineralogy, geochemistry and isotopic compositions, eruptive products were able to be fingerprinted. In conjunction with a knowledge of eruption ages and vent sites, Sutton et al. (1995, 2000) were able to recognise magmas from different sources and therefore new influxes of magma into the system. Hence, insights into the evolution of this magmatic system were obtained. Brown (1994) provided some insights into the evolution of the older Whakamaru Volcanic Centre in a study of the Whakamaru group ignimbrites and the Western Dome Belt rhyolite lavas, although in less detail than Sutton et al. (1995, 2000). These are the only two studies to date which have endeavoured to integrate data from lavas and pyroclastics, erupted at different times, to assess the overall spatial and temporal evolution of a silicic magmatic system in the TVZ.

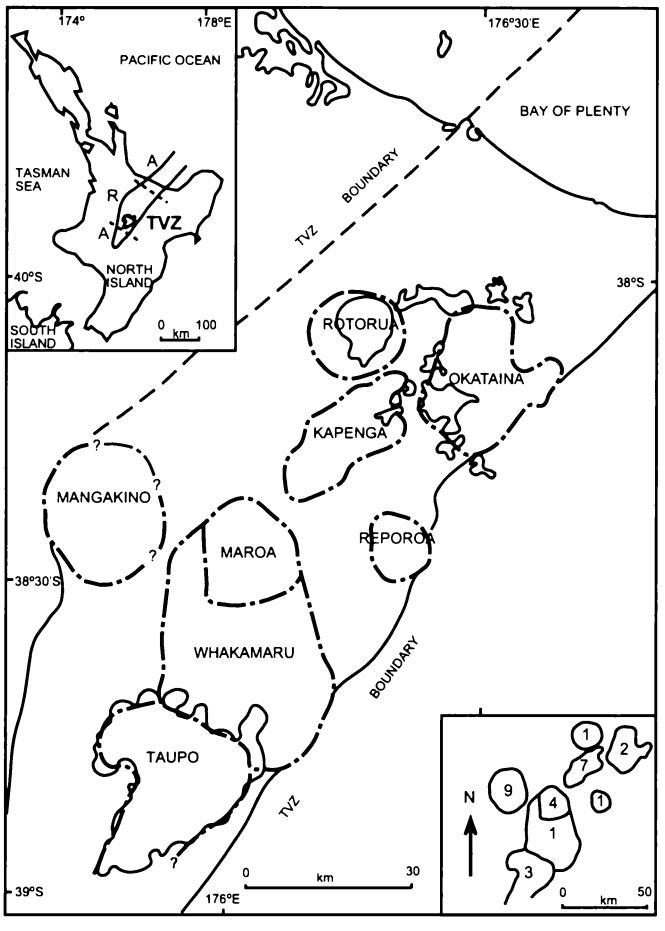

Figure 1.1: Map showing approximate boundaries of silicic volcanic centres in the central Taupo Volcanic Zone (TVZ). Top inset shows the three segments of the TVZ, andesitic-dacitic (A) to the northeast and southwest and the rhyolitic (R) central TVZ. Bottom inset shows the number of caldera forming events at each of the volcanic centres. Redrawn and modified from Houghton et al. (1995).

The primary aim of this thesis is to investigate the evolution of the magmatic system at the Okataina Volcanic Centre. Supporting data will also be obtained for the adjacent Rotorua and Kapenga volcanic centres.

1.2 OBJECTIVES OF THE STUDY

The rhyolite eruptives of the Okataina Volcanic Centre have been extensively studied in terms of age, distribution and vent location, particularly for the last c. 65 000 years (eg. Vucetich and Pullar, 1969; Nairn, 1972; Howorth, 1976; Nairn, 1980, 1981a, 1989; Froggatt and Lowe, 1990; Nairn, 1992; Lowe et al., 1999). This study focuses on the petrography,

mineralogy, geochemistry and isotopic composition of the eruptives, and uses the age data to put these petrological constraints into a geochronological and geological framework.

While other investigations into the evolution of silicic magmatic systems, including that of Sutton et al. (1995), have studied both the pyroclastics and lavas produced from a particular magmatic system, this study will focus on the lavas erupted from the Okataina Volcanic Centre. The primary reason for this is to restrict the scope of the study. The pyroclastics from Okataina, particularly those erupted during the post-caldera phase of activity, are numerous and complex, especially in proximal exposures. Any in-depth geochemical study of these pyroclastic deposits should involve a "pumice-by-pumice" approach to sampling, and indeed a detailed study of any one of these pyroclastic eruptive episodes could well comprise a PhD project on its own. Rhyolite lavas have been erupted throughout the history of Okataina, both prior to and following caldera collapse episodes. Therefore, confining this investigation to lavas will not preclude an assessment of the evolution of the Okataina Volcanic Centre over its entire life and this study will hopefully provide a framework into which later, detailed studies of the pyroclastics can be integrated.

The vents for post-caldera eruptions at the Okataina Volcanic Centre have occurred along two southwest-northeast lineations known as the Haroharo and Tarawera linear vent zones. During several of the post-caldera eruptive episodes, multiple vents along these lineations were active, and in some cases, simultaneous eruptions may have occurred. Consequently, pumice clasts derived from discrete vents may become intimately mingled. In these cases, it would be more reliable to determine the composition of the lavas, rather than the pyroclastics, as indicators of geochemical variation between magma batches.

The objectives of this project are:

1) To provide an extensive set of petrographic, mineralogical, geochemical and isotopic data for rhyolite lavas from the Okataina Volcanic Centre. Additional supporting data will be obtained for rhyolite lavas from the Rotorua and Kapenga volcanic centres.

2) To assess spatial and temporal variations in these parameters.

3) To use these data, together with existing geochronological data, to identify magma batches that have existed beneath the Okataina Volcanic Centre. An assessment will be

made of the number and volume of magma batches, distinguishing mineralogical and/or geochemical features, and residence times in the upper crust.

4) To use these data to aid in delineating the boundary between the Okataina and Kapenga volcanic centres, as there has traditionally been some confusion as to where the southwestern boundary of the Okataina Volcanic Centre lies.

5) To discuss the relevance of magmatic evolution at the Okataina Volcanic Centre to general models of continental rhyolite magmatism.

6) To use the petrological and geochemical data to constrain the nature of future eruptions from the Okataina Volcanic Centre.

1.3 LOCATION OF THE STUDY AREAS

1.3.1 Okataina Volcanic Centre

The Okataina Volcanic Centre (OVC) is the most northeastern of the rhyolitic caldera complexes in the Taupo Volcanic Zone (Figure 1.1). The OVC occurs to the east of Rotorua city (Figure 1.2) beneath a very picturesque area of lakes, surrounded by native and plantation forest covered hills. These topographic features occur as a result of the underlying volcanic activity. The forest covered hills are underlain by rhyolitic tephras, lava domes and flows. It is common for the lakes in the area to have been impounded by the growth of these dome complexes (eg. lakes Rotoiti, Rotoehu, Okataina, Tarawera, Okareka, Tikitapu and Rotokakahi) or to occupy volcanic craters (eg. lakes Rotomahana and Rotoma).

The OVC does not have a pronounced basin topography, seen at other rhyolitic caldera volcanic centres in the TVZ, as it has been largely filled by post-caldera rhyolite dome complexes. The Tarawera Volcanic Complex, the showpiece of the OVC, rises from beneath Lake Tarawera at 210 metres above sea level to the summit at 1 111 metres above sea level. The Tarawera Volcanic Complex is bisected by the deep and precipitous craters of the 1886 A.D. Tarawera Fissure, which extends for 8 km across the dome complex, and a further 9 km southwest across Lake Rotomahana to Waimangu. The largest 1886 A.D.

explosion craters are now filled by Lake Rotomahana (Nairn, 1989). To the north of Tarawera, the Haroharo Volcanic Complex rises to 914 metres above sea level. Both complexes have gently to moderately sloping flow surfaces and steep flow margins (Nairn, 1989).

Evidence of caldera collapse can be seen in the northern part of the OVC, north of Lake Tarawera and the Tarawera River. Caldera margins are less obvious to the south where collapse is considerably older and often obscured either by regional faulting or by burial beneath younger eruptives (Nairn, 1989). Where well expressed, the topographic caldera rim is strongly scalloped, interpreted as a series of coalescing slump scars (Nairn, 1989).

The OVC is the most recently active of the TVZ silicic volcanic centres. Due to its proximity to urban areas in the Bay of Plenty and Waikato Regions, it has been the subject of a number of studies concerning potential volcanic hazards (eg. Nairn, 1981b; Johnston and Nairn, 1993; Scott and Nairn, 1998; Becker, 1999). Evidence that the OVC is active to this day is seen in the thermal activity that is located throughout the area.

1.3.2 Rotorua Volcanic Centre

The Rotorua Volcanic Centre (RVC) occurs in the northern central Taupo Volcanic Zone to the west of the Okataina Volcanic Centre (Figure 1.1). A 20 km diameter basin containing Lake Rotorua topographically expresses the RVC. Its caldera is marked to the south, east and north by a roughly circular fault scarp approximately 17 km across, while to the west the ground surface is gently downwarped into the basin (Wilson et al., 1984). A large portion of the southern RVC is occupied by the city of Rotorua (Figure 1.2).

Rhyolite domes play an important role in the topographic expression of the RVC, although they are not as extensive and voluminous as at Okataina. Mokoia Island in the centre of Lake Rotorua, Kawaha Point and Hinemoa Point which protrude into Lake Rotorua, and Hospital Hill located near the centre of Rotorua city, are all rhyolite domes (Figure 1.3). The Rotorua landscape is dominated by Mount Ngongotaha, which rises to 757 metres above sea level and provides a boundary to northwest urban sprawl. The level of Lake Rotorua also controls the topography of the Rotorua area. Former lake levels, higher than the present day, have cut terraces and deposited large quantities of lake sediments, which are

now exposed between the present shore of the lake, the caldera margin and the edge of the Mamaku Plateau.

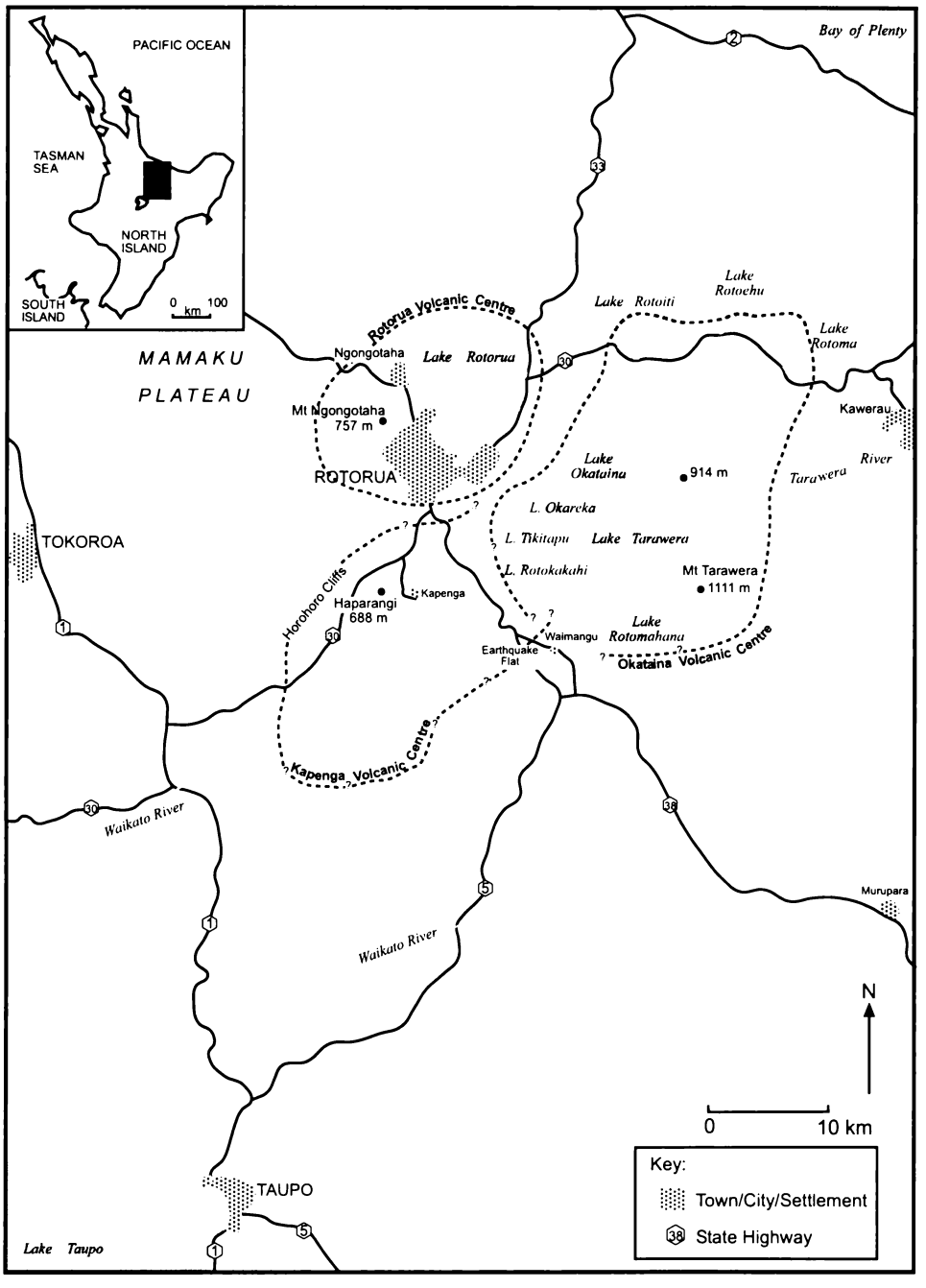

Figure 1.2: Map of part of the central North Island of New Zealand showing the location of the three silicic volcanic centres discussed in this study. Approximate boundaries of the volcanic centres are shown with dashed lines (after Thompson, 1974; Wilson et al., 1984; Nairn, 1989 and Houghton et al., 1995). Geographical features mentioned in section 1.3 are also shown.

Modern activity from the RVC is seen in the geothermal activity at Whakarewarewa, Kuirau Park, and around the southern shore of Lake Rotorua (Figure 1.3).

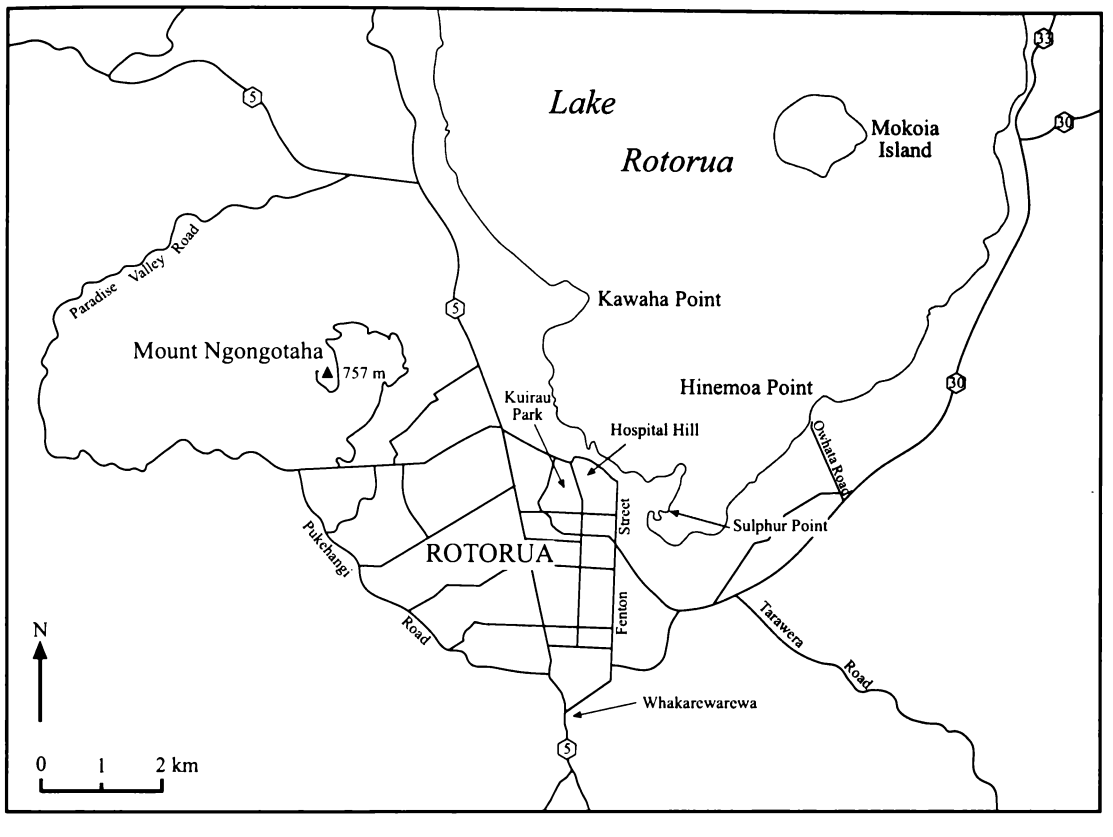

Figure 1.3: Map of the southern Rotorua Volcanic Centre showing the location of rhyolite domes and geothermal areas discussed in section 1.3.2. Main roadways in Rotorua City and state highways (numbered) in the area are also shown.

1.3.3 Kapenga Volcanic Centre

The Kapenga Volcanic Centre (KVC) is centred near Kapenga settlement, 9 km south of Rotorua city and the RVC, and southwest of the OVC (Figure 1.2). The KVC includes the Guthrie and Ngakuru Grabens, two extensively faulted, sediment-filled depressions (Rogan, 1982; Wilson et al., 1984). Tectonic activity has produced this young horst and graben topography, which has subsequently overprinted the Kapenga Caldera structure (Dunham, 1981; Langridge, 1990). In addition, the caldera has been partly infilled by younger ignimbrites derived from the KVC as well as the Whakamaru-group ignimbrites (Graham et al., 1995) from the Whakamaru Volcanic Centre.

The modern topography over the KVC is subdued and the average elevation is only slightly lower than that of the surrounding terrain (Rogan, 1982). Rhyolite domes form several landmarks in this area. Most notable are the Horohoro Cliffs, a rim-fracture dome that marks the northwestern edge of the KVC, and Haparangi, a late-stage intra-caldera dome that at 688 metres above sea level stands proud above the surrounding Guthrie and Ngakuru Grabens.

The KVC is considerably older than both the RVC and OVC (Houghton et al., 1995). Modern thermal activity is therefore less, in both frequency and strength, than at these younger centres.

1.4 A Review of Literature on Rhyolite Lavas in the Study Area

1.4.1 Introduction

There have been many studies undertaken on the volcanic geology of the Okataina, Rotorua and Kapenga areas. These studies tend to focus on mapping of the area (eg. Cole, 1966; Thompson, 1974; Dunham, 1981; Nairn, 1981a, 1989; Langridge, 1990; Bellamy, 1991; Lowther, 1997; Crosby, 1998; Dravitzki, 1999) or on the geochemistry and eruptive processes of the caldera-forming ignimbrites from these volcanic centres (eg. Nairn, 1972; Nairn and Kohn, 1973; Carr, 1984; Davis, 1985; Karhunen, 1993; Bailey and Carr, 1994; Schmitz, 1995; Ritchie, 1996; Lynch-Blosse, 1998; Beresford and Cole, 2000).

Mineralogical and geochemical analyses have been carried out on a number of the rhyolite lavas of the area (eg. Cole, 1966; Ewart et al., 1968; Ewart and Taylor, 1969; Ewart, 1971a; Ewart et al., 1971, 1975; Nairn, 1981a; Bellamy, 1991; Gaston, 1991; Shepherd, 1991; Nairn, 1992; Stevenson et al., 1994; Blattner et al., 1996; Dravitzki, 1999; Richnow, 1999). However, a major problem is that the available previous data are incomplete and analysed in many laboratories, and hence in this study all lavas have been resampled and analysed as a single analytical batch.

The petrography of the rhyolite lavas of the central Taupo Volcanic Zone has been studied extensively by Ewart (1968) who paid particular attention to phenocryst abundances and assemblages. This is the most recent publication to discuss the petrographic characteristics

of the rhyolite lavas of the OVC as a whole. More recently, Gaston (1991) and Shepherd (1991) provided some discussion of the rhyolite lavas of the Kapenga and Rotorua volcanic centres respectively.

In earlier studies the rhyolite lava domes and flows of the Taupo Volcanic Zone were referred to collectively as Haparangi Rhyolite, named after the Haparangi rhyolite dome in the central KVC (Figure 1.2). This term is still being used today, although it fails to associate rhyolite lavas with their source volcanic centre and hence, magmatic system. The terminology is currently being reviewed and will be discussed further in section 1.5.

1.4.2 Haparangi Rhyolite

The name Haparangi Rhyolite was first given to rhyolite flows/lavas of Pliocene-Pleistocene age by Grange (1937) in his study of the Rotorua-Taupo subdivision. Grindley (1959) used the term Haparangi Rhyolite Group for all the rhyolite domes and flows (ha) and associated pumice breccia, ash, lapilli and avalanche deposits (hap) of Pleistocene-Recent age.

Grindley (1960) divided the Haparangi Rhyolite domes into two groups based on physiographic evidence. Older domes (ha_1) are of mid-Pleistocene age (penultimate glaciation) and are characterised by their dissection and erosion of their pyroclastics and ash beds. The younger domes (ha), of late-Pleistocene age (last glaciation), are more numerous (as older domes become buried with time), are little dissected, and are accompanied by widespread pyroclastics and tephras. Preliminary petrographic studies showed that Haparangi Rhyolite domes generally consist of an intrusive core of lithoidal rhyolite, commonly with steeply dipping flow banding, chilled marginal zones of banded obsidian and perlitic rhyolite, and in the younger less eroded domes, a cap of pumiceous rhyolite grading laterally into pyroclastic deposits (Grindley, 1961). The rhyolites contain as essential minerals: plagioclase feldspar (oligoclase), quartz, hornblende, and as accessory minerals: orthopyroxene, augite, biotite and magnetite (Grindley, 1961).

Healy (1963) and Ewart (1967) noted that, in general, for the Maroa, Okataina and Rotorua volcanic centres, the rhyolite domes that occur on the rim of the volcanic centre are older than those within the centre. Healy et al. (1964) divided the rhyolite domes associated with the Okataina and Rotorua calderas into two groups:

(1) The glassy and lithoidal rhyolites of early dome building stages (mid-Pleistocene) are termed ha_1 and occur on the caldera-rim.

(2) The glassy orthopyroxene-hornblende rhyolites of the final stages of dome building (late-Pleistocene to Holocene) are termed ha_2 and occur within the caldera.

1.4.3 Okataina Volcanic Centre

Following on from the subdivision of Healy et al. (1964) into older (ha_1) and younger (ha_2) domes, based mainly on physiographic evidence, Ewart (1968) further subdivided the rhyolite lavas on the basis of geographic locations, mineralogy and relative ages into four complexes shown in Figure 1.4:

1)	Tikitapu Rhyolite Complex	- older and younger rhyolites of the area between Whakarewarewa, Lake Tarawera and Lake Rotokakahi.
2)	Rotoma Rhyolite Complex	- older rhyolites lying along the northern and northeastern part of the OVC.
3)	Tarawera Rhyolite Complex	- younger dome building rhyolites of the Tarawera Massif, occurring east of Lake Tarawera.
4)	Haroharo Rhyolite Complex	- younger rhyolites of the Haroharo Massif, extending north of Lake Tarawera to lakes Rotoiti and Rotoehu.

Ewart (1968) noted that, based on division into older (caldera-rim) and younger (intra-caldera) dome-building phases, the older rhyolites of this centre have slightly higher crystal contents than the younger group, and that it is clear that there are marked variations in the crystal contents between the complexes.

Considerable variation in phenocryst content and ferromagnesian assemblage occurs within the Tikitapu Rhyolite Complex. The majority of the rhyolites are orthopyroxene-hornblende bearing but there are several that contain significant amounts of biotite. Total phenocryst contents range from 5% to greater than 30% (Ewart, 1968).

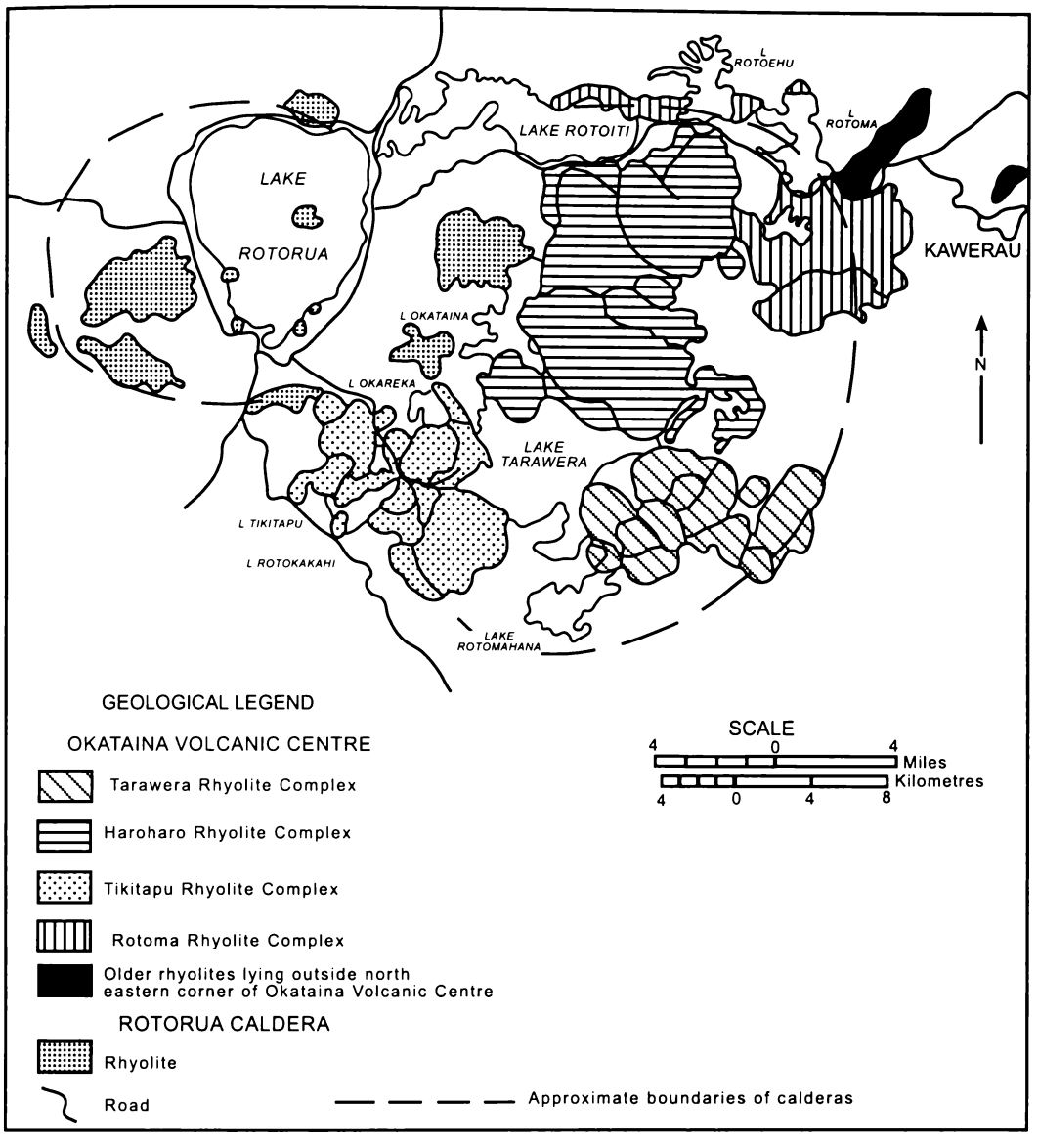

Figure 1.4: Generalised map showing the division of the rhyolite domes and flows of the Okataina Volcanic Centre into the various complexes. The Rotorua rhyolites are also shown for comparison. Redrawn and modified from Ewart (1968).

Rhyolites of the Rotoma Rhyolite Complex contain 5 - 25% phenocrysts. Ferromagnesian assemblages are either orthopyroxene + hornblende or biotite + hornblende ± orthopyroxene (Ewart, 1968). Ewart et al. (1975) noted that the rhyolite dome occurring north of Lake Rotoma contained cummingtonite and clinopyroxene in addition to hornblende and biotite.

In the Haroharo Rhyolite Complex, Ewart (1968) found that the ferromagnesian minerals present are orthopyroxene and hornblende, with some lavas also containing cummingtonite.

Total phenocryst contents are up to 15%. The most notable fact about the Haroharo rhyolites was the absence of biotite. Ewart (1968) also showed that the Haroharo rhyolites are very similar in terms of the ratios and percentages of modal quartz and plagioclase to the Matahina and Rotoiti Ignimbrites, which are considered to have been erupted from the Haroharo caldera now infilled by these younger rhyolites.

The phenocryst assemblages of the Tarawera Rhyolite Complex are much more varied than those at Haroharo, shown in an extensive study undertaken by Cole (1966, 1970a, 1970b) who identified 12 rhyolite domes/flows, and divided them into four ferromagnesian assemblages:

1) Orthopyroxene-hornblende rhyolite (crystal content ~20%)
2) Hornblende-biotite rhyolite (crystal content >30%)
3) Orthopyroxene rhyolite (crystal content <10%)
4) Biotite rhyolite (crystal content 20-30%)

The older rhyolites of the Tarawera Rhyolite Complex have low crystal contents with hornblende and orthopyroxene dominant, while the youngest domes, sitting on the top of the complex, have high crystal contents and contain biotite. Leonard (1999) found minor amounts of cummingtonite in some of these youngest domes, the first documented occurrence of this amphibole in Tarawera rhyolites.

The rhyolites of these four complexes within the OVC were considered to represent the eruptive products from separate magma sources or reservoirs, and therefore indicated the positions and extents of the higher-level magma bodies (Ewart, 1968; Nairn, 1981a).

Ewart et al. (1971, 1975) determined TVZ rhyolite temperatures using Fe-Ti oxide geothermometry and correlated these temperatures to ferromagnesian mineral assemblages. For mineral assemblages observed at the OVC, Ewart et al. (1975) calculated the following temperatures:

- Cummingtonite + Calcic Hornblende ± Orthopyroxene 725-755°C
- Calcic Hornblende + Orthopyroxene 750-825°C
- Biotite + Calcic Hornblende ± Cummingtonite ± Orthopyroxene 720-765°C

Since the studies of Ewart (1968), Ewart et al. (1975) and Cole (1966, 1970a, 1970b), Nairn (1981a, 1989) has used a three-fold classification system for the rhyolites of the Okataina Volcanic Centre. Rhyolites predating the widespread Mamaku Ignimbrite, which was erupted from the adjacent Rotorua Volcanic Centre at 220 ± 10 ka (age from Houghton et al., 1995), are denoted as ha_1. Rhyolites erupted between the Mamaku Ignimbrite and the Rotoiti Ignimbrite eruption at c. 65 ka (age from Houghton et al., 1995) are denoted as ha_2, and those younger than the Rotoiti Ignimbrite are denoted as ha_3. The rhyolites comprising the Rotoma Rhyolite Complex of Ewart (1968) are ha_1, as are two domes between lakes Okataina and Rotorua that Ewart (1968) identified incorrectly as being Rotorua eruptives. The Tikitapu Rhyolite Complex of Ewart (1968) comprises the ha_2 Moerangi and Tutaeheka Rhyolites, two ha_1 rhyolites near Lake Okareka and ha_3 rhyolites within the Okareka Embayment. The rhyolites of the Tarawera and Haroharo volcanic complexes are also ha_3. An age of 230 ± 12 ka was obtained by Shane et al. (1994) for the Mamaku Ignimbrite, however the age of Houghton et al. (1995) will be used in this study.

Although the petrography of the Okataina rhyolites has been extensively studied by Ewart (1968) and Cole (1966, 1970a, 1970b), later studies (Nairn, 1981a, 1989) have provided a more detailed division of the ha_3 rhyolite lavas comprising the Haroharo and Tarawera volcanic complexes. Volcanic activity has been subdivided into eruptive episodes, which will be discussed in Chapter Two. Some of the lava flows and domes of the Haroharo and Tarawera Complexes have also been renamed. Hence, there is reason to recalculate phenocryst percentages and ferromagnesian assemblages for the Okataina rhyolite lavas and to reassess any spatial and temporal variations.

The most recent studies of OVC rhyolite lavas have tended to focus on associations between domes and pyroclastics erupted in the same episode of activity. Bellamy (1991) related the Moerangi Rhyolites (ha_2) to the Te Wairoa Ignimbrites in the southwestern OVC. Leonard (1999) discussed the magmatic processes associated with the eruption of rhyolite domes and pyroclastics during the Kaharoa Eruptive Episode at the Tarawera Volcanic Complex. Richnow (1999) investigated the eruptional and post-eruptional processes in rhyolite domes of the Kaharoa episode. Wright (2000) studied the products of the Mamaku Eruptive Episode at Haroharo, and Speed (2001) studied the products of the Waiohau Eruptive Episode at Tarawera.

1.4.4 Rotorua Volcanic Centre

Healy et al. (1964) divided the Rotorua rhyolites into older (ha_1) and younger (ha_2) dome building phases. Ha_1 rhyolites, occurring on the caldera rim, consisted of a crescentic edifice west of Rotorua City, a dome at the northern end of Lake Rotorua, the Hemo Gorge ridge, and a large lava dome complex to the south of Ngongotaha. Also included in this group by Ewart (1968) were the domes of Whakapoungakau and Pukepoto, which are now accepted as being related to the OVC. These ha_1 rhyolites are now known to pre-date the caldera-forming Mamaku Ignimbrite. The ha_2 rhyolites, occurring within the caldera, consisted of the Ngongotaha, Kawaha Point, Hinemoa Point, Mokoia Island and Kuirau Reserve domes as well as another dome at the southeastern corner of Lake Rotorua. These are now known to post-date the Mamaku Ignimbrite.

Within the group of intra-caldera (ha_2) rhyolites, a subdivision was suggested by Healy (1963), and subsequently adopted by Ewart (1968), based upon the age of the domes relative to the formerly high level of Lake Rotorua (at ~100 metres above its present level after the Rotoiti Ignimbrite eruption from Okataina at c. 65 ka). Ewart (1968) postulated the Ngongotaha, Kawaha Point and Kuirau Reserve domes as pre-Rotoiti Ignimbrite (ha_2), and the domes of Mokoia Island, Hinemoa Point and the southeastern corner of Lake Rotorua as post-Rotoiti Ignimbrite (ha_3). Figure 1.5 shows the names and relative ages of the rhyolites of the Rotorua Caldera according to Ewart (1968).

Ewart (1968) noted that there are no consistent mineralogic differences based on the generalised division into older (ha_1) or younger (ha_2) dome-building phases. However, the division of younger domes into pre- and post- Rotoiti Ignimbrite groups is supported by significant differences in phenocryst contents. The ha_2 domes are crystal-poor (< 5%) and in terms of ferromagnesian minerals contain only orthopyroxene. The ha_3 domes are crystal-rich (15-30%) and contain orthopyroxene, hornblende, and with the exception of Mokoia Island, biotite (Ewart, 1968; Nairn and Wood, 1987). Wilson et al. (1984) considered the disparity in crystal contents between the Mamaku Ignimbrite and younger domes suggest that at least two separate magma batches have been erupted during the lifetime of the RVC.

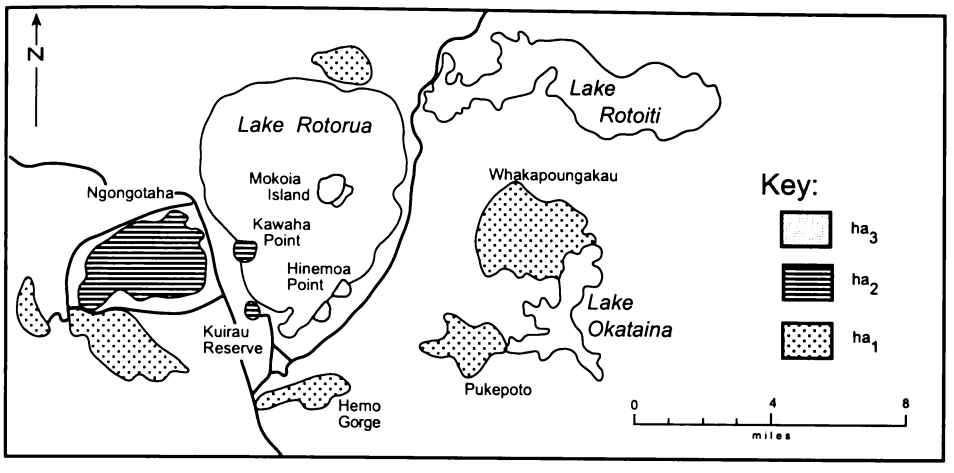

Figure 1.5: The rhyolites of the Rotorua Caldera and their division into three age groups. Redrawn and modified from Ewart (1968).

An apparent mis-identification by Healy et al. (1964) and Ewart (1968) was classifying the large lava dome complex to the south of Ngongotaha as ha_1. Thompson (1974) redefined this complex as ha_2 and it is now named Pukehangi.

Shepherd (1991) studied the volcanology, geochemistry and petrology of the post-caldera rhyolite domes in the RVC. He confirmed the mineral assemblages described by Ewart (1968) for the Rotorua rhyolites and found fayalitic olivine in tridymite lined lithophysal cavities within one of the Ngongotaha Dome Complex rhyolites. Grapes et al. (1994) describe an interesting assemblage of silicate and oxide vug minerals that also occur in this dome. Oxide equilibria magmatic temperatures of 711°C and 778°C were calculated for two of the Ngongotaha domes (Shepherd, 1991).

While Shepherd (1991) provided little discussion of the Pukehangi rhyolite domes because he considered them to be ha_1, Dravitzki (1999) provided a volcanological interpretation for the entire Ngongotaha-Pukehangi complex. In dividing the Ngongotaha-Pukehangi complex into a series of individual rhyolite domes, Dravitzki (1999) provided a more detailed picture of phenocryst contents and ferromagnesian mineral assemblages than Ewart (1968) with three assemblages present:

1) Plagioclase + Orthopyroxene + Fe-Ti Oxide ± Quartz
2) Plagioclase + Orthopyroxene + Biotite + Fe-Ti Oxide ± Quartz
3) Plagioclase + Orthopyroxene + Hornblende + Biotite + Fe-Ti Oxide ± Quartz

Dravitzki (1999) also noted the occurrence of secondary olivine in one of the Ngongotaha domes. Richnow (1999) investigated the eruptional and post-eruptional processes in the Quarry Dome of the Ngongotaha Complex and calculated magmatic temperatures of 784-823°C. Milner (2001) examined the petrography and geochemistry of rhyolite lavas associated with the RVC in an effort to determine any affiliation to the Mamaku Ignimbrite.

1.4.5 Kapenga Volcanic Centre

Healy et al. (1964) divided the rhyolites of the Ngakuru Graben area into older (ha_1) and younger (ha_2) dome building phases, with the western-most and eastern-most of the rhyolites occurring on the caldera rim being ha_1, and three domes occurring between these rhyolites being ha_2.

The rhyolite lavas of the KVC were included as part of the Mokai Ring Structure by Ewart (1968) as it was not until the study of Rogan (1982) that Kapenga was postulated as being a separate volcanic centre. The rhyolites of the Mokai Ring Structure were divided into seven groups, shown in Figure 1.6. Six of these groups comprise lavas associated with what are now known as the Reporoa, Maroa and Whakamaru volcanic centres. The remaining group, referred to as Rhyolites of Horohoro-Waiotapu, comprise lavas associated with what is now called the Kapenga Volcanic Centre. Ewart (1968) divided these rhyolites into two groups. The ha_1 rhyolites occur around the caldera rim and have low phenocryst contents (<10%) with the dominant ferromagnesian phenocryst being orthopyroxene. The ha_2 rhyolites occur within the caldera and have higher phenocryst contents (>25%) with biotite, hornblende and orthopyroxene present. Ewart (1968) considered that petrological evidence indicates that the rhyolites of this group may constitute a magmatically related group but noted that this is by no means certain. The names given to these rhyolites by Ewart (1968) are shown in Figure 1.6. The ha_1 domes are Horohoro in the west and Waikorapa, Tumunui, and Trig 8566 in the east. The ha_2 domes are Haparangi, Round Hill and Trig 8523. This latter dome is now known as Ongahoro.

Dunham (1981) provided some discussion of the petrography and mineralogy of the Horohoro, Haparangi, Ongahoro and Round Hill domes. He also identified an outcrop on the northern flank of Haparangi Dome that appeared to be of a buried crystal-poor ha_1 rhyolite. Nairn (1989) suggested the occurrence of several other intracaldera domes

occurring northeast of Ongahoro that are petrographically similar to the Earthquake Flat Ignimbrite, but topographically protrude above the ignimbrite surface.

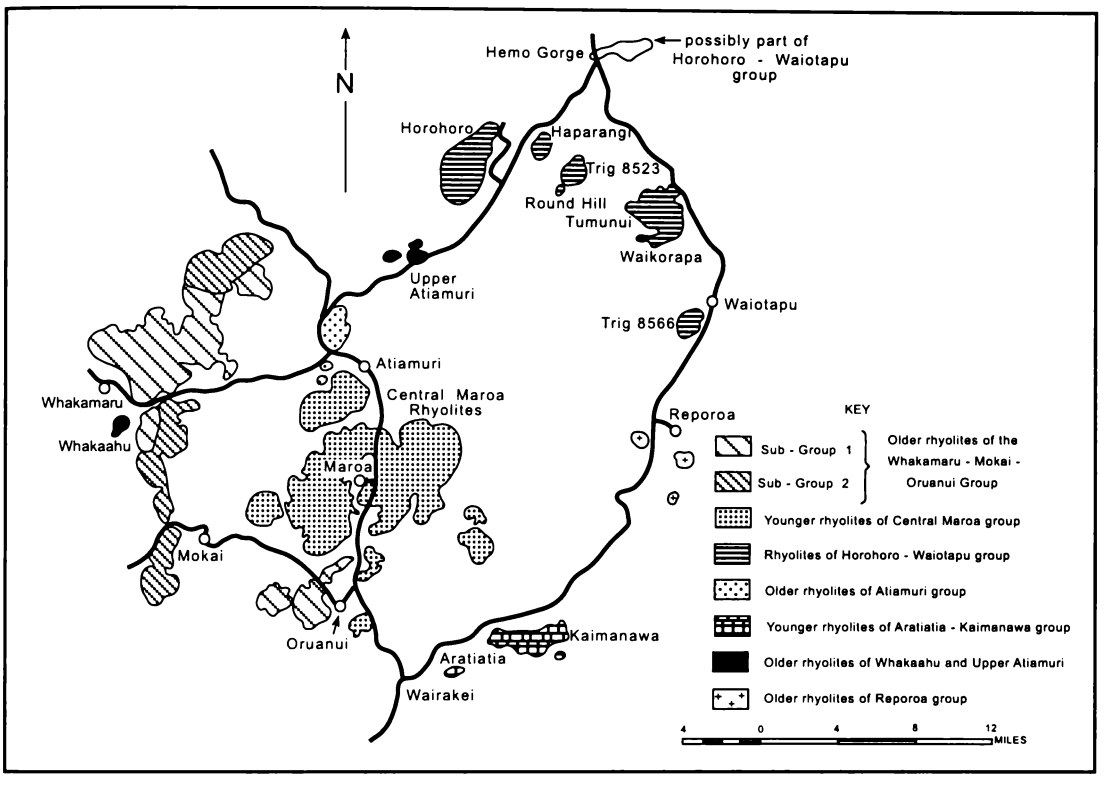

Figure 1.6: Rhyolite lavas and domes of the Mokai Ring Structure of Healy (1964) and Ewart (1967) showing their division into seven groups based on geographical and mineralogical similarities. Redrawn and modified from Ewart (1968).

Gaston (1991) studied the petrology and geochemistry of all the Kapenga Caldera rhyolites, the first such study since that of Ewart (1968). He noted that in addition to orthopyroxene, the ha_1 rhyolites may also contain small amounts of hornblende and/or biotite. An Fe-Ti oxide geothermometry temperature calculation for Tumunui dome suggested a temperature range of 810-950°C. Gaston (1991) highlighted some geochemical similarities between the Kapenga Rhyolites and those of the adjacent RVC and suggested a similarity of source for the two calderas. This theory has not been widely accepted.

1.5 NEW TERMINOLOGY FOR CLASSIFYING RHYOLITE LAVAS

The Haparangi Rhyolite (ha_1, ha_2, ha_3) classification system is no longer considered acceptable for the central TVZ rhyolites as it implies all the rhyolites have a common magmatic origin. This is not the case, with rhyolite lavas from each volcanic centre being derived from different magmatic systems. Hence the following terminology has now been proposed, and has been used in recent publications (eg. Dravitzki, 1999; Nairn, 2000). The "h" standing for Haparangi will remain but will be followed with a letter representing the volcanic centre from which the lava has been erupted. The numbers 1, 2 and 3 will still be used to denote pre-Mamaku Ignimbrite, between the Mamaku Ignimbrite and the Rotoiti Ignimbrite and post-Rotoiti Ignimbrite in age. The new terminology is presented in Table 1.1.

Table 1.1: New terminology for classifying the rhyolite lavas erupted from the Okataina, Rotorua and Kapenga volcanic centres.

Old Terminology (age range)*	New Terminology		
	Okataina Volcanic Centre	Rotorua Volcanic Centre	Kapenga Volcanic Centre
ha_1 (> 220 ± 10 ka.)	ho_1	hr_1	hk_1
ha_2 (220 ± 10 – c. 65 ka.)	ho_2	hr_2	hk_2
ha_3 (< c. 65 ka.)	ho_3	hr_3	

* Ages from Houghton et al. (1995).

Chapter Two:
Geologic Setting and Eruptive History

Chapter Two: Geologic Setting and Eruptive History

2.1 INTRODUCTION - THE TAUPO VOLCANIC ZONE

The Taupo Volcanic Zone (TVZ) is a volcano-tectonic complex, 300 km long and up to 60 km wide, reflecting northwest-directed subduction of the Pacific Plate beneath the North Island of New Zealand (Houghton et al., 1995). Houghton et al. (1995) defined the zone as an envelope around all vent locations known or inferred to have been active during the past 2.0 m.y., the time of onset of andesitic calc-alkaline volcanism in the zone, and associated with a northeast structural trend. The TVZ has been divided into three segments (Figure 1.1). The segments that occur northeast of Lake Rotorua and southwest of Lake Taupo contain andesitic to dacitic composite volcanoes and no rhyolitic calderas.

The central Taupo Volcanic Zone (125 x 60 km) is a region of intense Quaternary silicic volcanism (typically 70-77% SiO_2, Wilson et al., 1995) accompanying rapid extension of continental crust (Houghton et al., 1995). At least 34 caldera-forming ignimbrite eruptions have produced a complex sequence of relatively short-lived, nested and/or overlapping volcanic centres over 1.6 m.y. (Houghton et al., 1995). Eight rhyolitic caldera centres have so far been identified (Figure 1.1) of which Mangakino and Kapenga are composite features where collapse episodes related to independent periods of magmatism have coincided in geographic position (Wilson et al., 1995). Pyroclastic eruptions generating numerous but relatively small volume fall deposits and occasional ignimbrites, along with dome-building eruptions, have been present as a background between the major caldera-forming episodes. These eruptions have not been accompanied by significant caldera collapse and have occurred from vents within, or on the margins of, existing calderas (Wilson et al., 1995).

The central TVZ has a broad negative gravity anomaly upon which local anomalies, marking the caldera centres, are superimposed (Rogan, 1982; Wilson et al., 1984; Houghton et al., 1995).

This chapter reviews the eruptive history of the Okataina, Rotorua and Kapenga volcanic centres. The spatial and temporal distribution of rhyolite lavas at each volcanic centre, and their relationship to the caldera-forming ignimbrite eruptions, will be discussed. The sequence of basaltic eruptions at the Okataina Volcanic Centre will also be discussed, along

with the nature of modern hydrothermal activity at the Okataina and Rotorua volcanic centres. All ages reported in this and subsequent chapters are in calendar (cal.) years B.P., or thousands or millions of calendar (radiometric) years B.P. (ka and Ma respectively), unless otherwise stated.

2.2 OKATAINA VOLCANIC CENTRE

2.2.1 Introduction

The Okataina Volcanic Centre (OVC) is the most northeastern of the rhyolitic caldera complexes in the Taupo Volcanic Zone. The geology and geophysical expression of the OVC are known in some detail from the work of Rogan (1980, 1982) and Nairn (1981a, 1989). Okataina coincides with a major negative gravity anomaly whose contours are similar in shape to the geologically mapped Haroharo Caldera boundary (Figure 2.1). Gravity and magnetic modelling suggest that there is a caldera infill of magnetised rocks of about 600 km^3 (Wilson et al., 1984). The depth to basement at Haroharo is suggested by magnetic modelling to be no more than 2 km (Bailey and Carr, 1994).

There has been some confusion in the past over where the western and southwestern boundaries of the OVC lie in relation to the adjacent Rotorua and Kapenga volcanic centres. Ewart (1968) identified two rhyolite domes occurring between lakes Rotorua and Okataina as being part of the Rotorua Volcanic Centre (Figures 1.4 and 1.5). Subsequent studies (eg. Nairn, 1989) have redefined them as caldera-rim rhyolites of the OVC, which is now the widely accepted view. There is still debate over the specific location of the Okataina-Kapenga boundary.

2.2.2 Eruptive History

The eruptive history of the Okataina Volcanic Centre can be divided into two main periods:

1) A period of caldera formation, ending with the Rotoiti Ignimbrite eruption c. 65 ka (age from Houghton et al., 1995).
2) A period of post-caldera activity from c. 65 ka to the present, that intensified in the last c. 25 000 years, comprising caldera infilling pyroclastic and lava eruptions.

The OVC is considered to be highly active with an average of 0.08 $m^3 s^{-1}$ of erupted material over the past c. 65 ka, which makes it among the most productive rhyolitic centres documented on Earth (Wilson et al., 1995).

2.2.2.1 Caldera-forming Eruptions

Nairn (1981a, 1989) linked the OVC to at least four major and possibly two smaller caldera-forming pyroclastic eruptions in the last 400,000 years. Houghton et al. (1995) and Wilson et al. (1995) attributed only the 280 ± 10 ka Matahina Ignimbrite and the c. 65 ka Rotoiti Ignimbrite (ages from Houghton et al., 1995) to caldera collapse at this centre. However, these models may be too simplified and in the light of more recent studies (eg. Beresford and Cole, 2000) there may have been at least four caldera-forming ignimbrite eruptions at the OVC. Tables 2.1 and 2.2 give a summary of the history of rhyolitic eruptions at the OVC.

The Haroharo Caldera is defined by an elongated (28 x 16 km) area of subsidence between surrounding pre-caldera ignimbrite/rhyolite plateaus, and occupies most of the OVC (Figure 2.1). Subsidence of parts of the southern caldera floor is thought to have accompanied the eruption of the Matahina Ignimbrite, whereas subsidence of the caldera floor in the north accompanied the Rotoiti Ignimbrite eruption. The margins of the caldera have a clear topographic expression to the north, but are much less obvious to the south where collapse is considerably older and often obscured either by regional faulting or by burial beneath younger eruptives (Nairn, 1989). The eruption of the Matahina Ignimbrite may have been accompanied by shallow synchronous collapse along regional faults to form the Puhipuhi Basin (Beresford and Cole, 2000), which adjoins the eastern margin of the Haroharo Caldera. It is likely that the Matahina Ignimbrite was erupted, at least in part, from within this basin (Nairn, 1981a, 1989).

Beresford and Cole (2000) attributed eruption of the quartz-biotite ignimbrite (also known as the quartz-biotite tuffs) at 380 ± 40 ka (age from Nairn, 1989) to caldera formation at the OVC. They suggest that this unit was erupted during a large-scale volcano-tectonic event that probably affected the entire TVZ, and also included the eruption of the widespread Whakamaru Ignimbrites from the Whakamaru Volcanic Centre. Beresford and Cole (2000) also considered that caldera development accompanied the eruption of the Kawerau Ignimbrite from a source within the western part of the OVC. Outcrops of Kaingaroa

Ignimbrite occurring on the eastern side of the OVC, with an age of 240 ± 50 ka (Nairn, 1989), are now considered by Beresford and Cole (2000) to be outcrops of Kawerau Ignimbrite.

Table 2.1: Pre-65 ka rhyolitic eruptive history of the Okataina Volcanic Centre.

	Age (c. ka)	Lavas	Pyroclastics	Lava Volume (km^3)	Pyroclastics Volume (km^3)	EMV (km^3)
Rotoiti Tephra Formation	65		Rotoehu Ash		90	40
			Rotoiti Ignimbrite		150	80
			Matahi Scoria (basaltic)		1	0.5
(caldera formation)						
ho_2 Rhyolites	65 - 220 ± 10	Moerangi Rhyolites Tutaeheka Rhyolites South Rotomahana Rhyolites Lake Rotoiti Rhyolites	Te Wairoa Ignimbrites	?	?	
	220 ± 10		Mamaku Ignimbrite (Rotorua Volcanic Centre)			
	240 ± 50		Kawerau Ignimbrite (caldera formation)			?
	?		? Onuku-Pokopoko Pyroclastics			?40
	280 ± 10		Matahina Ignimbrite (caldera formation)			150
	380 ± 40		Quartz Biotite Ignimbrite (tuffs) (caldera formation)			90
ho_1 Rhyolites	>220 ± 10	Northeastern Rhyolites Western Rhyolites Southern Rhyolite		?		

Ages from Nairn (1989) and Houghton et al. (1995). Volume estimates from Nairn (1989) and Froggatt and Lowe (1990). EMV = Equivalent magma volume.

Table 2.2: Post-65 ka rhyolitic eruptive history of the Okataina Volcanic Centre.

	Age (c. cal. yrs B.P.)	Lavas	Pyroclastics	Lava Volume (km^3)	Pyroclastics Volume (km^3)	EMV (km^3)
ho_3 rhyolites Eruptive Episode*		Ruawahia, Tarawera and Wahanga Domes				
Kaharoa (T)	1314±11 A.D.	Green Lake Plug Crater Dome	Kaharoa Pyroclastics Kaharoa Ash (plinian)	2.5	5	4
Whakatane (H)	5 550	Tikorangi Dome Makatiti Dome Haroharo Dome Makatiti Flows Rotokohu Dome Okataina Flow Tapahoro Dome Tapahoro Flows Rotoroniu Flows	Minor Pyroclastic Eruptions Rotokohu Tuff Cone Whakatane Ash (plinian) Whakatane Pyroclastics	9	10	13.5
Mamaku (H)	8 050	Te Horoa Dome Hainini Dome Hainini Flow Te Matae Flow Parewhaiti Dome Ruakokopu Flow ? Otangimoana Flow ? Oruaroa Flow Waiti Flow Kaipara Flow	Te Whekau explosion breccia Local flow and surge deposits Hainini Pyroclastics Mamaku Ash (plinian)	15	6	17.5
Rotoma (H)	9 500	Te Pohue Flows Rotoma Flows	? Otamuri Pyroclastics Tuahu Pyroclastics Rotoma Ash (plinian)	2	12	7
Waiohau (T)	13 800	Kanakana Dome Pokohu Flows Waikakareao Flows Eastern Dome	 Waiohau Pyroclastics Waiohau Ash (plinian)	4	18	12
Rotorua (Ok)	15 800	Trig 7693 Dome# Middle Rhyolite#	Local flow and surge deposits Rotorua Ash (plinian)	1	7	4
Rerewha-kaaitu (T)	17 600	Southern Dome ? Te Puha Flow Western Dome ? Rotomahana Dome	 Rerewhakaaitu Pyroclastics (tuff cone) Rerewhakaaitu Ash (plinian)	2	7	5
Okareka (T)	22 500	? Patiti Island Dome ? Ridge Dome Ridge Flow Hawea Flow	 Okareka Ash (plinian)	5	8	8.5
Te Rere (H, Ok)	25 000	Eastern Rhyolite# Te Rere Dome# Haumingi Flow Te Koutu Flow Tuarae Flow ? Fenton's Mill Flow	 ? Tapuaeharuru Pyroclastics ? Te Haehaenga Pyroclastics Te Rere Ash (plinian)	8	6	11.5
Mangaone Pyroclastics Subgroup (caldera modification)	31 400 33 000 36 700 43 000		Unit L Unit K Unit J (Awakeri Tephra) Unit I (Mangaone Tephra) Unit H Unit G Unit F Unit E (Te Mahoe Tephra) Unit D (Maketu Tephra) Unit C Unit B Unit A		81 (total)	22 (total)
Rotoiti Tephra Formation (caldera formation)	c. 65 ka		Rotoehu Ash Rotoiti Ignimbrite Matahi Scoria (basaltic)		90 150 1	40 80 0.5

See following page for footnote.

Table 2.3: Ages for post-caldera eruptive episodes at the Okataina Volcanic Centre

Eruptive Episode	Nairn (1981a, 1989) ^{14}C yrs B.P.	Froggatt and Lowe (1990) ^{14}C yrs B.P.	Lowe et al. (1999) ^{14}C yrs B.P.#	Lowe et al. (1999) c. cal. yrs B.P.$^{\delta}$	Age Accepted in this Study (c. cal. yrs B.P.)
Kaharoa	800	770 ± 20	665 ± 15	1314±11 A.D.$^{\phi}$	1314±11 A.D.
Whakatane	5 500	4830 ± 20	4830 ± 20	5 550	5 550
Mamaku	7 500	7250 ± 20	7250 ± 20	8 050	8 050
Rotoma	9 000	8530 ± 10	8530 ± 10	9 500	9 500
Waiohau	11 000	11 850 ± 60	11 850 ± 60	13 800	13 800
Rotorua	13 000	13 080 ± 50		15 800$^{\phi}$	15 800
Rerewhakaaitu	15 000	14 700 ± 110	14 700 ± 95	17 600$^{\phi}$	17 600
Okareka	18 000	c. 18000		22 500$^{\phi}$	22 500
Te Rere	21 000	21 100 ± 320		25 000$^{\phi}$	25 000

\# The error weighted mean (EM) age obtained from cluster analysis.
δ The calibrated age (for details see Lowe et al., 1999) based on Stuiver et al. (1998).
ϕ D. Lowe pers. comm. (2001)

Two collapse features occurring adjacent to the Haroharo Caldera are attributed to withdrawal of underlying magma associated with the Rotoiti Ignimbrite eruption. Lake Rotoma occupies a 5 km diameter basin of subsidence, known as the Rotoma Caldera, which coalesces with the northeastern corner of the Haroharo Caldera (Nairn, 1981a, Nairn and Wood, 1987). In the southwestern OVC, lakes Okareka, Tikitapu and the northeastern part of Lake Rotokakahi occupy a basin known as the Okareka Embayment. The geological history and structure of this basin suggest that it may comprise a subsidiary embayment of the Haroharo Caldera with subsidence partly controlled by pre-existing regional faults (Nairn, 1981a).

Nairn (1989) and Beresford and Cole (2000) suggested that the Onuku-Pokopoko pyroclastics (also known as the Pokopoko Breccia, Pokopoko Ignimbrite and Onuku Pyroclastics) were also erupted from the OVC. However, Beresford and Cole (2000) did not associate these pyroclastics with caldera formation.

Footnote to Table 2.2:

Names of eruptive episodes, ho_3 lavas and associated pyroclastics from Nairn (1980, 1989). Mangaone terminology from Jurado-Chichay and Walker (2000) with the equivalent units of Howorth (1975) in brackets. Rotoiti terminology from Froggatt and Lowe (1990). Ages from Houghton et al. (1995), Lowe et al. (1999) (see Table 2.3) and Jurado-Chichay and Walker (2000). Volume estimates from Froggatt and Lowe (1990) and Jurado-Chichay and Walker (2000). EMV = Equivalent magma volume. * Volcanic complexes active given in brackets T = Tarawera, H = Haroharo, Ok = Okareka. # These rhyolites were not individually named by Nairn (1980) and the names shown here will be used in this study.

The eruption of the Mangaone Pyroclastics Subgroup is attributed to caldera modification (Nairn, 1989). Eight tephra formations comprising the Mangaone Pyroclastics Subgroup were identified and defined by Howorth (1975, 1976). More recently, Jurado-Chichay and Walker (2000) and Smith (2001) have identified new tephras within this subgroup. The revised sequence of eruptives according to Jurado-Chichay and Walker (2000) is given in Table 2.2. Only four of the tephra formations identified and defined by Howorth (1975, 1976) are equivalent to new units. Smith (2001) identified two additional units, the Pupuwharau and Pongakawa tephras, occurring between units C and D. Jurado-Chichay and Walker (2000) presented some new ^{14}C ages for some of the Mangaone Subgroup tephras. An age of c. 31 400 years B.P. was obtained for the youngest of the tephras (Unit L) along with an age of c. 36 700 years B.P. for the Te Mahoe tephra. These ages imply that the eight youngest tephras were erupted in only c. 5 000 years. Jurado-Chichay and Walker (2000) suggested that the earliest eruption (Unit A) may have been at c. 43 000 years B.P. and that the entire subgroup may have been erupted over a period of time shorter than originally estimated by Froggatt and Lowe (1990).

2.2.2.2 Rhyolite Lavas - ho_1 and ho_2

The ho_1 rhyolites were erupted prior to the eruption of the Mamaku Ignimbrite from the Rotorua Volcanic Centre at 220 ± 10 ka. Figure 2.1 shows the location of these rhyolites in relation to the collapse structures of the OVC. They generally occur on or adjacent to the caldera rim, and vents may mark the locations of underlying ring fractures up which magma was extruded early in the Okataina eruptive sequence (Nairn, 1989).

The ho_1 rhyolites can be divided spatially into three groups:

- The northeastern rhyolites of Maungawhakamana, North Rotoma, Waitangi, and Matawhaura
- The western rhyolites of Whakapoungakau, Pukepoto, Crater Farm and Stancorp Quarry
- The southern rhyolite of Wairua

Ages are not available for the ho_1 rhyolites. However, Nairn (1989) mapped all ha_1 (ho_1) OVC rhyolites as older than the Matahina Ignimbrite (280 ± 10 ka) and noted that this ignimbrite has been observed in outcrop overlying Maungawhakamana rhyolite. Such a relationship has not been observed for other ho_1 rhyolites. Nairn (1981a) thought that these

ha_1 rhyolites were probably extruded both prior to and following eruption of the "quartz-biotite tuffs" at 380 ± 40 ka. Hence the ho_1 rhyolites may include both pre-caldera and post-caldera eruptives and may be magmatically related to any of the three caldera-forming ignimbrites erupted from the OVC prior to 220 ± 10 ka.

The ho_2 rhyolites were erupted between 220 ± 10 and c. 65 ka. The majority of lavas erupted at this time occur adjacent to the caldera rim in the southwestern OVC. Two ho_2 rhyolites occurring in the northwestern OVC, south of Lake Rotoiti (Nairn, 1989), were not sampled in this study and will not be discussed further.

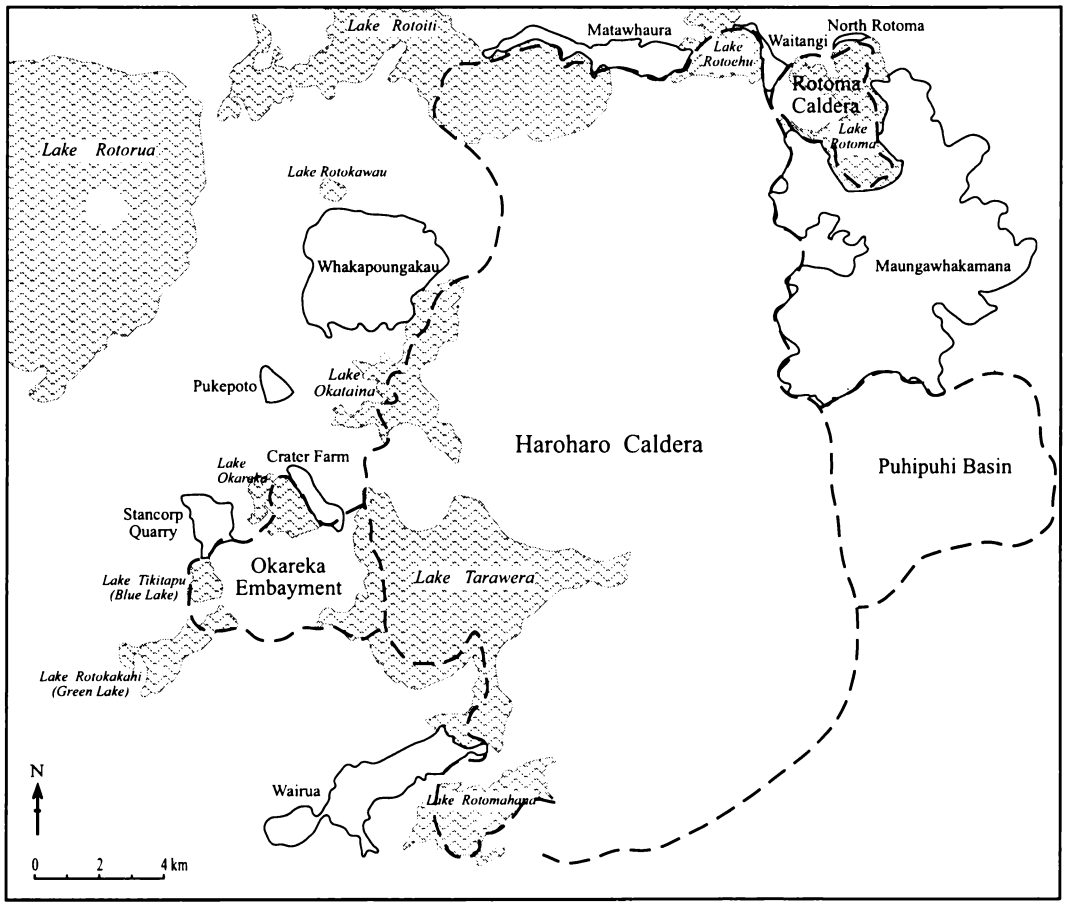

Figure 2.1: The distribution of ho_1 rhyolite lavas and their spatial relationships to the collapse features of the Okataina Volcanic Centre. Redrawn and modified from Nairn (1989).

Vents for the ho_2 rhyolites occur on a NW-SE trend and the rhyolites cluster spatially into three groups, shown in Figure 2.2:

- The Moerangi Rhyolites comprising the Direct Road, Hill Road, Moerangi Road, Chestnut Road, Green Lake, Blue Lake and Kakapiko domes
- The Tutaeheka Rhyolites which in this study have been numbered from northwest to southeast (1, 2 and 3)
- The South Rotomahana Rhyolites of Waimangu and Hapeotoroa

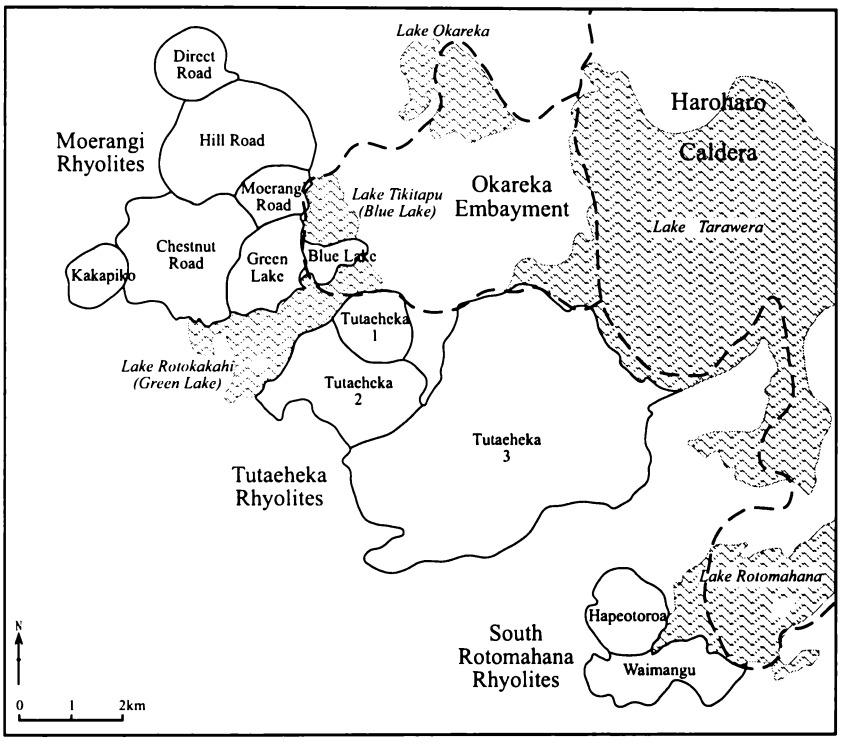

Figure 2.2: The distribution of ho_2 rhyolite lavas and their spatial relationships to collapse features in the southwestern Okataina Volcanic Centre. Complied from Ewart (1968), Nairn (1981a, 1989) and Bellamy (1991).

The Te Wairoa Ignimbrites described by Bellamy (1991) were erupted in association with the ho_2 rhyolites, and it is highly likely that there were other minor pyroclastic eruptions during this episode.

Ages are not available for the ho_2 rhyolites. However, the range of possible ages based on stratigraphy (220 ± 10 - c. 65 ka) suggests that they may have been erupted following the first episode of collapse at Okataina, associated with the eruption of the Matahina and

Kawerau Ignimbrites, or prior to the second collapse event associated with the Rotoiti Ignimbrite eruption. Some of the Moerangi domes are observed as being directly overlain by Rotoehu Ash (I. Nairn, pers. comm., 1999), which was erupted contemporaneously with the Rotoiti Ignimbrite. This suggests a temporal association with the second episode of collapse. However, the distance between the source of this ignimbrite in the northern OVC and the location of the ho_2 rhyolites may preclude a genetic relationship.

At approximately the same time as the Rotoiti Ignimbrite was being erupted in the northern OVC, the Earthquake Flat (EQF) Ignimbrite was being erupted in an area adjacent to the southwestern OVC that is currently considered to be a part of the Kapenga Volcanic Centre (see section 2.4.2.2). Therefore the ho_2 domes are spatially adjacent to the source of the EQF Ignimbrite and may be related to this eruption, which did not involve caldera collapse. Some studies have classed these ho_2 rhyolites as eruptives of the Kapenga Volcanic Centre (eg. Wilson et al., 1984) but others (eg. Ewart, 1968; Nairn, 1989) suggested they are part of the OVC. Nairn (2000) has classed these rhyolites as eruptives of Kapenga (hk_2) based primarily on structural interpretation of the Okataina and Kapenga boundaries. It is hoped that this study will shed some light on this problem.

The names used in this study for ho_1 and ho_2 rhyolites follow those used in previous studies (eg. Nairn, 1989; Bellamy, 1991) or have been named after geographic localities.

2.2.2.3 Post-Caldera Eruptive Sequence and ho_3 Rhyolite Lavas

The post-caldera sequence of events at the Okataina Volcanic Centre has been well established due to the work of Nairn (1980, 1981a), particularly for the last c. 25 000 years. Post-caldera activity at the OVC has involved the eruption of rhyolite lava domes and flows (ho_3), with interbedded pyroclastic flow and fall deposits, that have largely infilled the collapse structures. The eruptives can be divided spatially into three groups, shown in Figure 2.3:

- The Haroharo Volcanic Complex has grown on the northern and central floor of the Haroharo Caldera. Lavas and pyroclastics infilling the adjacent Rotoma Caldera are also considered part of this complex.
- The Tarawera Volcanic Complex has grown on the southeastern floor of the Haroharo Caldera.
- The Okareka Volcanic Complex has infilled the Okareka Embayment.

The post-caldera rhyolitic activity forming these volcanic complexes has occurred in nine eruptive episodes (Nairn, 1989) during the past c. 25 000 years separated by quiescent periods. Table 2.2 lists the lavas and pyroclastics erupted during each episode according to Nairn (1980, 1989), along with estimated volumes. Froggatt and Lowe (1990) proposed that all the primary pyroclastic products of one eruptive episode should be referred to as a tephra formation. This terminology will be adopted in subsequent discussions of the pyroclastics associated with the rhyolite lavas. For example, the pyroclastics of the Mamaku eruptive episode will be referred to collectively as the Mamaku Tephra Formation comprising the Mamaku Tephra (previously the Mamaku Ash) and other associated pyroclastics. The episodes are generally named after the major tephra erupted at that time.

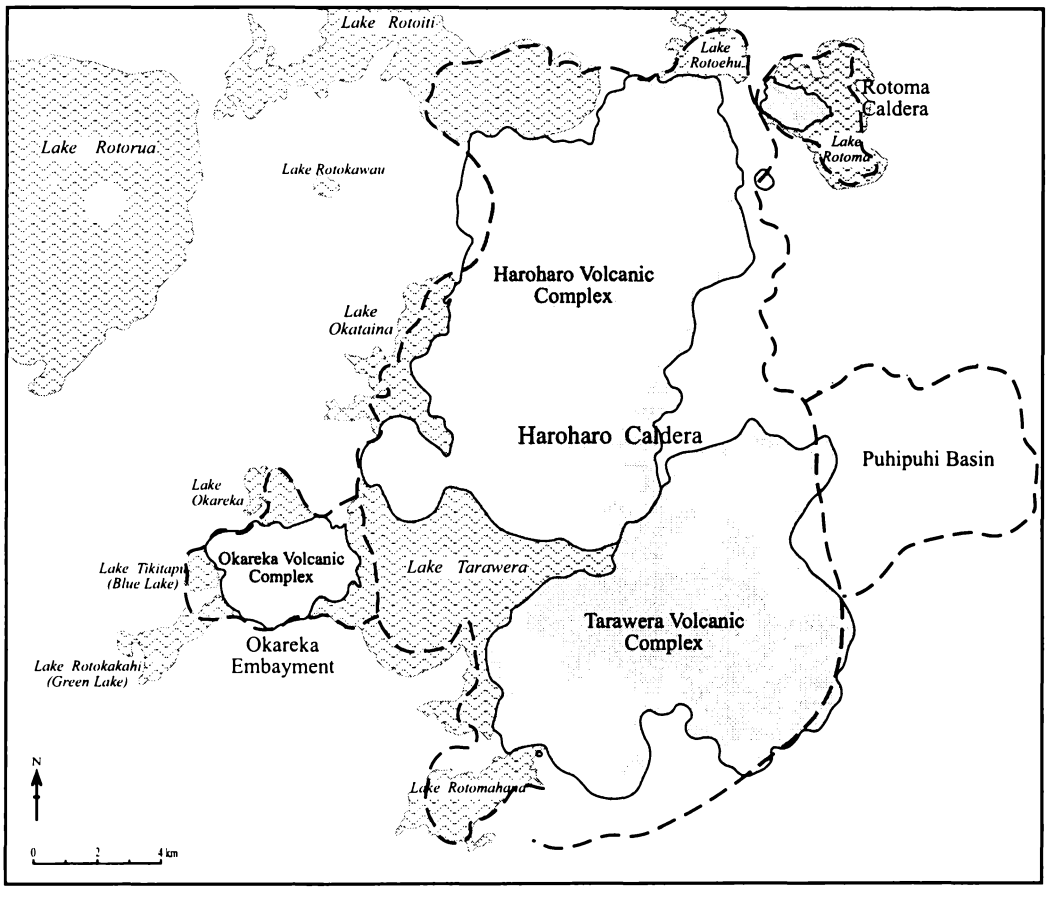

Figure 2.3: The distribution of ho_3 rhyolite lavas and their spatial relationship to the collapse features of the Okataina Volcanic Centre. Redrawn and modified from Nairn (1989).

It should be noted that no direct ages have yet been obtained for the ho_3 rhyolite lavas and that they have been dated based on their stratigraphic relationships to the ^{14}C-dated pyroclastics. Ages proposed for the eruptive episodes and those used in this study are given in Table 2.3. Figures 2.4 and 2.5 show the distribution of lavas comprising the Haroharo and Tarawera volcanic complexes, respectively. The names given to these lavas by Nairn (1989), which will be used in this study, and the episode in which they were erupted, are shown. Figure 2.6 shows the distribution of lavas comprising the Okareka Volcanic Complex. Nairn (1980) did not formally name these lavas and the names appointed and used in this study are given in Figure 2.6.

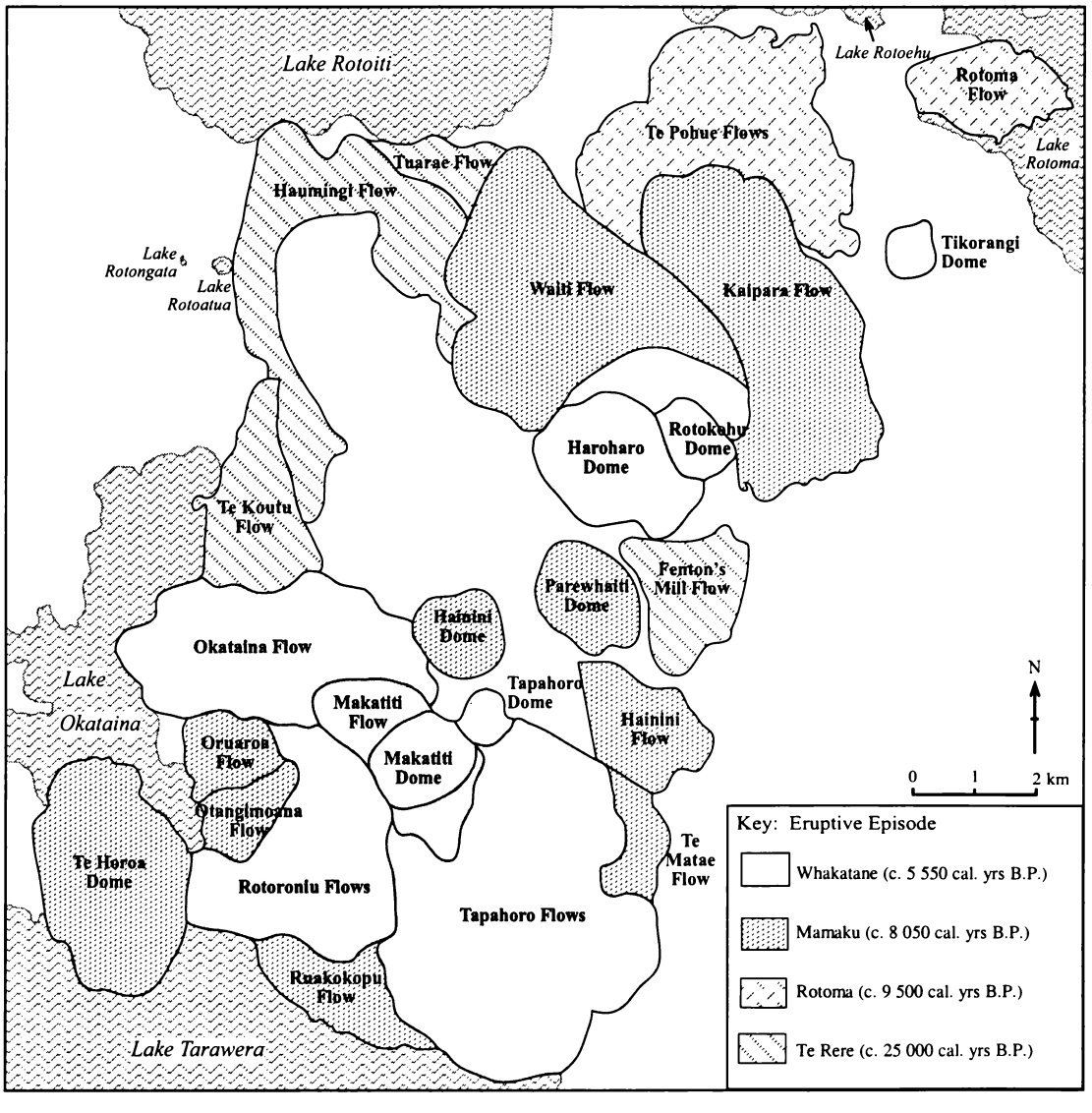

Figure 2.4: Rhyolite lavas of the Haroharo Volcanic Complex. Redrawn and modified from Nairn (1989).

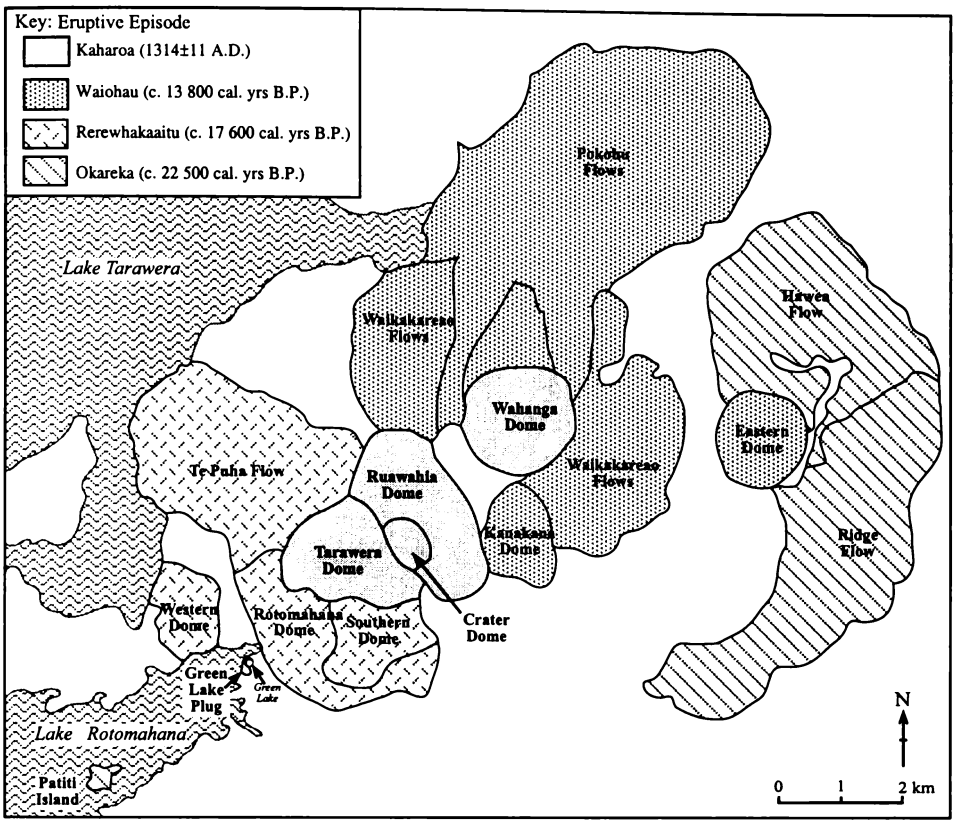

Figure 2.5: Rhyolite lavas of the Tarawera Volcanic Complex. Redrawn and modified from Nairn (1989).

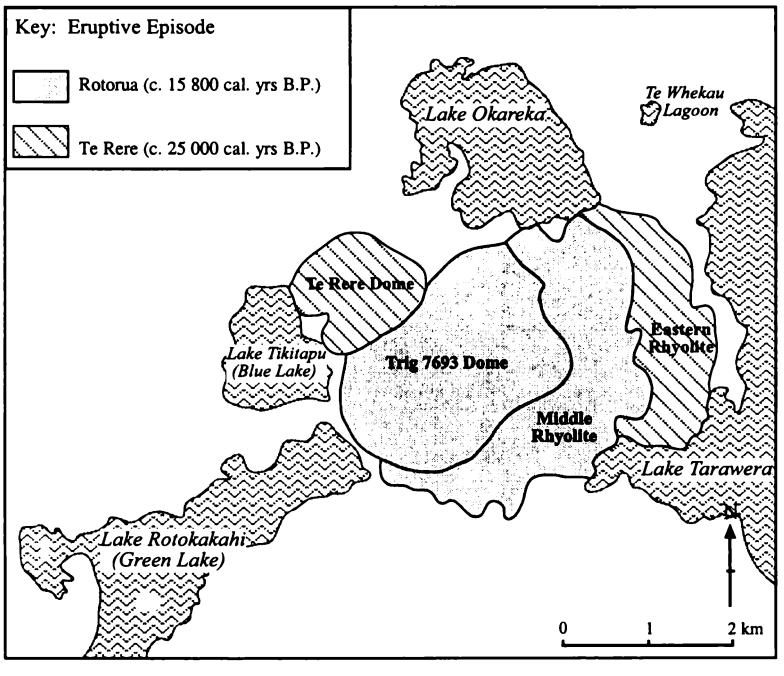

Figure 2.6: Rhyolite lavas of the Okareka Volcanic Complex. Redrawn and modified from Nairn (1980).

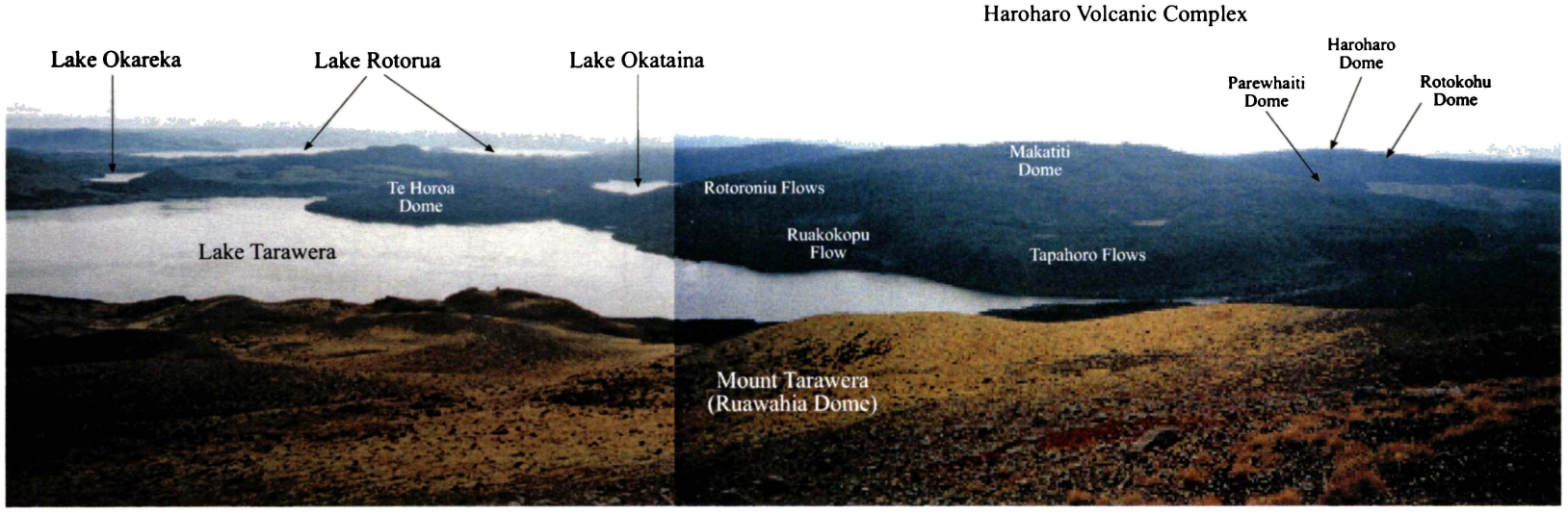

Plate 2.1: View looking northwest from the summit of Mount Tarawera, across Lake Tarawera to the Haroharo Volcanic Complex.

The Haroharo Volcanic Complex (shown in Plate 2.1) was built up in four rhyolitic eruptive episodes beginning c. 25 000 years B.P. The Okareka Volcanic Complex was built up in two eruptive episodes at c. 25 000 years B.P. (simultaneously with activity at Haroharo) and at c. 15 800 years B.P. The vents for these eruptions lie within a 4 km wide, 050° trending zone known as the Haroharo Linear Vent Zone (HLVZ) and shown in Figure 2.7. This zone extends between the Okareka Embayment and the Rotoma Caldera, and represents a deep seated basement fracture that has controlled the location of post-caldera activity (Nairn, 1989).

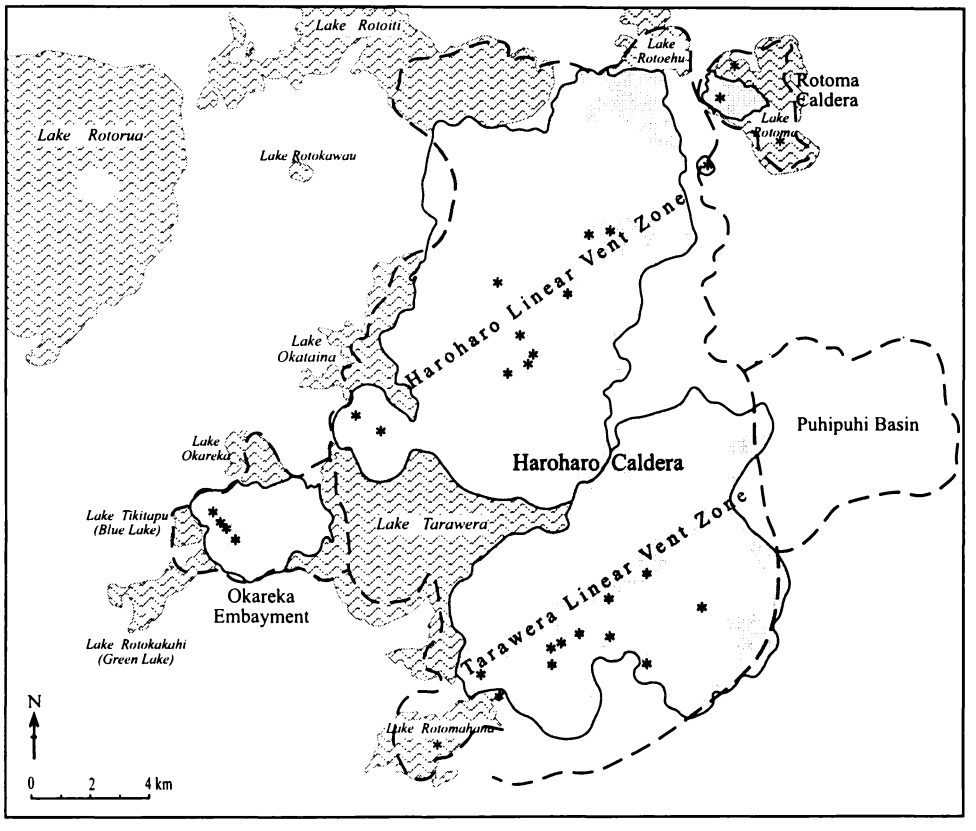

Figure 2.7: The Haroharo and Tarawera linear vent zones. The ho_3 rhyolite vent locations are marked with an asterisk. Redrawn and modified from Nairn (1989).

The Tarawera Volcanic Complex was built up in four different rhyolitic eruptive episodes beginning c. 22 500 years B.P. (Nairn, 1989). This complex is the site of the most recent rhyolitic eruption from the TVZ (Kaharoa Eruptive Episode, 1314±11 A.D.). The most recent activity from this complex occurred on 10 June 1886, and was basaltic in composition. As at Haroharo, the Tarawera Volcanic Complex vents appear to lie above a

deep-seated basement fracture zone known as the Tarawera Linear Vent Zone (TLVZ) and shown in Figure 2.7. All the known (both rhyolitic and basaltic) vent locations on the Tarawera Volcanic Complex lie within a 5 km wide, 057° trending zone that extends northeast from the basaltic phreatomagmatic/phreatic 1886 A.D. craters at Waimangu, through Lake Rotomahana and Mount Tarawera. The 17 km long Tarawera fissure, defined by the craters produced by the 1886 A.D. eruption, lies within the TLVZ (Nairn, 1989). The deep craters of the fissure bisect the rhyolite domes and flows of the Tarawera Volcanic Complex (Plates 2.2 and 2.3). At no time during the last c. 25 000 years have the Haroharo and Tarawera linear vent zones been active simultaneously.

During the c. 25 000 years B.P. Te Rere Eruptive Episode, eruption of the Te Rere Tephra Formation (Te Rere Tephra and associated pyroclastics) was followed by the extrusion of the oldest exposed lava flows at the Haroharo and Okareka volcanic complexes. The Te Rere Tephra Formation was erupted from multiple vents, now buried, along the HLVZ (Nairn, 1981a; Nairn and Wood, 1987; Nairn, 1992).

The c. 22 500 years B.P. Okareka Eruptive Episode marks commencement of growth of the Tarawera Volcanic Complex. Near-vent exposures of Okareka Tephra include a basal sub-plinian basalt lapilli layer indicating a basalt eruption may have triggered the much larger rhyolitic eruptions which followed (see section 2.2.2.4). The Okareka Eruptive Episode terminated with extrusion of the oldest exposed lavas of the Tarawera massif and the vent for the Okareka Tephra was probably the same as that for these lavas (Nairn, 1981a; 1992). The Patiti (Banded) Island rhyolite was probably also erupted around this time as it is overlain by Rerewhakaaitu Tephra (Nairn, 1981a).

The c. 17 600 years B.P. Rerewhakaaitu Eruptive Episode followed at Tarawera from vents to the southwest. Rotomahana Dome was extruded early, followed by major pyroclastic eruptions with widespread dispersal of the Rerewhakaaitu Tephra. These pyroclastic eruptions were terminated by extrusion of Southern Dome in the vent. Lavas were extruded from two other vents about this time forming Western Dome and the Te Puha Lava Flow (Nairn and Wood, 1987).

Plate 2.2: View northeast along the Tarawera fissure from Ruawahia Dome towards Wahanga Dome.

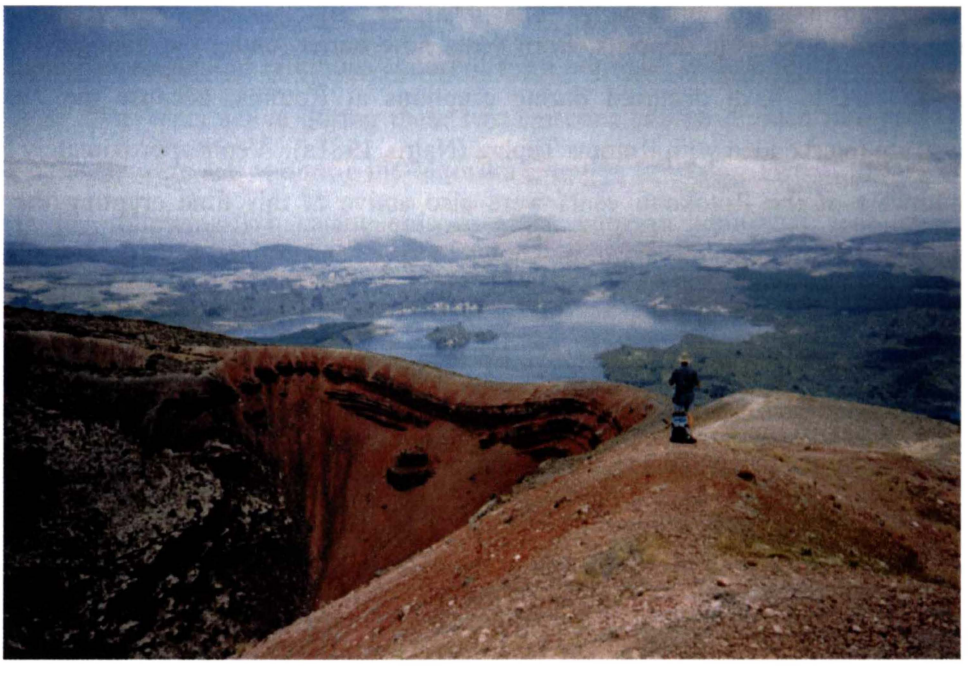

Plate 2.3: View southwest along the Tarawera fissure from the edge of Tarawera Dome across Lake Rotomahana towards the Waimangu Thermal Valley.

The next eruptions at the Okataina Volcanic Centre took place in the Okareka Embayment with the eruption of the c. 15 800 years B.P. Rotorua Tephra and associated local pyroclastics. Lava extrusion was the final phase of the eruption, filling the main pyroclastic vent (Nairn, 1980; Nairn and Wood, 1987).

During the c. 13 800 years B.P. Waiohau Eruptive Episode from Tarawera, Eastern Dome was extruded before the main pyroclastic eruptions from the Kanakana vent. Pyroclastic flows and voluminous lava flows (Waikakareao) accompanied the eruption of the widespread Waiohau Tephra (Nairn and Wood, 1987). The eruption of the Waiohau Tephra Formation was terminated by extrusion of Pokohu Lava Flows. The final event in this eruptive episode was the extrusion of Kanakana Dome to fill the source vent (Nairn, 1981a).

At Haroharo the c. 15 500 year quiescent interval which followed the Te Rere eruption was ended by the c. 9 500 years B.P. Rotoma Eruptive Episode. Within the Rotoma Caldera the Rotoma Lava Flow was extruded. Dome-shaped elevations on the floor of Lake Rotoma were assumed by Nairn (1981a) to be rhyolite domes extruded at the same time as the Rotoma Lava Flow. The eruption of the Rotoma Tephra continued after lava extrusion had ceased. Other lavas and pyroclastics were erupted from vents in the northern Haroharo Caldera at about this time (Nairn and Wood, 1987). Extrusion of the Te Pohue Lava Flows and associated pyroclastic deposits, from vents now buried under the younger Rotokohu Dome, appears to have occurred during eruptions at Rotoma, because the Te Pohue eruptives are interbedded with Rotoma Tephra (Nairn, 1981a). Vents approximately 5 km to the southwest of the Rotokohu vents were also active at this time erupting the Tuahu pyroclastics and tuff cone. No lavas are known to have been erupted from these vents.

The c. 8 050 years B.P. Mamaku Eruptive Episode began with northward extrusion of lavas from vents now buried under the younger Haroharo and Rotokohu domes, followed by eruption of the Mamaku Tephra, interbedded near source with small pyroclastic flow deposits. Other flows and domes were extruded at this time to the southwest. The Mamaku episode vents were spread over ~ 14 km of the Haroharo vent zone. The main pyroclastic vent was probably in the vicinity of Hainini Dome or the younger Makatiti Dome (Nairn and Wood, 1987).

The Whakatane Eruptive Episode at c. 5 550 years B.P. is the latest to have occurred from the Haroharo Volcanic Complex, with eruptions from at least five vents over ~ 11 km of the

Haroharo Linear Vent Zone. Pyroclastic eruptions depositing the Whakatane Tephra and Whakatane Pyroclastics began from a main vent later buried under Makatiti Dome. Voluminous lava flows and domes were extruded following the main pyroclastic eruptions from this vent. Eruptions at the vents for Haroharo and Rotokohu domes also commenced during the Makatiti sequence. Extrusion of Haroharo Dome followed the end of eruption of Whakatane Tephra. Extrusion of Tikorangi Dome to the northeast concluded this episode of activity (Nairn, 1981a; Nairn and Wood, 1987).

The Kaharoa Eruptive Episode (1314±11 A.D.) is the most recent rhyolitic episode to have occurred from the Tarawera Volcanic Complex and the Taupo Volcanic Zone. This episode involved the eruption of the Kaharoa Tephra Formation and the extrusion of Wahanga, Ruawahia, Crater and Tarawera domes, which are seen today capping the Tarawera massif. Crater Dome is considered to have been erupted first and has subsequently been "buried" by the younger Ruawahia and Tarawera domes (Cole, 1970a). The Green Lake Plug on the eastern shore of Lake Rotomahana was also erupted at this time. This episode of activity is also considered to have had a basaltic trigger (Leonard, 1999).

Within a particular eruptive episode it is common for more than one vent to be active. This is particularly the case for the Mamaku and Whakatane eruptive episodes when simultaneous or sequential eruptions occurred from multiple, widely separated vents along the HLVZ. The vents active during these two episodes can be divided into 'vent areas'. Three vent areas were active during the Mamaku Eruptive Episode. Two of these were also active in the following Whakatane episode along with an additional vent area to the northeast (Figure 2.8). The 'vent area' concept introduced here will form an important part of discussions in subsequent chapters.

2.2.2.4 Basaltic Eruptions

The most recent activity within the Okataina Volcanic Centre was the June 10 1886 basaltic plinian eruption from Mount Tarawera, producing pyroclastics with an equivalent magma volume of ~ 1.5 km^3 (Walker et al., 1984; Froggatt and Lowe, 1990). The eruption commenced at Ruawahia Dome and extended both southwest and northeast across the rhyolite domes and flows of the Tarawera Volcanic Complex (Keam, 1988). Phreatomagmatic and phreatic explosions followed at Lake Rotomahana and Waimangu (Nairn and Cole, 1981; Keam, 1988). Basaltic dikes can be seen exposed in the Tarawera

fissure representing feeders for the pyroclastic eruptions (Cole, 1970a; Nairn and Cole, 1981; Walker et al., 1984) although no basaltic lavas were erupted.

Although the eruption of basalt from the OVC in 1886 A.D. was originally considered unusual, six other pyroclastic eruptions involving a basaltic component have been identified in the eruptive history of the OVC in the last c. 65 000 years. No basaltic lavas have been erupted. The potential role of basalt in triggering rhyolitic eruptions at the OVC is not yet fully understood, but has been discussed in recent studies (eg. Leonard, 1999).

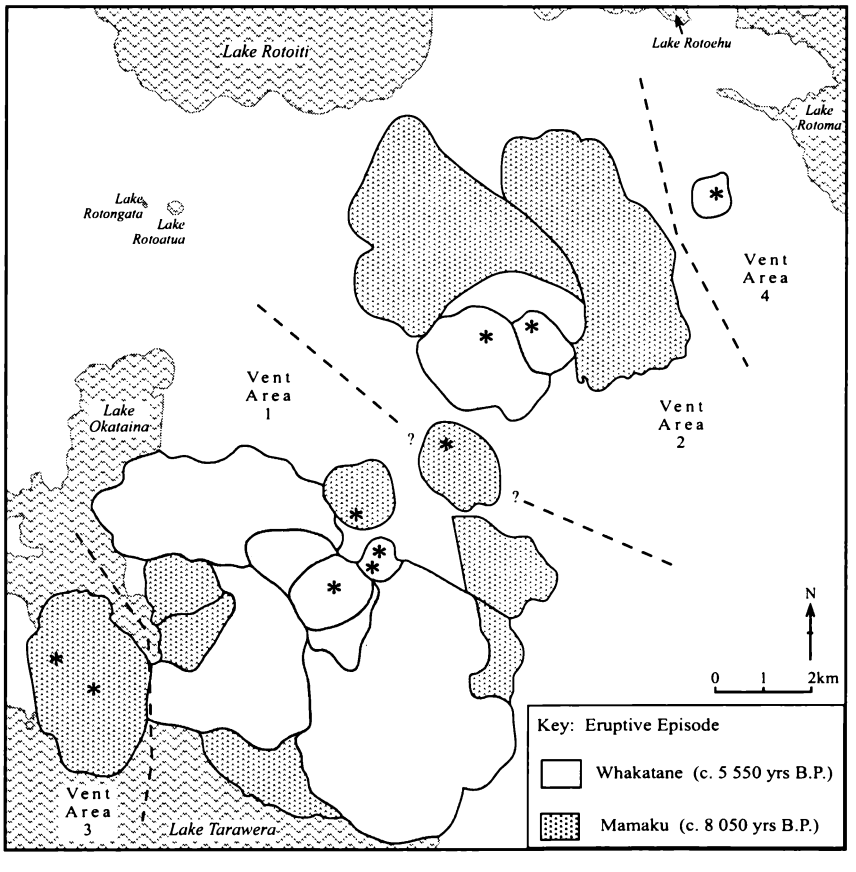

Figure 2.8: Rhyolite lavas of the Haroharo Volcanic Complex erupted during the Mamaku and Whakatane eruptive episodes. Vents that were active are marked with an asterisk (from Nairn, 1989). The vents have been divided into four vent areas.

The Matahi Scoria is the basal member of the Rotoiti Tephra Formation of Froggatt and Lowe (1990), also known as the Rotoiti Pyroclastics, erupted c. 65 ka. It consists of vesicular black basaltic ash and lapilli with a minor content of rhyolite ash and lapilli (Pullar and Nairn, 1972). The lack of basaltic clasts in the overlying rhyolitic deposits, as found by Davis (1985), implies a short time break (though not sufficient for erosion or soil formation) between the basaltic and rhyolitic events (Houghton et al., 1987). The scoria has a limited distribution occurring beneath the Rotoiti Ignimbrite only in exposures to the east and northeast of Lake Rotoma suggesting a source in the Rotoma area (Pullar and Nairn, 1972). The Matahi scoria is petrographically similar to other TVZ high-alumina basalts, but since it is contaminated by rhyolite, has an overall mixed "andesitic" chemistry (Nairn and Wood, 1987).

On the northwestern shore of Lake Rotomahana a basaltic scoria directly overlies a small rhyolitic tuff cone. This deposit has been named the Rotomakariri Scoria and contains black scoriaceous ash, lapilli and bombs with abundant rhyolite lithics. Rhyolite inclusions are common within the scoria bombs. Some assimilation of rhyolite magma has produced quartz-olivine hybrid rocks of andesitic composition. The source for the scoria and the underlying rhyolitic tuff cone is thought to have been located beneath the present-day Lake Rotomahana (Nairn, 1989). Nairn (1989) notes that Kawakawa Tephra mantles the upper surface of the scoria, and that the Mangaone Pyroclastics are absent. Hence, ages for the Kawakawa Tephra and the youngest of the Mangaone Pyroclastics (Unit L) constrain the age of the Rotomakariri Scoria eruption to between c. 26 500 and 31 400 years B.P. (ages from Wilson (1993) and Jurado-Chichay and Walker (2000)).

The c. 22 500 years B.P. eruption of the Okareka Tephra, from vents since buried beneath the Tarawera volcanic massif, was immediately preceded by a small basaltic scoria eruption, apparently from vents close to those for the rhyolite eruptions. The scoria consists of loosely shower bedded, well-sorted, dark grey to black, weakly vesicular dense clasts up to ~ 1-2 cm in dimension (Nairn, 1992). Some clasts are pure basalt while others include assimilated rhyolitic country rock. Many of the scoria clasts are coated with a grey rhyolitic ash fused to the surface. The scoria is typical TVZ high-alumina basalt. Dacitic pumice clasts and banded clasts also occur within the rhyolitic unit and represent basalt and rhyolite magma mixing and mingling respectively (Nairn, 1992). Nairn (1992) saw this scoria as analogous to the Matahi Scoria and suggested both rhyolitic eruptions were initiated by basaltic intrusion.

A basaltic component has been identified in the c. 9 500 years B.P. eruption of the Tuahu Pyroclastics (also known as Pukerimu Pyroclastics) during the Rotoma Eruptive Episode at the Haroharo Volcanic Complex (Nairn, 1981a; Houghton et al., 1987). Nairn (1981a) observed basaltic accessory lithics in the pyroclastics, while Houghton et al. (1987) suggested the eruptives show evidence for liquid-liquid mixing of basalt and rhyolite immediately prior to eruption.

Basaltic phreatomagmatic eruptions occurred on the northwestern margin of the OVC c. 3 700 years B.P. during the Rotokawau Eruptive Episode (Froggatt and Lowe, 1990). The four maars formed in these eruptions contain the lakes of Rotokawau, Rotoatua and Rotongata (Beanland, 1981; Beanland and Houghton, 1991).

A basaltic component has also been identified in pyroclastics from the Kaharoa Eruptive Episode (1314±11 A.D.). Pyroxene basalt was intruded into the Tarawera Volcanic Complex prior to the eruption, and was subsequently erupted as small pillowed inclusions in the eruptives and as rhyolite coated clasts (Nairn, 1981a; Nairn and Cole, 1981; Nairn and Wood, 1987). Cole (1970c) identified the blocks found in the Kaharoa deposits as basalt and dolerite, believing the dolerite to have formed from the sinking of olivine and augite phenocrysts within the basaltic intrusion. Leonard (1999) provided evidence for both mixing and mingling between basalt and rhyolite magmas in the Kaharoa eruption.

2.2.2.5 Modern Hydrothermal Activity

Evidence that the OVC remains active to this day is seen in hydrothermal activity that is located throughout the centre. The Waimangu Thermal Valley, a well-known tourist attraction, occurs in the southern OVC. At Lake Okataina bubbles of gas, dominantly CO_2, rise from the eastern side of the lake and a seepage of warm water occurs through the beach sands at times of low lake level (Nairn, 1989). Hydrothermal activity is known in three areas on the northern, eastern and southern shores of Lake Tarawera. The most intense activity occurs on the southern shore where steam rises from the surface of the lake. On shore, water can be seen discharging from rocks at a temperature of 37-90°C. This activity is associated with the two arms of the bifurcating Paeroa Fault (Nairn, 1989). Lake Rotomahana is up to 3°C warmer than Lake Tarawera in winter, both at the surface and at depth. Lake bottom temperatures are 4-5°C higher in Rotomahana than in other nearby

lakes of similar size and depth (Nairn, 1989). These elevated temperatures suggest the presence of submerged hot springs. On the southwestern shore of Lake Rotomahana are the "steaming cliffs" comprising hydrothermally altered rock with boiling springs, geysers and fumaroles.

Some minor fumarolic activity has been noted on Mount Tarawera within the craters of the 1886 A.D. fissure (Nairn, 1989). Warm springs are located on the northwest toe of the Hawea Lava Flow and on the southeast edge of the Fenton's Mill Lava Flow. These springs represent the highly diluted surface discharge of geothermal waters flowing outwards at depth from the Haroharo and Tarawera volcanic complexes (Nairn, 1989). Evidence of previous hydrothermal activity can been seen in areas of hydrothermally altered rocks, for example on the eastern edge of the Kaipara Lava Flow.

Nowhere in the OVC does modern hydrothermal activity occur at great intensity. This situation contrasts with that prior to 1886 A.D. when the Rotomahana Basin was the most intensely active hydrothermal field in the Rotorua region with many boiling springs, geysers, fumeroles and the siliceous sinter Pink and White Terraces (Nairn, 1989). Nairn (1981a, 1989) provided a more detailed discussion of hydrothermal fields associated with the OVC.

2.3 ROTORUA VOLCANIC CENTRE

2.3.1 Introduction

The Rotorua Volcanic Centre (RVC) occurs in the northern central Taupo Volcanic Zone to the west of the OVC (Figures 1.1 and 1.2). The geology and geophysics of the RVC are not known in as much detail as for the OVC. The RVC comprises the Rotorua Caldera which coincides with a modest negative gravity anomaly modelled by Rogan (1982) as a 500-1500 m deep, 200 km^3 basement depression whose lowest point is in the southwestern part of the caldera under Rotorua City. Basement highs clearly separate it from the adjacent Okataina and Kapenga volcanic centres (Wilson et al., 1984). A disparity between gravity and magnetic models implies the presence at depth of low-density nonmagnetic material (Rogan, 1982), which Wilson et al. (1984) thought likely to be hydrothermally altered. The caldera is marked to the south, east and north by a roughly circular fault scarp approximately 17 km

across, whereas to the west the ground surface is gently downwarped into the basin (Wilson et al., 1984).

2.3.2 Eruptive History

2.3.2.1 Caldera-forming Eruptions

Wilson et al. (1984) described Rotorua as a single-event caldera formed by collapse following the eruption of the Mamaku Ignimbrite at 220 ± 10 ka (age from Houghton et al., 1995). This ignimbrite covers a broad sector southwest to north of the caldera in a fan shape (Nairn and Wood, 1987) and caps the Mamaku Plateau (Figure 1.2). Its in situ volume is at least 300 km^3 (Wilson et al., 1984). The distribution and stratigraphy of the Mamaku Ignimbrite have been discussed in detail by Milner (2001). Recently, a more complex history for the RVC has been implied with the centre being linked to the eruption of the older Pokai Ignimbrite (Wood, 1992; Wilson et al., 1995). However, Karhunen (1993) and Lynch-Blosse (1998) suggested that this ignimbrite is more likely to be sourced from the Kapenga Volcanic Centre. Lynch-Blosse (1998) considered that Waimakariri Ignimbrite (estimated age of c. 290-300 ka) was erupted from the RVC prior to the Mamaku Ignimbrite. Any evidence of caldera collapse associated with the eruption of this ignimbrite has not yet been found and may have been overprinted or buried by the subsequent Mamaku Ignimbrite eruption (Lynch-Blosse, 1998). However, Milner (2001) considered the volume of the Rotorua Caldera insufficient to accommodate eruption of the Waimakariri Ignimbrite. Table 2.4 gives a summary of activity at the RVC and eruptive volume estimates.

2.3.2.2 Pre-Mamaku Ignimbrite Eruptions - hr_l Rhyolite Lavas

The only certain evidence of pre-Mamaku Ignimbrite activity at the RVC is the exposure of hr_l rhyolite lavas on the edges of the caldera. These rhyolites, shown in Figure 2.9, have a combined volume of 1.5 km^3 (Wilson et al., 1984). They can be divided spatially into three groups:

- The northern rhyolites of Hamurana and Fryer Road
- The western rhyolites of Endean Road and Umurua
- The southern rhyolites of Tokorangi and Hemo Gorge

Table 2.4: Summary of the eruptive history of the Rotorua Volcanic Centre.

Unit	Age (ka)	Volume (km^3)	EMV (km^3)	Caldera Collapse
hr_3 rhyolites Mokoia Island Hinemoa Point Vaughan Road	< c. 65 (> c. 15 800 yrs B.P.)$^{\phi}$	<0.2	<0.2	
Rotoiti Tephra Formation (Okataina Volcanic Centre)	c. 65			
hr_2 rhyolites Ngongotaha Complex Pukehangi Complex Kawaha Point Pukeroa Hill Paradise Valley Ignimbrites	c. 65 - 220 ± 10	4	4	
Mamaku Ignimbrite	220 ± 10	>300	~200	yes
hr_1 rhyolites Endean Road/Umurua Hamurana/Fryer Road Hemo Gorge/Tokorangi	> 220 ± 10	1.5	1.5	
?Waimakariri Ignimbrite	c. 290 - 300	?	?	no evidence to date

Ages for the Rotoiti and Mamaku Ignimbrites from Houghton et al. (1995), Waimakariri Ignimbrite from Lynch-Blosse (1998). ϕ Age from Table 2.3. Volume estimates from Wilson et al. (1984). EMV = Equivalent magma volume.

The Fryer Road rhyolite has not been sampled in this study and, other than initial identification (Dravitzki, 1999) and petrographic observations (Milner, 2001), little is known about this unit. The Umurua rhyolite, first identified by Dravitzki (1999), has also not been sampled in this study. The relationship of these two rhyolites to adjacent hr_1 rhyolites is not clear. Milner (2001) suggested that the Endean Road and Umurua rhyolites may be the same unit. Ewart (1968) noted that the Tokorangi/Hemo Gorge rhyolites may comprise part of the Haroharo-Waiotapu group rhyolites (Figure 1.6), which are now known to be associated with the Kapenga Volcanic Centre.

Lynch-Blosse (1998) proposed that at least some of these hr_1 lavas represent the effusion of degassed magma following the eruption of the Waimakariri Ignimbrite and considered that the current best estimate for the age of the hr_1 domes in the Rotorua Basin is c. 290-300 ka. Ages for the hr_1 rhyolites have either not yet been determined or published and so this possibility cannot be discounted.

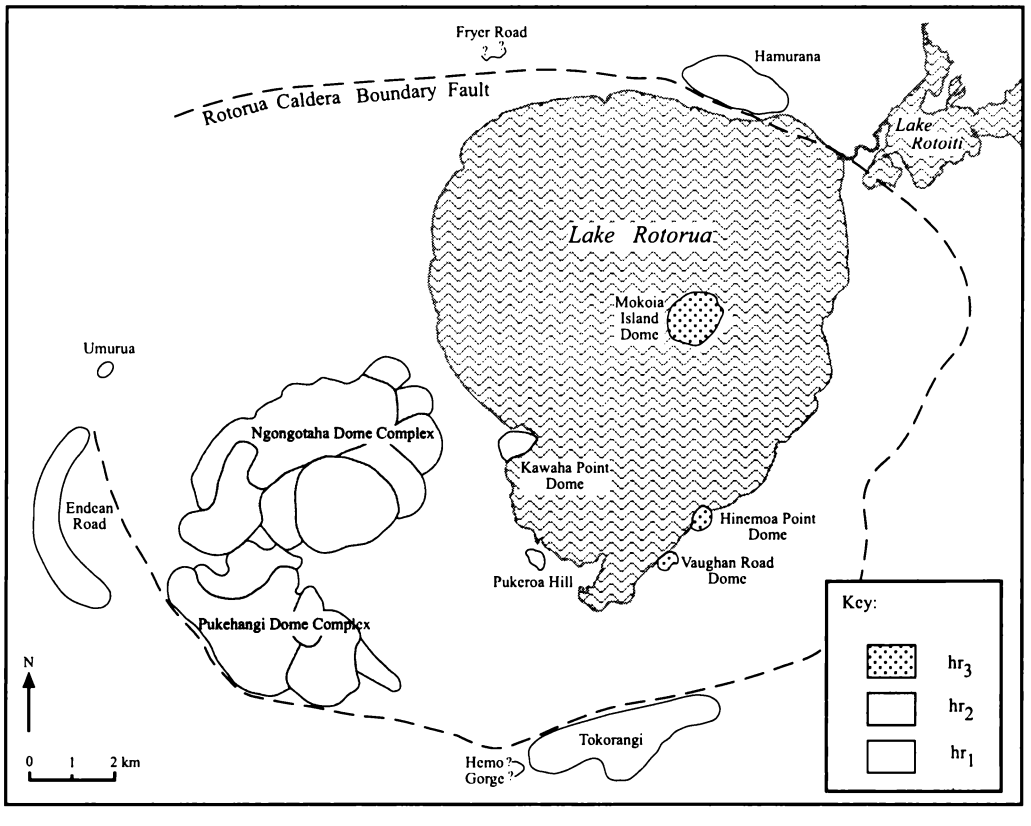

Figure 2.9: The distribution of rhyolite lavas associated with the Rotorua Volcanic Centre and their spatial relationship to the Rotorua Caldera boundary fault (of Thompson, 1974). Compiled from Ewart (1968) and Dravitzki (1999).

2.3.2.3 Post-Caldera Eruptions - hr_2 and hr_3 Rhyolite Lavas

Post-Mamaku Ignimbrite activity from the RVC has been limited to dome formation, unaccompanied by significant pyroclastic eruptions (Wilson et al., 1984). These domes occur within the caldera and are divided into two groups shown in Figure 2.9:

- The hr_2 rhyolites, erupted between the Mamaku and Rotoiti Ignimbrites (220 ± 10 - c. 65 ka), comprise the Ngongotaha and Pukehangi dome complexes, Kawaha Point Dome and the rhyolites which are dominantly buried beneath Rotorua City but outcrop at Pukeroa Hill.
- The hr_3 rhyolites, erupted after the Rotoiti Ignimbrite (in the last c. 65 ka), comprise the Mokoia Island, Hinemoa Point and Vaughan Road Domes. However, these domes are older than c. 15 800 years B.P. as they are mantled by Rotorua Tephra (Nairn and Wood, 1987; age from Table 2.3).

Several studies (eg. Wood, 1992) have suggested that the Ngongotaha and Pukehangi rhyolites may in fact be part of a very extensive rhyolite volcano complex which includes Kawaha Point and the concealed domes which lie beneath Rotorua City. Aeromagnetic data indicate the possible presence of another, largely buried, rhyolite complex in the southeast of the caldera, represented by outcrops at Hinemoa Point (Bibby et al., 1992; Wood, 1992).

The hr_2 Ngongotaha-Pukehangi domes, Kawaha Point and the rhyolites buried under the city are considered to represent the effusion of degassed magma following the Mamaku Ignimbrite eruption (Nairn and Wood, 1987; Wood, 1992). Any relationship between the hr_3 rhyolites and the Mamaku Ignimbrite has not yet been investigated, although Wilson et al. (1984) suggested that they were sourced from a separate magma batch.

Dravitzki (1999) noted four minor localised ignimbrites, collectively termed the Paradise Valley Ignimbrites, outcropping in the Paradise and Utuhina Valleys to the west of Rotorua City and adjacent to the Ngongotaha and Pukehangi complexes. These ignimbrites were suggested to represent pyroclastic episodes during the development of the dome complexes, similar to the Te Wairoa Ignimbrites identified in the southwestern OVC by Bellamy (1991).

Within the Ngongotaha and Pukehangi Dome complexes individual domes can be identified. Shepherd (1991) identified eight domes at Ngongotaha with a relative chronology inferred from morphology and weathering. Dravitzki (1999) revised the division of Shepherd (1991) and also provided a division of the Pukehangi Complex. Figure 2.10 shows the division of the Ngongotaha and Pukehangi Domes, their names and their relative ages. Dravitzki (1999) noted difficulty in integrating the Pukehangi domes into the Ngongotaha stratigraphic sequence due to lack of contacts between most of the domes, but concluded that Te Miri Dome (V) is younger than Dome 5 and Relph Dome (6).

The names given to hr_1, hr_2 and hr_3 rhyolites in this study follow those used previously. An exception is the Vaughan Road Dome, which has previously been known as the Owhata Dome (Shepherd, 1991). The Pukeroa Hill Dome, which has not been sampled in this study, has also been known as the Kuirau Reserve Dome (Ewart, 1968). Plate 2.4 is a view across the RVC from Mount Ngongotaha showing rhyolites of the Rotorua and Okataina Volcanic Centres.

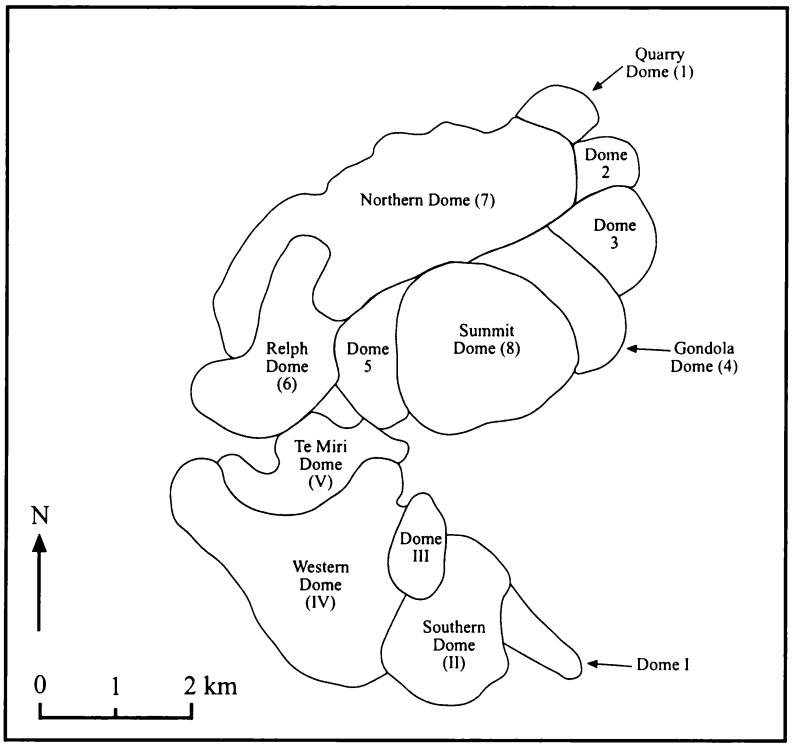

Figure 2.10: The names given to the domes of the Ngongotaha and Pukehangi dome complexes by Shepherd (1991) and Dravitzki (1999). Numbers indicate relative ages with Ngongotaha domes numbered from oldest (1) to youngest (8) and Pukehangi domes numbered from oldest (I) to youngest (V) (from Dravitzki, 1991).

2.3.2.4 Modern Hydrothermal Activity

The Rotorua Geothermal System is located in the southern part of the Rotorua Caldera. As defined by surface activity and shallow drillholes it covers an area of about 12 km^2 (Wood, 1992). The principal production aquifers are Mamaku Ignimbrite and the rhyolites buried beneath the city. New Zealand's last remaining geyser field occurs at Whakarewarewa, which contains the famous Pohutu Geyser. Boiling mud pools occur in Kuirau Park in the central city. A small phreatic eruption occurred at Kuirau Park in January 2001. In recent years there have been several occurrences of ground subsidence, mud pools, springs and steaming ground appearing on private property in the vicinity of Kuirau Park. An acidic spring feeds the Polynesian Pools, which are a popular tourist attraction. There is also thermal activity around the southern shore of Lake Rotorua, at Ohinemutu and Sulphur Point (Figure 1.3).

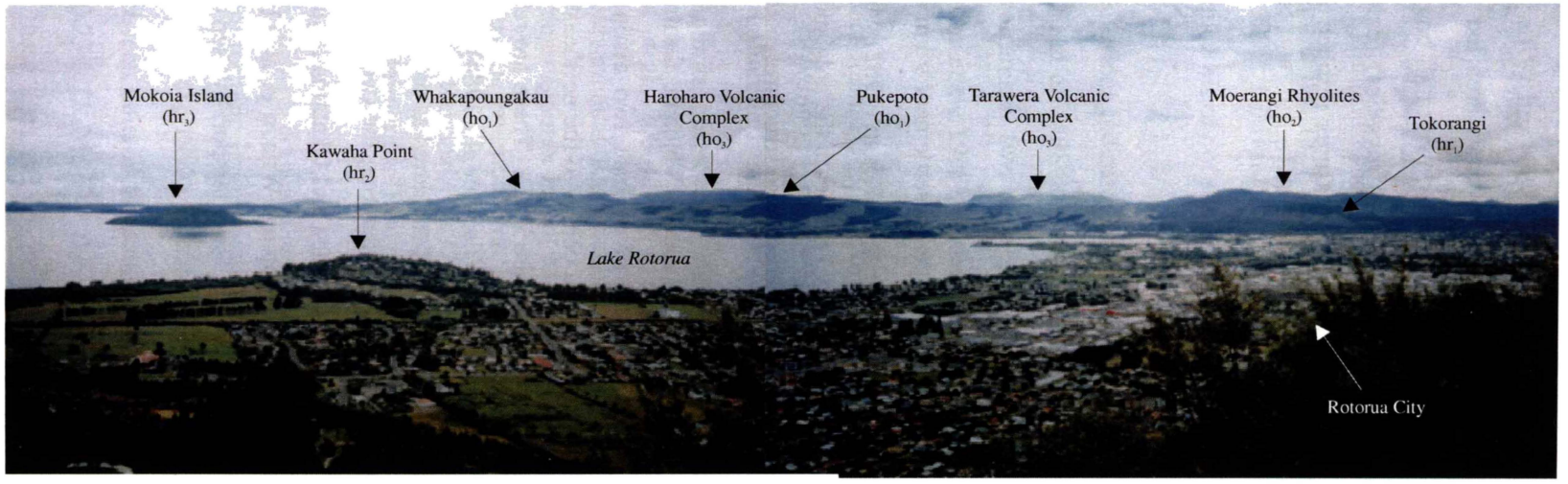

Plate 2.4: View looking east from near the summit of Mount Ngongotaha across the Rotorua Volcanic Centre (RVC) to the Okataina Volcanic Centre (OVC). Some of the rhyolite domes of the RVC can be seen, as well as the Haroharo and Tarawera volcanic complexes and older rhyolite domes of the OVC.

The Rotorua Geothermal Regional Plan (Environment Bay of Plenty, 1999) discussed the use of the Rotorua geothermal field. Population growth and energy crises contributed to significant increases in well drilling between the 1950s and 1970s. Increasing concern over the effect of fluid withdrawal on the Whakarewarewa area led the Government to take emergency measures in 1986. This included a shutdown of all bores within a 1.5 km radius of Pohutu geyser. A resource rental (geothermal royalties) regime was imposed by the Ministry of Energy from April 1987. These measures resulted in recovered geyser and spring activity.

2.4 KAPENGA VOLCANIC CENTRE

2.4.1 Introduction

The existence of a caldera centred near Kapenga settlement 9 km south of Rotorua (Figure 1.2) was postulated from geophysical evidence by Rogan (1982) who observed a large body, 2.5 km thick, of low density, magnetised rocks beneath the area and inferred that these were rhyolites and ignimbrites infilling a volcanic collapse structure.

The geophysical anomalies defining the Kapenga Volcanic Centre (KVC) cover 250 km^2 and suggest that the centre is composed of at least two distinct collapse structures of differing ages. A smaller 2.5 km deep basin occurs to the northeast with a larger 3 km deep basin in the central and southern parts (Figure 2.11). These are referred to as the northeast and central-southern centres respectively (Wilson et al., 1984). Wilson et al. (1984) stated that the northeast centre had previously been considered as part of Okataina, but gravity data indicates the presence of a basement ridge separating the two centres. They also noted that the relationships between northeastern Kapenga and Okataina require further study. On the basis of observations and unpublished mapping, Wilson et al. (1995) considered that the KVC as presently defined consists of four temporally separate but geographically overlapping volcanic centres.

2.4.2 Eruptive History

2.4.2.1 Caldera-forming Eruptions

Due to the age of the KVC and its complex history, the eruptive sequence and relationships between caldera-forming ignimbrites and rhyolite lavas are not known in any detail. Studies have focused on the ignimbrites (eg. Langridge, 1990; Karhunen, 1993; Ritchie, 1996; Bowyer, 1997; Spinks, 1998; Hildyard et al., 2000) and not on linking all the eruptives together to unravel a detailed history of the centre.

Mapping and age determinations indicate that the area termed Kapenga Volcanic Centre by Rogan (1982) and Wilson et al. (1984) is a composite structure that developed during at least three periods of volcanism, two of which were accompanied by inferred caldera-forming ignimbrites (Wilson et al., 1995), as shown in Table 2.5.

The first period of caldera-forming ignimbrite activity occurred from c. 0.89 - 0.68 Ma (Houghton et al., 1995). Houghton et al. (1995) identified the Tikorangi Ignimbrite as the earliest caldera-forming ignimbrite from the KVC (0.89 ± 0.04 Ma). They did not mention the older Pukerimu Ignimbrite but, due to the gradational contact between these units (Bowyer, 1997; Hildyard et al., 2000), it is likely to have been included under the name Tikorangi Ignimbrite. Hildyard et al. (2000) concluded that there is only one ignimbrite and formally adopted Tikorangi Ignimbrite as its name. The eruption of the Tikorangi Ignimbrite was followed by the eruption of at least three caldera-forming ignimbrites from source(s) within the KVC, the Rahopaka (0.77 ± 0.03 Ma), Waiotapu (0.71 ± 0.06 Ma) and Matahana (0.68 ± 0.04 Ma) ignimbrites (Houghton et al., 1995).

The second period of volcanism at Kapenga resulted in the eruption of the Waihou (Chimp), Pokai and Ohakuri caldera-forming ignimbrites. The Ohakuri Ignimbrite has been dated at 0.27 ± 0.03 Ma (Houghton et al., 1995). Lynch-Blosse (1998) used field stratigraphy and the nature of contacts between units in the southern Mamaku Plateau area to estimate ages of 0.26-0.25 Ma and 0.23-0.22 Ma for the Waihou (Chimp) and Pokai Ignimbrites, respectively. However, these ages are not in agreement with the ignimbrite stratigraphy implied by Houghton et al. (1995) and an age of 0.27 ± 0.03 Ma for the Ohakuri Ignimbrite (Table 2.5). More work on these ignimbrites is required to resolve their stratigraphic

associations and ages. This second period of caldera-forming activity at the KVC overlaps with the eruption of the Matahina and Kawerau ignimbrites from the OVC, and occurs prior to the eruption of the Mamaku Ignimbrite from the RVC. The southern portion of the KVC is now concealed beneath the Ohakuri Ignimbrite and pumiceous lacustrine sediments of the Huka Group (Wilson et al., 1984).

Table 2.5: Summary of the eruptive history of the Kapenga Volcanic Centre.

Unit	Age	Caldera Collapse
Earthquake Flat Tephra Formation Earthquake Flat Ignimbrite Rifle Range Ash	c. 65 ka	
Rotoiti Tephra Formation (Okataina Volcanic Centre)	c. 65 ka	
hk_2 rhyolites Haparangi Round Hill Ongahoro Domes 1 - 3	220 ± 10 - c. 65 ka	
Mamaku Ignimbrite (Rotorua Volcanic Centre)	220 ± 10 ka	
hk_1 rhyolites Horohoro Tumunui Waikorapa North Haparangi Ridge	> 220 ± 10 ka	
Ohakuri Ignimbrite	0.27 ± 0.03 Ma	yes
Pokai Ignimbrite	0.23 - 0.22 Ma*	yes
Waihou (Chimp) Ignimbrite	0.26 - 0.25 Ma*	yes
Matahana Ignimbrite	0.68 ± 0.04 Ma.	yes
Waiotapu Ignimbrite	0.71 ± 0.06 Ma	yes
Rahopaka Ignimbrite	0.77 ± 0.03 Ma	yes
Tikorangi Ignimbrite	0.89 ± 0.04 Ma	yes

Ages from Houghton et al. (1995). * Estimated ages from Lynch-Blosse (1998).

2.4.2.2 Non Caldera-forming Ignimbrite Eruptions

Wilson et al. (1995) stated that the youngest activity in the KVC occurred in its northeast portion generating numerous lava domes (presently classified as ho_2 in this study) and ending with the c. 65 ka. Earthquake Flat (EQF) Ignimbrite eruption, which was not accompanied by caldera collapse. This eruption is considered to have followed, without significant time interval, the Rotoiti Ignimbrite eruption in the northern OVC (Nairn and Kohn, 1973; Davis, 1985).

The northeastern portion of the KVC was originally considered part of the OVC (Wilson et al., 1984; Langridge, 1990) and is largely filled by the EQF Ignimbrite (Langridge, 1990). Schmitz (1995) considered that evidence existed to support a similar parental magma and mixing between the Rotoiti and EQF magmas and that this establishes connectivity between the OVC and northeastern KVC at the time of these eruptions. He therefore suggested that the EQF Ignimbrite should be grouped with other eruptives from Okataina, rather than Kapenga. Langridge (1990) suggested that the area known as Earthquake Flat might in fact be a separate caldera occurring at the junction of three major calderas. Neither of these concepts has been widely accepted.

2.4.2.3 Rhyolite Lavas - hk_1 and hk_2

KVC rhyolite lavas can be divided into two groups (Figure 2.11):

- The hk_1 rhyolites erupted prior to the Mamaku Ignimbrite (220 ± 10 ka) are Horohoro, Tumunui, Waikorapa and the ridge north of Haparangi. Trig 8566 of Ewart (1968), shown in Figure 1.6, is now associated with the Reporoa Volcanic Centre.
- The hk_2 rhyolites erupted between the Mamaku and Rotoiti Ignimbrites (220 ± 10 - c. 65 ka) are Haparangi, Round Hill, Ongahoro (formally Trig 8523) and Domes 1-3 northeast of Ongahoro.

The ridge north of Haparangi and Domes 1-3 were not identified in the earliest studies of this area (e.g. Ewart, 1968). Dunham (1981) first documented the ridge north of Haparangi. Domes 1-3 that protrude above the surrounding Earthquake Flat Ignimbrite were first suggested by Nairn (1989) and were subsequently mapped by Gaston (1991).

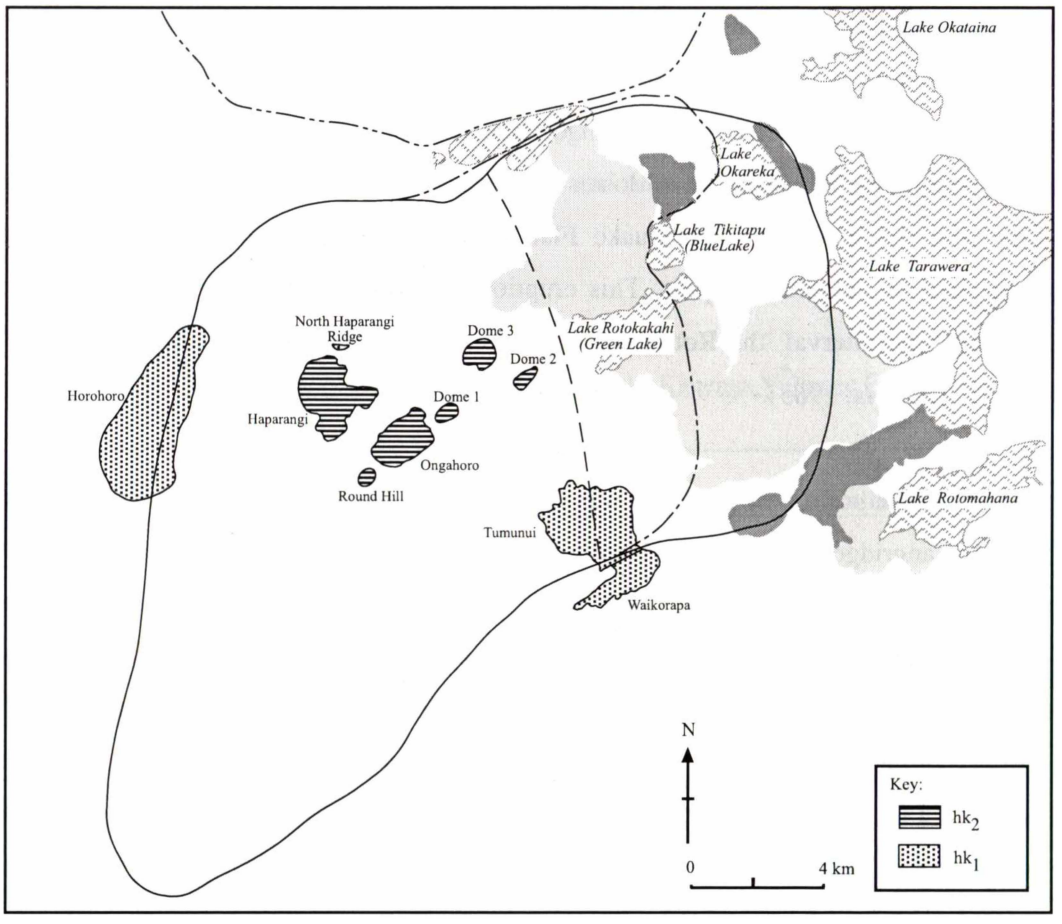

Figure 2.11: The distribution of rhyolite lavas associated with the Kapenga Volcanic Centre. Compiled from Ewart (1968), Dunham (1981) and Gaston (1991). Solid line gives the outline of the KVC according to Wilson et al. (1984) with the dashed line separating the central-southern and northeastern parts of the centre. Dot-dash line shows the approximate northeastern margin of the KVC according to Houghton et al. (1995). Shading indicates the distribution of ho_2 rhyolites (light) and ho_1 hyolites (dark) in the area (from Nairn, 1989). Double dot-dash line shows the location of the Rotorua Caldera Boundary Fault of Thompson (1974). Cross-hatch shading indicates hr_1 rhyolites in the southern Rotorua Volcanic Centre.

It is not known which of the two periods of caldera-forming ignimbrites the hk_1 rhyolites are associated with because no ages for the rhyolite lavas are available. Due to mineralogical similarities it would seem likely that the hk_2 rhyolites are genetically associated with the Earthquake Flat Ignimbrite eruption.

The names used in this study for hk_1 and hk_2 rhyolites follow those used in previous studies (Ewart, 1968; Dunham, 1981; Gaston, 1991). Of most interest is the hk_2 lavas and how they compare with the ho_2 lavas in this area.

Chapter Three: Petrography

Chapter Three: Petrography

3.1 INTRODUCTION

Rhyolite lavas comprise phenocrysts set in a silicic glass groundmass, which may contain quench crystals and vesicles. Fragments of foreign rocks and minerals, known as xenoliths and xenocrysts respectively, may also be present. This chapter discusses the petrography of rhyolite lavas erupted from the Okataina, Rotorua and Kapenga volcanic centres. The internal textural variations that occur within the glass groundmass of rhyolite domes and flows will be described along with the factors involved in their formation. Groundmass textures and phenocryst assemblages will then be discussed for rhyolites of each volcanic centre and age group. Several basaltic xenoliths have been identified and their petrographic characteristics will also be described. The characteristics of the phenocrysts, such as habit, colour and size, show little variation between volcanic centres and age groups, and will be discussed for the rhyolites collectively in Chapter Five.

3.2 INTERNAL TEXTURAL VARIATIONS IN RHYOLITE LAVAS

The interiors of subaerial silicic lava flows and domes display diverse textures, involving the distribution of coherent versus autoclastic facies, variations in vesicle size and abundance, and the effects of devitrification, crystallisation and hydration (McPhie et al., 1993). A simplified cross-section through a subaerial silicic lava flow (Figure 3.1) shows the distribution of four main textures - crystallised rhyolite, obsidian, pumiceous rhyolite and autobreccia. Within each of these textural groups variations in colour, vesicularity and degree of devitrification may occur. The contacts between textural zones may be inter-fingered or gradational, and can range in thickness from centimetres to metres.

Development of these textures reflects the interplay of pre-eruption conditions (composition, especially volatile and phenocryst content), processes that operate during extrusion (vesiculation, autobrecciation, crystallisation and devitrification) and post-emplacement changes (further crystallisation and devitrification, hydration and joint development) (McPhie et al., 1993). Primarily, textural variations are the product of cooling processes and hence rhyolite domes and flows of different volumes and thicknesses may show different textural patterns. For example small domes may cool relatively quickly and the central core

of crystallised rhyolite may be absent. The sequence of formation of many of the textural features observed in rhyolite lavas, and discussed in this study, is shown in Figure 3.2.

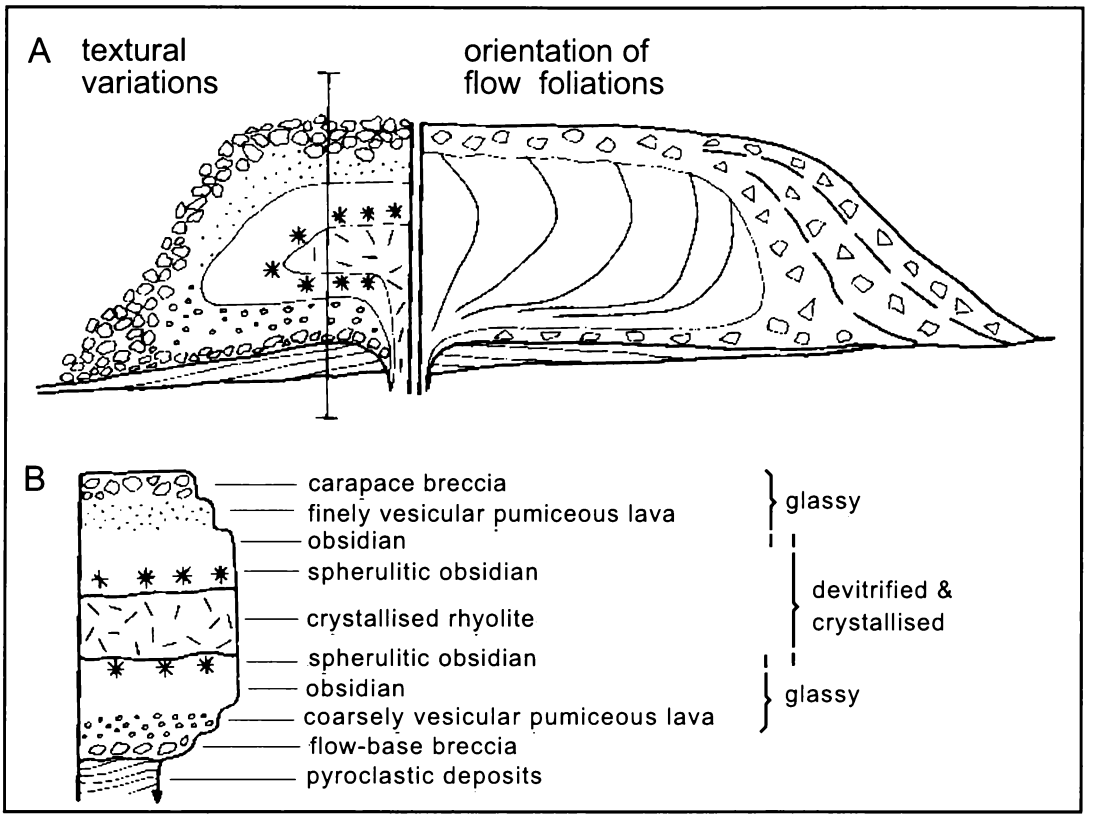

Figure 3.1: A) Simplified cross-section through a subaerial silicic lava flow. The left side shows the internal textural variations arising from vesiculation, devitrification and flow fragmentation. The right side shows the orientations of internal flow foliations, and crude layering in flow margin breccia. B) Vertical section through the flow at the position indicated in A, showing the major textural zones. Redrawn from McPhie et al. (1993).

In practice, the stratigraphic relationships between the main textural types can be much more complex than shown in Figure 3.1. For example, Fink and Manley (1987) observed coarsely vesicular pumice outcropping on the surface of Little Glass Mountain, a rhyolitic obsidian flow on the Medicine Lake Highland Volcano in northern California. A layer of coarsely vesicular pumice is considered to have formed within the upper obsidian layer of the flow as a result of gases released by crystallisation. The buoyancy of this layer subsequently gave rise to diapirs that rose to the surface through the overlying obsidian and finely vesicular pumice. Fink and Manley (1987) noted that the size of an extrusion is a decisive factor in

determining whether or not a coarsely vesicular pumice layer develops. Stevenson et al. (1994) present an interpretation of the textural stratigraphy of the Haumingi and Waiti lava flows in the northern Haroharo Volcanic Complex. They show both flows to be comprised of an upper finely vesicular pumice, overlying a layer of obsidian, with a crystalline, spherulitic flow centre. The coarsely vesicular pumice unit of Fink and Manley (1987) was not observed in either flow. However, the Haumingi Flow contained small pockets of coarsely vesicular foam at its surface.

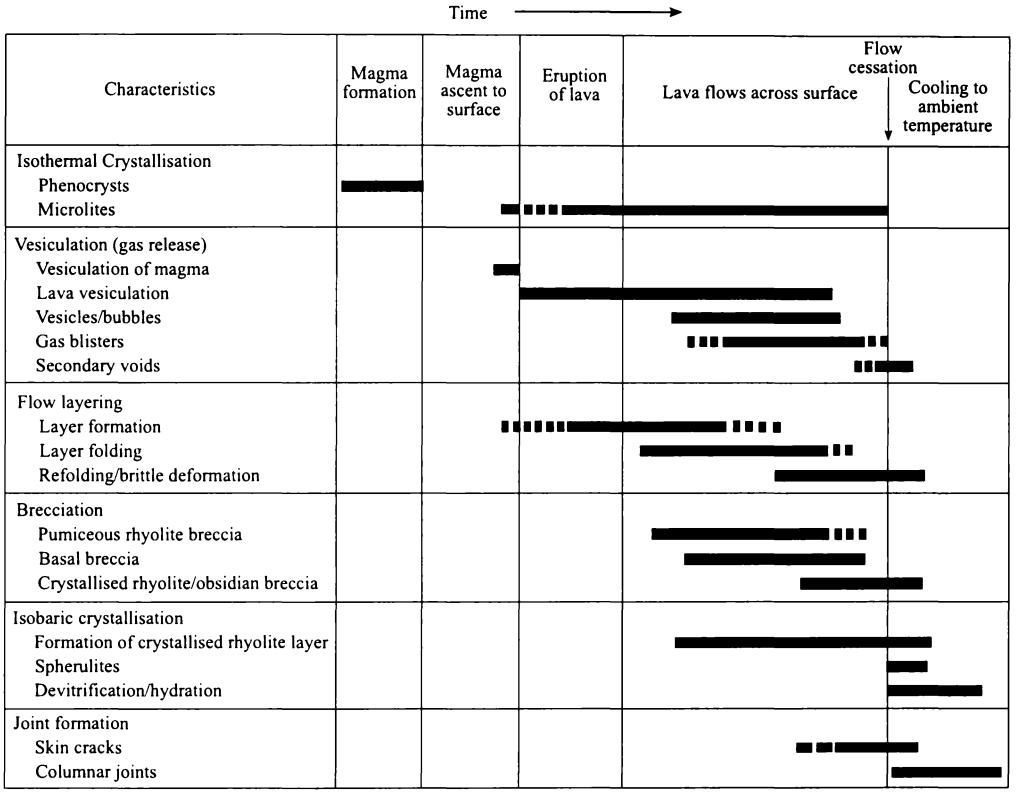

Figure 3.2: The sequence of formation of the textural features observed in rhyolite lavas, from magma generation to cooling of the lava to ambient temperature. Modified from Bonnichsen and Kauffman (1987) and Stevenson et al. (1993).

It is not the purpose of this study to provide an extensive discussion of the textures found in rhyolite lavas and their associated chemical and physical processes. The following is an overview and more detailed information can be obtained by consulting the references given. The texture of a particular sample of rhyolite lava can be used to give an idea of the approximate position in the dome or flow that the sample has come from, interior or exterior.

Samples are dictated by outcrop availability, which varies depending on a number of factors including the degree of erosion of the dome or flow, thickness of overlying pyroclastics and covering vegetation. Hence, even though a particular textural zone occurs within a lava dome or flow, obtaining a sample of it may not be possible.

3.2.1 Crystallised Rhyolite

Crystallised rhyolite occurs in the interior of a lava flow or dome. The slower rates of cooling in the interior of the lava are primarily responsible for the textural characteristics of these samples. The glass groundmass becomes thermodynamically unstable, resulting in devitrification and crystallisation (section 3.2.5). A spherulitic texture is most commonly formed, and other possible textures include lithophysae, orb, micropoikilitic and granophyric (Lofgren, 1971a, 1971b; McPhie et al., 1993). In some samples the glass has become hydrated and a perlitic texture has formed (section 3.2.6). Some of the crystallised rhyolites sampled are among the most phenocryst rich rhyolites obtained in this study. This may also be due to the slower rate of cooling in the interior of the lava flow or dome. In hand specimen, samples of crystallised rhyolite are very dense and non-vesicular. They may be a variety of colours, including grey, brown and pinkish brown, often a result of the colour of the products of glass devitrification (Plate 3.1).

3.2.2 Obsidian

Rapid quenching of silicic melt produces solid silicic glass. This glass may be non-vesicular obsidian, partially vesicular or highly vesicular and pumiceous (section 3.2.3). In some cases quenching includes a short period of very rapid crystallisation, and the glass is crowded with quench crystals (McPhie et al., 1993) (section 3.2.7). The samples of obsidian obtained in this study commonly contain quench crystals, which are often aligned into bands that define flow foliations within the lava (section 3.2.9). In hand specimen the obsidian appears black, and commonly contains white, grey or pink spherulitic balls (Plate 3.2), termed the glassy stage texture by Lofgren (1971b) (discussed further in section 3.2.5). The obsidian may be seen to contain bands that are slightly lighter (dark grey) in colour. Thin section investigation shows these to be bands comprised of densely packed, sub-parallel quench crystals. Under crossed-polarised light unmodified silicic volcanic glass is isotropic, but with inclusions of quench crystals small white/grey flecks may be seen in the glass.

Plate 3.1: Crystallised, spherulitic rhyolite. Blue Lake rhyolite, Okataina Volcanic Centre (sample number 152).

Plate 3.2: Spherulitic obsidian. Te Koutu Flow, Haroharo Volcanic Complex, Okataina Volcanic Centre (sample number 23).

While obsidian can occur on its own, it is also seen inter-fingered and flow banded with crystallised, spherulitic rhyolite. Obsidian has a pronounced conchoidal fracture. As a result, samples may not be found as smooth-surfaced glass but may instead have a coarse sugary texture where small sub-spherical pieces of glass can be easily pulled away from the sample, much like a clump of sugar grains. In thin section the conchoidal fracture is expressed as cracks in the glass. These cracks are relatively large, both in length and width, compared to other kinds of cracks that may form in volcanic glass (section 3.2.6) and commonly extend from phenocryst to phenocryst.

3.2.3 Pumiceous Rhyolite

Rapid quenching of silicic melt and vesiculation in the outer portions of the lava dome or flow produces a pumiceous texture. Vesicles may vary in abundance and size, and samples may be coarsely vesicular with large vesicles or finely vesicular with small vesicles. Vesicles may be round, oval, elongated and tubular. Elongation of vesicles in a dominant direction may result from stretching/shearing during flow of vesiculating lava. Some samples are highly vesicular and in hand specimen appear very much like pumice produced in pyroclastic eruptions (Plate 3.3), while others are only poorly, or even incipiently, vesicular (section 3.2.8). These latter samples have a texture intermediate between obsidian and pumiceous rhyolite. Occasionally crystal-rich pumiceous samples may have a coarse sugary texture, where the lava has a texture similar to a crystal-rich ash and lapilli tephra deposit. Pumiceous rhyolite is generally white, cream, light brown or light grey in colour.

In thin section, samples of pumiceous rhyolite are seen to contain quench crystals which may occur in bands, often aligned in the direction of elongation of the vesicles. These quench crystals are commonly aligned parallel to each other and to the vesicle walls. McPhie et al. (1993) noted that vesicle walls may consist of quench crystal-rich glass which may be folded and crenulated. Pumiceous rhyolite may also contain isolated small spherulites that commonly nucleate on phenocrysts.

3.2.4 Autobreccia

Silicic lava flows and domes typically have an upper, basal and marginal breccia composed of lava blocks in a granular matrix (McPhie et al., 1993). The formation of this breccia is due to temperature variations within the lava flow or dome. Minimum temperatures occur at the top surface and base of the lava with increases to near-eruption temperatures in the

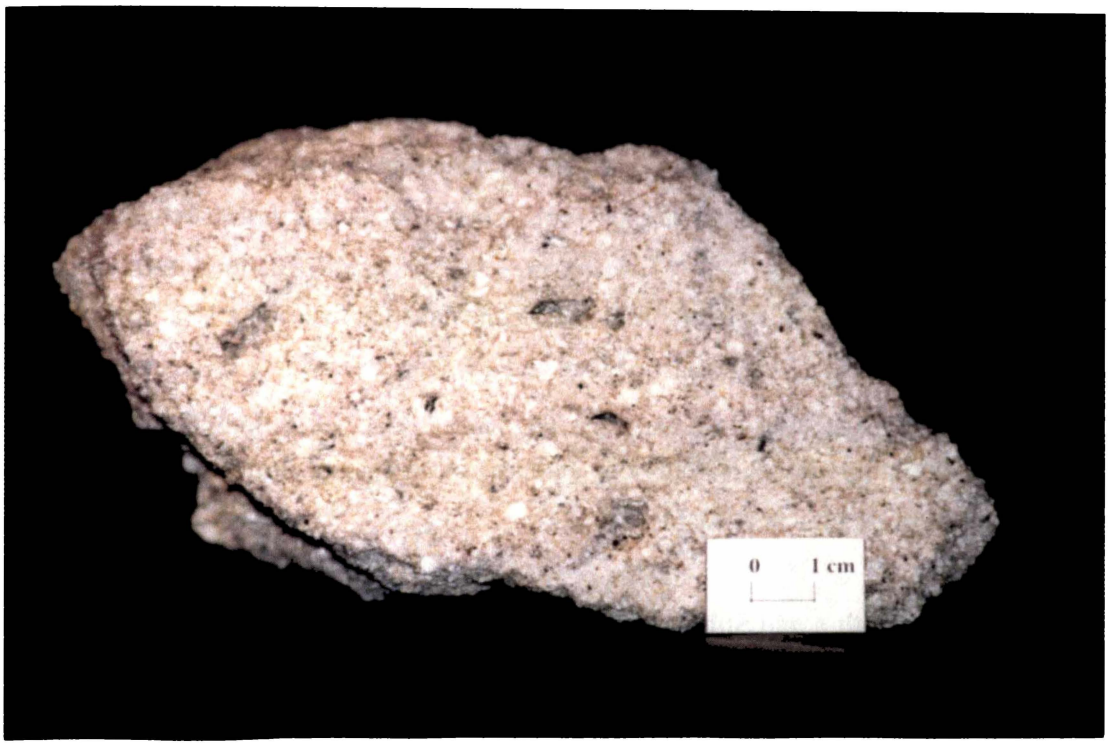

Plate 3.3: Pumiceous rhyolite. Middle rhyolite, Okereka Volcanic Complex, Okataina Volcanic Centre (sample number 175).

Plate 3.4: Autobreccia. Te Pohue Flows, Haroharo Volcanic Complex, Okataina Volcanic Centre (sample number 60).

centre (Fink, 1983; McPhie et al., 1993). Thus movement and deformation of the hot flow interior causes fragmentation of the rigid non-deforming top and base (McPhie et al., 1993). Obsidian and pumice have a strong tendency to fracture on cooling (Fink, 1983), and hence the lava blocks comprising the breccia are commonly pumiceous rhyolite and obsidian (Plate 3.4).

For a geochemical study it is preferable to sample the coherent facies of a lava flow or dome as problems may occur if a pyroclastic block and ash flow overlying a lava is mistaken for the autobreccia associated with the lava. Of the rhyolite lava domes and flows studied from Okataina, Rotorua and Kapenga, only one autobreccia was sampled due to outcrops of the coherent lava flow not being available.

3.2.5 Devitrification and Spherulitic Textures

As volcanic glass cools it becomes thermodynamically unstable and will eventually devitrify. Hence, all rhyolitic lavas are affected to some degree by devitrification. Devitrification involves the nucleation and growth of crystals in glasses at subsolidus temperatures (McPhie et al., 1993). Spherulites, lithophysae, orb texture and micropoikilitic texture are characteristic products of devitrification of silicic glass (Lofgren, 1971a, 1971b). Devitrification in the Okataina, Rotorua and Kapenga rhyolites is commonly seen in the formation of spherulites and a spherulitic texture. Spherulites consist of radiating arrays of crystal fibres. Each fibre is a single crystal that has only a slightly different crystallographic orientation from adjacent crystals (McPhie et al., 1993). Shelley (1993) notes that with such a high degree of undercooling, crystal habit is partly suppressed so that the minerals forming grow as radiating masses of acicular branches, rather than their usual crystal forms. Lofgren (1971a, 1974) demonstrated that spherulites are not always spherical (Figure 3.3) and that the morphology of spherulites in rhyolitic glass varies as a result of the temperature at which they formed. Axiolitic morphologies radiate from a line. Such a line may represent a boundary between flow bands in the pre-devitrified glass.

Spherulitic material dominates the groundmass of crystallised rhyolite, but it may also be found as a minor component of the groundmass in obsidian and pumiceous rhyolite. Lofgren (1971b) distinguished three textural associations among the experimental devitrification products of silicic glass. Glassy-stage texture consists of glass that contains isolated spherulites (eg. spherulitic obsidian, Plate 3.5). This texture represents rapidly cooled water undersaturated magma where little nucleation was possible. Spherulitic-stage texture is

when devitrification is complete and former glass is crystallised to spherulites (eg. crystallised rhyolite, Plate 3.6). Relatively slow cooling and maintenance of higher temperatures favour the development of spherulitic-stage textures (Lofgren, 1971b; McPhie et al., 1993). Hence, this texture occurs in the interior of lava flows and domes. A third stage was hypothesised, although not reproduced experimentally, as having a granophyric or granitic texture, with no evidence of glassy precursors.

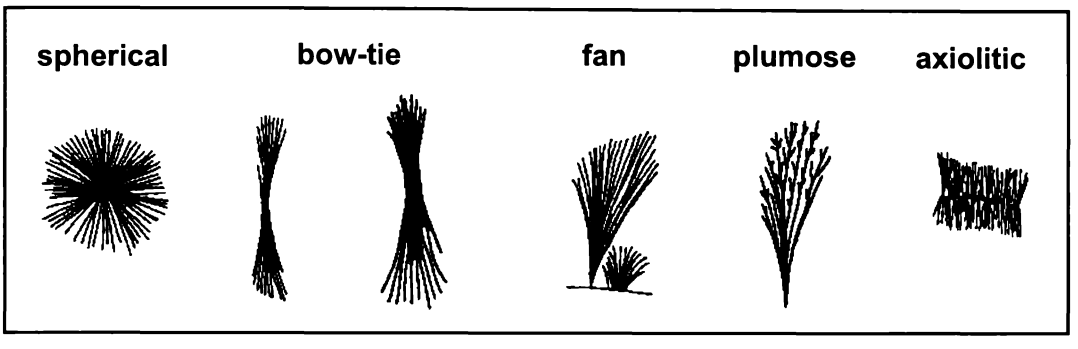

Figure 3.3: Spherulite morphologies seen in devitrified silicic glass. Note that fibres in axiolitic spherulites radiate from a line. Redrawn from McPhie et al. (1993).

In hand specimen the spherulitic material may be seen as complete balls (common in spherulitic obsidian), a mass of radiating fibres or as patches/bands of aphanitic material, which can only be distinguished as spherulitic in thin section. Spherulitic material is commonly grey, white, pink or light brown in colour. In thin section the different spherulite morphologies present can be identified. Spherulites occurring in obsidian and pumiceous rhyolite (glassy-stage texture) are commonly spherical in shape and the crystal fibres are different shades of brown in plane-polarised light (Plate 3.5), with some fibres being opaque. Under crossed-polarised light the crystal fibres comprising these spherulites appear almost black.

In plane-polarised light the spherulitic material comprising a spherulitic-stage texture also appears brown, with some opaque fibres. The spherulitic material may be spherical, fan, plumose, bow-tie or axiolitic in shape (Figure 3.3) and coalesces so as to overtake the entire groundmass. Small, poorly devitrified, irregular patches of interstitial residual glass may remain. Under crossed-polarised light the white/grey interference colours of alkali feldspar

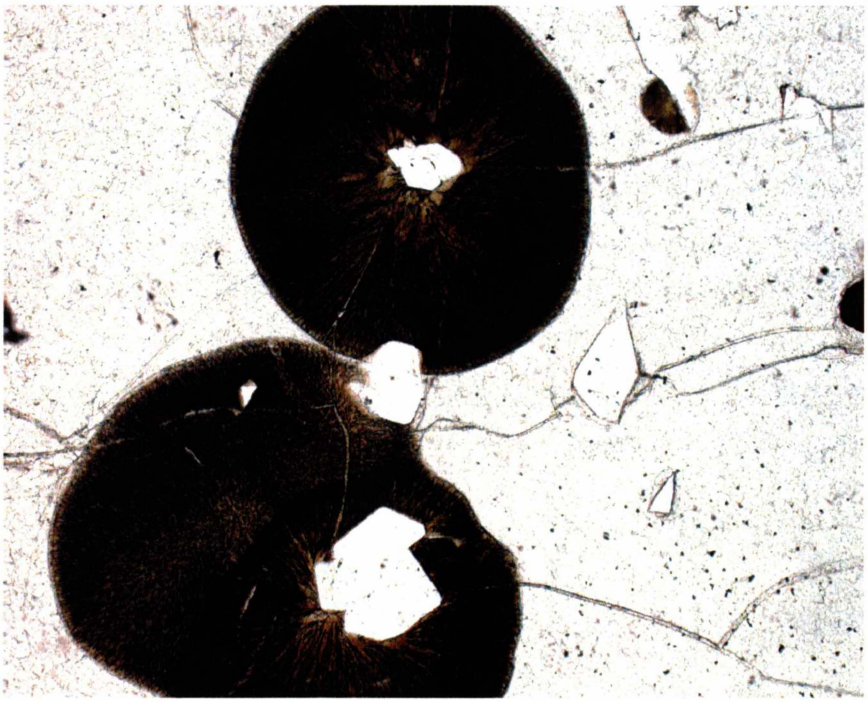

Plate 3.5: Glassy-stage texture of Lofgren (1971b) where the glass groundmass contains isolated spherulites. These spherulites have nucleated on plagioclase phenocrysts. The groundmass contains cracks reflecting the conchoidal fracture of volcanic glass. Okataina Flow, Haroharo Volcanic Complex, Okataina Volcanic Centre (sample number 25). Plane-polarised light. ~ 30x magnification.

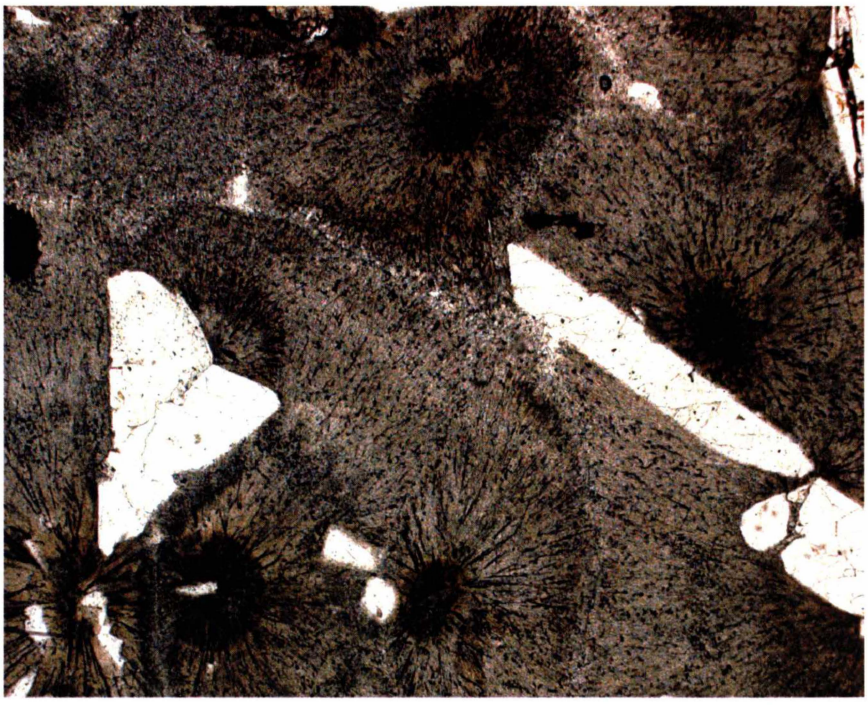

Plate 3.6: Spherulitic-stage texture of Lofgren (1971b) where devitrification is complete and former glass groundmass has crystallised to spherulites. Several of the spherulites have nucleated on plagioclase phenocrysts. Stancorp Quarry rhyolite, Okataina Volcanic Centre (sample number 63). Plane-polarised light. ~ 30x magnification.

and quartz polymorphs (cristobalite) can commonly be seen comprising the spherulitic material. Lofgren (1971a) noted that spherulites are not of a unique composition and in addition to alkali feldspar and cristobalite, they may also comprise plagioclase feldspar and pyroxene. Ewart (1971b) noted spherulites in Taupo Volcanic Zone rhyolite lavas consisted of cryptocrystalline intergrowths of cristobalite and alkali feldspar, with minute granules of magnetite, haematite and secondary goethite.

Spherulitic material, especially spherical balls, commonly shows concentric zoning highlighted by colour variations (commonly different shades of brown in plane-polarised light). This zoning may result from varying densities or compositions of the crystal fibres comprising the spherulites or different periods of spherulite growth.

A number of the crystallised rhyolite samples obtained in this study have a texture intermediate between the spherulitic-stage and granitic-stage of Lofgren (1971b). In these samples spherulitic material can be readily identified and a fine grained equigranular mosaic of crystals fills interstices between the spherulitic material. The interference colours and shapes of these equigranular crystals suggest that they may be comprised of cristobalite and alkali feldspars.

Cole (1966) noted that in some pumiceous rhyolites from the Tarawera Volcanic Complex, very small (< 1 mm in diameter) individual spherulites were present that have a granophyric appearance. These spherulites are near colourless in plane-polarised light but under crossed-polarised light are seen to comprise worm or finger-like intergrowths of quartz and alkali feldspar (anorthoclase). Cole (1966) also noted what he termed microspherulites in some Tarawera rhyolites. These spherulites are very small (< 0.2 mm in diameter) and are usually clear in plane-polarised light. In crossed-polarised light they show a black, well defined extinction cross or two "pseudo-isogyres" on a white background. These spherulite features are quite rare and can be seen in only a few samples obtained in this study.

In both glassy-stage and spherulitic-stage textures, spherulites commonly nucleate on phenocrysts. Some spherulite balls have a phenocryst centre whereas other incomplete balls, fan and plumose morphologies may nucleate on the corners of phenocrysts. While the majority of spherical spherulites occur as quite compact balls, occasionally they are seen to consist of long fingers of fan or plumose spherulitic material radiating from a more compact core (Plate 3.7). This type of spherulite can be seen as a star-shape in hand specimen. The size of spherulitic balls varies, with a maximum diameter of ~ 4 mm and a minimum of less

Plate 3.7: Star-shaped spherulites with fingers of spherulitic material radiating from a more compact core. Pokohu Flows, Tarawera Volcanic Complex, Okataina Volcanic Centre (sample number 5). Plane-polarised light. ~ 30x magnification.

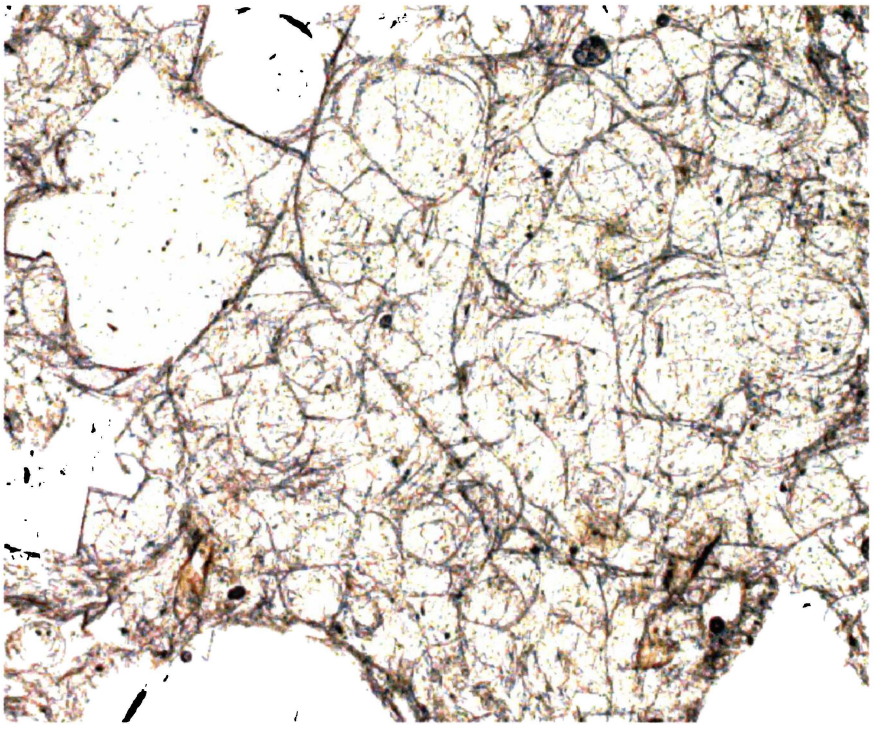

Plate 3.8: Glass groundmass exhibiting a classical perlite texture with arcuate cracks concentrically arranged around spherical, non-hydrated cores. North Rotoma rhyolite, Okataina Volcanic Centre (sample number 107). Plane-polarised light. ~70x magnification.

than 0.5 mm. The largest are commonly found in spherulitic obsidian where they have been free to grow unhindered by adjacent spherulites. Fan and plumose morphologies are commonly less than 1.25 mm in length. Axiolitic bands may extend beyond the length of a thin section slide (several centimetres) and may be up to several millimetres in width.

In addition to textural changes, devitrification can result in significant changes in the bulk rock chemistry, particularly affecting SiO_2, H_2O, Na_2O, K_2O and Al_2O_3 contents (Lipman, 1965; Lofgren, 1970) and, in some cases, trace and rare earth element abundances (Weaver et al., 1990). Ewart (1971b) concluded that progressive spherulitic devitrification of rhyolite lava results in a marked fractionation, especially of alkalis, between the spherulites and coexisting residual volcanic glass.

The least devitrified samples obtained in this study show evidence of minor devitrification with the formation of individual crystal fibres within an otherwise unaltered glass groundmass. In this case devitrification has not been sufficient to produce spherulitic material.

Lithophysae are spherulites that have a central vug resulting from nucleation of spherulites on small vesicles. The vugs vary from circular to star-shaped, and may remain open or be lined or filled with minerals. Lithophysae range up to larger diameters than spherulites, reaching a few tens of centimetres across (McPhie et al., 1993) and hence are often readily identified in hand specimen. Crosby (1998) identified lithophysae in the Hamurana rhyolite erupted from the Rotorua Volcanic Centre. Grapes et al. (1994) describe an interesting assemblage of silicate and oxide vug minerals that occur in lithophysal cavities within one of the Ngongotaha Dome Complex rhyolites, also erupted from the Rotorua Volcanic Centre. The occurrence of lithophysae is generally restricted to highly devitrified crystallised rhyolite and has not been observed in the rhyolite lavas obtained in this study.

Amygdales are former vesicles that have been partially or completely infilled with secondary minerals (McPhie et al., 1993). Rhyolite lava comprising such vesicles has an amygdaloidal texture, which is not common in the rhyolite lavas of this study.

3.2.6 Perlitic Textures

Perlite is the term given to volcanic glass in which there are abundant, delicate, intersecting, arcuate and gently curved cracks that surround cores of intact glass, generally less than a few

millimetres across (McPhie et al., 1993). Perlitic cracks develop in response to hydration of the glass, which involves the diffusion of water into the solid glass, accompanied by a volume increase. Strain associated with hydration is released by means of perlitic cracks (McPhie et al., 1993). In classical perlite (Figure 3.4) the cracks are distinctly arcuate and concentrically arranged around spherical, non-hydrated cores (Allen, 1988). In strongly flow banded glassy lava, perlitic fractures form a roughly rectilinear network, comprising cracks that are subparallel and strongly oblique to the banding, known as banded perlite (Allen, 1988). Classical perlite is easily identified but banded perlite may be confused with tension cracks, which are common in pumiceous rhyolite. Tension cracks are often small and delicate, occurring perpendicular to flow direction, and are caused by stretching of the glass during flow. Perlitic cracks may occur in the glassy domains between spherulites in partially devitrified obsidian (McPhie et al., 1993). In the rhyolites studied a perlitic texture is most readily identified in thin section (Plate 3.8).

Noble (1967) noted that hydrated glasses have lower Na/K and FeO/Fe_2O_3 ratios and lower silica contents. Lofgren (1970) noted that the rate of hydration is higher at higher temperatures. This may explain the occurrence of perlitic textures in crystallised rhyolites occurring in the interior of lava flows.

In this study the glass groundmass of rhyolite lavas will be referred to simply as cracked, unless the cracks are clearly perlitic.

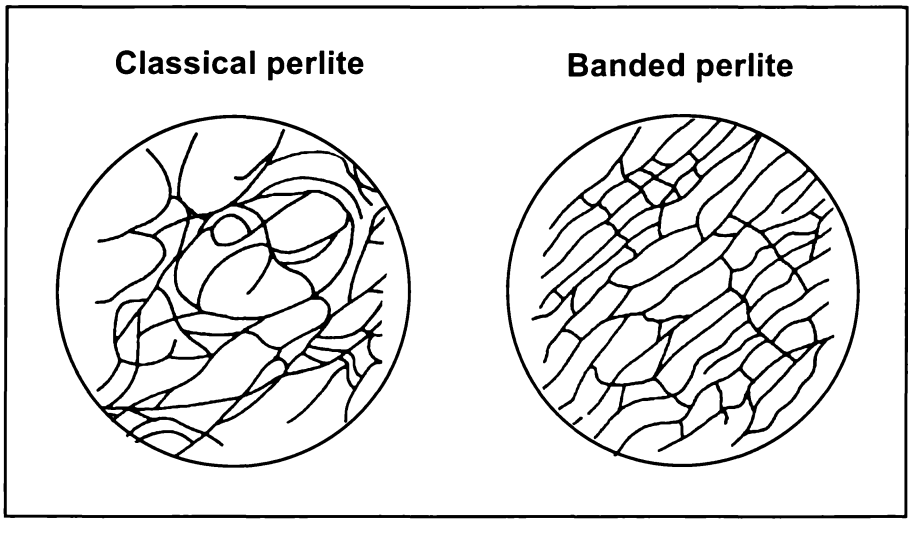

Figure 3.4: Fracture patterns for classical and banded perlite. Redrawn and modified from McPhie et al. (1993).

3.2.7 Quench Crystals

The rapid quenching of silicic melt which results in the formation of obsidian and pumiceous textures may include a short period of very rapid crystallisation, and the glass becomes crowded with microscopic quench crystals. These crystals have been referred to as microlites when they show birefringence and crystallites when they are so small as to be isotropic. Microlites have also been subdivided based on size (eg. Cashman, 1992; Sharp et al., 1996). Crystallisation of abundant microlites occurs in response to high degrees of undercooling and supersaturation related to degassing/loss of a vapour phase (H_2O) prior to and during the initial stages of eruption (Swanson et al., 1989; McPhie et al., 1993). Swanson et al. (1989) observed that bands of microlites were deflected around phenocrysts and crosscut by spherulites. Thus, microlites formed after the phenocrysts, but before the devitrification. The crystals formed during quenching have a variety of distinctive morphologies, which can be seen under the microscope using high-power magnification, including laths with swallow tail terminations, rods, prisms, chains and spider-like arrangements. The morphologies observed in the rhyolites of this study are shown in Figure 3.5 and Plate 3.9.

A variety of minerals comprise the microlites found in rhyolite flows with pyroxene being the most common. Sanidine, amphibole, biotite and magnetite microlites have also been noted (Ross, 1962). Pyroxene microlites were observed to have a very pale green colour (Richnow, 1999) and a very low apparent birefringence in thin section (Ross, 1962; Richnow, 1999). Positive identification of quench crystals may however be difficult due to their small size. Richnow (1999) noted that analysis by Electron Microprobe might not be possible due to the microlite not being exposed at the analysing surface but covered by a thin film of glass. Swanson et al. (1989) studied the crystallisation history of Obsidian Dome, Inyo Dome, California, and found the quench crystals to be pyroxene (ferroaugite) and feldspar (Ca-plagioclase). Sharp et al. (1996) studied microlites in obsidian from the Ben Lomond Dome, Taupo Volcanic Centre. Pyroxene microlites were dominant (orthopyroxene, augite, pigeonite) with some plagioclase feldspar also present. Magnetite and biotite compositions were also found and some microlites had a composition intermediate between amphibole and mica, known as biopyribole. Richnow (1999) noted that microlites in rhyolite lavas exposed in the Ngongotaha Quarry, Rotorua Volcanic Centre, were of the same mineral assemblage as the phenocrysts - pyroxene, feldspar and opaques (magnetite/ilmenite).

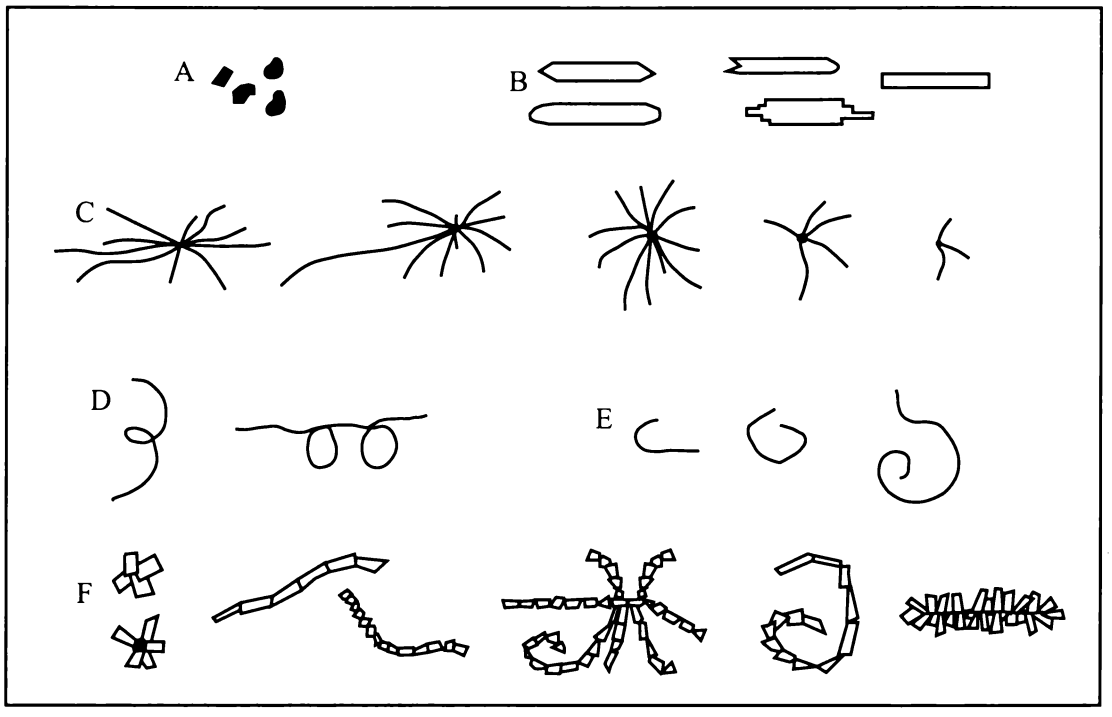

Figure 3.5: Quench crystal morphologies. A) Granular/globular - small and often isotropic, B) Laths/rods/prisms - may have pyramidal, rounded, swallow-tail or step-like terminations, C) Spider-like arrangements - comprise long, thin, hair-like strands (also known as trichites) that may or may not have a central crystal, D) Looped/coiled-spring shaped crystals, E) Hook shaped crystals, F) Bead-like/chain-like arrangements - small stout rods or prisms arranged together, may form clusters, strands, spider-like arrangements or hooks.

The shape of microlites has been related to their composition. Pyroxene microlites occur as slender prisms, chains of stout prisms and as spider-like (trichitic) groups. These spider-like groups may form around magnetite grains. Feldspar microlites occur as slender prisms or laths often with forked, jagged or swallow tail terminations (Ross, 1962; Swanson et al., 1989; Sharp et al. 1996; Richnow, 1999). Richnow (1999) found opaque microlites occurring as rounded, often shapeless blebs and as four-sided shapes occurring individually and in the centre of spider-like groups.

In a glassy matrix microlites are generally fresh and euhedral with well-defined crystal edges. However, they may be altered to opaque minerals and have corroded outlines if they are enclosed in spherulites or are in the vicinity of spherulites. This oxidation is facilitated by localised water enrichment and temperature increase resulting from the growth of quartz polymorphs and feldspars that constitute the spherulites (Richnow, 1999). Affected crystals are primarily those of pyroxene and Fe-Ti oxide in which the Fe becomes oxidised.

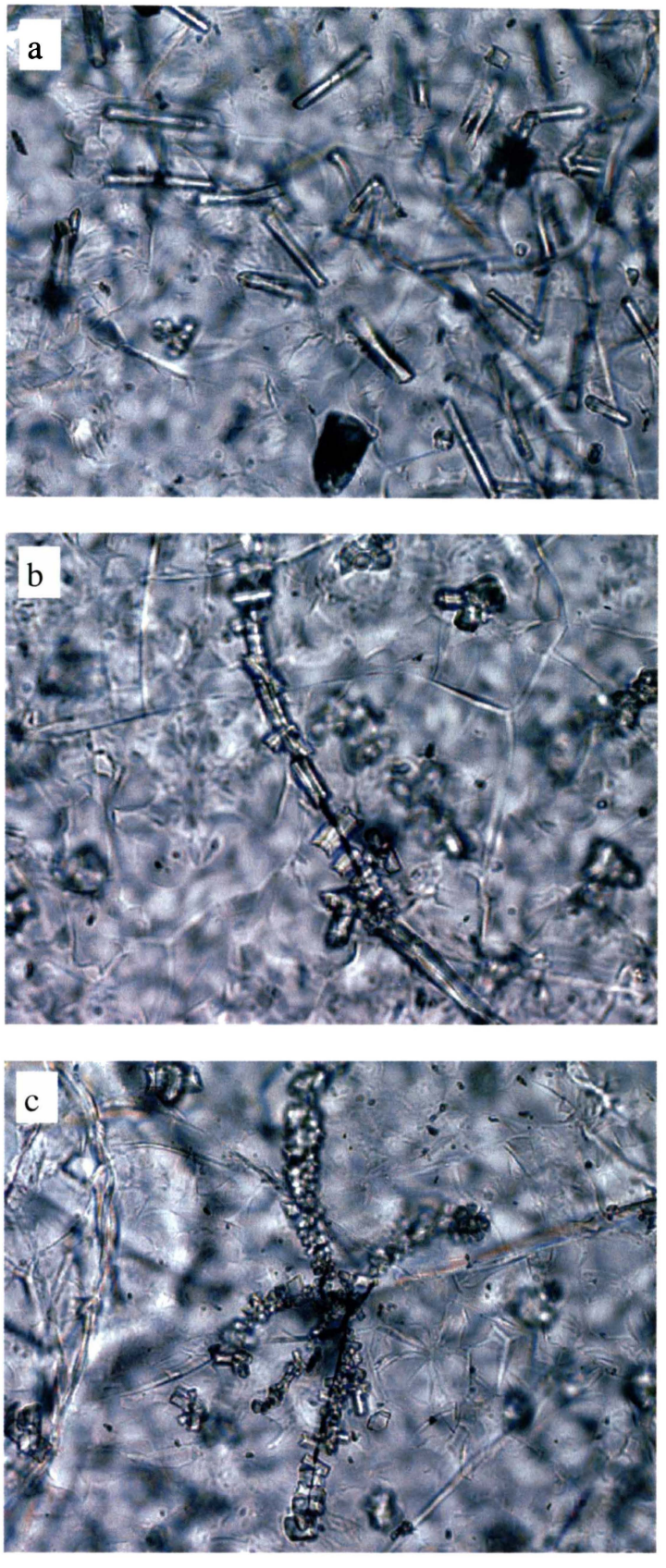

Plate 3.9: Quench crystals. a) Prismatic, lath and rod shaped. b) Stout rods and prisms forming a bead-like strand. c) Bead-like strands of stout rods and prisms joined in a spider-like arrangement. Eastern rhyolite, Okareka Volcanic Complex, Okataina Volcanic Centre (sample number 65). Plane-polarised light. ~ 800x magnification.

Pyroxene crystals will become opaque and lose birefringence (Richnow, 1999). Such opaque microlites are seen in some Okataina, Rotorua and Kapenga rhyolites. A similar process appears to be occurring to Fe-rich phenocrysts in some of the crystallised, spherulitic rhyolite lavas sampled.

It is important to note that these oxidised microlites are different from the opaque fibres commonly seen in crystallised, spherulitic rhyolite, which are products of rhyolitic glass devitrification. These fibres occur in blobs and dendritic strands and do not have the euhedral crystal form exhibited by many microlites. While microlites commonly show some alignment due to flow, opaque fibre strands commonly occur in a radial pattern within spherulites.

In this study all microlites and crystallites will be referred to collectively as quench crystals. It is likely that quench crystals in the Okataina, Rotorua and Kapenga rhyolites are of the same mineral assemblage as the phenocrysts - plagioclase feldspar, orthopyroxene, amphibole, biotite, magnetite and ilmenite. The majority of quench crystals are colourless and do not appear to have the very pale green colour that Richnow (1999) considered to indicate a pyroxene composition. Their very small size gives them a low birefringence such that the only interference colours observed are white and grey. Many crystals show no interference colours. While some crystals appear to have straight extinction, which would suggest an orthopyroxene composition, the majority of crystals that show interference colours have oblique extinction. In addition, the moderate to high relief of many crystals suggests that they are not plagioclase feldspar. While there is a lack of clinopyroxene in the phenocryst assemblage of these lavas, it is possible, based on morphology, extinction angles and relief, that quench crystals may be of clinopyroxene composition. Confirmation of the compositions of quench crystals would require careful analysis by Electron Microprobe, which was not undertaken in this study.

Quench crystals are most noticeable in samples of obsidian and pumiceous rhyolite, although they are also seen to occur in some crystallised, spherulitic lavas. They are commonly aligned in bands that are deflected around phenocrysts and may be deflected around, or cross-cut by, spherulites. Quench crystals are a dominant feature of the groundmass in many of the lavas sampled, although it is suspected that they are present in at least minor quantities in all rhyolite lavas.

3.2.8 Vesicularity

Rhyolite lavas show internal variations in vesicle abundance ranging from non-vesicular obsidian to highly vesicular pumiceous rhyolite. These variations may occur on a large scale as zones within a rhyolite lava flow or dome (Figure 3.1), or may occur on a small scale as variations between flow bands observed in thin section (Plate 3.10). Vesicularity percentages were determined for rhyolites obtained in this study that were seen in thin section to contain vesicles, following the procedure of Houghton and Wilson (1989). Results are given in Appendix II (Table II.1). These calculations give an idea of the overall vesicularity of a 2-5 cm chip of the lava, but do not reflect small-scale variations that may occur. Rhyolite lavas exhibiting a pumiceous texture in hand specimen contain ~30 - 70% vesicles and are classed as poorly to highly vesicular. Samples of obsidian generally contain less than 5% vesicles and are considered non-vesicular. Many rhyolite lavas can not be classed as either obsidian or pumiceous rhyolite, as their texture is intermediate between these two end members. Such rhyolites have ~5 - 30% vesicles and are classed as incipiently to poorly vesicular.

3.2.9 Flow Banding

Rhyolite lavas commonly exhibit flow bands or foliations that record the history of internal deformation and movement of the lava. The development of flow banding begins during flow in the conduit and continues during extrusion and outflow (McPhie et al., 1993). Flow banding can occur in crystallised rhyolite, obsidian and pumiceous rhyolite and is manifested in a number of forms, which may be observed in hand specimen and/or thin section:

- Alignment of spherulitic material, variations in spherulite morphology, or spherulitic and non-spherulitic bands. Alignment of spherical spherulites into trains and formation of axiolitic morphologies may be due to preferential devitrification of bands of susceptible glass, rather than a physical alignment due to flow.
- Varying degrees of glass devitrification, which may lead to colour variations.
- Alignment of quench crystals into bands or variations in the abundance or density of quench crystals (Plate 3.11).
- Variations in vesicle size, shape and abundance (Plate 3.10), or elongation of vesicles due to stretching/shearing during flow.
- Alignment of phenocrysts or variations in the abundance of phenocrysts.

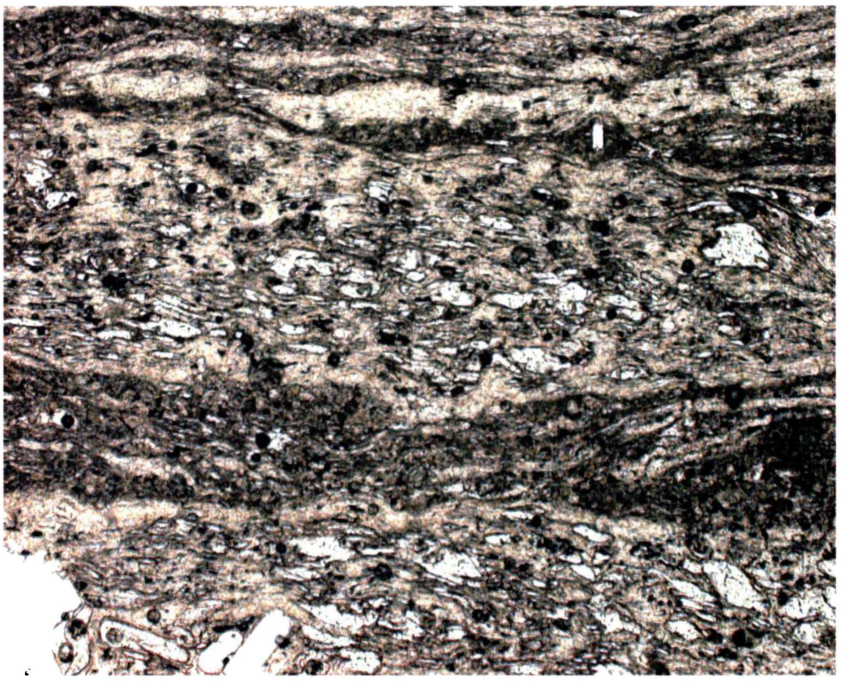

Plate 3.10: Flow banding defined by highly (coarsely) vesicular, poorly vesicular and devitrified glass bands. Bands show deflection around phenocrysts. Haumingi Flow, Haroharo Volcanic Complex, Okataina Volcanic Centre (sample number 56). Plane-polarised light. ~ 30x magnification.

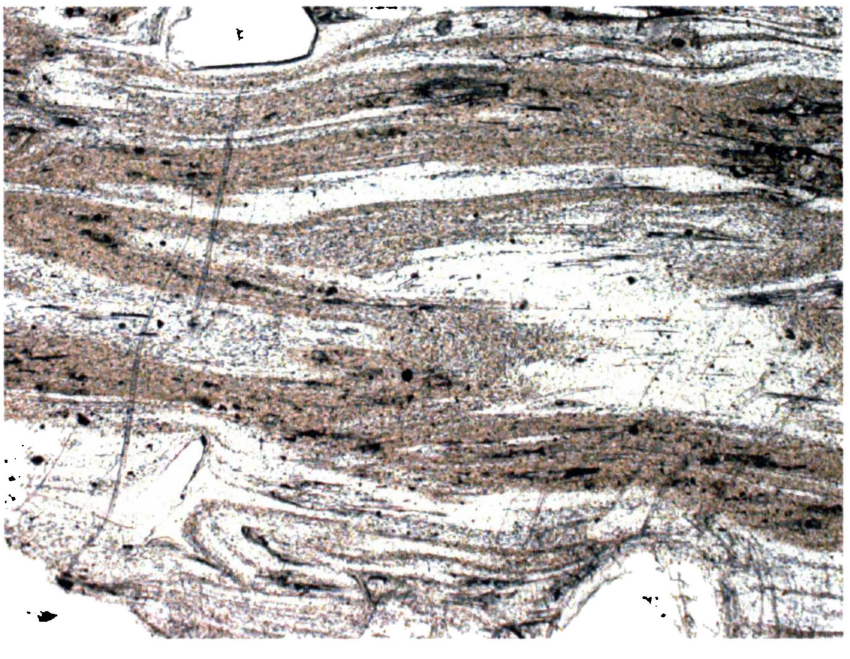

Plate 3.11: Flow banding defined by bands of densely packed and aligned quench crystals (brown and grey bands). Flow bands are folded and show deflection around phenocrysts. Waikakareao Flows, Tarawera Volcanic Complex, Okataina Volcanic Centre (sample number 38). Plane-polarised light. ~ 40x magnification.

Flow bands may be inter-fingered, lensoidal, continuous or discontinuous and the thickness of the bands can vary. Flow bands may be straight or folded. Folding is particularly noticeable when the bands are being defined by the alignment, abundance and density of quench crystals (Plate 3.11). The flow folds are commonly asymmetric with unequal limb angles, lengths and thicknesses. The folds may verge in different directions, with a single flow band forming both s- and z-shaped folds. Folded flow bands do not always parallel each other and disharmonic folding may occur where adjacent layers develop folding of different wavelengths, amplitudes and thicknesses.

Flow bands are commonly deflected around phenocrysts (Plates 3.10 and 3.11), and are rarely deflected around spherulites, indicating spherulite growth before flow cessation. Spherulites that overprint flow bands, indicating growth after flow cessation, are more common.

3.3 FERROMAGNESIAN PHENOCRYST ASSEMBLAGES

In addition to plagioclase feldspar, quartz and Fe-Ti oxide phenocrysts, the rhyolites of the Okataina, Rotorua and Kapenga volcanic centres may contain phenocrysts of the ferromagnesian minerals orthopyroxene, calcic amphibole, biotite and cummingtonite in varying quantities. Assigning a particular rhyolite lava or tephra to a ferromagnesian assemblage has become a useful tool for identification, particularly for tephras. Cole (1966) and Ewart (1968) first undertook the classifying of ferromagnesian assemblages for rhyolite lavas in the study area. Froggatt and Lowe (1990) applied the ferromagnesian assemblage principle to Quaternary silicic tephra formations of the Okataina Volcanic Centre.

Based on thin section point counting results given in Appendix III, the rhyolite lavas of the Okataina, Rotorua and Kapenga volcanic centres have been assigned a ferromagnesian phenocryst assemblage. Nineteen different assemblages are found within the rhyolites obtained in this study, seventeen in Okataina lavas, five in Rotorua lavas and six in Kapenga lavas. Mineral species have been listed in general order of abundance, followed by minerals that may or may not be present (±). Assemblages involving cummingtonite are generally restricted to the Haroharo Volcanic Complex. The abundance of a particular mineral may vary between thin sections and some degree of error is likely given the inaccuracies involved in point counting. Hence for a particular ferromagnesian phenocryst assemblage it is more important to note which mineral species are always present, which species occur in trace

amounts and which species are absent, rather than placing too much emphasis on the exact order in which minerals are listed.

Previous studies of the rhyolite lavas from the Okataina, Rotorua and Kapenga volcanic centres have found them to lack clinopyroxene phenocrysts. However, studies of the tephras erupted in conjunction with the ho_3 lavas (Lowe, 1988; Froggatt and Lowe, 1990; Nairn, 1992) have identified crystals of augite. Ewart (1967) noted that augite is only very rarely found in Taupo Volcanic Zone rhyolite lavas, and Ewart et al. (1975) note that this mineral species may only be seen in mineral concentrates. Hence Cole (1966) and Ewart (1968) defined ferromagnesian assemblages not including augite. This practice has been continued in this study, as the occurrence of clinopyroxene was not confirmed petrographically or by Electron Microprobe analysis (Chapter Five).

3.4 THE ho_1 RHYOLITES

3.4.1 Groundmass Textures

Petrographic descriptions of the ho_1 rhyolites are given in Appendix IV (Table IV.1). All samples are hypocrystalline and vitrophyric with phenocrysts set in a glass groundmass. These oldest rhyolite lavas from the Okataina Volcanic Centre generally have a crystallised, spherulitic glass groundmass. This is likely to be a result of age as any outer obsidian, pumice and autobreccia layers of the rhyolite have been eroded away over time. Alternatively they may comprise flow bands of crystallised, spherulitic glass and poorly devitrified, non-vesicular glass (obsidian). The ho_1 rhyolite lavas commonly contain quench crystals, often aligned with the flow banding, that were subsequently overprinted by the spherulitic texture. Many quench crystals have been altered to opaque minerals in the vicinity of spherulitic material. It is common for non-spherulitic glass, occurring between spherulites or in flow bands, to show evidence of hydration with the formation of perlitic cracks. The North Rotoma rhyolite is notable in that the spherulite content is minor and the groundmass has a classical perlitic texture (Plate 3.8). In both hand specimen and thin section the groundmass of Matawhaura rhyolite can be seen to contain large star-like spherulites.

3.4.2 Phenocryst Assemblages

Point counting results and ferromagnesian phenocryst assemblages for the ho_1 rhyolites are given in Appendix III (Table III.1). Phenocryst contents range from 5 - 36%. Average phenocryst contents and ferromagnesian phenocryst assemblages are given diagrammatically for the ho_1 rhyolites in Figure 3.6. Samples which contain biotite in significant quantities have the highest phenocryst contents (~22% and ~36%). Samples with orthopyroxene and calcic amphibole as the dominant ferromagnesian phenocrysts have lower phenocryst contents (<19%). Spatially, there are no clear patterns in terms of ferromagnesian phenocryst assemblage. The southern rhyolite, Wairua, contains significant quantities of biotite. The western rhyolites are dominated by orthopyroxene and calcic amphibole, as are the northeastern rhyolites. The exception is North Rotoma rhyolite, which contains both biotite and cummingtonite.

The five samples obtained of Maungawhakamana rhyolite show variations in phenocryst content from 5 - 16%. There are also variations in plagioclase (3.4 - 12%), quartz (0.3 - 2.4%) and amphibole (0 - 1.3%) contents. Maungawhakamana dominates the northeastern edge of the Okataina Volcanic Centre and Nairn (1989) identified six vents within this rhyolite edifice, which is likely to be comprised of a number of individual flows and/or domes. It is not clear on what basis Ewart (1968) divided the three rhyolites of this area. The variations in phenocryst contents noted here may represent individual flows and/or domes within this rhyolite, although sampling is insufficient to allow their identification. This may be a problem with other older rhyolites where the level of erosion and difficulty in obtaining fresh unaltered samples hampers identification of individual domes and flows. Ewart (1968) suggested that Whakapoungakau comprised two units, an older underlying part and a younger upper part, which have different phenocryst contents and ferromagnesian assemblages. Only the rhyolite outcropping on the northwestern shore of Lake Okataina, the older underlying part of Ewart (1968), has been sampled in this study. More recent maps of the Okataina Volcanic Centre (Nairn, 1981a, 1989) have made no subdivision of Maungawhakamana or Whakapoungakau.

While the phenocryst contents determined in this study are generally higher than those given by Ewart (1968), most likely a result of the different techniques used, the ferromagnesian phenocryst assemblages are in general agreement. The exceptions are Maungawhakamana, which Ewart (1968) found to contain biotite, and North Rotoma, which Ewart et al. (1975) found to contain clinopyroxene (augite).

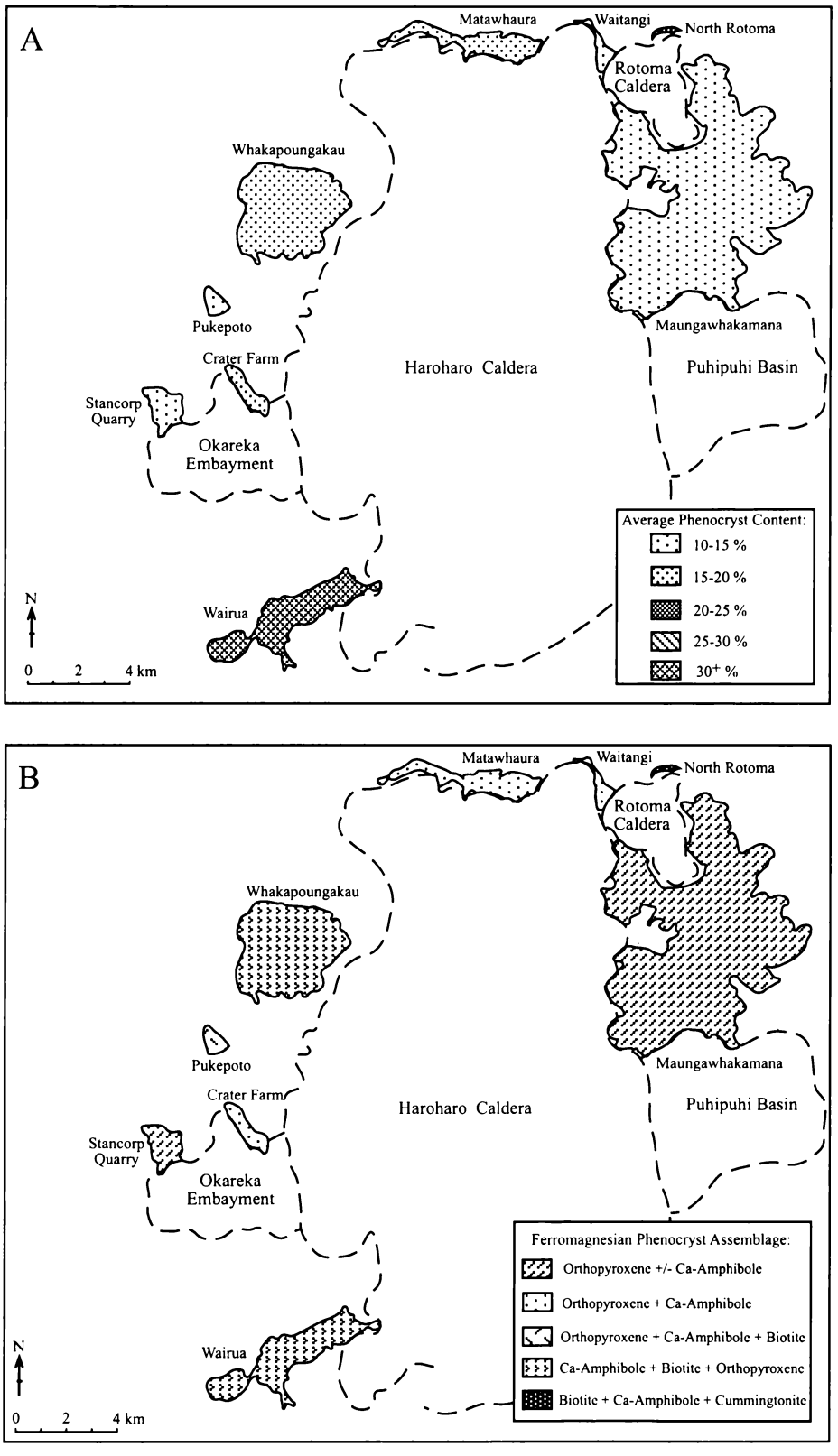

Figure 3.6: Phenocryst characteristics of the ho_1 rhyolites of the Okataina Volcanic Centre. A) Average phenocryst content as a percentage of the total rock. B) Ferromagnesian phenocryst assemblage. Collapse features from Nairn (1989).

Ferromagnesian phenocryst assemblages suggest that the ho_1 rhyolites can be divided into three groups:

Group 1 - Biotite, calcic amphibole and cummingtonite-bearing magma erupting in the northeastern Okataina Volcanic Centre as the North Rotoma rhyolite.

Group 2 - Orthopyroxene and calcic amphibole-bearing magma, with minor quantities of biotite, erupting in the northeastern and western Okataina Volcanic Centre as the Matawhaura, Waitangi, Maungawhakamana, Whakapoungakau, Pukepoto, Stancorp Quarry and Crater Farm rhyolites.

Group 3 - Calcic amphibole, biotite and orthopyroxene-bearing magma erupting in the southern Okataina Volcanic Centre as the Wairua rhyolite.

3.5 THE ho_2 RHYOLITES

3.5.1 Groundmass Textures

Petrographic descriptions of the ho_2 rhyolites are given in Appendix IV (Table IV.2). All samples are hypocrystalline and vitrophyric with phenocrysts set in a glass groundmass. These intermediate age rhyolite lavas from the Okataina Volcanic Centre fall into three textural groups. Several samples appear pumiceous in hand specimen and comprise poorly vesicular glass with vesicles commonly elongated or stretched due to flow. Individual flow bands may show a higher level of vesicularity. These pumiceous lavas commonly contain minor small spherulites. Many samples of ho_2 rhyolite have a crystallised, spherulitic glass groundmass comprising a mosaic of coalesced spherulitic material. The flow direction can be recognised by axiolitic textures, coalesced spherulites and variations in spherulite colour. The third group comprises rhyolites with a texture intermediate between pumiceous rhyolite and obsidian, with a groundmass comprising incipiently to poorly vesicular glass. One of these rhyolites is seen in hand specimen to contain black obsidian bands.

Waimangu rhyolite has a crystallised, spherulitic glass groundmass, except for non-devitrified glass occurring between the spherulites which has a classical perlitic texture. One sample of Tutaeheka 3 is notable in that recrystallisation of the glass groundmass has produced a fine grained equigranular texture, likely to be comprised of cristobalite and alkali feldspars, filling interstices between spherulitic material.

3.5.2 Phenocryst Assemblages

Point counting results and ferromagnesian phenocryst assemblages for the ho_2 rhyolites are given in Appendix III (Table III.1). Phenocryst contents range from 17 - 32%. Average phenocryst contents and ferromagnesian phenocryst assemblages are given diagrammatically for the ho_2 rhyolites in Figure 3.7. As with the ho_1 rhyolites there is a correlation between phenocryst assemblage and average phenocryst content. Samples which contain biotite in significant quantities have the highest phenocryst contents (~26 - 32%). Samples with orthopyroxene and calcic amphibole as the dominant ferromagnesian phenocrysts generally have lower phenocryst contents (~17 - 27%).

The Moerangi, Tutaeheka and South Rotomahana rhyolites cannot be distinguished based on ferromagnesian phenocryst assemblage or total phenocryst content. Spatially, spanning these three groups, there appears to be a broad trend of increasing phenocryst content and the introduction of biotite into the phenocryst assemblage towards the southeast. The northwestern rhyolites contain no biotite and have total phenocryst contents of 17 - 21%. The southeastern rhyolites of Hapeotoroa and Waimangu have phenocryst contents >30% and biotite is the dominant ferromagnesian phenocryst type. Spatially intermediate rhyolites have intermediate phenocryst contents and amounts of biotite.

While Ewart (1968) suggested subdivision of the rhyolite that is here called Tutaeheka 3, he also noted similar phenocryst contents and ferromagnesian assemblages for the individual units. The three samples of Tutaeheka 3 obtained in this study have similar phenocryst contents and ferromagnesian phenocryst assemblages. As for the ho_1 rhyolites, phenocryst contents determined in this study are generally higher than those given by Ewart (1968). The ferromagnesian phenocryst assemblages are in general agreement, with the additional discovery in this study of trace amounts of biotite in the Tutaeheka 2 and Tutaeheka 3 rhyolites.

Ferromagnesian phenocryst assemblages suggest that the ho_2 rhyolites can be divided into two groups:

Group 1 - Biotite-bearing magma erupting as the Kakapiko, Blue Lake, Tutaeheka 1, Hapeotoroa and Waimangu rhyolites.

Group 2 - Orthopyroxene and calcic amphibole-bearing magma, with trace amounts of biotite, erupting as the Direct Road, Hill Road, Moerangi Road, Chestnut Road, Green Lake, Tutaeheka 2 and Tutaeheka 3 rhyolites.

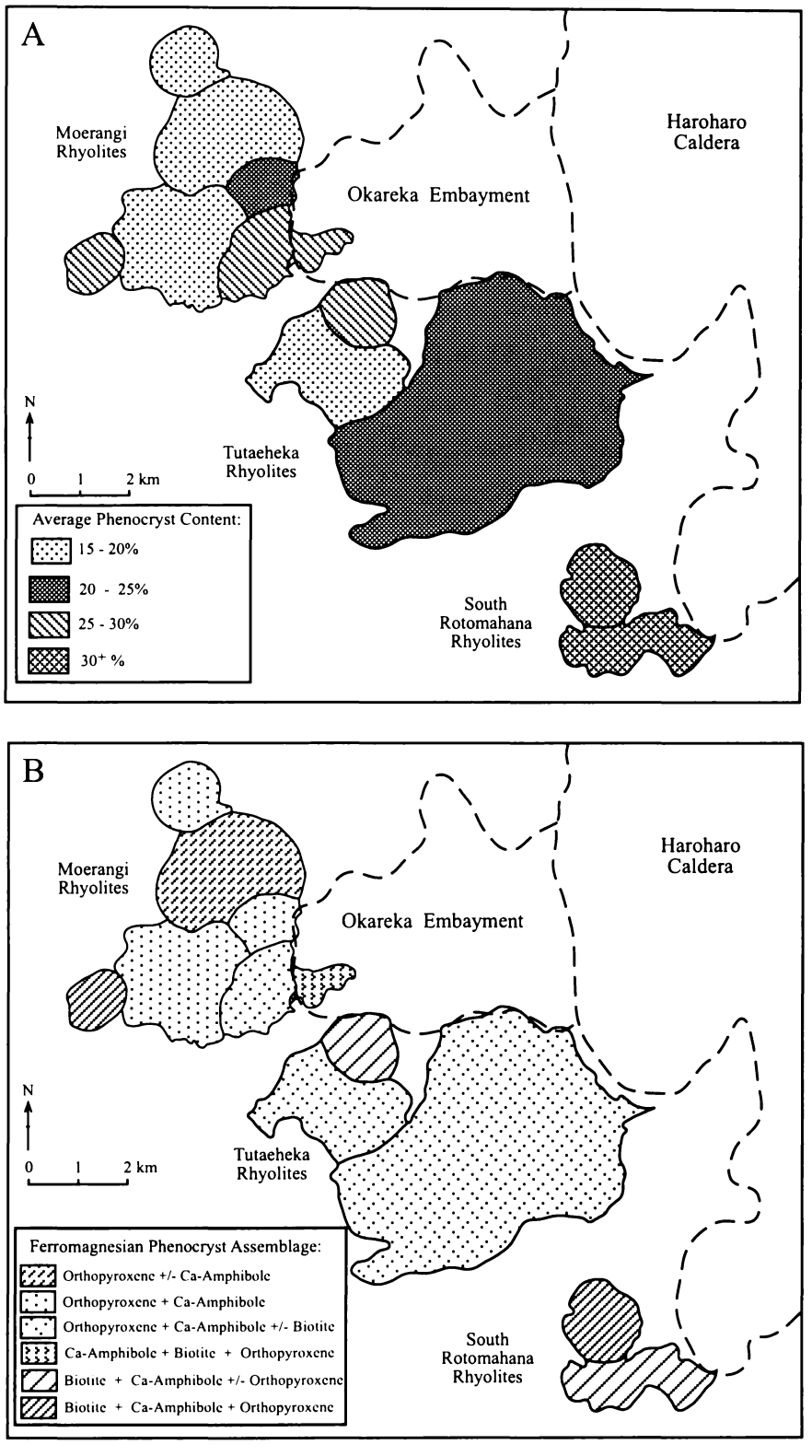

Figure 3.7: Phenocryst characteristics of the ho_2 rhyolites of the Okataina Volcanic Centre. A) Average phenocryst content as a percentage of the total rock. B) Ferromagnesian phenocryst assemblage. Collapse features from Nairn (1989).

3.6 HAROHARO VOLCANIC COMPLEX ho_3 RHYOLITES

Petrographic descriptions of the ho_3 rhyolites of the Haroharo Volcanic Complex are given in Appendix IV (Table IV.3). All samples are hypocrystalline and vitrophyric with phenocrysts set in a glass groundmass. Point counting results and ferromagnesian phenocryst assemblages are given in Appendix III (Table III.1). Average phenocryst contents and ferromagnesian phenocryst assemblages are given diagrammatically for the Haroharo Volcanic Complex rhyolites in Figures 3.8 and 3.9. The Haroharo Volcanic Complex lavas are the only rhyolites found in the Okataina Volcanic Centre, with the exception of the ho_1 North Rotoma rhyolite, that have ferromagnesian phenocryst assemblages containing the amphibole cummingtonite.

3.6.1 Te Rere Eruptive Episode

The oldest lavas of the Haroharo Volcanic Complex were found in outcrop as incipiently vesicular rhyolites and non-vesicular, spherulitic obsidian. A sample obtained from the Haumingi Flow is poorly vesicular overall, but contains highly (coarsely) vesicular flow bands (Plate 3.10). Stevenson et al. (1994) studied the textural stratigraphy of this flow in more detail. In Te Rere Eruptive Episode rhyolites spherulitic material is present as singular spherulite balls, coalesced masses, and axiolitic textures and is most abundant in the obsidian samples. Where quench crystals are present they are aligned and indicate the flow direction. These samples are commonly highly cracked due to the conchoidal nature of volcanic glass.

The Te Rere Eruptive Episode rhyolites are relatively phenocryst poor (7 - 12%) and all have the same ferromagnesian phenocryst assemblage of orthopyroxene + calcic amphibole. Quartz is a very minor component of these samples and occurs only in trace amounts in the Te Koutu and Haumingi flows. The petrographic and mineralogical similarity of the rhyolites of this episode is to be expected as they are considered to have been erupted from the same vent or vent area now buried beneath younger pyroclastics (Nairn, 1981a).

The eruption of rhyolite lavas at the Haroharo Volcanic Complex during this episode of activity was preceded by the eruption of the Te Rere Tephra. Nairn (1992) noted variations in thickness, lithology and grain size which show that the Te Rere Tephra has a complex eruptive origin from multiple vents along the Haroharo Linear Vent Zone (HLVZ). The thickest and/or coarsest deposits occur in exposures to the north and east of the Haroharo Caldera. Here the tephra is crystal-poor and characterised by a lack of phenocrystic quartz

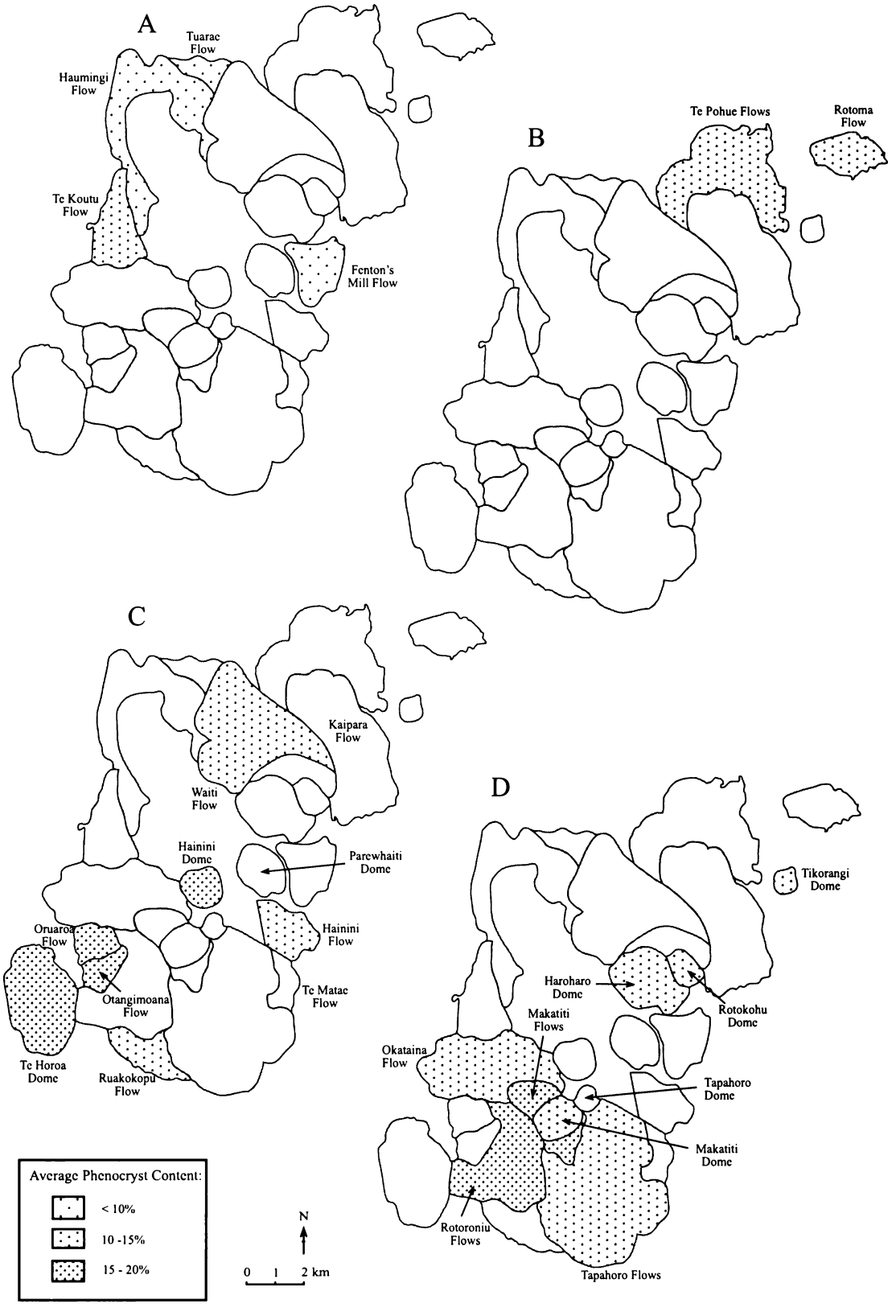

Figure 3.8: Average phenocryst content, as a percentage of the total rock, for Haroharo Volcanic Complex ho_3 rhyolites. A) Te Rere Eruptive Episode, B) Rotoma Eruptive Episode, C) Mamaku Eruptive Episode, D) Whakatane Eruptive Episode. Rhyolites erupted in each episode have been labelled. Rhyolites that have been labelled, but without shading, were not sampled in this study.

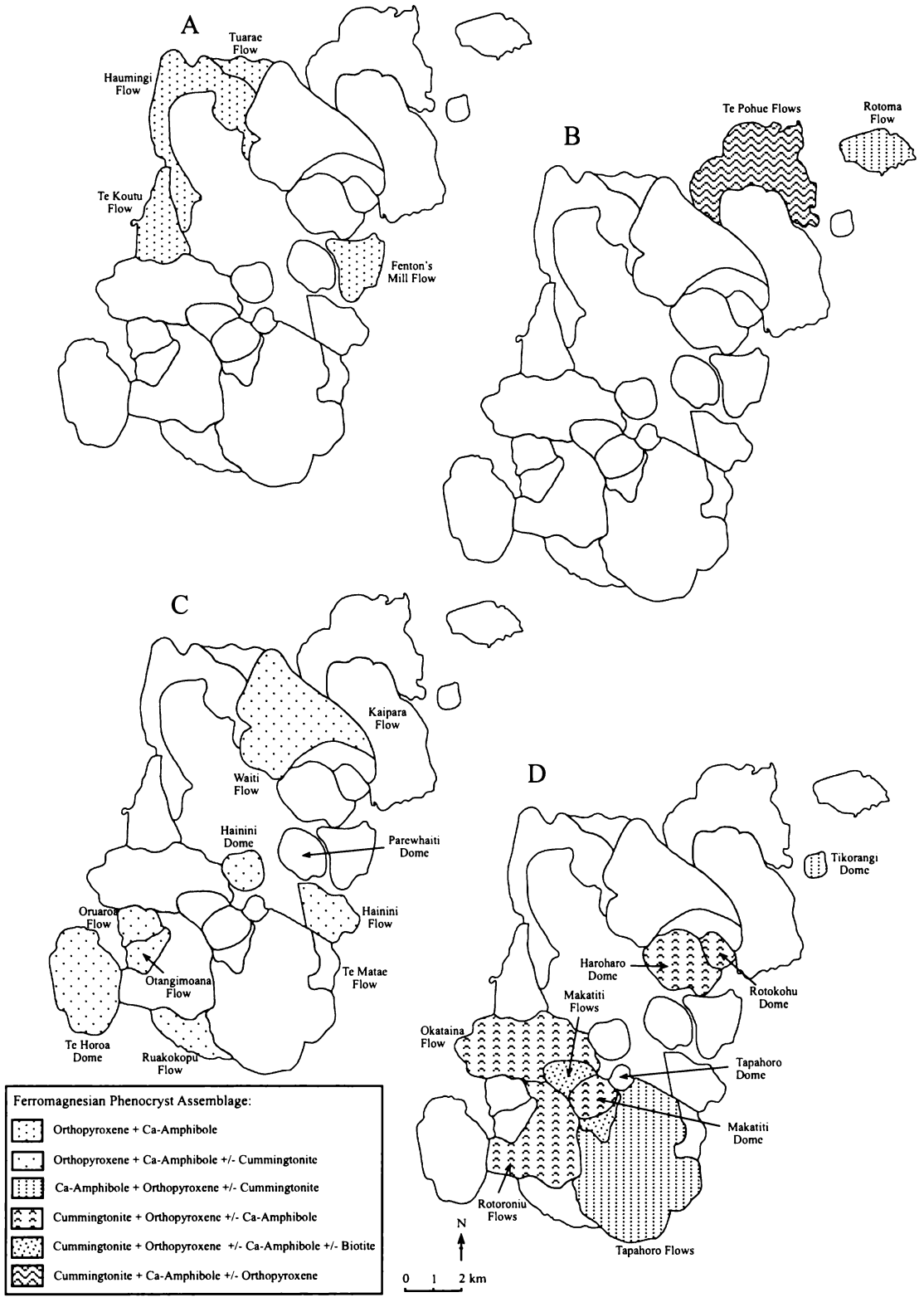

Figure 3.9: Ferromagnesian phenocryst assemblages for Haroharo Volcanic Complex ho_3 rhyolites. A) Te Rere Eruptive Episode, B) Rotoma Eruptive Episode, C) Mamaku Eruptive Episode, D) Whakatane Eruptive Episode. Rhyolites erupted in each episode have been labelled. Rhyolites that have been labelled, but without shading, were not sampled in this study.

and an orthopyroxene - hornblende - augite ferromagnesian assemblage. Biotite is absent. In exposures to the southwest of the caldera the Te Rere Tephra displays variations in texture and mineral content. The tephra has an orthopyroxene - hornblende - augite assemblage at its base and an ash-size distribution consistent with a distant source. However, upward in the sequence rare biotite and quartz phenocrysts appear and then become increasingly abundant, accompanied by small pumice lapilli with a biotite - hornblende ferromagnesian assemblage (Nairn, 1992). However, Nairn (1992) considers quartz-biotite ejecta in southwestern exposures of the Te Rere Tephra to have an accessory lithic origin.

The crystal-poor, quartz-free nature of the Te Rere Tephra in northern and eastern exposures is consistent with Te Rere episode lavas erupted at the Haroharo Volcanic Complex. Nairn (1992) noted that the lack of quartz makes the eruptives of this episode unique in the Haroharo Volcanic Complex.

3.6.2 Rotoma Eruptive Episode

During the Rotoma Eruptive Episode three vent areas were active, two of which erupted rhyolite lavas, one in the northeastern Haroharo Caldera and another in the Rotoma Caldera. The only outcrops of the Te Pohue Flow, erupted in the Haroharo Caldera, found in this study were of an autobreccia deposit assumed to overlie the coherent flow (as documented by Nairn (1981a)). This is the only autobreccia sampled in this study and the two samples obtained have petrographic differences. Both have a pinky-brown ash matrix but one sample contains large white/grey sub-angular rhyolite blocks (Plate 3.4) while the other contains smaller grey/black obsidian lapilli. These blocks and lapilli represent pieces of the underlying lava flow and both clast types have a ferromagnesian phenocryst assemblage of cummingtonite + calcic amphibole ± orthopyroxene. While the obsidian lapilli were too small to point count, phenocrysts comprise ~ 14% of the larger rhyolite blocks.

Also during this eruptive episode the Rotoma Flow was erupted in the Rotoma Caldera to the northeast. Samples obtained from this flow are pumiceous in hand specimen, comprising poorly to moderately vesicular glass, with vesicles stretched due to flow. Less vesicular areas of glass contain cracks. Spherulites are absent. This rhyolite contains ~10 - 11% phenocrysts and has a ferromagnesian phenocryst assemblage of calcic amphibole + orthopyroxene ± cummingtonite.

The ferromagnesian assemblages for these two rhyolites are consistent with observations that the Rotoma Tephra has a dominant ferromagnesian assemblage of orthopyroxene + cummingtonite ± hornblende (Froggatt and Lowe, 1990).

3.6.3 Mamaku Eruptive Episode

During the Mamaku Eruptive Episode rhyolite lavas were erupted from three vent areas within the Haroharo Volcanic Complex (Figure 2.8). In hand specimen these lavas range from obsidian (non-vesicular) to pumiceous rhyolite (moderately to highly vesicular), with many samples having an intermediate texture (incipiently to poorly vesicular). Vesicles are commonly stretched due to flow. Spherulites may occur singularly or as coalesced masses and are most common in obsidian. They are rare or absent in the majority of samples. Quench crystals are common and may be aligned in bands. All samples contain cracks in the glass groundmass, with the non-vesicular obsidian samples being the most highly cracked.

The phenocryst content of the Mamaku episode rhyolites varies from ~8 - 19%. There is little variation in phenocryst content between vent areas and all rhyolites have the same ferromagnesian phenocryst assemblage of orthopyroxene + calcic amphibole ± cummingtonite. Differences between vent areas occur in the abundance of individual minerals. The rhyolite erupted from vent area 2 (Waiti Flow) contains low amounts of quartz (< 0.7%) relative to the rhyolites of vent areas 1 and 3 (1.7 - 4.6%), and hence has a much higher plagioclase/quartz ratio. In addition, the Waiti Flow has higher amphibole contents (0.7 - 1.6%) than the vent area 1 and 3 rhyolites (0.4 - 0.9%).

A sample obtained of the Kaipara Flow was hydrothermally altered preventing determination of the original phenocryst content and assemblage. Parewhaiti Dome and Te Matae Flow were not sampled in this study. Ewart (1968) noted that these three lavas had a phenocryst assemblage similar to the other Haroharo rhyolites of orthopyroxene + hornblende. Ewart et al. (1975) noted the occurrence of cummingtonite in Parewhaiti Dome. Wright (2000) observed a ferromagnesian phenocryst assemblage of orthopyroxene + calcic amphibole ± clinopyroxene for Mamaku Eruptive Episode lavas and pyroclastics. However, clinopyroxene was only observed in ferromagnesian concentrates and its composition was not confirmed by Electron Microprobe analysis. The exception was the Kaipara Flow, in which Wright (2000) found cummingtonite to be the dominant ferromagnesian mineral coexisitng with trace amounts of orthopyroxene and calcic amphibole. In light of the

mineral assemblages determined in this study for other Mamaku Eruptive Episode lavas, it can be assumed that Parewhaiti Dome and the Te Matae Flow have an orthopyroxene + calcic amphibole ± cummingtonite assemblage. Stevenson et al. (1994) noted the presence of biotite in the Waiti Flow. Wright (2000) observed very rare biotite only in ferromagnesian concentrates, and not in thin section.

Froggatt and Lowe (1990) assigned the Mamaku Tephra a dominant ferromagnesian assemblage of orthopyroxene + hornblende ± augite. Lowe (1988) noted the occurrence of trace amounts of cummingtonite. This assemblage is consistent with the rhyolite lavas.

3.6.4 Whakatane Eruptive Episode

During the Whakatane Eruptive Episode rhyolite lavas were erupted from three vent areas within the Haroharo Volcanic Complex (Figure 2.8). In hand specimen these lavas range from obsidian (non-vesicular) to pumiceous rhyolite (poorly to moderately vesicular), with many samples having an intermediate texture (incipiently to poorly vesicular). Vesicles are commonly stretched due to flow. Spherulites may occur singularly or as coalesced masses in obsidian and obsidian flow bands. They are rare or absent in the majority of samples. Quench crystals are common and may be aligned in bands. All samples contain cracks in the glass groundmass, with samples of non-vesicular obsidian being the most highly cracked.

The phenocryst content of the Whakatane episode rhyolites varies from ~11 - 17% and there is little variation in phenocryst content between vent areas. Vent areas 1 and 2 erupted rhyolites with ferromagnesian mineral assemblages dominated by cummingtonite. The exception is the Tapahoro Flows, which have a calcic amphibole + orthopyroxene ± cummingtonite assemblage. The rhyolite erupted in vent area 4 (Tikorangi Dome) also has a calcic amphibole + orthopyroxene ± cummingtonite assemblage. A variation between the vent areas can be seen in the amphibole content. Vent area 1 lavas contain less amphibole (0.7 - 1.1%) than vent area 2 and 4 lavas (1.3 - 1.6%).

For vent area 2, comparing Whakatane and Mamaku lavas shows that the lavas have become richer in quartz and cummingtonite and poorer in orthopyroxene. For vent area 1, lavas of the Whakatane Eruptive Episode are richer in cummingtonite and poorer in orthopyroxene. There is little change in the quartz content. The orthopyroxene content of rhyolite lava appears to be a good predictor of the importance of cummingtonite in the phenocryst

assemblage. Rhyolites with a phenocryst assemblage dominated by cummingtonite have lower orthopyroxene contents.

Tapahoro Dome was not sampled in this study, or by Ewart (1968). In light of the mineral assemblages determined in this study for other Whakatane Eruptive Episode lavas, it can be assumed that this rhyolite contains calcic amphibole, orthopyroxene and cummingtonite.

Froggatt and Lowe (1990) assigned the Whakatane Tephra a dominant ferromagnesian assemblage of orthopyroxene + cummingtonite ± hornblende. Lowe (1988) noted the occurrence of small amounts of biotite. This assemblage for the Whakatane Tephra is consistent with the rhyolite lavas.

3.7 OKAREKA VOLCANIC COMPLEX ho_3 RHYOLITES

Petrographic descriptions of the ho_3 rhyolites of the Okareka Volcanic Complex are given in Appendix IV (Table IV.3). All samples are hypocrystalline and vitrophyric with phenocrysts set in a glass groundmass. Point counting results and ferromagnesian phenocryst assemblages are given in Appendix III (Table III.1). Average phenocryst contents and ferromagnesian phenocryst assemblages are given diagrammatically for the Okareka Volcanic Complex rhyolites in Figure 3.10.

3.7.1 Te Rere Eruptive Episode

The oldest lavas of the Okareka Volcanic Complex have a glass groundmass that may be crystallised and spherulitic or incipiently to poorly vesicular with vesicles stretched due to flow. Where quench crystals are present they are aligned. One sample of the Eastern Rhyolite contains notably large quench crystals. The rhyolites of this episode contain 12 - 21% phenocrysts and have orthopyroxene and calcic amphibole as dominant ferromagnesian phenocrysts. Eastern Rhyolite contains small amounts of biotite and quartz and Te Rere dome contains ~ 3% quartz.

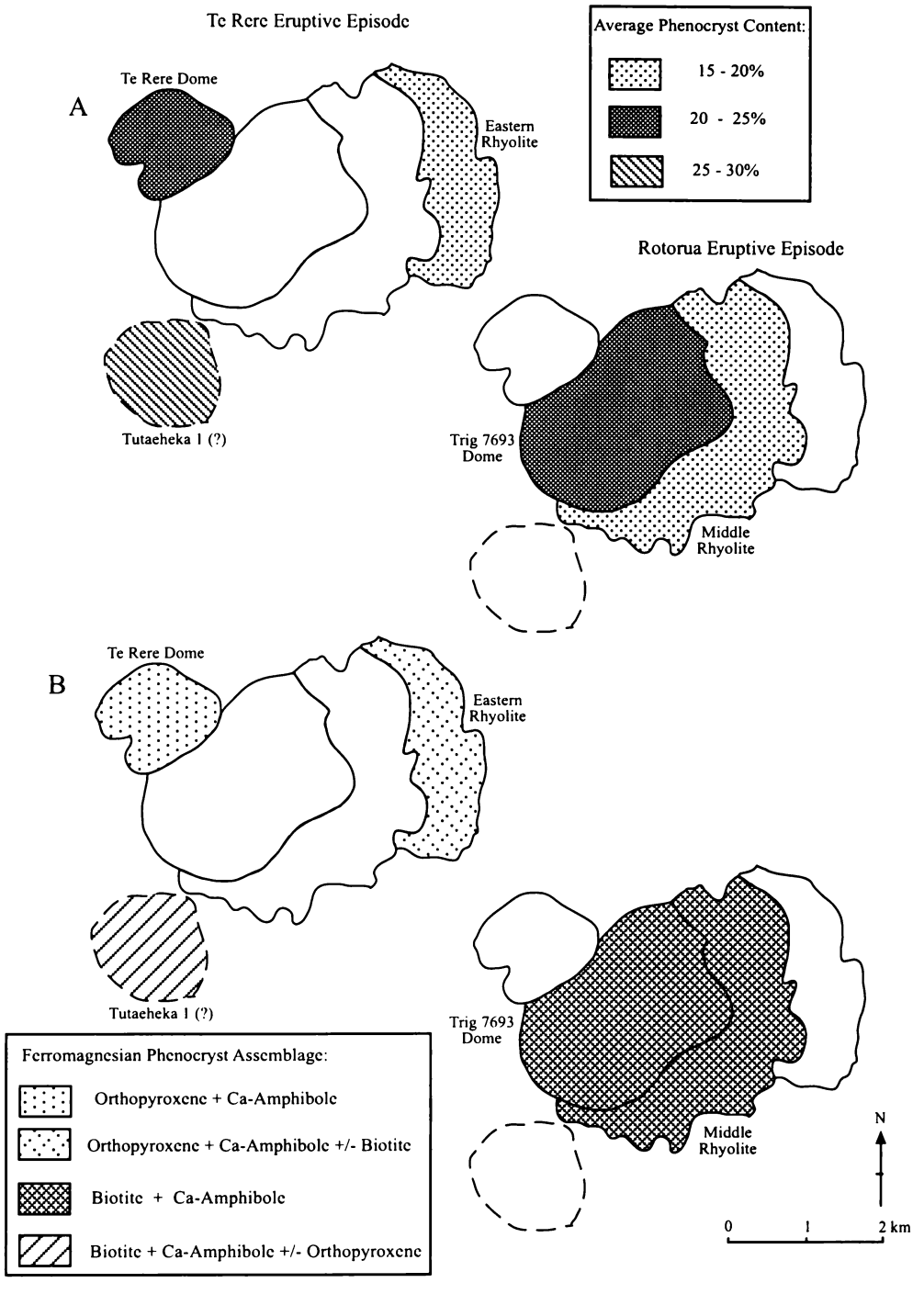

Figure 3.10: Phenocryst characteristics of the Okareka Volcanic Complex ho_3 rhyolites. A) Average phenocryst content as a percentage of the total rock. B) Ferromagnesian phenocryst assemblage.

Nairn (1992) also noted that a dome situated adjacent to the Okareka Embayment (classed as an ho_2 rhyolite in this and other studies) may have been erupted in this episode. A lack of deep exposures on Tutaeheka 1 means that it can only be dated as older than Rotorua Ash. The greatest evidence for its eruption as an ho_3 rhyolite is that it is morphologically young and outcrops are of a coarse-sugary textured rhyolite with obsidian bands. This study has found Tutaeheka 1 to have a ferromagnesian assemblage of biotite + calcic amphibole ± orthopyroxene with ~ 6% quartz. It is phenocryst rich and contains considerably more biotite and quartz than lavas erupted in the Okareka Embayment at this time.

Nairn (1992) considers that pyroclastic eruptions in the Okareka Embayment during the Te Rere episode were restricted to vent clearing phreatic explosions, with only accessory quartz-biotite lithic material erupted.

3.7.2 Rotorua Eruptive Episode

Outcrops of the youngest lavas of the Okareka Volcanic Complex are of pumiceous rhyolite. The glass groundmass is poorly to highly vesicular, with vesicles stretched due to flow and no spherulites present. These rhyolites contain ~17 - 20% phenocrysts and have biotite as the dominant ferromagnesian phenocryst. Small amounts of calcic amphibole are also present and orthopyroxene is absent. In comparison with lavas erupted during the Te Rere Eruptive Episode, these younger lavas are richer in biotite and quartz and poorer in amphibole and orthopyroxene.

Froggatt and Lowe (1990) assigned two dominant ferromagnesian mineral assemblages to the Rotorua Tephra, orthopyroxene + hornblende ± augite in the lower parts and orthopyroxene + hornblende + biotite in upper parts. Hence the upper parts of the tephra are more mineralogically consistent with the rhyolite lavas, which is to be expected as lava extrusion followed eruption of the tephra. Nairn (1980) noted the Rotorua Ash to have an orthopyroxene - hornblende - biotite assemblage and made no mention of a change in composition between upper and lower parts.

3.8 TARAWERA VOLCANIC COMPLEX ho_3 RHYOLITES

Petrographic descriptions of the ho_3 rhyolites of the Tarawera Volcanic Complex are given in Appendix IV (Table IV.3). All samples are hypocrystalline and vitrophyric with phenocrysts set in a glass groundmass. Point counting results and ferromagnesian phenocryst assemblages are given in Appendix III (Table III.1). Average phenocryst contents and ferromagnesian phenocryst assemblages are given diagrammatically for the Tarawera Volcanic Complex rhyolites in Figures 3.11 and 3.12.

3.8.1 Okareka Eruptive Episode

The oldest lavas of the Tarawera Volcanic Complex outcrop as non-vesicular obsidian or poorly vesicular rhyolite with some stretching of vesicles due to flow. The glass groundmass of these samples is cracked and contains quench crystals which are commonly aligned. Spherulitic material may be present in minor quantities. The two rhyolites sampled from this episode of activity were erupted from vents ~10 km apart along the Tarawera Linear Vent Zone (Nairn, 1992). Patiti Island contains 24% phenocrysts and has a calcic amphibole + orthopyroxene ferromagnesian assemblage. Ridge Flow contains 15% phenocrysts and, in addition to orthopyroxene and calcic amphibole, contains trace amounts of biotite. The Hawea Flow was not sampled in this study. Nairn (1992) notes that this lava has an orthopyroxene - hornblende assemblage with rare biotite, similar to that found in this study for the adjacent Ridge Flow.

The eruption of rhyolite lavas during this episode of activity was preceded by eruption of the Okareka Tephra. Nairn (1992) observed that the Okareka Tephra is quartz-bearing, characterised by the presence of biotite along with orthopyroxene and hornblende, and most likely has a vent buried under the Kanakana Dome - Ridge Dome area. Ridge Dome occurs to the west of the Ridge Flow and is buried under younger pyroclastics (Nairn, 1989). Nairn (1992) notes that a significant change in mineralogy must have occurred during the eruption sequence, as the lavas generally lack biotite, but noted that such changes are not unknown at the Tarawera Volcanic Complex, having also occurred in the Rerewhakaaitu Eruptive Episode.

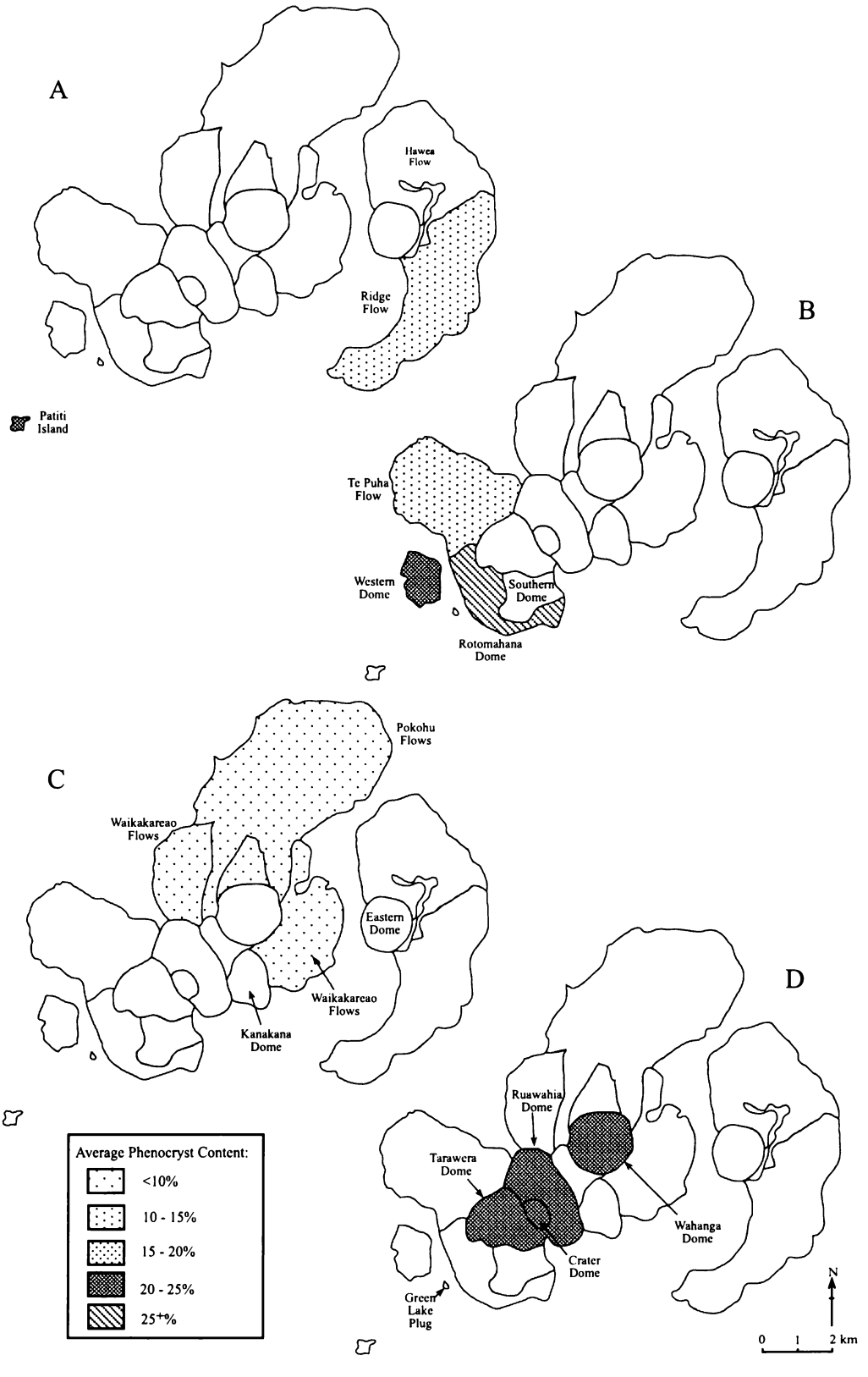

Figure 3.11: Average phenocryst content, as a percentage of the total rock, for the Tarawera Volcanic Complex ho_3 rhyolites. A) Okareka Eruptive Episode, B) Rerewhakaaitu Eruptive Episode, C) Waiohau Eruptive Episode, D) Kaharoa Eruptive Episode (Green Lake Plug contains 16% phenocrysts). Rhyolites erupted in each episode have been labelled. Rhyolites that have been labelled, but without shading, were not sampled in this study.

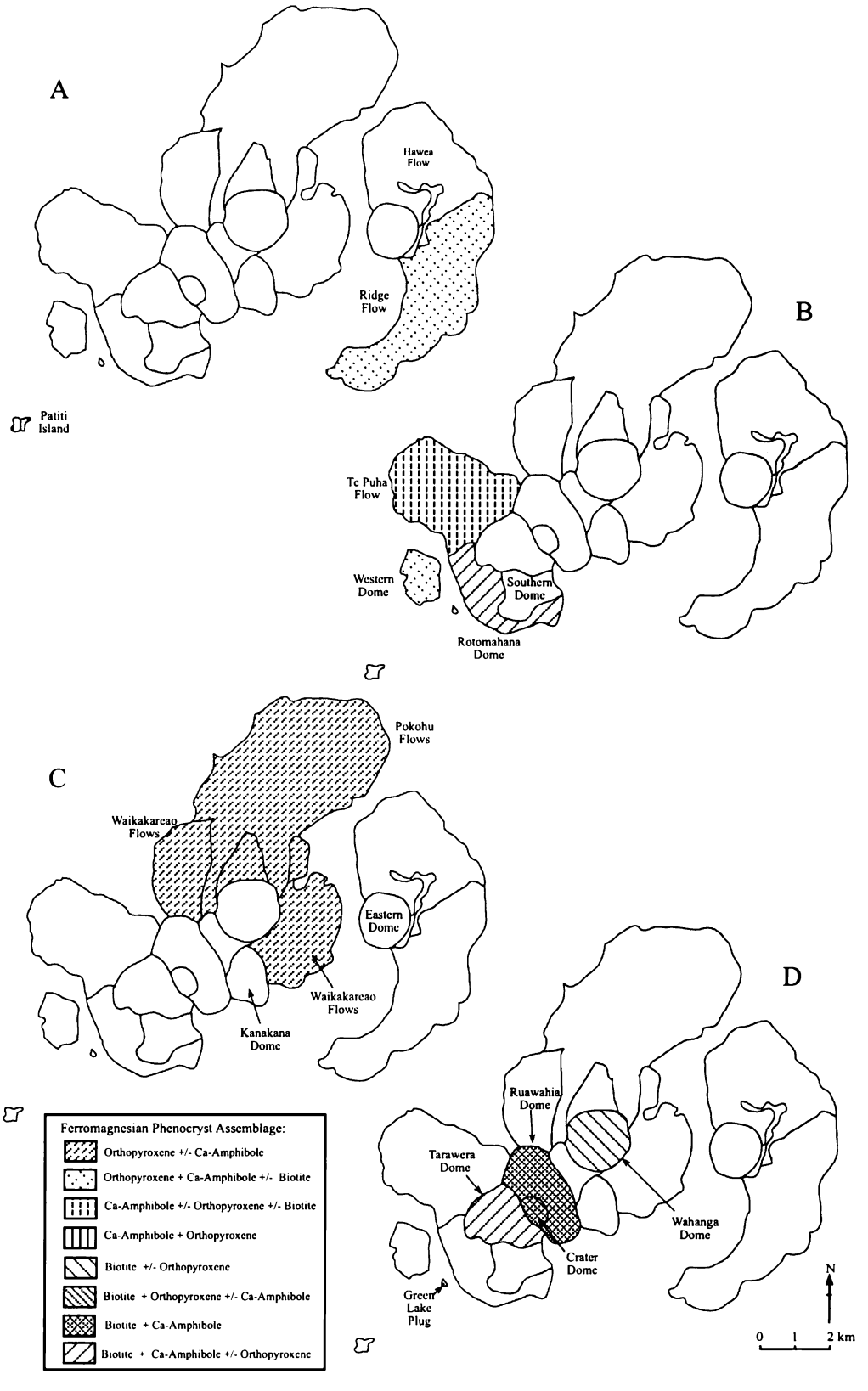

Figure 3.12: Ferromagnesian phenocryst assemblages for the Tarawera Volcanic Complex ho_3 rhyolites. A) Okareka Eruptive Episode, B) Rerewhakaaitu Eruptive Episode, C) Waiohau Eruptive Episode, D) Kaharoa Eruptive Episode (Green Lake Plug contains Bio + Opx ± Ca-Amph). Rhyolites erupted in each episode have been labelled. Rhyolites that have been labelled, but without shading, were not sampled in this study.

3.8.2 Rerewhakaaitu Eruptive Episode

During the Rerewhakaaitu Eruptive Episode rhyolite lavas were erupted from vents in the southwestern Tarawera Volcanic Complex. In hand specimen these lavas range from non-vesicular obsidian to incipiently to poorly vesicular rhyolite. Singular spherulites or areas of spherulitic material and devitrified glass may be present. The exception is Rotomahana Dome, which contains a crystallised, spherulitic glass groundmass consisting of a mosaic of coalesced spherulitic material. Non-vesicular glass occurring between spherulites contains perlitic cracks. The glass groundmass of all other samples is cracked and if quench crystals are present, they are commonly aligned.

Western Dome contains ~22% phenocrysts and has orthopyroxene and calcic amphibole as the main ferromagnesian phenocrysts. Rotomahana Dome contains ~29% phenocrysts and has biotite as the dominant ferromagnesian phenocryst. The two samples obtained of the Te Puha Flow have different phenocryst contents and assemblages. One sample contains ~22% phenocrysts and has biotite as the dominant ferromagnesian mineral (similar to Rotomahana Dome). Another sample contains ~7% phenocrysts and has orthopyroxene and calcic amphibole as the dominant ferromagnesian phenocrysts.

Cole (1966, 1970a) observed intimate mingling between a phenocryst-poor orthopyroxene lava and a phenocryst-rich hornblende-biotite lava in rhyolites erupted during the Rerewhakaaitu episode. This mingling was not directly observed in the rhyolites of this study, but the two lava types are represented in the samples obtained. The two samples obtained of the Te Puha Flow highlight the occurrence of both lava types in a single unit. Hence the overall ferromagnesian phenocryst assemblage shown for the Te Puha Flow in Figure 3.12 is calcic amphibole ± orthopyroxene ± biotite. However, it actually contains two lava types, one containing orthopyroxene + calcic amphibole and another containing biotite + calcic amphibole ± orthopyroxene.

Southern Dome was not sampled in this study. Cole (1970b) assigned the rhyolite now known as Southern Dome a ferromagnesian phenocryst assemblage of orthopyroxene (± hornblende + biotite). It was in this dome that Cole (1966) noted mingling between two lava types. Cole (1966) also noted the occurrence of two magma types within deposits of the Rerewhakaaitu Tephra, which contains two types of pumice occurring in approximately equal quantities throughout. Low crystal content pumice has orthopyroxene as the only ferromagnesian mineral present and quartz is absent. Higher crystal content pumice contains

hornblende, biotite and quartz. Such a bimodal pumice population is consistent with the lava compositions.

3.8.3 Waiohau Eruptive Episode

During the Waiohau Eruptive Episode rhyolite lavas were erupted from vents that now lie beneath Kanakana Dome and Eastern Dome. The samples obtained of lavas erupted in this episode have glass groundmass textures that span the range found in rhyolite lavas - crystallised and spherulitic glass, incipiently vesicular glass containing spherulitic material (spherulitic obsidian), incipiently and poorly vesicular coarsely flow banded glass, and moderately vesicular glass (pumiceous rhyolite). Vesicles are commonly elongated or stretched due to flow. Cracks are seen in the glass groundmass of non-crystallised samples. When present, quench crystals are aligned with this direction. One sample of the Pokohu Flows found at Tarawera Falls on the Tarawera River contains large star-like spherulites (Plate 3.7) which can be observed in hand specimen.

The Waikakareao and Pokohu flows have low phenocryst contents (<11%) and the same ferromagnesian phenocryst assemblage of orthopyroxene ± calcic amphibole. Kanakana Dome and Eastern Dome were not sampled in this study. Cole (1970b) found Eastern Dome and Plateau Dome to have an orthopyroxene ± hornblende ferromagnesian assemblage. Plateau Dome has subsequently been divided into Kanakana Dome and the Waikakareao flows. Speed (2001) observed orthopyroxene as the dominant ferromagnesian phenocryst in Waiohau Eruptive Episode pyroclastics and lavas (including Kanakana and Eastern domes), occurring in association with trace amounts of calcic amphibole. Speed (2001) also noted trace amounts of cummingtonite in Kanakana Dome.

The Waiohau Tephra was noted by Cole (1966) to be typified by the minerals orthopyroxene ± hornblende, with traces of augite in the top of the unit due to contamination from the overlying tephra sequence. Lowe (1988) also noted augite in the Waiohau Tephra and Froggatt and Lowe (1990) assigned the tephra a dominant ferromagnesian assemblage of orthopyroxene + hornblende ± augite.

3.8.4 Kaharoa Eruptive Episode

During the Kaharoa Eruptive Episode rhyolite lavas were erupted from vents along ~ 6 km of the TLVZ. The samples obtained of lavas erupted in this episode range from poorly vesicular rhyolites to poorly to moderately vesicular pumiceous rhyolites. Vesicles are elongated or stretched due to flow and when quench crystals are present in the glass groundmass they are aligned with this. The glass groundmass of these rhyolites is commonly cracked and the spherulite content is minor.

With the exception of Green Lake Plug the rhyolites of this episode have high phenocryst contents (~24 - 26%). All rhyolites have ferromagnesian phenocryst assemblages dominated by biotite. Calcic amphibole and orthopyroxene may or may not be present in small amounts.

The Kaharoa Tephra was given the ferromagnesian assemblage of orthopyroxene + hornblende ± biotite by Froggatt and Lowe (1990), which is consistent with the rhyolite domes. Leonard (1999) noted that the products of the Kaharoa episode contain rare cummingtonite.

3.9 ROTORUA VOLCANIC COMPLEX RHYOLITES

3.9.1 Groundmass Textures

Petrographic descriptions of the Rotorua Volcanic Centre rhyolites are given in Appendix IV (Table IV.4). All samples are hypocrystalline and vitrophyric with phenocrysts set in a glass groundmass. The oldest rhyolites erupted from the Rotorua Volcanic Centre (hr_1) have either a crystallised, spherulitic glass groundmass or comprise perlitically cracked non-vesicular glass (obsidian) with abundant spherulitic material. Alignment and morphology of spherulitic material commonly suggests the flow direction. Hamurana Dome was found by (Crosby, 1998) to be lithophysal, although such features were not observed in this study.

Intermediate age rhyolites erupted from the Rotorua Volcanic Centre (hr_2) exhibit a range of groundmass textures - crystallised and spherulitic glass, non-vesicular glass containing spherulitic material (spherulitic obsidian), and moderately vesicular glass with vesicles

elongated or stretched due to flow (pumiceous rhyolite). Where present, quench crystals show an alignment.

The youngest rhyolites erupted from the Rotorua Volcanic Centre (hr_3) are comprised of either crystallised, spherulitic glass or are pumiceous in hand specimen and comprise poorly vesicular glass with vesicles elongated or stretched due to flow. In pumiceous samples the glass groundmass is cracked and no spherulitic material is present.

3.9.2 Phenocryst Assemblages

Point counting results and ferromagnesian phenocryst assemblages for the Rotorua Volcanic Centre rhyolites are given in Appendix III (Table III.1). Average phenocryst contents and ferromagnesian phenocryst assemblages are given diagrammatically for the Rotorua Volcanic Centre rhyolites in Figure 3.13. Overall the rhyolites contain ~3.5 - 30% total phenocrysts. There is a correlation between phenocryst content and ferromagnesian mineral assemblage, with the most phenocryst-rich rhyolites generally containing significant amounts of biotite.

The hr_1 rhyolites have a range in phenocryst contents from ~3.5 - 23%, being most phenocryst poor in the southern rhyolites of Tokorangi and Hemo Gorge and most phenocryst rich in the western rhyolite of Endean Road. The northern rhyolite of Hamurana has an intermediate phenocryst composition. Endean Road has a ferromagnesian phenocryst assemblage of orthopyroxene + calcic amphibole + biotite, with biotite occurring in significant quantities. Hamurana contains orthopyroxene ± calcic amphibole. The southern phenocryst-poor rhyolite of Tokorangi contains only orthopyroxene. The sample of Hemo Gorge contains only plagioclase, quartz and Fe-Ti oxides as phenocrysts and therefore cannot be assigned a ferromagnesian phenocryst assemblage. The hr_1 rhyolites of Umurua and Fryer Road were not sampled in this study. Point counting by Dravitzki (1999) gives the Umurua rhyolite a biotite + orthopyroxene + calcic amphibole ferromagnesian phenocryst assemblage, similar to that for the adjacent Endean Road rhyolite. Milner (2001) observed orthopyroxene as the only ferromagnesian phenocryst type in the Fryer Road rhyolite, comparable to the adjacent Hamurana rhyolite.

The hr_2 rhyolites are relatively phenocryst poor containing ~ 4 - 9% phenocrysts. These rhyolites are quartz poor containing generally only trace amounts. Orthopyroxene is the dominant and often only ferromagnesian mineral present. Calcic amphibole may be present

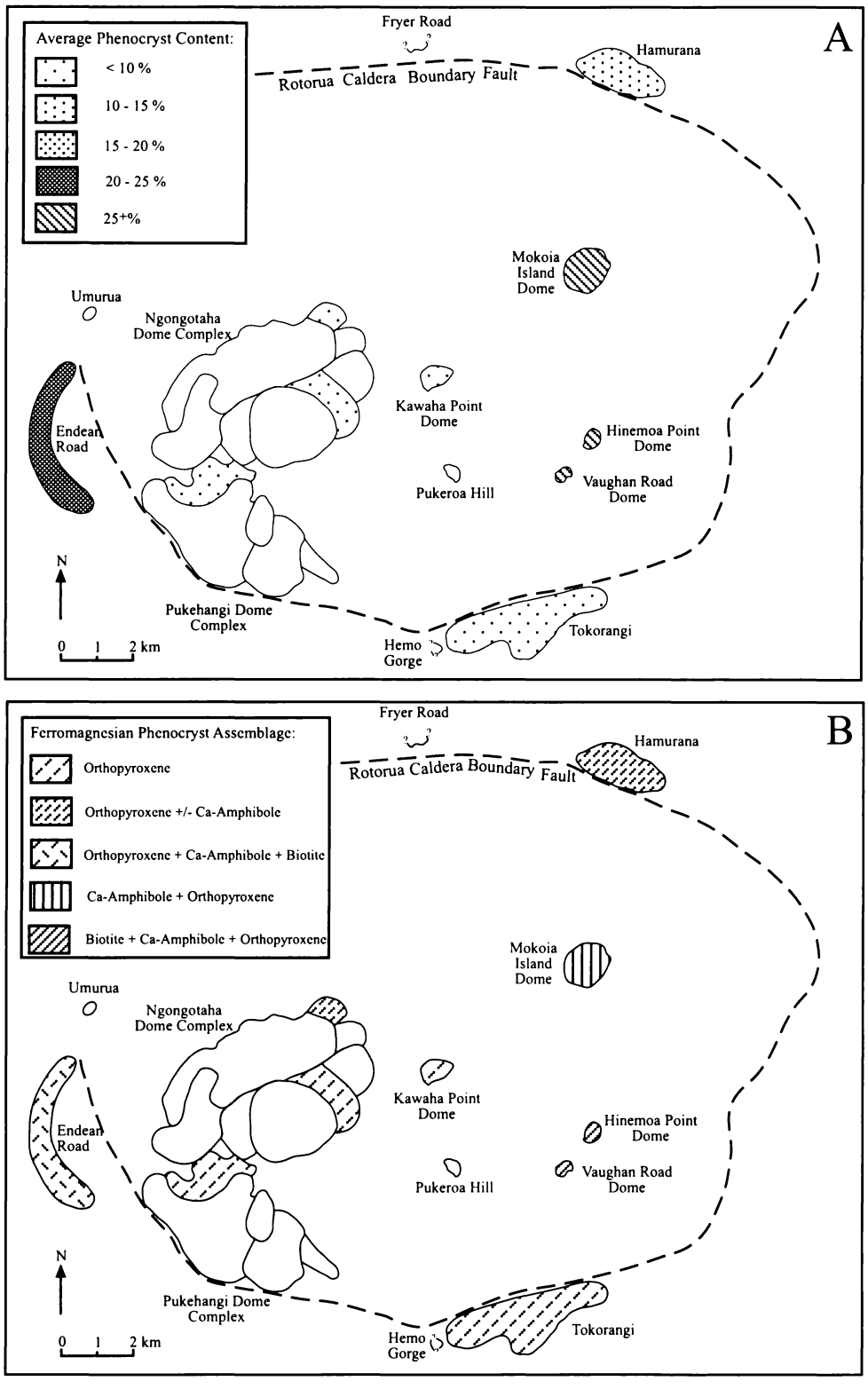

Figure 3.13: Phenocryst characteristics of the Rotorua Volcanic Centre rhyolites. A) Average phenocryst content as a percentage of the total rock. B) Ferromagnesian phenocryst assemblage. Hemo Gorge rhyolite contains < 10% phenocrysts, none of which are ferromagnesian minerals. Rotorua Caldera Boundary Fault from Thompson (1974).

in trace amounts. Dravitzki (1999) sampled many of the domes of the Ngongotaha and Pukehangi dome complexes that were not sampled in this study, finding orthopyroxene to be the dominant ferromagnesian phenocryst. Summit Dome (Ngongotaha) was found to contain biotite, and Te Miri Dome (Pukehangi) also contains calcic amphibole and biotite. This is in contrast to the sample of Te Miri Dome obtained in this study which contained only orthopyroxene. Dravitzki (1999) considered that the Summit and Te Miri domes are the last domes erupted from the Ngongotaha and Pukehangi complexes respectively, hence providing a possible explanation for their more diverse ferromagnesian assemblages. Milner (2001) notes that the Pukeroa Hill rhyolite contains orthopyroxene as the only ferromagnesian phenocryst type, similar to the other hr_2 rhyolite lavas.

The hr_3 rhyolites are relatively phenocryst rich containing ~29 - 30% phenocrysts and are quartz rich relative to the hr_2 rhyolites. The Hinemoa Point and Vaughan Road domes contain biotite + calcic amphibole + orthopyroxene. Mokoia Island lacks biotite and has a calcic amphibole + orthopyroxene assemblage.

3.10 KAPENGA VOLCANIC COMPLEX RHYOLITES

3.10.1 Groundmass Textures

Petrographic descriptions of the Kapenga Volcanic Centre rhyolites are given in Appendix IV (Table IV.5). All samples are hypocrystalline and vitrophyric with phenocrysts set in a glass groundmass. The oldest rhyolites erupted from the Kapenga Volcanic Centre (hk_1) have either a crystallised, spherulitic glass groundmass or comprise highly cracked non-vesicular glass (obsidian) with abundant spherulitic material. Alignment and morphology of spherulitic material commonly suggests the flow direction. Quench crystals are abundant in the obsidian and are aligned.

The youngest rhyolites erupted from the Kapenga Volcanic Centre (hk_2) exhibit two groundmass textures - crystallised, spherulitic glass and poorly to moderately vesicular glass with vesicles elongated or stretched due to flow (pumiceous rhyolite). The pumiceous lavas contain no spherulitic material. The flow direction in these lavas may be suggested by alignment of spherulitic material, stretching of vesicles or bands of quench crystals.

3.10.2 Phenocryst Assemblages

Point counting results and ferromagnesian phenocryst assemblages for the Kapenga Volcanic Centre rhyolites are given in Appendix III (Table III.1). Average phenocryst contents and ferromagnesian phenocryst assemblages are given diagrammatically for the Kapenga Volcanic Centre rhyolites in Figure 3.14. Overall the rhyolites contain ~ 5.5 - 29% phenocrysts and again there is a correlation between phenocryst content and ferromagnesian mineral assemblage, with the most phenocryst-rich rhyolites containing significant amounts of biotite.

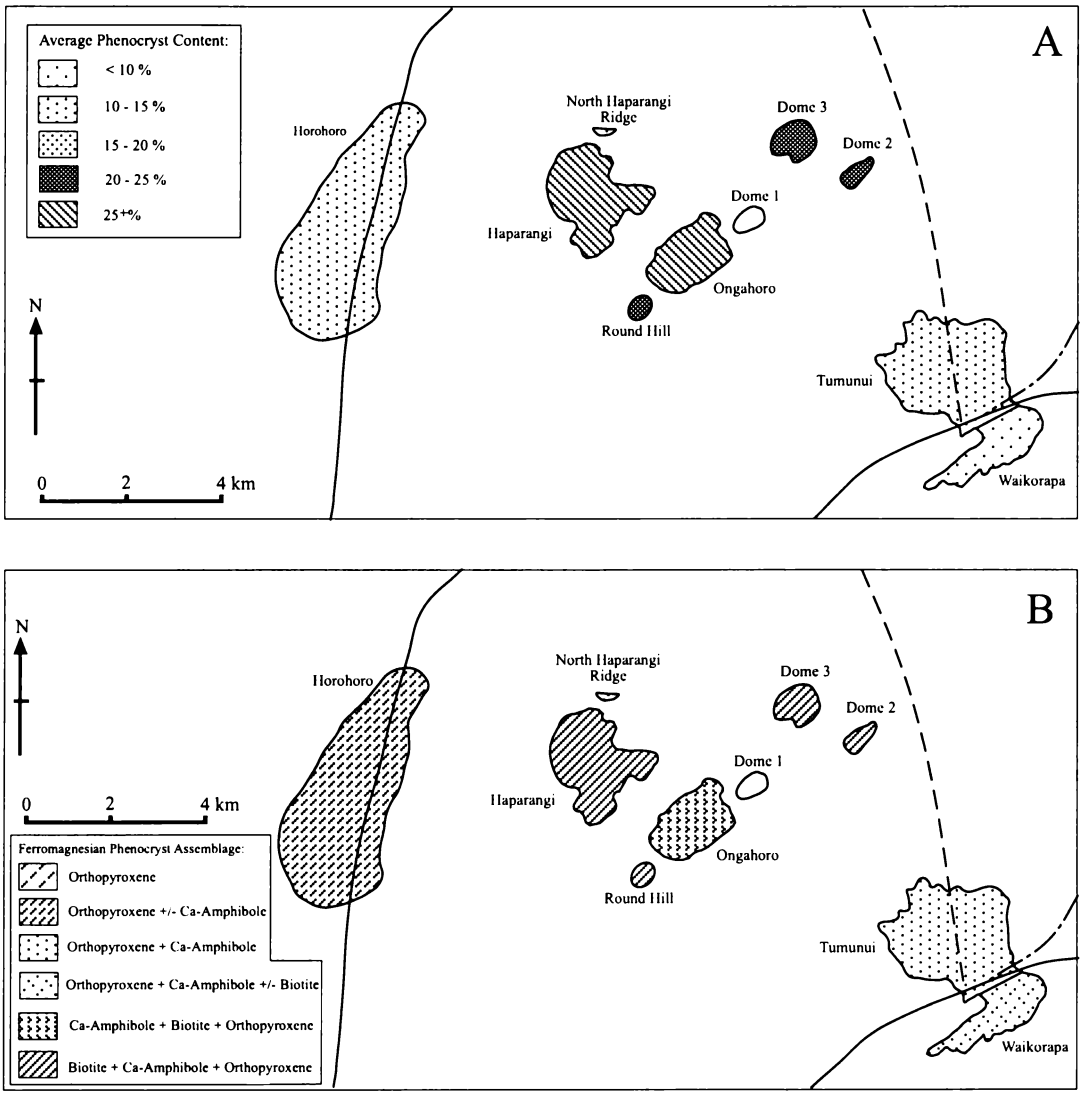

Figure 3.14: Phenocryst characteristics of the Kapenga Volcanic Centre rhyolites. A) Average phenocryst content as a percentage of the total rock. B) Ferromagnesian phenocryst assemblage. North Haparangi Ridge rhyolite contains < 10% phenocrysts and the only ferromagnesian phenocryst present is orthopyroxene. Outlines of the Kapenga Volcanic Centre according to Wilson et al. (1984) and Houghton et al. (1995).

The hk_1 rhyolites have a range in phenocryst contents from ~ 5.5 - 15%. These rhyolites contain orthopyroxene as the dominant ferromagnesian phenocryst. Horohoro, Tumunui and Waikorapa also contain varying amounts of calcic amphibole. Waikorapa contains trace amounts of biotite.

The hk_2 rhyolites are phenocryst rich compared to the hk_1 rhyolites, containing ~ 23 - 29% phenocrysts. The ferromagnesian phenocryst assemblage of these rhyolites is dominated by biotite with lesser amounts of calcic amphibole and orthopyroxene. The exception is Ongahoro in which calcic amphibole is the dominant ferromagnesian mineral. Dome 1 was not sampled in this study, although Gaston (1991) showed it to have a similar mineralogy to the other hk_2 rhyolites.

3.11 XENOLITHS

Xenoliths were found in three of the rhyolite lavas obtained in this study, all of which were erupted from the Okataina Volcanic Centre. Based on texture and mineralogy they appear to be of basaltic composition. They occur in the North Rotoma (ho_1), Te Koutu (ho_3 - Haroharo) and Green Lake Plug (ho_3 - Tarawera) rhyolites and range in size from 9-15 mm. The boundary between these xenoliths and the surrounding rhyolite lava is sharp and may be a site of spherulite nucleation in the rhyolite lava. The basalt xenoliths are hypocrystalline and porphyritic with a fine-grained intergranular groundmass comprised of plagioclase feldspar, pyroxene, Fe-Ti oxides and olivine with small amounts of glass.

The North Rotoma xenolith contains sparse phenocrysts, which are < 1 mm in length, of plagioclase feldspar, pyroxene, corroded/resorbed amphibole and Fe-Ti oxides. One very large plagioclase clot, 7.5 mm in length, is out of character for the otherwise fine-grained xenolith. The crystals comprising this clot are subhedral and show resorption features and internal melting. The xenolith found in the Te Koutu Flow contains phenocrysts up to 1 mm in length with the most common being clinopyroxene. Plagioclase phenocrysts are highly resorbed and some have been completely resorbed so all that remains is a brown glass occupying the prismatic shape of the phenocryst. The Green Lake Plug xenolith contains phenocrysts of olivine and pyroxene up to 1.5 mm in length. Quartz phenocrysts up to 1.75 mm have embayed and resorbed margins. Plagioclase phenocrysts are up to 1 mm. Some are highly resorbed and have a sieve-like texture while others have been entirely resorbed and a brown glass is all that remains.

The existence of quartz crystals in these olivine-bearing basaltic xenoliths suggests that the quartz is xenocrystic. The resorbed nature of the quartz, as well as the resorption seen in plagioclase and amphibole phenocrysts, suggests these crystals were out of equilibrium with the crystallising magma and hence the plagioclase and amphibole may also be xenocrystic.

Brown et al. (1998a) and Burt et al. (1998) discuss the nature and occurrence of plutonic lithics in ignimbrites derived from the Taupo Volcanic Zone and Okataina Volcanic Centre respectively. Rare crystal clusters observed in rhyolites obtained in this study show textural and mineralogial similarities to plutonic lithics documented by Brown et al. (1998a) and Burt et al. (1998). They have an equigranular texture and may exhibit intergrowth textures similar to those that are most commonly seen in plutonic rocks.

A crystal cluster found in the Tutaeheka 3 rhyolite (ho_2) is equigranular with fine grained crystals, most of which are < 0.25mm in length. The fine-grained nature of these crystals compared to the phenocrysts in the rhyolite lava suggests that this is not simply a phenocryst clot. The crystals are comprised of roughly equal amounts of plagioclase feldspar and amphibole (hornblende), with very small amounts of Fe-Ti oxides and apatite, and are subhedral to euhedral in shape. The cluster is 8 mm in length and has an irregular boundary with the surrounding rhyolite.

The mineralogy and texture of this crystal cluster is similar to fine grained microdiorite fragments found in the Rotoiti Ignimbrite and small (< 2 mm) mafic fragments found within the Earthquake Flat Ignimbrite (Burt et al., 1998). Both of these fragment types contain hornblende as the dominant mafic phase. Chemically and isotopically these fragments are very similar to Taupo Volcanic Zone high alumina basalts and andesites and are therefore interpreted as their plutonic equivalents. The differing mineralogy (Taupo Volcanic Zone high alumina basalts and andesites contain pyroxene as the dominant mafic phase) is a consequence of crystallisation under high P_{H_2O} conditions ($P_{H_2O} \approx P_{Total}$) at relatively shallow levels in the crust (< 2 kbar pressure, < 6 km depth) (Burt et al., 1998).

Two equigranular crystal clusters were seen that exhibit intergrowth textures. The Waikorapa rhyolite (hk_1) contains a cluster of feldspar and quartz with apparent graphic, myrmekitic and perthitic intergrowths between quartz and alkali feldspar, quartz and plagioclase feldspar and two feldspar species respectively. Without electron microprobe analyses the species involved in the intergrowths cannot be positively determined. The cluster is 5 mm in length and has an irregular boundary with the surrounding rhyolite lava,

on which spherulites have nucleated. The cluster is medium-grained with subhedral to anhedral crystals. Rotomahana Dome (ho_3 - Tarawera) contains a cluster of crystals 2.5 mm in length comprising feldspar exhibiting apparent perthitic intergrowth textures. Small flakes of biotite (< 0.25 mm) occur in the centre of the cluster and appear to be intergrown with the plagioclase. Sparse Fe-Ti oxides, quartz and amphibole are also present. Plagioclase crystals around the edge of the cluster are subhedral. Plagioclase crystals in the interior of the cluster, along with biotite, Fe-Ti oxides, quartz and amphibole are generally anhedral.

Burt et al. (1998) document granitoid lithic fragments within the Rotoiti Ignimbrite that have a similar mineralogy and show similar intergrowth textures. Lowenstern et al. (1997) note that degassing of a shallow magma, perhaps due to eruption of a portion of the magma or migration towards the surface, forces undercooling of the magma. As a result, feldspar and quartz intergrowths may crystallise from the magma remaining in the intrusion.

Similar processes of formation to those suggested for microdiorite and granitoid lithic fragments in the ignimbrites can be invoked for the crystal clusters observed in the rhyolite lavas. In the absence of any chemical or isotopic data for the crystal clusters seen in the Waikorapa rhyolite and Rotomahana Dome, it is unknown whether they represent chilled portions of the same magma or whether they are true xenoliths. However, their rarity may suggest a xenolithic origin. The implications of the nature and composition of lithic fragments in ignimbrites for the evolution of the Okataina Volcanic Centre will be discussed further in Chapter Seven.

3.12 FERROMAGNESIAN ASSEMBLAGES OF ASSOCIATED PYROCLASTIC ERUPTIVES

The ferromagnesian assemblages of the pyroclastics erupted in association with rhyolite lavas (ho_3) during the post-caldera eruptive sequence at the Okataina Volcanic Centre have already been discussed for each eruptive episode (sections 3.6 - 3.8). Pyroclastics erupted earlier in caldera-forming and caldera-modifying eruptions at Okataina have similar ferromagnesian assemblages to the ho_1 and ho_2 rhyolite lavas.

The Quartz-Biotite Ignimbrite (tuffs) contains abundant biotite in addition to hornblende and orthopyroxene (Nairn, 1981a), which is a similar assemblage to the ho_1 southern Wairua rhyolite. Pumice clasts in the Matahina Ignimbrite contain orthopyroxene and, towards the

top of the unit, hornblende (Carr, 1984). This assemblage is similar to some of the northeastern and western ho_1 rhyolites. Bailey and Carr (1994) also note the occurrence of rare clinopyroxene in the Matahina Ignimbrite. Studies of the Onuku-Pokopoko pyroclastics (Nairn, 1989; Crosby, 1998) have shown them to have a similar assemblage of orthopyroxene ± calcic amphibole. The Kawerau Ignimbrite also has a similar assemblage with pumice clasts containing hornblende + orthopyroxene, with less than 1% of the clasts erupted being of dacitic composition and also containing augite (Beresford and Cole, 2000).

Schmitz (1995) observed cummingtonite to be the dominant ferromagnesian mineral in the Rotoiti Ignimbrite, which also contains smaller amounts of orthopyroxene and calcic amphibole, and biotite in upper units. The ho_1 North Rotoma rhyolite has a ferromagnesian assemblage similar to the Rotoiti Ignimbrite. This may be coincidence or perhaps the North Rotoma rhyolite, located on the northern edge of the Rotoma caldera that is attributed to the Rotoiti Ignimbrite eruption, is genetically related to this ignimbrite.

Smith (2001) discusses ferromagnesian assemblages for the Mangaone Pyroclastics Subgroup tephras. All tephras contain orthopyroxene. Calcic amphibole dominates the ferromagnesian mineralogy of Unit A and Unit B and is abundant in Units G - L. It is found in lesser proportions in the Pupuwharau and Pongakawa tephras and Unit E, and is scarce in Unit D and Unit F. Clinopyroxene is found in the Pupuwharau and Pongakawa tephras, Units D - F and occasionally in Unit A and Unit B. Biotite is very rare and was observed in trace amounts in Unit E. A mineralogical feature of the Mangaone Pyroclastics Subgroup is the occurrence of clinopyroxene only in the older units (Units A - F). These ferromagnesian assemblages for the Mangaone Pyroclastics are similar to some of the younger ho_3 rhyolites comprising the Haroharo Volcanic Complex. However, the Mangaone Pyroclastics do not contain cummingtonite, which dominates Haroharo Volcanic Complex assemblages, and the rhyolite lavas lack clinopyroxene.

None of the previously mentioned pyroclastic eruptives are known to have a source in the southwestern Okataina Volcanic Centre and for this reason, despite possible mineralogical similarities, it is considered unlikely that they are genetically related to the ho_2 rhyolite lavas in this area. Bellamy (1991) used mineralogical similarities between the Te Wairoa Ignimbrites, outcropping in this area, and the non-biotite bearing ho_2 Moerangi rhyolites to suggest a genetic relationship. The biotite-bearing ho_2 rhyolites have similar ferromagnesian assemblages to the Earthquake Flat Ignimbrite (Nairn, 1981a; Froggatt and Lowe, 1990), erupted in an area adjacent to the southwestern Okataina Volcanic Centre that is considered

to be part of the Kapenga Volcanic Centre. This is one of the lines of evidence for associating these rhyolite lavas with the Kapenga Volcanic Centre. The hk_2 rhyolite lavas also have ferromagnesian assemblages similar to the Earthquake Flat Ignimbrite.

The caldera-forming ignimbrites erupted from the Kapenga Volcanic Centre generally have ferromagnesian assemblages dominated by orthopyroxene. In addition, the Tikorangi and Waiotapu Ignimbrites contain clinopyroxene (augite) and rare hornblende (Bowyer, 1997; Ritchie, 1996; Lynch-Blosse, 1998; Hildyard et al.,2000), the Pokai Ignimbrite contains augite (Lynch-Blosse, 1998) and the Waihou Ignimbrite contains small amounts of augite and hornblende (Lynch-Blosse, 1998). Langridge (1990) noted that the Ohakuri Ignimbrite contains orthopyroxene and calcic amphibole, and that biotite is an important mineral in upper parts. Murphy and Seward (1981) and Spinks (1998) note that the abundance of hornblende is a characteristic feature of the Rahopaka Ignimbrite. These assemblages are consistent with the hk_1 rhyolites which have assemblages dominated by orthopyroxene and calcic amphibole.

Lynch-Blosse (1998) observed that orthopyroxene is the dominant ferromagnesian mineral in the Waimakariri Ignimbrite and that biotite occurs in trace amounts. This assemblage is comparable to the hr_1 Endean Road rhyolite. Milner (2001) observed that orthopyroxene is the dominant ferromagnesian mineral in the Mamaku Ignimbrite and that clinopyroxene (augite) and calcic amphibole occur in generally trace amounts. This is comparable to the hr_2 rhyolite lavas. In addition, the low phenocryst contents of Mamaku Ignimbrite pumice clasts (4 - 7 %) are comparable to low phenocryst contents in the hr_2 rhyolite lavas. No pyroclastic eruptives have been identified from the Rotorua Volcanic Centre that match the biotite dominant ferromagnesian assemblage of the hr_3 Hinemoa Point and Vaughan Road domes. Dravitzki (1999) used mineralogical similarities between the Paradise Valley Ignimbrites and the hr_2 rhyolites to suggest a genetic relationship.

Chapter Four: Geochemistry

Chapter Four: Geochemistry

4.1 INTRODUCTION

A study of the major and trace element compositions of rhyolite lavas can provide important information for identifying magma batches, assessing magma source characteristics, and determining evolutionary paths. This chapter examines the geochemistry of rhyolite lavas from the Okataina, Rotorua and Kapenga volcanic centres, and attempts to distinguish lavas both within and between volcanic centres, and to place them into spatial and temporal groups.

Major and trace element X-ray Fluorescence (XRF) analyses were obtained for 113 rhyolite lava samples from the Okataina, Rotorua and Kapenga volcanic centres (Appendix V, Table V.1). These analyses have been used to classify the lavas as dominantly peraluminous, medium-K calc-alkaline rhyolites and have formed the basis of a division of the lavas into possible magma batches. In addition, 43 of these samples, representative of different rhyolite groups identified by age, ferromagnesian phenocryst assemblages and whole rock geochemistry (XRF), were analysed by Laser Ablation, Inductively Coupled Plasma Mass Spectrometry (LA-ICPMS) for trace and rare earth elements (Appendix V, Table V.1).

Geochemical data available in the literature for the caldera-forming ignimbrites and pyroclastics erupted in association with the lavas have also been used and compared with data obtained in this study.

4.2 SUMMARY OF RHYOLITE LAVA GEOCHEMISTRY

This chapter presents new geochemical data for the rhyolite lavas erupted from the Okataina, Rotorua and Kapenga volcanic centres. Representative samples were analysed for whole rock major and trace elements by XRF (113 samples), and trace and rare earth elements by LA-ICPMS (43 samples).

4.2.1 Geochemical Characteristics

SiO_2 contents for the majority of rhyolite lavas sampled from the Okataina, Rotorua and Kapenga volcanic centres range from ≈ 73 - 78 wt. %, and the lavas are classified as medium-K calc-alkaline rhyolites (Figure 4.5). On the basis of Shand's index the lavas are predominantly peraluminous (Figure 4.5).

Chondrite-normalised multi-element patterns (Figure 4.1) show enrichment in large-ion lithophile elements (eg. Ba, Rb, Th and K) relative to the high-field-strength elements (eg. Sm, Zr and Hf) and depletion in Nb, P and Ti. These features are typical of arc-related magmas (Pearce, 1983; Wilson, 1989; Pearce and Peate, 1995). The patterns may be controlled at least in part by fractionation of minerals seen in the phenocryst and accessory assemblage of these lavas, and modeling of possible crystal fractionation and other magmatic processes is discussed in Chapter Six. Rhyolite lavas from the Okataina, Rotorua and Kapenga volcanic centres overlap in their trace element abundances and chondrite-normalised multi-element patterns.

Chondrite-normalised REE abundance patterns (Figure 4.1) are typical of TVZ silicic eruptives observed in other studies (e.g. Reid, 1983; Briggs et al., 1993; Brown, 1994; Beresford, 1997; Wright, 2000), characterised by a strongly enriched light REE pattern with steep slopes (La_N/Sm_N = 2.82 - 5.43), a pronounced negative Eu anomaly (Eu_N/Eu_N^* = 0.43 - 0.86), and flat heavy REE pattern (Gd_N/Yb_N = 0.99 - 1.34). Generally the most REE depleted lavas have the smallest negative Eu anomalies. Overall, there is no systematic correlation between Eu anomaly and SiO_2. However, increasing Eu anomalies are accompanied by increasing Rb/Sr. The negative Eu anomaly is generally attributed to fractionation of plagioclase feldspar. It is unlikely that the fractionation of calcic amphibole and orthopyroxene alone could produce the strong enrichment in light REE relative to heavy REE, and hence this is largely attributed to fractionation of the accessory phases zircon and apatite. REE abundances and chondrite-normalised patterns for Okataina, Rotorua and Kapenga lavas overlap (Figure 4.1).

4.2.2 Okataina Volcanic Centre

Rhyolite lavas erupted over time at the Okataina Volcanic Centre (ho_1, ho_2, ho_3) have similar major, trace and rare earth element compositions. There are no systematic changes in

composition over time that would suggest the lavas have tapped a single, magma body evolving in the crust. Analysing the data for each age group and volcanic complex separately has facilitated characterisation of individual magma types. A number of elements and element ratios have been plotted, but it was found that Rb and Zr are the most suitable elements for characterising the magma types, and they are therefore used in this summary. Rb is one of the most incompatible elements, and Zr is compatible, in these zircon-bearing rhyolite lavas. Characterisation of magma types using these elements allows use of the larger XRF data set.

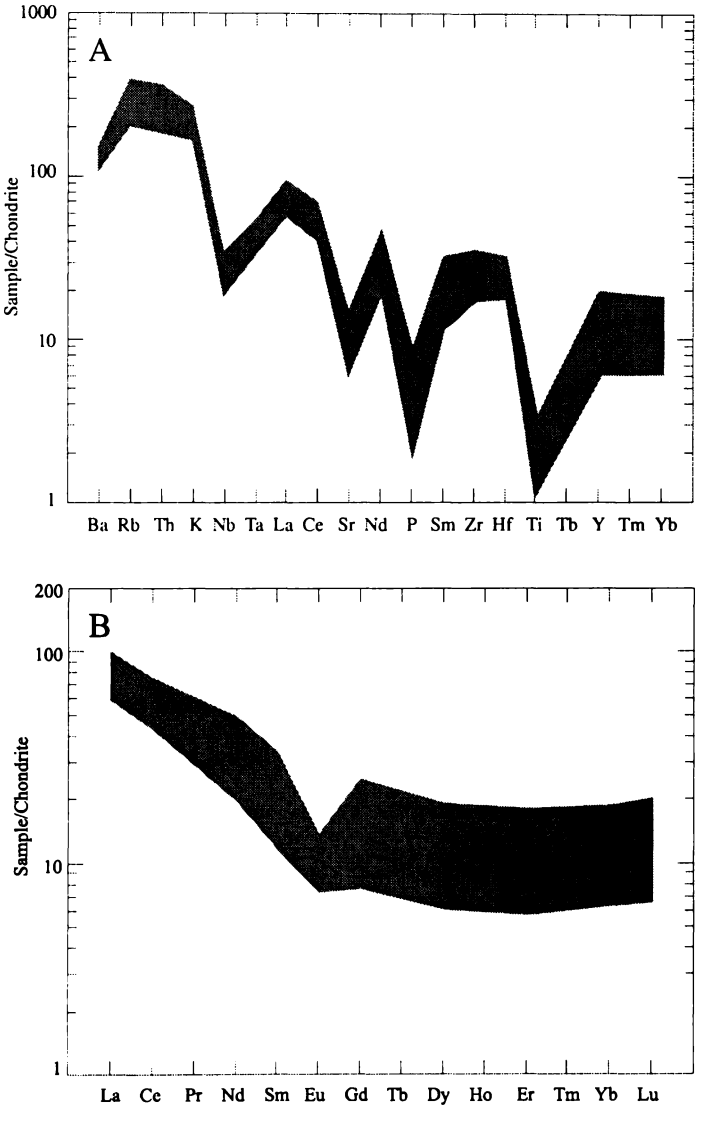

Figure 4.1: Range in chondrite-normalised a) multi-element (spider) patterns (normalisation values from Thompson et al., 1984), and b) REE abundance patterns (normalisation values from Boynton, 1984) for the Okataina, Rotorua and Kapenga rhyolite lavas.

4.2.2.1 The ho_1 rhyolite lavas

There are no distinct groupings in major or trace element compositions for the ho_1 rhyolite lavas that coincide with either spatial position or ferromagnesian phenocryst assemblage (Figures 4.2, 4.6 and 4.7). Hence geochemistry cannot be used as a means to identify magma types for the lavas of this age group. Some of the orthopyroxene and calcic-amphibole bearing ho_1 lavas have major and trace element compositions similar to pumice clasts from the Matahina Ignimbrite (Carr, 1984; Figures 4.6 and 4.7). This group of samples shows a reduction in Zr and an increase in Rb with increasing SiO_2, trends that are typical of fractional crystallisation processes involving the phenocryst and accessory phases in these lavas. Hence, on the basis of available major and trace element contents, these lavas and the Matahina Ignimbrite may record the evolution of a single magma body beneath the OVC during this time period.

4.2.2.2 The ho_2 rhyolite lavas

The ho_2 lavas fall into two geochemical groups that coincide with ferromagnesian phenocryst assemblages (Figures 4.2, 4.9 and 4.10). The biotite-bearing lavas have lower Zr than the biotite-free/poor lavas. Within each of the two groups a reduction in Zr and an increase in Rb accompany increasing SiO_2, trends typical of fractional crystallisation processes involving the phenocryst and accessory phases in these lavas. REE abundance patterns for the two groups are distinct (Figure 4.11), with biotite-bearing lavas having lower REE abundances. However, there is a lack of consistent trends in REE compositions, or SiO_2 content, between the two groups. These geochemical characteristics provide support for the existence of two separate magma types, initially suggested by ferromagnesian phenocryst assemblages. The biotite-bearing lavas have comparable major and trace element compositions to the Earthquake Flat Ignimbrite (Davis, 1985; Figures 4.9 and 4.10) and hk_2 rhyolite lavas (Figure 4.31). The biotite-free/poor lavas have comparable major and trace element compositions to the Te Wairoa Ignimbrites (Bellamy, 1991; Figures 4.9 and 4.10). Although the Rotoiti Ignimbrite was also erupted at this time it is geochemically distinct (particularly in terms of incompatible elements) from the ho_2 rhyolite lavas (Schmitz, 1995; Figures 4.9 and 4.10). Hence the ho_2 and hk_2 lavas, and geochemically associated pyroclastics, may record the evolution of two spatially adjacent magma bodies beneath the southwestern OVC - northeastern KVC during this time period.

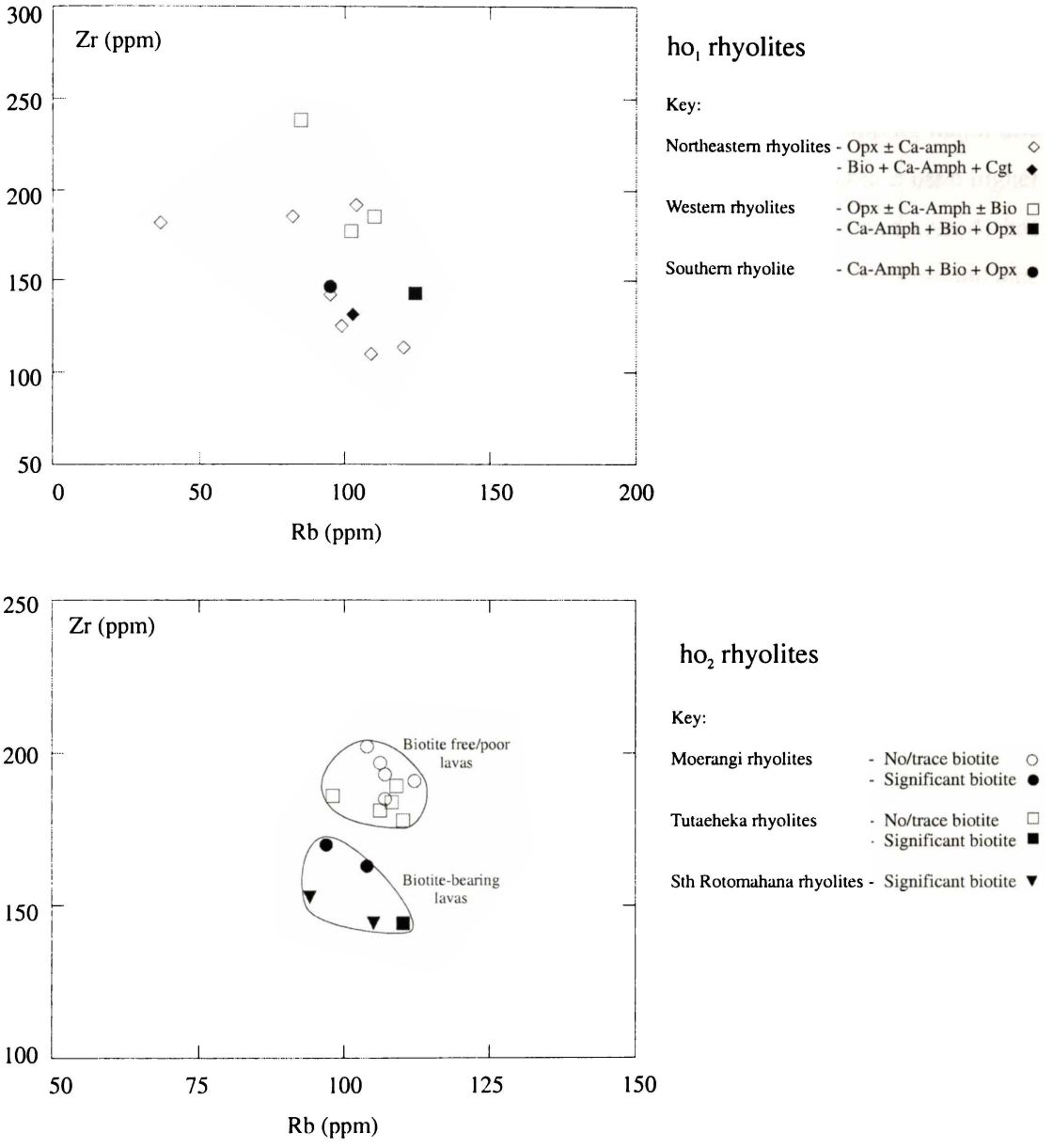

Figure 4.2: Rb vs. Zr plots for ho_1 and ho_2 rhyolite lavas from the Okataina Volcanic Centre.

4.2.2.3 Haroharo Volcanic Complex ho_3 rhyolite lavas

There are no systematic trends in major and trace element compositions over time in the Haroharo Volcanic Complex rhyolite lavas. Within the lavas erupted in each episode, geochemical groups can be identified which correspond with vent position (Figures 4.3, 4.12 and 4.13). The lavas erupted in the Te Rere episode (from a single vent) have very similar

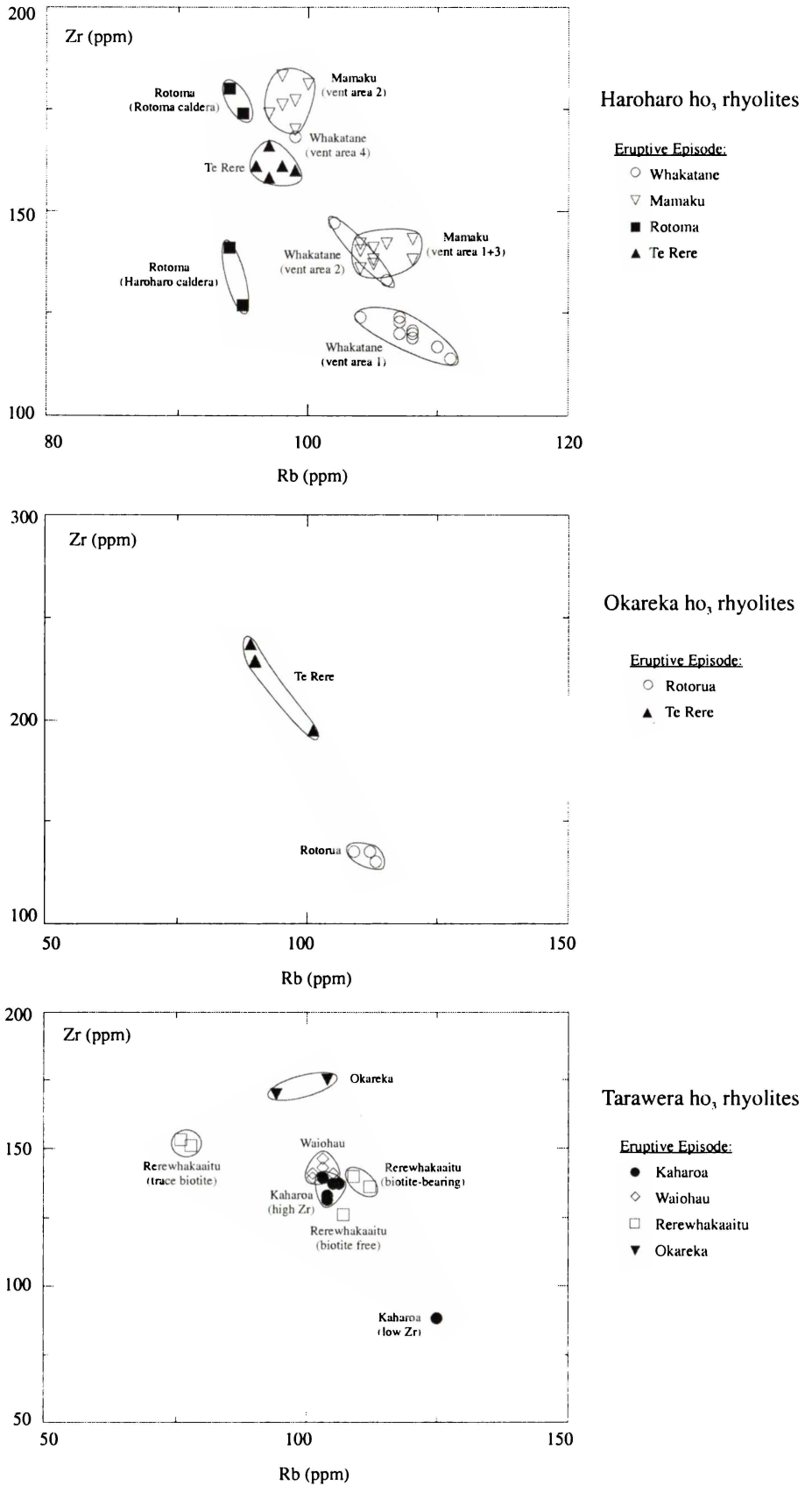

Figure 4.3: Rb vs. Zr plots for Haroharo, Okareka and Tarawera volcanic complex rhyolite lavas from the Okataina Volcanic Centre.

compositions in terms of all major and trace elements. During the Rotoma episode, lavas erupted in the Rotoma caldera have higher Zr than lavas erupted in the northern Haroharo caldera. During the Mamaku episode the Waiti Lava Flow (vent area 2) has lower Rb and higher Zr than the lavas erupted from vent areas 1 and 3, which have overlapping major and trace element compositions. Whakatane episode lavas erupted from vent area 2 have higher Zr than the group of lavas erupted from vent area 1. Tikorangi Dome (vent area 4) has higher Zr and lower Rb than all other lavas erupted during this episode. REE abundance patterns for Haroharo lavas are very similar and no distinction can be made between the Rotoma, Mamaku and Whakatane episodes (Figure 4.14). One lava erupted in the Te Rere episode has a slightly enriched REE pattern. While there are no systematic trends in lava compositions over time for the Haroharo Volcanic Complex as a whole, lavas erupted from vent areas 1+3 and 2 during the Mamaku and Whakatane eruptive episodes show compositional changes typical of fractional crystallisation of the observed phenocryst and accessory phases. A comparison of the geochemical data available in the literature (Wright, 2000) shows lavas and pyroclastics erupted in each of the Rotoma and Mamaku episodes have comparable major and trace element compositions.

4.2.2.4 Okareka Volcanic Complex ho_3 rhyolite lavas

At the Okareka Volcanic Complex, lavas erupted during the Rotorua episode have very similar major and trace element compositions (Figures 4.18 and 4.19). They have high Rb and low Zr compared to Te Rere episode lavas (Figure 4.3). Such compositional changes in addition to differences in REE abundance patterns (Figure 4.20) suggest that the Rotorua and Te Rere episode lavas may be genetically related by fractional crystallisation of the observed phenocryst and accessory phases.

4.2.2.5 Tarawera Volcanic Complex ho_3 rhyolite lavas

There are no systematic trends in major and trace element compositions over time in the Tarawera Volcanic Complex rhyolite lavas (Figures 4.3, 4.21 and 4.22). Lavas erupted during the Okareka episode differ in many of their major and trace element compositions, particularly SiO_2, but have similar Rb and Zr contents (Figure 4.3). During the Rerewhakaaitu episode three groups of lavas were erupted that correspond with ferromagnesian phenocryst assemblages. A low Rb, high Zr group comprises samples of Western Dome, which contains only trace biotite. A high Rb, intermediate Zr group

comprises samples of Rotomahana Dome and the Te Puha Flow, which contain significant amounts of biotite. A biotite-free, phenocryst poor sample from the Te Puha Flow comprises the third group with the lowest Zr content. These two latter groups are consistent with previous studies that have observed an intimate mingling between two lava types in the Rerewhakaaitu eruptives (Cole, 1966; 1970a). Rhyolite lavas erupted during the Waiohau episode cluster together with very similar compositions for all major and trace elements. Rhyolite lavas erupted during the Kaharoa episode generally cluster together with very similar compositions for all major and trace elements. The exception is a sample taken from Green Lake Plug, which has high Rb and low Zr. REE abundance patterns for Tarawera lavas are very similar and are neither distinct for particular eruptive episodes nor biotite-bearing and biotite-poor/free lavas (Figure 4.23). Geochemical differences between eruptive episodes, in association with mineralogical differences, suggest that eruptions at Tarawera may have tapped a number of discrete magma types. A comparison of the geochemical data available in the literature (Leonard, 1999; Speed, 2001) shows lavas and pyroclastics erupted in each of the Waiohau and Kaharoa episodes have comparable major and trace element compositions.

4.2.3 Rotorua Volcanic Centre

There are no systematic trends in major and trace element compositions over time in the Rotorua Volcanic Centre rhyolite lavas that would suggest the lavas have tapped a single, magma body evolving in the crust (Figures 4.4, 4.27 and 4.28). Instead, the lavas appear to have tapped several individual magma types, which can be characterised by their major and trace element compositions, and are summarised here using Rb and Zr abundances.

4.2.3.1 The hr_1 rhyolite lavas

The hr_1 rhyolites have a wide range in composition (Figures 4.4, 4.27 and 4.28). Samples from the Tokorangi and Hemo Gorge lavas on the southern rim of the RVC have lower Zr than the Endean Road and Hamurana rhyolites, and are geochemically similar to hk_1 lavas erupted from the Kapenga Volcanic Centre (Figure 4.4). Comparable major and trace element compositions for some of the hr_1 lavas and the Waimakariri Ignimbrite (Lynch-Blosse, 1998; Figures 4.27 and 4.28) may suggest the lavas represent the eruption of

degassed magma following the ignimbrite eruption, and support a Rotorua source for the Waimakariri Ignimbrite.

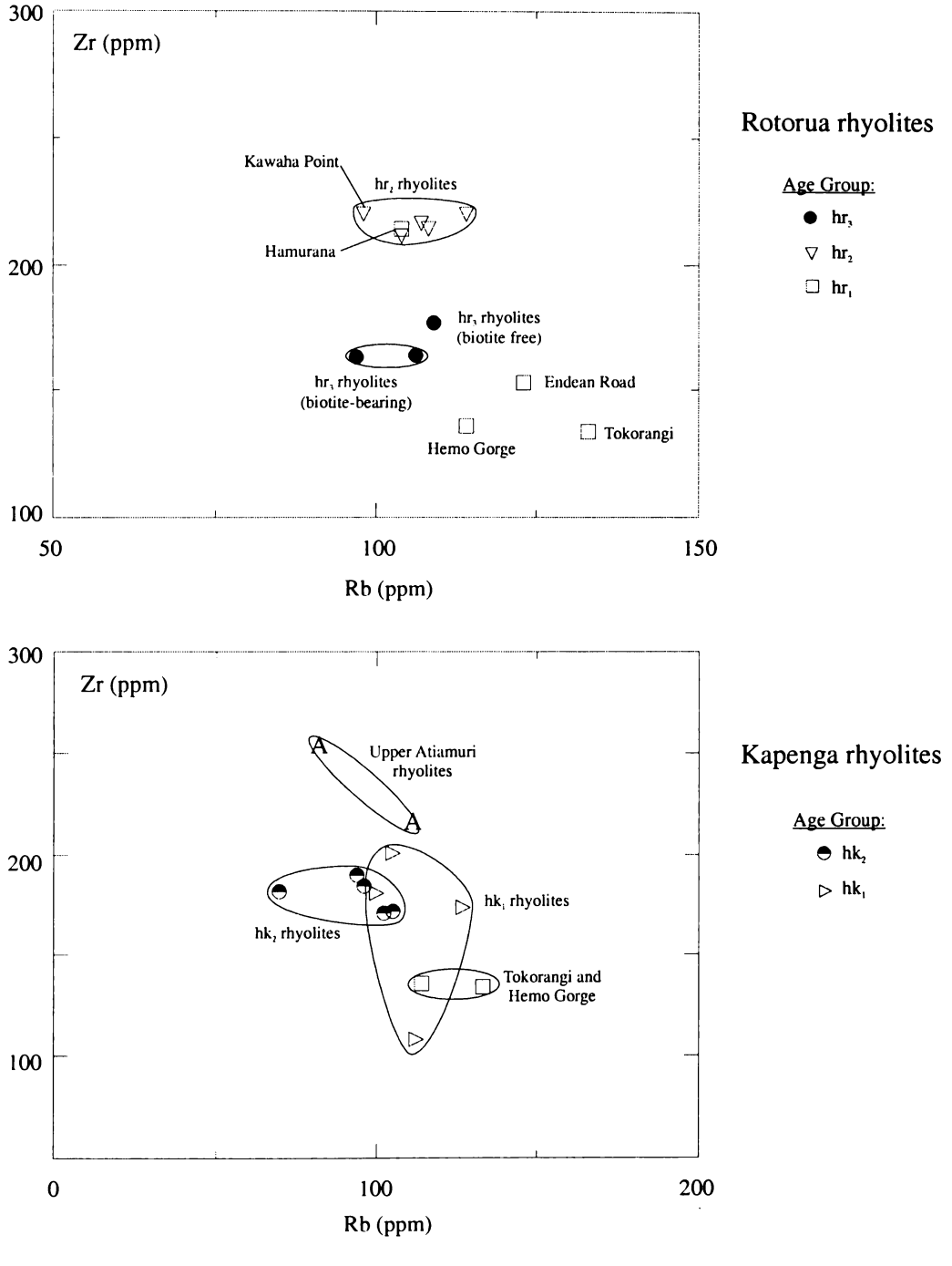

Figure 4.4: Rb vs. Zr plots for rhyolite lavas from the Rotorua and Kapenga volcanic centres.

4.2.3.2 *The hr_2 rhyolite lavas*

The hr_2 rhyolites have very similar major and trace element compositions (Figures 4.4, 4.27 and 4.28). The rhyolite dome at Kawaha Point has a composition indistinguishable from the Ngongotaha-Pukehangi lavas. This lends support to the theory that these rhyolites are all part of an extensive, partially buried rhyolite volcano complex. Geochemical similarities between the hr_2 rhyolite lavas and the Mamaku Ignimbrite (Milner, 2001; Figure 4.30), in association with mineralogical similarities, support a genetic relationship.

4.2.3.3 *The hr_3 rhyolite lavas*

The hr_3 rhyolites fall into two geochemical groups that coincide with ferromagnesian phenocryst assemblages (Figures 4.4, 4.27 and 4.28). The biotite-bearing lavas have lower Zr and Rb contents than the biotite-free lava, suggesting two magma types may have been tapped during these most recent eruptions from the RVC.

4.2.4 Kapenga Volcanic Centre

The two groups of rhyolite lavas erupted from the Kapenga Volcanic Centre (hk_1, hk_2) differ in their major and trace element compositions (Figures 4.4, 4.31 and 4.32) and there is no geochemical evidence to suggest a genetic relationship between these two groups of lavas.

4.2.4.1 *The hk_1 rhyolite lavas*

There are no distinct groupings in major or trace element compositions for the hk_1 rhyolite lavas that coincide with spatial position (Figures 4.4, 4.31 and 4.32). Geochemical similarities to the Tokorangi and Hemo Gorge rhyolites, previously classed as hr_1, may suggest a genetic relationship. The Upper Atiamuri rhyolites, which lie on or just beyond the southwestern edge of the Kapenga Volcanic Centre, have compositions with notably higher Zr than the hk_1 rhyolites. The hk_1, Tokorangi and Hemo Gorge rhyolites show geochemical similarities to the Pokai Ignimbrite (Karhunen, 1993; Lynch-Blosse, 1998; Figure 4.34).

4.2.4.2 *The hk_2 rhyolite lavas*

The hk_2 lavas have similar major and trace element compositions to the biotite-bearing ho_2 rhyolites erupted in the southwestern OVC and the EQF Ignimbrite (Davis, 1985; Figure 4.34), suggesting a genetic relationship.

Hence, geochemical data for rhyolite lavas erupted from the Okataina, Rotorua and Kapenga volcanic centres show no clear trends over time and do not suggest that each of these centres has tapped a large progressively evolving magma body. Instead the data suggest that eruptions from each of these centres have tapped a number of smaller, discrete magma types. In some cases, spatially and/or temporally associated magma types may have similar geochemical characteristics, but differ in their ferromagnesian phenocryst assemblages. This may be due to differences in the intensive parameters of the magmas (eg. temperature, pressure, oxygen fugacity, water content), which are discussed further in Chapter Five. Geochemical variations between spatially and/or temporally associated magma types will be discussed further and modeled in Chapter Six.

4.3 ANALYTICAL TECHNIQUES

Major and trace element concentrations were determined at the University of Canterbury by X-ray Fluorescence spectrometry (XRF), using a Philips PW 2400 automatic X-ray Fluorescence Spectrometer. Lithium tetraborate glass fusion beads (major element analysis) and pressed powder pellets (trace element analysis) were prepared following the general methods of Norrish and Hutton (1969). Volatile loss on ignition (LOI) was determined by weight loss after fusing at 1000°C for 20 minutes. Estimates of analytical uncertainty for major and trace elements determined by this machine are published in Weaver et al. (1990), and are generally < 1% for major elements and < 5% for trace elements.

Trace and rare earth element concentrations were determined by Laser Ablation-Inductively Coupled Plasma Mass Spectrometry (LA-ICPMS) at the Research School of Earth Sciences, Australian National University, Canberra. Samples were prepared as Li-borate glasses following standard procedures for fusion discs employed for XRF analyses. A pre-ignited (dehydrated) 12:22 mixture of Li-tetraborate and Li-metaborate (Sigma Chemicals) was used as a flux, in a 3:1 mixture with powdered sample. Analyses were preformed on a

polished, scratch-free surface cut through the disc (cross section). The ArF (193nm) EXCIMER laser sampling system and ICPMS instrumentation (Agilent 7500s) have been described by Eggins et al. (1998a; 1998b). All standards and unknowns were analysed using a scanning procedure (scanning across the glass with a 100μm circular spot, at a laser pulse repetition rate of 10 pulses/second, for a period of 120 seconds) which, when combined with optimal laser power, produces precisely controlled ablation and delivers exceptionally stable analyte signals to the ICPMS. Down-ablation pit element fractionation and the transient variations in signal intensities associated with conventional laser ablation analysis are circumvented. NIST 612 glass was used for external calibration of the instrument. BCR2g glass was used as a secondary reference standard. ^{44}Ca was employed as the internal standard, based on CaO concentrations previously measured by XRF for the samples. Data reduction was performed following the methods outlined by Longerich et al. (1996). Eggins et al. (1998b) note that the limits of detection are typically in the range 0.2 - 2 ppb for most high-mass elements (>80 amu) and 1 - 100 ppb for lower mass elements. Kamenetsky et al. (2000) note an analytical precision in the range 1 - 5% for most elements.

For samples analysed by both XRF and LA-ICPMS methods, some of the trace element analyses have been duplicated. In this study it was decided to use Rb, Ba, Zr and Sr concentrations obtained from XRF analyses and all other trace elements and REE from LA-ICPMS analyses. The analytical precision for Rb, Ba, Zr and Sr analyses by XRF is good and hence the larger data set (113 samples) can be utilised. The remaining trace elements and REE are more accurately determined by LA-ICPMS and in many cases the detection limits are lower. Hence the smaller LA-ICPMS data set (43 samples) will be used for these elements. Analyses for the major elements have been normalised to 100%, volatile free (Appendix V, Table V.1). All further discussions of major element compositions, including values plotted on variation diagrams, will involve these normalised values.

4.4 RHYOLITE CLASSIFICATION

One of the most useful classification schemes for fresh, unweathered, unaltered, non-metamorphosed volcanic rocks is the total alkalis ($Na_2O + K_2O$) versus silica (SiO_2) or TAS diagram of Le Bas et al. (1986). Figure 4.5a shows the TAS diagram for lavas from the Okataina, Rotorua and Kapenga volcanic centres. As expected, these lavas plot in the rhyolite field. SiO_2 contents range from ~ 72.5 - 79.5 wt. % and total alkali contents range

from ~ 5.7 - 8.0 wt. %. The K_2O versus SiO_2 diagram of Le Maitre (1989) and Rickwood (1989) classifies the lavas as medium-K calc-alkaline rhyolites (Figure 4.5b) with K_2O contents ranging from ~ 2.0 - 3.8 wt. %. On the basis of Shand's index (Maniar and Piccoli, 1989) the lavas are predominantly peraluminous (Figure 4.5c). On all classification diagrams the compositions for lavas from the Okataina, Rotorua and Kapenga volcanic centres overlap. Several samples show some scatter away from the main group, and this is likely to be a result of post-depositional alteration processes such as weathering, devitrification or hydrothermal alteration. A sample from the Kaipara Flow, Haroharo Volcanic Complex (sample no. 145, indicated on Figure 4.5a), showed evidence in thin section of hydrothermal alteration and has been omitted from further diagrams and discussions of rhyolite geochemistry.

4.5 OKATAINA VOLCANIC CENTRE

The preparation of preliminary variation diagrams to display the geochemistry of rhyolite lavas from the Okataina Volcanic Centre showed that lavas of the three age groups (ho_1, ho_2, ho_3) overlap in their major and trace element compositions. Within the ho_3 rhyolites, lavas from the Haroharo, Tarawera and Okareka volcanic complexes overlap in major and trace element compositions. Hence geochemistry cannot be used to distinguish between rhyolite lavas of these three age groups, or the ho_3 volcanic complexes, and there are no coherent trends over time in major and trace element compositions. In addition, several groupings were identified within the ho_2 and ho_3 rhyolites that required further investigation. Therefore, the geochemistry of rhyolite lavas from the Okataina Volcanic Centre will be discussed for each age group, and for the ho_3 rhyolites for each volcanic complex, individually. This will facilitate characterisation of magma batches erupted in each time period and possible processes operating within these magma batches.

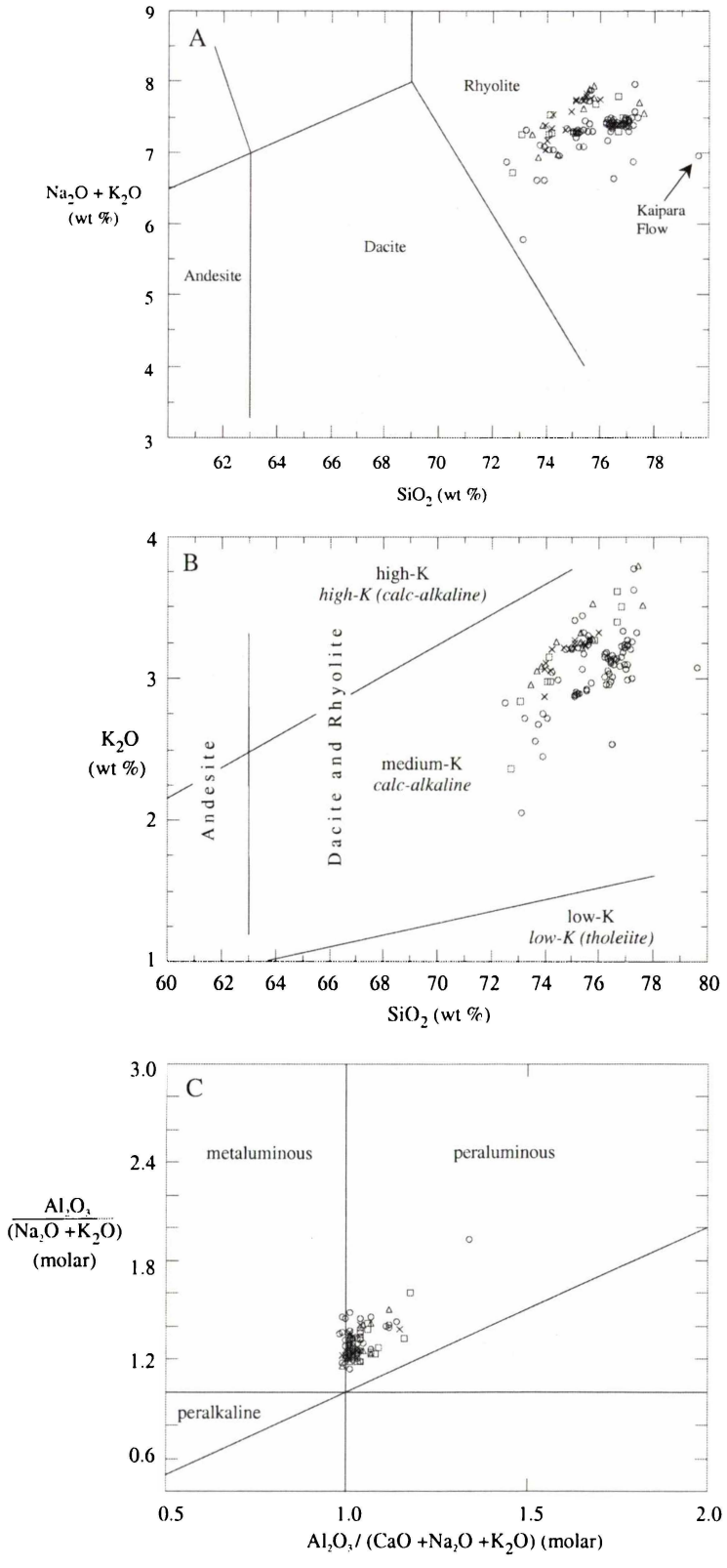

Figure 4.5: a) Classification of lavas from the Okataina, Rotorua and Kapenga volcanic centres (open circles, triangles and squares respectively) according to the total alkalis versus silica (TAS) diagram of Le Bas et al. (1986). Crosses indicate the ho_2 rhyolites occurring in the transition zone between the Okataina and Kapenga volcanic centres. b) Subdivision of the subalkalic rhyolite lavas following Le Maitre (1989) (plain font) and Rickwood (1989) (italics). c) Classification using Shand's Index following Maniar and Piccoli (1989).

4.5.1 The ho_1 Rhyolites

Major and trace element compositions for the ho_1 rhyolites are shown in Figures 4.6 and 4.7 respectively. These rhyolites have been divided into five groups based on spatial position and ferromagnesian phenocryst assemblage (see section 2.2.2.2 and Figure 3.6) and have SiO_2 compositions ranging from ~ 73.1 - 77.2 wt. %. There are no distinct groupings in major or trace element compositions that coincide with either spatial position or ferromagnesian phenocryst assemblage.

Two samples have anomalous high Al_2O_3 contents and this may be attributed to weathering/alteration and the formation of secondary minerals, although this was not evident in thin section. Anomalous geochemical compositions for rhyolite lavas (or scatter seen on variation diagrams) may also be attributed to vapour-phase alteration and/or crystallisation/devitrification of the lava during cooling. Samples of the ho_1 rhyolites obtained were either completely or partially crystallised and spherulitic (discussed in Chapter Three). Lipman (1965), Lofgren (1970) and Weaver et al. (1990) have investigated the effects of devitrification on bulk rock chemistry. Lipman (1965) and Lofgren (1970) noted that, in terms of the major elements, SiO_2, Na_2O, K_2O and Al_2O_3 are particularly affected. From a study of peralkaline silicic lavas Weaver et al. (1990) compared crystalline and glassy samples from the same lava flow. Crystalline samples were found to have suffered a loss in Na_2O, F, Cl, Cs, Y and REE and a gain in Al_2O_3, MgO, and Sr. Changes in bulk rock chemistry may also result from silicic glass hydration as Noble (1967) observed that hydrated glasses have lower Na/K and silica contents.

Where multiple samples have been obtained from the same rhyolite lava, and include glassy and crystallised/devitrified textures, a comparison of compositions can be made. A similar calculation procedure was followed to that used in Weaver et al. (1990) where the compositional differences are expressed as numbers of standard deviations. The standard deviations given in Weaver et al. (1990) are referred to throughout the literature as being indicative of analytical precision for the XRF spectrometer at the University of Canterbury. The results of these calculations are given in Appendix V, Table V.3. The compositional differences seen in the lavas of this study are not as great as those observed by Weaver et al. (1990). This may in part be due to the dominantly peraluminous nature of these lavas, although it is more likely to be due to a smaller degree of crystallisation/devitrification in these samples than those studied by Weaver et al. (1990).

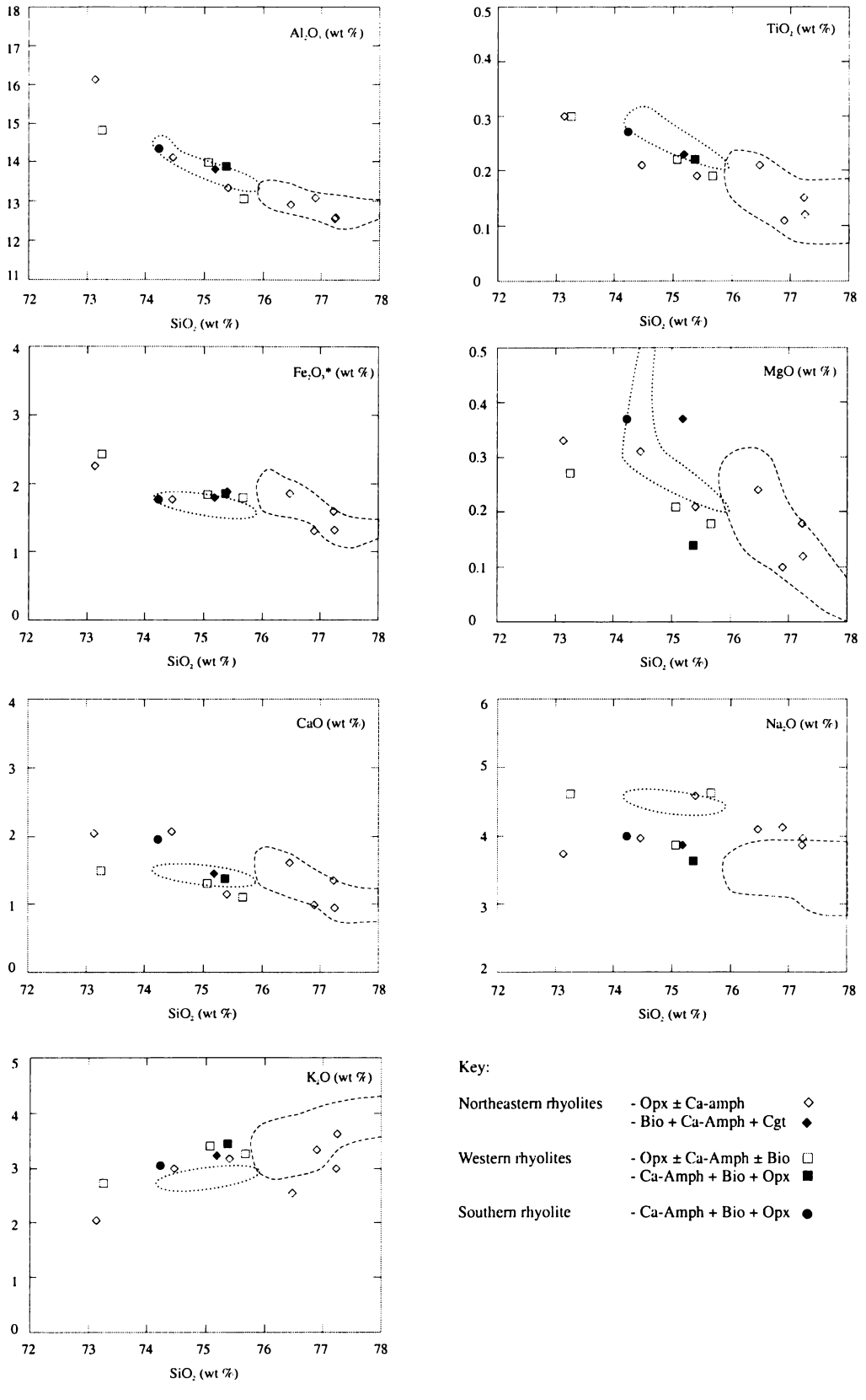

Figure 4.6: Selected major element variation diagrams for the ho_1 rhyolite lavas from the Okataina Volcanic Centre. Compositions for the Matahina Ignimbrite from Carr (1984) are enclosed by the dashed line. Rhyolitic compositions for the Kawerau Ignimbrite from Beresford (1997) are enclosed by the dotted line.

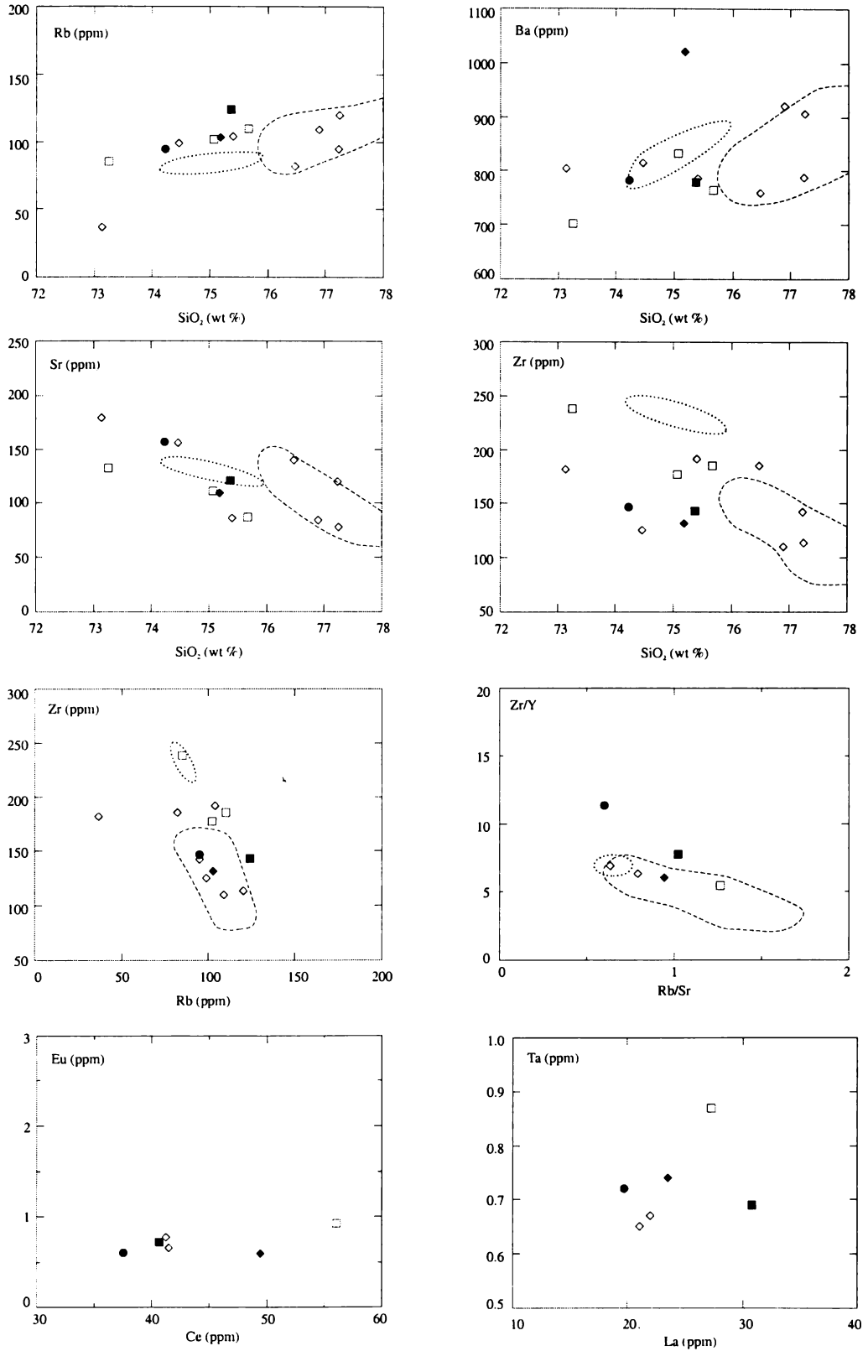

Figure 4.7: Selected trace element variation diagrams for the ho_1 rhyolite lavas from the Okataina Volcanic Centre. Symbols as in Figure 4.6. Compositions for the Matahina Ignimbrite from Carr (1984) are enclosed by the dashed line. Rhyolitic compositions for the Kawerau Ignimbrite from Beresford (1997) are enclosed by the dotted line.

In this study crystallised/devitrified portions of the rhyolite lavas were avoided where at all possible during sample collection. In terms of the ho_1 lavas, glassy equivalents of the crystallised samples obtained were not available and hence comparisons could not be made. With the exception of a sample from Tutaeheka 3 (117) none of the lavas used in these calculations can be classed as completely crystalline. Many contain only singular spherulites or coalesced spherulites with interstitial areas remaining undevitrified. Hence the compositional differences between glassy lavas and these partially crystallised lavas will be much less obvious. From Table V.3 it would seem that whether an element is enriched or depleted in these partially crystallised lavas is very much lava dependent and in many cases the documented gains or losses equate to less than the standard deviation. Such small variations may be due to minor compositional variations within the lava or analytical error, and not devitrification of the glassy groundmass. Notably, some of the largest differences are seen in the Tutaeheka 3 lava. Hence, scatter on variation diagrams for lavas that show some degree of crystallisation/devitrification (e.g. the ho_1 rhyolites) may be attributed to variable gains and losses in major and trace elements due to the devitrification process.

It is thought that the biotite-bearing southern rhyolite (Wairua) and the biotite and cummingtonite-bearing northeastern rhyolite (North Rotoma) are representative of two magma compositions which are separate from that which erupted as the orthopyroxene and calcic amphibole-bearing lavas (sometimes with small amounts of biotite) of this age group. This division is based entirely on ferromagnesian phenocryst assemblages as no distinctions can be made between these three groups geochemically. This distinction is somewhat hindered by the lack of data for the two biotite-bearing lavas, with only one sample of each rhyolite obtained. However, eleven samples are available from the orthopyroxene and calcic amphibole-bearing lavas. The range in major element compositions within this group of samples shows a reduction in Al_2O_3, TiO_2, Fe_2O_3, MgO, CaO and increase in K_2O with increasing SiO_2, trends which are typical of fractional crystallisation processes involving the phenocryst and accessory phases in these lavas. Na_2O remains fairly constant over the range in SiO_2 shown by these lavas. The range in trace element compositions within this group of samples shows an increase in incompatible elements (Rb and Ba) and a decrease in compatible elements (Sr and Zr) with increasing SiO_2, trends which are also typical of fractional crystallisation processes. Hence these lavas may record the evolution of a magma batch beneath the Okataina Volcanic Centre during this time period.

Of note is the wide range in compositions for samples from the Maungawhakamana rhyolite (e.g. SiO_2 = 73.1 - 77.2 wt. %, Sr = 78 - 179 ppm). It has been noted previously that this rhyolite, despite being treated as a single unit in this study, has been erupted from multiple vents and is likely to be comprised of a number of individual flows and/or domes. The wide range in major and trace element compositions supports this observation, and this edifice may have been erupted over a period of time that allowed evolution of the magma between eruptions.

Figure 4.8 shows chondrite-normalised multi-element (spider) and REE abundance patterns for representative ho_1 rhyolite lavas. These patterns are typical for Taupo Volcanic Zone (TVZ) silicic eruptives seen in other studies (e.g. Reid, 1983; Briggs et al., 1993; Brown, 1994; Beresford, 1997; Wright, 2000). The REE abundance patterns are characterised by a strongly enriched light REE pattern with steep slopes (La_N/Sm_N = 3.23 - 5.43), a pronounced negative Eu anomaly (Eu_N/Eu_N^* = 0.54 - 0.86), and flat heavy REE pattern (Gd_N/Yb_N = 1.01 - 1.33). The negative Eu anomaly seen in the lavas can be attributed to fractionation of plagioclase feldspar, as it is the most abundant phenocryst phase and mineral/melt partition coefficients for Eu in plagioclase range from ~ 2 - 5 (Arth, 1976; Nash and Crecraft, 1985), significantly higher than for the other REE. One sample (110) shows a small negative Ce anomaly, which was noted by Briggs et al. (1993) as a possible effect of weathering or vapour-phase alteration.

In silicic melts accessory phases such as zircon and apatite may strongly influence the REE pattern. Although they may be present in only small quantities, their very high partition coefficients for the REE lead to a disproportionate influence on the REE pattern (Nagasawa, 1970; Arth, 1976; Watson and Green, 1981; Mahood and Hildreth, 1983; Henderson, 1984; Rollinson, 1993). Both of these mineral species are found as accessory phases in the rhyolite lavas of the Okataina, Rotorua and Kapenga volcanic centres. The fractionation of zircon will deplete the heavy REE, and fractionation of apatite will deplete the middle REE relative to the light and heavy REE. The implications of REE geochemistry for rhyolite petrogenesis will be discussed further in Chapter Six.

There is no systematic variation in REE abundance with silica content. However, the most REE enriched lava (63) has the highest Rb/Sr ratio and the most REE depleted lava (119) has the lowest Rb/Sr ratio. Rb/Sr ratios tend to increase with increasing REE content for the other lavas. Rb/Sr also shows a correlation with the Eu anomaly. Increasingly negative Eu

anomalies are generally accompanied by increasing Rb/Sr. The largest Eu anomaly (Eu_N/Eu_N^* = 0.55) is seen in the most REE enriched lava and the smallest anomaly (Eu_N/Eu_N^* = 0.86) in the most REE depleted lava. There is no clear distinction in REE patterns between spatial groups or biotite-bearing and biotite-free/poor lavas.

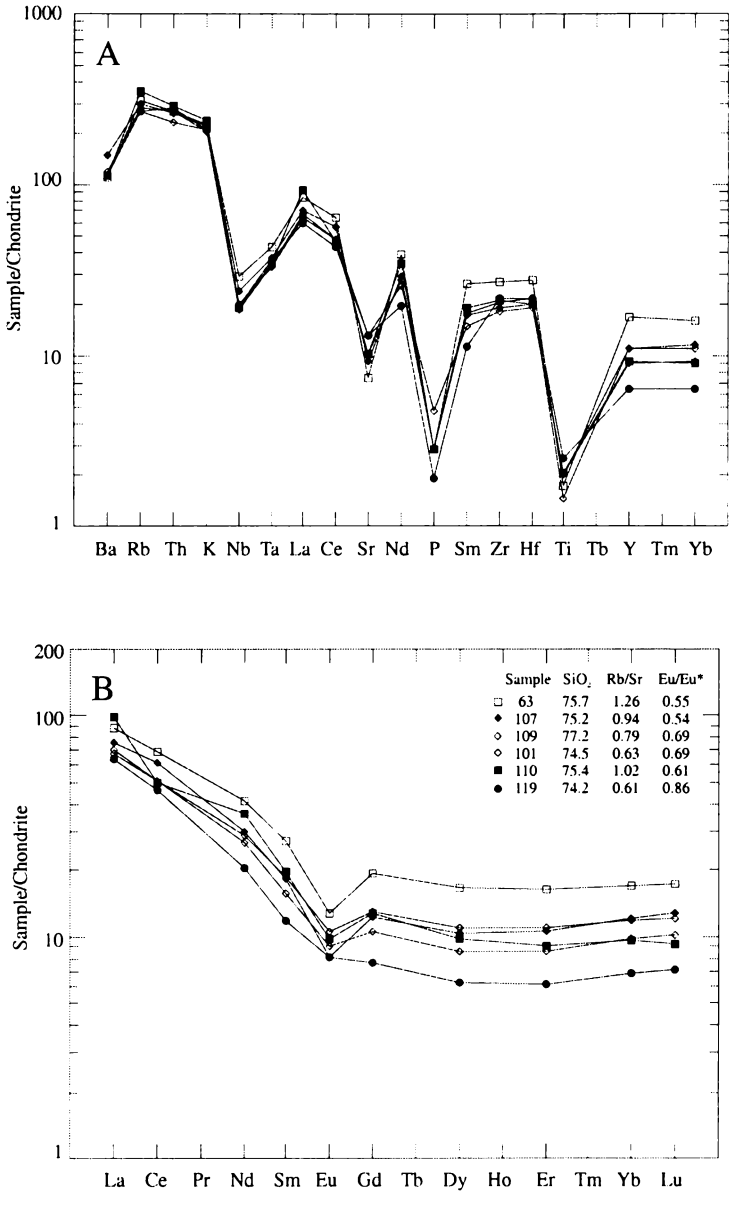

Figure 4.8: a) Chondrite-normalised multi-element (spider) patterns for the ho_1 rhyolite lavas from the Okataina Volcanic Centre (normalisation values from Thompson et al., 1984). b) Chondrite-normalised REE abundance patterns for the ho_1 rhyolite lavas (normalisation values from Boynton, 1984). Symbols as in Figure 4.6.

The multi-element (spider) patterns show more troughs and peaks due to the wider range of elements included. The patterns show enrichment in large-ion lithophile elements (e.g. Ba, Rb, Th and K) relative to the high-field-strength elements (e.g. Sm, Zr and Hf) and depletion in Nb, P and Ti. These features are typical of arc-related magmas (Pearce, 1983; Wilson, 1989; Pearce and Peate, 1995). The troughs are likely to be controlled at least in part by fractionation of minerals seen in the phenocryst and accessory assemblage of these lavas - Sr (plagioclase), P (apatite), Ti (Fe-Ti oxides, hornblende) and Nb (hornblende, biotite, Fe-Ti oxides). Ba, Rb and K are concentrated in the continental crust and the high abundance of these elements may reflect crustal involvement in magma genesis. Any depletion in Ba, Rb and K that may be caused by fractionation of biotite in some samples is not evident in the multi-element patterns. The implications of trace element geochemistry for rhyolite petrogenesis will be discussed further in Chapter Six.

Eruption of the Quartz Biotite, Matahina and Kawerau ignimbrites resulted in caldera-formation during this period of activity at the Okataina Volcanic Centre. To establish an overall picture of the chemical evolution of the centre during this time requires a comparison of all eruptives, however there are several problems when trying to achieve this. Firstly, no absolute ages are available for the ho_1 rhyolites, therefore their ages relative to each other and the three caldera-forming ignimbrites are unknown. Hence which ignimbrite they are temporally associated with, and their status as pre- or post-caldera eruptives, is unknown. Nairn (1989) mapped all ha_1 (ho_1) Okataina Volcanic Centre rhyolites as older than the Matahina Ignimbrite and noted that this ignimbrite has been observed in outcrop overlying Maungawhakamana rhyolite. Such a relationship has not been observed for other ho_1 rhyolites. Nairn (1981a) thought that these ha_1 rhyolites were probably extruded both prior to and following eruption of the "quartz-biotite tuffs".

In addition, geochemical data for these caldera-forming ignimbrites is limited. Data for the Quartz Biotite Ignimbrite exists as singular analyses in several studies (Nairn, 1981a; Dravitzki, 1999) that have been obtained from either whole rock or matrix samples. Carr (1984) provided major and trace element data for pumice clasts from the Matahina Ignimbrite, which are compared to the ho_1 rhyolites in Figures 4.6 - 4.7. Matahina Ignimbrite pumice clasts have higher SiO_2 contents than most of the ho_1 rhyolites and are most geochemically similar, in terms of major and trace elements, to several samples from the northeastern rhyolites (Maungawhakamana and Matawhaura). A possible hypothesis is that the orthopyroxene and calcic amphibole-bearing lavas may record the evolution of a

magma batch beneath the Okataina Volcanic Centre prior to eruption of the Matahina Ignimbrite, which has a similar ferromagnesian phenocryst assemblage to the lavas and more evolved major and trace element composition. However, without better age control on the ho_1 rhyolites and isotopic data for the Matahina Ignimbrite (discussed in Chapter Six) it becomes difficult to draw conclusions as to the geochemical sequence erupted during this period and the genetic relationship between the rhyolite lavas and the Matahina Ignimbrite. Data for the Kawerau Ignimbrite is limited to five preliminary analyses obtained for pumice clasts by Beresford (1997), which should not be considered representative of the whole ignimbrite. Three of these analyses are of rhyolitic composition and are compared to the ho_1 rhyolites in Figures 4.6 and 4.7. While these pumice samples have compositions similar to many of the ho_1 rhyolite lavas, such a small data set prevents any meaningful conclusions being drawn.

4.5.2 The ho_2 Rhyolites

Major and trace element compositions for the ho_2 rhyolites are shown in Figures 4.9 and 4.10 respectively. These rhyolites have been divided into five groups based on spatial position and ferromagnesian phenocryst assemblage (see sections 2.2.2.2 and 3.5.2) and have SiO_2 compositions ranging from ~ 73.9 - 76.0 wt. %. There are no distinct groupings in major or trace element compositions that coincide with spatial position, although the lavas fall into two groups that coincide with ferromagnesian phenocryst assemblages.

These two groups, for biotite-bearing and biotite-free/poor lavas, are seen in Figures 4.9 and 4.10 to be most distinct in terms of their MgO, CaO, Sr, Zr, Ce, La and Ta compositions. Generally the biotite-bearing lavas have lower SiO_2, Zr, Ce, La and Ta contents and higher MgO, CaO and Sr contents than the biotite-free/poor lavas. The more mineralogically evolved biotite-bearing lavas have lower SiO_2 and Rb/Sr, and are hence geochemically less evolved than the biotite-free/poor lavas. These characteristics provide support for the existence of two separate magma batches, initially suggested by ferromagnesian phenocryst assemblages. Evolution of the biotite-free/poor lavas from the biotite-bearing lavas seems unlikely, since the biotite-free/poor lavas are not relatively depleted in Rb and Ba. One sample from the biotite-free/poor Moerangi rhyolites has elevated Al_2O_3 and Ba and reduced SiO_2 compared to the other biotite-free/poor lavas. This may be due to weathering/alteration and the concentration of Al_2O_3 and Ba in secondary minerals. In a plot of Rb versus Sr this lava falls neatly into the biotite-free/poor group.

The range in major element compositions within each of the two groups shows a reduction in Al_2O_3, TiO_2, Fe_2O_3, MgO, CaO and increase in Na_2O and K_2O with increasing SiO_2, trends typical of fractional crystallisation processes involving the phenocryst and accessory phases in these lavas. Na_2O remains fairly constant over the range in SiO_2 shown by the biotite-bearing lavas. The range in trace element compositions within each of the two groups shows an increase in incompatible elements (Rb and Ba) and a decrease in compatible elements (Sr and Zr) with increasing SiO_2, trends which are also typical of fractional crystallisation processes. Hence these lavas may record the evolution of two spatially adjacent magma batches beneath the southwestern Okataina Volcanic Centre during this time period.

Figure 4.11 shows chondrite-normalised multi-element (spider) and REE abundance patterns for representative ho_2 rhyolite lavas. Once again these patterns are typical for TVZ silicic eruptives seen in other studies. Similar observations can be made regarding the shape of the patterns, and controls on pattern shapes, to those made for the ho_1 rhyolites. The REE abundance patterns are characterised by a strongly enriched light REE pattern with steep slopes (La_N/Sm_N = 2.82 - 4.61), a pronounced negative Eu anomaly (Eu_N/Eu_N^* = 0.43 - 0.71), and flat heavy REE pattern (Gd_N/Yb_N = 1.03 - 1.34). The two groups have distinct REE abundance patterns, with the biotite-bearing lavas having lower REE abundances than the biotite-free/poor lavas. Within each of these two groups the negative Eu anomaly is related to SiO_2 content. For the biotite-bearing lavas small decreases in SiO_2 accompany small increases in the negative Eu anomaly. In addition, the lava with the highest SiO_2 content (64) has the most depleted REE pattern. For the biotite-free/poor lavas small increases in SiO_2 accompany increases in the negative Eu anomaly and the lava with the highest SiO_2 content (72) has the most enriched REE pattern. Lack of consistent trends in REE compositions, and their relationship to SiO_2, for these two groups provides further evidence that they have been derived from discrete magma batches. In terms of the multi-element (spider) patterns the two groups have distinct compositions for most of the elements displayed, the exceptions being Ba, Rb, Th, K, P, Zr and Ti.

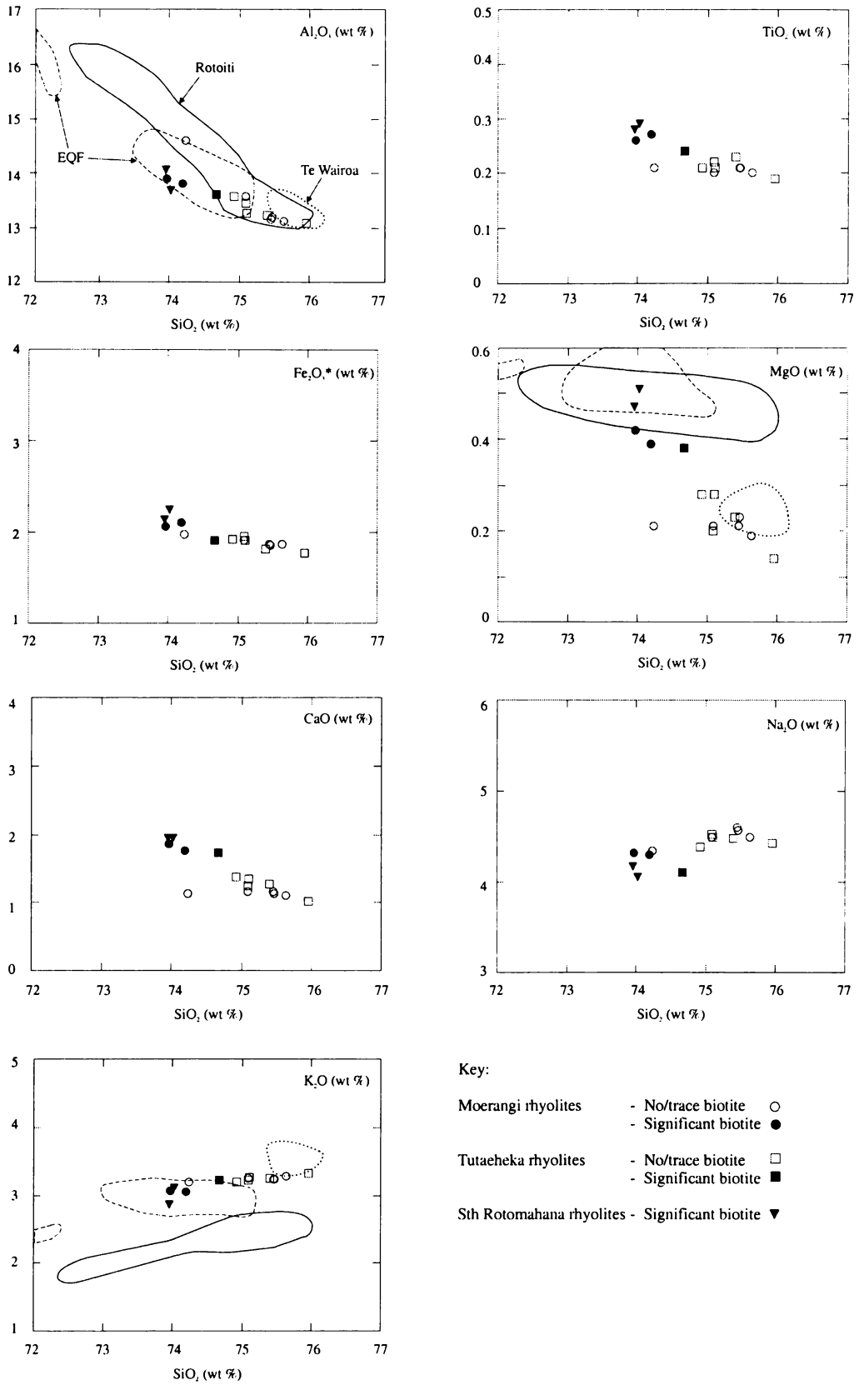

Figure 4.9: Selected major element variation diagrams for the ho_2 rhyolite lavas from the Okataina Volcanic Centre. Compositions for the Rotoiti, Earthquake Flat and Te Wairoa ignimbrites, from Schmitz (1995), Davis (1985) and Bellamy (1991) respectively, are enclosed by the plain, dashed and dotted lines respectively.

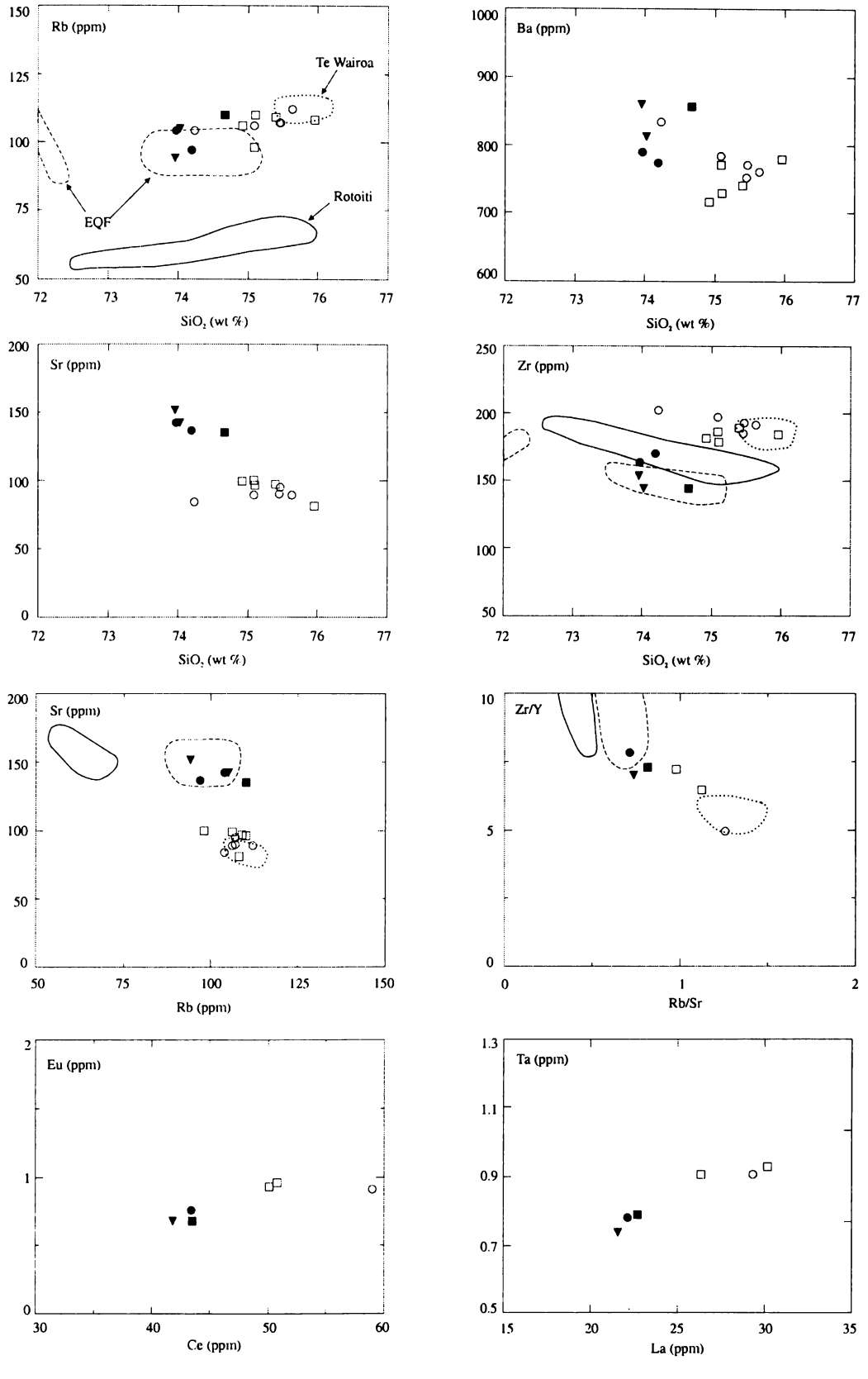

Figure 4.10: Selected trace element variation diagrams for the ho_2 rhyolite lavas from the Okataina Volcanic Centre. Symbols as in Figure 4.9. Compositions for the Rotoiti, Earthquake Flat and Te Wairoa ignimbrites, from Schmitz (1995), Davis (1985) and Bellamy (1991) respectively, are enclosed by the plain, dashed and dotted lines respectively.

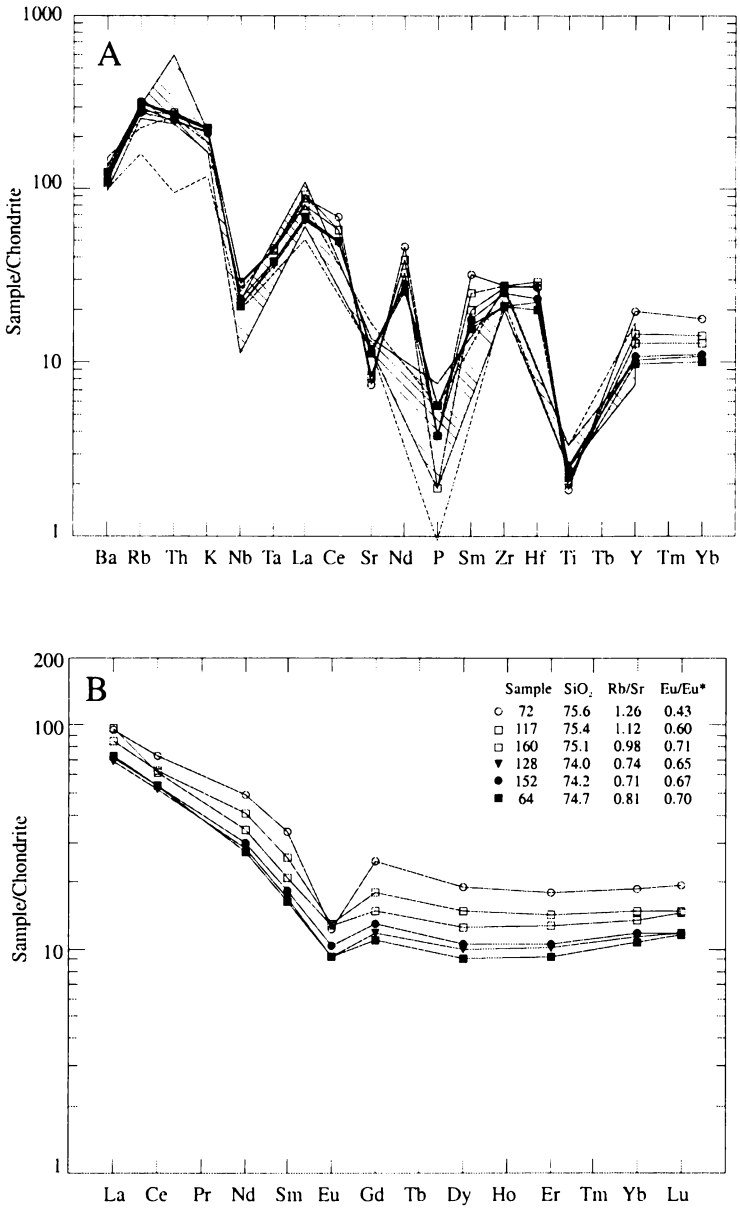

Figure 4.11: a) Chondrite-normalised multi-element (spider) patterns for the ho_2 rhyolite lavas from the Okataina Volcanic Centre (normalisation values from Thompson et al., 1984). Dashed outline and diagonal fill indicate the range in patterns for available Te Wairoa and Earthquake Flat ignimbrite data respectively (from Bellamy (1991) and Davis (1985)). b) Chondrite-normalised REE abundance patterns for the ho_2 rhyolite lavas (normalisation values from Boynton, 1984). Symbols as in Figure 4.9.

Eruption of the Rotoiti Ignimbrite resulted in caldera formation during this period of activity at the Okataina Volcanic Centre. In addition, two pyroclastic eruptions that did not result in caldera formation have been identified as occurring at this time. The Te Wairoa Ignimbrites consist of a series of small ignimbrites, lying stratigraphically between the Mamaku and Rotoiti ignimbrites, confined to stream valleys between lakes Rotorua and Okareka

(Bellamy, 1991). Because of the small, localised nature of these units Bellamy (1991) considered them to be related to the growth of the adjacent Moerangi rhyolites. The Earthquake Flat (EQF) Ignimbrite was erupted at approximately the same time as the Rotoiti Ignimbrite in an area adjacent to the southwestern Okataina Volcanic Centre that is currently postulated to be part of the Kapenga Volcanic Centre. These three ignimbrites have been compared to the ho_2 rhyolites in Figures 4.9 - 4.11.

At least some of the Moerangi rhyolites were erupted immediately prior to the Rotoiti Ignimbrite, as Rotoehu Ash directly overlies Kakapiko Dome (I. Nairn, pers. comm., 1999). Initial support for the theory that these rhyolites are not genetically related to the Rotoiti Ignimbrite magma is gained from the distance between their vent areas. Further evidence is obtained from the lack of geochemical similarity particularly seen in their K_2O, Rb, Sr, Rb/Sr and Zr/Y compositions.

Bellamy (1991) established a geochemical relationship between the Te Wairoa Ignimbrites and the Moerangi rhyolites, which is supported by data collected in this study. Pumices from the Te Wairoa Ignimbrites have similar major and trace element compositions to several of the biotite-free/poor Moerangi and Tutaeheka rhyolites. Bellamy (1991) did not study the Tutaeheka rhyolites, and from the data presented in this study no conclusion can be reached as to whether the Te Wairoa Ignimbrites accompanied Moerangi or Tutaeheka rhyolite dome growth, or both.

Davis (1985) identified two compositionally distinct magma types within the EQF Ignimbrite with Type 1 being enriched in SiO_2 and K_2O and depleted in Zr relative to Type 2. These two groups are shown in Figures 4.9 and 4.10. Similar Rb, Sr, Rb/Sr and Zr/Y compositions for these two magma types means they plot as one group on several diagrams. Of these two magma types, Type 1 has similar major element compositions to the biotite-bearing ho_2 rhyolites and both types have similar trace element compositions to these lavas. Davis (1985) proposed that these two magma types were erupted from a single layered chamber with Type 1 overlying Type 2. This seems consistent with eruption of the biotite-bearing lavas, similar in composition to the Type 1 magma, from the top of the chamber prior to the ignimbrite eruption. In addition to a geochemical similarity to the EQF Ignimbrite, the biotite-bearing ho_2 rhyolites are geochemically similar to the hk_2 rhyolites erupted during the same time period but well within the Kapenga Volcanic Centre (see section 4.7, Figures 4.31 - 4.33).

A comparison of chondrite-normalised multi-element (spider) abundance patterns for the ho_2 rhyolites with patterns for the Te Wairoa and EQF ignimbrites (Figure 4.11) shows that the patterns for these two ignimbrites overlap. A lack of data for many element abundances in the ignimbrites prevents a detailed comparison, although based on available data the patterns for each rhyolite group and its associated ignimbrite are similar. However, the element abundances available for the ignimbrites are generally those in which the two groups show little difference (Ba, Rb, Th, K, P, Zr and Ti). Differences in Y and Nb for the two groups are mirrored by slight differences in the ignimbrites.

4.5.3 The Haroharo Volcanic Complex (ho_3) Rhyolites

Major and trace element compositions for the Haroharo Volcanic Complex ho_3 rhyolites are shown in Figures 4.12 and 4.13. The rhyolites of this complex have SiO_2 compositions ranging from ~ 75.1 - 77.4 wt. %. A sample taken from the Kaipara Lava Flow (145) showed evidence in thin section of hydrothermal alteration. It contains ~ 79.6 wt. % SiO_2 and has been omitted from all diagrams and will not be discussed further. In Figures 4.12 and 4.13 the rhyolites have been divided into four groups based on eruptive episode. The range in compositions and compositional groupings within each episode are indicated on the enlarged SiO_2 versus Al_2O_3 plot in Figure 4.12. However, these groups are seen on all plots and within each eruptive episode they correspond to particular vents or vent areas that were active at that time. Of note is that there are no systematic trends in geochemical composition over time in the Haroharo Volcanic Complex rhyolite lavas.

The lavas erupted during the Te Rere episode have very similar compositions in terms of all major and trace elements with SiO_2 contents of ~ 76.2 - 76.5 wt. % (negligible difference given the analytical precision). These lavas are considered to have been erupted from the same vent or vent area now buried beneath younger pyroclastics (Nairn, 1981a). In addition to their petrographic and mineralogic similarity, noted in Chapter Three, they are also geochemically similar.

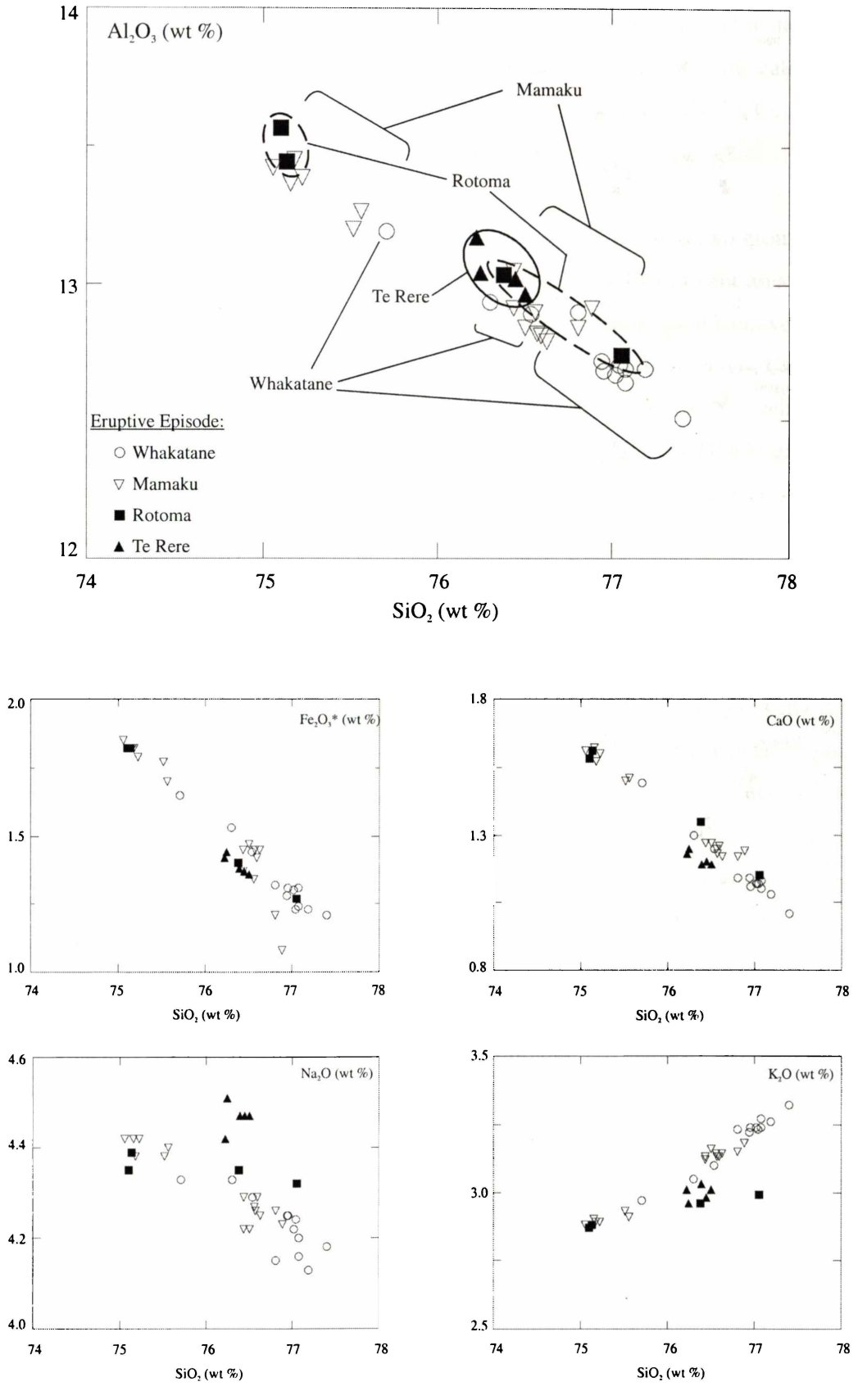

Figure 4.12: Selected major element variation diagrams for the Haroharo Volcanic Complex ho_3 rhyolite lavas from the Okataina Volcanic Centre.

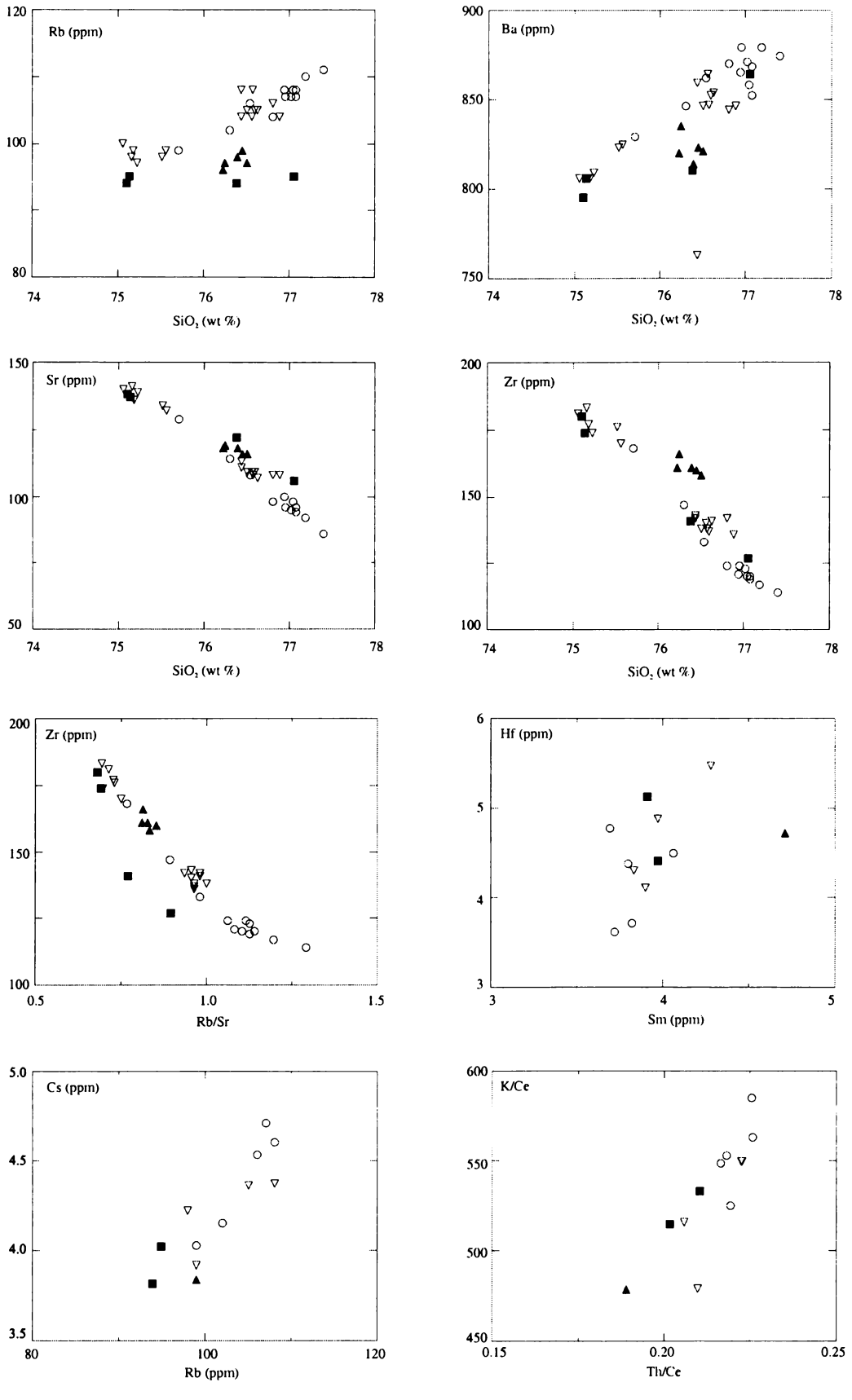

Figure 4.13: Selected trace element variation diagrams for the Haroharo Volcanic Complex ho_3 rhyolite lavas from the Okataina Volcanic Centre. Symbols as in Figure 4.12.

During the Rotoma episode lavas were erupted from two vent areas. These lavas have different major and trace element compositions. Lavas erupted in the Rotoma caldera have lower SiO_2, K_2O, Ba, Rb/Sr and higher Al_2O_3, Fe_2O_3, CaO, Sr, Zr, Hf, Cs, Th/Ce and K/Ce than lavas erupted in the northern Haroharo caldera at this time.

The compositions of lavas erupted during the Mamaku episode fall into two groups, which correspond to the vent areas shown in Figure 2.8. Lavas erupted from vent areas 1 and 3 have compositions that overlap. The Waiti Lava Flow, which was erupted from vent area 2, has lower SiO_2, K_2O, Rb, Ba, Rb/Sr, Cs, K/Ce, Th/Ce and higher Al_2O_3, Fe_2O_3, CaO, Na_2O, Sr, Zr, Hf and Sm than the group of lavas erupted from vent areas 1 and 3. The relative ages of lavas erupted during the Mamaku episode was proposed by Nairn (1989) and this is shown in Table 2.2. Within the lavas erupted from vent areas 1 and 3 there is no systematic change in composition from oldest to youngest.

The compositions of lavas erupted during the Whakatane episode fall into three groups, which correspond to vent areas 1, 2 and 4 in Figure 2.8. The two lavas erupted from vent area 2 have lower SiO_2, K_2O, Rb/Sr, Hf, K/Ce, Th/Ce and higher Al_2O_3, Fe_2O_3, CaO, Na_2O, Sr, Zr and Cs than the group of lavas erupted from vent area 1. Tikorangi Dome, erupted in vent area 4, has higher Al_2O_3, Fe_2O_3, CaO, Sr, Zr, Hf and lower SiO_2, K_2O, Rb, Ba, Rb/Sr and Cs than all other lavas erupted during this episode. The relative ages for lavas erupted in the Whakatane episode are shown in Table 2.2. Within the lavas erupted from vent area 1 there is no systematic or significant change in composition from oldest to youngest.

Of interest is the compositional variation in samples taken from the same lava dome or flow. Multiple samples were obtained of nine lavas from the Haroharo Volcanic Complex (Appendix V, Table V.1). The difference in SiO_2 between samples is generally less than 0.3 wt. %. Considering that the analytical uncertainty in XRF measurements of SiO_2 is ~ 0.2 wt. % (Weaver et al., 1990) these differences are negligible. The exceptions are the Waiti, Te Pohue and Makatiti lava flows where differences of 0.5 - 0.7 wt. % are seen. In many samples the differences between other elements are also negligible.

Figure 4.14 shows chondrite-normalised multi-element (spider) and REE abundance patterns for representative Haroharo Volcanic Complex rhyolite lavas. Once again these patterns are typical for TVZ silicic eruptives seen in other studies. Similar observations can be made regarding the shape of the patterns, and controls on pattern shapes, to those made for the ho_1

and ho_2 rhyolites. The REE abundance patterns are characterised by a strongly enriched light REE pattern with steep slopes (La_N/Sm_N = 3.35 - 3.96), a pronounced negative Eu anomaly (Eu_N/Eu_N^* = 0.61 - 0.72), and flat heavy REE pattern (Gd_N/Yb_N = 1.02 - 1.10).

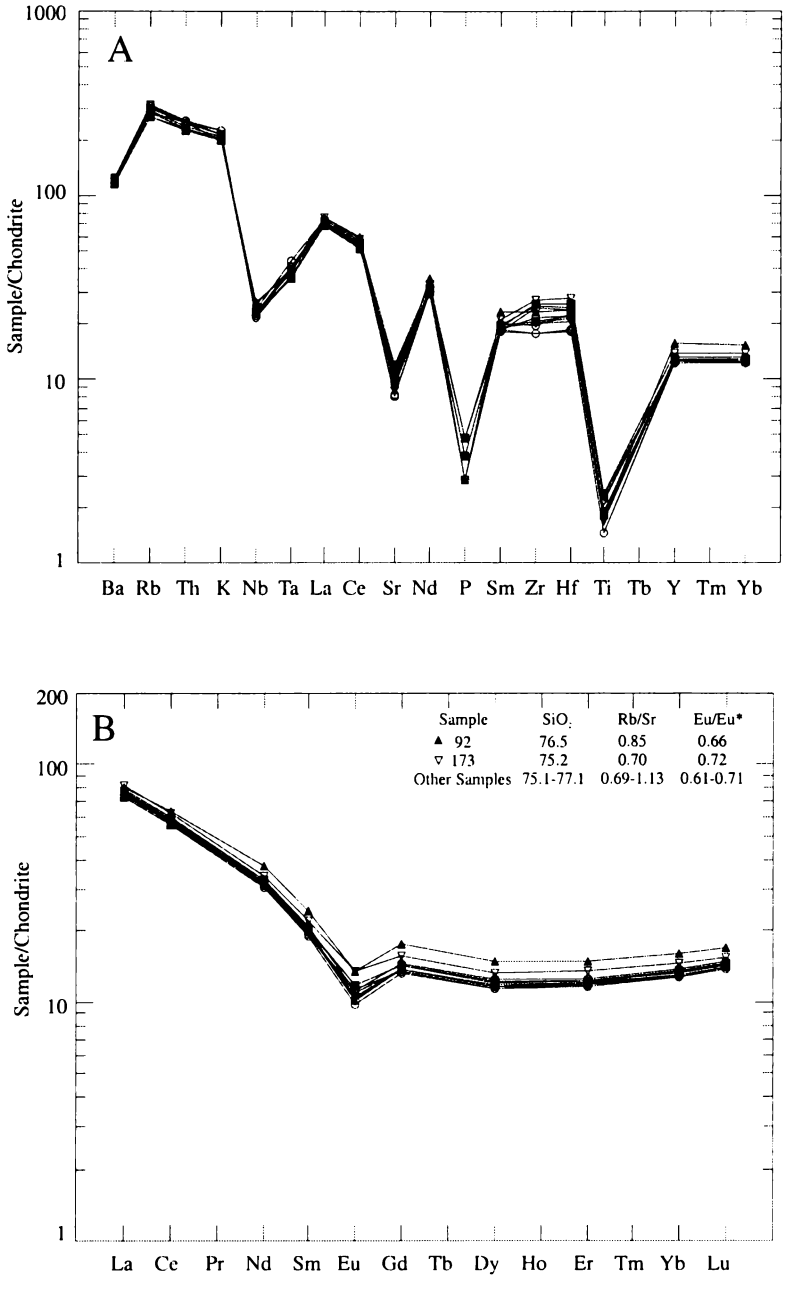

Figure 4.14: a) Chondrite-normalised multi-element (spider) patterns for the Haroharo Volcanic Complex ho_3 rhyolite lavas from the Okataina Volcanic Centre (normalisation values from Thompson et al., 1984). b) Chondrite-normalised REE abundance patterns for the Haroharo Volcanic Complex ho_3 rhyolite lavas (normalisation values from Boynton, 1984). Symbols as in Figure 4.12.

The patterns for all the lavas overlap and are nearly identical except for the Fenton's Mill Flow from the Te Rere episode (92) and the Waiti Flow from the Mamaku episode (173), which have slightly enriched REE patterns. For the Rotoma, Mamaku and Whakatane episodes, lavas erupted at the same time but from different vent areas have nearly identical REE abundance patterns. All of the lavas have very similar negative Eu anomalies, which show no relationship to SiO_2, Rb/Sr or REE abundance. In terms of the multi-element (spider) patterns the lavas also have nearly identical patterns, showing the widest range in compositions for Zr and Hf, which may be due to variable zircon fractionation as both Zr and Hf are highly compatible in this accessory phase.

While there are no systematic trends in lava compositions over time for the Haroharo Volcanic Complex as a whole, lavas erupted from vent areas 1+3 and 2 during the Mamaku and Whakatane eruptive episodes show compositional changes typical of fractional crystallisation of the observed phenocryst and accessory phases. Figure 4.15 shows in more detail two of the plots from Figures 4.12 and 4.13. Over the ~ 2 500 years between eruptions the magma erupted from vent area 2 has become more evolved with increased SiO_2, Rb/Sr and decreased Al_2O_3 and Zr. A similar change in magma composition has occurred at vent area 1. Also of interest is how the different groups of magmas erupted in each episode are related. For example, the vent area 1+3 magma erupted in the Mamaku episode may have evolved from the vent area 2 magma. These variations between and within the Mamaku and Whakatane eruptive episode lavas will be discussed further and assessed by fractional crystallisation modelling in Chapter Six.

Pyroclastic eruptions accompanied rhyolite lava extrusion during the four eruptive episodes that built up the Haroharo Volcanic Complex. There is a lack of published geochemical data for these pyroclastic deposits. Nairn (1981a, 1992) present analyses which cover all four eruptive episodes, but they are few in number and no indication is given as to whether they represent single or multiple clasts. To date the only data set of any size is that presented by Wright (2000) for the Mamaku episode.

Figure 4.16 compares data obtained in this study for Mamaku episode lavas with the data obtained by Wright (2000) for pyroclastics erupted at this time. In addition, Wright (2000) also obtained samples of Parewhaiti Dome and the Te Matae Flow, which were not sampled in this study, and unaltered samples of the Kaipara Flow. These compositions are also indicated in Figure 4.16. The Te Matae Flow has similar compositions to other vent area 1

eruptives, which is consistent with its spatial position. The composition of Parewhaiti Dome, which lies spatially between vent areas 1 and 2 (Figure 2.8), is also similar to the vent area 1 lavas. The Mamaku episode pyroclastics are most comparable to the vent area 1+3 lavas, especially in terms of their trace element (Rb/Sr, Zr) compositions. This is consistent with observations made by Nairn and Wood (1987) that the main pyroclastic vent was probably in the vicinity of Hainini Dome or the younger Makatiti Dome (vent area 1).

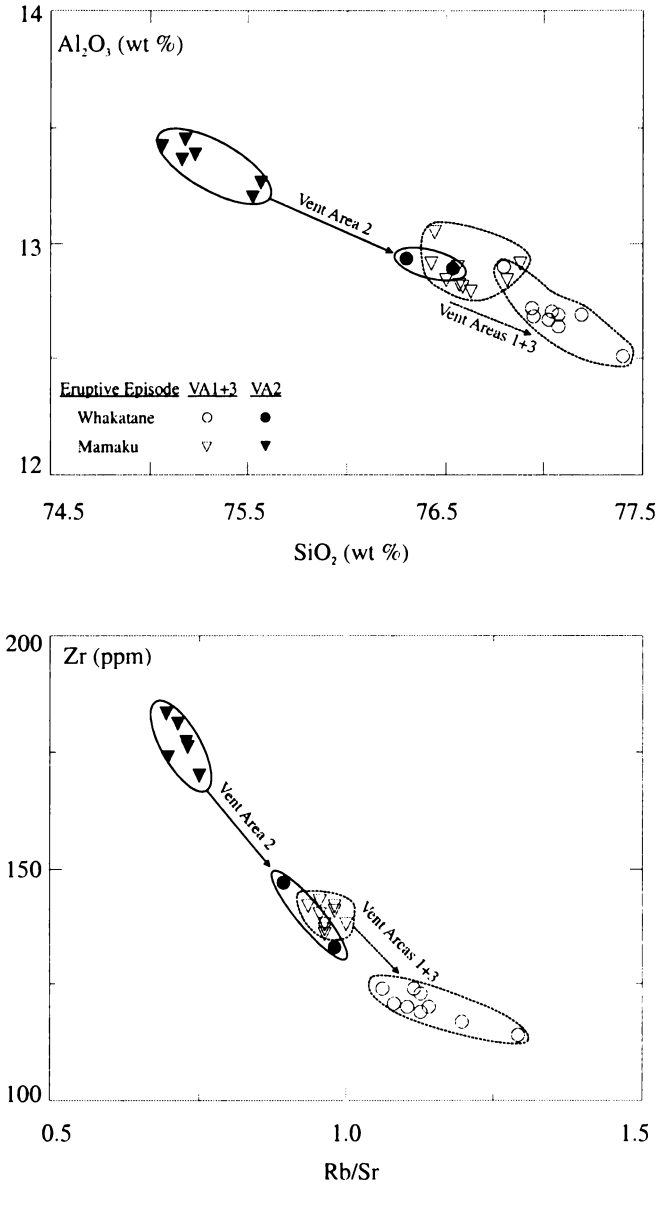

Figure 4.15: Selected major and trace element variation diagrams showing the changes in composition between rhyolite lavas erupted from vent areas 1, 2 and 3 in the Mamaku and Whakatane eruptive episodes at the Haroharo Volcanic Complex.

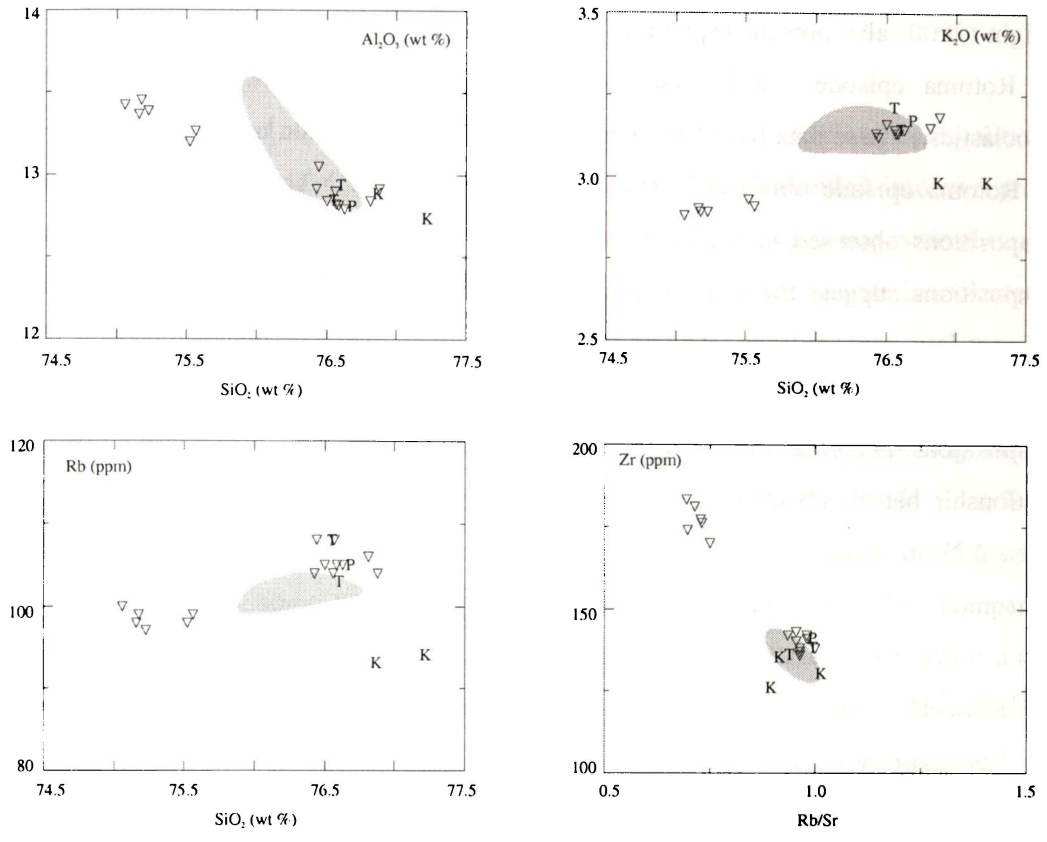

Figure 4.16: Selected major and trace element variation diagrams for rhyolite lavas erupted during the Mamaku episode at the Haroharo Volcanic Complex (open triangles). Also shown are the compositions of Parewhaiti Dome (P) and the Te Matae (T) and Kaipara (K) flows from Wright (2000). The shaded area indicates compositions for the Mamaku episode pyroclastics from Wright (2000).

The Kaipara Flow is unusual as its composition differs from other Mamaku episode eruptives, in particular the Waiti Flow that was erupted almost immediately after from the same vent. Wright (2000) noted that its ferromagnesian phenocryst assemblage differed from the other Mamaku lavas in that it is dominated by cummingtonite with minor amounts of orthopyroxene and calcic amphibole. This ferromagnesian phenocryst assemblage is similar to the older Te Pohue Flow, erupted from the same vent area in the Rotoma episode. Comparison of Figure 4.16 with Figures 4.12 and 4.13 shows that samples of the Kaipara Flow are also geochemically similar to Te Pohue Flow.

Wright (2000) also presented previously unpublished data from I. Smith for eruptives from the Rotoma episode. It is unknown whether this data set includes both lavas and pyroclastics. These data have been compared to compositions for lava flows erupted during the Rotoma episode obtained in this study in Figure 4.17. The data span the range of compositions observed in the Rotoma and Te Pohue flows. In addition, CaO, Zr and Sr compositions suggest the possibility of two compositional groups that coincide with the different lava compositions. Taking into account this previously unpublished data, the gap in compositions between the two possible magma batches represented by the lava compositions becomes much smaller, and this allows for the possibility of a genetic relationship between batches.

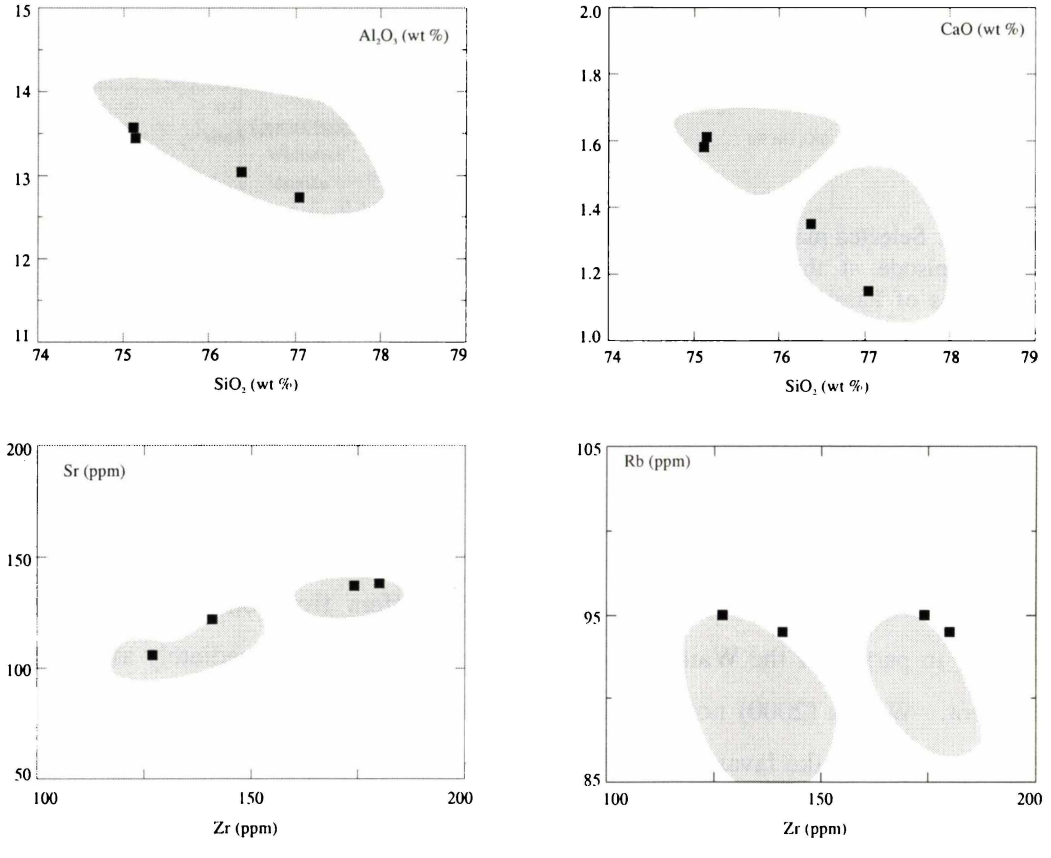

Figure 4.17: Selected major and trace element variation diagrams comparing rhyolite lavas erupted during the Rotoma episode at the Haroharo Volcanic Complex (filled squares) with unpublished data for Rotoma episode eruptives from I. Smith and discussed in Wright (2000) (shaded areas).

4.5.4 The Okareka Volcanic Complex (ho_3) Rhyolites

Major and trace element compositions for the Okareka Volcanic Complex ho_3 rhyolites are shown in Figures 4.18 and 4.19, where the rhyolites have been divided into two groups based on eruptive episode. The rhyolites of this complex have SiO_2 compositions ranging from ~73.7 - 75.6 wt. % and the range of compositions within each episode is indicated on the enlarged SiO_2 versus Al_2O_3 plot in Figure 4.18.

Two lavas were erupted during the Te Rere episode. Samples of the Eastern Rhyolite plot together on all major and trace element plots with a SiO_2 content of ~ 73.7 - 74.1 wt. %. Te Rere Dome was also erupted at this time and has an elevated SiO_2 content of 75.6 wt. %. However, in terms of some trace elements (e.g. Rb, Ba, Zr) this dome has comparable compositions to the Eastern Rhyolite. The possibility that the Te Rere Dome lava is a more evolved equivalent of the Eastern Rhyolite lava cannot be ruled out. However, the compositional differences may also be due to post-depositional alteration processes. The sample of Te Rere dome (174) is highly crystallised and devitrified. Samples of the Eastern Rhyolite are either non-spherulitic or comprise spherulites which reside in an unaltered, undevitrified glass. In addition these compositional differences in Te Rere dome are similar to differences seen in the Kaipara Flow (Haroharo Volcanic Complex), which was observed in thin section to be hydrothermally altered. Comparing Figures 4.18 and 4.19 with major and trace element variation diagrams for the Haroharo Volcanic Complex (Figures 4.12 and 4.13) shows that lavas erupted during the Te Rere episode at Okareka are compositionally distinct from lavas erupted during the same episode at Haroharo. The Okareka lavas generally have lower SiO_2, K_2O, Rb, Rb/Sr and higher Al_2O_3, Fe_2O_3, CaO, Sr and Zr. In addition, the distance between vents suggests the eruption of two separate magma batches.

During the Rotorua episode the Trig 7693 Dome and Middle Rhyolite were erupted. These two lavas, which are petrographically and mineralogically identical, have very similar major and trace element compositions with SiO_2 contents of ~ 74.8 - 75.6 wt. %. The Middle Rhyolite has a slightly lower SiO_2 content than the two samples of Trig 7693 Dome.

Only one sample from each eruptive episode was analysed by LA-ICPMS for trace and rare earth elements. The differences between these two samples are most readily seen in chondrite-normalised multi-element (spider) and REE abundance patterns (Figure 4.20).

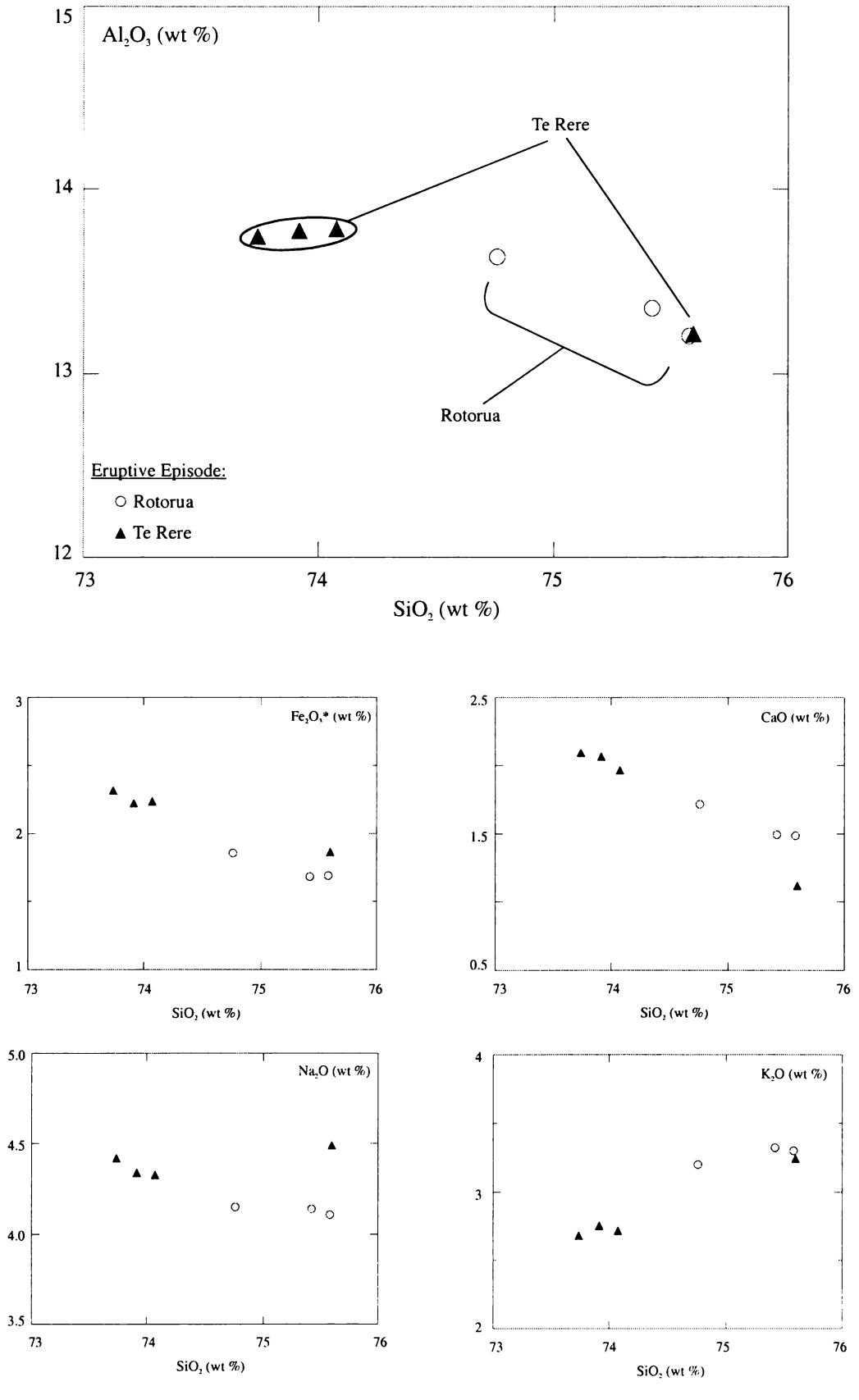

Figure 4.18: Selected major element variation diagrams for the Okareka Volcanic Complex ho_3 rhyolite lavas from the Okataina Volcanic Centre.

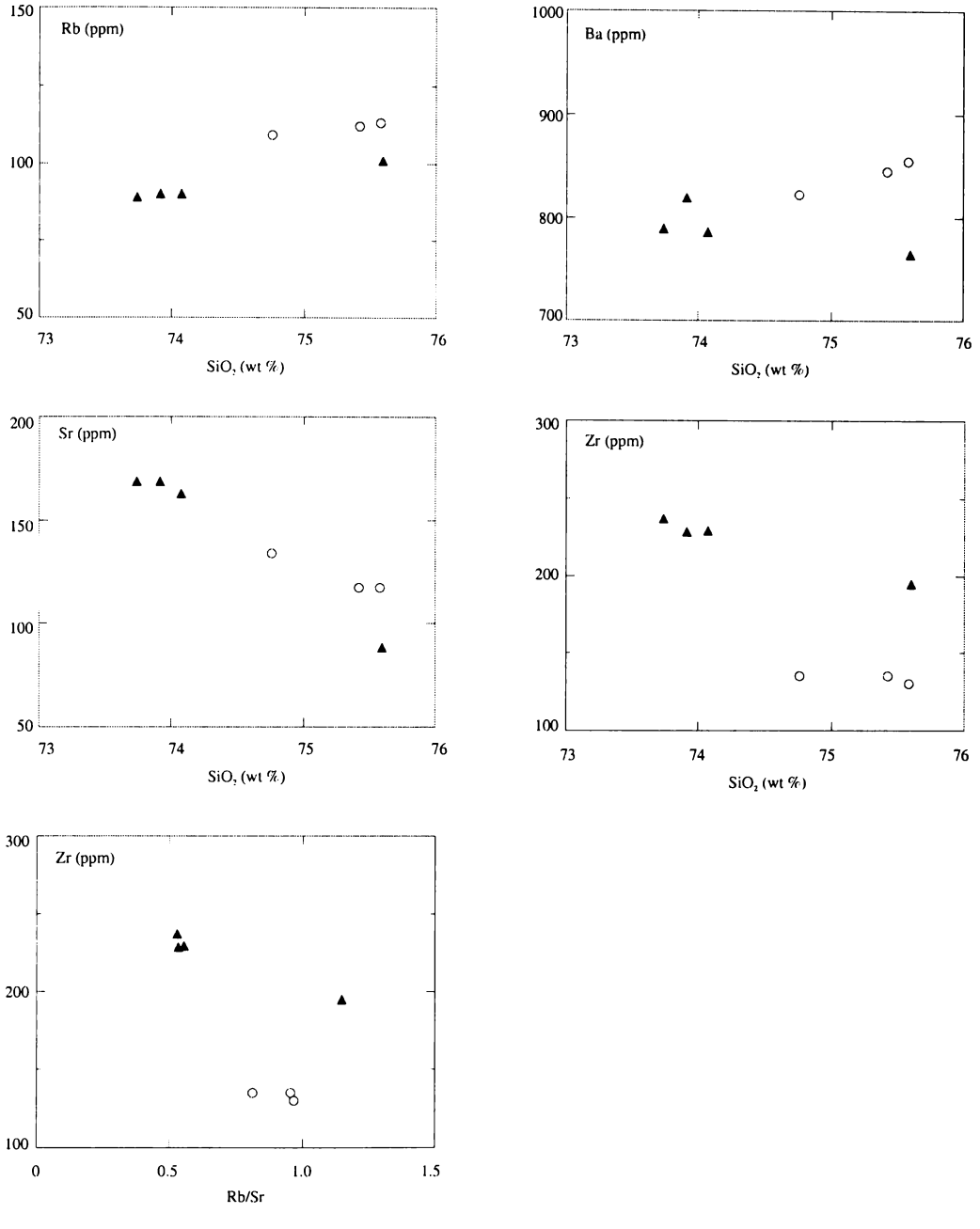

Figure 4.19: Selected trace element variation diagrams for the Okareka Volcanic Complex ho_3 rhyolite lavas from the Okataina Volcanic Centre. Symbols as in Figure 4.18.

The REE patterns are similar to those for the ho_1, ho_2 and Haroharo (ho_3) rhyolites and are characterised by a strongly enriched light REE pattern with steep slopes (La_N/Sm_N = 3.32 - 4.47), a pronounced negative Eu anomaly (Eu_N/Eu_N^* = 0.64 - 0.76), and flat heavy REE pattern (Gd_N/Yb_N = 1.03 - 1.13). Trig 7693 Dome (176) is depleted in most REE (except La and Ce) relative to the Eastern Rhyolite (113). The largest negative Eu anomaly is seen in the lava with the highest SiO_2 and Rb/Sr and most depleted REE pattern. Comparison with

the pattern for the Fenton's Mill Flow erupted during the Te Rere episode at Haroharo shows that the Okareka lavas are relatively depleted in REE. In terms of the multi-element (spider) patterns, Eastern Rhyolite is enriched in all elements from Sr - Yb and depleted in all elements from Ba - Ce (except Nb) relative to Trig 7693 Dome.

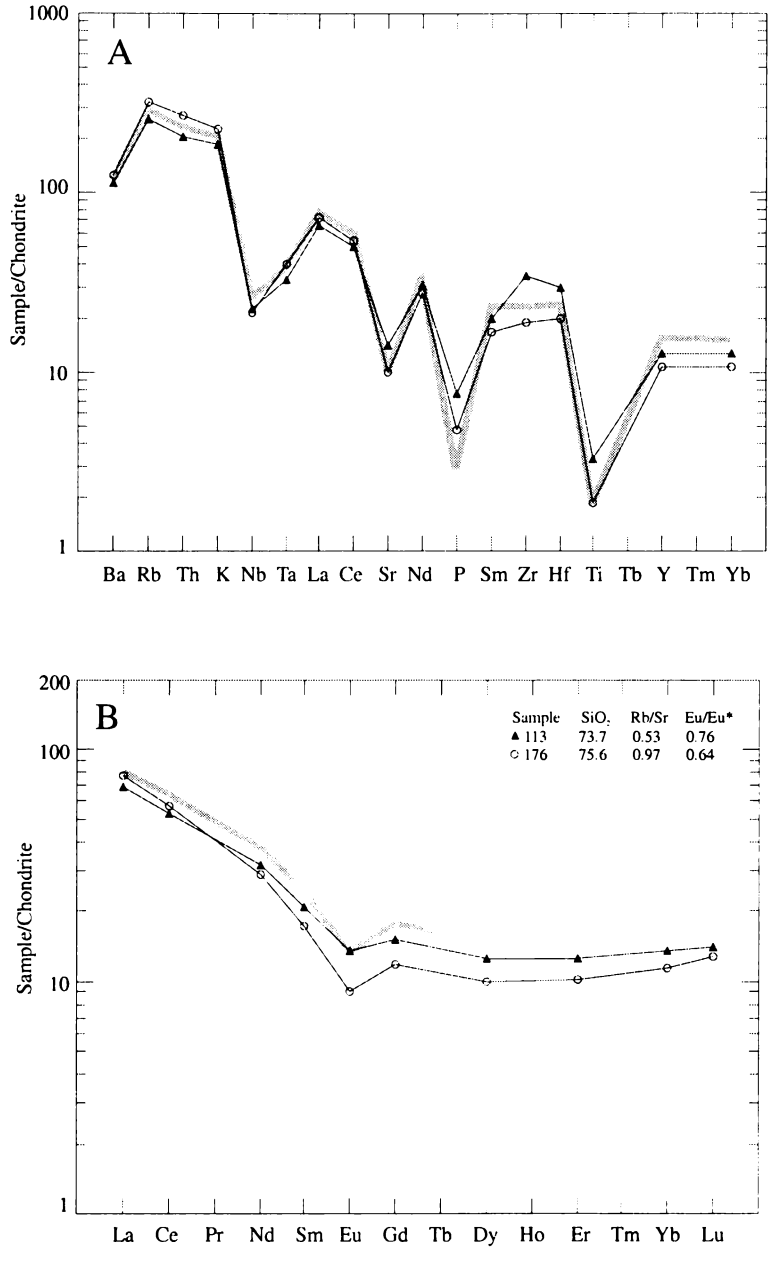

Figure 4.20: a) Chondrite-normalised multi-element (spider) patterns for the Okareka Volcanic Complex ho_3 rhyolite lavas from the Okataina Volcanic Centre (normalisation values from Thompson et al., 1984). b) Chondrite-normalised REE abundance patterns for the Okareka Volcanic Complex ho_3 rhyolite lavas (normalisation values from Boynton, 1984). Symbols as in Figure 4.18. Grey shading indicates the pattern for the Fenton's Mill flow (sample number 92) erupted from the Haroharo Volcanic Complex during the Te Rere episode (see Figure 4.14).

Compositional changes on major and trace element variation diagrams and differences in multi-element and REE abundance patterns suggest that the Rotorua episode magma (Trig 7693) may have evolved from Te Rere episode magma (Eastern Rhyolite) over the ~ 9 200 years between eruptions by fractional crystallisation of the observed phenocryst and accessory phases. Some input from the crust may also have been involved. The lower REE, Zr, P and Hf composition of the Rotorua lava can be attributed to fractionation of accessory phases such as zircon and apatite. Lower Ti and Sr compositions can be attributed to titanomagnetite, ilmenite, hornblende and plagioclase feldspar fractionation. An increase in the abundance of Ba, Rb, K suggests that the effect of any biotite fractionation may have been offset by crustal assimilation. This will be discussed further in Chapter Six.

Major and trace element geochemistry do not support eruption of the Tutaeheka 1 Dome during the Te Rere Eruptive Episode (see section 3.7.1), as this dome is geochemically comparable to the biotite-bearing ho_2 rhyolites (see section 4.5.2).

Pyroclastic eruptions accompanied rhyolite lava extrusion during the Rotorua Eruptive Episode at the Okareka Volcanic Complex. To date no data set of any size has been published for these pyroclastics.

4.5.5 The Tarawera Volcanic Complex (ho_3) Rhyolites

Major and trace element compositions for the Tarawera Volcanic Complex ho_3 rhyolites are shown in Figures 4.21 and 4.22. The rhyolites of this complex have SiO_2 compositions ranging from ~ 72.5 - 77.5 wt. %. In Figures 4.21 and 4.22 the rhyolites have been divided into four groups based on eruptive episode. The range in compositions and compositional groupings within each episode are indicated on the enlarged SiO_2 versus Al_2O_3 plot in Figure 4.21, however these groups are seen on all plots. Of note is that there are no systematic trends in geochemical composition over time in the Tarawera Volcanic Complex rhyolite lavas.

Samples have been obtained of two lavas erupted during the Okareka episode. The Ridge Flow contains ~ 75.4 wt. % SiO_2. Patiti Island has lower SiO_2 (~ 72.5 wt. %), Na_2O, K_2O, Rb, Ba, Rb/Sr, Sm, Hf and higher Al_2O_3, Fe_2O_3, CaO, Sr, Cs, K/Ce. It is possible that this lava has suffered some effects of weathering due to its elevated Al_2O_3 content.

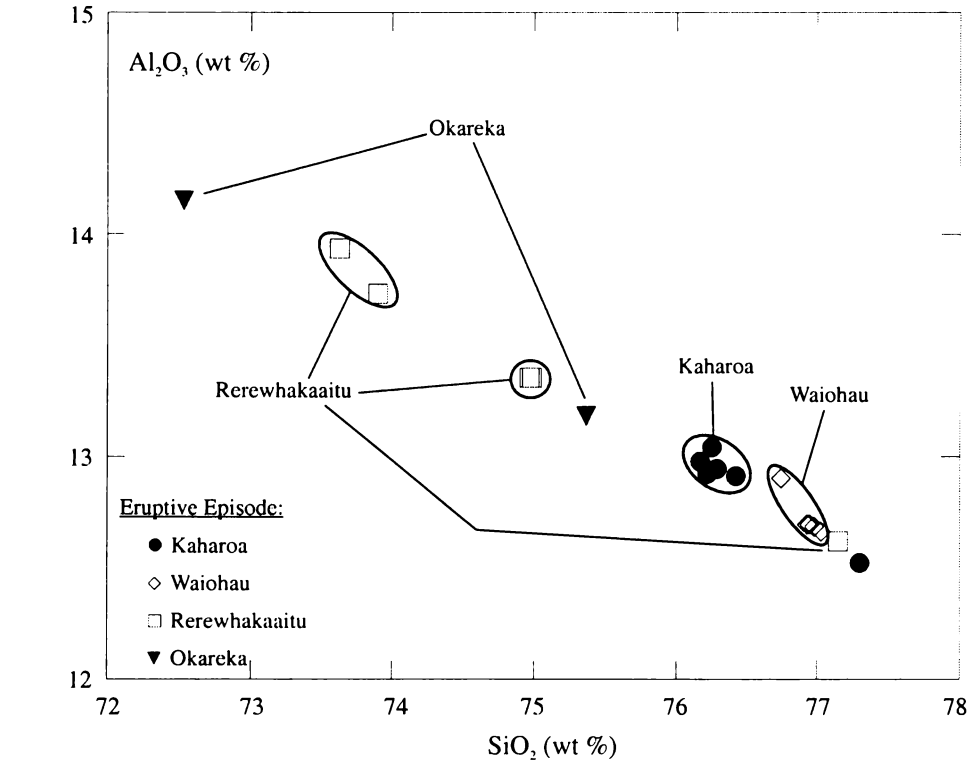

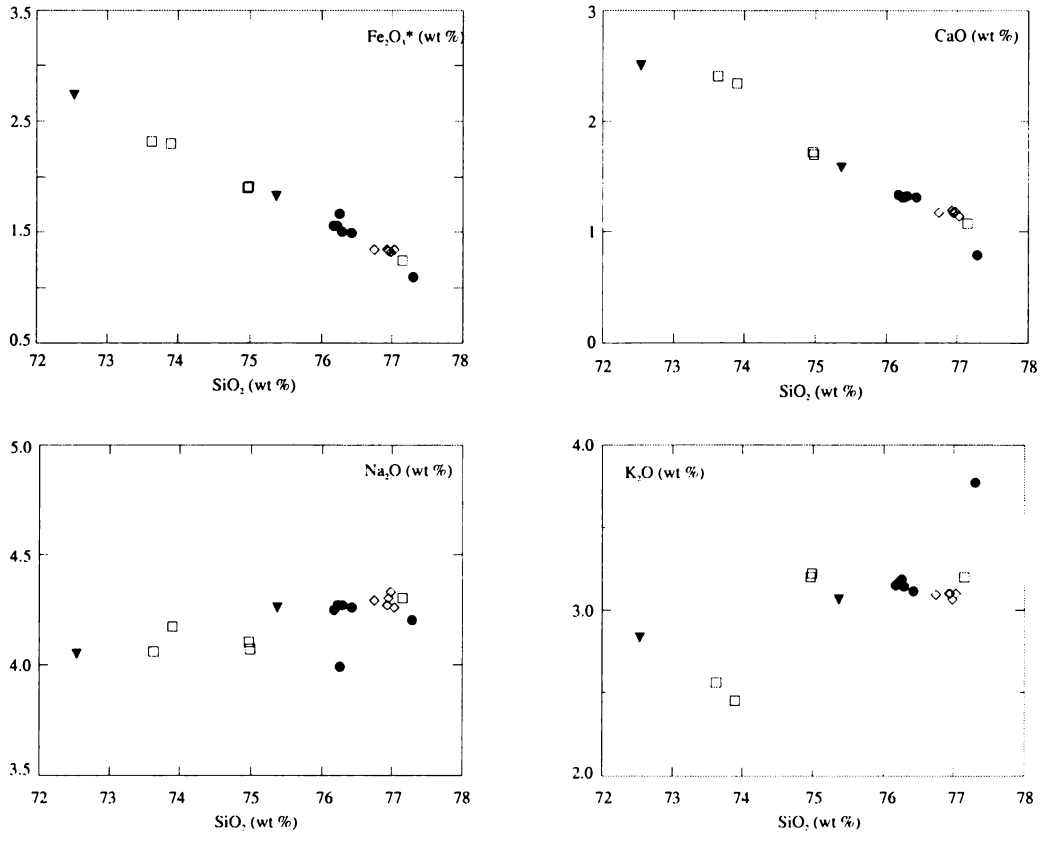

Figure 4.21: Selected major element variation diagrams for the Tarawera Volcanic Complex ho_3 rhyolite lavas from the Okataina Volcanic Centre.

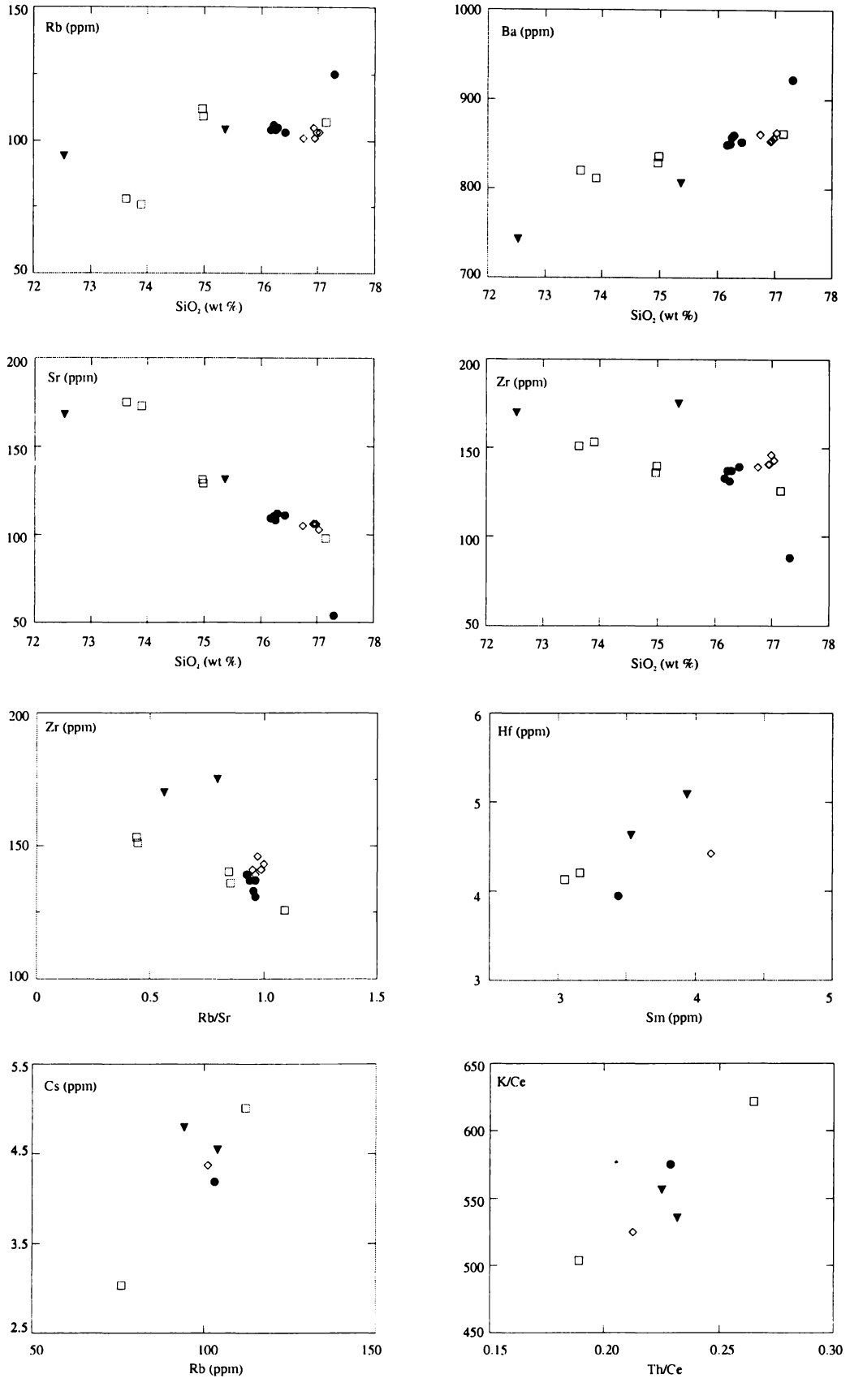

Figure 4.22: Selected trace element variation diagrams for the Tarawera Volcanic Complex ho_3 rhyolite lavas from the Okataina Volcanic Centre. Symbols as in Figure 4.21.

During the Rerewhakaaitu episode three groups of lavas were erupted that correspond with ferromagnesian phenocryst assemblages. The low SiO_2, K_2O, Rb, Rb/Sr and high Al_2O_3, Fe_2O_3, CaO, Sr, Zr group comprises samples of Western Dome, which contains only trace biotite. The intermediate group comprises samples of Rotomahana Dome and the Te Puha Flow, which contain significant amounts of biotite. A sample from the Te Puha Flow (40) comprises the third group with a high SiO_2 content of ~ 77.1 wt. %. This lava is biotite-free and phenocryst-poor, containing only ~ 7 % phenocrysts (Chapter Three, Appendix III). These two latter groups are consistent with previous studies that have observed an intimate mingling between two lava types in the Rerewhakaaitu eruptives (see section 3.8.2). Compositional differences between the three lava types erupted during the Rerewhakaaitu episode suggest that the biotite-bearing magma or the biotite-free phenocryst-poor magma may have evolved from the biotite-poor Western Dome magma by fractional crystallisation of the observed phenocryst and accessory phases. This will be discussed further in Chapter Six.

Rhyolite lavas erupted during the Waiohau episode cluster together with SiO_2 contents ranging from 76.8 - 77.0 wt. % (negligible difference given the analytical precision) and very similar compositions for all major and trace elements. These lavas (Pokohu and Waikakareao flows) were erupted from the same vent beneath Kanakana Dome and also have similar total phenocryst contents and ferromagnesian phenocryst assemblages. The relative ages for lavas erupted in this episode are shown in Table 2.2. There is no systematic change in composition from oldest to youngest lavas.

Rhyolite lavas erupted during the Kaharoa episode generally cluster together with SiO_2 contents ranging from 76.2 - 76.4 wt. % (negligible difference given the analytical precision) and very similar compositions for all major and trace elements. The exception is a sample taken from Green Lake Plug (133) which has a SiO_2 content of ~ 77.3 wt. %. This lava has a slight white colouration in hand specimen suggestive of minor hydrothermal alteration, although no evidence for this was seen in thin section. Leonard (1999) also observed this compositional difference between the Green Lake Plug and other Kaharoa rhyolite lavas. The rhyolite lavas erupted during the Kaharoa episode have similar total phenocryst contents, ferromagnesian phenocryst assemblages dominated by biotite and were erupted from several vents up to ~ 6 km apart in the central Tarawera Linear Vent Zone. The relative ages for lavas erupted in this episode are shown in Table 2.2. There is no systematic or significant change in composition from oldest to youngest lavas.

Where multiple samples have been taken from the same lava dome or flow they are found to be compositionally similar. Multiple samples obtained from Western Dome (Rerewhakaaitu episode), Pokohu Flow and Waikakareao Flow (Waiohau episode) and Crater Dome (Kaharoa episode) have SiO_2 content differences of less than 0.3 wt. %. The exception, as discussed previously, is the two samples obtained of the Te Puha Flow.

Figure 4.23 shows chondrite-normalised multi-element (spider) and REE abundance patterns for representative Tarawera Volcanic Complex rhyolite lavas. The REE patterns are similar to those for the ho_1, ho_2, Haroharo (ho_3) and Okareka (ho_3) rhyolites and are characterised by a strongly enriched light REE pattern with steep slopes (La_N/Sm_N = 3.74 - 4.42), a pronounced negative Eu anomaly (Eu_N/Eu_N^* = 0.64 - 0.74), and flat heavy REE pattern (Gd_N/Yb_N = 0.99 - 1.11). The patterns show some degree of overlap and are not distinct for particular eruptive episodes nor biotite-bearing and biotite-poor/free lavas. The most REE enriched samples are those from the Ridge (Okareka episode) and Waikakareao (Waiohau episode) flows. The most REE depleted samples are those from the Rerewhakaaitu Eruptive Episode (Western and Rotomahana domes). All of the lavas have very similar negative Eu anomalies, which show a relationship to Rb/Sr, with increasing Rb/Sr generally accompanying increasingly negative Eu anomalies. Multi-element (spider) patterns also show some degree of overlap for the Tarawera Volcanic Complex rhyolite lavas. The most variation is seen in Sr, P and Ti, which will be affected by variable degrees of fractionation of observed phenocryst and accessory phases. In the Rerewhakaaitu episode the biotite-bearing lava (134) has notably higher Ba, Rb, Th and K than the biotite-free/poor lava (44).

As at the Haroharo Volcanic Complex, pyroclastic eruptions accompanied rhyolite lava extrusion during the four eruptive episodes that built up the Tarawera Volcanic Complex. Cole (1966) and Nairn (1992) present geochemical analyses which include the pyroclastic deposits all four eruptive episodes but, as for analyses of Haroharo pyroclastics, they are few in number and no indication in given as to whether they represent single or multiple clasts. Two recent studies have presented data sets for the Waiohau episode (Speed, 2001) and Kaharoa episode (Leonard, 1999).

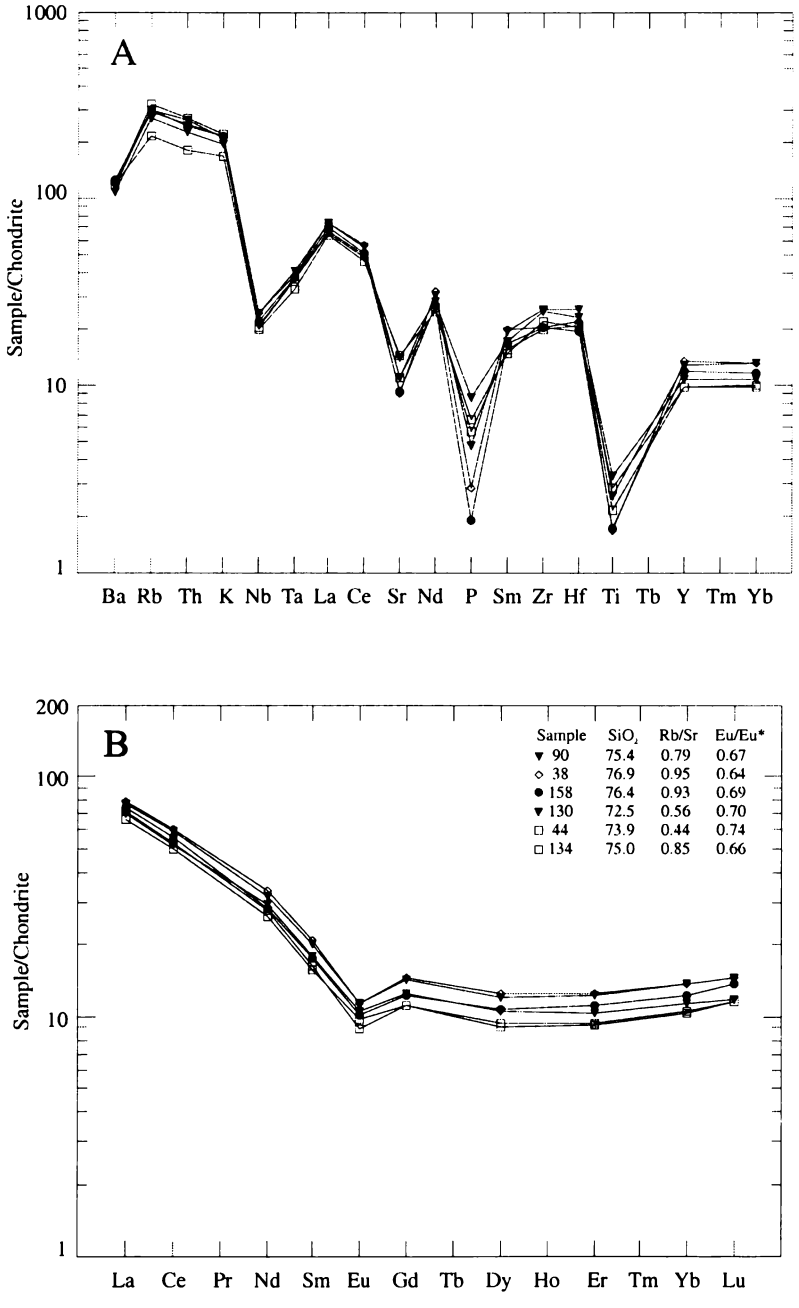

Figure 4.23: a) Chondrite-normalised multi-element (spider) patterns for the Tarawera Volcanic Complex ho_3 rhyolite lavas from the Okataina Volcanic Centre (normalisation values from Thompson et al., 1984). b) Chondrite-normalised REE abundance patterns for the Tarawera Volcanic Complex ho_3 rhyolite lavas (normalisation values from Boynton, 1984). Symbols as in Figure 4.21.

Figure 4.24 compares data obtained in this study for Waiohau episode lavas with the data obtained by Speed (2001) for pyroclastics erupted at this time. In addition, Speed (2001) also obtained samples of Eastern Dome and Kanakana Dome, which were not sampled in this study. These compositions are also indicated in Figure 4.24. Eastern Dome and Kanakana Dome have similar compositions to other lava flows erupted during this episode and sampled in this study. All of the lavas are compositionally similar to the Waiohau episode pyroclastics. There is no compositional difference between Eastern Dome and the lavas and pyroclastics erupted from the vent beneath Kanakana Dome. Speed (2001) noted that all eruptives from the Waiohau episode were derived from a magma that lacked a compositional or physical gradient, suggesting that the magma may have been vigorously convecting prior to eruption and/or did not reside in the crust for a prolonged period.

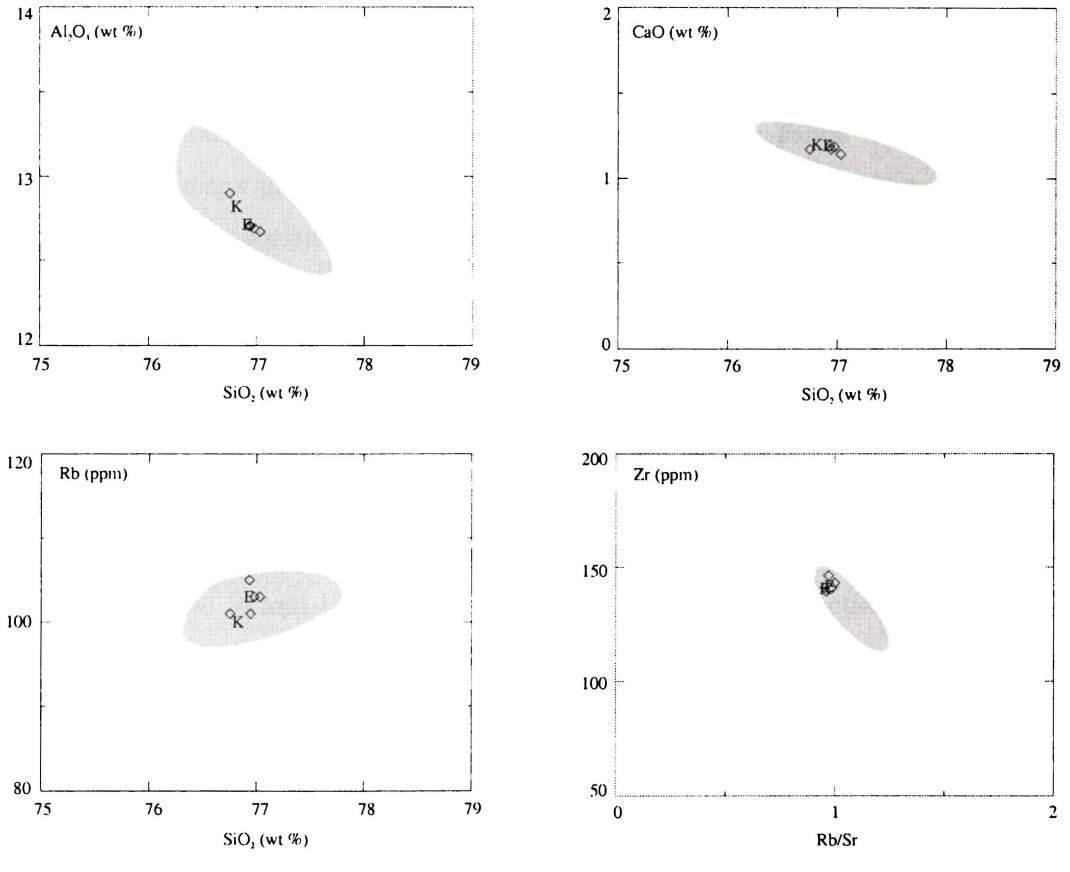

Figure 4.24: Selected major and trace element variation diagrams for rhyolite lavas erupted during the Waiohau episode at the Tarawera Volcanic Complex (open diamonds). Also shown are the compositions of Eastern Dome (E) and Kanakana Dome (K) from Speed (2001). The shaded area indicates compositions for the Waiohau episode pyroclastics from Speed (2001).

Figure 4.25 compares data obtained in this study for Kaharoa episode lavas with the data obtained by Leonard (1999) for lavas and pyroclastics erupted at this time. Leonard (1999) noted that block and ash flow rhyolites are petrographically and chemically identical to the outer carapace of the rhyolite lava domes, confirming their origin. He also found airfall rhyolite clasts to comprise two compositional groups, which generally correspond to the two groups of lavas. He went on to suggest that the range in compositions for the Kaharoa lavas and pyroclastics was the result of eruption from a stratified magma chamber with low-Zr and high-Zr layers. The low-Zr layer may have been depleted towards the end of the eruption, as the rhyolite domes are dominantly of the high-Zr magma type.

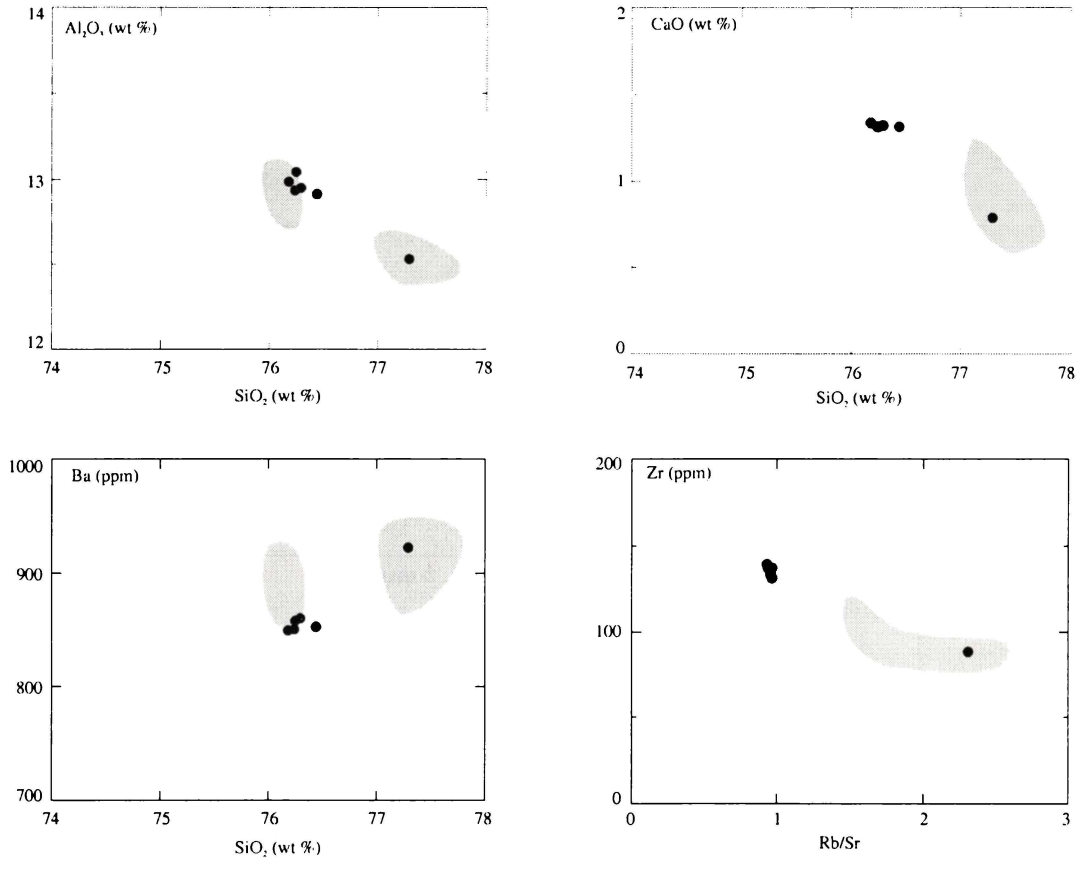

Figure 4.25: Selected major and trace element variation diagrams comparing rhyolite lavas erupted during the Kaharoa episode at the Tarawera Volcanic Complex (filled circles) with data for the Kaharoa lavas and pyroclastics from Leonard (1999) (shaded areas).

Figure 4.26 compares data obtained in this study for the oldest rhyolite lavas from the Haroharo, Okareka and Tarawera volcanic complexes, erupted in the Te Rere and Okareka episodes, with data for the Rotoiti Ignimbrite (from Schmitz, 1995) and the Mangaone Pyroclastics Subgroup (from Smith, 2001). Smith (2001) divided the Mangaone Pyroclastics into two main geochemical groups, which correlate with the stratigraphic sequence of eruptions and vent locations. The Old Mangaone Subgroup comprises Unit A - Unit F, erupted from a general north-south trending zone within the central part of the Haroharo Caldera. The Young Mangaone Subgroup comprises Unit I - Unit L, erupted from an east-west trending zone in the upper Puhipuhi Basin. Units G and H have compositions intermediate between the Old and Young Mangaone Subgroup (Smith, 2001).

Trends are observed in both major and trace elements with time for the Mangaone Pyroclastics. However, least squares modelling (Smith, 2001) indicates that the change in composition between the Old Mangaone Subgroup and Young Mangaone Subgroup is inconsistent with the expected effects of closed-system fractional crystallisation. Smith (2001) therefore concluded that the Old and Young Mangaone Subgroup tephras were derived from completely different magma systems with separate sources. Linear relationships in major and trace element compositions within each of these two groups are most likely to be associated with fractionation of the two individual magmatic systems (Smith 2001).

A comparison of the Rotoiti Ignimbrite and the Old Mangaone Subgroup shows that there are geochemical inconsistencies between these eruptives, with the Old Mangaone Subgroup erupting less evolved magma. There are also mineralogical and thermal differences, as the Old Mangaone Subgroup represents high temperature clinopyroxene-bearing magma (Smith, 2001), whereas the Rotoiti Ignimbrite contains cummingtonite and biotite and represents a lower temperature magma (Shane, 1998). Hence, it is unlikely that the Old Mangaone Subgroup tapped residual magma from the Rotoiti Ignimbrite eruption.

Geochemistry does not preclude a genetic relationship between the Young Mangaone Subgroup and the rhyolite lavas of subsequent eruptions, particularly the Te Rere lavas from Haroharo that are more evolved in terms of major and trace elements. However, Smith (2001) considered that the spatial separation of vent locations is compelling evidence for a lack of genetic relationship between the Young Mangaone Subgroup eruptives and the first eruptions from the Haroharo, Okareka and Tarawera volcanic complexes. In addition there

are temporal and thermal inconsistencies between the Young Mangaone Subgroup and subsequent eruptions (discussed further in Chapter Seven).

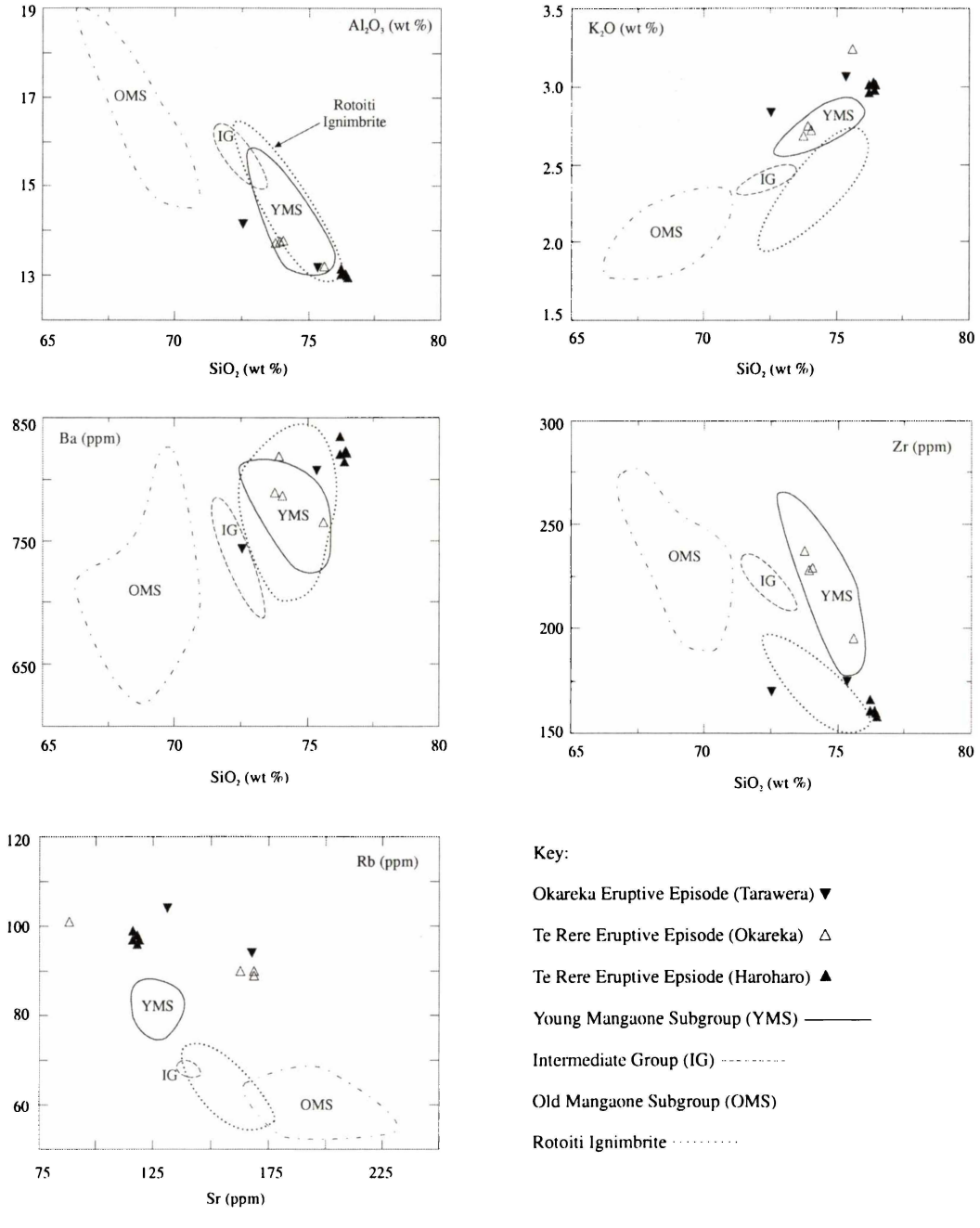

Figure 4.26: Selected major and trace element variation diagrams comparing rhyolite lavas erupted in the Te Rere and Okareka episodes, at the Haroharo/Okareka and Tarawera volcanic complexes respectively, with compositions for the Rotoiti Ignimbrite (from Schmitz, 1995) and the Mangaone Pyroclastics Subgroup (from Smith, 2001).

4.6 ROTORUA VOLCANIC CENTRE

Major and trace element compositions for the Rotorua Volcanic Centre rhyolite lavas are shown in Figures 4.27 and 4.28 respectively, where the rhyolites have been divided into three groups based on age. A small data set for the Rotorua Volcanic Centre rhyolite lavas facilitates plotting and discussion of the rhyolites as a group. Also shown in Figures 4.27 and 4.28 are compositions for the Endean Road and Umurua hr_1 rhyolites and the compositional field for the hr_2 rhyolites from Dravitzki (1999). There are no systematic trends in major and trace element compositions between the three age groups for the Rotorua Volcanic Centre rhyolite lavas.

The lavas obtained in this study have SiO_2 compositions ranging from ~ 73.5 - 77.6 wt. %. The hr_1 rhyolites have a wide range in compositions with SiO_2 ranging from ~ 73.7 - 77.6 wt. %. Samples from the Tokorangi and Hemo Gorge lavas on the southern rim of the Rotorua Volcanic Centre have higher SiO_2, K_2O, Ba, Rb/Sr and lower Al_2O_3, Fe_2O_3, CaO, Sr and Zr than the Endean Road and Hamurana rhyolites. Both of these rhyolites are phenocryst-poor (~3 - 5 %) and Tokorangi contains minor amounts of orthopyroxene while Hemo Gorge contains no ferromagnesian phenocrysts. These two factors are likely contributors to the elevated SiO_2 content and relatively depleted Al_2O_3, Fe_2O_3 and CaO contents of these lavas. In addition, the Tokorangi and Hemo Gorge lavas are geochemically similar to hk_1 lavas erupted from the Kapenga Volcanic Centre (section 4.7, Figures 4.31 and 4.32) and the possibility that they are Kapenga eruptives cannot be ruled out. Compositions from Dravitzki (1999) for the Endean Road and Umurua hr_1 rhyolites are similar to the Hamurana and Endean Road samples obtained in this study. In particular the two Endean Road samples are nearly identical in terms of their Fe_2O_3, CaO, K_2O, Rb, Sr and Zr compositions. The Endean Road, Hamurana and Tokorangi lavas have distinct compositions on plots of Sm vs. Hf and Ce vs. Eu. A small data set for the hr_1 rhyolites prevents a possible spatial subdivision based on geochemistry.

The hr_2 rhyolites sampled in this study have a restricted range in compositions and cluster into a single group with SiO_2 ranging from ~ 75.3 - 75.8 wt. %. Dravitzki (1999) sampled a larger number of the lavas comprising the Ngongotaha and Pukehangi dome complexes and compositions for these samples overlap with the compositions of samples obtained in this study. He noted a lack of substantial variation in major element compositions with Al_2O_3 and K_2O varying by 0.5 wt. % and all other major elements by less than 0.2 wt. %.

Dravitzki (1999) also observed that no clear distinction could be made between Ngongotaha and Pukehangi lavas based on their geochemistry and that there are no consistent trends in composition with age within either of these dome complexes, suggesting the domes were erupted over a relatively short period of time. In addition, no geochemical evidence was found to support the suggestion of evolution associated with fractionation of biotite and hornblende within the Summit and Te Miri domes (Chapter Three, section 3.9.2).

The rhyolite dome at Kawaha Point has a composition indistinguishable from the Ngongotaha-Pukehangi lavas. This lends support to the theory, suggested by Wood (1992), that these rhyolites are all part of an extensive, partially buried rhyolite volcano complex. The Pukeroa Hill rhyolite, which is also considered to be part of this complex, lies adjacent to the Kuirau Park geothermal area. Previous studies have found it to be hydrothermally altered both in outcrop and at depth in drill cores and consequently it was not sampled in this study. However, its composition can be expected to be similar to the other hr_2 rhyolites.

The hr_3 rhyolites fall into two groups. The sample of biotite-free Mokoia Island has a SiO_2 content of ~ 75.4 wt. % and has a generally similar composition to the hr_2 rhyolite lavas. The biotite-bearing lavas from Hinemoa Point and Vaughan Road have lower SiO_2, Rb/Sr and higher Al_2O_3, Fe_2O_3, CaO, Ba, Sr contents. While many major and trace elements show differences for these two groups of lavas, they have similar Ce, Eu, Th/Ce and K/Ce compositions.

Figure 4.29 shows chondrite-normalised multi-element (spider) and REE abundance patterns for representative Rotorua Volcanic Centre rhyolite lavas. These patterns are similar to those seen for the Okataina Volcanic Centre rhyolite lavas. The REE abundance patterns are characterised by a strongly enriched light REE pattern with steep slopes (La_N/Sm_N = 3.33 - 4.97), a pronounced negative Eu anomaly (Eu_N/Eu_N^* = 0.48 - 0.77), and flat heavy REE pattern (Gd_N/Yb_N = 1.01 - 1.28). With the exception of the sample of Tokorangi (84) the Eu anomaly varies systematically with REE abundance, with the most depleted lavas having the smallest negative Eu anomalies and the most REE enriched lavas having the largest negative Eu anomalies. The Eu anomaly shows no relationship to SiO_2 content or Rb/Sr. The hr_2 rhyolite lavas have the most enriched REE patterns while the hr_1 and hr_3 rhyolite lavas show overlapping patterns. The two biotite-bearing lavas (Endean Road (87) and Vaughan Road (104)) have the lowest compositions of most REE, with Endean Road being depleted relative to Vaughan Road. With the exception of La, Ce and Lu, Vaughan

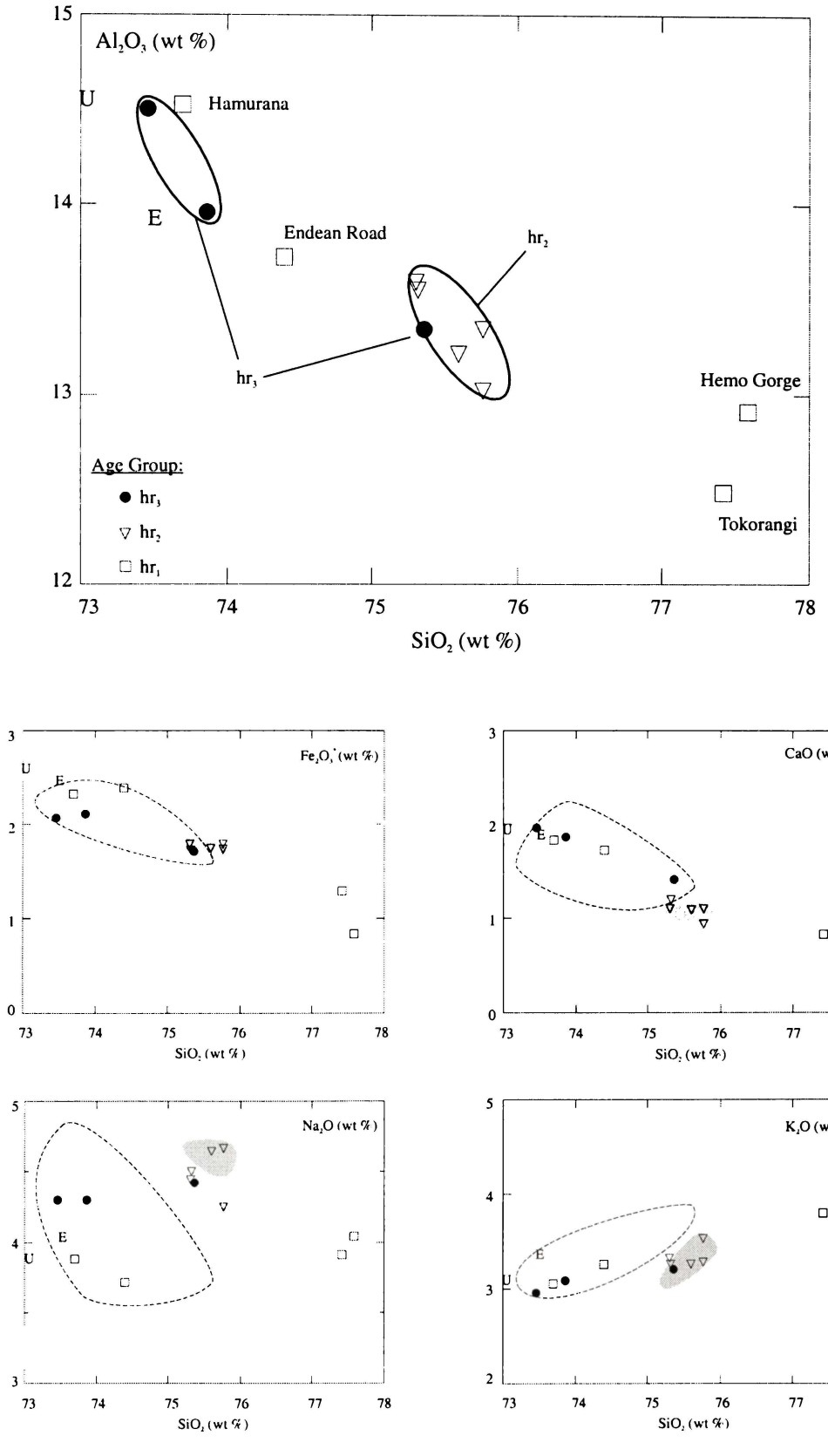

Figure 4.27: Selected major element variation diagrams for rhyolite lavas from the Rotorua Volcanic Centre. Also shown are compositions for the Endean Road (E) and Umurua (U) hr_1 rhyolites and the hr_2 rhyolites (shaded area) from Dravitzki (1999). Compositions for the Waimakariri Ignimbrite (from Karhunen (1993) and Lynch-Blosse (1998)) are enclosed by the dashed line.

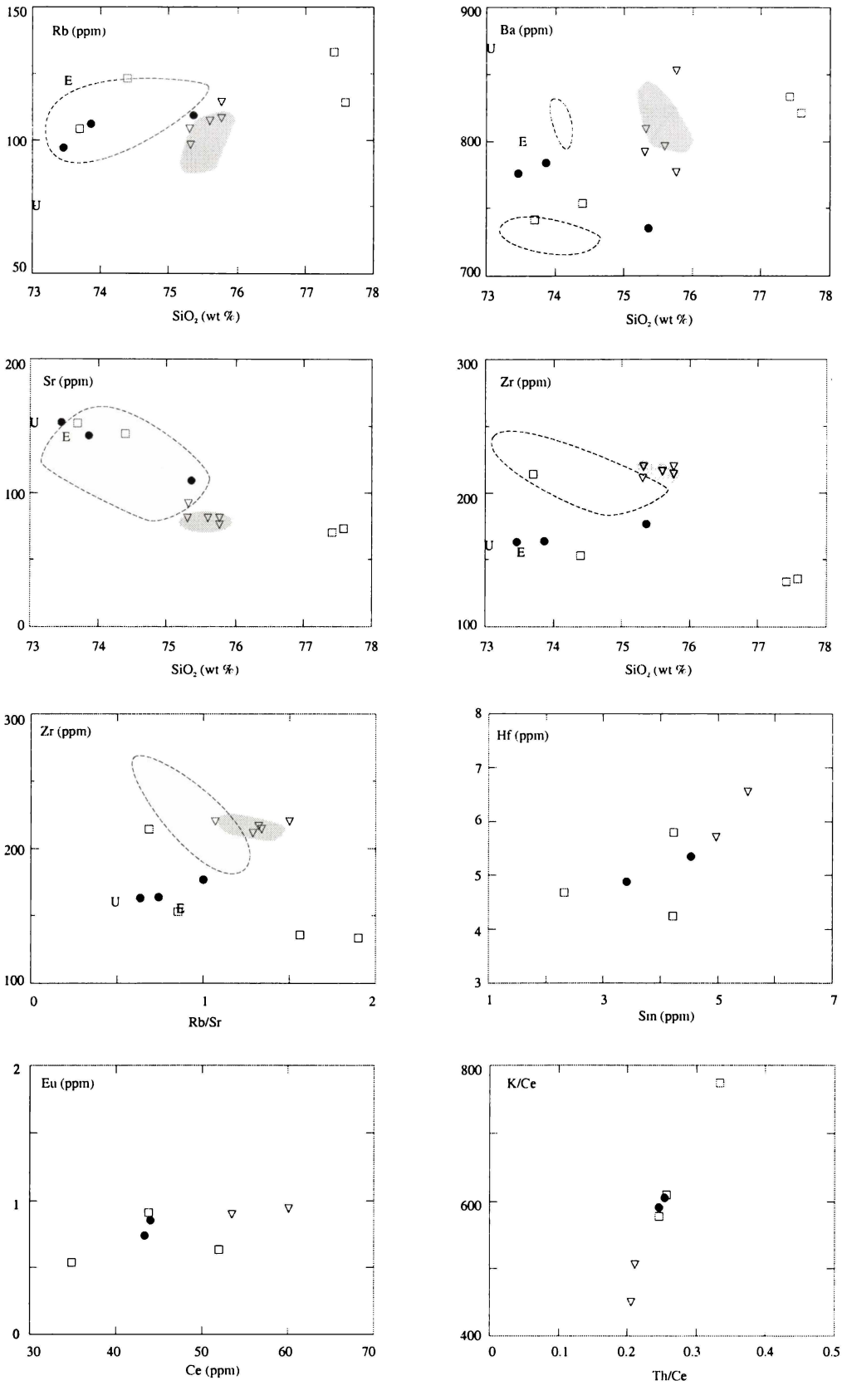

Figure 4.28: Selected trace element variation diagrams for rhyolite lavas from the Rotorua Volcanic Centre. Symbols as in Figure 4.27. Compositions for the Waimakariri Ignimbrite (from Karhunen (1993) and Lynch-Blosse (1998)) are enclosed by the dashed line.

Road has lower REE contents than the temporally similar but biotite-free Mokoia Island lava (103). Multi-element (spider) patterns show the same relative abundances of the elements as the REE patterns. Once again the most variation between patterns is seen in Sr, P and Ti. The sample from the Endean Road rhyolite stands out as having lower Yb, Y, Sm, P, Nd, Ce and La than the rest of the Rotorua rhyolite lavas.

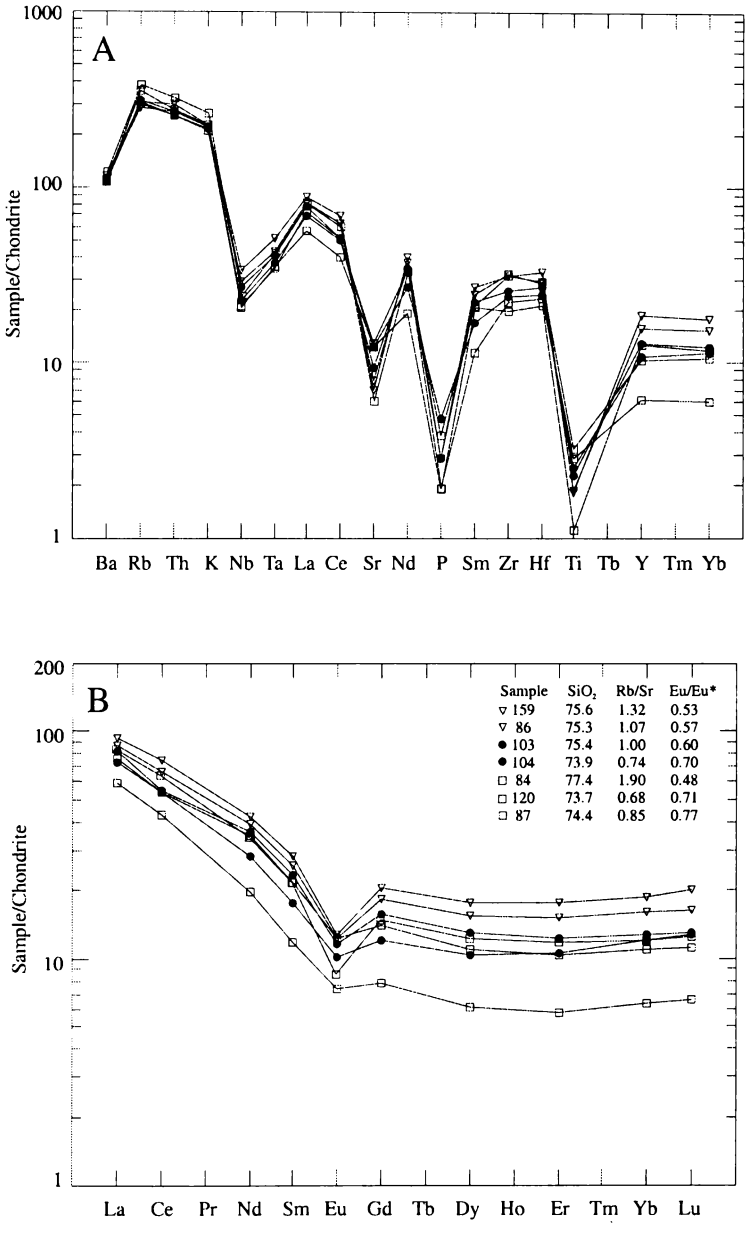

Figure 4.29: a) Chondrite-normalised multi-element (spider) patterns for rhyolite lavas from the Rotorua Volcanic Centre (normalisation values from Thompson et al., 1984). b) Chondrite-normalised REE abundance patterns for rhyolite lavas from the Rotorua Volcanic Centre (normalisation values from Boynton, 1984). Symbols as in Figure 4.27.

To date three pyroclastic units have been attributed to the Rotorua Volcanic Centre. Dravitzki (1999) noted four minor localised ignimbrites, collectively termed the Paradise Valley Ignimbrites, outcropping in the Paradise and Utuhina Valleys to the west of Rotorua City and adjacent to the Ngongotaha and Pukehangi complexes. Dravitzki (1999) noted that, although they show greater scatter resulting from higher crystal contents and LOI values, the compositions of these ignimbrites are similar to the Ngongotaha and Pukehangi rhyolites providing strong evidence for a genetic relationship. Lynch-Blosse (1998) attributes the Waimakariri Ignimbrite to the Rotorua Volcanic Centre. The range in composition for pumice clasts from the Waimakariri Ignimbrite is indicated in Figures 4.27 and 4.28. A small data set for the hr_1 rhyolites, a lack of absolute ages and hence uncertainty as to whether the lavas represent pre- or post-ignimbrite eruptives, prevents a detailed comparison. However, Lynch-Blosse suggested that at least some of the hr_1 rhyolites represent the eruption of degassed magma following the Waimakariri Ignimbrite eruption. Comparable compositions for the hr_1 lavas and the ignimbrite may be consistent with such a theory.

Figure 4.30 compares data obtained in this study for the Rotorua Volcanic Centre rhyolite lavas with data obtained by Milner (2001) for pumice clasts from the Mamaku Ignimbrite, which is attributed to caldera collapse at the Rotorua Volcanic Centre.

Milner (2001) notes that geochemistry reveals the occurrence of three silicic pumice types. Types 1 and 2 are rhyolitic, with Type 2 being the most common pumice type, and Type 3 is dacitic. No large compositional gaps exist between the pumice types hence providing support for the evacuation of a gradationally zoned magma chamber. Modelling by Milner (2001) suggests that the more silicic pumice compositions were probably derived by ~ 20% plagioclase dominated fractionation from the dacitic magma. Pumice clasts from the Mamaku Ignimbrite have compositions similar to many of the rhyolite lavas erupted from the Rotorua Volcanic Centre. However, differences in ferromagnesian mineralogy preclude a genetic relationship between most of the hr_1 and hr_3 rhyolite lavas and the Mamaku Ignimbrite. Milner (2001) considers that geochemical similarities between the hr_2 rhyolite lavas and the Mamaku Ignimbrite, in association with mineralogical similarities (which have also been noted in this study), support a genetic relationship.

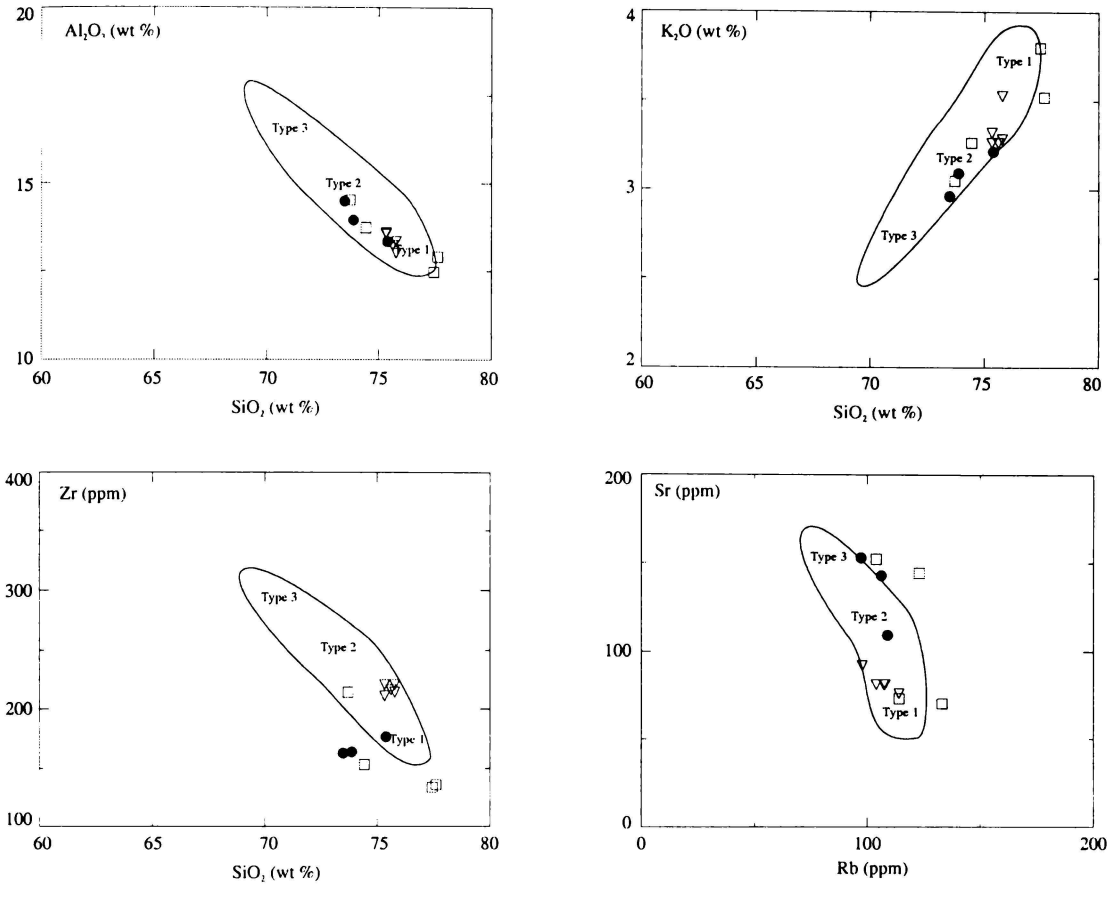

Figure 4.30: Selected major and trace element variation diagrams for rhyolite lavas from the Rotorua Volcanic Centre. Symbols as in Figure 4.27. Also shown are the compositions of pumice clasts (Types 1 - 3, see text for explanation) in the Mamaku Ignimbrite (from Milner, 2001).

4.7 KAPENGA VOLCANIC CENTRE

Major and trace element compositions for the Kapenga Volcanic Centre rhyolite lavas are shown in Figures 4.31 and 4.32 respectively, where the rhyolites have been divided into two groups based on age. Also shown are compositions for the Tokorangi and Hemo Gorge hr_1 rhyolites, the Upper Atiamuri rhyolites and the compositional field for the biotite-bearing ho_2 rhyolites. A small data set facilitates plotting and discussion of the Kapenga Volcanic Centre rhyolite lavas as a group.

Rhyolite lavas obtained in this study from the Kapenga Volcanic Centre have SiO_2 compositions ranging from ~ 72.7 - 76.8 wt. %. The hk_1 rhyolites have compositions ranging from ~ 75.8 - 76.8 wt. % SiO_2. Samples of the Tokorangi and Hemo Gorge

rhyolites, which have been previously classed as hr_1 eruptives, have slightly higher SiO_2 compositions but very similar Fe_2O_3, CaO, Na_2O, K_2O, Rb, Sr, La, Ce and Th/Ce compositions to the hk_1 rhyolites. The Upper Atiamuri rhyolites, which lie on or just beyond the southwestern edge of the Kapenga Volcanic Centre, have compositions with notably lower SiO_2 and higher CaO, Sr and Zr than the hk_1 rhyolites. The Horohoro and North Haparangi Ridge rhyolites have very similar major and trace element compositions. Spatially adjacent Tumunui and Waikorapa show some differences in composition, particularly in SiO_2, Fe_2O_3, Na_2O, Ba and Zr, which may be suggestive of minor magmatic evolution over the time that they were erupted. The highly elevated Ba in Waikorapa suggests post-depositional alteration of this lava. There is no geochemical data on which to base a spatial subdivision of the hk_1 rhyolites.

The hk_2 rhyolites have compositions ranging from ~ 72.7 - 74.2 wt. % SiO_2. Two samples have elevated Al_2O_3 from the other lavas (one of these has a highly elevated Ba content), which suggests that weathering, or other post-depositional alteration processes, have affected their composition. The hk_2 lavas that show no geochemical evidence of alteration have very similar major and trace element compositions to the biotite-bearing ho_2 rhyolites erupted in the southwestern Okataina Volcanic Centre, or area of possible overlap between the Okataina and Kapenga volcanic centres. This suggests a genetic relationship between these ho_2 lavas and lavas which occur well inside the Kapenga Volcanic Centre.

Figure 4.33 shows chondrite-normalised multi-element (spider) and REE abundance patterns for representative Kapenga Volcanic Centre rhyolite lavas. These patterns are similar to those seen for rhyolite lavas from the Okataina and Rotorua volcanic centres. The REE abundance patterns are characterised by a strongly enriched light REE pattern with steep slopes (La_N/Sm_N = 3.48 - 4.44), a pronounced negative Eu anomaly (Eu_N/Eu_N^* = 0.55 - 0.81), and flat heavy REE pattern (Gd_N/Yb_N = 1.02 - 1.11). The Eu anomaly shows no relationship to REE abundance, SiO_2 content or Rb/Sr. The biotite-free hk_1 rhyolites generally have higher REE contents than the biotite-bearing hk_2 rhyolites. Horohoro (126) has the most enriched REE pattern and the largest negative Eu anomaly. The pattern for the Tokorangi rhyolite shows that it has REE compositions similar to those for the hk_1 rhyolites. A comparison with the range of compositions for the biotite-bearing ho_2 rhyolites shows that the hk_2 rhyolites and the biotite-bearing ho_2 rhyolites have very similar REE abundances. The inclusion of more trace elements in the multi-element (spider) patterns results in overlapping patterns for the hk_1 and hk_2 rhyolites.

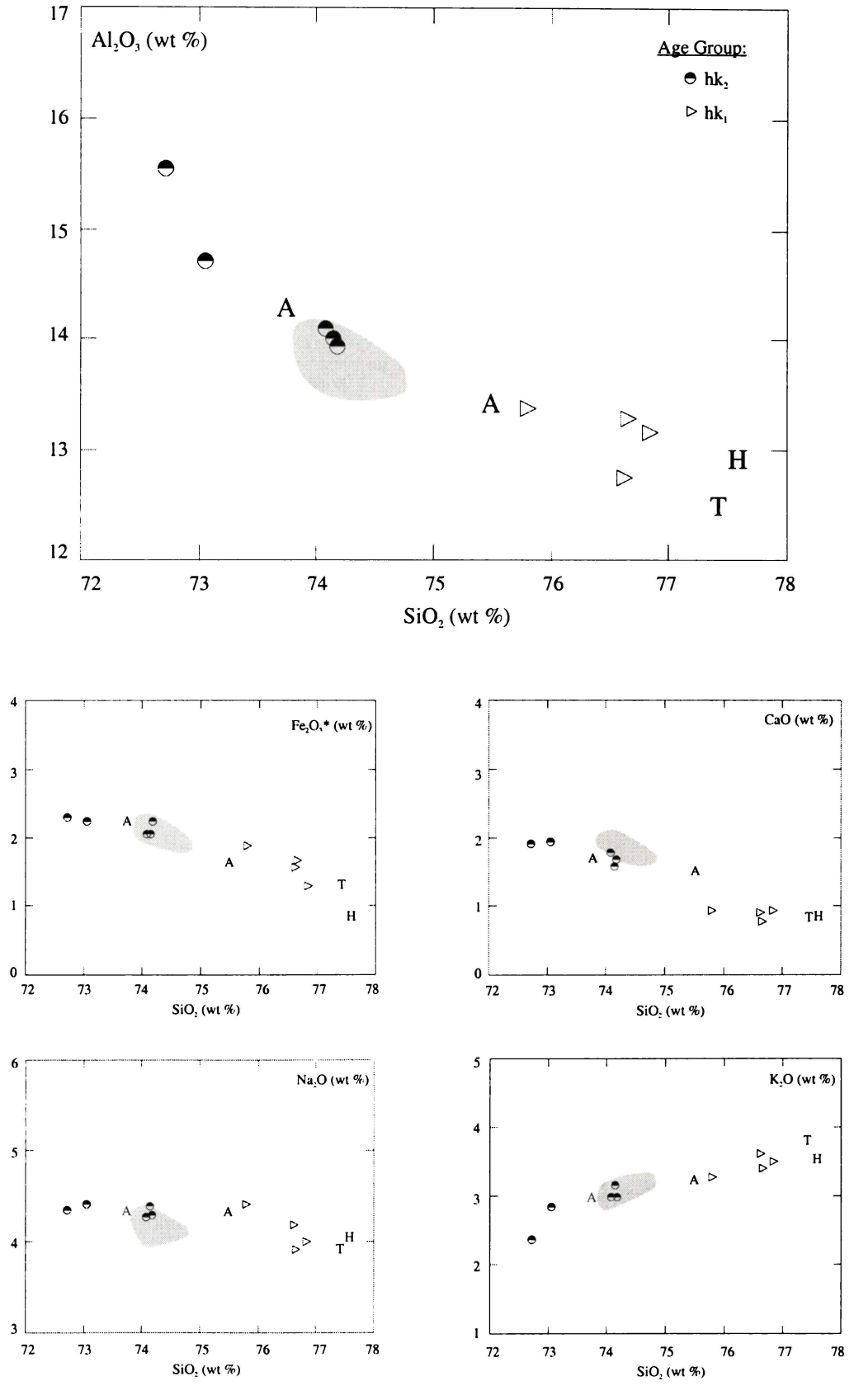

Figure 4.31: Selected major element variation diagrams for rhyolite lavas from the Kapenga Volcanic Centre. Also shown are compositions for the Tokorangi (T) and Hemo Gorge (H) hr_1 rhyolite lavas, the Upper Atiamuri (A) rhyolite lavas and the biotite-bearing ho_2 rhyolite lavas (shaded area).

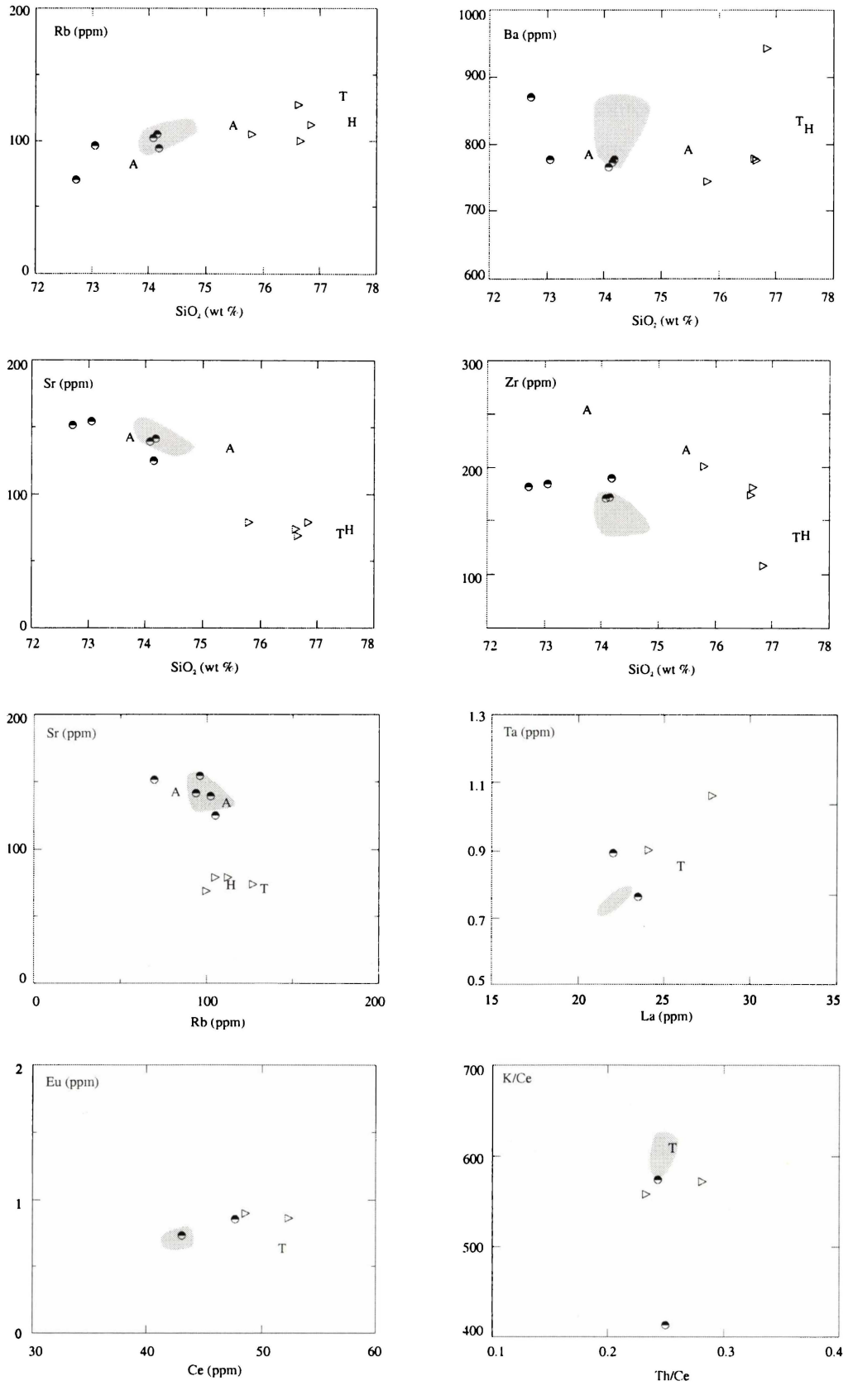

Figure 4.32: Selected trace element variation diagrams for rhyolite lavas from the Kapenga Volcanic Centre. Symbols as in Figure 4.31. Also shown are compositions for the biotite-bearing ho_2 rhyolite lavas (shaded area).

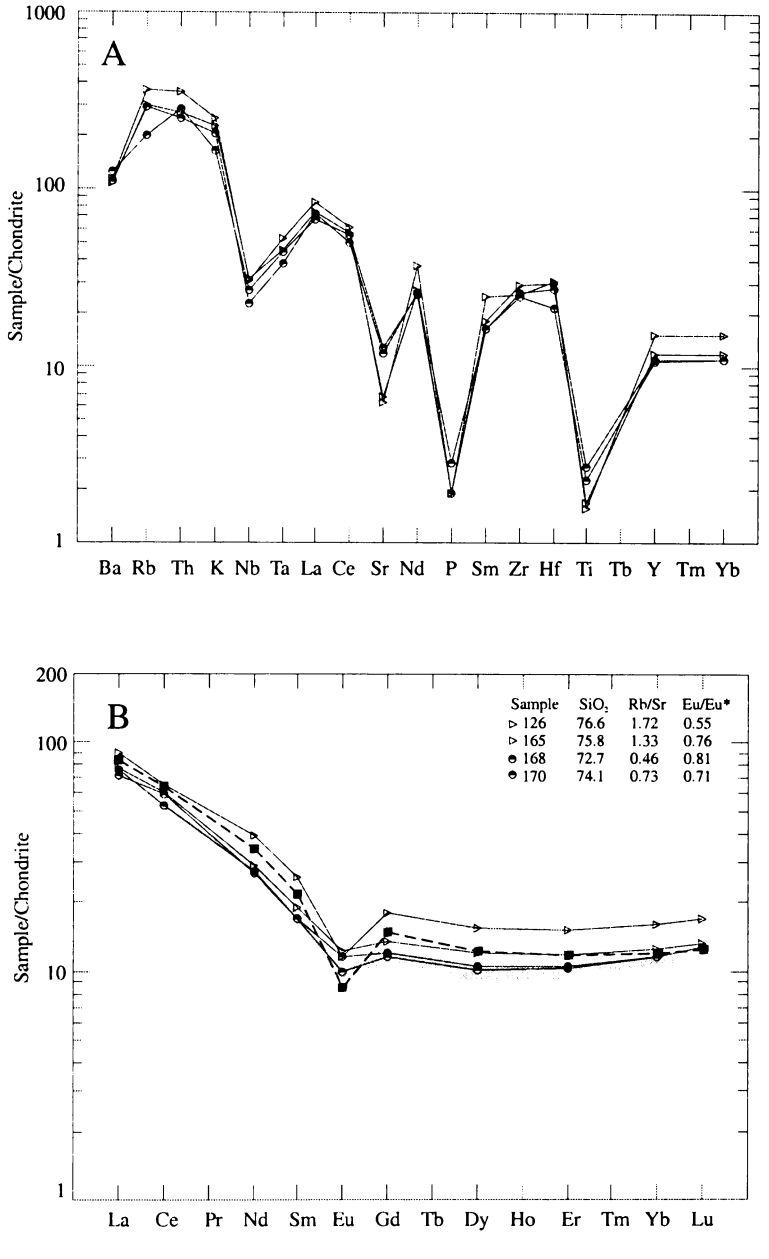

Figure 4.33: a) Chondrite-normalised multi-element (spider) patterns for rhyolite lavas from the Kapenga Volcanic Centre (normalisation values from Thompson et al., 1984). b) Chondrite-normalised REE abundance patterns for rhyolite lavas from the Kapenga Volcanic Centre (normalisation values from Boynton, 1984). Symbols as in Figure 4.31. Shaded area indicates the range in patterns for the biotite-bearing ho_2 rhyolite lavas. Dashed line indicates the pattern for Tokorangi (hr_1) rhyolite.

A comparison between the hk_1 rhyolites and the caldera-forming ignimbrites of the Kapenga Volcanic Centre is hindered by a lack of knowledge regarding the age of the rhyolite lavas relative to the seven caldera-forming ignimbrites currently attributed to Kapenga. Figure 4.34 shows the Rb, Sr, Zr and Na_2O/CaO composition of the hk_1, hk_2, Tokorangi, Hemo

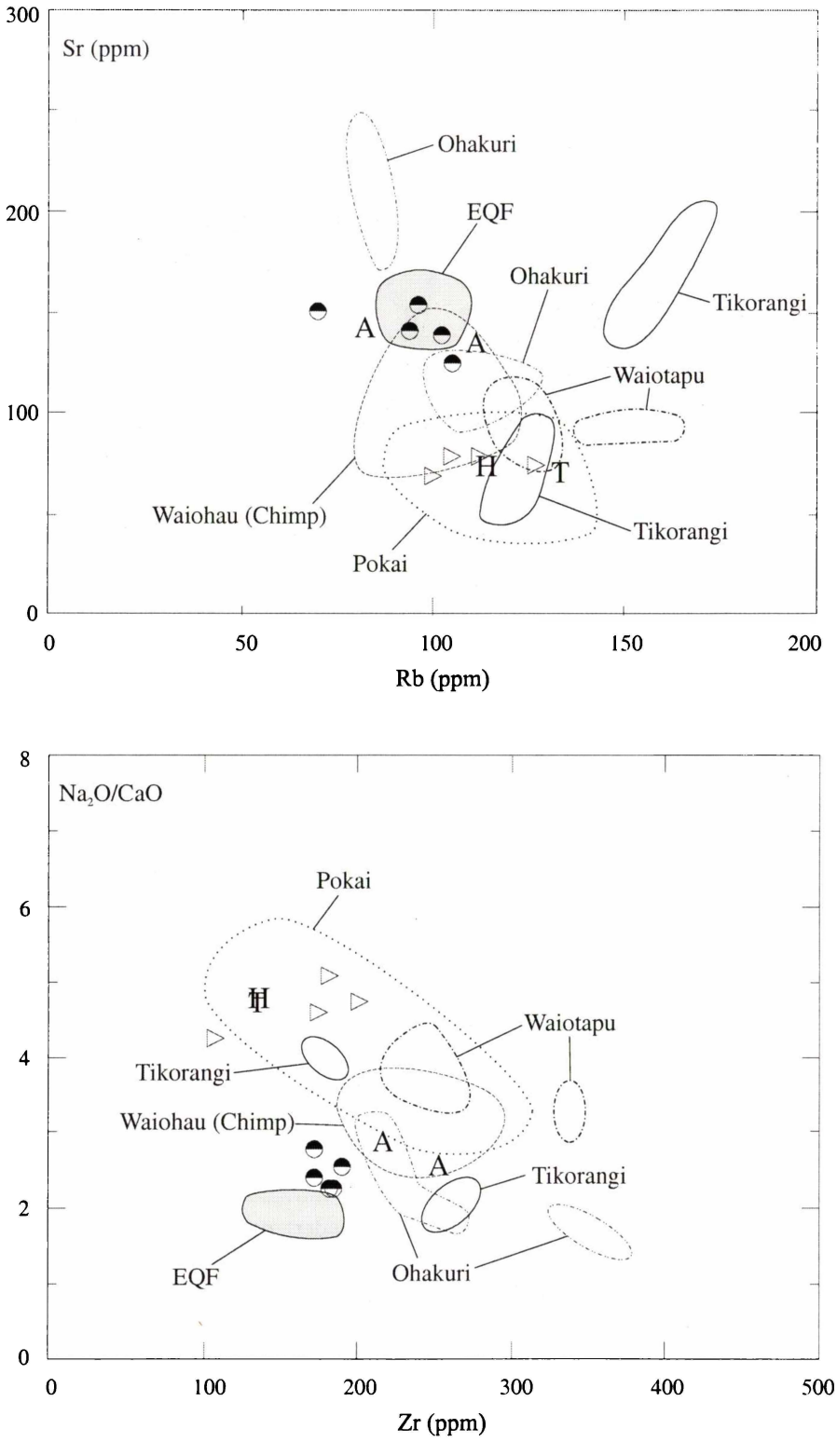

Figure 4.34: Rb vs Sr and Zr vs Na_2O/CaO plots comparing compositions of the Kapenga Volcanic Centre rhyolite lavas and the Tokorangi, Hemo Gorge and Upper Atiamuri rhyolite lavas (symbols as in Figure 4.31) to the caldera-forming ignimbrites attributed to the Kapenga Volcanic Centre and the Earthquake Flat Ignimbrite. Data for the ignimbrites from Davis (1985), Langridge (1990), Karhunen (1993), Bowyer (1997), Ritchie (1996), Lynch-Blosse (1998) and Hildyard et al. (2000). Only rhyolitic compositions are shown for the Tikorangi Ignimbrite.

Gorge and Upper Atiamuri rhyolite lavas and available data for the caldera-forming ignimbrites attributed to the Kapenga Volcanic Centre. The hk_1, Tokorangi and Hemo Gorge rhyolites show geochemical similarities to the Pokai Ignimbrite. However, the significantly larger data set for the Pokai Ignimbrite compared to the other caldera-forming ignimbrites may predispose such a similarity. In addition only the Pokai Ignimbrite was found to contain pumice clasts with SiO_2 > 76 wt. % (Karhunen, 1993; Lynch-Blosse, 1998), similar to most of these rhyolite lavas. The hk_2 rhyolites not only show geochemical similarities to the biotite-bearing ho_2 rhyolites, but both groups show similarities to the non-caldera forming Earthquake Flat Ignimbrite (see also Figures 4.9 and 4.10). A comparison of available data for the ignimbrites suggests that there has been no systematic variation in compositions erupted over the early history of the Kapenga Volcanic Centre. However, a much more thorough study of the ignimbrites would be required to ratify such conclusions.

4.8 Comparison Between Volcanic Centres

As can be seen in Figures 4.5 - 4.33, major and trace element compositions for rhyolite lavas from the Okataina, Rotorua and Kapenga volcanic centres are very similar. In summarising REE data for Taupo Volcanic Zone rhyolites, Graham et al. (1995) note that there are no clear trends in REE patterns or overall abundances which correlate with age, volcanic centre or bulk rock composition. They suggest that the similarity in REE patterns from magmas which were widely separate in time and space indicates essentially similar processes of magma generation have operated at all Taupo Volcanic Zone rhyolitic centres. Lack of compositional differences between the Okataina, Rotorua and Kapenga volcanic centres and significant compositional variability in samples obtained from a particular centre prevents a distinction between these centres using geochemistry. This is seen in Figure 4.35, which shows selected major and trace element variation diagrams for the rhyolites of the Okataina, Rotorua and Kapenga volcanic centres. Although a large group of Okataina rhyolites commonly cluster together or fall on a linear trend, outlying samples and scatter in samples from the Rotorua and Kapenga volcanic centres prevent distinctions being made. A volcanic centre distinction similar to that obtained by Shane (2000) for Okataina and Taupo, although he used tephra glass shard analyses, is not possible using the whole rock compositions of rhyolite lavas obtained in this study. Adding geochemical data for the pyroclastics to these plots would only serve to create further confusion as they commonly show more scatter than the lavas.

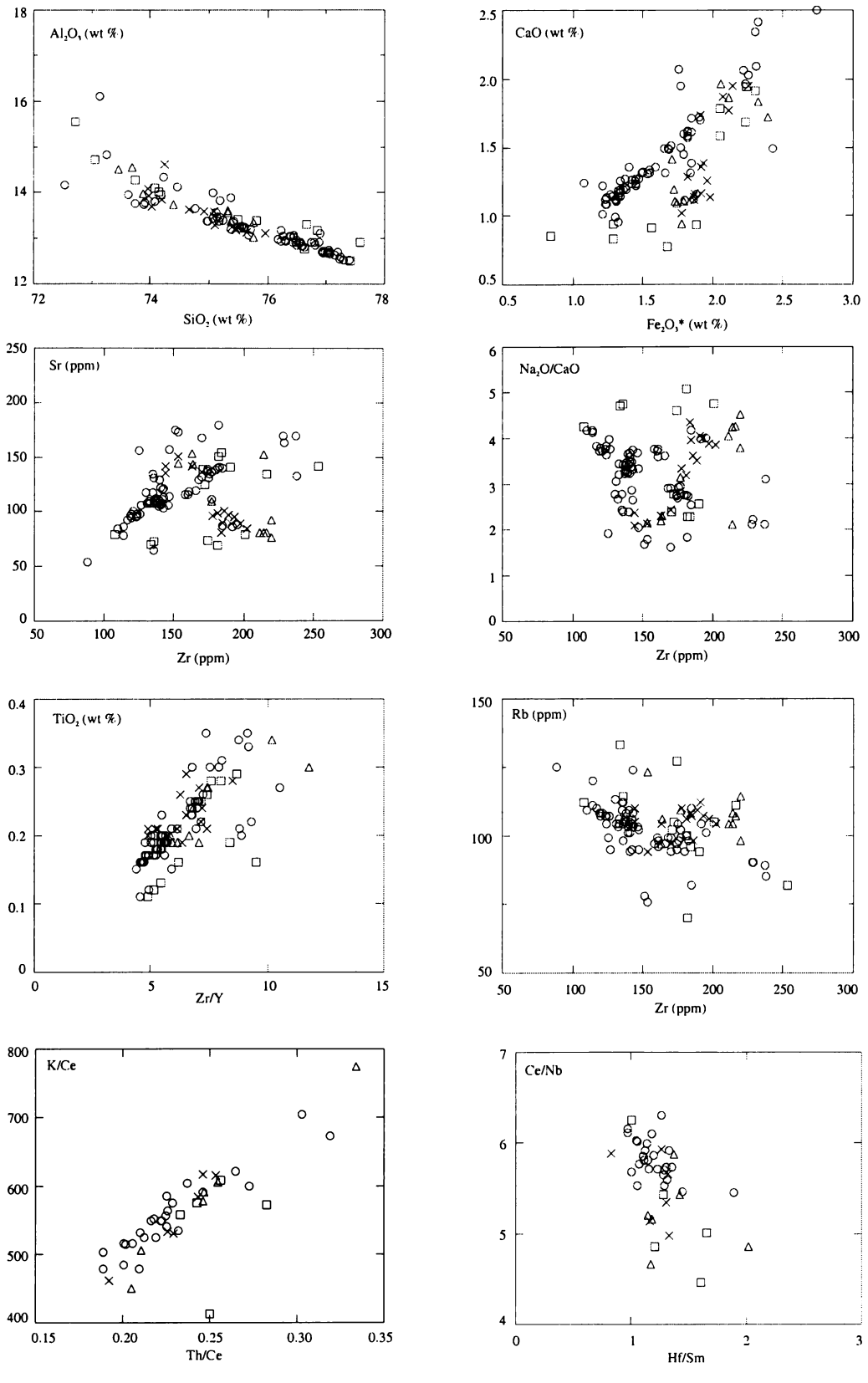

Figure 4.35: Selected major and trace element variation diagrams comparing the compositions of rhyolites from the Okataina, Rotorua and Kapenga volcanic centres (open circles, triangles and squares respectively). Crosses indicate the ho_2 rhyolites occurring in the transition zone between the Okataina and Kapenga volcanic centres.

Hence in this study, no geochemical means has been found on which to base a classification scheme for rhyolites from these three volcanic centres. A particular geochemical signature cannot be ascribed to a particular volcanic centre and therefore such signatures cannot be used as a means of classifying the ho_2 rhyolites as being eruptives of either the Okataina or Kapenga volcanic centres.

4.9 BASALTS OF THE OKATAINA AND KAPENGA VOLCANIC CENTRES

During the early stages of this research a possible aim was to study basalt-rhyolite relationships at the Okataina Volcanic Centre. This has been the subject of other studies (e.g. Leonard, 1999) and hence this line of research was not pursued. However, several samples were obtained of basaltic scoria deposits erupted from the Okataina and Kapenga volcanic centres and these were analysed for major and trace elements by XRF (Appendix V, Table V.2). Purely for comparative purposes these data are shown along with the compositions of the rhyolite lavas in Figure 4.36. The scoria deposits can be classified as either basalt or basaltic-andesite with SiO_2 contents ranging from ~ 50.6 - 55.7 wt. %. For the Tarawera Basalt (sample number 47) and the Rotomakariri Scoria (136) two samples were analysed. One sample had all rhyolitic clasts or inclusions removed (picked) and the remaining sample (unpicked) was analysed without any clasts or inclusions being removed. Unpicked samples have slightly higher SiO_2 contents (up to ~ 0.7 wt. % higher) and incompatible elements (e.g. Rb, Ba, Zr) and slightly lower compatible elements (e.g. Sr) than picked samples.

Most basaltic scoria samples cluster together on variation diagrams. The exceptions are the Matahi Scoria which has a higher SiO_2 content and plots away from the main group, and the Johnson Road Basalt (the only Kapenga Volcanic Centre basalt sampled) which has similar SiO_2 but higher Zr and Sr. The Rotokawau Basalt also has a higher Sr content than the other Okataina Volcanic Centre scoria deposits. These basalts have compositions typical for Taupo Volcanic Zone high-alumina basalts (Gamble et al., 1993; Graham et al., 1995). The composition of the rare basaltic deposits erupted in the Taupo Volcanic Zone may be the best approximation we have to a mantle source component for the rhyolite lavas. This will be discussed further in Chapter Six.

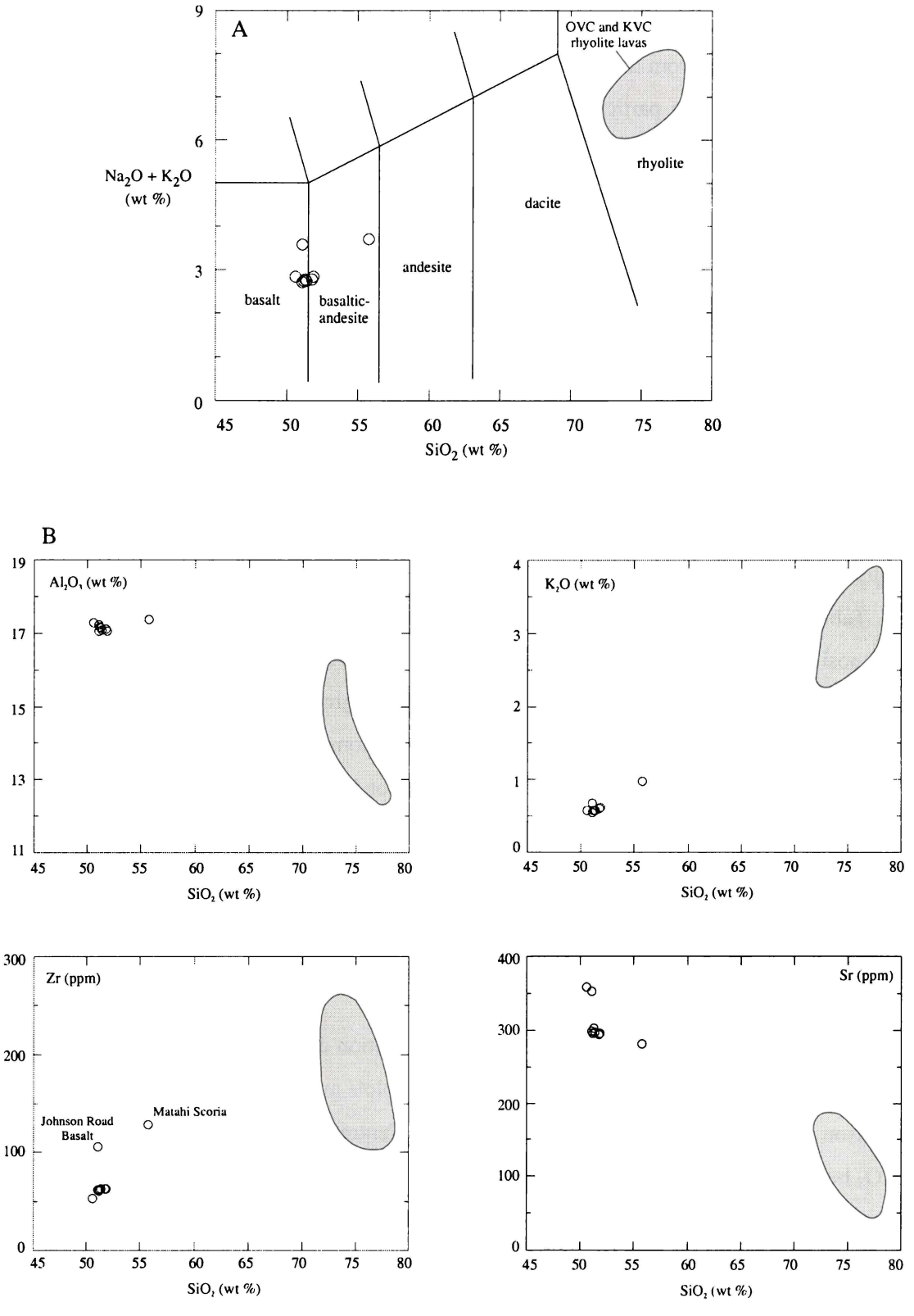

Figure 4.36: Comparison of the composition of basaltic scoria and rhyolite lavas erupted from the Okataina and Kapenga volcanic centres. a) Classification according to the total alkalis versus silica (TAS) diagram of Le Bas et al. (1986). b) Selected major and trace element variation diagrams.

4.10 MELT INCLUSION STUDIES

The major element composition of melt inclusions in quartz phenocrysts from rhyolite lavas of the Haroharo Volcanic Complex were determined by electron probe microanalysis using the JEOL 733 Superprobe in the Analytical Facility, Victoria University of Wellington (Appendix VIII). The rhyolite lavas were crushed and felsic phenocrysts were concentrated using standard magnetic separation techniques. The grains were then mounted in epoxy resin, the mounts were ground down to reveal melt inclusions and finally the surface of the mounts were polished. As a means of comparison, the composition of the glass groundmass of the host rhyolite lava was also determined by analysing multiple points on a polished whole rock thin section slide (Appendix VIII). For glass and melt inclusion analyses an electron beam diameter of 10μm was used in order to minimise the effects of alkali migration.

Melt inclusions represent quenched samples of non-degassed magma that became entrapped during phenocryst growth prior to eruption. The compositions of melt inclusions preserve the composition of the melt at different stages during magma evolution and crystal fractionation processes, and may hence record compositions along the liquid line of descent of a magma (Roedder, 1984). Hervig et al. (1989) note that while melt inclusions represent the composition of the magma at the time and place of entrapment, they may not necessarily be representative of the entire magma chamber.

As all melt inclusions analysed in this study were entrapped in quartz phenocrysts, which only crystallise from silicic melts, they will only record melt compositions at the more silicic end of the magmatic evolution spectrum. Many of the melt inclusions have compositions comparable to the glass groundmass of the rhyolite lavas, which corroborate this. Hence, use of these melt inclusions in tracing magmatic liquid lines of descent is limited. In addition, their use in fingerprinting the possible interaction of silicic magmas with less silicic melts is also limited. Certainly this latter case is a potentially very interesting area of study, particularly as it is considered that basaltic and rhyolitic magmas interact beneath the volcanic centres of the Taupo Volcanic Zone (including the Okataina Volcanic Centre). This is a possible area of future in-depth study.

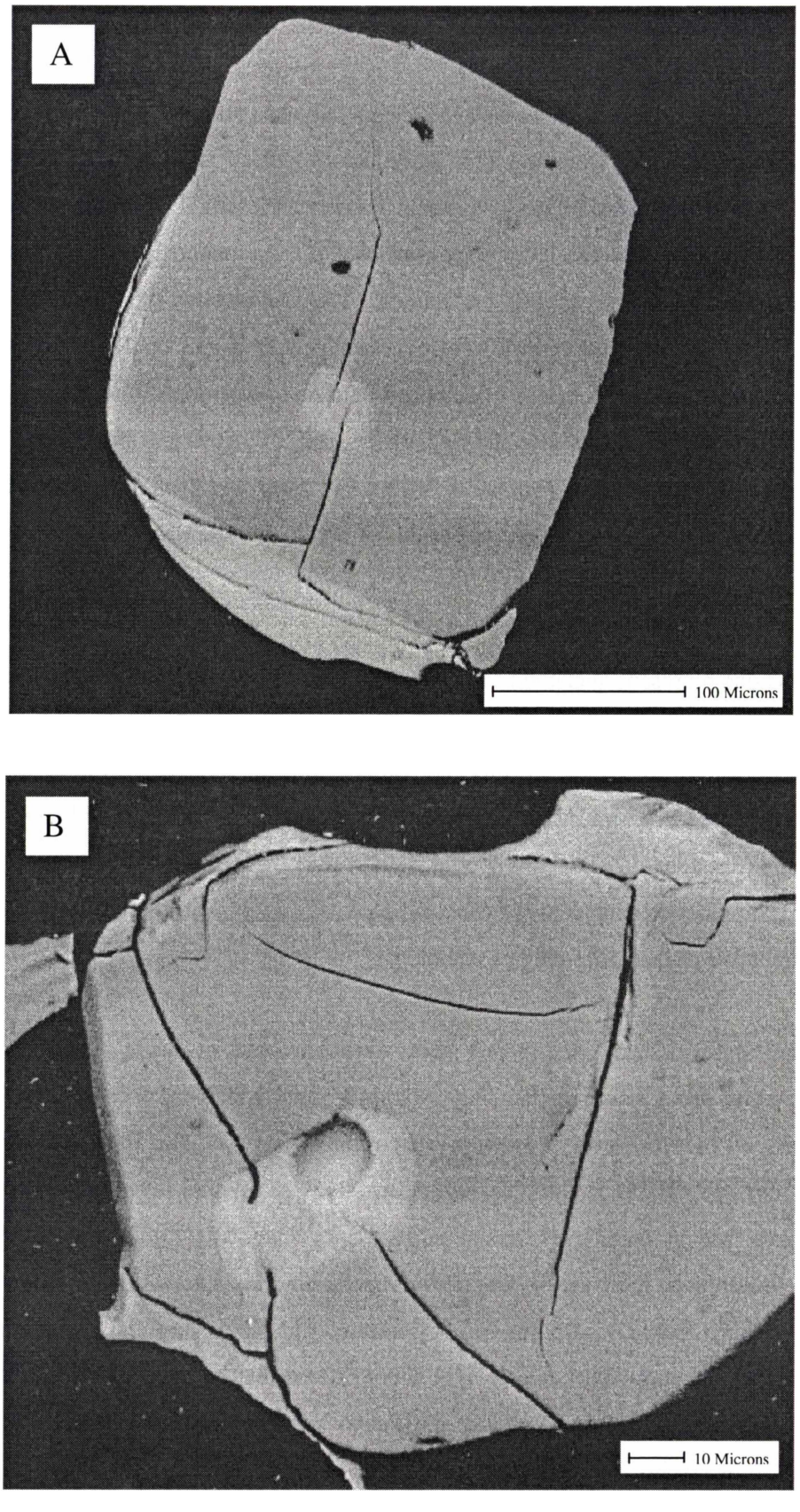

Plate 4.1: Back scattered electron images of melt inclusions in quartz phenocrysts. a) Waiti Flow (sample number 173), melt inclusion 3. b) Hainini Dome (7), melt inclusion 5. Note the cracks terminating in the melt inclusions and the vapour bubble in b).

The melt inclusions observed in quartz phenocrysts in the Haroharo Volcanic Complex rhyolite lavas contain clear to pale brown/purple glass in plane-polarised light. In a back scattered electron image they are slightly paler in colour than the host quartz crystal (Plate 4.1). The inclusions may contain vapour bubbles (Plate 4.1b), which were avoided during analysis. Most melt inclusions were seen to occur at the termination point of cracks running through the quartz crystals (Plate 4.1). This is likely to be as a result of the melt inclusion or melt inclusion-quartz boundary being a point of weakness within the crystal. In some cases the melt inclusion appeared to be elongated in shape along these cracks, which suggests possible leakage of the melt. This type of inclusion was avoided during analysis.

Numerous studies have utilised melt inclusion compositions to determine the pre-eruptive volatile contents of magmas such as H_2O, F and Cl (e.g. Dunbar et al., 1989; Hervig et al., 1989). This line of investigation was not carried out in this study.

The compositions of melt inclusions are compared to glass groundmass compositions and lava whole rock compositions in Figures 4.37 - 4.39. The melt inclusions range in SiO_2 composition from those comparable to the glass groundmass to those with SiO_2 less than the whole rock compositions. However, all melt inclusions are of rhyolitic composition (> 70 wt % SiO_2). Melt inclusions with compositions comparable to the glass groundmass suggest entrapment at a late stage in magma evolution. There are no discrete melt inclusion compositions for lavas erupted in a particular episode or from a particular vent area. For similar SiO_2 compositions, the melt inclusions are enriched in Al_2O_3 and K_2O and depleted in CaO relative to the whole rock compositions. For CaO this is consistent with crystallisation processes occurring in the magma that would incorporate CaO into crystallising phases (e.g. plagioclase feldspar, calcic amphibole), leaving the melt relatively depleted. The differences in K_2O are also consistent with crystallisation since K_2O is incompatible in the crystallising phases and is hence concentrated in the melt. The effects of such crystallisation are less obvious on Al_2O_3 contents.

As expected, due to concentration of compatible elements in crystallising phases and concentration of incompatible elements in the melt, the glass groundmass compositions have elevated SiO_2 and K_2O, and depleted Al_2O_3 and CaO relative to whole rock compositions. Glass groundmass compositions overlap for lavas erupted during a particular episode. For the Whakatane episode, lavas erupted in vent areas 1, 2 and 4 have a glass groundmass with comparable SiO_2, Al_2O_3, CaO and K_2O compositions. For the Mamaku episode, lavas

erupted in vent areas 1 and 2 have a glass groundmass with comparable SiO_2, Al_2O_3 and CaO compositions. However, the glass groundmass is becoming depleted in K_2O towards the northeast. For the Rotoma episode, lavas erupted in the Rotoma and Haroharo calderas have a glass groundmass with comparable SiO_2, Al_2O_3, CaO and K_2O compositions. In addition, there is no notable difference in glass groundmass compositions for lavas erupted in different episodes.

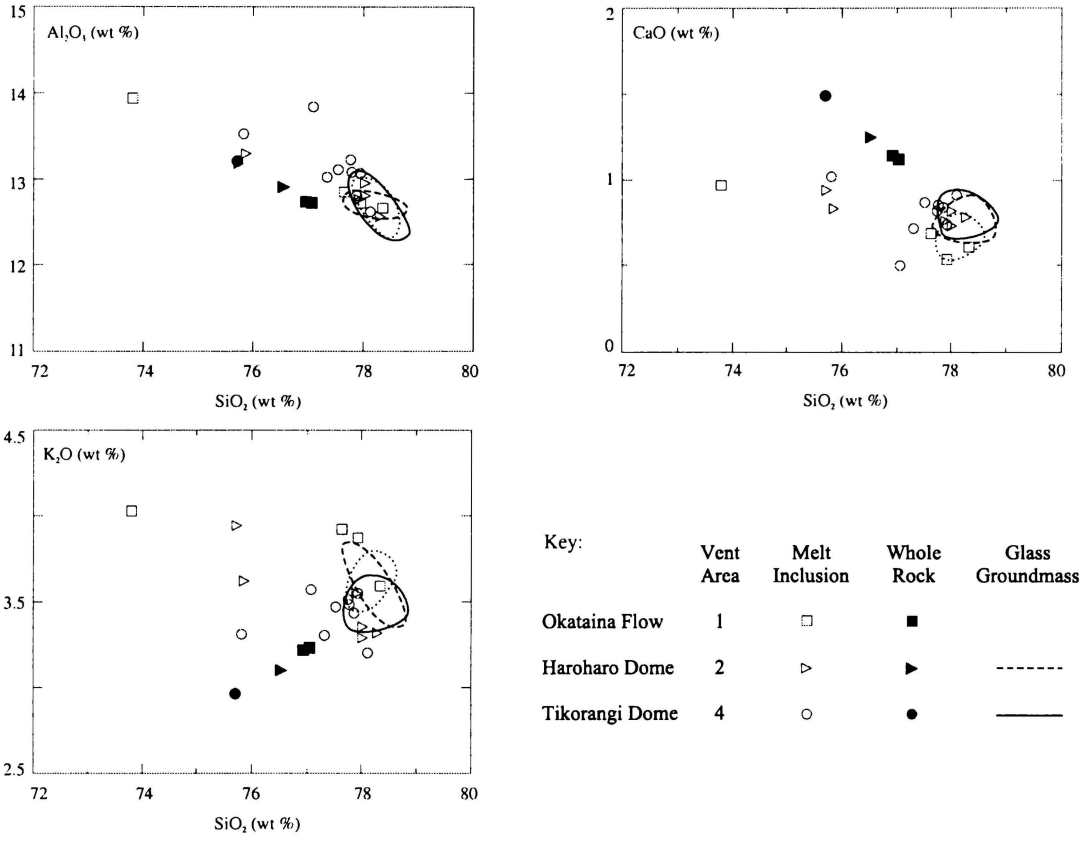

Figure 4.37: Selected major element variation diagrams for lavas erupted during the Whakatane episode at the Haroharo Volcanic Complex, showing melt inclusion, whole rock and glass groundmass compositions.

The composition of melt inclusions in quartz phenocrysts in lavas erupted during the Whakatane, Mamaku and Rotoma episodes may record the composition of the rhyolitic melts as they evolved from ~ 74 wt. % SiO_2 to ~ 78 wt. % SiO_2. Melt inclusion compositions may also reflect minor compositional heterogeneity in the melts.

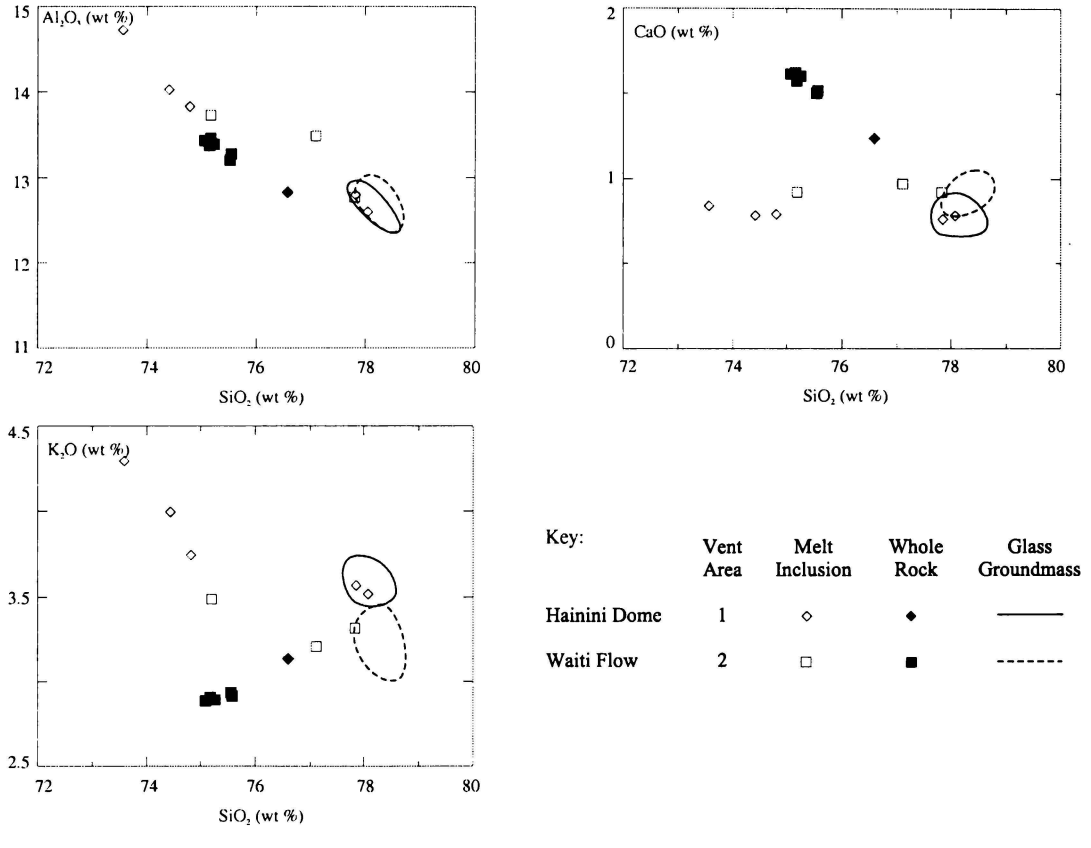

Figure 4.38: Selected major element variation diagrams for lavas erupted during the Mamaku episode at the Haroharo Volcanic Complex, showing melt inclusion, whole rock and glass groundmass compositions.

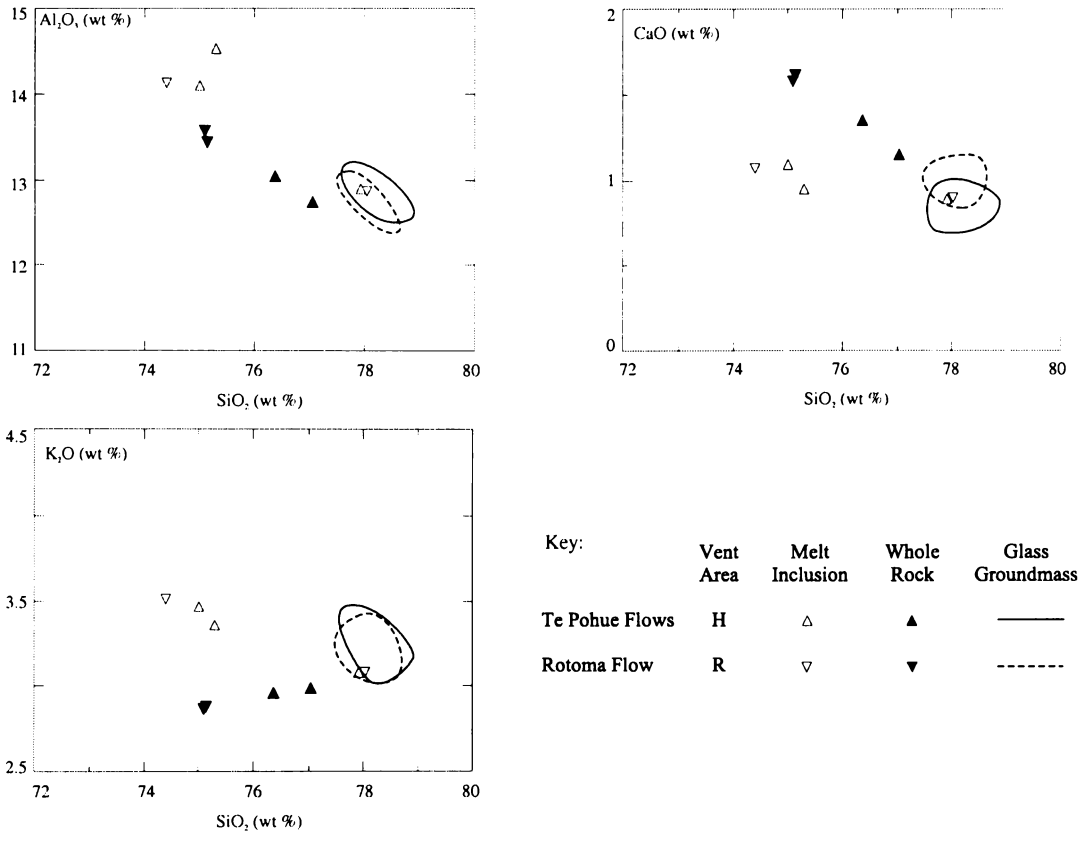

Figure 4.39: Selected major element variation diagrams for lavas erupted during the Rotoma episode at the Haroharo Volcanic Complex, showing melt inclusion, whole rock and glass groundmass compositions. Vent area: H = Haroharo, R = Rotoma.

Chapter Five: Mineralogy and Intensive Parameters

Chapter Five: Mineralogy and Intensive Parameters

5.1 INTRODUCTION

All rhyolite lavas of the Okataina, Rotorua and Kapenga volcanic centres contain phenocrysts of plagioclase feldspar, quartz and Fe-Ti oxides, and may also contain phenocrysts of the ferromagnesian minerals orthopyroxene, calcic amphibole, cummingtonite and biotite in varying quantities. This chapter discusses the occurrence, characteristics and compositions of these phenocrysts. Characteristics such as habit, colour and size show little variation between volcanic centres and age groups, and hence will be discussed for the rhyolites collectively. The composition of plagioclase feldspar, orthopyroxene, amphibole, biotite and Fe-Ti oxide phenocrysts from twenty-nine rhyolite lavas have been determined by electron probe microanalysis on polished thin sections using the JEOL 733 Superprobe in the Analytical Facility, Victoria University of Wellington (operating at 8 or 12 nanoamps and 15kV, with a spot size of 1 micron and analysis time of 30 seconds per element). Samples for analysis were chosen as representative of the different groups of rhyolite lavas suggested by age, ferromagnesian phenocryst assemblages and whole rock geochemistry. The compositions of these phenocrysts will be discussed and comparisons will be made between volcanic centres and age groups. The intensive parameters of the rhyolite lavas, such as temperature, crystallisation pressure and H_2O content, have been modelled using phenocryst compositions.

5.2 PLAGIOCLASE FELDSPAR

5.2.1 Occurrence and Characteristics

Plagioclase feldspar is the most common phenocryst type in the rhyolite lavas comprising ~ 3 - 21 % of the total rock and ~ 52 - 84 % of the total phenocrysts. Matawhaura (ho_1) is the exception, with plagioclase feldspar comprising only ~ 33 % of the total phenocrysts.

Plagioclase feldspar phenocrysts are most commonly less than 3 mm in length, although they can reach up to 5 mm in length. They are prismatic and subhedral to anhedral in shape and occur either singularly or in clusters, which may also include ferromagnesian minerals.

Plagioclase feldspar phenocrysts are colourless in plane-polarised light, although resorption may form embayments around crystal edges and areas of internal melting that are filled with a light brown glass. Under crossed-polarised light they show polysynthetic twinning which may be simple, multiple (Plate 5.1a), concentric (Plate 5.1b) or sector/hourglass in nature. Some plagioclase feldspar phenocrysts may be highly resorbed and embayed with a sieve texture while others in the same sample show no resorption features. Such a high level of resorption suggests that the phenocryst is out of equilibrium with the surrounding liquid/magma. The lack of resorption in co-existing phenocrysts suggests two plagioclase populations. Patiti Island contains phenocrysts with extensively resorbed sieve texture cores and non-resorbed euhedral rims (Plate 5.1c). This suggests that a phenocryst initially out of equilibrium with the surrounding liquid/magma, and possibly xenocrystic (see section 5.9), continued to crystallise in equilibrium. It is quite common for plagioclase phenocrysts to contain glass inclusions, which may occur in distinct bands coinciding with twin bands (Plate 5.1d). Such inclusions represent melt trapped within the phenocryst as it crystallised and which subsequently solidified to glass during the rapid cooling that accompanied eruption.

Following Page

Plate 5.1: a) Plagioclase feldspar phenocryst showing multiple polysynthetic twinning (sample number 109). Crossed-polarised light. ~ 35x magnification. b) Plagioclase feldspar phenocryst showing concentric zoning (109). Crossed-polarised light. ~ 35x magnification. c) Plagioclase feldspar phenocryst with a heavily resorbed sieve textured core and an unresorbed euhedral rim (130). Crossed-polarised light. ~ 25x magnification. d) Plagioclase feldspar phenocryst containing bands of glass inclusions (indicated by the red arrows) which coincide with twin bands (85). Crossed-polarised light. ~ 25x magnification. e) Quartz phenocryst with a subhedral pseudohexagonal form (103). The irregular fracture of quartz can be seen. Crossed-polarised light. ~ 30x magnification. f) Resorbed and embayed quartz phenocryst (74). Isotropic glass has filled areas of internal melting. Crossed-polarised light. ~ 45x magnification. g) Cluster of prismatic orthopyroxene phenocrysts showing parallel crystal growth and association with Fe-Ti oxides (117). Plane-polarised light. ~ 35x magnification. h) Oxidation rim on a prismatic pyroxene phenocryst (58). Plane-polarised light. ~ 45x magnification.

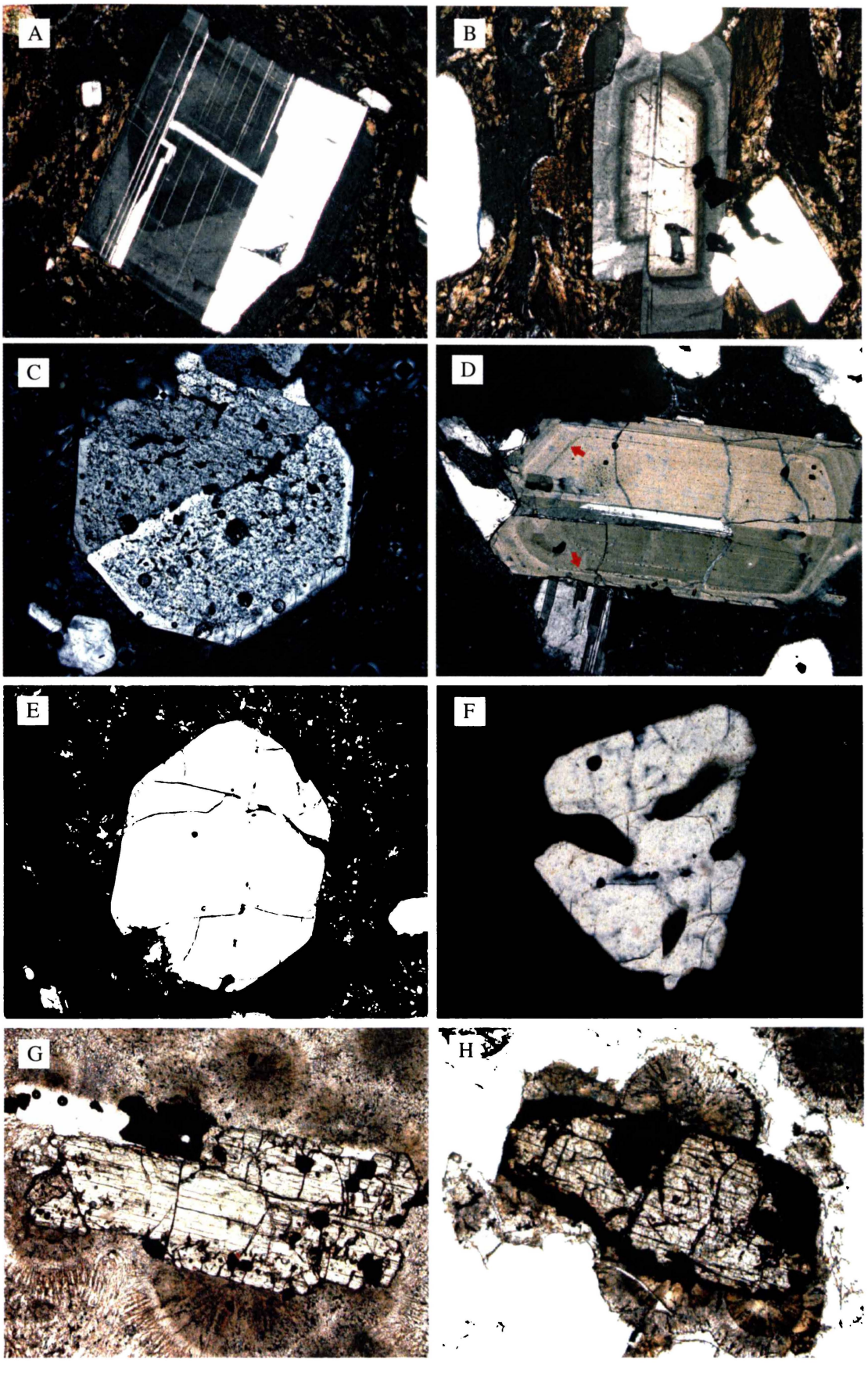
A
B
C
D
E
F
G
H

5.2.2 Composition

Analyses of plagioclase feldspar phenocrysts are given in Appendix VI (Tables VI.1 - VI.3). Or-Ab-An ternary diagrams for classifying feldspars according to Deer et al. (1966) are given in Figure 5.1. Plagioclase compositions range from oligoclase (An_{15}) to labradorite (An_{54}).

Plagioclase feldspars comprise a solid-solution series varying in composition from albite ($NaAlSi_3O_8$) to anorthite ($CaAl_2Si_2O_8$). Normal zoning, a variation in plagioclase composition from more An-rich core to more Ab-rich rim, is very common in volcanic rocks and occurs as crystallisation proceeds with falling temperature. However, it is often interrupted by oscillations in composition resulting in a sequence of normal zones that are separated by sharp reversals in composition, known as oscillatory zoning. Oscillatory zoning has not been investigated in any detail by electron microprobe analyses in this study. True reverse zoning, with more Ab-rich feldspar towards the centre of a crystal, is rare (Shelley, 1993). Hence in this study when analyses show plagioclase phenocrysts to have cores that are more Ab-rich than their rims, it is assumed that the rim analysis represents a zone that shows a sharp reversal in composition within an otherwise normally zoned phenocryst. In plagioclase feldspar and pyroxene analyses "core" implies the central point of the crystal as seen in thin section and may not be the true centre of the crystal. "Rim" is used to describe a point near the edge of the crystal as seen in thin section.

Plagioclase compositions range from oligoclase (An_{22}) to andesine (An_{34}) in the ho_1 rhyolites. Lava at Stancorp Quarry contains oligoclase, with one Ca-rich core having an andesine composition. Matawhaura lava contains phenocrysts with andesine cores and oligoclase rims. Wairua lava contains phenocrysts with cores and rims of both oligoclase and andesine. The plagioclase phenocrysts may exhibit normal zoning, oscillatory zoning or little change in composition from core to rim. Plagioclase compositions show some correlation with coexisting ferromagnesian assemblage, for example lava at Stancorp Quarry (opx ± calcic amph) contains the most An-poor plagioclase, Wairua lava (calcic amph + bio + opx) contains the most An-rich plagioclase and Matawhaura lava, with an intermediate assemblage of opx + calcic amph, contains plagioclase of intermediate composition.

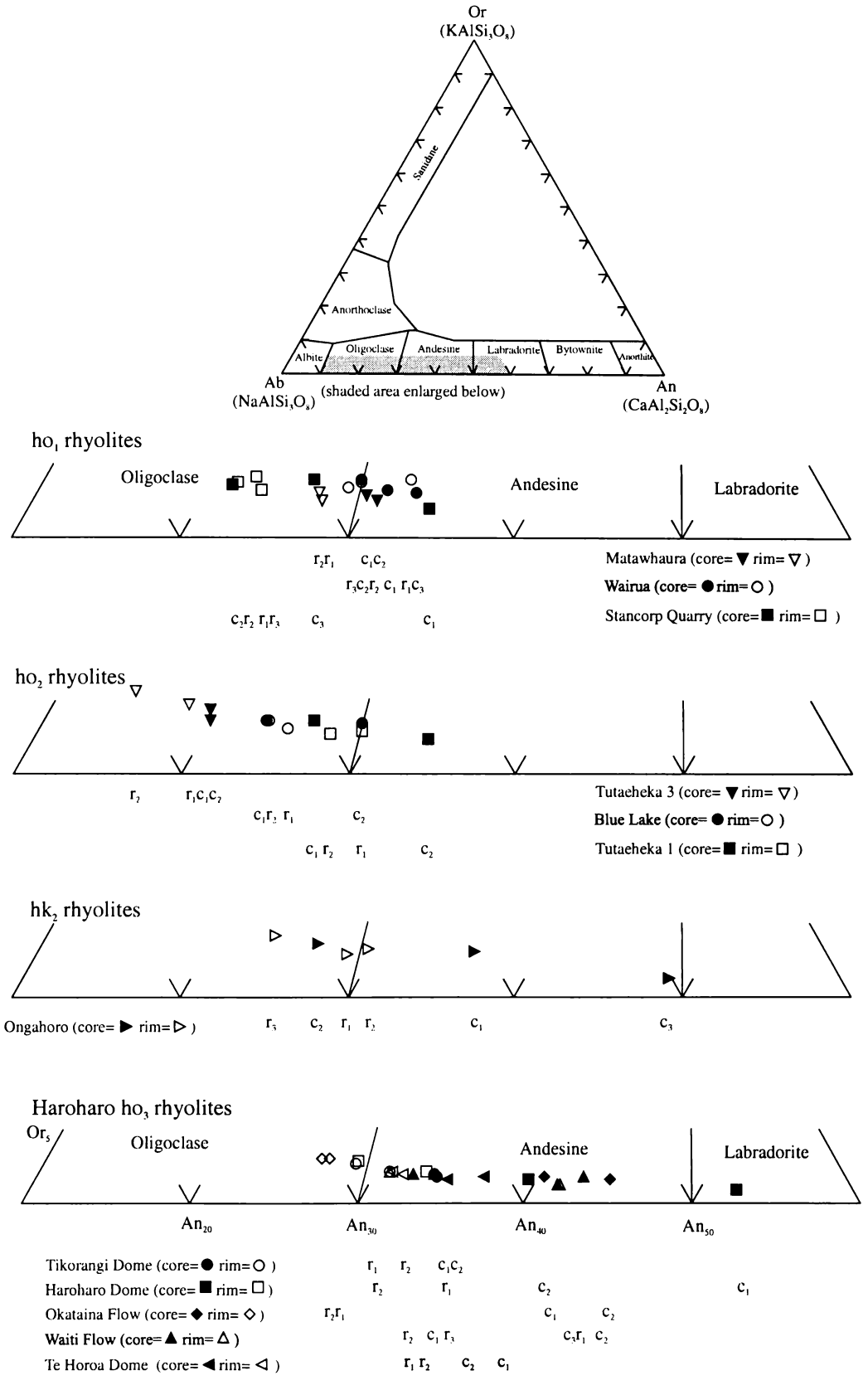

Figure 5.1: Classification of plagioclase feldspar phenocrysts in representative rhyolite lavas according to Deer et al. (1966). Core (c) and corresponding rim (r) compositions are indicated.

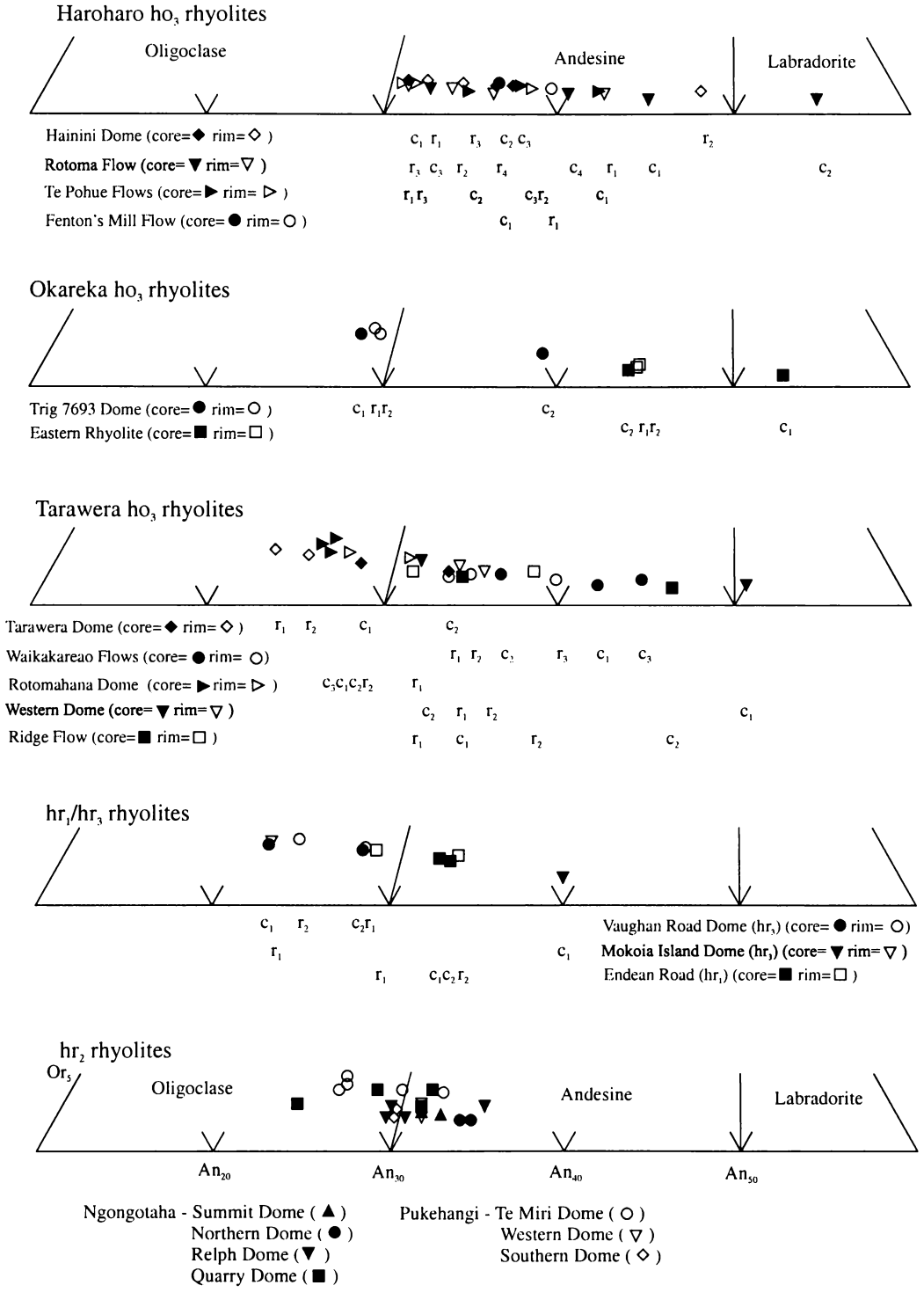

Figure 5.1 (continued): Classification of plagioclase feldspar phenocrysts in representative rhyolite lavas according to Deer et al. (1966). Core (c) and corresponding rim (r) compositions are indicated. Analyses for hr_2 rhyolites from Dravitzki (1999), cores and rims have not been distinguished.

In the ho_2 rhyolites plagioclase compositions range from An_{15} to An_{34} and core and rim compositions are dominantly oligoclase except for Tutaeheka 1 which contains a phenocryst with an andesine core. The plagioclase phenocrysts may exhibit normal or oscillatory zoning. In comparison, compositions for a representative hk_2 rhyolite, Ongahoro, range from An_{24} to An_{48} and show both normal and oscillatory zoning. As for the ho_1 rhyolites, plagioclase compositions are related to coexisting ferromagnesian phenocrysts. Tutaeheka 3 contains only trace amounts of biotite and An-poor plagioclase compared to the other ho_2 rhyolites and Ongahoro, which contain significant quantities of biotite.

Haroharo Volcanic Complex ho_3 rhyolites contain plagioclase feldspar phenocrysts with compositions ranging from An_{26} to An_{54} and are dominantly andesine. No distinctions can be made between rhyolites from different eruptive episodes or vent areas. There is no clear trend in plagioclase feldspar composition with age, although oligoclase was only found in rhyolites of the Whakatane Eruptive Episode. Although the most An-poor plagioclase feldspars occur in association with significant amounts of cummingtonite, there is no clear difference in plagioclase compositions between rhyolites that contain cummingtonite in significant quantities and those that do not. Plagioclase feldspar phenocrysts in Haroharo Volcanic Complex rhyolites exhibit both normal and oscillatory zoning.

Okareka Volcanic Complex ho_3 rhyolites contain plagioclase feldspar phenocrysts with compositions ranging from oligoclase (An_{27}) to labradorite (An_{53}). Plagioclase phenocrysts from the Eastern rhyolite, erupted in the Te Rere episode with a coexisting ferromagnesian assemblage of opx + calcic amph ± bio, are An-rich compared to phenocrysts from the Trig 7693 Dome, erupted in the Rotorua episode and coexisting with bio + calcic amph. This correlation is opposite to that seen in plagioclase phenocrysts in the ho_1 and ho_2 rhyolites. Both the Eastern rhyolite and the Trig 7693 Dome contain plagioclase phenocrysts that show normal zoning or little compositional change from core to rim.

Tarawera Volcanic Complex ho_3 rhyolites contain plagioclase feldspar phenocrysts with compositions ranging from oligoclase (An_{22}) to labradorite (An_{50}) but are dominantly andesine. No clear distinctions can be made between rhyolites from different eruptive episodes and there is no clear trend in plagioclase feldspar compositions with age. For the Rerewhakaaitu Eruptive Episode rhyolites, two groups of plagioclase feldspar phenocrysts occur. Rotomahana Dome (bio + calcic amph ± opx) contains plagioclase ranging from

An_{25} - An_{30} and Western dome (opx + calcic amph ± bio) contains plagioclase ranging from An_{31} - An_{50}. There is a trend of plagioclase phenocrysts being An-poor in rhyolites containing significant amounts of biotite, compared to those samples that contain orthopyroxene and calcic amphibole as the dominant ferromagnesian minerals. Plagioclase feldspar phenocrysts in Tarawera Volcanic Complex rhyolites exhibit both normal and oscillatory zoning.

Rotorua Volcanic Centre rhyolites contain plagioclase feldspar phenocrysts with compositions ranging from oligoclase (An_{21}) to andesine (An_{39}). Analyses from Dravitzki (1999) for hr_2 rhyolites have been used to supplement those obtained in this study for hr_1 and hr_3 rhyolites. No clear distinction can be made in plagioclase compositions between the three age groups. There appears to be no relationship between plagioclase feldspar compositions and ferromagnesian assemblage. Both hr_1 and hr_3 rhyolites contain plagioclase phenocrysts that exhibit both normal and oscillatory zoning. Dravitzki (1999) noted that generally zoning within plagioclase phenocrysts in Ngongotaha and Pukehangi rhyolites is rare. He considered this to imply that the phenocrysts had little time to react with the cooling lava, consistent with a rapidly cooling lava body erupted at close to solidus temperatures.

5.3 QUARTZ

5.3.1 Occurrence and Characteristics

Phenocrysts of quartz may be present in only trace amounts or may comprise up to ~ 9 % of the total rock and ~ 48 % of the total phenocrysts. There is a broad correlation between the occurrence of quartz and biotite, with samples containing significant amounts of biotite having higher amounts of quartz. Of note is the quartz-poor nature of hr_2 lavas and ho_3 lavas erupted from the Haroharo Volcanic Complex during the Te Rere episode.

Quartz phenocrysts may be up to 4.5 mm in diameter, although they occur most commonly in the 1 - 2 mm size range. They are most often subhedral to anhedral, ranging from quite prismatic (Plate 5.1e) to very rounded. Quartz occurs singularly and is commonly cracked/fractured. These phenocrysts are also commonly resorbed and embayed to varying degrees (Plate 5.1f). Quartz is colourless in plane-polarised light although resorption may

form embayments around crystal edges and areas of internal melting that are filled with a light brown glass. It is also common for quartz phenocrysts to contain glass inclusions.

5.4 PYROXENE

5.4.1 Occurrence and Characteristics

Pyroxene is the most common ferromagnesian phenocryst type in rhyolites of the Okataina, Rotorua and Kapenga volcanic centres, comprising up to ~ 2.5 % of the total rock and ~ 21 % of the total phenocrysts. In lavas that contain significant amounts of biotite, pyroxene may be absent or occur in only trace amounts. This is noticeable in ho_3 rhyolite lavas of the Rotorua and Kaharoa eruptive episodes at the Okareka and Tarawera volcanic complexes respectively.

Pyroxene phenocrysts are most commonly less than 1.5 mm in length, but may range up to 2.5 mm. Pyroxenes may occur singularly or in clusters and almost always occur in association with Fe-Ti oxides (Plate 5.1g). The dominant pyroxene present is orthopyroxene, which has been identified by its weak pale green-pale pink pleochroism and straight extinction. Clinopyroxene was not positively identified in thin section or by electron microprobe analysis (see section 5.4.2). Orthopyroxenes are subhedral to anhedral in shape and may occur as prismatic crystals with a single cleavage or as four or eight sided cross-sections of prisms showing two sets of cleavage at 90°. Pyroxene crystals with overgrowths or intergrowths of amphibole are rare (Plate 5.2a). Even more rarely, amphibole may be overgrown by pyroxene. Such overgrowths may be referred to as a corona texture and are often presumed to result from incomplete reaction of the inner mineral with melt/magma to produce the outer mineral (MacKenzie et al., 1982). Red - orange - brown - black oxidation rims may occur on pyroxene phenocrysts and are most common in older crystallised rhyolites (Plate 5.1h). Richnow (1999) considered that oxidation similar to this occurring in quench crystals was due to water enrichment and temperature increases resulting from devitrification and crystallisation of the glass groundmass. These oxidation rims may be minor or completely replace the crystal so that identification is no longer possible. In some samples the pyroxene phenocrysts appear to be resorbed or embayed.

5.4.2 Composition

Analyses of pyroxene phenocrysts are given in Appendix VI (Tables VI.4 - VI.6). Wo-En-Fs ternary diagrams for classifying pyroxenes according to Morimoto et al. (1988) are given in Figure 5.2. All pyroxene phenocrysts analysed are orthopyroxenes (less than 5% wollastonite) and both enstatite (formerly known as hypersthene) and ferrosilite (formerly known as ferrohypersthene) compositions occur.

Orthopyroxene phenocrysts in ho_1 rhyolites range in composition from ferrosilite (En_{39}) to enstatite (En_{55}). Matawhaura lava contains ferrosilite showing En depletion from core to rim. The one pyroxene analysed from Wairua is enstatite showing En depletion from core to rim. Stancorp Quarry lava contains ferrosilite showing very little change in composition from core to rim and a second orthopyroxene phenocryst has an enstatite core and ferrosilite rim. Generally orthopyroxenes in the biotite-bearing Wairua rhyolite are En-rich compared to those in the biotite-free ho_1 rhyolites.

Following Page

Plate 5.2: a) Pyroxene phenocryst with green amphibole overgrowth (sample number 134). Plane-polarised light. ~ 45x magnification. b) Diamond/lozenge shaped cross section of a pale pinky-brown cummingtonite phenocryst showing two sets of cleavage at 120° (107). Plane-polarised light. ~ 45x magnification. c) Prismatic calcic amphibole phenocryst and Fe-Ti oxides (134). Plane-polarised light. ~ 25x magnification. d) Calcic amphibole phenocryst with intergrowths of yellow-brown biotite (indicated by red arrows) (44). Plane-polarised light. ~ 40x magnification. e) Flakes of dark brown biotite (64). Plane-polarised light. ~ 45x magnification. f) Biotite flake showing red-brown and yellow-green brown bands (128). Plane-polarised light. ~ 35x magnification. g) Opaque Fe-Ti oxide phenocryst and accessory zircon crystal (indicated by the red arrow) (107). Plane-polarised light. ~ 95x magnification. h) Acicular apatite crystals occurring in association with plagioclase feldspar (105). Crossed-polarised light. ~ 45x magnification.

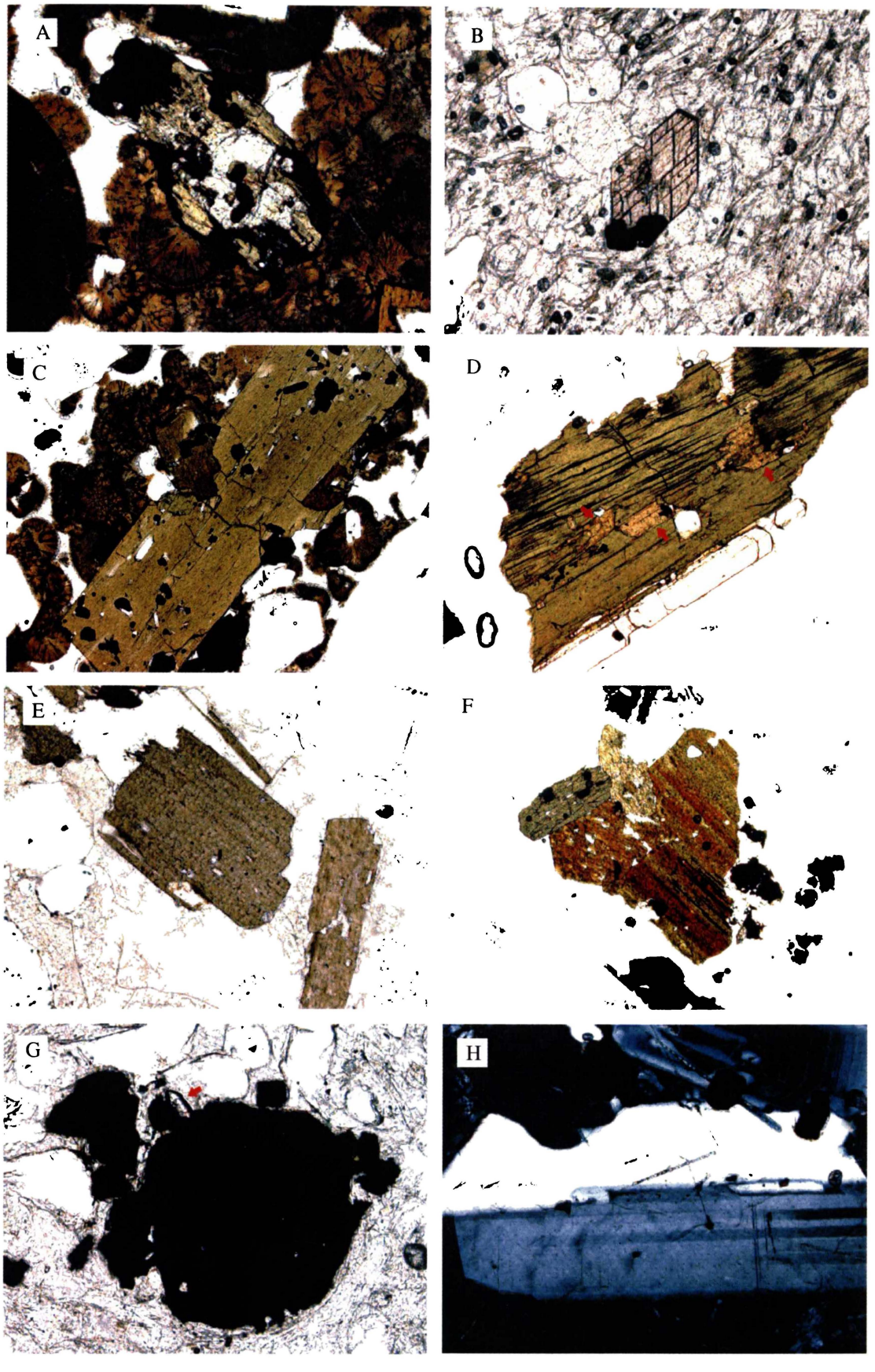
A
B
C
D
E
F
G
H

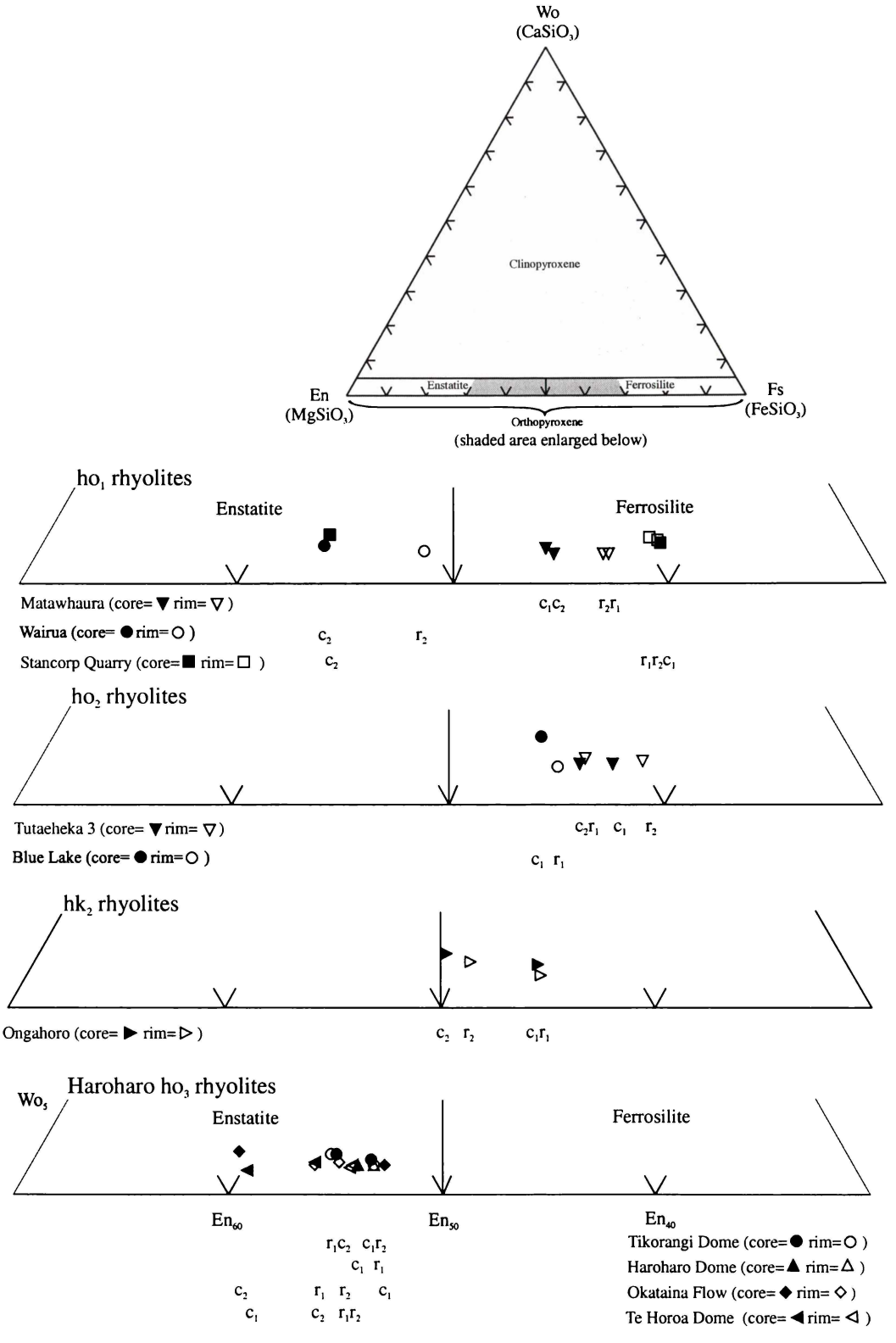

Figure 5.2: Classification of orthopyroxene phenocrysts in representative rhyolite lavas according to Morimoto et al. (1988). Core (c) and corresponding rim (r) compositions are indicated.

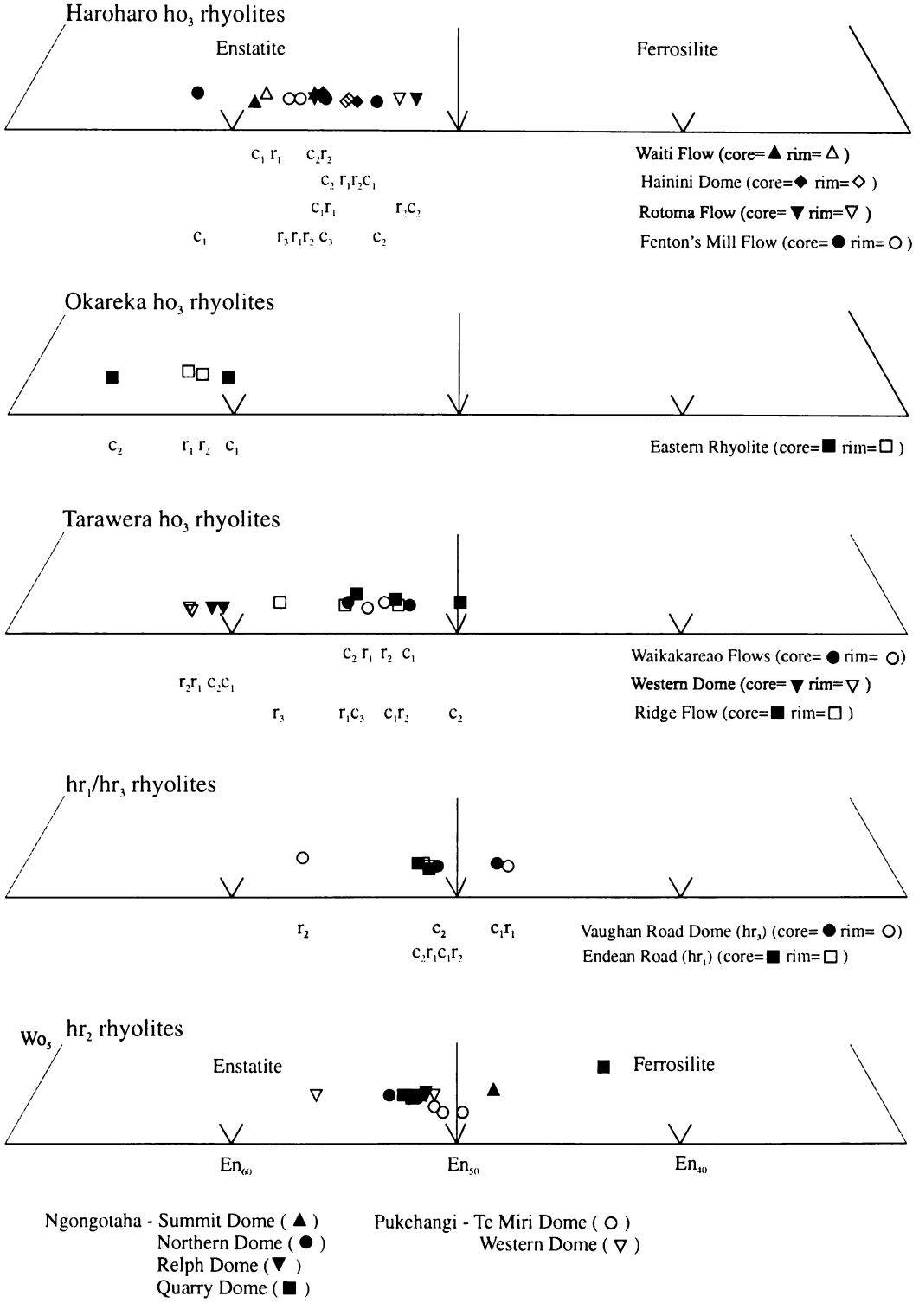

Figure 5.2 (continued): Classification of orthopyroxene phenocrysts in representative rhyolite lavas according to Morimoto et al. (1988). Core (c) and corresponding rim (r) compositions are indicated. Analyses for hr_2 rhyolites from Dravitzki (1999), cores and rims have not been distinguished.

All orthopyroxenes analysed in ho_2 rhyolites are ferrosilite with compositions ranging from En_{39} to En_{44}. The ferrosilite may exhibit both En enrichment and depletion, or little change in En content, from core to rim. Orthopyroxene compositions for Ongahoro (hk_2) are relatively En-rich, ranging from En_{44} to En_{49}, and show either En depletion from core to rim or little change. For the ho_2 and hk_2 rhyolites, those that contain significant amounts of biotite have more En-rich orthopyroxenes than those that contain only trace amounts.

Haroharo Volcanic Complex ho_3 rhyolites contain orthopyroxene phenocrysts with compositions ranging from En_{51} to En_{61} (enstatite). No distinctions can be made between rhyolites from different eruptive episodes or vent areas and there is no clear trend in orthopyroxene composition with age. There is no difference in the composition of orthopyroxene phenocrysts between rhyolites that contain significant amounts of cummingtonite and those that do not. Orthopyroxenes exhibit both En enrichment and depletion, or little composition change, from core to rim.

Rhyolite lavas erupted during the Rotorua episode at the Okareka Volcanic Complex were found not to contain orthopyroxene and hence analyses are only available for phenocrysts from the Eastern rhyolite erupted during the earlier Te Rere episode. These orthopyroxenes are enstatites with compositions ranging from En_{59} to En_{65}. They exhibit both En enrichment and depletion from core to rim and are some of the most En-rich orthopyroxenes analysed in this study.

Tarawera Volcanic Complex ho_3 rhyolites contain orthopyroxene phenocrysts that are dominantly enstatite with compositions ranging from En_{49} to En_{61}. While orthopyroxene phenocrysts in the Ridge and Waikakareao lava flows are very similar, the orthopyroxenes in Western Dome have a distinct En-rich composition. Orthopyroxenes in these lavas may show En enrichment or depletion from core to rim.

Of note is that the ho_3 rhyolites from the Haroharo, Okareka and Tarawera volcanic complexes are dominated by orthopyroxene phenocrysts of enstatite composition, whereas the ho_1, ho_2 and hk_2 rhyolites contain dominantly ferrosilite.

Rotorua Volcanic Centre rhyolites contain orthopyroxene phenocrysts with compositions ranging from En_{41} (ferrosilite) to En_{56} (enstatite). Analyses from Dravitzki (1999) for hr_2 rhyolites have been used to supplement those obtained in this study for hr_1 and hr_3 rhyolites.

No clear distinction can be made in orthopyroxene compositions between the three age groups and there appears to be no relationship between composition and ferromagnesian assemblage. Orthopyroxenes in both the hr_1 and hr_3 rhyolites exhibit both En enrichment and depletion from core to rim.

5.5 AMPHIBOLE

5.5.1 Occurrence and Characteristics

Amphibole is the second most common ferromagnesian phenocryst type in rhyolite lavas of the Okataina, Rotorua and Kapenga volcanic centres, comprising up to ~ 3 % of the total rock and ~ 16 % of the total phenocrysts. Of note is its presence, along with orthopyroxene, in all lavas of the Haroharo Volcanic Complex. The absence, or low abundance, of amphibole phenocrysts is noticeable in ho_3 lavas erupted during the Waiohau episode from the Tarawera Volcanic Complex and the hr_2 lavas from the Rotorua Volcanic Centre.

Amphibole phenocrysts are commonly less than 1.5 mm in length, although they may range up to 8 mm. They commonly occur singularly although may be found in clusters and in both instances commonly occur with Fe-Ti oxides. Amphiboles are subhedral to anhedral in shape and may be found in prismatic form (Plate 5.2c) or as diamond/lozenge shaped cross-sections showing two sets of cleavage at 120° (Plate 5.2b). In some samples they appear to be resorbed or embayed.

Two types of amphibole occur and may be tentatively identified in thin section by their colour in plane-polarised light. Calcic amphibole (commonly referred to as hornblende) exhibits a range of colours and is strongly pleochroic in shades of green - olive green - lime green - yellow brown - orange brown - red brown - dark brown (Plate 5.2c). Cummingtonite, a Mg-Fe-Mn amphibole, exhibits much paler colours and is weakly pleochroic from colourless to shades of pale green - pale yellow - pale pink - pale pinky brown (Plate 5.2b). Generally, electron microprobe analyses are the best method to confirm the occurrence of cummingtonite (see section 5.5.2). Under crossed-polarised light amphibole crystals may show simple twins. Comparable to pyroxene phenocrysts, oxidation rims may also occur on amphibole phenocrysts and may completely replace the crystal so that identification is no longer possible. Amphibole phenocrysts have been observed with

biotite intergrowths (Plate 5.2d) and orthopyroxene overgrowths and intergrowths. Inclusions of Fe-Ti oxides and rare zircon may be found in amphibole phenocrysts.

5.5.2 Composition

Analyses of amphibole phenocrysts are given in Appendix VI (Tables VI.7 - VI.9). Amphiboles have been classified using the procedure of Leake et al. (1997) (Figures 5.3 - 5.6) who divide the amphiboles into four principal groups on the basis of the B group cation occupancy:

$(Ca+Na)_B < 1.00$, $(Mg,Fe,Mn,Li)_B \geq 1.00$	Magnesium-iron-manganese-lithium group
$(Ca+Na)_B \geq 1.00$, $Na_B < 0.50$	Calcic amphibole group
$(Ca+Na)_B \geq 1.00$, $0.50 \leq Na_B < 1.50$	Sodic-calcic amphibole group
$Na_B \geq 1.50$	Sodic amphibole group

The rhyolites of this study contain amphiboles that fall into the magnesium-iron-manganese-lithium (Mg-Fe-Mn-Li) and calcic (Ca) amphibole groups. Further subdivision within each group is based on the magnesium number of the amphibole ($Mg/(Mg + Fe^{2+})$) and TSi (Si per formula unit), in addition to crystal system for the Mg-Fe-Mn-Li amphiboles, and A group cation occupancy $(Na + K)_A$ for the calcic amphiboles. In this precise nomenclature 'hornblende' is always used with a prefix (magnesio- or ferro-). Hawthorne (1981) states that it is acceptable to use the term 'hornblende' to name calcic amphiboles that have been identified by physical and/or optical properties but for which chemical data are not available to allow a precise name to be given.

Classification of amphibole phenocrysts in the ho_1 rhyolites is shown in Figure 5.3. Matawhaura and Wairua lavas contain calcic amphiboles of magnesio-hornblende and edenite composition. North Rotoma lava contains calcic amphibole of magnesio-hornblende composition as well as Mg-Fe-Mn-Li amphibole of cummingtonite composition. A ternary plot of CaO-MgO-FeO shows that these co-existing calcic amphibole and cummingtonite phenocrysts are in equilibrium. The compositions of amphibole phenocrysts show no relationship to the ferromagnesian assemblage of the rhyolite lava.

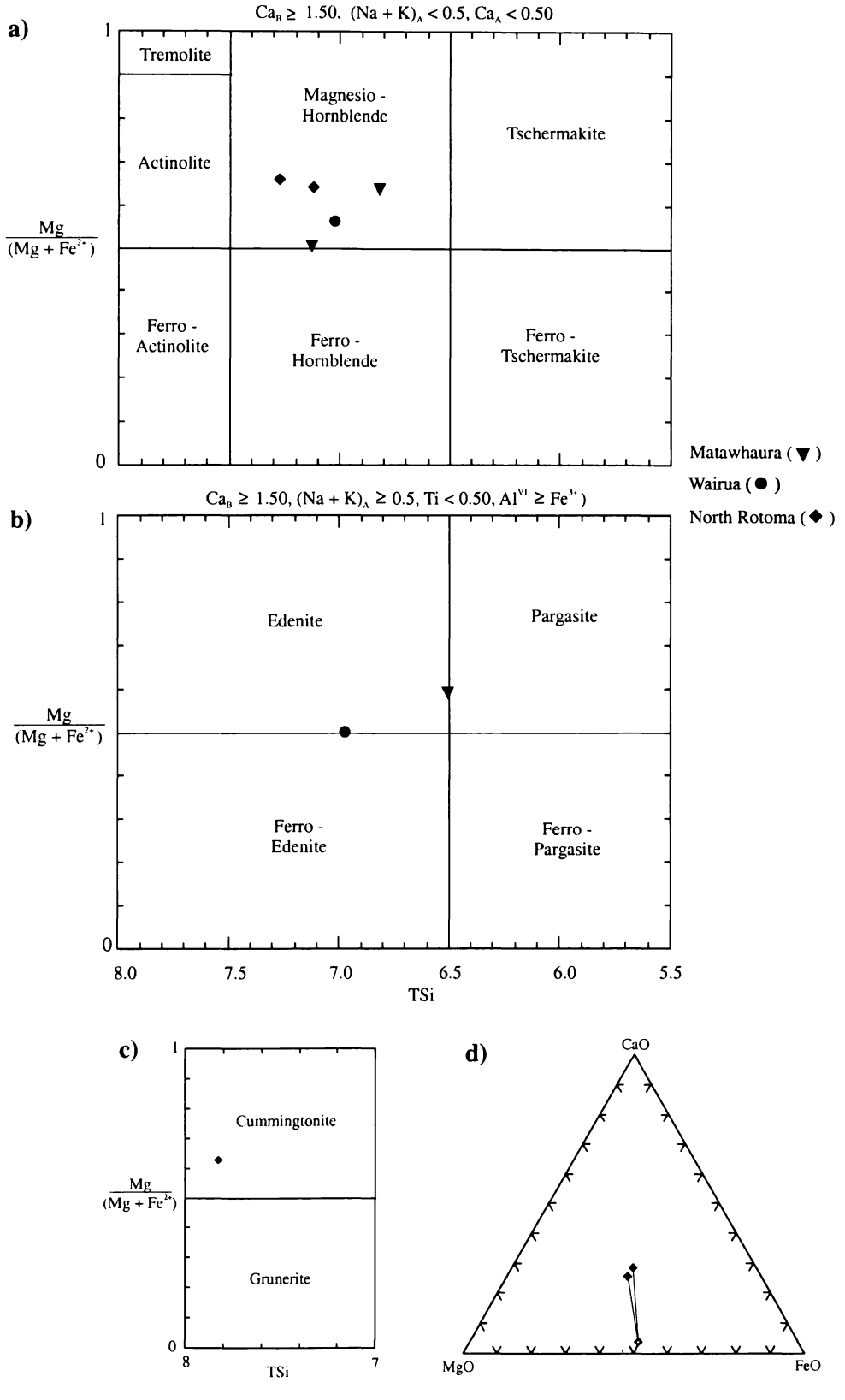

Figure 5.3: Classification of amphibole phenocrysts in representative ho_1 rhyolite lavas from the Okataina Volcanic Centre according to Leake et al. (1997). a) and b) Classification of calcic amphiboles. c) Classification of monoclinic Mg-Fe-Mn-Li amphiboles. d) CaO-MgO-FeO ternary plot showing compositions of co-existing calcic amphibole (filled diamonds) and cummingtonite (unfilled diamond) phenocrysts in the North Rotoma rhyolite.

Classification of amphibole phenocrysts in the ho_2 rhyolites is shown in Figure 5.4. All are calcic amphiboles of either magnesio-hornblende or edenite composition. In comparison, Ongahoro (hk_2) also contains magnesio-hornblende, in addition to one phenocryst that plots on the edenite - ferro-edenite boundary. There is no difference in amphibole compositions between rhyolites that contain biotite in significant amounts and those that are biotite-free/poor.

Classification of amphibole phenocrysts in Haroharo and Okareka volcanic complex ho_3 rhyolites is shown in Figure 5.5. Haroharo rhyolites contain calcic amphiboles of magnesio-hornblende and edenite composition. One amphibole from the Rotoma lava flow is of pargasite composition. There is no significant difference in calcic amphibole compositions between eruptive episodes or vent areas. Haroharo Dome, Okataina Flow, Te Horoa Dome and Te Pohue Flows contain cummingtonite, which shows no significant change in composition over time or between vent areas. All amphibole phenocrysts analysed in two of the youngest rhyolites, Haroharo Dome and Okataina Flow, were of cummingtonite composition. A ternary plot of CaO-MgO-FeO (Figure 5.5d) shows that co-existing calcic amphibole and cummingtonite phenocrysts in Te Horoa Dome and the Te Pohue Flows are in equilibrium. Okareka rhyolites contain only calcic amphibole. Trig 7693 Dome, the only Haroharo or Okareka lava to contain significant amounts of biotite, contains amphiboles with distinctly lower $Mg/(Mg+Fe^{2+})$ contents than other Okareka and Haroharo amphiboles.

Classification of amphibole phenocrysts in Tarawera Volcanic Complex ho_3 rhyolites is shown in Figure 5.6. Tarawera rhyolites contain only calcic amphiboles, the compositions of which show a relationship to the ferromagnesian assemblage of the rhyolite. Rotomahana Dome, which contains significant amounts of biotite, contains magnesio-hornblende and edenite phenocrysts with distinctly lower $Mg/(Mg+Fe^{2+})$ contents than those occurring in Western Dome and Ridge Flow, which contain only very minor amounts of biotite. Hence, the amphiboles of Western Dome and Rotomahana Dome, which were erupted during the same episode, have clearly distinct compositions.

Classification of amphibole phenocrysts in Rotorua Volcanic Centre rhyolites is also shown in Figure 5.6. Analyses from Dravitzki (1999) for hr_2 rhyolites have been used to supplement those obtained in this study for hr_1 and hr_3 rhyolites. Rotorua rhyolites contain calcic amphiboles of magnesio-hornblende and edenite composition. No clear distinction

can be made in amphibole compositions between the three age groups and there appears to be no relationship between amphibole composition and ferromagnesian assemblage.

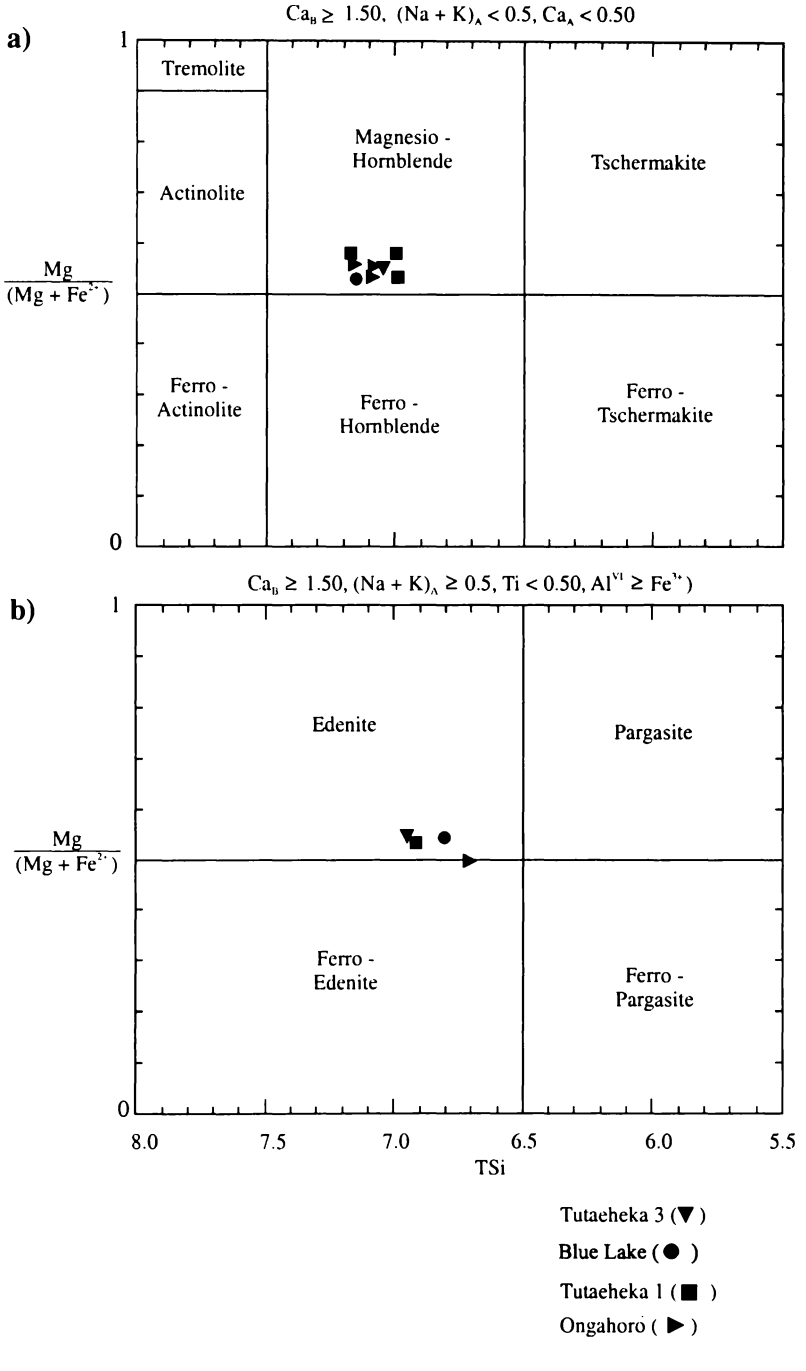

Figure 5.4: Classification of calcic amphibole phenocrysts in representative ho_2 and hk_2 rhyolite lavas, from the Okataina and Kapenga volcanic centres respectively, according to Leake et al. (1997).

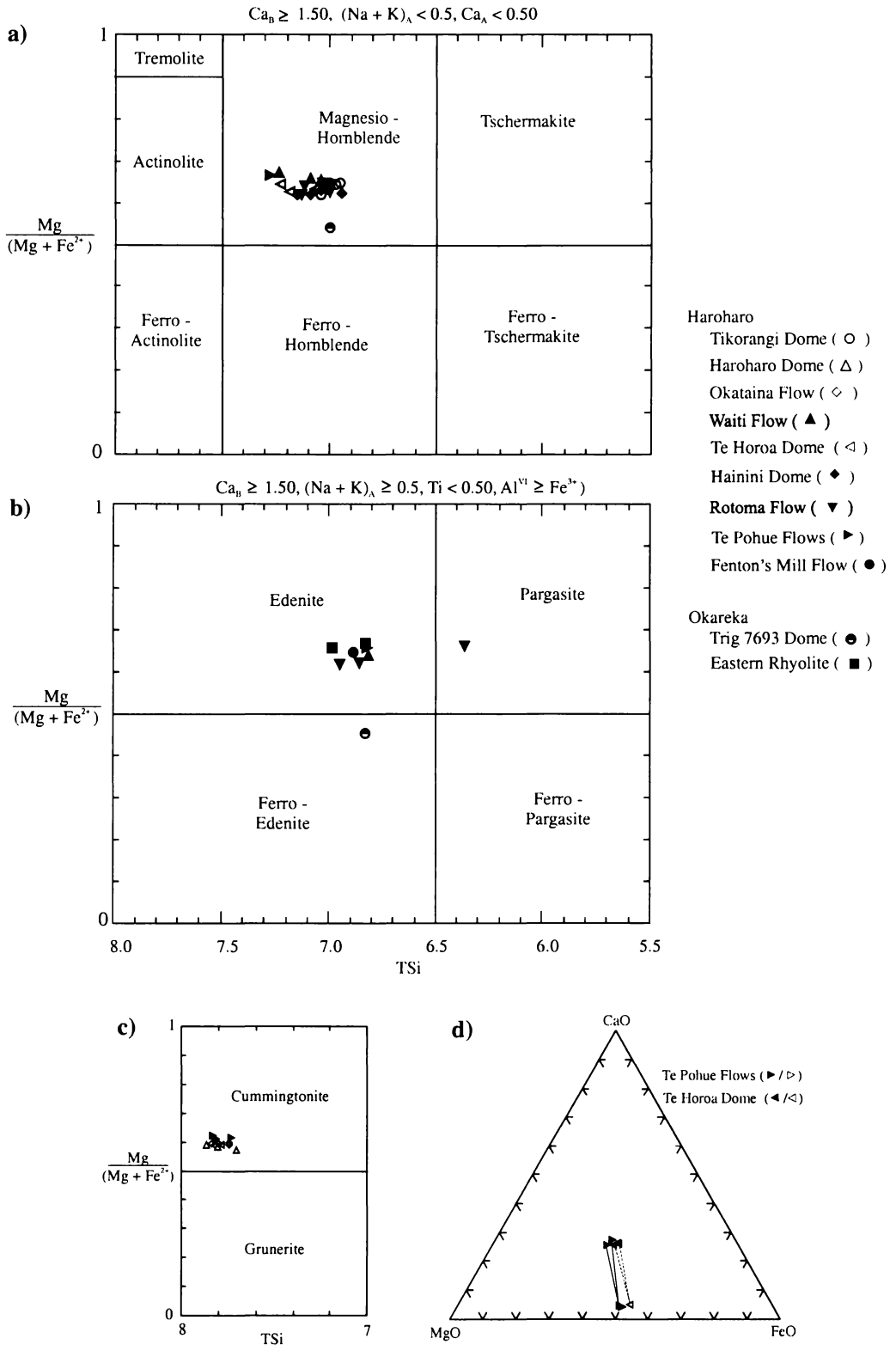

Figure 5.5: Classification of amphibole phenocrysts in representative Haroharo Volcanic Complex and Okareka Volcanic Complex ho_3 rhyolite lavas from the Okataina Volcanic Centre according to Leake et al. (1997). a) and b) Classification of calcic amphiboles. c) Classification of monoclinic Mg-Fe-Mn-Li amphiboles. d) CaO-MgO-FeO ternary plot showing compositions of co-existing calcic amphibole (filled symbols) and cummingtonite (unfilled symbols) phenocrysts.

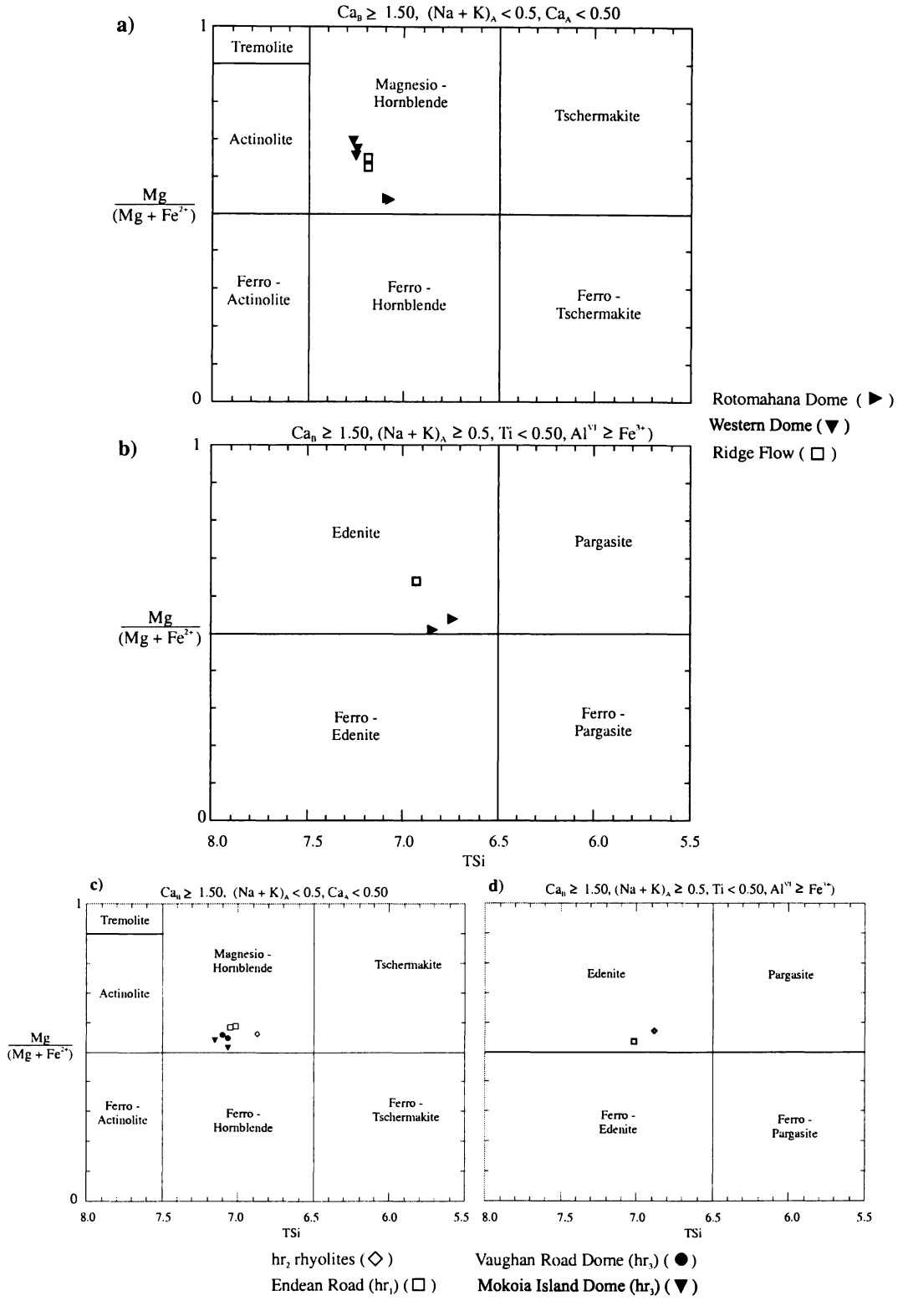

Figure 5.6: a) and b) Classification of calcic amphibole phenocrysts in representative Tarawera Volcanic Complex ho_3 rhyolite lavas from the Okataina Volcanic Centre according to Leake et al. (1997). c) and d) Classification of calcic amphibole phenocrysts in representative Rotorua Volcanic Centre rhyolite lavas according to Leake et al. (1997). Analyses for the hr_2 lavas from Dravitzki (1999).

As previously noted, calcic amphibole phenocrysts may exhibit a wide range of colours in plane-polarised light. However, these colour differences are not clearly related to phenocryst composition or classification. Magnesio-hornblende phenocrysts may be pleochroic in shades of green - olive green - lime green - yellow brown - orange brown - red brown - dark brown. While edenite phenocrysts may also be pleochroic in shades of green and brown, it is common for them to occur in shades of orange - brown and red -brown.

5.6 BIOTITE

5.6.1 Occurrence and Characteristics

Rhyolite lavas of the Okataina, Rotorua and Kapenga volcanic centres can be divided into three groups based on the occurrence of biotite. In samples that contain significant amounts of biotite, these phenocrysts comprise ~ 1 - 4 % of the total rock and ~ 5 - 16 % of the total phenocrysts. In samples that contain small amounts of biotite, these phenocrysts comprise < 1 % of the total rock and < 3 % of the total phenocrysts. The third group comprises lavas that contain no biotite phenocrysts. Of note is the lack of biotite phenocrysts in the Haroharo Volcanic Complex rhyolite lavas.

Biotite phenocrysts occur as subhedral to anhedral plates and flakes up to 2.5 mm in length. Biotite has eminent basal cleavage although some phenocrysts have been cut parallel to the (001) cleavage direction and therefore no cleavage can be seen in thin section. Biotite flakes may occur singularly or in clusters, and are commonly found in association with Fe-Ti oxides (Plate 5.2f). In plane-polarised light biotite exhibits a range of colours and is strongly pleochroic in shades of red brown - orange brown - yellow brown - green brown - light brown - dark (chocolate) brown (Plate 5.2e). Within a particular lava the biotite phenocrysts can exhibit a wide range of colours, and even in particular phenocrysts colour variations can be seen with red - brown and yellow - green brown bands (Plate 5.2f). In crossed-polarised light biotite phenocrysts have straight mottled/twinkly extinction. They have been observed with small plagioclase, zircon and apatite inclusions and some show evidence of resorption and embayments. Biotite may be intergrown with amphibole.

5.6.2 Composition

Analyses of biotite phenocrysts obtained from rhyolite lavas of the Okataina and Rotorua volcanic centres are given in Appendix VI (Table VI.10). Figure 5.7 shows the relationship of biotite phenocryst compositions to the principal components of biotite compositions according to Deer et al. (1992). The biotite phenocrysts have Fe/(Fe+Mg) compositions ranging from ~ 0.49 - 0.57. No distinction can be made between biotite phenocrysts in Okataina and Rotorua rhyolites. There is no clear relationship between biotite compositions and age for the Okataina rhyolite lavas.

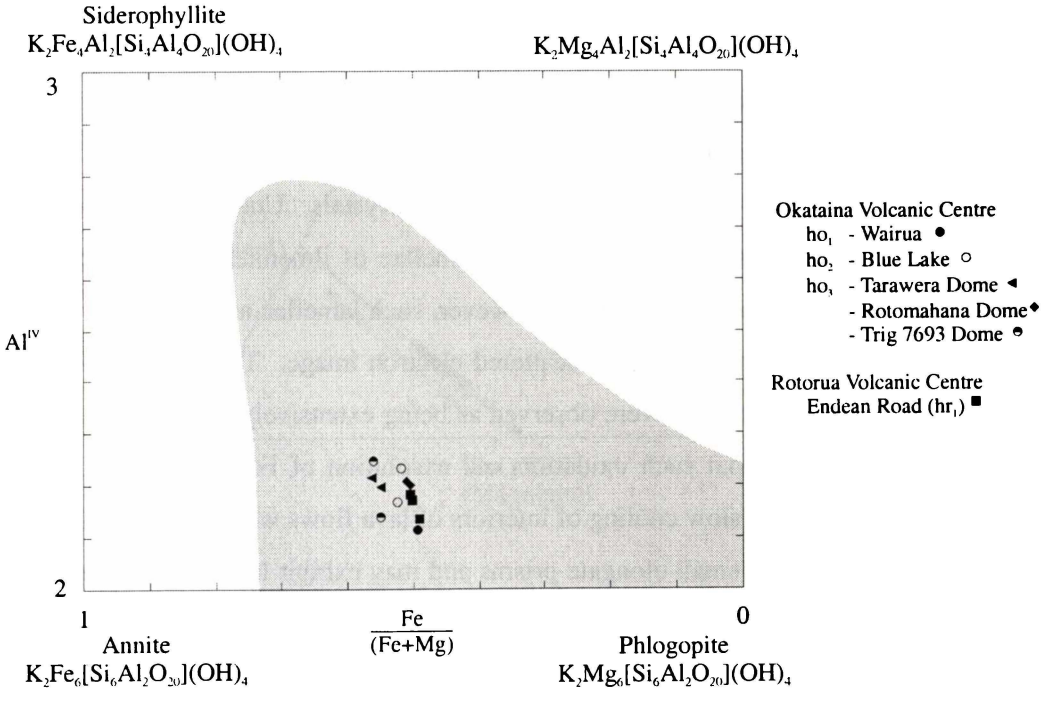

Figure 5.7: The composition of biotite phenocrysts in representative Okataina and Rotorua volcanic centre rhyolite lavas in relation to the principal components of biotite compositions and the field in which most natural biotites lie (shaded) from Deer et al. (1992).

5.7 FE-TI OXIDES

5.7.1 Occurrence and Characteristics

Fe-Ti oxides are present in all rhyolite lavas and comprise up to ~ 1.5 % of the total rock and ~ 13 % of the total phenocrysts. The proportion of total phenocrysts that Fe-Ti oxides comprise is highest when the ferromagnesian phenocryst composition of the lavas is low. In the hr_2 rhyolites, which lack biotite and amphibole in addition to containing very small amounts of quartz, Fe-Ti oxides comprise ~ 9 - 13 % of the total phenocrysts.

Fe-Ti oxides may occur as discrete phenocrysts or small clusters. As previously noted it is common for these phenocrysts to be found in association with ferromagnesian minerals (Plates 5.1g, 5.2b and 5.2f). Fe-Ti oxide phenocrysts are subhedral, anhedral and rarely euhedral. Although they may be up to 1 mm in length/diameter, they most commonly occur as small granular crystals less than 0.5 mm in length/diameter. Fe-Ti oxides commonly occur in association with zircon (Plate 5.2g), apatite and occasionally pyrite, and may also have inclusions of these minerals. Two types of Fe-Ti oxide minerals are present. Titanomagnetite commonly occurs as cubic or granular crystals. Under reflected light they may be seen to contain exsolution or oxidation lamellae of ilmenite, although this is not common in the rhyolite lavas of this study. However, such lamellae are seen to be common when the oxides are examined in a back scattered electron image. Titanomagnetites in the Mokoia Island Dome in particular were observed as being extensively exsolved. Bacon and Hirschmann (1988) noted that such oxidation and exsolution of Fe-Ti oxides most likely took place during relatively slow cooling of interiors of lava flows when a vapour phase was present. Ilmenite occurs as small elongate prisms and may exhibit lamellar twinning. Both titanomagnetite and ilmenite are present in all rhyolite lavas, although titanomagnetite is more common, and may show evidence of resorption and embayments.

5.7.2 Composition

Analyses of Fe-Ti oxide phenocrysts are given in Appendix VI (Tables VI.11 - VI.13). Electron microprobe analyses give total iron as FeO* and analyses have been recalculated according to Droop (1987) to give FeO and Fe_2O_3.

Fe-Ti oxides occur as complex solid solutions. Figure 5.8 shows these solid solutions in the system FeO-Fe_2O_3-TiO_2 along with the compositions of Fe-Ti oxides from representative Okataina, Rotorua and Kapenga volcanic centre rhyolite lavas. Fe-Ti oxides termed titanomagnetite in this study are actually solid solutions of magnetite and ulvospinel, being richer in TiO_2 and poorer in Fe_2O_3 than pure magnetite. Fe-Ti oxides termed ilmenite in this study have compositions richer in Fe_2O_3 than pure ilmenite and sit slightly above the hematitie-ilmenite solid solution series composition line. This is likely to be a result of the recalculation method used.

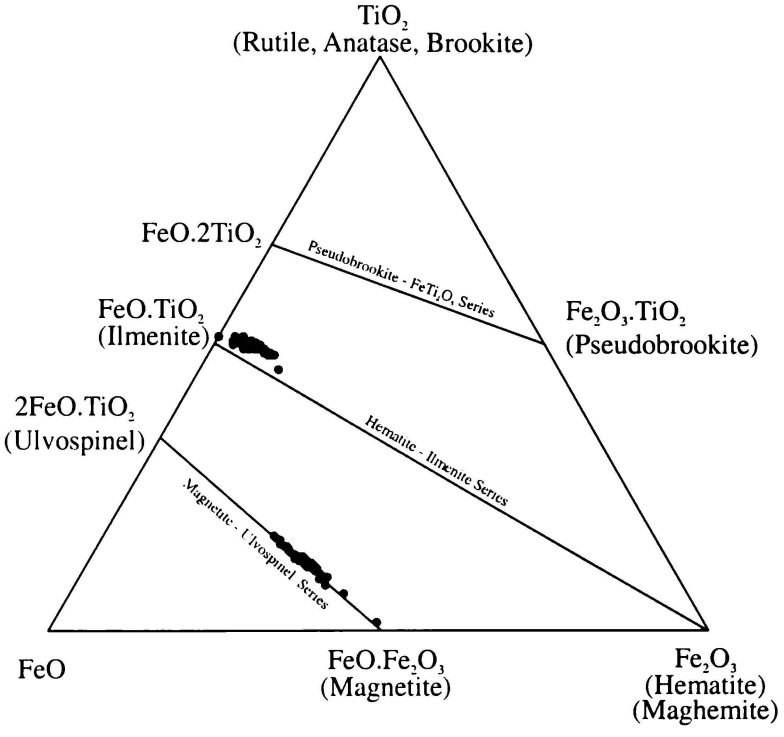

Figure 5.8: The system FeO-Fe_2O_3-TiO_2 showing the major high-temperature solid solution series magnetite-ulvospinel, hematite-ilmenite and psudobrookite-$FeTi_2O_5$ plotted on a mol percent basis (from Deer et al., 1992). The composition of Fe-Ti oxide phenocrysts in representative Okataina, Rotorua and Kapenga volcanic centre rhyolite lavas are shown.

Ternary plots of the composition of Fe-Ti oxides in terms of the minor elements Al_2O_3-MnO-MgO are given in Figure 5.9. The titanomagnetites are more Al_2O_3 rich, while ilmenites may be richer in MnO and MgO. Minor element compositions of Fe-Ti oxides in the Haroharo rhyolite lavas are very similar with no distinctions possible on the basis of age or ferromagnesian phenocryst assemblage. The Okareka rhyolites have two distinct

compositions of both titanomagnetites and ilmenites, one for the older biotite-poor Eastern rhyolite and one for the younger biotite-rich Trig 7693 rhyolite. There are also two distinct compositions of both titanomagnetite and ilmenite in Tarawera rhyolites, which correspond to lavas that contain biotite and those that are biotite-free/poor. This difference is not seen in the ho_1 and ho_2 lavas where Fe-Ti oxide compositions are indistinguishable between biotite-rich and biotite-free lavas.

Shane (1998) used titanomagnetite (spinel-phase) compositions to distinguish between eruptives of the Okataina and Taupo volcanic centres. Figure 5.10 indicates that such compositions are of no clear use in distinguishing between rhyolite lavas of the Okataina, Rotorua and Kapenga volcanic centres. However, rhyolites containing titanomagnetite with < 9 wt. % TiO_2 are generally restricted to the Okataina Volcanic Centre. Shane (1998) also used titanomagnetite compositions to distinguish between selected tephra beds erupted from the Okataina Volcanic Centre. Figure 5.10c shows that such compositions cannot be used to distinguish clearly between the ho_3 rhyolite lavas in terms of eruptive episode or vent area. The compositions of titanomagnetite phenocrysts are seen to be related to whether they coexist with biotite, as noted in Figure 5.9. Rhyolites which contain significant amounts of biotite contain titanomagnetite phenocrysts with TiO_2 > ~ 8.5 wt. % and Fe_2O_3 < ~ 51 wt. %. Biotite-free/poor rhyolites contain titanomagnetite phenocrysts with TiO_2 < ~ 9 wt. % and Fe_2O_3 > ~ 49.5 wt. %. This is most noticeable in the Rerewhakaaitu episode during which both biotite-bearing and biotite-free/poor lavas were erupted.

5.8 ACCESSORY MINERALS - APATITE AND ZIRCON

5.8.1 Occurrence and Characteristics

Apatite and zircon occur as accessory crystals in the rhyolite lavas. Apatite occurs as tiny euhedral crystals with a hexagonal or acicular habit and may reach up to 0.75 mm in length, although they are commonly much smaller. They are colourless in plane-polarised light and are most noticeable in crossed-polarised light as white-grey crystals occurring in association with plagioclase phenocrysts (Plate 5.2h). They may also be found in association with ferromagnesian phenocrysts such as biotite.

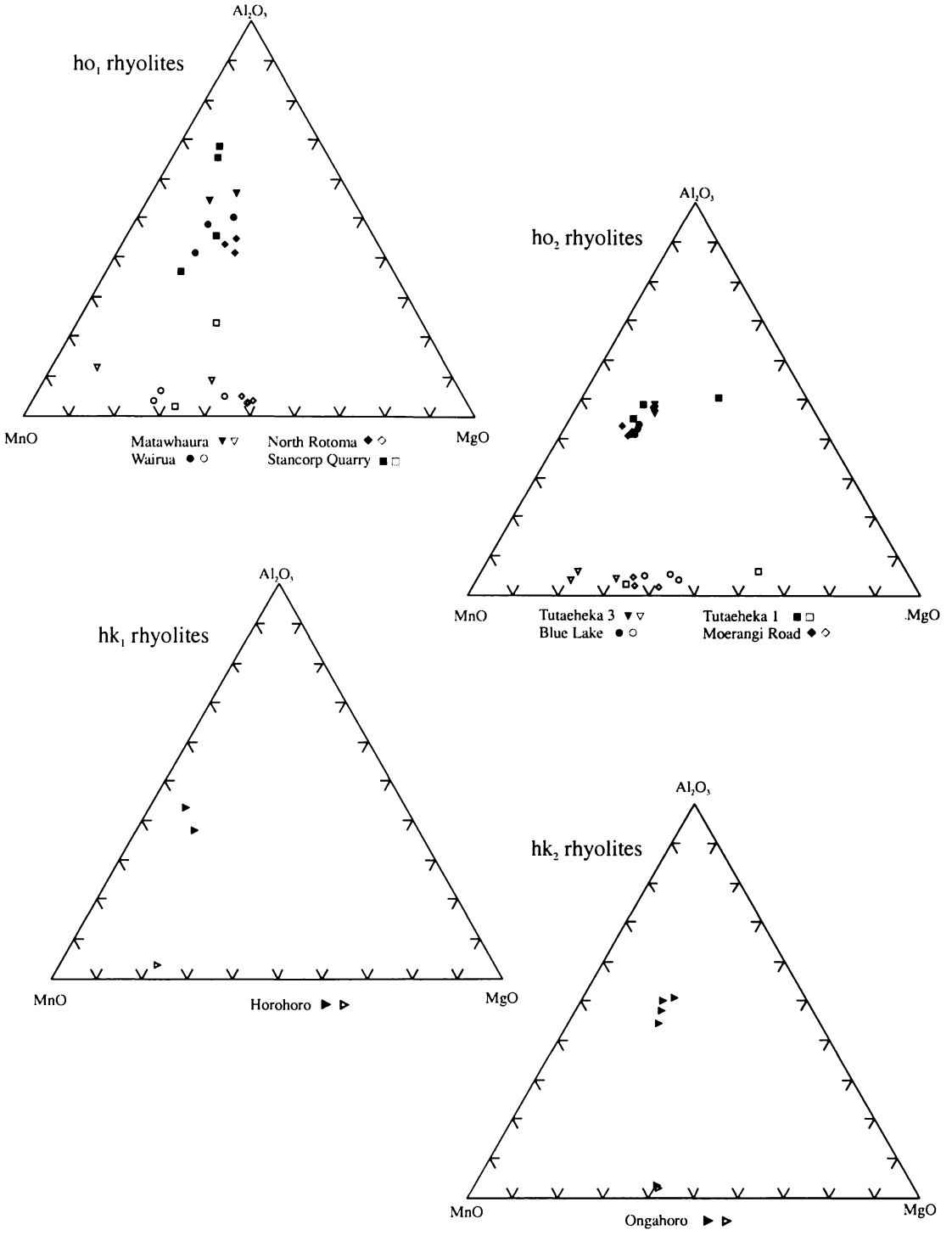

Figure 5.9: The distribution of minor elements between co-existing phenocrysts of titanomagnetite and ilmenite in representative rhyolite lavas. Titanomagnetites (filled/first symbols) are relatively enriched in Al_2O_3 compared to ilmenites (unfilled/second symbols).

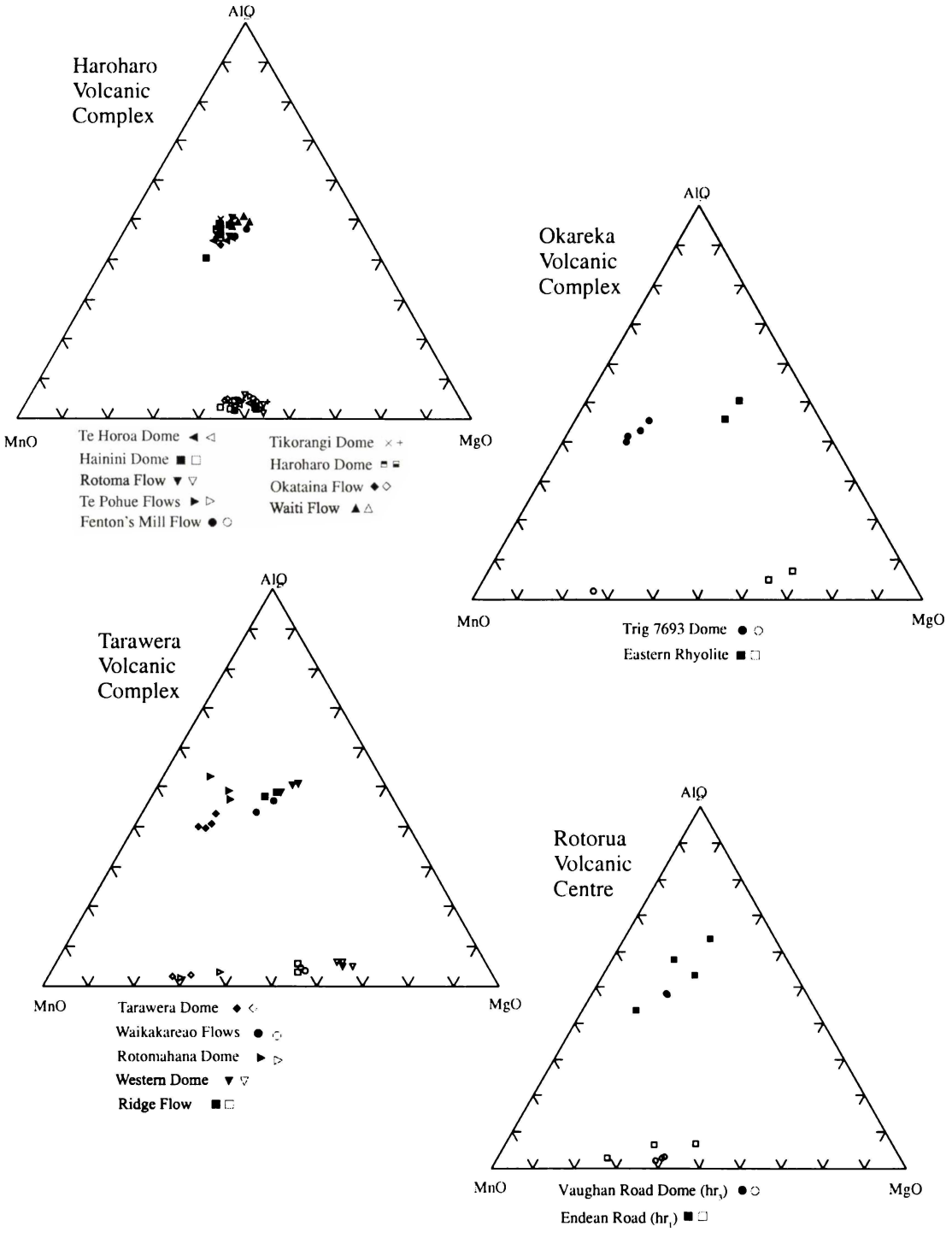

Figure 5.9 (continued): The distribution of minor elements between co-existing phenocrysts of titanomagnetite and ilmenite in representative rhyolite lavas. Titanomagnetites (filled/first symbols) are relatively enriched in Al_2O_3 compared to ilmenites (unfilled/second symbols).

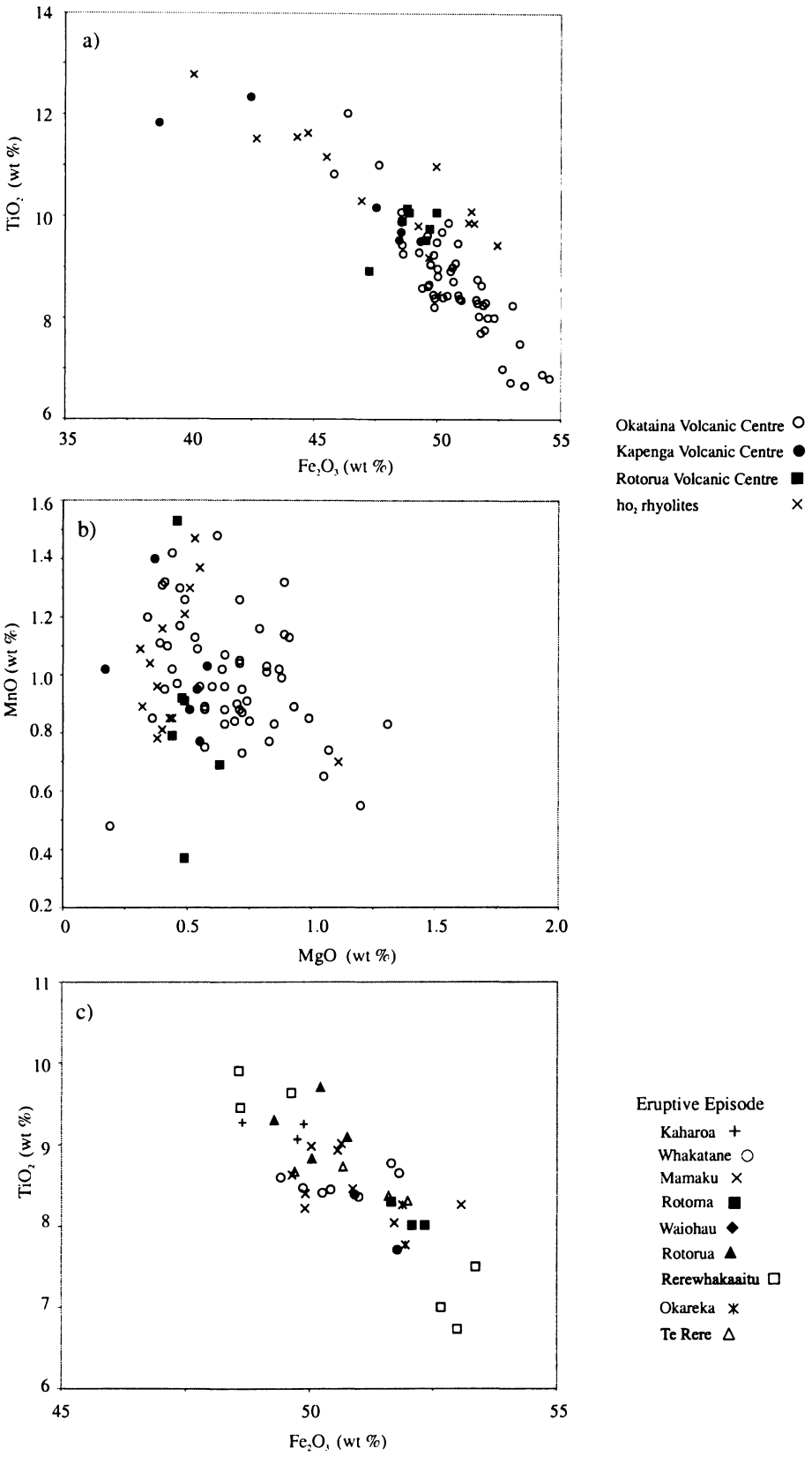

Figure 5.10: Composition of titanomagnetite (spinel-phase) phenocrysts in representative rhyolite lavas classified according to volcanic centre (a and b) and post-caldera eruptive episodes at the Okataina Volcanic Centre (c).

Zircon occurs as tiny euhedral prismatic crystals with extreme relief and very bright interference colours in crossed-polarised light. They occur most commonly in association with Fe-Ti oxide phenocrysts (Plate 5.2g) but may also be seen as individual crystals or in association with ferromagnesian minerals such as biotite. Zircons are generally less than 0.25 mm in length.

5.9 XENOCRYSTS

Xenocrysts (foreign crystals) can often be difficult to distinguish from phenocrysts. An obvious indication of a xenocryst is when it is comprised of a mineral that is out of equilibrium with the phenocryst assemblage and chemistry of the rhyolite lava. An example is augite and olivine crystals occurring in quartz-bearing rhyolite lavas of the Kaharoa Eruptive Episode at the Tarawera Volcanic Complex (Leonard, 1999). Leonard (1999) considered that this disequilibrium mineral assemblage was due to mixing of basaltic and rhyolitic magma. Such a combination of minerals is not seen in any of the rhyolite lavas obtained in study. Extensive resorption of a crystal, and the formation of a sieve texture, suggests that the crystal was out of equilibrium with the surrounding melt and may be xenocrystic. A sieve texture is seen in some plagioclase crystals in the Patiti Island rhyolite, Tarawera Volcanic Complex (Plate 5.1c). These crystals commonly have a non-resorbed euhedral rim suggesting that if they were xenocrysts, then subsequent crystallisation has occurred, in equilibrium with the melt, after their incorporation into the magma.

5.10 INTENSIVE PARAMETERS

5.10.1 Fe-Ti Oxide Geothermometry

Fe-Ti oxide minerals provide important paragenetic information on the rocks containing them and can serve as a useful geological thermometer and oxygen barometer. The basis of such an Fe-Ti oxide geothermometer is that the compositions of co-existing solid solutions of magnetite-ulvospinel and hematite-ilmenite in mutual equilibrium are dependent on temperature and oxygen fugacity (fo_2) (Buddington and Lindsley, 1964).

Oxygen fugacity is a variable used in geologic systems to indicate the potential for iron to occur in a more oxidised or reduced state. At very low oxygen fugacities iron is likely to be found in its native state (Fe^0). At progressively higher oxygen fugacities iron may be found as a divalent ion in a silicate (fayalite (Fe_2SiO_4)) or as a divalent or trivalent ion in an oxide (magnetite ($FeO.Fe_2O_3$), hematite (Fe_2O_3)) (Frost, 1991). However, in natural systems the presence of Mg and Ti also play an important role in determining the relative stabilities of silicates, magnetite and ilmenite. Mg and Fe^{2+} substitute for each other in a variety of silicates. Ti and Fe^{2+} will substitute for Fe^{3+} in both magnetite and hematite. This substitution stabilises these minerals to higher oxygen fugacities (Frost, 1991). As a result the Fe/Mg ratio of the silicates, the Ti content and the ferrous/ferric ratios of the oxides, and oxygen fugacities are all interrelated. In many rocks it is appropriate to say that oxygen fugacity is a function of the Fe/Mg ratio of the silicates and the Ti content of the oxides, for it is more likely that oxygen fugacity is a variable that is governed by the mineral assemblages in the rock, rather than one that is imposed from the environment (Frost, 1991).

Temperature (T) and oxygen fugacity (fo_2) were estimated for coexisting titanomagnetite (spinel) and ilmenite (rhombohedral) phases using a program provided by M. Ghiorso and described by Ghiorso and Sack (1991). Oxide pairs used for such calculations passed the Mg-Mn equilibrium criteria of Bacon and Hirschmann (1988) (Figure 5.11) who found a linear relationship between $\log(Mg/Mn)_{sp}$ and $\log(Mg/Mn)_{rhomb}$. An oxide pair that falls beyond the arbitrarily specified conservative error limits (2σ), determined on the basis of typical electron microprobe precision, may be said to fail the test for equilibrium. Bacon and Hirschmann (1988) note that commonly the composition of phenocrysts that have been oxidised and exsolved do not plot within the error envelope for equilibrium Mg/Mn distribution. For this reason exsolved Fe-Ti oxides were avoided during electron microprobe analysis.

Ghiorso and Sack (1991) note that the majority of quartz-bearing silicic volcanic rocks plot in the temperature range 650° to 900°C. When comparing their calculated temperatures and oxygen fugacities with those of Lindsley et al. (1990) for the same oxide pairs, they observe that their range in calculated temperatures is wider while the range in oxygen fugacity is essentially the same. Comparison of the two distributions reveals that the temperature estimates are highly correlated and that the relative ordering of samples in temperature is preserved using either technique. Ghiorso and Sack (1991) note that both their model and

that of Lindsley et al. (1990) yield nearly identical results for oxide pairs equilibrated close to 800°C and that the difference between results becomes greater at progressively lower and higher temperatures. They consider that part of the inconsistency may lie in alternative formulations for the entropy of exchange reactions involved in the calculations. Differences may also arise through the treatment of minor constituents of the oxides in the thermodynamic models.

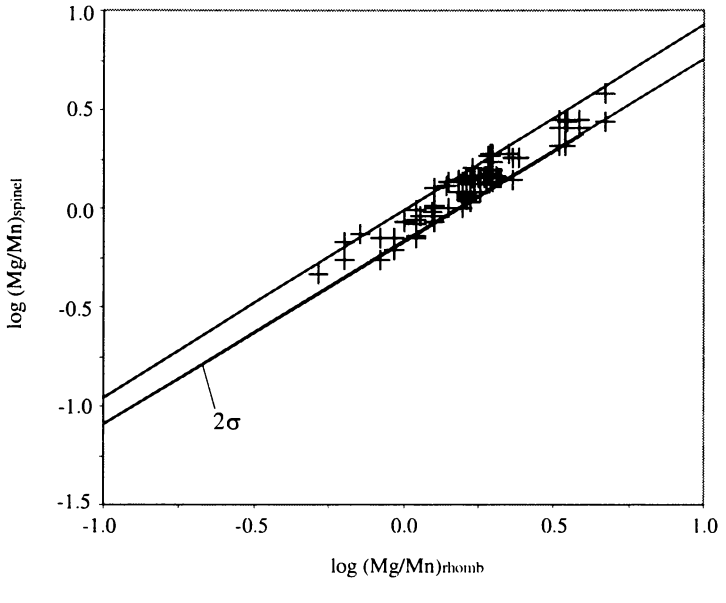

Figure 5.11: Log (Mg/Mn) plot for spinel and rhombohedral pairs used in temperature and oxygen fugacity calculations. The error limits of Bacon and Hirschmann (1988) for the composition of pairs in equilibrium are shown (2σ).

Hence, due to differences that may exist in the formulation of different Fe-Ti oxide geothermometers, care should be taken when comparing results calculated using different models. The model of Ghiorso and Sack (1991) is being used in this study to allow comparison of temperatures and oxygen fugacities for rhyolite lavas with those obtained for pyroclastic eruptives by Shane (1998).

The values of temperature and oxygen fugacity for the equilibration of each titanomagnetite-ilmenite pair are given in Appendix VII (Table VII.1). Temperatures range from 650°C to 835°C. Oxygen fugacity (measured as log fo_2) ranges from -18.53 to -12.28. The errors in temperature and oxygen fugacity calculations when using Fe-Ti geothermometry are

generally ±30°C and ±1.0 log units respectively. Table 5.1 provides a summary of temperature and oxygen fugacity calculations for each of the rhyolite lavas. Figure 5.12 shows a comparison of temperature and oxygen fugacity calculations according to Ghiorso and Sack (1991) with those of Spencer and Lindsley (1981), which use mole fraction recalculations of Stormer (1982), for the same oxide pairs (Table VII.1). Observations can be made regarding the comparative ordering and spread of results that are similar to those made by Ghiorso and Sack (1991) when comparing their results to Lindsley et al. (1990). Calculations that fall into the 800 - 850°C range show little difference between the two models. Fe-Ti oxide pairs with temperature calculations < 800°C according to Spencer and Lindsley (1981) show a drop in temperature when calculated using Ghiorso and Sack (1991). The greatest reduction (45 - 50°C) occurs in pairs that gave the lowest temperatures. However, considering errors of ±30°C involved in these calculations, temperatures calculated using both methods can be considered similar.

Figure 5.13 shows values of temperature and oxygen fugacity for the equilibration of each titanomagnetite-ilmenite pair in relation to the FMQ buffer. Frost (1991) noted that most felsic rocks crystallised at oxygen fugacities one or two log units above the FMQ buffer, which is the case for Okataina, Rotorua and Kapenga rhyolite lavas. Such an observation is sensible given that the substitution of Mg and Ti into silicates and oxides is known to stabilise them to higher oxygen fugacities. At lower temperatures samples lie approximately one log unit above the FMQ buffer and, as the temperature increases, the differences between estimated oxygen fugacity values and those of the FMQ buffer increase.

Temperatures for Haroharo rhyolites range from 661°C to 800°C. There is a general trend of decreasing temperature over time with the oldest lava (Fenton's Mill) having the highest temperatures and the youngest lavas (Okataina and Haroharo) having the lowest temperatures. Tikorangi Dome, which is also one of the youngest lavas, has a temperature similar to the older Waiti Flow. Temperatures for Hainini Dome are very widely spread between 696°C and 766°C. At the Okareka Volcanic Complex the older Eastern rhyolite (828 - 835°C) and younger Trig 7693 rhyolite (651 - 667°C) show large differences in temperature. Tarawera Volcanic Complex rhyolites range from 650°C to 830°C and also become progressively cooler over time. However, biotite-bearing lavas (Rotomahana Dome) are even cooler than the temperature-age trend would suggest.

Table 5.1: Mean Fe-Ti oxide geothermometry calculations for rhyolite lavas of the Okataina, Rotorua and Kapenga volcanic centres.

	Rhyolite Lava	Sample Number	Temperature (°C)	±	log fo_2	±	*N*
Okataina Volcanic Centre							
ho_3							
Kaharoa Episode							
	Tarawera Dome	158	652	3	-18.50	0.05	2
Whakatane Episode							
	Haroharo Dome	6	679	6	-17.19	0.23	6
	Okataina Flow	24	678	16	-17.18	0.60	4
	Tikorangi Dome	98	718	6	-15.85	0.13	2
Mamaku Episode							
	Hainini Dome	7	727	35	-15.35	1.16	5
	Te Horoa Dome	32	700	4	-16.35	0.12	4
	Waiti Flow	173	721	3	-15.77	0.06	8
Rotoma Episode							
	Te Pohue Flows	60	741	9	-14.83	0.28	8
	Rotoma Flow	105	742	16	-14.90	0.56	3
Waiohau Episode							
	Waikakareao Flows	38	744	9	-14.72	0.22	3
Rotorua Episode							
	Trig 7693 Dome	176	658	8	-18.20	0.19	3
Rerewhakaaitu Episode							
	Western Dome	44	802	11	-12.66	0.24	11
	Rotomahana Dome	134	724	5	-15.92	0.08	2
Okareka Episode							
	Ridge Flow	90	824	6	-12.41	0.12	4
Te Rere Episode							
	Fenton's Mill Flow	92	788	14	-13.52	0.38	4
	Eastern Rhyolite	113	832	4	-12.35	0.10	3
ho_2	Tutaeheka 1	64	687	7	-17.17	0.15	2
	Blue Lake	152	743	1	-15.21	0.03	2
ho_1	North Rotoma	107	715	10	-15.29	0.32	9
	Wairua	119	727	30	-15.71	1.00	2
Kapenga Volcanic Centre							
hk_2	Ongahoro	170	710	7	-16.47	0.19	5
hk_1	Horohoro	126	832		-13.39		1
Rotorua Volcanic Centre							
hr_3	Vaughan Road	104	661	7	-18.22	0.27	3
hr_1	Endean Road	87	736	3	-15.55	0.06	2

Temperature and oxygen fugacity (fo_2) represent means from number (*N*) of Fe-Ti oxide pairs and are calculated following Ghiorso and Sack (1991). Errors (±) are one standard deviation from the mean.

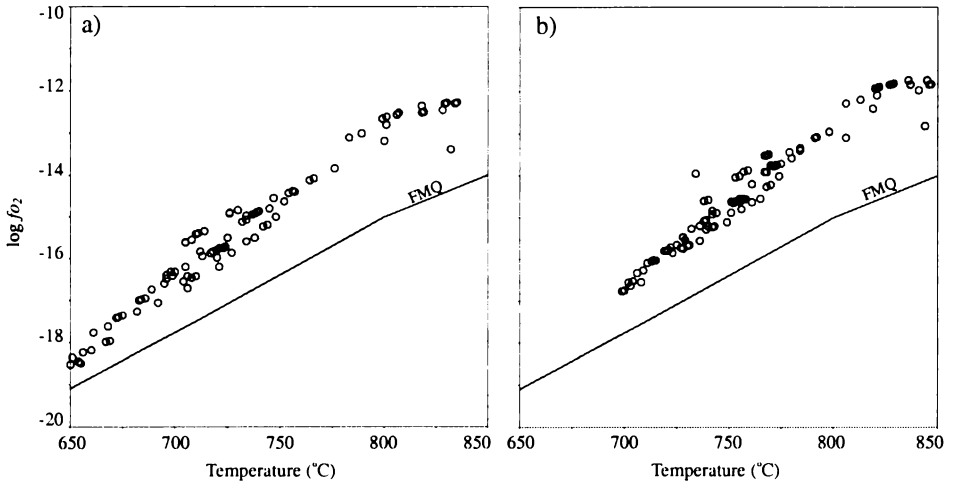

Figure 5.12: Temperature vs. oxygen fugacity for each oxide pair according to a) Ghiorso and Sack (1991) and b) Spencer and Lindsley (1981) using mole fraction recalculations of Stormer (1982). FMQ buffer curve from Carmichael (1967) and Wones and Gilbert (1969).

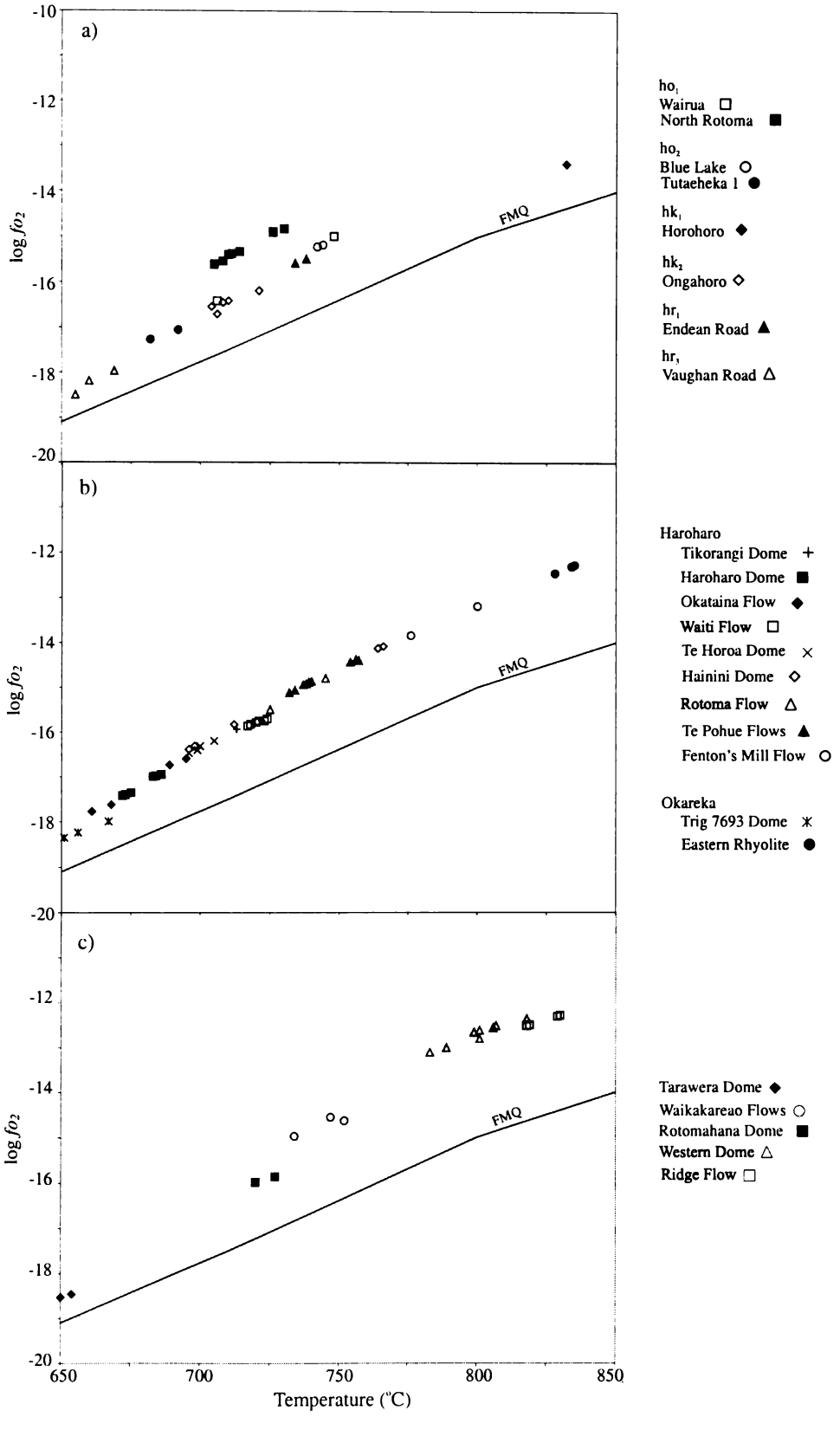

Figure 5.13: Temperature vs. oxygen fugacity for each oxide pair according to Ghiorso and Sack (1991). a) Representative ho_1, ho_2, hk_1, hk_2, hr_1 and hr_3 rhyolite lavas. b) Representative Haroharo and Okareka volcanic complex ho_3 rhyolite lavas. c) Representative Tarawera Volcanic Complex ho_3 rhyolite lavas. FMQ buffer curve from Carmichael (1967) and Wones and Gilbert (1969).

Temperatures for Rotorua rhyolites fall into two groups. The older Endean Road rhyolite has a temperature of 734 - 738°C, while the younger Vaughan Road dome has a temperature of 655 - 669°C. Shepherd (1991) obtained temperatures of 711°C and 778°C for hr_2 rhyolites of the Ngongotaha Dome Complex and Richnow (1999) calculated temperatures of 784 - 823°C for Quarry Dome. The Kapenga rhyolites also fall into two groups, Horohoro at 832°C and the younger Ongahoro at 704 - 721°C. This temperature for Horohoro is comparable to a temperature of 810 - 950°C obtained by Gaston (1991) for Tumunui, another hk_1 rhyolite.

Temperatures available for two ho_2 rhyolite lavas form two groups at 682 - 692°C and 742 - 744°C, while those available for two ho_1 rhyolite lavas are essentially the same (705 - 748°C). However, the North Rotoma rhyolite has significantly higher log fo_2 than Wairua for similar temperatures. This feature is also apparent in Figure 5.14a, which plots temperature and log fo_2 for all rhyolite lavas in relation to their ferromagnesian phenocryst assemblage. The data falls onto three curves that run essentially parallel to the experimental FMQ buffer curve, and which are related to ferromagnesian phenocryst assemblage. Lavas in which biotite is present in significant quantities lie on a curve closest to the FMQ buffer with temperatures ranging from 650 - 748°C. Lavas in which both biotite and cummingtonite are present fall on a curve furthest from the FMQ buffer with temperatures ranging from 705 - 730°C. An intermediate curve comprises lavas which contain orthopyroxene + calcic amphibole at higher temperatures (734 - 835°C), forming a continuous trend with orthopyroxene + calcic amphibole ± cummingtonite bearing lavas at intermediate temperatures (696 - 766°C) and cummingtonite dominated lavas at lower and intermediate temperatures (661 - 695°C and 732 - 756°C). Ewart et al. (1971, 1975) also correlated Fe-Ti oxide geothermometry temperatures for Taupo Volcanic Zone rhyolites to ferromagnesian mineral assemblages: cummingtonite + calcic hornblende ± orthopyroxene (725 - 755°C), calcic hornblende + orthopyroxene (750 - 825°C), biotite + calcic hornblende ± cummingtonite ± orthopyroxene (720 - 765°C). These temperature ranges of Ewart et al. (1971, 1975) are in agreement with those calculated in this study.

Figures 5.14b and 5.14c show the relationship of Δlog fo_2 (FMQ), displacement of the estimated oxygen fugacity relative to the FMQ buffer, to temperature for Haroharo, Okareka and Tarawera volcanic complex rhyolites. Such a relationship was used by Shane (1998) to

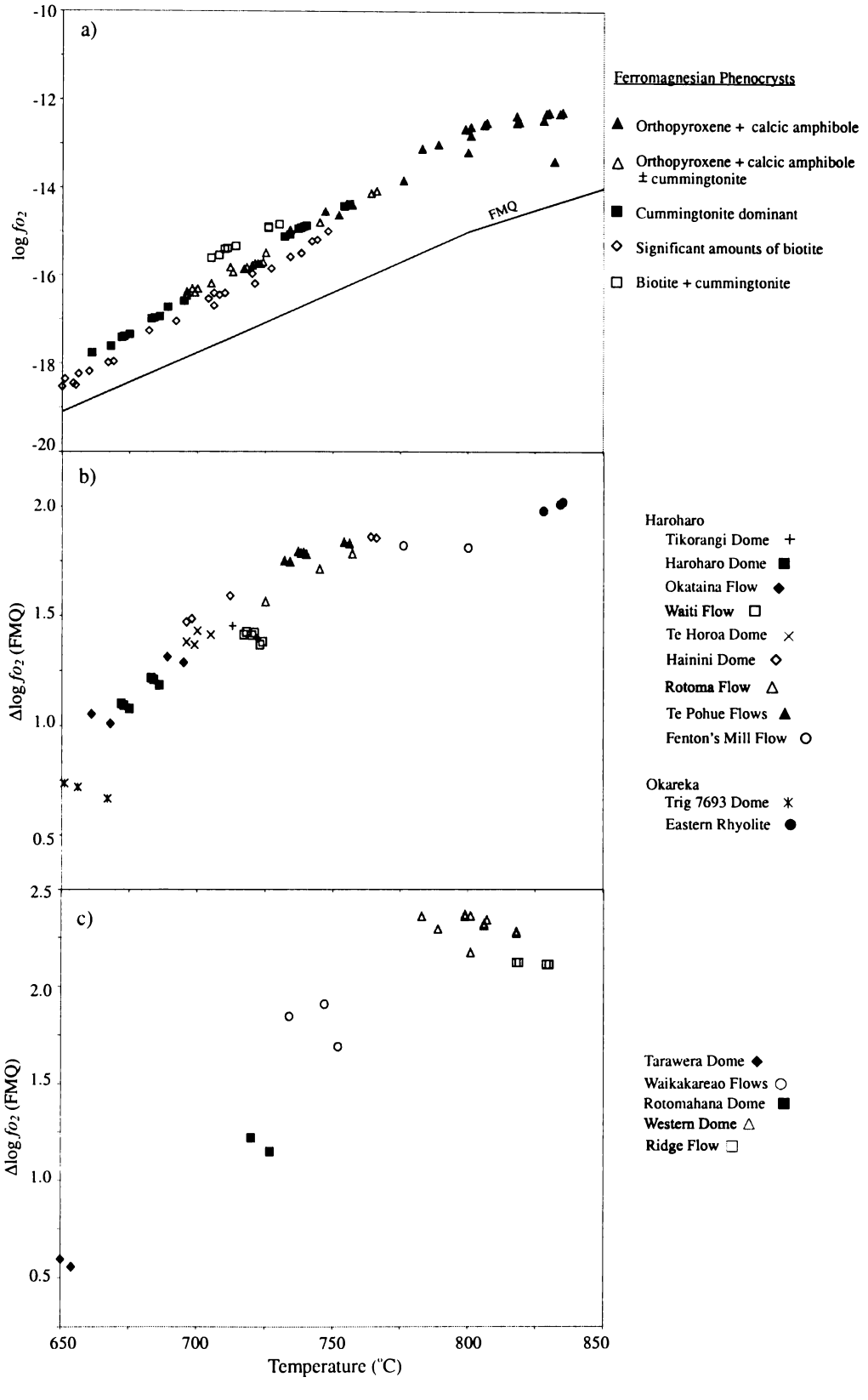

Figure 5.14: a) Temperature vs. oxygen fugacity for Fe-Ti oxide pairs according to Ghiorso and Sack (1991) in relation to the co-existing ferromagnesian phenocryst assemblage. b) Temperature and Δlog fo_2 (FMQ) estimates for Haroharo and Okareka volcanic complex ho_3 rhyolite lavas. c) Temperature and Δlog fo_2 (FMQ) estimates for Tarawera Volcanic Complex ho_3 rhyolite lavas. FMQ buffer curve from Carmichael (1967) and Wones and Gilbert (1969).

identify magma batches for the pyroclastic eruptive units of the Okataina Volcanic Centre. A closer inspection reveals that such identification was more successful for the older Mangaone, Rotoiti and Earthquake Flat eruptives than for the younger post caldera pyroclastics erupted in association with ho_3 rhyolite lavas. It is evident from Figures 5.14b and 5.14c that it is possible to use these parameters to identify some eruptive episodes, but further subdivision between vent areas at the Haroharo Volcanic Complex is not possible.

Apparent in Figure 5.14a is that Δlog fo_2 (FMQ) appears to be related to coexisting ferromagnesian phenocryst assemblages. This is not a new observation, and the correlation has been interpreted previously in terms of mineral assemblages defining the thermodynamic intensive variables of the magmatic liquid (Carmichael, 1967; Ghiorso and Sack, 1991).

When taking into consideration the errors involved in such calculations (±30°C), temperatures for the ho_3 lavas are in agreement with those calculated by Shane (1998) for associated pyroclastic eruptives (Table 5.2). The exception is the mean temperature of 856°C obtained by Shane (1998) for the Rotorua Tephra, which is ~ 200°C above the temperatures obtained in this study (658°C) for Rotorua Eruptive Episode lavas. Ghiorso and Sack (1991) reported temperatures of ~ 740 - 860°C for selected Okataina Volcanic Centre rhyolite lavas, which are also in agreement with those obtained in this study.

Table 5.2: Mean temperature and oxygen fugacity calculations for tephra units of the Okataina Volcanic Centre (from Shane, 1998).

Eruptive Unit	Temperature (°C)	±	log fo_2	±	*N*
Kaharoa	724	16	-15.65	0.54	9
Mamaku	750	5	-14.60	0.19	6
Rotoma	745	6	-14.56	0.18	4
Waiohau	761	13	-14.31	0.34	5
Rotorua	856	16	-11.60	0.34	6
Rerewhakaaitu	770	9	-14.04	0.24	5

Temperature and oxygen fugacity (fo_2) represent means from number (*N*) of Fe-Ti oxide pairs and are calculated following Ghiorso and Sack (1991). Errors (±) are one standard deviation from the mean.

Figure 5.15 compares average temperature estimates for ho_3 rhyolite lavas from the Okataina Volcanic Centre to whole rock geochemistry, phenocryst chemistry and age. Over the small range in SiO_2 compositions for these rhyolites (~ 3 wt. %) there is a broad trend of lower temperature lavas containing higher SiO_2 contents and lower Al_2O_3 and Fe_2O_3 contents. Shane (1998) observed a relationship between temperature and the composition of orthopyroxene crystals in pyroclastic eruptives from the Okataina Volcanic Centre. He noted that as temperature increased so did the En content of orthopyroxene cores, from c. En_{45} to En_{65} over a temperature range of ~ 700 - 980°C. Such a trend is not obvious in orthopyroxene phenocrysts in the ho_3 rhyolite lavas. Ewart et al. (1975) noted a drop in the An content of plagioclase phenocrysts in rhyolites of the Taupo Volcanic Zone with a drop in temperature. However, a similar trend is not seen for the ho_3 rhyolites, with lavas of a particular temperature containing plagioclase phenocrysts with a wide range in An compositions. As previously mentioned, the ho_3 rhyolites have become cooler over time with the youngest lavas of the Tarawera and Haroharo volcanic complexes having the lowest temperatures, and the oldest lavas at Haroharo, Tarawera and Okareka having the highest temperatures. Two outliers fall below the trend for other samples. These are Rotomahana Dome at Tarawera and Trig 7693 Dome at Okareka, which contain significant amounts of biotite, and as previously noted, they are cooler than the temperature-age trend would predict.

5.10.2 Hornblende - Plagioclase Thermometry

The use of hornblende-plagioclase thermometry (Holland and Blundy, 1994) has been possible for samples in which both species were analysed by electron microprobe. The edenite-tremolite thermometer (thermometer A) has been used as the rhyolite lavas contain quartz. Temperature calculations for individual calcic amphibole phenocrysts, and an average plagioclase composition for each sample, are given in Appendix VII (Table VII.2). Such calculations are dependent on equilibration pressure and the temperature calculations for 0, 5 and 10 kbar are given. The error in temperature calculations when using hornblende-plagioclase thermometry is ±40°C (Holland and Blundy, 1994). Pressure estimates for these rhyolite lavas are in the range 1 - 5 kbar (see section 5.10.3) and for this reason further discussion of hornblende-plagioclase thermometry temperatures will refer to

the average temperature for 0 and 5 kbar. Such average temperatures range from 677°C to 846°C.

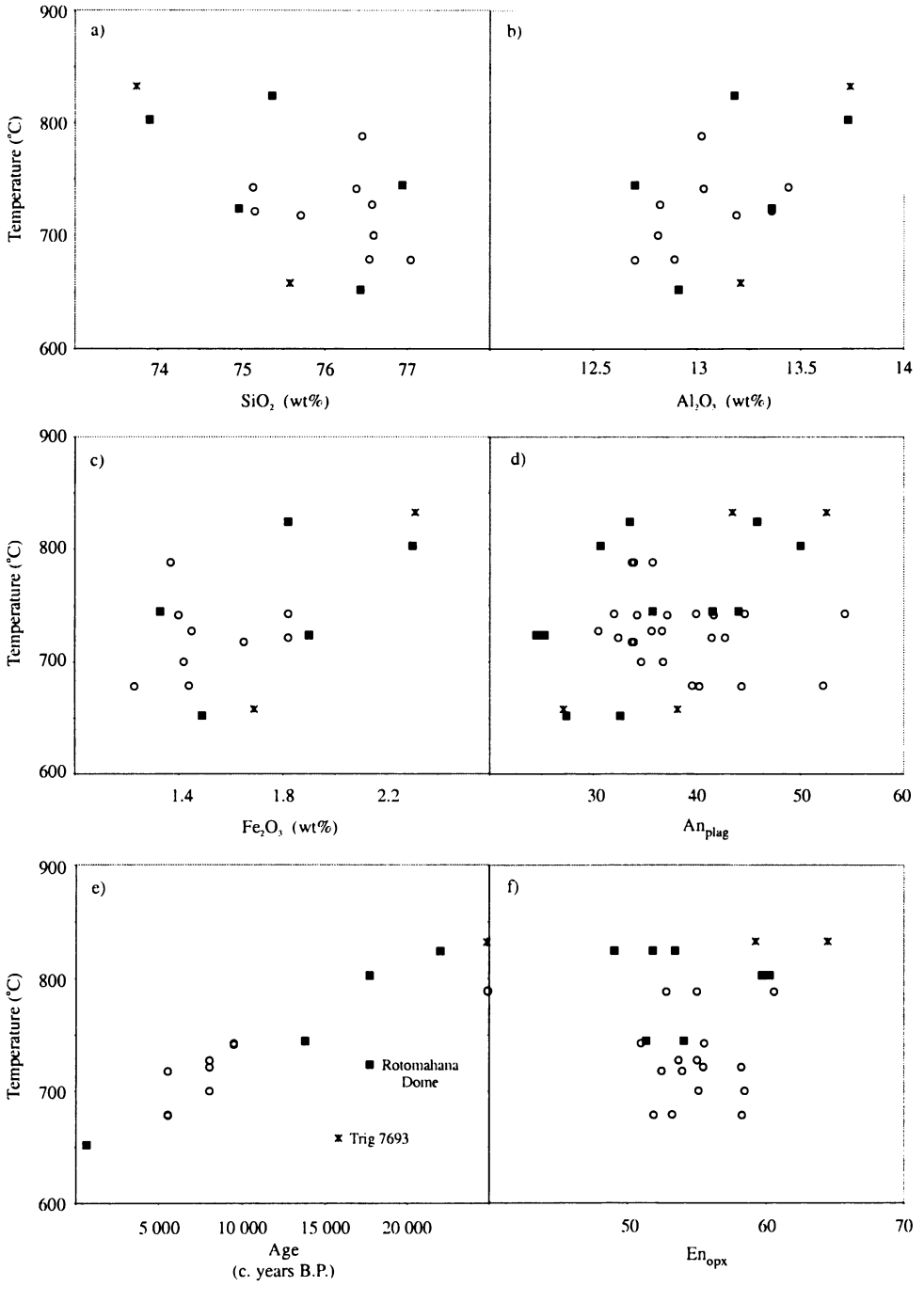

Figure 5.15: Comparison of mean temperature estimates for ho_3 rhyolite lavas from the Okataina Volcanic Centre with whole rock geochemistry (a-c), phenocryst chemistry (d and f) and age (e). Temperature calculated according to Ghiorso and Sack (1991) (Table 5.1). Ages from Table 2.3. Open circles, filled squares and asterisks are Haroharo, Tarawera and Okareka volcanic complex lavas respectively. For An and En compositions each point represents a single plagioclase or orthopyroxene core analysis.

This technique would appear to have an advantage over Fe-Ti oxide geothermometry in that the mineral species do not have to be checked for equilibrium and temperatures can be calculated for lavas in which the Fe-Ti oxides are oxidised and exsolved. However, the crystallisation of hornblende and plagioclase in equilibrium is still implied and it would seem logical that this technique would be most reliable when applied to hornblende and plagioclase crystals that have crystallised in contact with one another. In this study the average composition of plagioclase crystals analysed in each sample has been used, excluding outliers noted in Figure 5.1, since no plagioclase and amphibole phenocrysts in contact with one another were analysed. As the composition of plagioclase phenocrysts can be quite variable in some samples, this places important limitations on the use of this method.

Table 5.3 provides a summary of temperature calculations for each of the rhyolite lavas. Considering the errors involved in both this method and Fe-Ti oxide geothermometry, the temperatures calculated by both methods are generally in agreement (Figure 5.16) for the Fe-Ti oxide geothermometry calculations of both Ghiorso and Sack (1991) and Spencer and Lindsley (1981). However, the correlation is better for the calculations of Spencer and Lindsley (1981). The exception is Western Dome, from the Tarawera Volcanic Complex, which gives a high Fe-Ti oxide temperature (> 800°C, Table 5.1) yet a low hornblende-plagioclase temperature (680°C). This lava contains orthopyroxene and calcic amphibole as dominant ferromagnesian minerals and the Fe-Ti oxide temperatures calculated are considered consistent with this assemblage. The average plagioclase composition used in calculations for this sample (Xab = 0.65) excluded an Ab-poor outlier.

Hornblende-plagioclase thermometry is sensitive to the Ab content of plagioclase and, for a particular hornblende composition, a reduction in Xab increases the calculated temperature. Calculations were repeated for Western Dome using the Xab content of the Ab-poor outlier (Xab = 0.49, Table VII.2) and the average temperature rose by 32°C. However, this is still not high enough to be considered similar to the Fe-Ti oxide temperature, even when taking errors into consideration. Hence, it is suggested that the calcic amphibole phenocrysts analysed in Western Dome are out of equilibrium with the plagioclase phenocrysts and hence do not provide reliable temperature estimates.

Table 5.3: Mean hornblende-plagioclase thermometry calculations for rhyolite lavas of the Okataina, Rotorua and Kapenga volcanic centres.

	Rhyolite Lava	Sample Number	Temperature (°C)	±	*N*
Okataina Volcanic Centre					
ho_3	Whakatane Episode				
	Tikorangi Dome	98	759	20	4
	Mamaku Episode				
	Hainini Dome	7	750	25	4
	Te Horoa Dome	32	736	16	3
	Waiti Flow	173	755	29	5
	Rotoma Episode				
	Te Pohue Flows	60	738	80	2
	Rotoma Flow	105	772	28	8
	Rotorua Episode				
	Trig 7693 Dome	176	769	24	2
	Rerewhakaaitu Episode				
	Western Dome	44	680	4	3
	Rotomahana Dome	134	756	31	4
	Okareka Episode				
	Ridge Flow	90	804		1
	Te Rere Episode				
	Fenton's Mill Flow	92	804	25	2
	Eastern Rhyolite	113	829	19	2
ho_2	Tutaeheka 1	64	750	26	4
	Tutaeheka 3	117	752	11	2
	Blue Lake	152	768	48	2
ho_1	Matawhaura	109	832	19	2
	Wairua	119	758	14	2
Kapenga Volcanic Centre					
hk_2	Ongahoro	170	722	18	3
Rotorua Volcanic Centre					
hr_3	Mokoia Island	103	734	28	2
	Vaughan Road	104	728	2	2
hr_1	Endean Road	87	766	10	3

Temperatures represent means from number (*N*) of 0-5 kbar mean calculations using individual amphibole phenocrysts and an average plagioclase content for each sample, and are calculated following Holland and Blundy (1994). Errors (±) are one standard deviation from the mean.

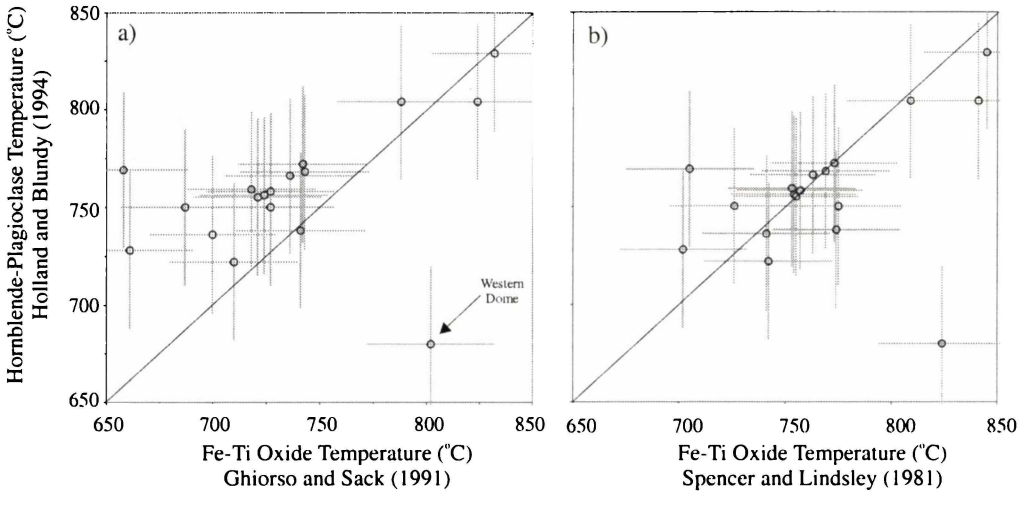

Figure 5.16: Comparison of mean Fe-Ti oxide and hornblende-plagioclase temperatures for rhyolite lavas from the Okataina, Rotorua and Kapenga volcanic centres. Errors of ± 30°C in Fe-Ti oxide calculations and ± 40°C in hornblende-plagioclase calculations are indicated.

5.10.3 Pressure Estimates

The Al-in-hornblende geobarometer of Johnson and Rutherford (1989) has been used to estimate crystallisation pressures for the Okataina, Rotorua and Kapenga rhyolite magmas and results are given in Appendix VII (Table VII.3). The estimated pressures are those at the time of hornblende crystallisation. This geobarometer requires hornblende to be in equilibrium with biotite, quartz, sanidine, plagioclase, sphene and magnetite or ilmenite. Estimates of pressure for hornblende and biotite bearing lavas obtained in this study range from 0.7 - 3.0 kbar with an average of 1.6 kbar. The error in these pressure calculations is ± 0.5 kbar. Based on a pressure gradient of 3 km/kbar (similar to pressure gradients used in other studies of Okataina eruptives, eg. Leonard, 1999; Smith, 2001; Speed, 2001) this suggests crystallisation depths up to ~ 10 km.

More recently, Anderson and Smith (1995) have made modifications to the Al-in-hornblende geobarometer to account for the temperature of the system. Estimates of pressure made using average temperatures calculated by the method of Holland and Blundy (1994) (Table 5.3) range from 0.6 - 3.5 kbar, with an average of 1.7 kbar (Table VII.3). The error in pressure calculations is ± 0.6 kbar, although uncertainty in temperatures of ± 50°C leads to an additional average uncertainty of ± 0.8 kbar. Hence, taking these errors into account, the crystallisation depth could be up to ~ 15 km. However, the temperature estimates of Holland and Blundy (1994) are themselves pressure dependant. Using independent temperature estimates from Fe-Ti oxide geothermometry (Table 5.1) in the calculations of Anderson and Smith (1995) gives pressure estimates of 1.0 - 3.7 kbar with an average of 2.3 kbar (Table VII.3).

Differences between pressure estimates for hornblende crystals in the same sample that are greater than the errors associated with the calculations, suggests that hornblende has crystallised at multiple pressures (polybaric crystallisation), and hence depths, within the crust. This may be indicative of a pressure gradient within a magma batch or crystallisation of hornblende at different pressures as the magma batch migrated through the crust.

It should be noted that none of the Okataina, Rotorua and Kapenga lavas contain primary sanidine and therefore the validity of such pressure estimates may be limited. In addition, temperature estimates from co-existing Fe-Ti oxides were calculated from the compositions

of primarily discrete crystals, and not those occurring as inclusions within amphibole phenocrysts. Hence these temperatures better reflect those at the time Fe-Ti oxides were crystallising and not necessarily at the time of hornblende crystallisation. However, estimates of pressure made in this study are comparable with estimates documented in other studies. Ewart et al. (1975) calculated an average P_{total} of 2.2 kbar for rhyolites of the Taupo Volcanic Zone, corresponding to an equilibration depth of ~ 7 - 8 km. Ghiorso and Sack (1991) inferred equilibration pressures from coexisting oxide and silicate phenocrysts for a variety of silicic volcanic rocks, which included lavas from the Okataina Volcanic Centre at pressures of ~ 1.5 - 5 kbar.

Other studies have indicated that cummingtonite-bearing lavas crystallised at comparable pressures to those calculated above for hornblende and biotite-bearing lavas. Evans and Ghiorso (1995) note that cummingtonite-bearing volcanic rocks are indicative of shallow magma chambers (< 4 kbar) and a H_2O-rich fluid close to or at saturation. Nicholls et al. (1992) considered that cummingtonite-bearing rhyolites of the Okataina Volcanic Centre formed under conditions close to saturation in water and that the cummingtonite could have crystallised only at pressures ≤ 3 kbar (depths ≤ 10 km), probably in the roof zone of a shallow crustal magma.

Brown (1994) applied the geobarometer of Johnson and Rutherford (1989) to the sanidine-free Western Dome Belt rhyolite lavas associated with the Whakamaru Volcanic Centre, and calculated crystallisation pressures up to 1.5 kbar, indicating shallow crustal reservoirs (~ 2.5 - 4.5 km). Leonard (1999) calculated an average pressure of 1.3 kbar (± 1 kbar) for the Kaharoa eruptives from Tarawera and, based on a pressure gradient of 3.3 km/kbar, suggested emplacement depths of 1.0 - 7.6 km for the magma chamber. Wright (2000) used the geobarometer of Johnson and Rutherford (1989) to calculate pressures of 0.7 - 4.6 kbar for the biotite and sanidine-free Mamaku Eruptive Episode lavas and pyroclastics from the Haroharo Volcanic Complex.

Crystallisation pressure and depth calculations made in this study are more or less consistent with a crustal thickness of ~ 15 km beneath the Taupo Volcanic Zone, which has been determined on the basis of geophysical data (Stern and Davey, 1987; Beanland and Haines, 1998).

5.10.4 H_2O Content Estimates

The H_2O content of Haroharo Volcanic Complex rhyolite melts has been estimated using a program provided by T. Housh and described by Housh and Luhr (1991). Calculations relate the composition of a plagioclase phenocryst rim, melt composition, temperature and the H_2O content of the melt. If plagioclase phenocryst and melt (groundmass glass) compositions are known, in this case from electron microprobe analyses, and an independent estimate of the temperature of the system can be made, for example from Fe-Ti oxide geothermometry, then the H_2O content of the melt can be estimated. The calculations also require an estimate of the pressure of the system. Two calculations are made, one based on the Ab content of the plagioclase and another based on the An content. Housh and Luhr (1991) note that under optimal conditions the uncertainties in estimated H_2O contents are 0.54 and 0.33 wt. % for the Ab and An calculations respectively.

H_2O estimates for rhyolite melts from the Haroharo Volcanic Complex at a pressure of 2 kbar are given in Appendix VII (Table VII.4) and range from ~ 2.8 - 11.6 wt. %. The melt (groundmass glass) composition used for these calculations was an average for each sample from analyses given in Appendix VIII (Table VIII.1). H_2O contents were calculated for each plagioclase phenocryst rim composition at two temperatures, which represent the upper and lower temperature limits based on average Fe-Ti oxide temperatures given in Table 5.1 and applying an error of ± 30°C. Calculations were also carried out at pressures of 4 and 6 kbar. H_2O content estimates for these higher pressures were within 0.1 wt. % of the values given in Table VII.4. Hence varying the pressure by 4 kbar has little effect on the estimated water content of these rhyolite magmas.

However, it is apparent that varying the temperature of the melt has quite a significant effect on estimates of water content. Housh and Luhr (1991) note that successful estimates of H_2O content require a good estimate of pre-eruptive temperature. The importance of temperature can be seen in Table VII.4 where increasing the temperature by 60°C results in the estimated H_2O content decreasing by ~ 1.5 - 3.5 wt. % depending on the original temperature. Given that Fe-Ti oxide geothermometry temperature estimates following Ghiorso and Sack (1991) are known to be slightly lower than other methods (e.g. Spencer and Lindsley, 1981), the best estimates of H_2O contents in Haroharo magmas would be those calculated at the higher temperature for each plagioclase phenocryst. These higher temperatures are well within the range calculated for these rhyolites following Spencer and Lindsley (1981) (Table VII.1).

The An content of the plagioclase also has an effect on estimated H_2O contents. For example, in sample number 105 at 770°C plagioclase phenocrysts with An contents of 31, 33, 36 and 42 give H_2O (Ab) contents of ~ 5.2, 5.4, 5.6 and 6.1 wt. % respectively and H_2O (An) contents of ~ 4.6, 4.3, 4.0 and 3.5 wt. % respectively.

Many of the H_2O content estimates given in Table VII.4 show a difference between calculations based on Ab content and An content that is well beyond the expected errors in these calculations under optimal conditions. The most agreeable H_2O content estimates for each sample are highlighted (bold font) in Table VII.4. Interestingly, the most agreeable estimates occur for calculations using the higher temperature and plagioclase with the lowest An content. Considering only these most agreeable calculations, H_2O content estimates for Haroharo Volcanic Complex rhyolite melts range from ~ 2.8 - 7.6 wt. %.

Estimated H_2O contents show some correlation with the ferromagnesian phenocryst assemblage of the rhyolites. The orthopyroxene and calcic amphibole bearing Fenton's Mill rhyolite (sample number 92) has the lowest estimated H_2O content of ~ 2.8 - 4.4 wt. %. Rhyolites which contain small or trace amounts of cummingtonite (Hainini Dome (7), Tikorangi Dome (98), Rotoma Flow (105) and Waiti Flow (173)) have estimated water contents ranging from ~ 4.3 - 6.1 wt. %. Rhyolites that have cummingtonite as the dominant ferromagnesian phenocryst (Haroharo Dome (6), Okataina Flow (24) and Te Pohue Flow (60)) have estimated water contents ranging from ~ 4.5 - 7.6 wt. %.

These estimated water contents for the Haroharo Volcanic Complex rhyolites are comparable to estimations in other studies. Experiments in a synthetic system show that the presence of hornblende requires a minimum of ~ 4 wt. % H_2O at 2 kbar and ~ 2.5 wt. % at 8 kbar (Naney, 1983). Calculations for amphibole and biotite-bearing rhyolites by Ewart et al. (1975) indicate that magmas were water saturated, with water contents of ~ 6 wt. % prior to eruption.

Taylor et al. (1983) determined water contents of young (≤ 2000 years old) obsidian domes and flows in North America. The measured H_2O contents are those at the time the glass cooled, hence in the case of a dome or flow, after emplacement. Water contents > 0.4 wt. % were rare and values close to 0.2 wt. % were more common. Stevenson et al. (1994) provided the first detailed analyses of the physical properties of Taupo Volcanic Zone rhyolite lavas. This included estimates of the water content of the Haumingi Lava Flow,

Haroharo Volcanic Complex, which varies between 0.12 and 0.36 wt. % H_2O. Hence, as these Haroharo Volcanic Complex rhyolite lava domes and flows have low post-eruption water contents compared to calculations for magmatic water contents (as above, ~ 3 - 8 wt. %), there must have been significant degassing between the magma chamber and the surface.

5.10.5 Flow Viscosity and Velocity Estimates

Stevenson et al. (1994) provided the first estimates of the viscosity and velocity of Taupo Volcanic Zone rhyolite lavas. A physiochemical method, which incorporates the composition of the lava, eruptive temperature and water content, estimates the viscosity of the interior of the Haumingi and Waiti lava flows, Haroharo Volcanic Complex, during emplacement as 10^{10} Pa·s and 10^{11} Pa·s respectively (1 Pa·s = 10 poise (P)). These calculations are supported by a morphological method, based on the morphology of the arrested flows, which gives viscosity estimates of 10^{10} - 10^{11} Pa·s for both flows. The mean velocity of both lavas was estimated as ~ 10^{-4} m/s, giving between 0.5 and 2.0 years for the Haumingi and Waiti flows to advance 6.7 and 5 km respectively. Stevenson et al. (1994) also estimated the time it would take for the Haumingi Flow to cool below the brittle glass transition temperature, ~ 3 years for the flow carapace (upper 20 metres) and > 30 years for the core of the flow.

Chapter Six:
Sr-Nd-Pb Isotopes and Rhyolite Petrogenesis

Chapter Six: Sr-Nd-Pb Isotopes & Rhyolite Petrogenesis

6.1 INTRODUCTION

The genesis of silicic magmas is considered to be a complex multi-stage process that may involve fusion or partial melting of crustal rocks, fractional crystallisation of mantle-derived basaltic magma, and crustal assimilation. The components involved in either partial melting or assimilation may be from the upper or lower crust. This chapter discusses the petrogenesis of rhyolite lavas from the Okataina, Rotorua and Kapenga volcanic centres. Current models for rhyolite magma genesis in the Taupo Volcanic Zone (TVZ) will be reviewed, and new isotopic data for the rhyolite lavas will be used to provide some insights into magma genesis at the Okataina, Rotorua and Kapenga volcanic centres. Thirty-three representative samples were analysed for Sr isotopes, eleven for Nd isotopes and six for Pb isotopes on a Finnigan Mat 262 thermal ionisation mass spectrometer (TIMS) at VIEPS, La Trobe University, Melbourne, Australia. Petrogenetic modelling will assess the role of fractional crystallisation and combined assimilation-fractional crystallisation (AFC) processes in the genesis of these rhyolite lavas.

6.2 ISOTOPES

6.2.1 Analytical Procedure

Samples were prepared for analysis in a low-blank clean laboratory. Approximately 100 mg of sample powder was weighed into either a PFA teflon beaker (Sr) or Krogh-style PTFE teflon bomb (Nd), followed by dissolution with HF-HNO_3 and HCl. Sample powders for Pb analysis (50 mg) were leached with hot 6M HCl (30 minutes) prior to dissolution. The Sr fraction was separated from the sample solution by one of two methods:

a) Cation exchange resin (AG 50W-X8 200-400 mesh) packed into Si-glass columns using HCl gradient elution.

b) Eichrom^{TM} Sr.spec resin (an element specific "filter") following the method of Pin et al. (1994).

Nd was purified from REE fractions collected by method (a) on 3 ml beds of HDEHP-coated Kel-F material following Richard et al. (1976). Pb was purified using conventional HBr-HCl anion exchange methods on 0.1 ml resin beds.

Sr samples were loaded as phosphates onto single Ta filaments, or onto single Re filaments with a Ta emitter. Nd was picked up in H_3PO_4-doped 1M HNO_3 and loaded onto the Ta side of a Re-Ta filament assembly. Pb was loaded onto a single Re filament in a suspension of silica gel with phosphoric acid, following the method of Gerstenberger and Haase (1997).

All three elements were analysed in static multi-collection mode. Instrumental mass fractionation for Sr and Nd was corrected by normalizing to $^{86}Sr/^{88}Sr = 0.1194$ and $^{146}Nd/^{144}Nd = 0.7219$, respectively, while a ^{207}Pb-^{204}Pb double spike was used for Pb (Woodhead et al., 1995). Sr and Nd isotope ratios are reported relative to SRM987 Sr = 0.71023 and La Jolla Nd = 0.511860, respectively. Internal precisions for Sr were $\leq \pm 0.000035$ ($2\sigma_{mean}$); external precision based on multiple analyses of geological standards (BCR-1, BHVO-1) is ± 0.000040 (2σ). Internal precision for Nd is ≤ 0.000015; external precision is ± 0.000020 (2σ). External precisions for Pb isotope ratios are ± 0.05 %. Blanks are ≤ 0.2 ng (Sr, Nd, Pb) and negligible in all cases.

6.2.2 Strontium Isotopes

$^{87}Sr/^{86}Sr$ ratios for the thirty-three representative rhyolite lavas are given in Table 6.1. The rhyolite lavas have a narrow range in $^{87}Sr/^{86}Sr$ values from 0.70503 - 0.70583 (with most lying between 0.70525 and 0.70545) which are within the range of other TVZ silicic eruptives (Briggs et al., 1993; McCulloch et al., 1994; Sutton et al., 1995; Beresford, 1997; Brown et al., 1998b). Figure 6.1 shows the relationship of $^{87}Sr/^{86}Sr$ to the Rb/Sr ratio of the lavas. The Rb/Sr ratio serves as an index of differentiation and this combination of parameters was used by Sutton et al. (1995) to distinguish between rhyolite lavas of the Taupo Volcanic Centre. In this study, the interpretation of trends in Rb/Sr versus $^{87}Sr/^{86}Sr$ is that shown in Figure 6.2.

Table 6.1: Strontium and neodymium isotope ratios for rhyolite lavas of the Okataina, Rotorua and Kapenga volcanic centres.

	Eruptive Episode	Rhyolite Lava	Sample Number	$^{87}Sr/^{86}Sr$	±	$^{143}Nd/^{144}Nd$	±	ε_{Nd}
Okataina Volcanic Centre								
ho_3	Kaharoa	Tarawera	158	0.705304	23	0.512725	19	1.70
	Whakatane	Haroharo	6	0.705334	21			
		Okataina	24	0.705306	29	0.512705	13	1.31
		Tikorangi	98	0.705305	26			
	Mamaku	Hainini	7	0.705314	28	0.512690	12	1.01
		Te Horoa	32	0.705328	17			
		Waiti	173	0.705317	28			
	Rotoma	Te Pohue	60	0.705365	21			
		Rotoma	105	0.705321	29			
	Waiohau	Waikakareao	38	0.705340	26			
	Rotorua	Trig 7693	176	0.705435	23			
	Rerewhakaaitu	Western	44	0.705394	18			
		Rotomahana	134	0.705361	24			
	Okareka	Ridge	90	0.705384	24	0.512700	12	1.21
		Patiti Island	130	0.705349	21			
	Te Rere	Fentons Mill	92	0.705463	24			
		Eastern Rhyolite	113	0.705294	25			
ho_2		Tutaeheka 1	64	0.705424	24			
		Moerangi Rd	72	0.705162	29	0.512716	14	1.52
		Blue Lake	152	0.705328	20	0.512684	13	0.90
		Tutaeheka 2	160	0.705180	22			
ho_1		North Rotoma	107	0.705578	26			
		Matawhaura	109	0.705832	26	0.512639	11	0.02
		Whakapoungakau	110	0.705216	27			
		Wairua	119	0.705391	31	0.512669	13	0.60
Rotorua Volcanic Centre								
hr_3		Mokoia Island	103	0.705276	26			
		Vaughan Road	104	0.705249	33	0.512730	13	1.79
hr_2		Kawaha Point	86	0.705031	26	0.512740	14	1.99
hr_1		Endean Road	87	0.705409	25			
		Hamurana	120	0.705364	27			
Kapenga Volcanic Centre								
hk_2		Dome 3	168	0.705293	26			
		Ongahoro	170	0.705287	25	0.512708	12	1.37
hk_1		Horohoro	126	0.705531	24			

Lavas that are genetically related via closed-system fractional crystallisation processes will have the same $^{87}Sr/^{86}Sr$ composition with increasing Rb/Sr. Lavas that are genetically related via assimilation - fractional crystallisation (AFC) processes will have increasing $^{87}Sr/^{86}Sr$ compositions with increasing Rb/Sr. If the rate of assimilation to fractional crystallisation is constant, then the trend for AFC will be a straight line with a positive slope. A curved path would indicate that the rate of assimilation to fractional crystallisation has varied during magmatic evolution. A path for closed-system equilibrium partial melting would be the reverse of that for closed-system fractional crystallisation.

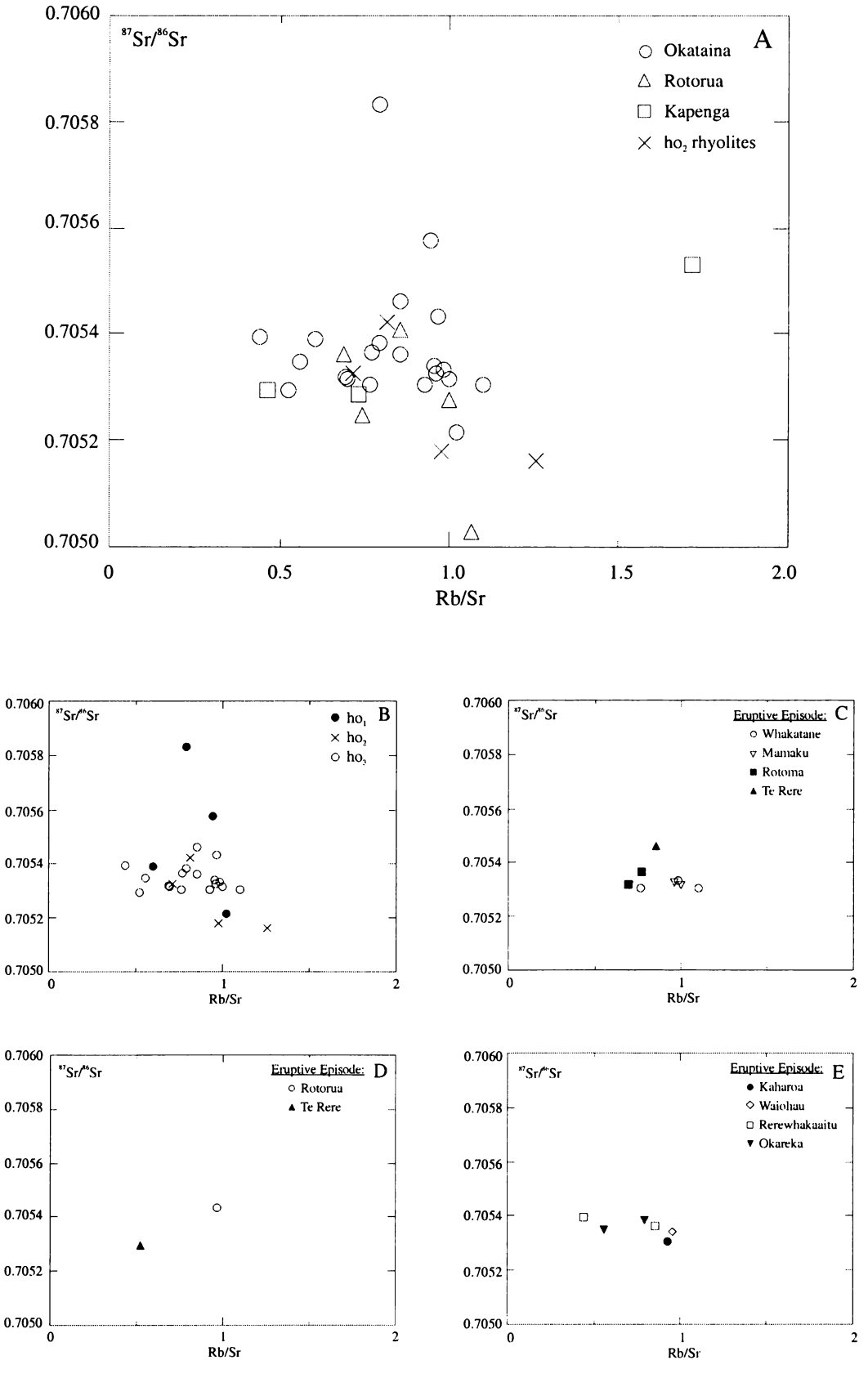

Figure 6.1: Rb/Sr vs. $^{87}Sr/^{86}Sr$ plots for rhyolite lavas from a) Okataina, Rotorua and Kapenga volcanic centres, b) Okataina Volcanic Centre, c) Haroharo Volcanic Complex, d) Okareka Volcanic Complex, e) Tarawera Volcanic Complex.

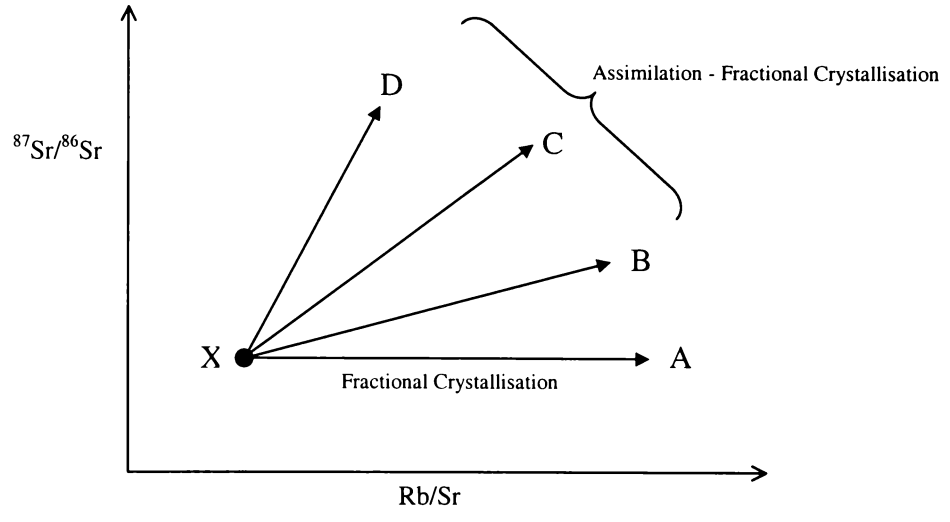

Figure 6.2: Schematic diagram illustrating trends in Rb/Sr vs. $^{87}Sr/^{86}Sr$ for lavas genetically related via fractional crystallisation or assimilation-fractional crystallisation (AFC) processes. Path XA represents samples related via closed-system fractional crystallisation processes, which leave $^{87}Sr/^{86}Sr$ unchanged with increasing Rb/Sr. Any path with a positive slope, eg. XB, XC and XD, represents samples related via AFC processes, which increase $^{87}Sr/^{86}Sr$ with increasing Rb/Sr. Each of these paths represent a particular constant rate of assimilation to fractional crystallisation.

Figure 6.1a shows that compositions for the majority of Okataina, Rotorua and Kapenga volcanic centre lavas overlap, and hence strontium isotopes cannot be used to distinguish between the eruptives of these volcanic centres. Figure 6.1b shows that within the Okataina Volcanic Centre, the isotopic compositions of rhyolite lavas from the three age groups overlap and that there is no systematic change in $^{87}Sr/^{86}Sr$ with age. Such a wide range in $^{87}Sr/^{86}Sr$ within the whole Okataina Volcanic Centre data set, and within each time period, precludes an origin for the rhyolites by closed-system partial melting of the same crustal source or closed-system fractional crystallisation of the same parental magma. In addition there is an overall lack of correlation between Rb/Sr and $^{87}Sr/^{86}Sr$, which suggests the magmas have not evolved along a single assimilation-fractional crystallisation (AFC) path.

The ho_1 rhyolites show a wide range in $^{87}Sr/^{86}Sr$ compositions with a particularly high value for Matawhaura (0.705832) compared to other samples. There is no relationship between $^{87}Sr/^{86}Sr$ and Rb/Sr, which precludes an origin for the ho_1 rhyolite lavas by AFC of a common parent, as AFC processes involving likely crustal assimilants would systematically

increase $^{87}Sr/^{86}Sr$ as well as Rb/Sr. This lack of relationship provides support for the existence of several isolated batches of magma beneath the Okataina Volcanic Centre at this time.

Major and trace element compositions suggest that the orthopyroxene and calcic amphibole-bearing ho_1 lavas might record the evolution of a magma batch beneath the Okataina Volcanic Centre prior to the eruption of the Matahina Ignimbrite. However, the difference in $^{87}Sr/^{86}Sr$ compositions for Matawhaura and Whakapoungakau preclude a common magma source for these lavas or any relationship involving closed-system fractional crystallisation or AFC processes. The acquisition of further isotopic data for the ho_1 rhyolites is required to investigate this situation, and to determine the range in $^{87}Sr/^{86}Sr$ compositions for all of the orthopyroxene and calcic amphibole-bearing ho_1 lavas. Only limited isotopic data are available for the Matahina Ignimbrite: Ewart and Stipp (1968) give values of 0.7060 and 0.7067 corresponding to Rb/Sr values of 1.05 and 1.14 respectively, and more recently, Blattner et al. (1996) give a $^{87}Sr/^{86}Sr$ composition of 0.70587±6. This latter value is comparable to the $^{87}Sr/^{86}Sr$ composition of Matawhaura. Given that in terms of major and trace elements the Matahina Ignimbrite was most similar to the northeastern rhyolites, including Matawhaura (Figures 4.2 and 4.3), this may provide further evidence for a genetic relationship. The Matahina Ignimbrite has Rb/Sr contents similar to and higher than Matawhaura and the other northeastern rhyolites (Figure 4.7). Hence Matawhaura and the Matahina Ignimbrite may be related by fractional crystallisation processes that increased Rb/Sr and left $^{87}Sr/^{86}Sr$ relatively unchanged.

The much lower $^{87}Sr/^{86}Sr$ composition for Whakapoungakau compared to Matawhaura and the Matahina Ignimbrite suggests that not all of the orthopyroxene and calcic amphibole-bearing lavas erupted at this time are sourced from the same magma. Whakapoungakau occurs in the western Okataina Volcanic Centre, and contains small amounts of biotite, which set it apart from the northeastern lavas. However, a relationship between the biotite-free western rhyolites (Stancorp Quarry and Crater Farm) and the northeastern rhyolites cannot be ruled out.

$^{87}Sr/^{86}Sr$ compositions provide further support for the existence of two magma batches beneath the southwestern Okataina Volcanic Centre that erupted as the ho_2 rhyolite lavas (Figure 6.1b). The biotite-bearing lavas have lower Rb/Sr and higher $^{87}Sr/^{86}Sr$ compared to the biotite-free/poor lavas. These differences preclude evolution of the more

mineralogically evolved biotite-bearing magma by AFC from the biotite-free/poor magma, as this process would be expected to increase both $^{87}Sr/^{86}Sr$ and Rb/Sr. The difference in $^{87}Sr/^{86}Sr$ also precludes closed-system fractional crystallisation. In addition to being inconsistent with observed trace element contents, the evolution of the biotite-free/poor magma from the biotite-bearing magma is also precluded by the reduction in $^{87}Sr/^{86}Sr$ composition.

Within the biotite-free/poor magma, similar $^{87}Sr/^{86}Sr$ compositions over a range in Rb/Sr (0.98 - 1.26) suggest evolution by closed-system fractional crystallisation. Within the biotite-bearing magma, increased Rb/Sr (from 0.71 - 0.81) is accompanied by increased $^{87}Sr/^{86}Sr$ (from 0.705328 - 0.705424). This compositional change has been modelled by AFC processes (section 6.6). The biotite-bearing ho_2 rhyolites have similar $^{87}Sr/^{86}Sr$ compositions to the hk_2 rhyolite lavas (Figures 6.1a and 6.3b). Burt et al. (1998) give a $^{87}Sr/^{86}Sr$ composition for the Earthquake Flat Ignimbrite of 0.70532, corresponding to Rb/Sr of 0.70, which is also similar to the biotite-bearing ho_2 rhyolites. Hence, isotopic data provides further evidence for a common source for these lavas and the Earthquake Flat Ignimbrite.

Figure 6.1c shows $^{87}Sr/^{86}Sr$ compositions for Haroharo Volcanic Complex rhyolite lavas. Within these lavas there is no systematic relationship between $^{87}Sr/^{86}Sr$ and Rb/Sr. The lava erupted in the Te Rere episode has the highest $^{87}Sr/^{86}Sr$ content. In the Rotoma episode the Te Pohue and Rotoma lavas have similar $^{87}Sr/^{86}Sr$ for a small change in Rb/Sr (0.08). Hence the differences between these two magma types in terms of major and trace elements may be due to closed-system fractional crystallisation (modelled in section 6.5). For rhyolite lavas erupted during the Mamaku and Whakatane eruptive episodes there is little variation in $^{87}Sr/^{86}Sr$ (0.705305 - 0.705334; negligible when taking into account the errors), with changing Rb/Sr (0.70 - 1.10). This suggests that compositional variations between magmas erupted in these two episodes were produced by closed-system fractional crystallisation processes which would alter the Rb/Sr ratio without changing the $^{87}Sr/^{86}Sr$ composition (modelled in section 6.5).

Figure 6.1d shows the $^{87}Sr/^{86}Sr$ composition for two rhyolite lavas from the Okareka Volcanic Complex. Over the c. 9 200 years between the Te Rere and Rotorua eruptive episodes, the magma has become more evolved (with increased Rb/Sr and SiO_2 contents)

and has a higher $^{87}Sr/^{86}Sr$ composition. These changes are consistent with AFC processes (see section 6.6, Figure 6.11).

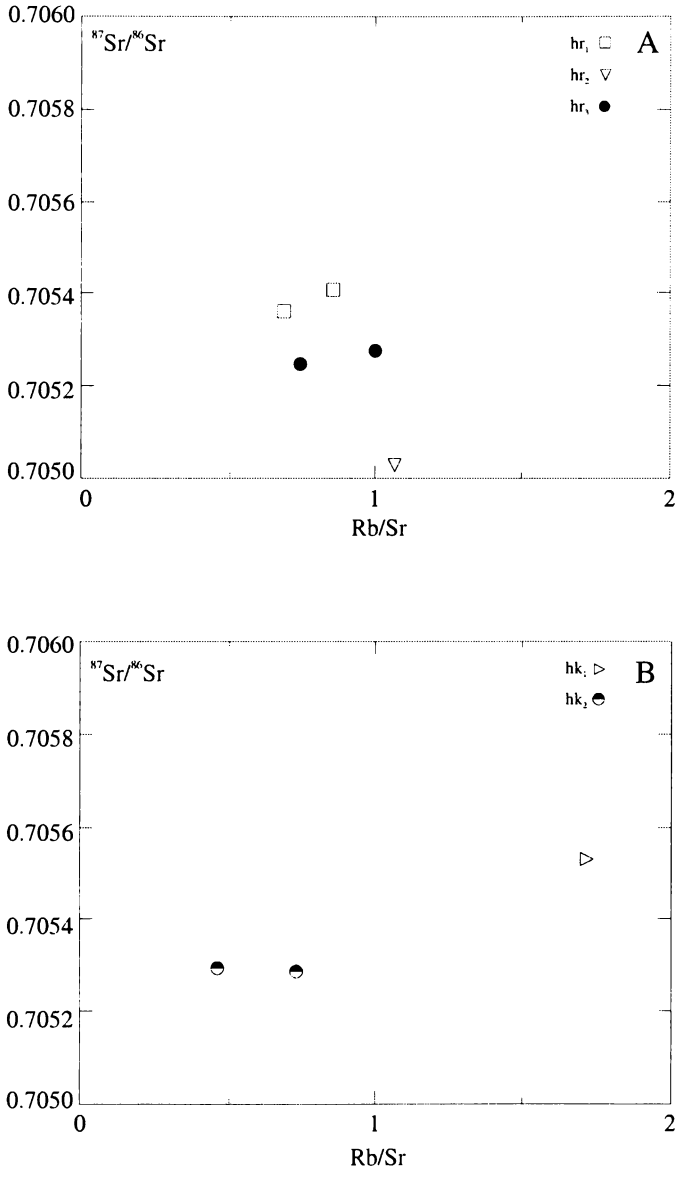

Figure 6.3: Rb/Sr vs. $^{87}Sr/^{86}Sr$ plots for rhyolite lavas from a) Rotorua Volcanic Centre, b) Kapenga Volcanic Centre.

Figure 6.1e shows $^{87}Sr/^{86}Sr$ compositions for rhyolite lavas from the Tarawera Volcanic Complex. Rhyolite lavas erupted during the Okareka episode have similar $^{87}Sr/^{86}Sr$ compositions (0.705349 - 0.705384) when taking into account errors. If it is assumed that the Rb/Sr ratios reflect magmatic compositions, and have not been affected by possible post-

depositional alteration in the Patiti Island rhyolite, then the possibility that the Ridge flow magma evolved from the Paiti Island magma by closed-system fractional crystallisation cannot be ruled out (discussed further in section 6.5). Rhyolite lavas erupted in the Rerewhakaaitu episode have similar $^{87}Sr/^{86}Sr$ compositions (0.705361 - 0.705394) although they differ in Rb/Sr by ~ 0.4, hence suggesting a possible relationship by closed-system fractional crystallisation processes (also discussed further section 6.5). Representative samples from the Waiohau and Kaharoa eruptive episodes have similar Rb/Sr and $^{87}Sr/^{86}Sr$ compositions.

Although there is neither a systematic relationship between $^{87}Sr/^{86}Sr$ and Rb/Sr for the ho_3 rhyolite lavas, nor between $^{87}Sr/^{86}Sr$ and SiO_2, there are slight trends in $^{87}Sr/^{86}Sr$ for lavas of each of the volcanic complexes when compared with their age (Figure 6.4). Within the Haroharo Volcanic Complex the older Te Rere episode lava has the highest $^{87}Sr/^{86}Sr$ composition. Lavas erupted during the Rotoma, Mamaku and Whakatane episodes show overlapping ranges in $^{87}Sr/^{86}Sr$ compositions. At the Okareka Volcanic Complex the lavas have become enriched in both SiO_2 and $^{87}Sr/^{86}Sr$ over time. At the Tarawera Volcanic Complex the younger Kaharoa episode lava has the lowest $^{87}Sr/^{86}Sr$ composition.

The slight decrease in $^{87}Sr/^{86}Sr$ compositions over time for lavas from the Haroharo and Tarawera volcanic complexes may be an indication of decreasing amounts of crustal assimilation over time and the increasing importance of fractional crystallisation processes in magma evolution. The difference between the Te Rere episode lava and younger lavas from Haroharo may reflect a longer residence time in the crust for the Te Rere magma, at higher temperatures (Table 5.1), and hence increased time and potential for assimilation.

Figure 6.3a shows the variation in $^{87}Sr/^{86}Sr$ compositions for rhyolite lavas from the Rotorua Volcanic Centre. The hr_1 rhyolites have the highest $^{87}Sr/^{86}Sr$ compositions (0.705364 and 0.705409) and the hr_2 rhyolite has the lowest $^{87}Sr/^{86}Sr$ composition (0.705031). The hr_3 rhyolites have intermediate compositions (0.705249 and 0.705276). Differences in isotopic compositions and Rb/Sr preclude the evolution of the hr_2 rhyolite magma from magma represented by either of the hr_1 rhyolites by fractional crystallisation or AFC processes. In addition, the evolution of the hr_3 rhyolite magmas from the hr_2 rhyolite magma is also precluded.

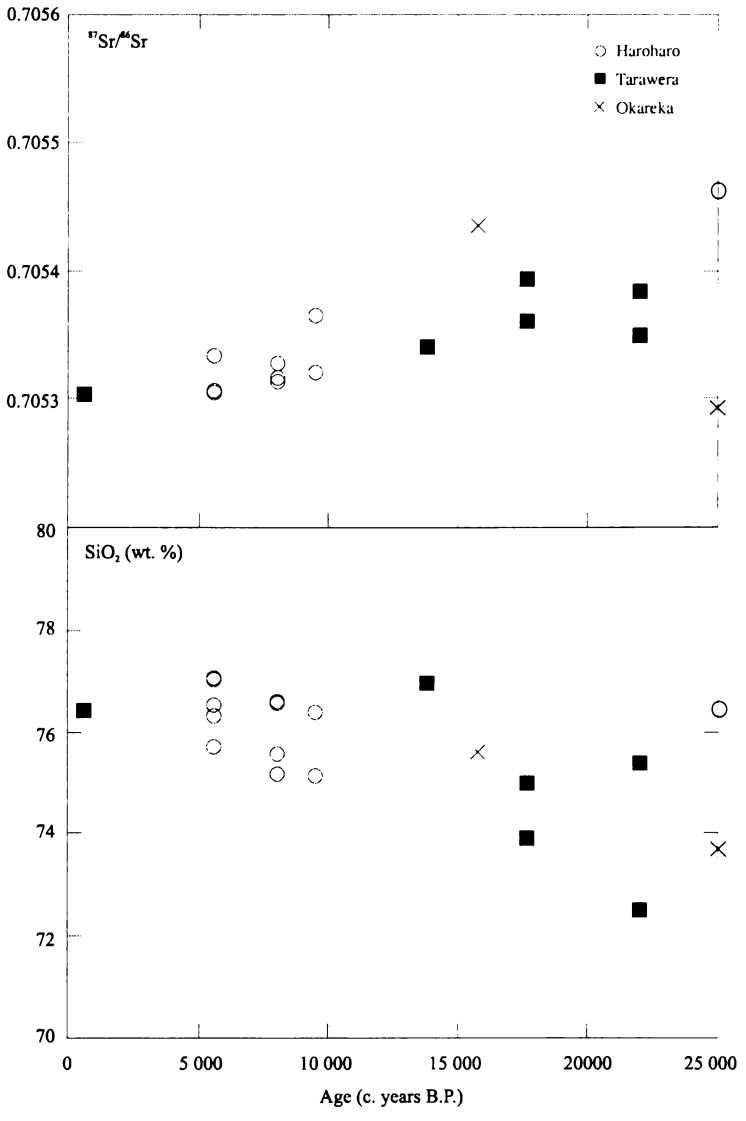

Figure 6.4: Variation in $^{87}Sr/^{86}Sr$ and SiO_2 (wt. %) with age for the ho_3 rhyolite lavas from the Okataina Volcanic Centre.

The hr_1 rhyolites of Hamurana and Endean Road have similar $^{87}Sr/^{86}Sr$ compositions, and could be genetically related, eg. by fractional crystallisation processes. Major and trace element compositions are consistent with this, although a significant amount of crystallisation would be involved. The available whole rock and phenocryst data are insufficient to properly assess if any genetic relationship exists between these two lava types.

$^{87}Sr/^{86}Sr$ analyses for the Ngongotaha Quarry Dome and the Mamaku Ignimbrite by Blattner et al. (1996) range from 0.70482±6 - 0.70508±4 and 0.70505±6 - 0.70512±5 respectively. These two ranges overlap and are comparable with the analysis of hr_2 rhyolite (Kawaha Point) in Figure 6.3a. Further geochemical and isotopic data are required for the hr_2 rhyolites and the Mamaku Ignimbrite to enable any further assessment of a possible genetic relationship between them.

The Vaughan Road and Mokoia Island hr_3 rhyolites have similar $^{87}Sr/^{86}Sr$ compositions. However, the mineralogically more evolved Vaughan Road rhyolite (biotite-bearing) is geochemically less evolved (lower Rb/Sr, SiO_2) than the Mokoia Island rhyolite, and unlikely to be genetically related via fractional crystallisation processes.

Figure 6.3b shows the variation in $^{87}Sr/^{86}Sr$ compositions for rhyolite lavas from the Kapenga Volcanic Centre. Two representative hk_2 rhyolite lavas have lower $^{87}Sr/^{86}Sr$ and Rb/Sr than a sample of hk_1 rhyolite (Horohoro). As previously discussed, these hk_2 lavas have similar $^{87}Sr/^{86}Sr$ compositions to the biotite-bearing ho_2 rhyolite lavas. Isotopic data for ignimbrites from the Kapenga Volcanic Centre are limited to two analyses in Blattner et al. (1996) for the Pukerimu and Tikorangi ignimbrites (now known collectively as the Tikorangi Ignimbrite). These analyses of 0.70528±6 and 0.70540±8 are lower than the $^{87}Sr/^{86}Sr$ composition of the hk_1 rhyolite, although further analyses for the hk_1 lavas and Kapenga ignimbrites are required to assess possible genetic relationships.

6.2.3 Neodymium Isotopes

A smaller set of eleven $^{143}Nd/^{144}Nd$ ratios were obtained for representative rhyolite lavas (Table 6.1). The rhyolite lavas have a range in $^{143}Nd/^{144}Nd$ values from 0.51264 - 0.51274 and ε_{Nd} from 1.99 - 0.02 which are within the ranges of other TVZ silicic eruptives (e.g. Briggs et al., 1993; McCulloch et al., 1994, Sutton et al., 1995; Beresford, 1997). Figure 6.5 compares $^{87}Sr/^{86}Sr$ and ε_{Nd} compositions for the eleven representative rhyolite lavas with Waipapa and Torlesse metasediments (considered to form the basement beneath the TVZ), TVZ basaltic eruptives and a general field for TVZ rhyolites. Representative rhyolites from the Okataina, Rotorua and Kapenga volcanic centres, along with all TVZ silicic volcanics, show a trend of decreasing ε_{Nd} with increasing $^{87}Sr/^{86}Sr$. Such a trend has been thought

consistent with derivation of TVZ silicic magmas by AFC processes from a basaltic magma, and this has been modelled in section 6.6 (Figure 6.8).

Consistent with its elevated $^{87}Sr/^{86}Sr$ composition, Matawhaura (ho_1) has the lowest ε_{Nd} of 0.02. Kawaha Point (hr_2) has the lowest $^{87}Sr/^{86}Sr$ and the highest ε_{Nd} of 1.99. Bearing in mind the errors associated with $^{143}Nd/^{144}Nd$ analyses, the differences in ε_{Nd} between the two samples from Haroharo (Hainini Dome and Okataina Flow) are negligible. This is also the case for the two samples from Tarawera (Ridge Flow and Tarawera Dome). Such a small data set precludes the use of a combination of $^{87}Sr/^{86}Sr$ and ε_{Nd} compositions to make any possible distinction between volcanic centres.

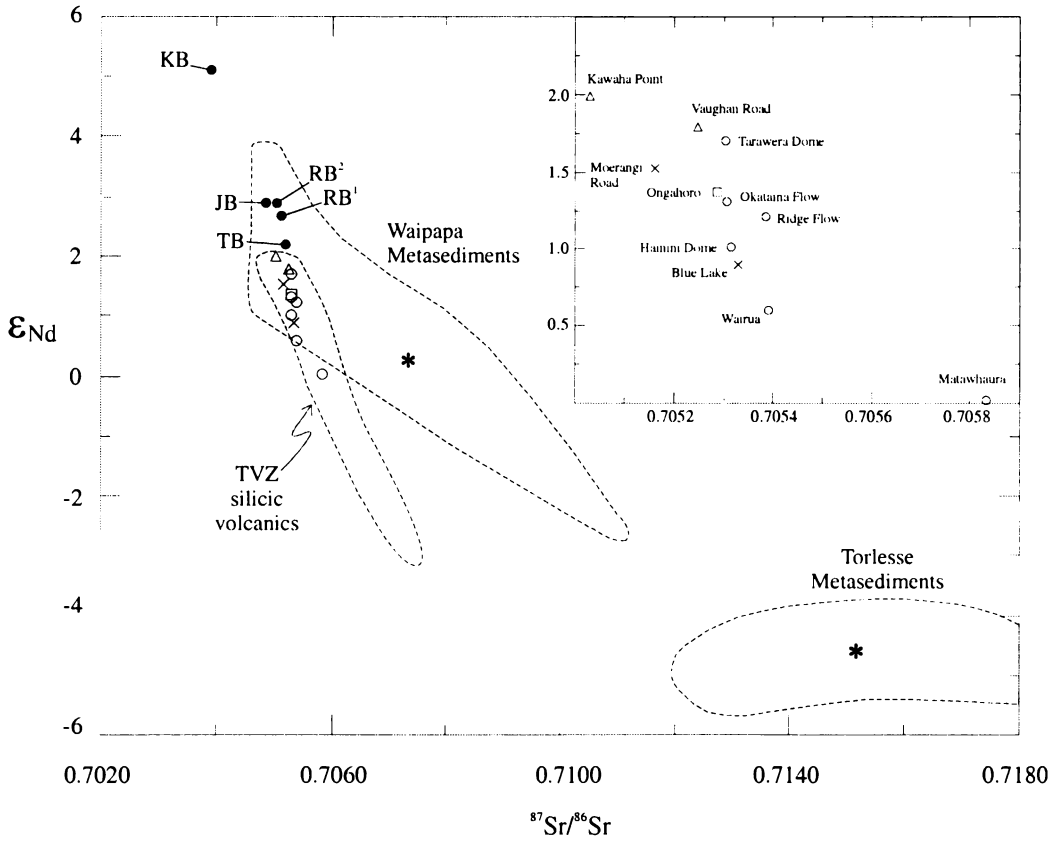

Figure 6.5: $^{87}Sr/^{86}Sr$ vs. ε_{Nd} for rhyolite lavas from the Okataina, Rotorua and Kapenga volcanic centres (open circles, triangles and squares respectively). Crosses indicate ho_2 rhyolites in the Okataina - Kapenga transition zone. Fields for Waipapa and Torlesse metasediments from Graham et al. (1992) and Gamble et al. (1993). Field for TVZ silicic volcanics modified from Graham et al. (1992) and Gamble et al. (1993) to accommodate high $^{87}Sr/^{86}Sr$, low ε_{Nd} rhyolites from Sutton et al. (1995). Asterisks represent average metasedimentary basement compositions from Graham et al. (1992). Filled circles are compositions of selected TVZ basalts from Gamble et al. (1993). TB = Tarawera basalt, RB = Rotokawau basalt, JB = Johnson Road basalt, KB = Kakuki basalt. Insert shows an expanded plot of the data and rhyolite lava names.

6.2.4 Lead Isotopes

Six representative rhyolite lavas were analysed for Pb isotopes and these are given in Table 6.2. $^{206}Pb/^{204}Pb$ ratios range from 18.750 - 18.857, $^{207}Pb/^{204}Pb$ from 15.548 - 15.635 and $^{208}Pb/^{204}Pb$ from 38.419 - 38.739. Most of these rhyolite lavas fall within the ranges of Pb isotopes for other TVZ silicic volcanics (e.g. Graham et al., 1992; McCulloch et al., 1994). The exceptions are Kawaha Point (hr_2), which has slightly higher $^{206}Pb/^{204}Pb$, and Matawhaura (ho_1), which has much lower Pb isotope ratios than the other rhyolites in this study and TVZ silicic volcanics generally (Figure 6.6).

Pb isotopic data show wide scatter and less definable trends than seen in Sr and Nd isotopes. Graham et al. (1995) note that the TVZ rhyolites as a whole have a relatively wide range of Pb isotopic values and that rocks from specific volcanic centres may have a much more restricted range. The small data set prevents any possible systematic distinction between the Okataina, Rotorua and Kapenga volcanic centres in this study.

Pb isotopic compositions for Matawhaura are different to the other rhyolite lavas analysed in this study and TVZ silicic volcanics in general. When taking errors into account, Matawhaura has similar Pb isotopic compositions to Kakuki basalt. Matawhaura contains ~ 12 ppm Pb which, while comparable to other rhyolite lavas, is significantly higher than Kakuki basalt. Such comparable isotopes yet differing trace element compositions can signify evolution of the rhyolite by fractional crystallisation processes that changed trace element compositions and left isotopic ratios unaltered. However, such an observation is inconsistent with Sr and Nd isotopes that show Matawhaura to be the most radiogenic rhyolite lava sampled, with notably distinct compositions from Kakuki basalt. Hence, Matawhaura is unique among rhyolite lavas analysed in this study, and possibly TVZ silicic volcanics in general, in terms of its Sr-Nd-Pb isotopic composition.

The $^{206}Pb/^{204}Pb$ and $^{207}Pb/^{204}Pb$ compositions of TVZ silicic volcanics overlap with the field for Waipapa metasediments, with a small overlap with the Torlesse metasediments field at the more radiogenic compositions. Of the six representative samples analysed for Pb isotopes in this study, three show $^{206}Pb/^{204}Pb$ and $^{207}Pb/^{204}Pb$ compositional similarities to Torlesse compositions and two show similarities to Waipapa compositions. Pb isotopes have been utilised in modelling AFC processes involving these two possible assimilants in section 6.6 (Figures 6.9 and 6.10).

Table 6.2: Lead isotope ratios for rhyolite lavas of the Okataina, Rotorua and Kapenga volcanic centres.

	Rhyolite Lava	Sample Number	Pb 206/204	Pb 207/204	Pb 208/204
Okataina Volcanic Centre					
ho_3					
Kaharoa Episode	Tarawera	158	18.830	15.622	38.701
Whakatane Episode	Okataina	24	18.844	15.635	38.739
ho_2	Moerangi Road	72	18.838	15.622	38.705
ho_1	Matawhaura	109	18.750	15.548	38.419
Rotorua Volcanic Centre					
hr_2	Kawaha Point	86	18.857	15.635	38.737
Kapenga Volcanic Centre					
hk_2	Ongahoro	170	18.845	15.632	38.736

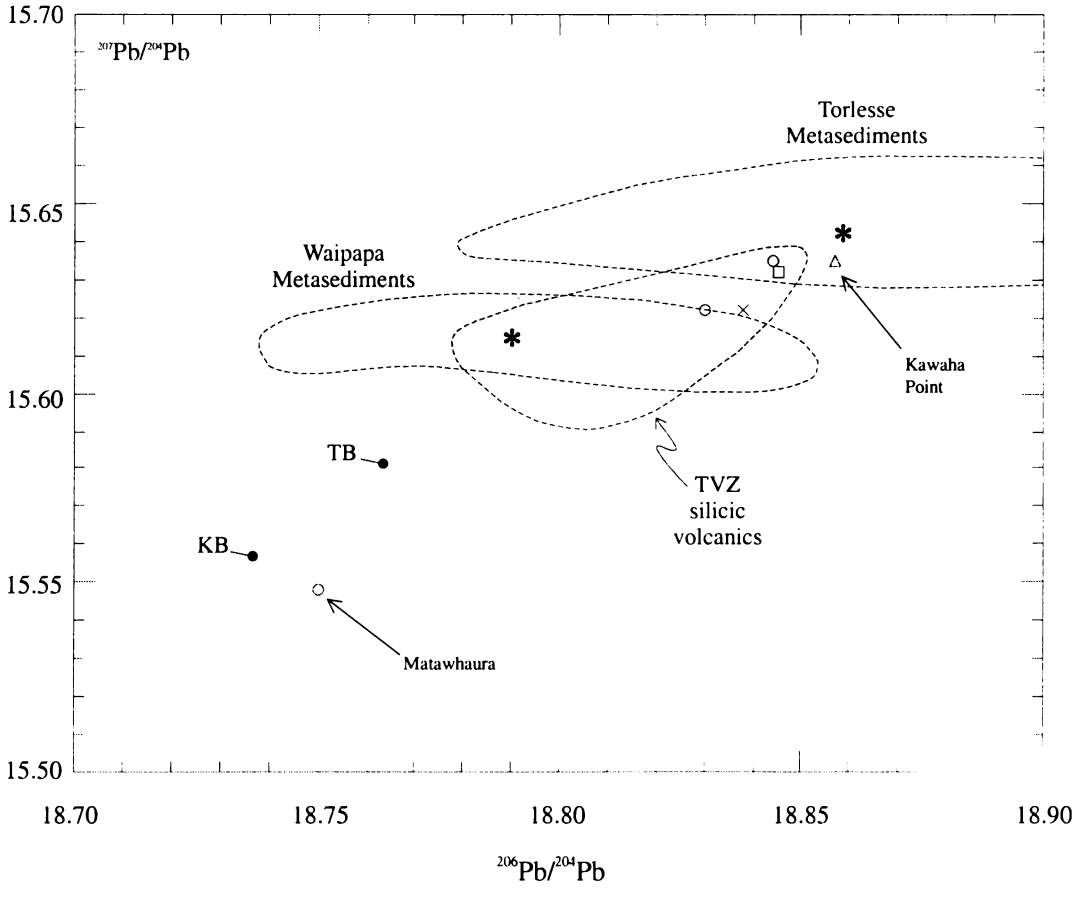

Figure 6.6: $^{206}Pb/^{204}Pb$ vs. $^{207}Pb/^{204}Pb$ for rhyolite lavas from the Okataina, Rotorua and Kapenga volcanic centres (open circles, triangles and squares respectively). Cross indicates ho_2 rhyolite in the Okataina - Kapenga transition zone. Fields for Waipapa and Torlesse metasediments, TVZ silicic volcanics and selected TVZ basalts from Graham et al. (1992). TB = Tarawera basalt, KB = Kakuki basalt. Asterisks represent average metasedimentary basement compositions from Graham et al. (1992).

6.3 Models for Rhyolite Magma Genesis in the Taupo Volcanic Zone

Petrogenetic models for TVZ rhyolitic magmas have been reviewed by Graham et al. (1995). Two opposing generalised models for rhyolite magma genesis have been proposed:

1. Crustal fusion either by massive transfer of heat from the mantle to the crust via magma movement or by injection of mantle-derived magmas into a crust already heated by plastic deformation (eg. Ewart, 1966; Ewart and Stipp, 1968; Ewart et al., 1975; Reid, 1983; Graham et al., 1992; Hochstein et al., 1993; Graham et al., 1995).

2. Fractional crystallisation of basaltic magma accompanied by assimilation of crust (AFC) (eg. Blattner and Reid, 1982; Graham et al., 1992; Nicholls et al., 1992; McCulloch et al., 1994; Graham et al., 1995).

Various lines of circumstantial evidence can be advanced to support or refute either model (Graham et al., 1995). Waipapa and Torlesse metasediments comprise the pre-Cenozoic basement west and east of the TVZ respectively, it is accepted that they comprise the basement under most of the North Island (Graham et al., 1995), and are potential assimilants or sources of crustal melts. The isotopic (Sr, Nd, Pb, O) compositions of TVZ rhyolites and Torlesse meta-greywackes are generally distinct, which effectively eliminates the latter as the sole source of the rhyolites through crustal melting. Waipapa meta-greywackes have similar isotopic compositions to the rhyolites, although the degree of overlap is slight. This also eliminates Waipapa (or a mixture of Waipapa and Torlesse) rocks as the primary source (Blattner and Reid, 1982; Graham et al., 1995). Conrad et al. (1988) showed that crustal melting models are inconsistent with experimental melting studies which show that the dominantly peraluminous (corundum normative) meta-greywackes are poorly suited as partial melting source rocks for the dominantly metaluminous (diopside-normative) rhyolites.

Graham et al. (1992) and McCulloch et al. (1994) both considered the possibility that rhyolite magmas are derived from primary mantle-derived basaltic magmas by crystallisation-differentiation or AFC processes (Graham et al., 1995). Reid (1983) used least-squares mixing models to show that high-degree (~90 %) crystal fractionation of high-alumina basalt (HAB) can produce liquids of rhyolitic composition. However, the results were inconsistent with calculated trace element and REE concentrations. This was also

found to be true for andesitic parental magmas. Furthermore, the vast volumes of rhyolite would require >100,000 km^3 of basalt to evolve by crystal fractionation, yet basalt comprises only about 0.1 % of the total volume of exposed volcanics in the TVZ (Graham et al., 1995). Robinson et al. (1981) give no indication of large volumes of molten rock below the TVZ, which Reid (1983) noted was difficult to reconcile with the large amount of cooling magma that would be required to produce rhyolites by crystal fractionation.

If crustal contamination is introduced to the least-squares mixing models the situation is not so clear-cut. For all the isotopic systems considered, the composition of TVZ rhyolites lie close to the theoretical curves between Kakuki HAB and Torlesse meta-greywacke (Graham et al., 1995) (see section 6.6, eg. Figure 6.8). Kakuki basalt is petrographically and chemically the most primitive volcanic rock in the TVZ, and is the only one likely to approach a primary basalt composition (Gamble et al., 1990; Graham et al., 1992). However, neither Kakuki basalt - Torlesse AFC nor Kakaki basalt - Waipapa AFC can entirely explain all the data satisfactorily.

Graham et al. (1995) consider that petrogenetic models to generate TVZ rhyolites from associated HAB magmas by assimilation - fractional crystallisation processes are internally consistent, given the inherent uncertainties in end member compositions, contamination rate, bulk liquid-crystal distribution coefficients and, especially, the differentiation processes operating. AFC processes have been suggested for rhyolite magma genesis at silicic volcanic fields elsewhere in the world but, as with the TVZ, they fail to adequately explain the dominance of evolved compositions and apparent compositional bimodality. Examples are those discussed by Hildreth (1981); the Timber Mountain/Oasis Valley Caldera Complex, SW Nevada (Farmer et al., 1991); Yellowstone Plateau volcanic field, Wyoming (Hildreth et al., 1991) and the Valles Caldera, New Mexico (Spell et al., 1993).

Since chemical, isotopic and experimental evidence suggests pre-Cenozoic metasedimentary basement rocks (Torlesse and Waipapa metagreywackes) are unsuitable as the major crustal fusion/partial melting source rock, Graham et al. (1992) suggest that the answer may lie in the lower crust. TVZ rhyolites have generally uniform compositions as would be expected after large-scale melting of lower crustal rocks (Graham et al., 1995). Two possibilities have been considered:

1. Remelting of igneous forerunners (early formed intrusive or extrusive rocks) in a thick volcanic pile may be promoted by increases in the rate of intrusion of ascending mafic magmas and by hydrothermal alteration of the pile (Hildreth, 1981; Graham et al., 1992). This process is likely to be multi-stage wherein successive basaltic pulses result in partial remelting of progressively more evolved compositions until, over time, a predominantly bimodal basalt-rhyolite field is generated (Hildreth, 1981; Graham et al., 1995). Early-formed andesitic rocks are known to occur along the eastern margin of the TVZ, underlying rhyolites and overlying metasedimentary basement (Stern, 1986; Browne et al., 1992; Graham et al., 1995). The Pb isotopic compositions of TVZ rhyolites are strikingly similar to those of contemporary TVZ andesites, supporting a close genetic relationship through partial melting (Graham et al., 1995). If the isotopic composition of the igneous forerunners to the rhyolites is assumed to be similar to those of the recent andesite eruptives, then only a small addition of a more radiogenic component (perhaps Torlesse metagreywacke) would be required to explain all the rhyolitic compositions (Graham et al., 1995). Much supporting evidence is still required for this model, including the extent and composition of the buried andesitic rocks (Graham et al., 1995).

2. Processes similar to partial fusion of lower crustal granulite basement have been promoted to explain the occurrence of the rhyolitic rocks of the Sierra Madre Occidental (Ruiz et al., 1988) and Yellowstone Plateau volcanic field (Doe et al., 1982). However, lower crustal granulite basement has yet to be identified within the rhyolitic centres of the TVZ, although it occurs as xenoliths in some andesitic lavas (Graham et al., 1990; Graham et al., 1995). In addition, these rocks are isotopically distinct from TVZ rhyolites and cannot represent their source by direct partial melting (Graham et al., 1995).

It is likely that a number of processes are responsible for the production of rhyolite magmas beneath the TVZ and that several different crustal components are involved in addition to a mantle-derived component. Models have been established to evaluate fractional crystallisation and assimilation-fractional crystallisation processes in magmas (which have been applied to the lavas obtained in this study in sections 6.5 and 6.6). However, processes involving varying degrees of partial melting are not as easily modelled especially when the composition of the source of the melt, the crust, is not well known and likely to be heterogeneous. The complexity of processes involved in the production of rhyolite magmas

and an inadequate knowledge of component compositions limit the usefulness of current petrogenetic modelling to positively identify components or processes.

6.4 TRACE ELEMENT IMPLICATIONS FOR RHYOLITE PETROGENESIS

Chondrite-normalised multi-element (spider) patterns of the Okataina, Rotorua and Kapenga rhyolite lavas show enrichment in large-ion lithophile elements (eg. Ba, Rb, Th and K) relative to the high-field-strength elements (eg. Sm, Zr and Hf) and depletion in Nb, P and Ti. These features are typical of arc-related magmas (Pearce, 1983; Wilson, 1989; Pearce and Peate, 1995). McCulloch and Gamble (1991) note that the depletion of Nb has remained a perplexing and contentious problem, and that one possible explanation for the Nb "deficiency" is the presence of a residual titanate phase such as rutile, titanite (sphene), ilmenite or perovskite to retain Nb in the source region (subducted slab or overlying mantle wedge) during partial melting. Ewart and Hawkesworth (1987) and Ewart et al. (1994) explained the observed HFSE depletion within arc lavas as due to melt extraction during back-arc extension (Ewart et al., 1998). The relative enrichment in the large-ion lithophile elements has been attributed to metasomatism of the mantle source of arc magmas by fluids released from the subducted slab (Wilson, 1989; Pearce and Peate, 1995; Ewart et al., 1998). However, the occurrence of a depletion in Nb need not preclude an entirely crustal origin for silicic magmas in the Taupo Volcanic Zone. Such a Nb depletion may be inherited by a magma resulting from fusion or partial melting of metasedimentary crustal rocks that are themselves comprised of the eroded remains of typical arc-related andesitic and basaltic eruptives.

In addition to subduction related controls on trace element compositions in the Okataina, Rotorua and Kapenga volcanic centre rhyolite lavas, the troughs seen in multi-element patterns are likely to be controlled at least in part by fractionation of minerals seen in the phenocryst and accessory assemblage of these lavas - Sr (plagioclase), P (apatite), Ti (Fe-Ti oxides, hornblende) and Nb (hornblende, biotite, Fe-Ti oxides). Ba, Rb and K are concentrated in the continental crust and the high abundance of these elements may reflect crustal involvement in magma genesis. Any depletion in Ba, Rb and K that may be caused by fractionation of biotite in some samples is not evident in the multi-element patterns.

Chondrite-normalised REE patterns are also of use in evaluating the importance of fractionating phenocryst and accessory phases in magma evolution. Figure 6.7 compares REE mineral/melt partition coefficients for phenocryst and accessory phases present in the lavas with a typical chondrite-normalised REE pattern for the rhyolite lavas. The pronounced negative Eu anomaly seen in the lavas can be attributed to fractionation of plagioclase feldspar, as it is the most abundant phenocryst phase and mineral/melt partition coefficients for Eu in plagioclase range from ~ 2 - 5 (Arth, 1976; Nash and Crecraft, 1985), significantly higher than for the other REE. Fractionation of calcic amphibole and orthopyroxene may account for a slight depletion of heavy REE relative to light REE. However, it is unlikely that the fractionation of these phenocryst phases alone could produce the strong enrichment in light REE relative to heavy REE seen in the REE patterns. Mineral/melt partition coefficients for the REE in the accessory phases zircon and apatite range from 1 - 2 orders of magnitude greater than coefficients for orthopyroxene and calcic amphibole (Figure 6.7). Although zircon and apatite may be present in only small quantities, their very high partition coefficients for the REE lead to a disproportionate influence on the REE pattern (all of the REE are highly compatible in these accessory phases). The fractionation of zircon will deplete the heavy REE relative to the light REE, and fractionation of apatite will slightly deplete the middle REE relative to the light and heavy REE.

Settling curves calculated for a convecting granitic magma show that accessory minerals are too small to settle appreciably unless included within larger minerals (Bea, 1996). Biotite, which has small abundances of REE, is the mineral which shows the greatest tendency to include REE-rich accessory phases (Bea, 1996). Hence lavas in which biotite is a fractionating phase will have REE patterns relative to biotite-free/poor lavas that reflect removal of REE by accessory phases. This is seen to be the case for the Okataina, Rotorua and Kapenga volcanic centre rhyolite lavas, as generally those lavas containing biotite have depleted REE patterns relative to biotite-free/poor lavas. This is particularly seen in the biotite-bearing ho_2 rhyolite lavas. However, the rhyolite lavas sampled in this study contain REE-rich accessory phases (zircon and apatite) as inclusions in other phenocryst phases, such as orthopyroxene, plagioclase feldspar and titanomagnetite. The fractionation of these phases may therefore also have a significant effect on the REE patterns.

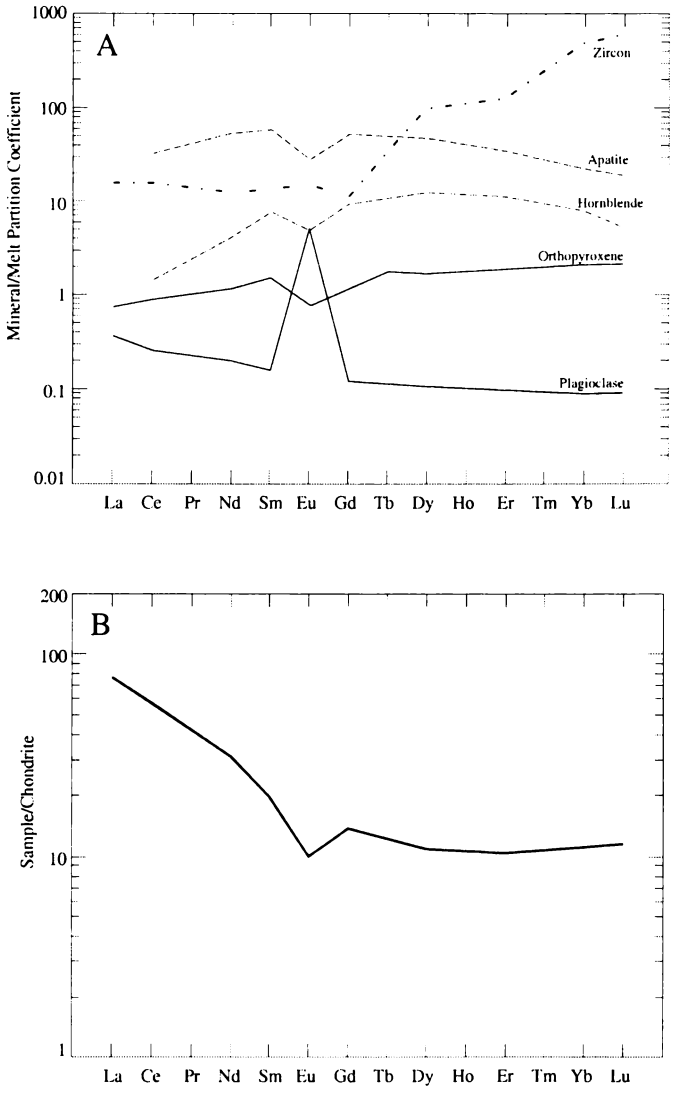

Figure 6.7: a) Mineral/melt partition coefficients for the REE in plagioclase feldspar, orthopyroxene, hornblende, apatite and zircon. Coefficients from Arth (1976) (dashed line), Nash and Crecraft (1985) (solid line) and Mahood and Hildreth (1983) (dot-dash line). b) Average chondrite-normalised REE abundance pattern for rhyolite lavas from the Okataina, Rotorua and Kapenga volcanic centres (normalisation values from Boynton, 1984).

If zircon was significant in the fractionating mineral assemblage, as suggested by REE patterns, it would be expected that there would be a depletion in Zr in these rhyolite lavas. Figure 4.13 shows that over a range in SiO_2 of ~ 2.5 wt. % and Rb/Sr of ~ 0.6, Haroharo Volcanic Complex rhyolite lavas exhibit a significant decrease in Zr from ~ 180 - 110 ppm. This is consistent with fractionation of zircon. However, multi-element patterns show no evidence for zircon fractionation (there is no trough in the patterns at Zr or Hf, which are both highly compatible in zircon). A possible reason for this is that these silicic magmas had a high initial abundance of Zr and Hf and fractionation of zircon has

caused a depletion in these elements, but not so significant as to result in visible depletions on multi-element diagrams.

6.5 FRACTIONAL CRYSTALLISATION MODELLING

Least squares regression modelling can be used to quantitatively evaluate the role of crystal fractionation in magmatic evolution for rhyolite lavas of the Okataina, Rotorua and Kapenga volcanic centres. Calculations were made using an Excel version of the XLFRAC program of Stormer and Nicholls (1978). This program utilises a least squares mass balance approach to calculate the proportions of mineral phases that need to be subtracted from the parent magma to produce a magma with a major element composition comparable to the daughter magma. A measure of the "fit" of the model is given in the value of Σr^2, the calculated sum of the squares of the residuals. In this study only Σr^2 values less than 0.3 have been considered acceptable. Higher values suggest that magmatic evolution from parent to daughter compositions cannot be modelled by simple closed-system fractional crystallisation. Phenocryst compositions used in this modelling were an average of compositions given in Appendix VI for a particular mineral phase in each parent sample or, if not available, for mineral phases in the daughter sample.

The concentration of trace elements in the daughter samples are then calculated using the proportions of subtracted phases determined by least squares regression modelling in the equation:

$$\text{TE concentration}_{\text{daughter}} = \text{TE concentration}_{\text{parent}} \times F^{(D-1)}$$

where F = fraction of liquid remaining
D = bulk partition coefficient of crystallising phases, where $D = \Sigma(w \times K_D)$
w = weight proportion of crystallising phase
K_D = partition coefficient of crystallising phase (Appendix IX)

These calculated trace element concentrations are compared to the observed concentrations in the daughter samples to provide a further assessment of the "fit" of the model. The results of fractional crystallisation modelling are given in Appendix X. Only the results of successful modelling, in which all phases are being subtracted and the Σr^2 value is acceptable, are given.

There are several potential problems when applying fractional crystallisation models to silicic magmas (and specifically the rhyolite lavas of this study) and hence there is cause for caution when interpreting the results. These problems include:

1. In the course of modelling rhyolite lavas in this study it was found that in order to obtain acceptable Σr^2 values and modelling results in which all mineral phases were being subtracted from the parent magma, orthopyroxene and cummingtonite could not both be included in the fractionating assemblage. Models give acceptable results by fractionating plagioclase + orthopyroxene + calcic amphibole + Fe-Ti oxides, or plagioclase + cummingtonite + calcic amphibole + Fe Ti oxides, but not with both orthopyroxene and cummingtonite together (e.g. Appendix X, Table X.1). In each of these acceptable cases the total fractionating percentage is similar, and the amount of orthopyroxene fractionating is similar to cummingtonite in the alternative model. In addition, calculated trace element compositions are similar. The inability of the model to accept both orthopyroxene and cummingtonite in the fractionating assemblage is most likely due to their similar compositions. However, this should not be seen as evidence to preclude fractional crystallisation processes from magma evolution.

2. Calculated trace element concentrations are extremely sensitive to the mineral-melt partition coefficients that are used. This is a critical factor in modelling silicic liquids as the partition coefficients for trace elements in silicic liquids vary, are different from those in less silicic magmas, and the behaviour of some trace elements is poorly understood. This is particularly true for REE. Partition coefficients for Sr and Ba in plagioclase were calculated for the Okataina, Rotorua and Kapenga rhyolites following Blundy and Wood (1991). The values are dependent on plagioclase composition and temperature and are hence sample specific. However, calculated Sr concentrations still differ from those observed, in that Sr is generally behaving more compatibly. Mineral-melt partition coefficients used in fractional crystallisation modelling are given in Appendix IX.

3. As previously discussed, the occurrence of accessory phases in silicic magmas such as zircon and apatite, for which no compositional analyses are available, can greatly affect trace element concentrations. In the case of zircon, abundances of Zr, Hf, U and the REE are particularly affected. Apatite will also have a significant affect on the REE. An example is the difference between observed and calculated Zr and Hf

concentrations in Appendix X. With the modelled subtracted phases as listed, Zr and to a lesser extent Hf, are being treated as too incompatible with calculated concentrations in excess of observed values. If the high partition coefficients of Zr and Hf in zircon could be incorporated into these models, calculated values would be lower and possibly in line with those observed. An attempt to incorporate analyses for zircon and apatite from the literature into fractional crystallisations modelling revealed that the model is not robust enough to accommodate these extra phases and the minor element oxides that they contain.

4. The introduction of calcic amphibole as a fractionating phase in least squares regression modelling can result in an artificially good value of Σr^2. This is because calcic amphibole contains significant amounts of a range of major elements and hence can act as a "sink", to which surplus portions of major elements can be attributed.

5. Quartz occurs in significant quantities in some samples and has not been included in the model. In addition, partition coefficients for magnetite are being used whereas these silicic magmas contain titanomagnetite.

6. Mobility of elements such as Rb, Ba and Sr during post-eruptive alteration of the lavas, and/or their loss by volatile-rich phases, could alter their concentrations in a way that the model would not account for.

7. In addition to crystal fractionation, crustal assimilation and partial melting processes may also fundamentally affect trace element concentrations. This is particularly important in silicic magmas and can affect Rb, Ba, Nb and K_2O in particular.

The results of fractional crystallisation modelling in Appendix X suggest that closed-system fractional crystallisation of the observed phenocryst phases could theoretically explain the range in compositions between rhyolites erupted from the same eruptive episode and over time at the Haroharo Volcanic Complex. Modelling of magma compositions erupted during the Rotoma episode (Table X.1) is consistent with evolution of the Te Pohue magma through closed-system fractional crystallisation of plagioclase + calcic amphibole + titanomagnetite + ilmenite + orthopyroxene (or cummingtonite) from the Rotoma magma. This is consistent with a previously unpublished data set for eruptives from the Rotoma episode shown in Figure 4.17, that shows an almost continuous range in composition. Modelling of the evolution of the Waiti magma, erupted in the following

Mamaku episode, from the Rotoma magma did not yield acceptable results, which suggests that they may be discrete and unrelated magmas.

Modelling involving magmas erupted during the Mamaku episode (Table X.2) is consistent with evolution of the vent area 1 and 3 magmas erupted at this time (Hainini and Te Horoa) from the vent area 2 magma (Waiti) by closed-system fractional crystallisation of plagioclase + orthopyroxene + calcic amphibole + titanomagnetite + ilmenite. Cummingtonite occurs in only trace amounts in these samples (Appendix III) and hence was not included in the model. Modelling using an average analysis for the Kaipara flow from Wright (2000) is consistent with evolution of the Kaipara magma from the Waiti magma by closed-system fractional crystallisation of plagioclase + calcic amphibole + titanomagnetite + ilmenite + orthopyroxene (or cummingtonite). Hence, as suggested by Wright (2000), the Kaipara magma may represent an isolated system at one end of the Waiti magma chamber, or alternatively may overlie the Waiti magma in a vertically stratified magma chamber.

The composition of rhyolite lavas erupted in vent areas 2 (Haroharo) and 4 (Tikorangi) during the Whakatane episode can be modelled by closed-system fractional crystallisation of plagioclase + calcic amphibole + titanomagnetite + ilmenite + orthopyroxene (or cummingtonite) from the older Waiti magma also erupted in this area (Table X.3). The magma erupted in vent area 1 during the Whakatane episode (Okataina) can be modelled by closed-system fractional crystallisation of plagioclase + calcic amphibole + titanomagnetite + ilmenite + orthopyroxene (or cummingtonite) from the older but spatially comparable Hainini magma, or plagioclase + cummingtonite + titanomagnetite from the vent area 2 magma erupted at this time (Haroharo) (Table X.3).

Hence fractional crystallisation modelling suggests considerable lateral/spatial compositional zonation within magmas beneath the Haroharo Volcanic Complex such that lavas erupted from the Haroharo Linear Vent Zone during the same eruptive episode are of different compositions related by closed-system fractional crystallisation processes. Within the Mamaku episode, with the exception of the Kaipara flow, the magma is becoming more evolved to the southwest. This is also the case for the Whakatane episode lavas.

Although variations in $^{87}Sr/^{86}Sr$ composition suggest that magmas erupted over c. 9 200 years from the Okareka Volcanic Complex have evolved by AFC processes (section 6.6), fractional crystallisation modelling was also carried out (Table X.4). This modelling is consistent with evolution of the Trig 7693 magma from the older Eastern Rhyolite magma by closed-system fractional crystallisation of plagioclase + orthopyroxene + calcic amphibole + titanomagnetite + ilmenite. Introducing biotite into the fractionating assemblage (the dominant ferromagnesian mineral in the Trig 7693 lava) requires the exclusion of orthopyroxene, titanomagnetite and ilmenite as fractionating phases and results in $\Sigma r^2 > 0.3$. These discrepancies may be explained by crustal involvement in magma evolution.

Modelling of two rhyolite lavas erupted during the Okareka episode at the Tarawera Volcanic Complex (Patiti Island and Ridge Flow) did not yield acceptable results and suggests that these two magmas are not related by closed-system fractional crystallisation. However, modelling is consistent with the evolution of the magma of Western Dome, erupted in the following Rerewhakaaitu episode, from the Patiti Island magma by closed-system fractional crystallisation of plagioclase + orthopyroxene + calcic amphibole + titanomagnetite + ilmenite (although Σr^2 is only marginally acceptable) (Table X.5). Within the Rerewhakaaitu episode, the more evolved biotite-bearing Rotomahana magma cannot be derived by closed-system fractional crystallisation from the biotite-poor Western Dome magma. The biotite-free Te Puha magma cannot be derived from either the Western Dome magma or the Rotomahana magma by closed-system fractional crystallisation.

The magma erupted in the Waiohau episode (Waikakareao) can be modelled by closed-system fractional crystallisation of plagioclase + titanomagnetite + ilmenite + orthopyroxene (or calcic amphibole) from the Ridge magma erupted earlier in the Okareka episode (Table X.5). Models incorporating both orthopyroxene and calcic amphibole were unacceptable in this case. Phenocryst contents suggest evolution of the Waikakareao magma from the Ridge magma would involve fractionation of both orthopyroxene and calcic amphibole (Appendix III). In addition, the eruption of spatially adjacent but geochemically unrelated magmas during the intervening Rerewhakaaitu episode may preclude a common magma source for the Ridge and Waikakareao lavas.

Modelling involving the two biotite-bearing magmas erupted from the Tarawera Volcanic Complex allows for the possibility that the Kaharoa episode magma (Tarawera) evolved by

closed-system fractional crystallisation of plagioclase + calcic amphibole + biotite from the Rerewhakaaitu episode magma (Rotomahana) (Table X.5). However, eruption of the intervening biotite-free Waiohau episode magma suggests that the existence of biotite-bearing Rotomahana magma in a liquid state beneath the Tarawera Volcanic Complex over this period of time is unlikely.

6.6 ASSIMILATION - FRACTIONAL CRYSTALLISATION (AFC) MODELLING

Assimilation-Fractional Crystallisation (AFC) processes are most commonly modelled to account for the compositions of silicic magmas in the TVZ. Waipapa and Torlesse metasediments comprise the pre-Cenozoic basement west and east of the TVZ respectively and are potential assimilants. They are commonly used as end-member compositions in crustal contamination and AFC modelling (eg. Graham et al., 1992; Gamble et al., 1993; Brown, 1994; McCulloch et al., 1994). Kakuki basalt is petrographically and chemically the most primitive volcanic rock in the TVZ, and the only one likely to approach a primary basalt composition (Gamble et al., 1990; Graham et al., 1992). Hence it is commonly used as an end-member in modelling of AFC processes (Graham et al., 1992; Gamble et al., 1993). The end-member compositions used in AFC modelling in this study are given in Table 6.3.

Figures 6.8 - 6.10 show the results of AFC modelling. The AFC modelling hyperbolae or trajectories generally replicate those produced in other studies using similar end-member compositions. Figure 6.8 shows, as has been found in previous studies, that the compositions of TVZ silicic volcanics as a whole can be best modelled in terms of $^{87}Sr/^{86}Sr$ vs. ε_{Nd} by AFC processes involving Kakuki basalt and Torlesse metasediments. Assuming a value of r = 0.2 (the rate of assimilation relative to crystal fractionation) and D_{Nd} = 0.25 (bulk partition coefficient for Nd), the compositions of the rhyolite lavas of this study are most closely replicated by hyperbolae representing D_{Sr} = 0.2 - 0.5, and requiring 60 - 90 % crystallisation. Several samples occur beyond these hyperbolae, but they could be reached by a small increase in r.

Table 6.3: Compositions of Torlesse and Waipapa metasedimentary basement and selected basalts from the Taupo Volcanic Zone.

	Torlesse Average	Waipapa Average	Tarawera basalt	Rotokawau basalt 1	Rotokawau basalt 2	Johnson Road basalt	Kakuki basalt
$^{87}Sr/^{86}Sr$	0.71459	0.70718	0.70520	0.705064	0.705002	0.704717	0.703878
ε_{Nd}	-4.5	+0.4	+2.2	+2.7	+2.9	+2.9	+5.1
$^{206}Pb/^{204}Pb$	18.859	18.788	18.763*				18.737*
$^{207}Pb/^{204}Pb$	15.646	15.618	15.581*				15.557*
Rb (ppm)	152	85	15	13	20	22	4
Sr (ppm)	217	309	318	372	382	357	350
Nd (ppm)	35	22	10.45	10.80	13.60	18.30	12.70
Pb (ppm)	19	17	3*	3	3		2*
SiO_2	65.0	61.1	50.63	51.06	53.24	51.74	48.52
Al_2O_3	16.6	15.8	17.17	17.75	16.86	17.21	18.09

Torlesse and Waipapa metasediment averages from Graham et al. (1992). Tarawera, Rotokawau, Johnson Road and Kakuki basalt analyses from Gamble et al. (1993) except those marked with an asterisk, which are from Graham et al. (1992).

This model is limited in that it assumes a constant D_{Sr} and assimilation rate throughout the evolution process and both of these parameters, in particular D_{Sr}, are likely to be variable. Graham et al. (1995) note that inconsistencies between Al_2O_3 and Sr contents in the rhyolites, which would require extensive plagioclase dominated fractionation with a net $D_{Sr} > 1$, and modelling involving $^{87}Sr/^{86}Sr$ vs. ε_{Nd} could be resolved if there was a gradual increase in D_{Sr} throughout the differentiation process. This might be expected with increased plagioclase crystallisation as the magmas become more silicic. For the rhyolites collected in this study, D_{Sr} values for plagioclase of ~ 5 - 14 (mean ~ 9) have been calculated following Blundy and Wood (1991) (Appendix IX).

Of note is that the TVZ basalts associated with the Okataina (Rotokawau and Tarawera) and Kapenga (Johnson Road) volcanic centres also lie on these AFC hyperbolae suggesting some degree of crustal contamination. Tarawera basalt is the most radiogenic, suggesting the highest degree of contamination. However, the degree of crystallisation implied for the Tarawera basalt by the $^{87}Sr/^{86}Sr$ vs. ε_{Nd} model (~ 60 %) is somewhat at variance with values

for Pb isotopes (~ 15 %) (Figures 6.9 and 6.10). This paradox can be resolved by a different choice of r or partition coefficient (Graham et al., 1992).

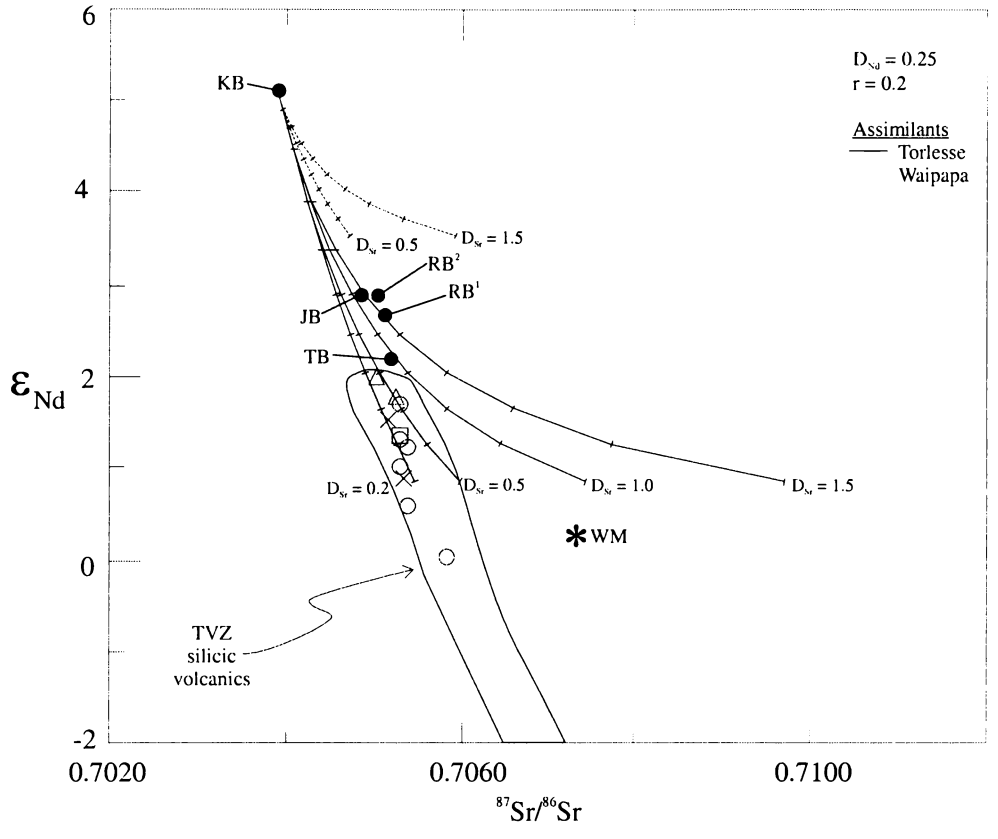

Figure 6.8: Enlargement of Figure 6.5 showing $^{87}Sr/^{86}$ Sr and ε_{Nd} compositions for rhyolite lavas from the Okataina, Rotorua and Kapenga volcanic centres and selected TVZ basalts (symbols as in Figure 6.5). Asterisk represents the average Waipapa metasedimentary basement composition from Graham et al. (1992). Field for TVZ silicic volcanics modified from Graham et al. (1992) and Gamble et al. (1993) to accommodate high $^{87}Sr/^{86}Sr$, low ε_{Nd} rhyolites from Sutton et al. (1995). Representative AFC mixing hyperbolae are constructed (after DePaolo, 1981) for parental Kakuki Basalt and either Waipapa or Torlesse metasediments as assimilants. D_{Nd} = 0.25, D_{Sr} indicated next to hyperbolae. r = Ma/Mc = 0.2 (where Ma = mass of assimilant and Mc = mass of crystals). Tick marks indicate the degree of crystallisation and are given in intervals of 0.1 to a maximum of 0.9.

TVZ silicic volcanics have similar lead isotopic compositions to both Waipapa and Torlesse metasediments. However, as has been found in previous studies, AFC modelling using parental Kakuki basalt indicates that the more likely assimilant is the Torlesse metasediments. Figure 6.9 shows that for r = 0.2 and D_{Pb} = 0.1, the AFC trajectory for Torlesse assimilant enters the field of TVZ silicic volcanics (at ~30 % crystallisation) and

approaches compositions for rhyolite lavas obtained in this study. Increasing the value of r slightly will extend the trajectory towards the more radiogenic compositions. Trajectories involving Waipapa metasediments fail to replicate the compositions of most TVZ silicic volcanics. Figure 6.10 utilises similar values of r and D_{Pb} and shows the failure of both assimilant types to replicate compositions of rhyolite lavas obtained in this study at these values. However, increasing r from 0.2 to 0.4 for Torlesse metasediments extends the hyperbolae to higher $^{207}Pb/^{204}Pb$ compositions and closer to the rhyolite lava compositions. Modelling involving lead isotopes suffers from the same limitations as models utilising $^{87}Sr/^{86}Sr$ and ε_{Nd}, in that it is assumed there is a constant D_{Pb} and rate of assimilation relative to crystal fractionation (r) throughout the evolution process.

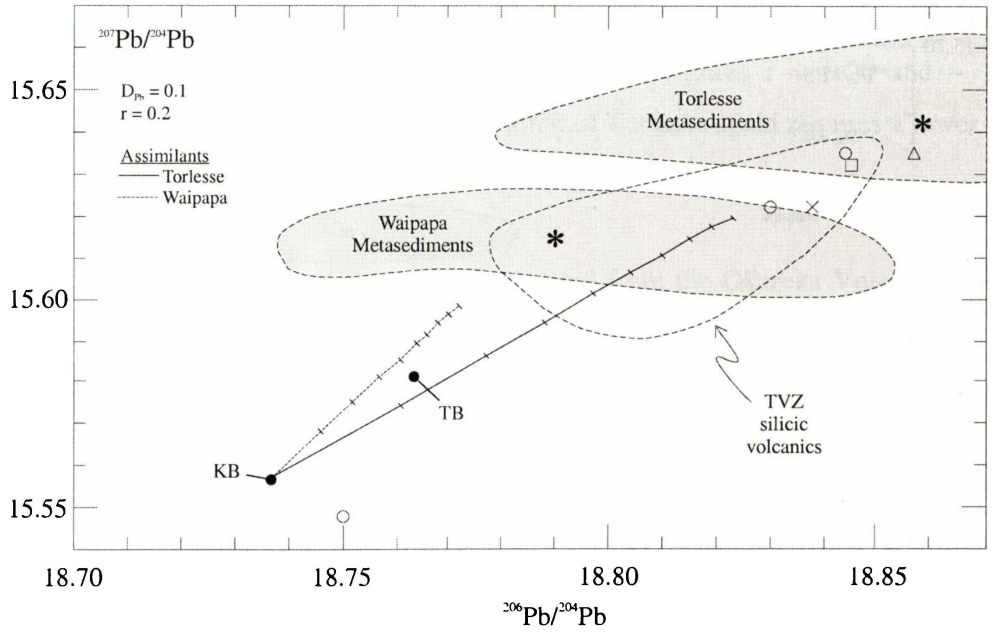

Figure 6.9: Enlargement of Figure 6.6 showing $^{206}Pb/^{204}Pb$ and $^{207}Pb/^{204}Pb$ compositions for rhyolite lavas from the Okataina, Rotorua and Kapenga volcanic centres and selected TVZ basalts (symbols as in Figure 6.6). Fields for Waipapa and Torlesse metasediments and TVZ silicic volcanics from Graham et al. (1992). Asterisks represent average metasedimentary basement compositions from Graham et al. (1992). Representative AFC mixing hyperbolae are constructed (after DePaolo, 1981) for parental Kakuki Basalt and either Waipapa or Torlesse metasediments as assimilants. D_{Pb} = 0.1, r = 0.2. Tick marks indicate the degree of crystallisation and are given in intervals of 0.1 to a maximum of 0.9.

It is clearly evident that there are inconsistencies when using Torlesse or Waipapa metasediments in AFC modelling of TVZ silicic magmas. However, as yet compositions for other possible crustal components are not well known.

AFC modelling can also be used to assess the relationship between the compositions of rhyolite lavas obtained in this study. There are two cases that warrant further investigation by AFC modelling. For the rhyolite lavas erupted from the Okareka Volcanic Complex and the biotite-bearing ho_2/hk_2 rhyolite lavas, increases in $^{87}Sr/^{86}Sr$ are accompanied by increases in Rb/Sr. In addition, the differences in $^{87}Sr/^{86}Sr$ are considered significant as they are beyond the errors associated with these analyses. Hence AFC modelling has been used to assess the assimilation rate and degree of crystallisation required to produce the range in compositions in these two groups of lavas.

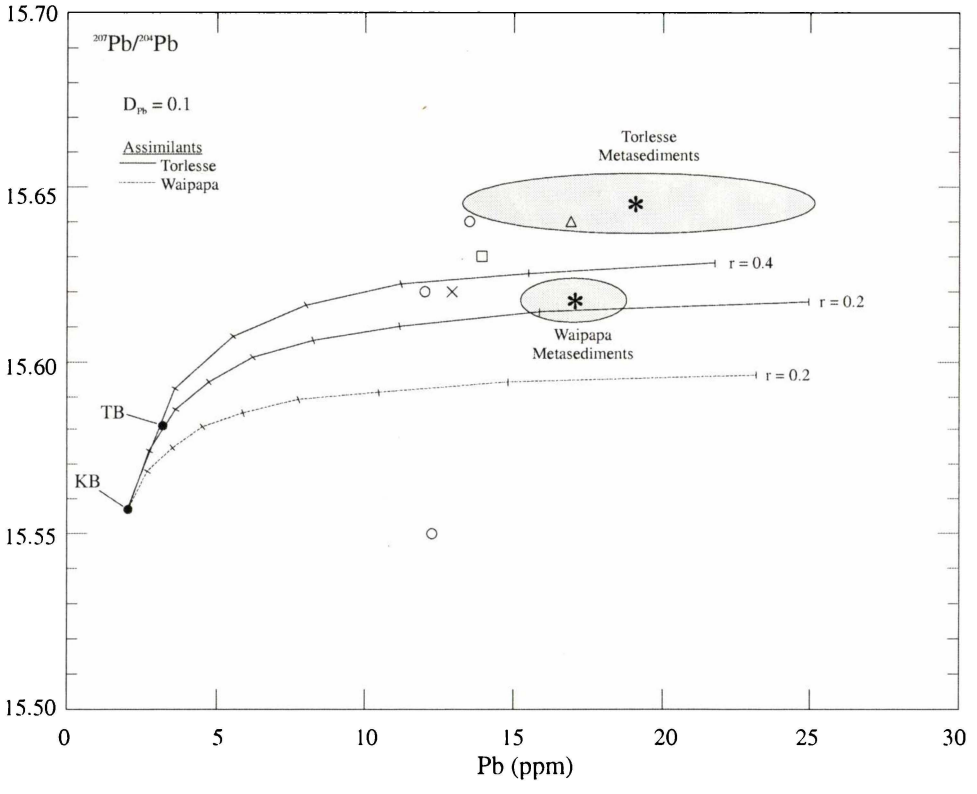

Figure 6.10: Pb (ppm) vs. $^{207}Pb/^{204}Pb$ for rhyolite lavas from the Okataina, Rotorua and Kapenga volcanic centres (open circles, triangle and square respectively). Cross indicates ho_2 rhyolite in the Okataina - Kapenga transition zone. Fields for Waipapa and Torlesse metasediments and compositions for selected TVZ basalts from Graham et al. (1992). TB = Tarawera basalt, KB = Kakuki basalt. Asterisks represent average metasedimentary basement compositions from Graham et al. (1992). Representative AFC mixing hyperbolae are constructed (after DePaolo, 1981) for parental Kakuki Basalt and either Waipapa or Torlesse metasediments as assimilants. D_{Pb} = 0.1, r = 0.2 or 0.4. Tick marks indicate the degree of crystallisation and are given in intervals of 0.1 to 0.8 (r = 0.2) or 0.1 to 0.6 (r = 0.4).

Figure 6.11 shows AFC model trajectories using Rb/Sr and $^{87}Sr/^{86}Sr$ compositions for rhyolite lavas from the Okareka Volcanic Complex. The sample of Eastern Rhyolite, erupted in the Te Rere episode (113), has been used as the parent composition and trajectories represent assimilation of either Torlesse or Waipapa metasediment. For each trajectory different values of D_{Sr} and r have been used until a fit was obtained with the daughter composition (Trig 7693 Dome, Rotorua episode (176)). In each case Sr has been considered strongly compatible (D_{Sr} = 2.5 - 4.0) and Rb has been considered incompatible (D_{Rb} = 0.1) in the fractionating assemblage. These values are realistic considering the fractionating phenocryst assemblage. The trajectories that best simulate the evolution of sample 176 from sample 113 are those numbered 2, 5 and 7. Note that trajectory 7 represents assimilation of both Waipapa and Torlesse metasediments at different values of r. The results are dependent on D_{Sr}. If D_{Sr} = 3.0, assimilation of Waipapa requires r = 0.15 and ~ 17 % crystallisation to produce sample 176. Assimilation of Torlesse requires a lower rate of assimilation relative to crystal fractionation (r = 0.05) but a similar amount of crystallisation. If D_{Sr} = 4.0, assimilation of Waipapa requires r = 0.20 and ~ 12 % crystallisation to produce sample 176. Assimilation of Torlesse again requires a lower value of r (0.06), but a similar amount of crystallisation.

Hence, the evolution in magma compositions erupted from the Okareka Volcanic Compex can be modelled by AFC processes. Dependent on the values of D_{Sr} and r that are used, either Waipapa or Torlesse metasediments could be possible assimilants. However, given previous constraints on assimilants from Nd and Pb isotopes for the rhyolite lavas as a whole, the most likely assimilant is considered to be Torlesse. Therefore, for a value of D_{Sr} from 3.0 - 4.0, a value of r = 0.05 - 0.06 and ~ 12 - 17 % crystallisation is required to produce the magma represented by sample 176 from the magma represented by sample 113 over the c. 9 200 years between eruptions.

Figure 6.12 shows AFC model trajectories using Rb/Sr and $^{87}Sr/^{86}Sr$ compositions for the biotite-bearing ho_2 and hk_2 rhyolite lavas. Modelling has been carried out in two steps. In step 1, Dome 3 (168) has been used as the parent composition and trajectories model the evolution of the Blue Lake rhyolite (152). In step 2, the Blue Lake rhyolite becomes the parent composition and trajectories model the evolution of Tutaeheka 1 (64). A value of D_{Rb} = 0.3 has been used in this modelling to reflect the increased importance of biotite in the fractionating assemblage, although overall, Rb is still behaving incompatibly (Figure 4.10). Values for D_{Sr} from 4.0 - 5.0 have been used, compared to slightly lower values for

trajectories in Figure 6.11, to reflect higher calculated values for D_{Sr} in plagioclase in these lavas (Appendix IX).

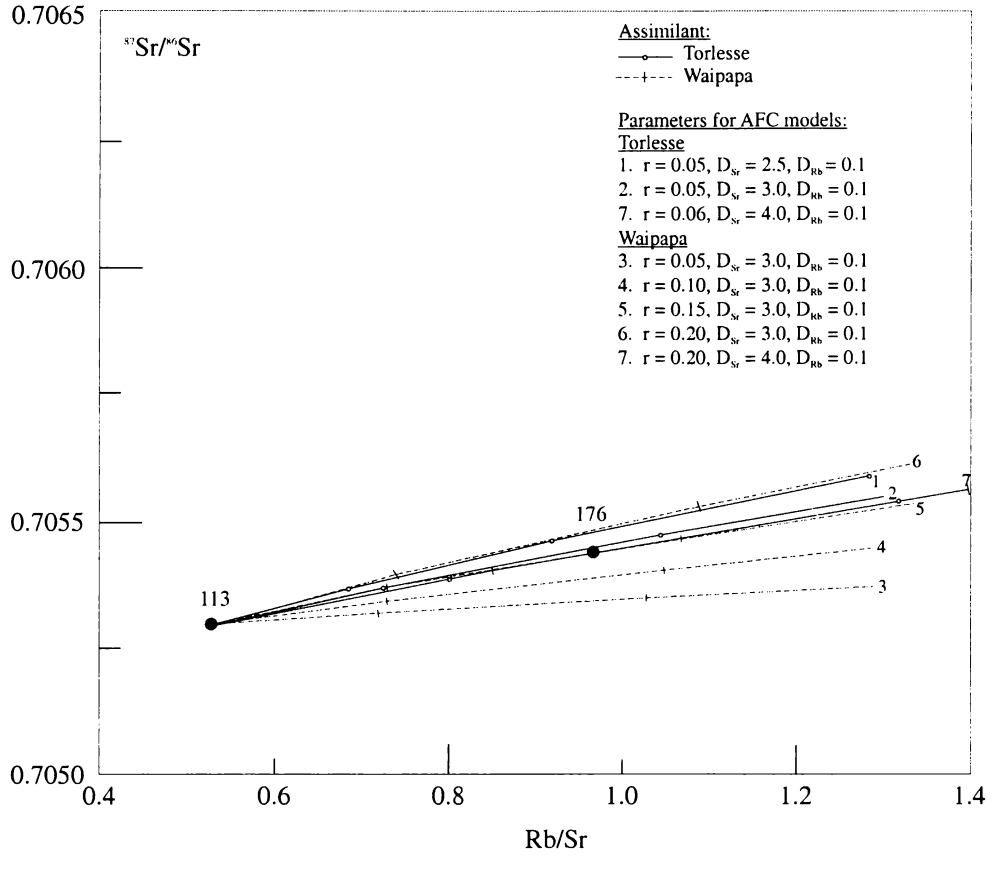

Figure 6.11: AFC model trajectories for Rb/Sr vs. $^{87}Sr/^{86}Sr$, using the equations of DePaolo (1981), for samples from the Okareka Volcanic Complex (113 = Eastern Rhyolite, Te Rere episode; 176 = Trig 7693 Dome, Rotorua episode). 113 is the parent composition and trajectories represent assimilation of Torlesse or Waipapa metasedimentary basement with variable values of r and D_{Sr}.

For step 1, the evolution of sample 152 from sample 168 can be modelled by assimilation of either Waipapa or Torlesse metasediments at low values of r (0.02 - 0.03 for Torlesse and 0.06 - 0.07 for Waipapa) and ~ 8 - 11 % crystallisation. For step 2, the evolution of sample 64 from 152 can be modelled by assimilation of Torlesse with r = 0.17 - 0.25 and up to 2 % crystallisation. Hence this step requires a higher level of assimilation and significantly less crystallisation than step 1. Models involving Waipapa assimilant for step 2 require high rates of assimilation relative to crystal fractionation (r = 0.50). Such high values of r have

not been considered as appropriate in other studies that have modelled TVZ silicic magma compositions by AFC. Again it is evident that the results are dependent on D_{Sr}, with increased D_{Sr} requiring slightly higher values of r and slightly lower crystallisation percentages for both assimilant types in steps 1 and 2.

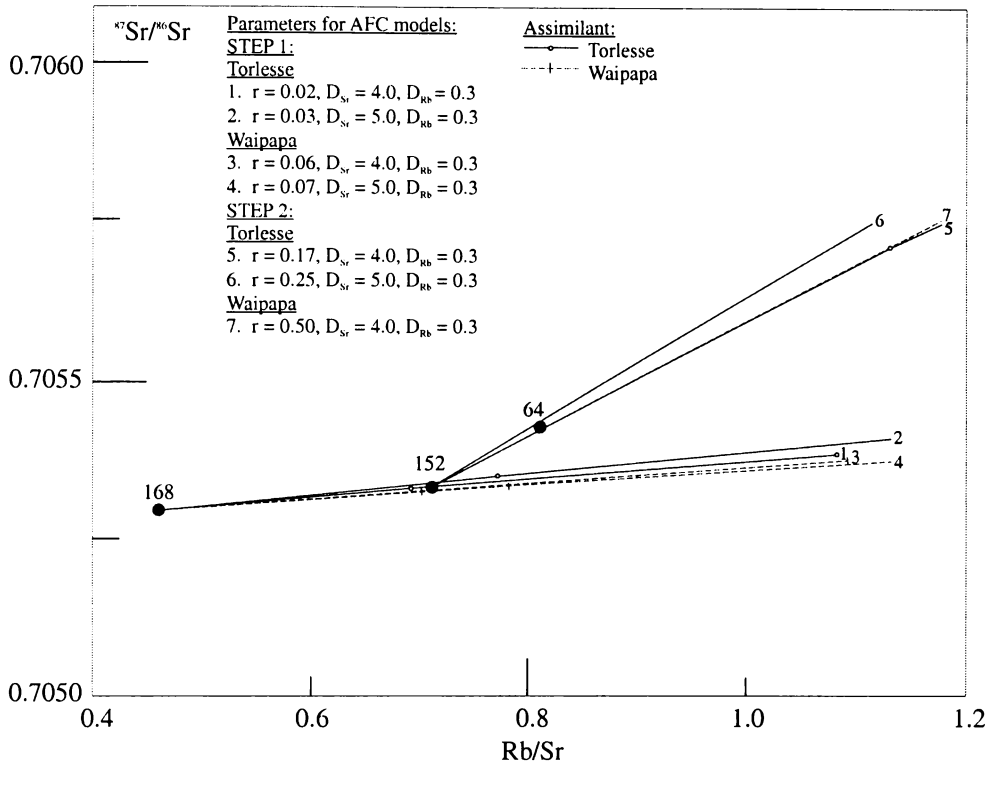

Figure 6.12: AFC model trajectories for Rb/Sr vs. $^{87}Sr/^{86}Sr$, using the equations of DePaolo (1981), for samples of ho_2 and hk_2 rhyolite lavas. Step 1: 168 to 152. Step 2: 152 to 64. Trajectories represent assimilation of Torlesse or Waipapa metasedimentary basement with variable values of r and D_{Sr}. 168 = Dome 3 (hk_2), 152 = Blue Lake rhyolite (ho_2), 64 = Tutaeheka 1 (ho_2).

Hence, the range in magma compositions erupted as the ho_2 and hk_2 rhyolite lavas can be modelled by AFC processes. As it is unlikely that assimilant lithologies have changed between steps 1 and 2, the unacceptably high value of r for assimilation of Waipapa metasediments in step 2 precludes their involvement in the evolution of these magmas. For D_{Sr} values of 4.0 - 5.0, an assimilation rate for Torlesse metasediments of r = 0.02 - 0.25 is required to replicate the lava compositions. This is accompanied by up to 11 % crystallisation. A possible scenario to explain the variable rates of assimilation and

crystallisation between steps 1 and 2 is that the Tutaeheka 1 lava (64) may be derived from the roof or side of a magma body where assimilation of crust was actively occurring. Dome 3 (168) and the Blue Lake rhyolite (152) may be derived from the interior of the magma body.

In summary, TVZ rhyolites as a whole and Okataina, Rotorua and Kapenga volcanic centre rhyolite lavas collected in this study have compositions that may be consistent with evolution of silicic magmas from basaltic magmas by crustal assimilation and fractional crystallisation processes (AFC). However, closed-system fractional crystallisation processes best model the small variations between spatially and temporally adjacent rhyolite lavas erupted from these centres. This is seen in particular for the ho_3 rhyolite lavas from the Okataina Volcanic Centre. This observation provides support for the McCulloch et al. (1994) model for silicic magma genesis in the TVZ, where basaltic magmas derived from the mantle assimilate crust, then evolve by closed-system fractional crystallisation processes with insignificant amounts of further assimilation.

Chapter Seven: Spatial and Temporal Evolution of the Okataina, Rotorua and Kapenga Volcanic Centres

Chapter Seven: Spatial and Temporal Evolution of the Okataina, Rotorua and Kapenga Volcanic Centres

7.1 INTRODUCTION

This chapter incorporates petrographic, geochemical, mineralogic and isotopic data presently available to provide a model for the spatial and temporal evolution of the magmatic system at the Okataina Volcanic Centre. Some insights will also be gained of the evolution of the magmatic systems at the adjacent Rotorua and Kapenga volcanic centres. Models for the evolution of large silicic magmatic systems will be outlined along with a comparison of silicic magmatic systems in North America and the Taupo Volcanic Zone. The timescales of magma generation and residence at the Okataina Volcanic Centre, and the implications of this study for the nature of future eruptions, will also be discussed.

7.2 SPATIAL AND TEMPORAL EVOLUTION OF THE OKATAINA VOLCANIC CENTRE

The eruptive history of the Okataina Volcanic Centre can be divided into two main periods:

1) A period of caldera formation, ending with the Rotoiti Ignimbrite eruption c. 65 ka (age from Houghton et al., 1995).

2) A period of post-caldera activity from c. 65 ka to the present, that intensified in the last c. 25 000 years, comprising caldera infilling pyroclastic and lava eruptions.

The rhyolite lavas erupted from the Okataina Volcanic Centre, which have been used in this study as the basis on which to assess the spatial and temporal evolution of the centre, have been erupted in three time periods:

1) Those pre-dating the widespread Mamaku Ignimbrite, which was erupted from the adjacent Rotorua Volcanic Centre at 220 ± 10 ka (age from Houghton et al., 1995) (known as the ho_1 rhyolites).

2) Those erupted between the Mamaku Ignimbrite and the Rotoiti Ignimbrite eruption at c. 65 ka (known as the ho_2 rhyolites).

3) Those younger than the Rotoiti Ignimbrite (known as the ho_3 rhyolites).

Hence it is these temporal divisions that are used in discussions of the evolution of the Okataina Volcanic Centre.

7.2.1 Pre-Mamaku Ignimbrite (> 220±10 ka)

The early history of the Okataina Volcanic Centre is recorded in lavas erupted adjacent to caldera margins (ho_1 rhyolites) and in the eruption of several caldera-forming ignimbrites. The lavas display considerable mineralogical, geochemical and isotopic heterogeneity, which suggests the occurrence of multiple batches of magma. This early period of activity is poorly constrained by age data, particularly for the rhyolite lavas. In addition there is a lack of geochemical and isotopic data for the Quartz Biotite Ignimbrite, Onuku-Pokopoko Pyroclastics and Kawerau Ignimbrite. These factors preclude the determination of genetic relationships between the rhyolite lavas and the pyroclastics. On the basis of spatial position, ferromagnesian phenocryst assemblages and isotopic composition, the ho_1 rhyolite lavas have been divided into four magma types. The characteristics of these magma types are summarised in Table 7.1.

The Matawhaura-Matahina type magma comprises all orthopyroxene and calcic amphibole-bearing rhyolite lavas erupted in the northern and western Okataina Volcanic Centre (Matawhaura, Maungawhakamana, Waitangi, Stancorp Quarry and Crater Farm rhyolites, see Figure 2.1). Also included in this group is the magma erupted during the eruption of the Matahina Ignimbrite. Similarities in ferromagnesian phenocryst assemblages, magmatic temperatures, geochemistry, and isotopic composition suggest a possible genetic relationship between the Matahina Ignimbrite and the Matawhaura-Matahina type rhyolite lavas. However, a lack of age data for the ho_1 rhyolites prevents a temporal comparison. Comparable $^{87}Sr/^{86}Sr$ compositions for Matawhaura rhyolite (0.705832, see Table 6.1) and the Matahina Ignimbrite (eg. 0.70587 ± 6; Blattner et al., 1996) suggest that geochemical variations within this magma type may be due to fractional crystallisation processes that

Table 7.1: Summary of the petrographic and isotopic characteristics of rhyolite magma types erupted from the Okataina Volcanic Centre pre-c. 25 000 years B.P.

Magma Type	Ferromagnesian Mineral Assemblage	Phen. %	Temperature (°C)	$^{87}Sr/^{86}Sr$	ε_{Nd}	Special Features or Extra Notes	Representative Sample (No.)
Post-Rotoiti Ignimbrite (< c. 65 ka)							
Young Mangaone Subgroup type	*Opx + Ca-Amph*[#]		*720-820*[#]			*Possibly some interaction between these two magma types resulting in eruptives of an intermediate composition.*[#]	
Old Mangaone Subgroup type	*Ca-Amph + Opx + Cpx*[#]		*850-950*[#]				
Post-Mamaku Ignimbrite and pre-Rotoiti Ignimbrite (220 ± 10 - c. 65 ka)							
Moerangi type	Opx + Ca-Amph (trace Bio)	17-27	752	0.70516 - 0.70518	1.52	Includes *Te Wairoa Ignimbrites*	72 117 160
Blue Lake - *Earthquake Flat* Type **(Kapenga eruptive ?)**	Bio + Ca-Amph + Opx	23-32	687-743	0.70529 - 0.70542	0.90 - 1.37	Includes *Earthquake Flat Ignimbrite* and the hk_2 rhyolite lavas	64 (ho_2) 152 (ho_2) 168 (hk_2) 170 (hk_2)
Rotoiti Type	*Cgt + Opx + Ca-Amph ± Bio*[φ]	*25*[φ]	*760-790*[φ]			*Mineralogical and geochemical inconsistencies preclude a genetic relationship with the Moerangi and Blue Lake-Earthquake Flat magma types.*	
Lake Rotoiti Rhyolites Type						*Not sampled in this study, hence a possible genetic relationship with the Rotoiti type magma cannot be assessed.*	
Pre-Mamaku Ignimbrite (> 220 ± 10 ka)							
Matawhaura - *Matahina* type	Opx + Ca-Amph	5-16	832	0.70583	0.02	Includes *Matahina Ignimbrite*	109
Whakapoungakau type	Ca-Amph + Bio + Opx	11-19		0.70522			110
Wairua type	Ca-Amph + Bio + Opx	36	727	0.70539	0.60	Erupted adjacent to the southern caldera rim	119
North Rotoma type	Bio + Ca-Amph + Cgt	22	715	0.70558		Coexisting biotite and cummingtonite	107
Quartz-Biotite type	*Bio + Ca-Amph + Opx*					*Lack of data prevents the determination of any genetic relationship between these pyroclastic eruptives and the rhyolite lavas erupted during this period.*	
Onuku-Pokopoko type	*Opx ± Ca-Amph*						
Kawerau type	Ca-Amph + Opx *± Cpx*						

Magma type characteristics are based on data obtained in this study for rhyolite lavas and do not specifically include data for associated pyroclastic eruptives from the literature (except where indicated). Age groups are listed in order of increasing age, however within each age group the magma types are listed in no particular order. Units in italics were not sampled in this study. Temperatures are Fe-Ti oxide estimates unless unavailable in which case hornblende-plagioclase estimates are given. Data for the Rotoiti Ignimbrite and Mangaone Pyroclastics Subgroup from Schmitz (1995) (φ) and Smith (2001) (#) respectively. Ferromagnesian phenocryst assemblages for pyroclastics from references cited in section 3.12.

increased Rb/Sr and left $^{87}Sr/^{86}Sr$ relatively unchanged, although further isotopic data for the rhyolite lavas and the Matahina Ignimbrite are required to substantiate this. Further isotopic data are also required to determine whether the unique isotopic composition of Matawhaura rhyolite (see section 6.2.4) is shared by the Matahina Ignimbrite and other rhyolite lavas ascribed to this magma type.

Within the Matawhaura-Matahina type magma, Maungawhakamana lavas show a wide range in major and trace element compositions in addition to variations in phenocryst abundances. Further work on determining vent locations and the extent of individual lava domes/flows comprising this edifice is required to properly interpret the geochemical and mineralogical data.

Different $^{87}Sr/^{86}Sr$ compositions distinguish the Matawhaura-Matahina type magma from the Whakapoungakau type magma, which was erupted in the western Okataina Volcanic Centre as the Whakapoungakau and Pukepoto rhyolites (Figure 2.1). In addition, the Whakapoungakau type magma contains small amounts of biotite (<3% of total phenocrysts).

The Wairua type magma is biotite-bearing (~5% of total phenocrysts) and phenocryst rich compared to other lavas erupted during this period. This magma type was erupted from a vent adjacent to the southern rim of the Haroharo Caldera and is spatially separate from other ho_1 rhyolite lavas.

The North Rotoma type magma, erupted in the northern Okataina Volcanic Centre spatially adjacent to the Matawhaura-Matahina type magma, is unique among magmas erupted during this period as it contains cummingtonite in addition to calcic amphibole and biotite.

The lack of geochemical and isotopic data for the Quartz Biotite Ignimbrite, Onuku-Pokopoko Pyroclastics and Kawerau Ignimbrite prevents an investigation of any genetic relationship between these pyroclastics or to the ho_1 rhyolite lavas. However, similarities in ferromagnesian phenocryst assemblages allude to possible relationships, which further mineralogical, geochemical and isotopic data are required to substantiate.

The volume of magma erupted as rhyolite lavas in this earliest period of activity at the Okataina Volcanic Centre is difficult to determine due to burial of lavas by younger deposits and possible destruction during caldera collapse. Wilson et al. (1984) estimated a volume of

40 km^3 for all rhyolite lavas erupted from the Okataina Volcanic Centre prior to the Rotoiti Ignimbrite. Volume estimates for the pyroclastics erupted during this period are given in Table 2.1. The Matahina Ignimbrite has an estimated equivalent magma volume of 150 km^3. However, the volume of the Matawhaura-Matahina type magma must have been in excess of this to account for the volume of rhyolite lavas also erupted from this magma type.

Hence this early period of activity at the Okataina Volcanic Centre involved eruption of multiple rhyolite magma types as caldera-forming ignimbrites, from relatively large magma batches (~ 90 - 150 km^3), and as lavas, which at this stage appear to have been erupted from smaller, spatially discrete magma batches confined to particular areas. The exception is the orthopyroxene and calcic amphibole-bearing rhyolite lavas erupted in the northern and western Okataina Volcanic Centre, which may represent pre- or post-Matahina Ignimbrite magma. Further geochemical and isotopic studies on the other caldera-forming ignimbrites erupted during this period may highlight a genetic relationship with one of the other three magma types identified from lava compositions.

The occurrence of multiple rhyolite magma types as identified in the ho_1 rhyolite lavas can be interpreted to reflect the absence of a single large magma chamber evolving beneath the Okataina Volcanic Centre during its early history. It is suggested that at least four discrete magma batches, based on the composition of rhyolite lavas, were erupted during this period and they may or may not have coexisted. Age data for the ho_1 rhyolite lavas would be required to shed more light on the coexistence of these magma batches and their longevity. Sutton (1995) drew similar conclusions regarding the early history of the Taupo Volcanic Centre, proposing that eruptions of multiple small volume magma types were confined to restricted areas and reflected the lack of a single large magma chamber. Sutton (1995) noted that this interpretation contrasts with explanations proposed for other lava dome fields (eg. Coso Volcanic Field, California (Bacon et al., 1981), Taylor Creek Rhyolite, New Mexico (Duffield and Ruiz, 1992)) in which dome compositions were interpreted as reflecting tapping of a large zoned/evolving magma chamber. However, Sutton (1995) considered that these cases differ from Taupo in that the eruption of different rhyolite types was not spatially restricted but distributed in a random fashion.

There is a significant interval of time between this earliest period of activity from the Okataina Volcanic Centre (> 220 ± 10 ka) and the next documented eruption at c. 65 ka (the Rotoiti Ignimbrite). The ho_2 rhyolite lavas were erupted during the intervening period, but

stratigraphic relationships suggest that they were erupted relatively close to c. 65 ka (see section 2.2.2.2). Other eruptions may have occurred during this period and currently remain unidentified due to the deposits being buried or destroyed by subsequent eruptions. However, based on the currently established stratigraphy for the Okataina Volcanic Centre, in association with current knowledge of vent locations and eruptive geochemistry, it is suggested that magma batches erupted prior to 220 ± 10 ka were exhausted during eruption or any residual magma solidified in the crust.

A temporal division, in addition to geochemical differences, is the reason that no genetic relationship has been suggested in this study between the biotite and cummingtonite-bearing North Rotoma magma type and the biotite and cummingtonite-bearing Rotoiti Ignimbrite, even though their vents are spatially associated.

Burt et al. (1998) provide some insights into the existence of the Matahina Ignimbrite magma during this intervening period, documenting granitoid lithic fragments within the Rotoiti Ignimbrite that have identical isotope ratios to the host ignimbrite, yet a similar chemistry to the Matahina Ignimbrite. The isotopic similarity of these granitoid fragments to the Rotoiti Ignimbrite, suggesting that they are chilled portions of the same magma, is considered by Burt et al. (1998) to be a coincidence given the limited isotopic variation in Taupo Volcanic Zone silicic volcanics. They suggest that these fragments represent a portion of the Matahina magma system, which remained at depth (3.5 - 5 kbar) and formed an isolated cupola to the main ignimbrite-forming magma chamber (Figure 7.1). Burt et al. (1998) consider that migration of this magma towards the surface, likely to have been initiated during the upheaval coincident with migration and eruption of the Rotoiti Ignimbrite, led to the development of fragments with a granitoid texture.

The conclusions of Burt et al. (1998) have implications for the longevity of magmas beneath the Okataina Volcanic Centre, suggesting that residual Matahina magma remained partially molten for the duration of the period between the Matahina and Rotoiti ignimbrite eruptions (c. 200 000 years). Burt et al. (1998) note that this is an order of magnitude longer than estimates by Sutton et al. (1995) for the Oruanui magma system at the Taupo Volcanic Centre, but within the mid-range of estimates for magma systems elsewhere. However, many of these systems are now being reinterpreted in terms of shorter magma residence times (see section 7.2.4.1).

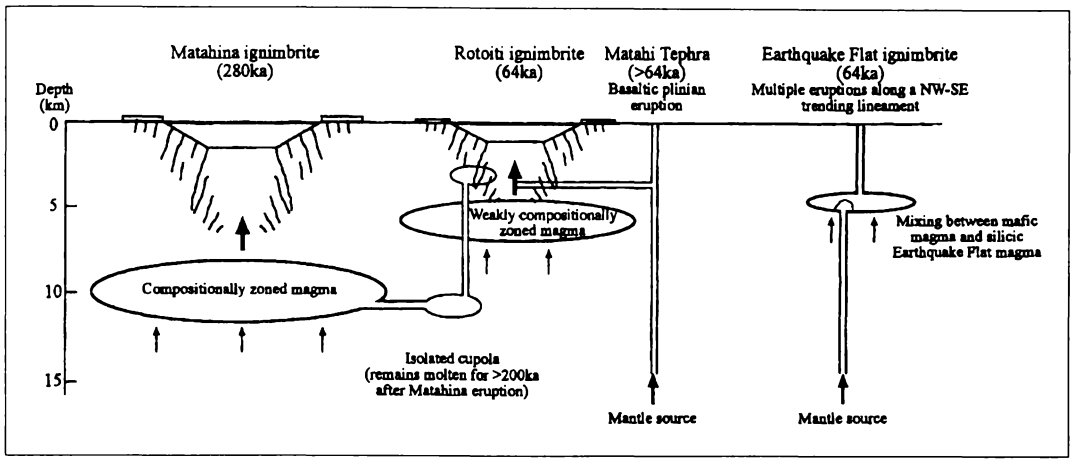

Figure 7.1: Cartoon model for the evolution of the Okataina Volcanic Centre from c. 280 - 64 ka from Burt et al. (1998). Note that the age for the Rotoiti Ignimbrite (64 ka) differs slightly from that used in this study (c. 65 ka).

Nairn (1989) considers that the Puhipuhi Dacite, outcropping in the Puhipuhi Basin, was also erupted during this early period of activity at the Okataina Volcanic Centre. However, it is younger than the post-Matahina Ignimbrite subsidence of the Puhipuhi Basin. This dacite was not sampled in this study, and its relationship to any of the rhyolite magma types erupted during this period is unknown.

7.2.2 Post-Mamaku Ignimbrite and Pre-Rotoiti Ignimbrite (220 ±10 - c. 65 ka)

This intermediate period in the history of the Okataina Volcanic Centre is recorded in the ho_2 rhyolite lavas and associated small volume pyroclastic deposits, erupted dominantly from vents in the southwestern Okataina Volcanic Centre in an area of possible overlap with the Kapenga Volcanic Centre, and ended with the caldera-forming Rotoiti Ignimbrite eruption. On the basis of ferromagnesian phenocryst assemblages, geochemistry and isotopic compositions presently available, the ho_2 rhyolite lavas are considered to represent two spatially adjacent magma types (Table 7.1).

The Moerangi type magma comprises all of the orthopyroxene and calcic amphibole-bearing lavas of the Moerangi and Tutaeheka rhyolites (Direct Road, Hill Road, Moerangi Road, Chestnut Road, Green Lake, Tutaeheka 2 and Tutaeheka 3 rhyolites, see Figure 2.2). Also included in this group are the Te Wairoa Ignimbrites, which show mineralogical and geochemical similarities to the lavas (Bellamy, 1991). Within the Moerangi type magma, similar $^{87}Sr/^{86}Sr$ compositions over a range in Rb/Sr (see Figure 6.1) are consistent with evolution by closed-system fractional crystallisation processes.

Mineralogical, geochemical and isotopic differences distinguish the Moerangi type magma from the Blue Lake - Earthquake Flat type magma. This latter magma type includes all of the biotite-bearing lavas of the Moerangi, Tutaeheka and South Rotomahana rhyolites (Kakapiko, Blue Lake, Tutaeheka 1, Hapeotoroa and Waimangu rhyolites, see Figure 2.2). Also included in this group are the Earthquake Flat Ignimbrite and the hk_2 rhyolite lavas, which show mineralogical, geochemical and isotopic similarities to the biotite-bearing ho_2 lavas. Davis (1985) identified two compositionally distinct magma types within the Earthquake Flat Ignimbrite with Type 1 being enriched in SiO_2 and K_2O and depleted in Zr relative to Type 2. These two groups are shown in Figures 4.5 and 4.6. Davis (1985) proposed that these two magma types were erupted from a single layered chamber with Type 1 overlying Type 2. This may be consistent with eruption of the biotite-bearing ho_2 and hk_2 lavas, similar in composition to the Type 1 magma, from the top of the chamber prior to the ignimbrite eruption. Within the Blue Lake - Earthquake Flat type magma, increasing Rb/Sr (from 0.46 - 0.81) is accompanied by increasing $^{87}Sr/^{86}Sr$ (from 0.705293 - 0.705424) (see Figure 6.12). These variations in magma compositions have been modelled by AFC processes. For D_{Sr} = 4.0 - 5.0, a variable assimilation rate of r = 0.02 - 0.25 is required to replicate the lava compositions, accompanied by up to 11% crystallisation (see Figure 6.12). A possible scenario to explain the variable rates of assimilation and crystallisation required within this magma type is that some of the lavas may be derived from the roof or side of a magma body where assimilation of crust was actively occurring. Other rhyolites may be derived from the interior of the magma body.

Mineralogical and geochemical data for the Rotoiti Ignimbrite distinguishes it from both magma types erupted in the southwestern Okataina Volcanic Centre as the ho_2 rhyolite lavas. In addition, the distance between vents provides support for the lack of a genetic relationship. The introduction of biotite into the ferromagnesian phenocryst assemblage of the Rotoiti Tephra Formation midway through the eruption sequence led Schmitz (1995) to

suggest a genetic relationship with the Earthquake Flat Ignimbrite. Both ignimbrites were erupted at approximately the same time but from vents ~ 25 km apart. The distance over which the Earthquake Flat magma type would have to migrate to substantiate such a scenario has precluded its wide acceptance. In addition, Burt et al. (1998) appeal to geochemical differences as evidence to discount the model of Schmitz (1995) and suggest that the geochemical and mineralogical variation in the Rotoiti Ignimbrite is a feature of a weakly zoned magma chamber. The Matahi Scoria is the basal member of the Rotoiti Tephra Formation, and intrusion of mafic magma is considered to have triggered the rhyolitic eruption (Nairn, 1992).

Burt et al. (1998) consider that hornblende-dominant microdiorite and mafic fragments found in the Rotoiti and Earthquake Flat ignimbrites represent almost totally crystallised (90 - 95%) mafic magma that mingled with largely molten silicic magma prior to its eruption. Chemically and isotopically these fragments are very similar to Taupo Volcanic Zone high alumina basalts and andesites and are therefore interpreted as their plutonic equivalents. The differing mineralogy (Taupo Volcanic Zone high alumina basalts and andesites contain pyroxene as the dominant mafic phase) is a consequence of crystallisation under high P_{H_2O} conditions ($P_{H_2O} \approx P_{Total}$) at relatively shallow levels in the crust (< 2 kbar pressure, < 6 km depth) (Burt et al., 1998). Burt et al. (1998) suggest that prior to the eruption of the Rotoiti Ignimbrite, part of the mafic Matahi magma system (which erupted immediately prior to the Rotoiti magma) became isolated from the main system and was injected laterally westwards where it was incorporated into the Rotoiti Ignimbrite eruption as microdiorite fragments (Figure 7.1). Smaller and more common mafic fragments in the Earthquake Flat Ignimbrite suggest that they represent mingling between largely solidified mafic and largely molten silicic magmas (Figure 7.1).

No specific estimates have been made of the volume of magma erupted as the ho_2 rhyolite lavas. Volumes of ~ 3.7 km^3 (dense rock equivalent) have been estimated for the Earthquake Flat Ignimbrite (Froggatt and Lowe, 1990). Given that this study has suggested that the Earthquake Flat Ignimbrite and the biotite-bearing ho_2 and hk_2 rhyolite lavas are derived from the same magma type, the volume of the Blue Lake - Earthquake Flat magma type must have been considerably larger than that estimated for the Earthquake Flat Ignimbrite alone. The Rotoiti Ignimbrite and associated Rotoehu Ash have a combined estimated equivalent magma volume of 120 km^3.

Hence this intermediate period of activity at the Okataina Volcanic centre involved eruption of multiple rhyolite magma types. One type of relatively large volume (~ 120 km^3) was erupted as a caldera-forming ignimbrite. Another two smaller volume rhyolite magma types were erupted dominantly as rhyolite lavas in the southwestern Okataina - Kapenga area, and as associated small volume non-caldera forming pyroclastics (the Te Wairoa and Earthquake Flat ignimbrites). Hence while a relatively large magma batch lay beneath the northern Okataina Volcanic Centre during this time, two smaller magma batches may have resided adjacent to each other beneath the southwestern Okataina Volcanic Centre.

Determining whether these two smaller batches may have co-existed with each other, or the larger Rotoiti type magma, requires age data for the ho_2 rhyolite lavas, which is not currently available. Insufficient studies have been carried out on the ho_2 rhyolite lavas to resolve the existence of any possible mingling of the two magma types which would also suggest that they coexisted (comparable to mingling between biotite-bearing and biotite-free/poor magmas in the Rerewhakaaitu eruptives from the Tarawera Volcanic Complex). In addition, consistent ages for the biotite-bearing ho_2 rhyolites and the hk_2 rhyolites would provide further support for a genetic relationship.

Data obtained in this study do not facilitate the drawing of a boundary between the Okataina and Kapenga volcanic centres. It is not possible to define such a boundary geochemically. Given the biotite-bearing ho_2 rhyolite lavas are comparable to hk_2 lavas well within the Kapenga Volcanic Centre, the southwestern Okataina Volcanic Centre area could perhaps be best defined as a northeastern part of the Kapenga Volcanic Centre. However, it has not been possible to relate the biotite-free/poor ho_2 lavas to other eruptives from either the Okataina or Kapenga volcanic centres. Their spatial relationship to the biotite-bearing lavas cannot be considered as evidence of a Kapenga Volcanic Centre origin. It is possible that this area is truly an overlap between the Okataina and Kapenga volcanic centres, with the biotite-bearing lavas having a strictly Kapenga origin and the biotite-free/poor lavas having an Okataina origin.

7.2.3 Post-Rotoiti Ignimbrite (c. 65 ka - present)

The post-Rotoiti Ignimbrite eruptive history of the Okataina Volcanic Centre can be divided into two periods:

1) A period from c. 43 000 - 31 400 years B.P., during which the Mangaone Pyroclastics Subgroup was erupted.

2) A period from c. 25 000 years B.P. to the present, during which the rhyolite lavas and pyroclastics comprising the Haroharo, Okareka and Tarawera volcanic complexes were erupted, largely infilling the collapse structures of the Okataina Volcanic Centre.

Although the lavas and pyroclastics comprising the Haroharo, Okareka and Tarawera volcanic complexes have been erupted over the same period of time, there are several factors which suggest that these complexes have not been derived from a single, large magma body evolving beneath the Okataina Volcanic Centre:

i) In terms of ferromagnesian phenocryst assemblages, many of the rhyolite lavas erupted from the Haroharo Volcanic Complex are cummingtonite-bearing, whereas many of those erupted from the Tarawera Volcanic Complex are biotite-bearing. Only very rarely is cummingtonite found at Tarawera or biotite found at Haroharo (Chapter Three). This suggests that the physical conditions involved in magma generation and evolution at the Haroharo and Tarawera volcanic complexes differ to a certain degree.

ii) Vent locations for the Haroharo and Tarawera volcanic complexes lie along the Haroharo and Tarawera linear vent zones, respectively, which lie on parallel NE-SW trends ~ 12 km apart (Figure 2.7). These spatially adjacent volcanic complexes have never been in eruption at the same time during the past c. 25 000 years. If they were being fed by a single, large magma body, simultaneous eruptions would be likely and vent locations may not be so clearly separated.

iii) The Okareka Volcanic Complex lies at the southern end of the Haroharo Linear Vent Zone, although the vents for this complex fall on a NW-SE trend perpendicular to the vent zone (Figure 2.7). Eruptions occurred at both the Haroharo and Okareka volcanic complexes during the Te Rere episode, although the distance between vents

(~ 14 km) suggests that the magmas erupted at these two complexes are not genetically related. In addition, rhyolite lavas erupted from the Okareka Volcanic Complex are biotite-bearing.

The approach used in this study to define the evolution of the Haroharo, Okareka and Tarawera volcanic complexes has involved identifying spatially or temporally comparable rhyolite lavas with similar mineralogical, geochemical and isotopic characteristics, which hence define the nature of the magma batch from which they were erupted. Possible genetic relationships between magma batches have then been assessed.

7.2.3.1 The Mangaone Subgroup (c. 43 000 - 31 400 years B.P.)

Newly identified tephra beds in the Mangaone Pyroclastics Subgroup (Jurado-Chichay and Walker, 2000; Smith, 2001) confirm that the Okataina Volcanic Centre was more productive between the Rotoiti Ignimbrite and Te Rere Eruptive Episode eruptions than previously thought, with at least 14 separate plinian or phreatoplinian eruptions occurring.

The Mangaone Subgroup can be divided into two main groups (Table 7.1). The Old Mangaone Subgroup (Unit A - Unit F) comprises clinopyroxene-bearing, high temperature (850-950°C), low SiO_2 rhyodacites (Smith, 2001). The Young Mangaone Subgroup (Unit I - Unit L) comprises orthopyroxene-dominated, low to medium temperature (720-820°C), high SiO_2 rhyolites. Units G and H have intermediate temperatures and compositions (Smith, 2001).

The major change in the glass, whole rock and phenocryst chemistry between the Old and Young Mangaone Subgroup can be correlated to changes in geographic position of the vents. The vent locations for the Old Mangaone Subgroup eruptions are in a general north-south trending zone within the central part of the Haroharo Caldera. Vents for the Young Mangaone Subgroup eruptions appear to migrate with time along an east-west trending zone in the upper Puhipuhi Basin (Jurado-Chichay and Walker, 2000) (Figure 7.2). The change in the geographic positions of vents suggests a change in source between the Old and Young Mangaone Subgroup. Fractional crystallisation modelling (Smith, 2001) revealed that the Young Mangaone Subgroup could not theoretically be derived from the same magma system as the Old Mangaone Subgroup. It is suspected that the last major eruption from the Old Mangaone Subgroup (Unit F) almost emptied the magma system and a new system derived

from a different source emerged. This new system, located to the east of the previous system, fed the Young Mangaone Subgroup eruptions. Linear relationships in major and trace element compositions within each of the two groups are most likely to be associated with fractionation of the two individual magmatic systems (Smith 2001). Smith (2001) also suggests that the intermediate compositions of Units G and H may reflect interaction of the two magma systems.

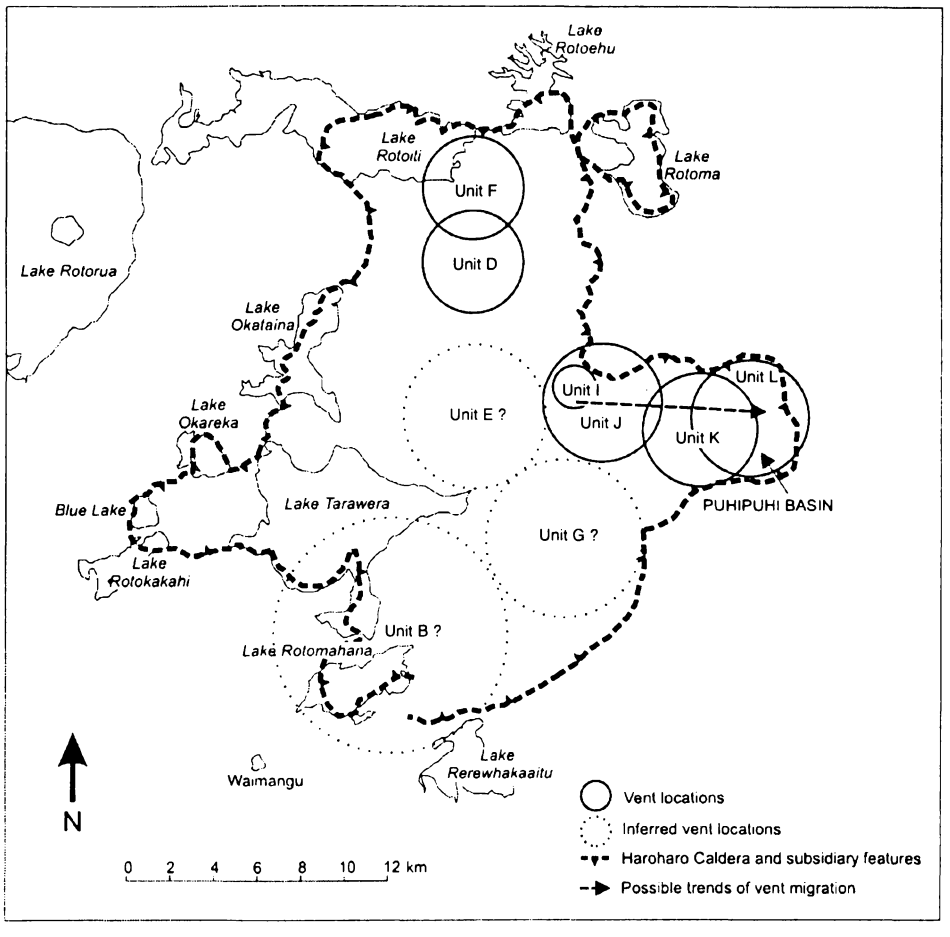

Figure 7.2: Vent locations for the Mangaone Pyroclastics Subgroup tephras, estimated by Jurado-Chichay and Walker (2000). The vents for Units A and C and the Pupuwharau and Pongakawa tephras are not shown, as their locations are unknown (modified from Smith, 2001).

Discrepancies in ages for the Mangaone Subgroup tephras mean that it is difficult to determine the period of time between eruptions of the Old and Young Mangaone Subgroup. Smith (2001) notes that the time interval could be as short as 2 ka, or as long as 9 ka, depending on the age estimates that are used. Support for a long time break between eruption of the Old and Young Mangaone Subgroup comes from pumice clast characteristics. Young Mangaone Subgroup pumice clasts are pale grey-white in colour and tend to be harder than the very weathered yellow-brown pumice from the Old Mangaone Subgroup tephras (Smith, 2001).

Given current age estimates for the oldest of the Mangaone Pyroclastics Subgroup tephras (c. 43 000 years B.P., Jurado-Chichay and Walker (2000)), the time interval between this eruption and the preceding Rotoiti Ignimbrite eruption is c. 20 000 years. This may be a realistic timeframe over which magma could reside in a liquid state in the crust beneath the Okataina Volcanic Centre. However, a comparison of the Rotoiti Ignimbrite with the Old Mangaone Subgroup shows that there are geochemical differences between these eruptives, with the Old Mangaone Subgroup erupting less evolved magma (Figure 4.26). There are also mineralogical and thermal differences, as the Old Mangaone Subgroup represents high temperature clinopyroxene-bearing magma (Smith, 2001), whereas the Rotoiti Ignimbrite contains cummingtonite and biotite, and represents lower temperature magma (Shane, 1998). Hence, it is unlikely that the Old Mangaone Subgroup tapped residual magma from the Rotoiti Ignimbrite eruption.

Geochemical compositions do not preclude a genetic relationship between the Young Mangaone Subgroup and the rhyolite lavas of subsequent eruptions, particularly the Te Rere Eruptive Episode lavas from the Haroharo Volcanic Complex which are more evolved in terms of major and trace element compositions. However, Smith (2001) considered that the spatial separation of vent locations is compelling evidence for lack of a genetic relationship between the Young Mangaone Subgroup and the first eruptions from the Haroharo, Okareka and Tarawera volcanic complexes. All post-Mangaone Subgroup eruptions from the Okataina Volcanic Centre have occurred from the Haroharo or Tarawera linear vent zones (Figure 2.7). The vents for the Young Mangaone Subgroup eruptions are spatially discrete, occurring in an east-west trending zone in the upper Puhipuhi Basin.

In addition, thermal and temporal differences may preclude a genetic relationship. Temperature estimates for the Young Mangaone Subgroup range from 720 - 820°C (Smith,

2001). Fe-Ti oxide temperature estimates determined in this study for Te Rere and Okareka eruptive episode lavas are comparable, ranging from ~ 780 - 830°C. If these latter magmas had evolved from the Young Mangaone Subgroup magma, these temperature estimates allow for little cooling of the magma during the c. 6 000 - 9 000 years between eruptions. Given that the fourteen eruptions currently identified within the Mangaone Pyroclastics Subgroup are considered to have occurred over c. 12 000 years (Jurado-Chichay and Walker, 2000), the existence of sufficient amounts of residual magma from the eruption of Unit L in a liquid state for c. 6 000 - 9 000 years may be unlikely.

No single eruption within the Mangaone Pyroclastics Subgroup exceeds 6 km^3 (dense rock equivalent) in volume (Jurado-Chichay and Walker, 2000). The Old Mangaone Subgroup erupted the equivalent of ~ 8.6 km^3 of magma and the Young Mangaone Subgroup erupted the equivalent of ~ 12.6 km^3 of magma (Jurado-Chichay and Walker, 2000). Hence the magma batches underlying the Okataina Volcanic Centre during this period of time were relatively small.

7.2.3.2 The Haroharo Volcanic Complex (c. 25 000 - 5 550 years B.P.)

The Haroharo Volcanic Complex was built up on the northern and central floor of the Haroharo Caldera, and on the floor of the adjacent Rotoma Caldera, in four rhyolitic eruptive episodes beginning c. 25 000 years B.P. Each of these episodes has involved the eruption of lavas and pyroclastics (Table 2.2). The vents for these eruptions lie within a 4 km wide, 050° trending zone known as the Haroharo Linear Vent Zone (HLVZ) (Figure 2.7). This zone represents a deep-seated basement fracture that has controlled vent locations (Nairn, 1989).

Te Rere Eruptive Episode

The lavas erupted during the Te Rere episode (c. 25 000 years B.P.) have the same ferromagnesian phenocryst assemblage (orthopyroxene + calcic amphibole) and very similar compositions in terms of all major and trace elements, with SiO_2 contents of ~ 76.2 - 76.5 wt. %. These lavas are considered to have been erupted from the same vent or vent area now buried beneath younger pyroclastics, and derived from a single magma, termed the Te Rere A type magma (Table 7.2, Figure 7.3), which lacked any significant compositional gradient. Although the pyroclastics erupted at this time (Te Rere Tephra, Te

Table 7.2: Summary of the petrographic and isotopic characteristics of rhyolite magma types erupted from the Okataina Volcanic Centre in the last c. 25 000 years.

Magma Type	Ferromagnesian Mineral Assemblage	Phen. %	Temperature (°C)	$^{87}Sr/^{86}Sr$	ε_{Nd}	Special Features or Extra Notes	Representative Sample (No.)
Kaharoa type (T)	Bio ± Ca-Amph ± Opx	16-26	652	0.70530	1.70		158
Whakatane type (H)	Cgt + Opx ± Ca-Amph (trace biotite in Makatiti Flows)	11-17	678-718	0.70531 - 0.70533	1.31	May have evolved from residual Mamaku A type.	6, 24, 98
Mamaku A type (H)	Opx + Ca-Amph ± Cgt	8-19	700-727	0.70531 - 0.70533	1.01	May have evolved from residual Rotoma type.	7, 32, 173
Mamaku B type (H)	*Cgt (trace Opx + Ca-Amph)*[x]	*5-20*[x]	*695-775*[x]			*Erupted as the Kaipara Flow. May have evolved from Mamaku A type.*	
Rotoma type (H)	Ca-Amph + Opx + Cgt	10-14	741-742	0.70532 - 0.70537		Erupted as the Rotoma and Te Pohue flows.	105 60
Waiohau type (T)	Opx ± Ca-Amph	7-11	744	0.70534		Contains only trace Ca-Amph.	38
Rotorua type (O)	Bio + Ca-Amph	17-20	658	0.70544		May have evolved from residual Te Rere B type.	176
Rerewhakaaitu A type (T)	Bio + Ca-Amph (trace Opx)	22-29	724	0.70536		Erupted as Rotomahana Dome. Mingled with Rerewhakaaitu C type in the Te Puha Flow.	134
Rerewhakaaitu B type (T)	Opx + Ca-Amph (trace Bio)	22	802	0.70539		Erupted as Western Dome. May have evolved from residual Okareka B type.	44
Rerewhakaaitu C type (T)	Opx + Ca-Amph	7				Mingled with Rerewhakaaitu A type in the Te Puha Flow.	40
Okareka A type (T)	Opx + Ca-Amph (trace Bio)	15	824	0.70538	1.21	Erupted as Ridge Flow.	90
Okareka B type (T)	Ca-Amph + Opx	24		0.70535		Erupted as Patiti Island lava.	130
Te Rere A type (H)	Opx + Ca-Amph	7-12	788	0.70546		Contains only minor amounts of quartz.	92
Te Rere B type (O)	Opx + Ca-Amph (trace Bio)	12-21	832	0.70529			113

Magma type characteristics are based on data obtained in this study for rhyolite lavas and do not specifically include data for associated pyroclastic eruptives from the literature. Magma types are listed in order of increasing eruptive episode age. Eruptive episodes are separated by horizontal lines, and within an episode the magma types are listed in no particular order. Units in italics were not sampled in this study. Temperatures are Fe-Ti oxide estimates. Volcanic complexes where the magmas were erupted are given in brackets: H = Haroharo, O = Okareka, T = Tarawera. [x] Data for the Kaipara Flow from Wright (2000).

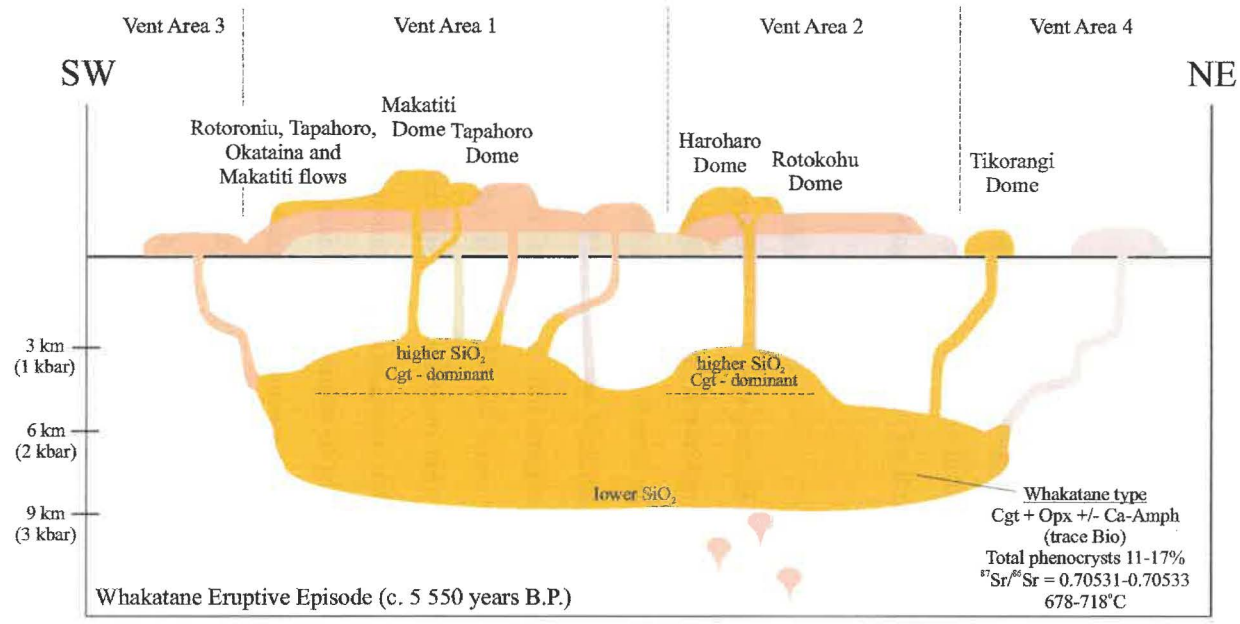

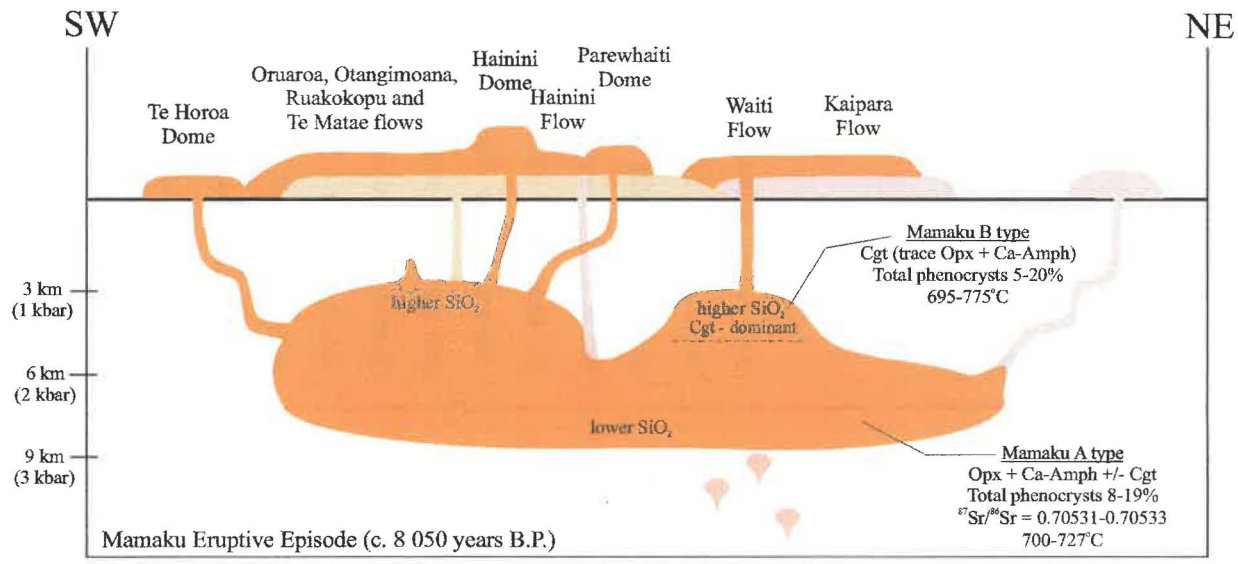

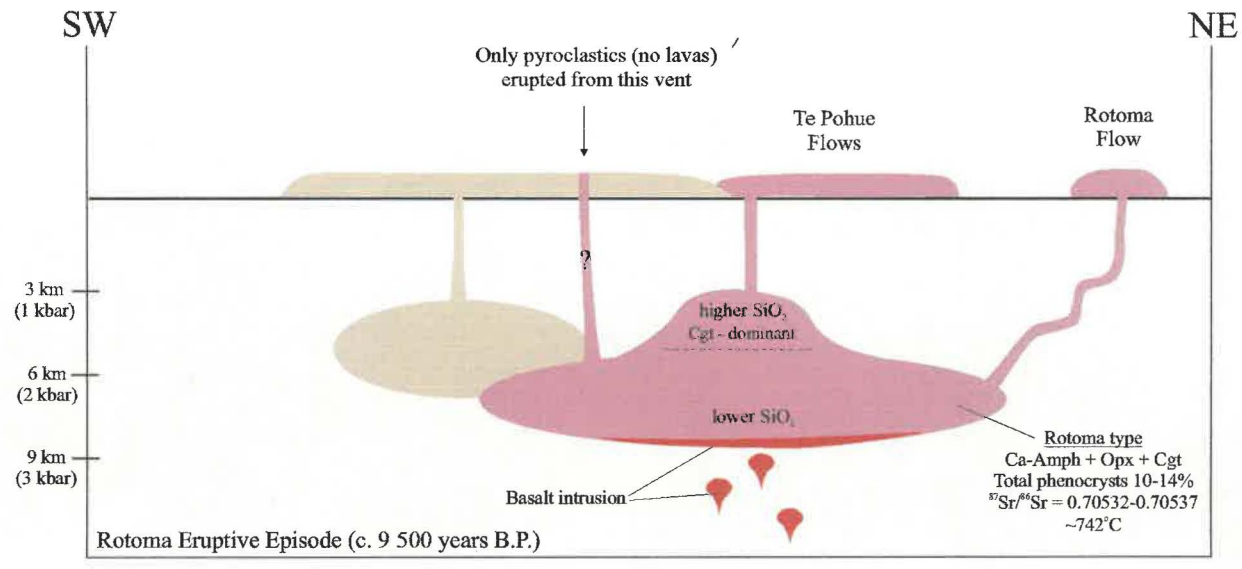

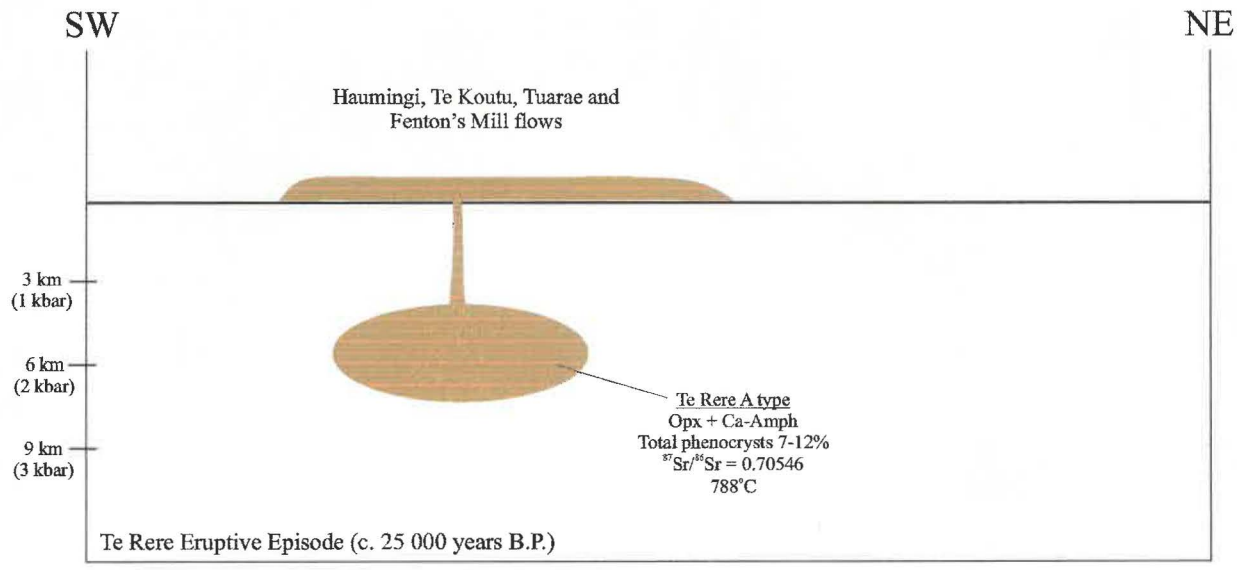

Figure 7.3: Conceptual cartoon of rhyolitic magma types erupted from the Haroharo Volcanic Complex, Okataina Volcanic Centre, in the last c. 25 000 years. Magma type characteristics from Table 7.2. The characteristics and surficial distribution of pyroclastic eruptives are not shown. The depth and pressure of magma batches are estimates only.

Haehaenga Pyroclastics and Tapuaeharuru Pyroclastics) have a similar ferromagnesian phenocryst assemblage to the lavas, geochemical and isotopic data are required to confirm their origin from the Te Rere A type magma.

The Te Rere A type magma is distinct from the Te Rere B type magma, erupted at this time in the Okareka Volcanic Complex (section 7.2.3.3), in terms of mineralogy, geochemistry and isotopic composition. In addition, the distance between vents (~ 14 km) suggests that two discrete and unrelated magmas may have been erupted.

The estimated volume of magma erupted during the Te Rere episode is 11.5 km^3 (Table 2.2), and suggests that the Te Rere A type magma was relatively small in volume. This volume estimate may also include the small volume of rhyolite lavas erupted from the Okareka Volcanic Complex during this episode (Te Rere B type magma).

Rotoma Eruptive Episode

During the Rotoma episode (c. 9 500 years B.P.) rhyolite lavas were erupted from two vent areas. These lavas have different ferromagnesian phenocryst assemblages and major and trace element compositions. The Te Pohue Flows erupted in the northern Haroharo Caldera have higher SiO_2 and Rb/Sr than the Rotoma Flows erupted in the Rotoma Caldera at this time, in addition to having a ferromagnesian phenocryst assemblage dominated by cummingtonite. The Rotoma Flows were found to contain only trace cummingtonite. However, these two rhyolite lavas have very similar $^{87}Sr/^{86}Sr$ compositions, and modelling of these lava compositions is consistent with evolution of the Te Pohue magma through closed-system fractional crystallisation of plagioclase + calcic amphibole + titanomagnetite + ilmenite + orthopyroxene (or cummingtonite) from the Rotoma magma. This is consistent with a previously unpublished data set for Rotoma episode eruptives, discussed in Wright (2000) (see Figure 4.17), that shows an almost continuous range in composition.

Hence, although two vent areas were active during this eruptive episode, it is considered that they both tapped a single compositionally zoned magma, termed the Rotoma type magma (Table 7.2, Figure 7.3). An additional vent was active at this time from which only pyroclastics were erupted (Tuahu Pyroclastics). It is unknown whether the previously unpublished data set shown in Figure 4.17 includes samples of these pyroclastics. However, further geochemical and isotopic data for the Tuahu pyroclastics, as well as the Rotoma Tephra and Otamuri Pyroclastics, are required to substantiate their eruption from the

Rotoma type magma. The estimated volume of Rotoma type magma erupted is 7 km^3 (Table 2.2).

A basaltic component has been identified in the Tuahu Pyroclastics and Houghton et al. (1987) suggested the eruptives show evidence for liquid-liquid mixing of basalt and rhyolite immediately prior to eruption. Hence it is likely that the eruption of the rhyolitic Rotoma type magma may have been triggered by the intrusion of more mafic magma.

Geochemical and isotopic inconsistencies may preclude the evolution of Rotoma type magma from the older Te Rere A type magma. In addition, temporal constraints on the longevity of small magma batches beneath the Okataina Volcanic Centre may also preclude a genetic relationship.

Mamaku Eruptive Episode

During the Mamaku episode (c. 8 050 years B.P.) rhyolite lavas were erupted from three vent areas (Figures 2.8 and 7.3) spread over ~ 14 km of the Haroharo Linear Vent Zone. Geochemically the lavas fall into two groups, which correspond to the vent areas. Lavas erupted from vent areas 1 and 3 have compositions that overlap. The Waiti Flow, which was erupted from vent area 2, has lower SiO_2 and Rb/Sr than the group of lavas erupted from vent areas 1 and 3. Within the lavas erupted from vent areas 1 and 3 there is no systematic change in composition from oldest to youngest. Rhyolite lavas erupted in this episode have the same ferromagnesian phenocryst assemblage of orthopyroxene + calcic amphibole ± cummingtonite. The Kaipara Flow was also erupted from vent area 2 during this eruptive episode. Data for this rhyolite from Wright (2000) (the sample obtained in this study was hydrothermally altered) showed that it is mineralogically different, with a ferromagnesian phenocryst assemblage dominated by cummingtonite.

Mamaku episode rhyolite lavas sampled in this study show little variation in $^{87}Sr/^{86}Sr$ compositions (0.705314 - 0.705328). Modelling of these lava compositions is consistent with evolution of the vent area 1 and 3 magmas from the vent area 2 magma (Waiti Flow) by closed-system fractional crystallisation of plagioclase + orthopyroxene + calcic amphibole + titanomagnetite + ilmenite. Hence, although three vent areas were active during this eruptive episode, it is considered that they tapped a single compositionally zoned magma, termed the Mamaku A type magma (Table 7.2, Figure 7.3). No isotopic data are available for the Kaipara Flow. However, modelling using an average major and trace element

analysis for the Kaipara Flow from Wright (2000) is consistent with evolution of the Kaipara magma from the Waiti magma by closed-system fractional crystallisation of plagioclase + calcic amphibole + titanomagnetite + ilmenite + orthopyroxene (or cummingtonite). Hence, as suggested by Wright (2000), the Kaipara magma may represent an isolated system at one end of the Waiti magma chamber, or alternatively may overlie the Waiti magma in a vertically stratified magma chamber. However, until more data becomes available to substantiate a relationship between the Mamaku A type magma and the magma erupted as the Kaipara Flow, this latter magma will be termed Mamaku B type.

Wright (2000) presented a data set for pyroclastics erupted during the Mamaku episode, which are geochemically comparable to vent area 1 and 3 lavas. This is consistent with observations made by Nairn and Wood (1987) that the main pyroclastic vent was probably in the vicinity of Hainini Dome or the younger Makatiti Dome (vent area 1). Wright (2000) also sampled Parewhaiti Dome and the Te Matae Flow, which were not sampled in this study. These lavas are geochemically comparable to vent area 1 lavas, which is consistent with their spatial position.

The estimated volume of magma erupted during the Mamaku episode is 17.5 km^3 (Table 2.2). It is evident that the majority of the magma erupted at this time was of Mamaku A type. In the absence of a volume estimate for the Kaipara Flow, the volume of the Mamaku B type magma cannot be estimated.

Fractional crystallisation modelling of the Waiti lava composition (Mamaku A type magma) from the older Rotoma lava composition (Rotoma type magma) did not yield acceptable results. However there are several factors that support a possible genetic relationship between magma erupted in the Rotoma and Mamaku episodes. The Rotoma and Waiti lavas have similar major and trace element compositions, which may account for the failure of fractional crystallisation modelling. In addition, they have the same ferromagnesian phenocryst assemblage, similar $^{87}Sr/^{86}Sr$ compositions, and similar Fe-Ti oxide geothermometry temperature estimates. The Te Pohue (Rotoma type magma) and Kaipara (Mamaku B type magma) lavas have similar major and trace element compositions, and the same ferromagnesian phenocryst assemblage. The short period of time between the Rotoma and Mamaku eruptive episodes (c. 1 450 years) is consistent with a genetic relationship, and may account for the similar major and trace element compositions, phenocryst assemblages, isotopic compositions, and temperatures of the magmas erupted.

Whakatane Eruptive Episode

During the Whakatane episode (c. 5 550 years B.P.) rhyolite lavas were erupted from three vent areas (Figures 2.8 and 7.3) spread over ~ 11 km of the Haroharo Linear Vent Zone. Geochemically the lavas fall into three groups, which correspond to the vent areas. The two lavas erupted from vent area 2 have lower SiO_2 and Rb/Sr than the group of lavas erupted from vent area 1. Tikorangi Dome, erupted in vent area 4, has lower SiO_2 and Rb/Sr than all other lavas erupted during this episode. Within the lavas erupted from vent area 1 there is no systematic or significant change in composition from oldest to youngest. Most of the lavas erupted in this episode have ferromagnesian phenocryst assemblages dominated by cummingtonite. The exceptions are Tikorangi Dome and the Tapahoro Flows, which contain more calcic amphibole than cummingtonite. Rhyolite lavas erupted in the Whakatane episode show little variation in $^{87}Sr/^{86}Sr$ (0.705305 - 0.705334). Modelling of these lava compositions is consistent with evolution of the Whakatane episode lavas erupted in vent areas 1, 2 and 4 by closed-system fractional crystallisation of plagioclase + calcic amphibole + titanomagnetite + ilmenite + orthopyroxene (or cummingtonite) from the older Waiti and/or Hainini lavas (Mamaku A type magma).

Hence, although three vent areas were active during this eruptive episode, it is considered that they tapped a single compositionally zoned magma, termed the Whakatane type magma (Table 7.2, Figure 7.3), that is considered to have evolved from the older Mamaku A type magma. Further geochemical and isotopic data for the pyroclastics erupted at this time (Whakatane Tephra, Whakatane Pyroclastics, Rotokohu Tuff Cone) are required to determine their relationship to the Whakatane type magma.

Several factors are consistent with evolution of the Whakatane type magma from the Mamaku A type magma. In the c. 2 500 years between eruptions the magma has become richer in cummingtonite, and estimated Fe-Ti oxide geothermometry temperatures show a slight decrease. The magma erupted at vent areas 1 and 2 shows increased SiO_2 and Rb/Sr with time. Similar $^{87}Sr/^{86}Sr$ compositions for eruptives of these two episodes are consistent with magmatic evolution by closed-system fractional crystallisation processes.

The estimated volume of Whakatane type magma erupted is 13.5 km^3 (Table 2.2). However, the Whakatane type magma is considered to represent the third eruption from a magma body that also incorporates the Rotoma, Mamaku A and Mamaku B type magmas. The estimated volume of magma erupted from this combined magma body (~ 38km^3) is still relatively

small in terms of silicic magmatic systems, but it is the largest volume of genetically related magma to be erupted from the Okataina Volcanic Centre during the post-caldera activity.

In summary, the Haroharo Volcanic Complex was built up in four rhyolitic eruptive episodes beginning c. 25 000 years B.P. The lavas and pyroclastics erupted in the Te Rere episode were derived from a single, relatively volumetrically small magma batch. The lavas and pyroclastics erupted in the Rotoma, Mamaku and Whakatane episodes record the evolution of a relatively larger single magma batch over c. 4 000 years by closed-system fractional crystallisation processes (Figure 7.3). Such a magma batch could theoretically still remain at depth in the crust beneath the Haroharo Volcanic Complex (see section 7.2.5.1).

The most recent eruption from the Haroharo area occurred strictly outside the northwestern margin of the Okataina Volcanic Centre, northwest of the Haroharo Linear Vent Zone. This eruption at c. 3 700 years B.P. involved maar-forming basaltic phreatomagmatic eruptions (Beanland, 1981; Froggatt and Lowe, 1990; Beanland and Houghton, 1991).

7.2.3.3 The Okareka Volcanic Complex (c. 25 000 - 15 800 years B.P.)

The Okareka Volcanic Complex was built up in two rhyolitic eruptive episodes at c. 25 000 years B.P. and c. 15 800 years B.P., and has infilled the Okareka Embayment. The vents for the eruptions are relatively closely spaced and lie at the southwestern end of the Haroharo Linear Vent Zone (Figure 2.7), but are located along a NW-SE trend perpendicular to the vent zone. Nairn (1981a) and Nairn and Wood (1987) note that this vent alignment parallels a northwest trending cross fault that forms the northeastern shore of Lake Okareka, and may indicate the location of a buried feeder dike.

Te Rere Eruptive Episode

The lavas erupted during the Te Rere episode (c. 25 000 years B.P.) have ferromagnesian phenocryst assemblages dominated by orthopyroxene and calcic amphibole, and the Eastern Rhyolite contains trace biotite. Geochemically, the Te Rere Dome differs in composition from the Eastern Rhyolite with increased SiO_2 content and Rb/Sr. These compositional differences may reflect post-depositional alteration, although the possibility that the Te Rere

Dome lava is a more evolved equivalent of the Eastern Rhyolite lava cannot be ruled out. These lavas are considered to have been erupted from a single magma, termed the Te Rere B type magma (Table 7.2). As previously noted, the Te Rere B type magma is distinct from the magma erupted at this time in the Haroharo Volcanic Complex (section 7.2.3.2). No volume estimates are available for the Te Rere episode lavas erupted in the Okareka Embayment and hence the volume of the Te Rere B type magma batch cannot be assessed. Nairn (1992) considers that only accessory lithics were ejected during pyroclastic eruptions in the Okareka Embayment during the Te Rere episode.

Rotorua Eruptive Episode

The lavas erupted during the Rotorua episode (c. 15 800 years B.P.) have ferromagnesian phenocryst assemblages dominated by biotite with small amounts of calcic amphibole also present. These lavas have very similar major and trace element compositions, with SiO_2 contents of ~ 74.8 - 75.6 wt. %, and are considered to have been erupted from a single magma, termed the Rotorua type magma (Table 7.2). The Rotorua Tephra erupted at this time has a similar ferromagnesian assemblage to the rhyolite lavas and is considered to have also been erupted from this magma batch, although no geochemical or isotopic data are available to support this. The estimated volume of Rotorua type magma erupted is 4 km^3 (Table 2.2).

Several factors support evolution of the Rotorua magma from the older Te Rere B magma during the c. 9 200 years between eruptions. The magma erupted in the Rotorua episode was mineralogically and geochemically more evolved than the magma erupted in the Te Rere episode. Fe-Ti oxide geothermometry temperatures show a reduction of ~ 200°C over this period of time. Plagioclase phenocrysts in the younger Trig 7693 Dome are An-poor relative to those in the Eastern Rhyolite (Figure 5.1). $^{87}Sr/^{86}Sr$ compositions are increased in the younger lava (0.705435) relative to the older lava (0.705294). The difference in composition between Te Rere and Rotorua episode lavas erupted at the Okareka Volcanic Complex can be modelled by AFC processes. For D_{Sr} = 3.0 - 4.0, an assimilation rate of r = 0.05 - 0.06, accompanied by ~ 12 - 17% crystallisation (Figure 6.11), is required to produce the Trig 7693 Dome composition from the Eastern Rhyolite composition.

Hence, mineralogical, geochemical, thermal and isotopic factors support evolution of the younger Rotorua magma from the older Te Rere B magma during the c. 9 200 years between eruptions at the Okareka Volcanic Complex. Because volume estimates are not available for

the Te Rere B type magma, the volume of this combined magma can only be estimated as > 4 km^3.

7.2.3.4 The Tarawera Volcanic Complex (c. 22 500 years B.P. - 1314 ± 11 A.D.)

The Tarawera Volcanic Complex was built up on the southeastern floor of the Haroharo Caldera in four rhyolitic eruptive episodes beginning c. 22 500 years B.P. Each of these episodes has involved the eruption of lavas and pyroclastics (Table 2.2). The vents for these eruptions lie within a 5 km wide, 057° trending zone known as the Tarawera Linear Vent Zone (TLVZ) (Figure 2.7). This zone represents a deep-seated basement fracture that has controlled vent locations (Nairn, 1989).

Okareka Eruptive Episode

The lavas erupted during the Okareka episode (c. 22 500 years B.P.) are mineralogically similar, but differ in terms of their major and trace element compositions. The Ridge Flow has higher SiO_2 and Rb/Sr compositions than the Patiti Island lava. It is possible that the elevated Al_2O_3 content in this latter lava indicates the effect of weathering. Even though these two lavas were erupted in the same episode and have similar ferromagnesian phenocryst assemblages and $^{87}Sr/^{86}Sr$ compositions, the distance between their vents (~ 10 km) means that the existence of discrete magma batches cannot be ruled out. The latter is suggested by the geochemical differences and unacceptable results for fractional crystallisation modelling (see section 6.5).

Hence, the magma that erupted as the Ridge Flow has been termed Okareka A type and the magma that erupted as the Patiti Island lava has been termed Okareka B type (Table 7.2, Figure 7.4). Two lavas erupted at this time that were not sampled in this study (Hawea Flow and Ridge Dome) are considered to have been erupted from the same vent as Ridge Flow, as is the Okareka Tephra (Nairn, 1992). A significant change in ferromagnesian mineralogy occurred during the Okareka Eruptive Episode, as the Okareka Tephra is characterised by the presence of biotite, yet the lavas are biotite-free/poor (Nairn, 1992). Geochemical and isotopic data are required for the two unsampled lavas and the Okareka Tephra to confirm their origin from the Okareka A magma type, and to characterise geochemical zoning that may have accompanied the variable ferromagnesian phenocryst assemblage. The estimated volume of rhyolitic magma erupted during the Okareka episode is 8.5 km^3 (Table 2.2),

and suggests that the Okareka A magma type was relatively small in volume. This volume estimate probably also includes the small volume of magma erupted as Patiti Island (Okareka B type magma).

The eruption of the Okareka Tephra was immediately preceded by a small basaltic scoria eruption, apparently from vents close to those for the rhyolite eruptions (Nairn, 1992). Dacitic pumice clasts and banded clasts occur within the rhyolitic unit and represent basalt and rhyolite magma mixing and mingling respectively (Nairn, 1992). Hence the eruption of the rhyolitic Okareka A type magma may have been triggered by the intrusion of more mafic magma.

Rerewhakaaitu Eruptive Episode

During the Rerewhakaaitu episode (c. 17 600 years B.P.) rhyolite lavas were erupted from vents at the southwestern end of the Tarawera Linear Vent Zone. These lavas show differences in total phenocryst content, ferromagnesian phenocryst assemblage and geochemistry, and three distinct magma types have been identified. The characteristics of these magma types are presented in Table 7.2 and Figure 7.4. Southern Dome was erupted during this episode of activity but was not sampled in this study. Cole (1966) noted a mingling between two lava types in this dome (similar to that noted for the Te Puha Flow in this study). Cole (1966) also noted a bimodal pumice population in the Rerewhakaaitu Tephra, with the two pumice types being mineralogically similar to the Rerewhakaaitu A and Rerewhakaaitu C type magmas identified in this study. Geochemical and isotopic data are required for the Rerewhakaaitu Tephra and Rerewhakaaitu Pyroclastics to confirm their origin from one or more of the three magma batches identified from lava compositions. It is not possible to divide the estimated total volume of magma erupted during the Rerewhakaaitu episode (5 km^3) between the three magma types identified as being erupted at this time.

$^{87}Sr/^{86}Sr$ compositions for the Rerewhakaaitu A and Rerewhakaaitu B type magmas are similar, although fractional crystallisation modelling does not support evolution of the biotite-bearing Rerewhakaaitu A type magma by closed-system fractional crystallisation from the biotite-poor Rerewhakaaitu B type magma. In addition, modelling does not support evolution of the biotite-free Rerewhakaaitu C type magma from either the Rerewhakaaitu A or Rerewhakaaitu B type magmas by closed-system fractional crystallisation. However, modelling is consistent with evolution of the Rerewhakaaitu B type magma from the older

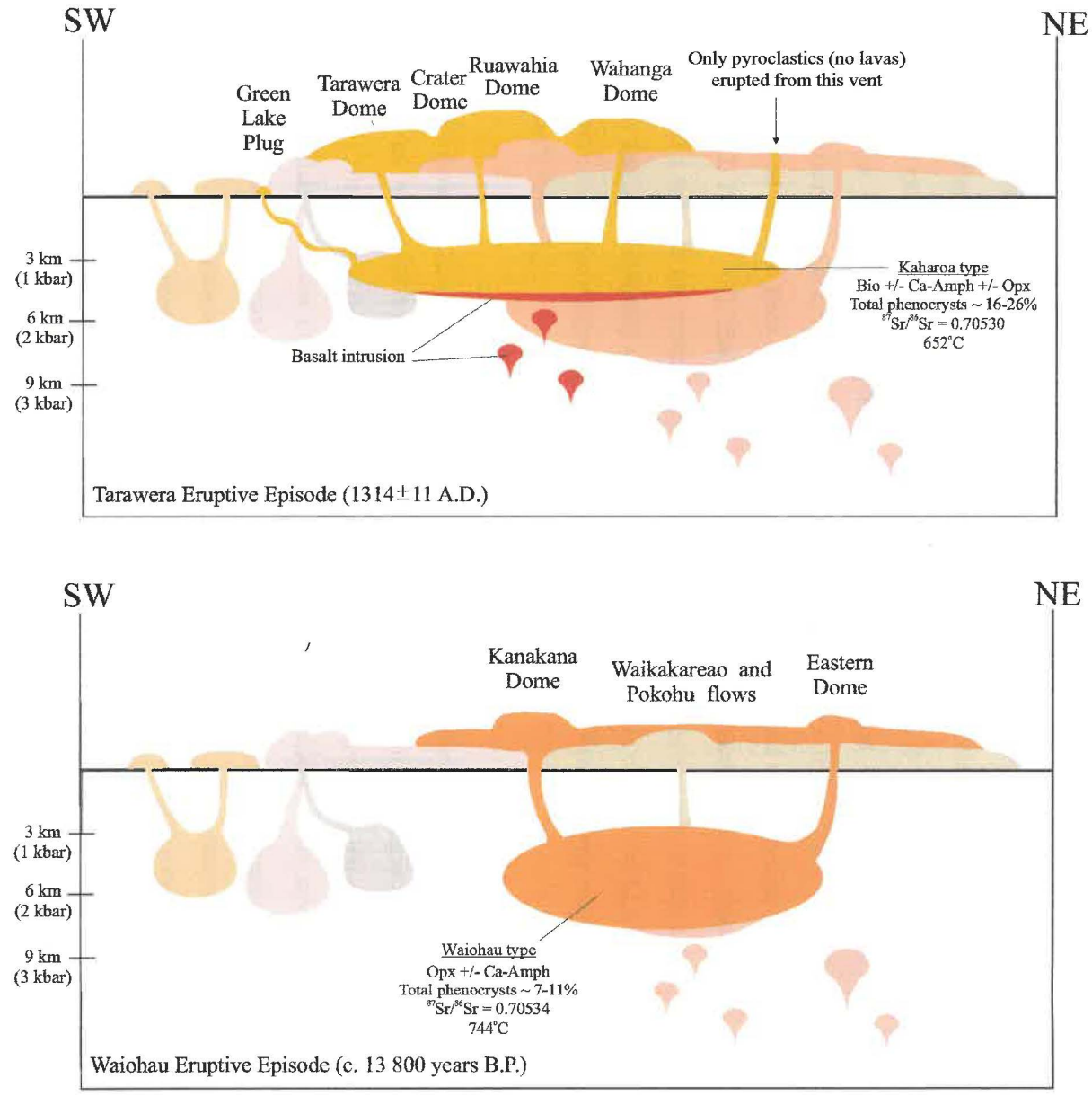

Figure 7.4: Conceptual cartoon of rhyolitic magma types erupted from the Tarawera Volcanic Complex, Okataina Volcanic Centre, in the last c. 22 500 years. Magma type characteristics from Table 7.2. The characteristics and surficial distribution of pyroclastic eruptives are not shown. The depth and pressure of magma batches are estimates only.

Okareka B type magma by closed-system fractional crystallisation of plagioclase + orthopyroxene + calcic amphibole + titanomagnetite + ilmenite (although Σr^2 is only marginally acceptable, see section 6.5).

Waiohau Eruptive Episode

During the Waiohau episode (c. 13 800 years B.P.) rhyolite lavas were erupted from vents at the northeastern end of the Tarawera Linear Vent Zone. The lava flows erupted from the Kanakana Dome vent (Waikakareao and Pokohu flows) have the same ferromagnesian phenocryst assemblage (orthopyroxene ± calcic amphibole) and very similar compositions in terms of all major and trace elements, with SiO_2 contents of ~ 76.8 - 77.0 wt. %. Kanakana Dome and Eastern Dome were sampled by Speed (2001) and found to also have this ferromagnesian assemblage and near identical major and trace element compositions. These lavas are considered to have been erupted from a single magma, termed the Waiohau type magma (Table 7.2, Figure 7.4), that lacked any significant compositional gradient. Speed (2001) presented a data set for pyroclastics erupted during the Waiohau episode, which are mineralogically and geochemically comparable to the lavas, and they are considered to have been erupted from this same magma type. The estimated volume of Waiohau type magma erupted is 12 km^3 (Table 2.2).

Fractional crystallisation modelling does not preclude evolution of the Waiohau magma from the Okareka A magma by closed-system fractional crystallisation of plagioclase + titanomagnetite + ilmenite + orthopyroxene (or calcic amphibole). However, phenocryst contents suggest that evolution of the Waiohau magma by such processes would involve fractionation of both orthopyroxene and calcic amphibole. In addition, the eruption of spatially adjacent but geochemically unrelated magmas during the intervening Rerewhakaaitu episode may preclude a common magma source for eruptives of the Okareka and Waiohau episodes.

Kaharoa Eruptive Episode

The Kaharoa episode (1314 ± 11 A.D.) is the most recent rhyolitic eruption to have occurred from the Taupo Volcanic Zone. Four rhyolite lava domes were erupted that cap the Tarawera massif, as well as the Green Lake Plug on the eastern shore of Lake Rotomahana. All of the lavas erupted at this time have ferromagnesian phenocryst assemblages dominated by biotite. The four domes capping the massif have very similar compositions in terms of

all major and trace elements, with SiO_2 contents of ~ 76.2 - 76.4 wt. %. Green Lake Plug has a higher SiO_2 content of ~ 77.3 wt. %. and differs in its major and trace element composition from the other Kaharoa lavas. All of these lavas are considered to have been erupted from a single magma, termed the Kaharoa type magma (Table 7.2, Figure 7.4), that Leonard (1999) considered to be stratified to account for the compositional differences seen in the Green Lake Plug lava. Leonard (1999) showed the pyroclastics erupted during this episode to be geochemically comparable to the rhyolite lavas, and they are considered to have been erupted from this same magma type. The estimated volume of Kaharoa type magma erupted is 4 km^3 (Table 2.2).

Fractional crystallisation modelling does not preclude evolution of the Kaharoa magma from the Rerewhakaaitu A magma by closed-system fractional crystallisation of plagioclase + calcic amphibole + biotite (see section 6.5). However, eruption of the temporally intervening biotite-free Waiohau magma from vents in the same area, suggests that biotite-bearing Rerewhakaaitu A magma may not have existed in a liquid state beneath the Tarawera Volcanic Complex over this period of time. A genetic relationship between the Kaharoa type magma and the Waiohau type magma is unlikely given the ferromagnesian phenocryst and major and trace element compositions of these magma types.

A basaltic component has been identified in pyroclastics erupted during the Kaharoa episode. Leonard (1999) provided evidence for both mixing and mingling between basaltic and rhyolitic magmas. Hence eruption of the Kaharoa type magma may have been triggered by intrusion of more mafic magma.

In summary, the Tarawera Volcanic Complex was built up in four rhyolitic eruptive episodes beginning c. 22 500 years B.P. During the two earlier episodes (Okareka and Rerewhakaaitu), multiple, relatively volumetrically small magma batches were erupted (Figure 7.4). The Rerewhakaaitu B type magma may be genetically related to the Okareka B type magma. The lavas and pyroclastics erupted in each of the two youngest episodes (Waiohau and Kaharoa) were derived from single, relatively volumetrically small, genetically discrete magma batches.

The most recent eruption from the Tarawera Volcanic Complex (and the Okataina Volcanic Centre) was the fissure-forming June 10 1886 basaltic plinian eruption. Basaltic dikes can

be seen exposed in the Tarawera fissure, representing feeders for the pyroclastic eruptions, although no basaltic lavas were erupted (Cole, 1970a; Nairn and Cole, 1981; Walker et al., 1984). The Kaharoa type magma could theoretically still remain at depth in the crust beneath the Tarawera Volcanic Complex. However, the 1886 A.D. eruption of basalt from the Tarawera Linear Vent Zone, with no juvenile rhyolitic component involved, suggests that this is unlikely. Nairn (1981b) considered that continuing solidification of rhyolitic magmas beneath the Tarawera Volcanic Complex may have allowed the upward passage of basaltic dikes.

7.2.3.5 Timescales of Magma Generation and Residence

The history of the Okataina Volcanic Centre in the last c. 25 000 years is well constrained by age data. These data, in combination with available estimates of eruptive volumes (Table 2.2), can be used to estimate generation and residence times, and generation rates, for magma batches erupted from the Okataina Volcanic Centre during this most recent period of its history.

The maximum time available to generate a magma batch can be estimated as the time between the first eruption of the magma (in most cases at Okataina this is the only eruption) and the preceding eruption involving genetically unrelated magma (Table 7.3). Along with an estimate of magma volume, this can be used to estimate the minimum magma generation rate (Table 7.3). Minimum generation times for the magma batches are unconstrained by the data. The minimum residence time in the crust of a particular magma batch is the time between the first and last eruptions of the magma. Such minimum residence times can only be estimated for magmas that have erupted more than once (Table 7.3). The maximum residence time in the crust of a particular magma batch is the time between preceding and following eruptions involving genetically unrelated magma (Table 7.3). For the purposes of estimating magma generation and residence times, the Haroharo, Okareka and Tarawera volcanic complexes are considered separate, and it is assumed that the generation and residence of magma at one centre does not place constraints on the generation and residence of magma at another.

Table 7.3: Summary of estimated generation and residence times, and generation rates, for magma batches erupted during the post-caldera sequence at the Okataina Volcanic Centre.

Magma Batch	Estimated Maximum Generation Time (years)	Estimated Magma Volume Erupted (km^3)	Estimated Minimum Generation Rate (km^3/year)	Estimated Minimum Residence Time (years)	Estimated Maximum Residence Time (years)
Kaharoa	13 100	4	3.1×10^{-4}	?	13 800* (13 100)
Whakatane + Mamaku A + Mamaku B + Rotoma	15 500	38	2.5×10^{-3}	3 950	25 000* (19 450)
Waiohau	3 800	12	3.2×10^{-3}	?	16 900
Rotorua + Te Rere B	6 400	> 4	$> 6.3 \times 10^{-4}$	9 200	31 400* (15 600)
Rerewhakaaitu A	4 900	?	?	?	8 700
Rerewhakaaitu C	4 900	?	?	?	8 700
Okareka B + Rerewhakaaitu B	8 900	?	?	4 900	17 600
Okareka A	8 900	8.5	9.6×10^{-4}	?	13 800
Te Rere A	6 400	11.5	1.8×10^{-3}	?	21 900

Magma volume estimates from Froggatt and Lowe (1990) (Table 2.2).
* Assumes the possibility that the magma still occurs at depth. Maximum residence times given in brackets assume the last/only eruption exhausted the magma supply.

No dating of the times of magma crystallisation/residence have been carried out in this study (eg. dating of phenocryst or accessory phases). All generation and residence times and generation rates in Table 7.3 are estimates based on available eruption ages and should be considered as a general guide only. Estimated generation rates utilise available estimates of erupted volumes, and cannot include the volume of unerupted magma remaining in the crust.

Estimated maximum generation times for the post-caldera magma batches erupted from the Okataina Volcanic Centre in the last c. 25 000 years range from c. 3 800 - 15 500 years, with estimated minimum magma generation rates from 3.1×10^{-4} - 3.2×10^{-3} km^3/year. Residence times are of the order of c. 4 000 - 31 000 years. However, if the Rotorua, Whakatane and Kaharoa eruptions are considered to have exhausted the available magma

supply beneath the Okareka, Haroharo and Tarawera volcanic complexes respectively (see section 7.2.5), estimated residence times range from c. 4 000 - 22 000 years. There are no clear differences between estimated magma generation times, generation rates and residence times at the Haroharo, Okareka and Tarawera volcanic complexes.

A comparison of these estimates with those made by Sutton et al. (2000) for the rhyolitic post-Oruanui magma batches erupted from the Taupo Volcanic Centre (see section 7.2.4.1), indicates that many magma batches at Okataina may have had longer generation and residence times, although magma generation rates are comparable.

Although these relatively small batches of magma erupted from the Okataina Volcanic Centre in the last c. 25 000 years have relatively short magma generation and residence times, it is likely that larger magma batches involved in earlier caldera-forming eruptions had a relatively longer time to generate. Assuming that estimated minimum magma generation rates for the last c. 25 000 years are comparable to those during the early history of the Okataina Volcanic Centre, on average ~ 2×10^{-3} km^3/year, then the Matahina and Rotoiti ignimbrites could have had maximum generation times on the order of c. 75 000 and c. 60 000 years, respectively. These estimated residence times for the Matahina and Rotoiti ignimbrites also assume that the accumulation of large magma bodies is not due to increased generation rates (see section 7.2.4.2).

7.2.3.6 The Relative Importance of Lava and Pyroclastic Eruptions

In many large silicic magmatic systems, the volume of extruded lava is subordinate to the volume of the pyroclastics. Hence the composition of the lavas may only represent a small proportion of the magma from which they were erupted. This is the case during the early caldera-forming activity at the Okataina Volcanic Centre, where the volume of pyroclastics (Table 2.1) is in excess of lava volume. This is also the case for the post-Oruanui eruptions from the Taupo Volcanic Centre (20.5 ka - 1740 years B.P.; Sutton et al., 1995), where only 4 out of 28 eruptions have involved lava extrusion. However, in this respect, post-caldera activity at Okataina differs from that at Taupo. Volume estimates from Froggatt and Lowe (1990; Table 2.2) for the nine post-caldera eruptive episodes that have built up the Haroharo, Tarawera and Okareka volcanic complexes, indicate that during many of these episodes, lavas comprised >60% of the magma erupted (Table 7.4). Hence, the rhyolite

lavas have been the dominant component, and the composition of lavas therefore represent a significant proportion of the magma from which they were erupted.

Nevertheless, it is recognised that sampling the lavas may not necessarily represent the full range of compositions from the OVC, and data for the pyroclastics have been used where presently available. Many more individual studies of the pyroclastics are required, but are beyond the scope of this study.

Table 7.4: Volume estimates for lavas and pyroclastics erupted during the post-caldera activity at the Okataina Volcanic Centre.

Eruptive Episode	Lava Volume (km^3)	Total EMV Erupted (km^3)	Lava %
Kaharoa	2.5	4	63
Whakatane	9	13.5	67
Mamaku	15	17.5	86
Rotoma	2	7	29
Waiohau	4	12	33
Rotorua	1	4	25
Rerewhakaaitu	2	5	40
Okareka	5	8.5	59
Te Rere	8	11.5	70

Volume estimates from Froggatt and Lowe (1990). EMV = equivalent magma volume.

7.2.3.7 The Effect of Post-depositional Alteration Processes on Rhyolite Lava Compositions

It may be claimed that pyroclastic materials are commonly quenched on eruption but lava bodies remain hot and vulnerable to post-depositional alteration for some time. This argument has been used to support sampling of pyroclastic rather than effusive phases of eruptions. However, a large portion of the samples of the younger lavas obtained in this study are of glassy pumiceous and obsidian textures, which suggest quenching soon after eruption. Some of the samples obtained of the devitrified interiors of lava domes/flows show small compositional variations relative to non-devitrified samples (Table V.3). However, these variations are not consistent and are generally insignificant when considering the range in compositions for a particular magma type. That is, post-depositional devitrification does not make a sample geochemically distinct from other samples obtained from the same magma type. For example, compositional variations

between all six samples obtained from the Waiti Flow (Figures 4.8 and 4.9) are greater than between non-devitrified and spherulitic samples of this lava. Differences in composition between non-spherulitic pumiceous samples and crystallised spherulitic samples of the Pokohu Flows are negligible given analytical precision. Given the lack of significant compositional variation between devitrified and non-devitrified portions of the younger lavas, it is a reasonable assumption that the devitrified portions of the older lavas (for which there are no non-devitrified samples) are representative of the magma from which they were erupted.

Pyroclastic material is just as likely to suffer the effects of weathering as coherent lava, perhaps even more so given its unconsolidated, vesicular and porous nature. Every effort was made during sample selection to avoid weathered material, and to remove weathered rinds from any samples obtained. Rare samples had anomalously high Al_2O_3 and Ba compositions, which may be considered indicative of weathering, and this has been noted in discussions of the geochemistry of these lavas (Chapter Four).

Hence, the geochemical record obtained in this study is not considered to have been biased by any post-depositional alteration of the lavas. This is supported by the comparable compositions of rhyolite lava data with that in the literature for the associated pyroclastics (Figures 4.12, 4.13, 4.20 and 4.21).

7.2.3.8 Validity of Temperature Calculations

Some of the lavas have very low calculated temperatures of less than 700°C (section 5.10.1), which lie below the probable solidus (eg. Best and Christiansen, 2001). These low temperatures may be partially attributed to the calculation procedure of Ghiorso and Sack (1991), whose method consistently calculates temperatures up to 50°C lower than others (eg. Spencer and Lindsley, 1981) for temperature calculations <800°C.

A comparison of lava temperatures with those obtained by Shane (1998) for the pyroclastics (also using Ghiorso and Sack (1991), Table 5.2) shows that the pyroclastics have calculated temperatures slightly higher than the lavas, but are still low.

All oxide pairs used in lava temperature calculations passed the Mg-Mn equilibrium criteria of Bacon and Hirschmann (1988), and were visually checked for exsolution under reflected light microscopy and backscattered images on the microprobe. However, they may represent titanomagnetite grains that are incipiently altered, but which is not observable petrographically or from backscattered images.

7.2.3.9 Evidence to Suggest that the Rotoma, Mamaku and Whakatane Eruptions Tapped a Single Magma Batch

Based on mineralogical and geochemical data presently available, the Rotoma, Mamaku and Whakatane eruptive episodes are considered to have tapped a single magma batch because of the following reasons:

- Their similarity of ferromagnesian phenocryst assemblages and total phenocryst contents, and an increase in the abundance of cummingtonite in younger eruptives. In contrast, Tarawera eruptives show variable phenocryst contents and ferromagnesian assemblages between eruptive episodes, suggesting a number of discrete magma types.

- A comparison of the geochemical data for the Mamaku and Whakatane eruptive episodes (including pyroclastic data from Wright (2000) for the Mamaku episode) show that at vent areas 1+3 and 2, the magma erupted becomes more evolved over time (increased SiO_2, Rb and decreased Sr, Zr). Rotoma lavas have very similar major and trace element compositions to Mamaku episode lavas.

- Rotoma, Mamaku and Whakatane lavas have similar phenocryst compositions (plagioclase, orthopyroxene, calcic amphibole, Fe-Ti oxides) compared to Tarawera lavas, where phenocryst compositions differ between adjacent eruptive episodes.

- Temperature data for Rotoma, Mamaku and Whakatane lavas suggest a tendency toward cooler temperatures over time. However, temperature data for the Mamaku pyroclastics from Wright (2000) indicate a slightly wider range in temperatures for the Mamaku eruptive episode than that suggested by the lavas, spanning the range for all Haroharo lavas. The addition of this pyroclastic data suggests that the magma body may have been more thermally zoned than originally thought, and that the apparent cooling over time as suggested by the lavas may not be so significant. However, it does not preclude

derivation of these eruptives from the same magma body, which is supported by the data for lavas and pyroclastics erupted in the three episodes falling on the same T-fo_2 trend.

- Very similar Sr isotopic compositions (within 2σ error) for lavas from the Rotoma, Mamaku and Whakatane episodes.

- Fractional crystallisation modelling indicates that Whakatane lava compositions can theoretically be derived by closed-system fractional crystallisation of phenocryst phases from Mamaku lava compositions, although modelling from Mamaku lavas to derive Rotoma lavas gave larger Σr^2 values.

- The short period of time between the eruptions (c. 1450 years between Rotoma and Mamaku, c. 2500 years between Mamaku and Whakatane) supports tapping of the same magma body. It seems unlikely that these eruptive episodes tapped discrete magmas that solidified sufficiently in such short periods of time to allow movement of new magma to the surface. It does not seem unreasonable that a body of magma could reside in the crust in this area for c. 4000 years.

The magma body tapped during the Rotoma, Mamaku and Whakatane eruptive episodes is the largest body of magma to have been erupted from the Okataina Volcanic Centre during the post-caldera activity. The eruption of such a large magma body represents a change in the post-caldera eruptive style at the Okataina Volcanic Centre. However, eruptives from the Haroharo, Tarawera and Okareka volcanic complexes exhibit differences in ferromagnesian phenocryst assemblages and lie along different structural trends, which suggest that these complexes should be considered separately. In this case, there is little prior activity from Haroharo on which to judge whether this large magma body represents a change in eruptive style.

Along similar lines, during the post-Oruanui eruptions from the Taupo Volcanic Centre three rhyolitic magma types were erupted, with the two oldest being considerably smaller (2.4 km^3 and 6.6 km^3 erupted) than the most recent (15-35 km^3) (volumes from Sutton et al., 2000).

7.2.4 Implications for General Models of Continental Rhyolite Magmatism

7.2.4.1 Models for the Evolution of Large Silicic Magmatic Systems

In Chapter Six the possible crustal and mantle-derived components involved in rhyolite magma genesis were characterised. Also of interest is the behaviour of the sub-volcanic magmatic system between magma formation and eruption. The evolution of large silicic magmatic systems, such as those found in the central Taupo Volcanic Zone, is poorly understood. Of interest, is (i) whether eruptions record the evolution of a single magma chamber, or of multiple magma bodies or batches, (ii) the length of time silicic magmas reside in the upper crust, and (iii) the nature and time-frame of magma chamber replenishment.

Models range from those in which rhyolites are derived from a single, relatively large, long-lived (> 100 000 years) magma chamber (eg. Halliday et al., 1989; Christensen and De Paolo, 1993) which underlies the volcano during repose periods, to those in which multiple relatively smaller silicic magma batches are produced rapidly by crustal melting. These batches then rise to the surface with only temporary development of small, short-lived (< 1 000 years) magma chambers just prior to the eruption (eg. Huppert and Sparks, 1988; Sparks et al., 1990, Sutton et al., 1995, 2000).

The Pliocene to Recent Long Valley magmatic system, California, occurs between the eastern front of the Sierra Nevada and the western margin of the Basin and Range Province (Heumann and Davies, 1997). This system can be considered as an example of the first model, in which magma chambers are long-lived, and may be an extreme case. Magma residence times ranging from c. 0.3 - 1.1 million years have been suggested (eg. Halliday et al., 1989; Metz and Mahood, 1991; Christensen and DePaolo, 1993; van den Bogaard and Schirnick, 1995; Christensen and Halliday, 1996; Reid et al., 1997; Davies and Halliday, 1998). Rhyolites from Long Valley may show extreme fractionation with Sr < 1 ppm and Rb/Sr > 2000 (Halliday et al., 1991). Halliday et al. (1991) consider that the only plausible mechanism for the production of such rhyolites is fractional crystallisation involving substantial volumes of cumulates. Such a process would be facilitated by long magma residence times. Halliday et al. (1989) implied that magma remained in a stable, stratified state for up to 0.7 million years. However, Sparks et al. (1990) point out that there are thermal constraints imposed upon the state of a magma chamber if it were to exist for this

long. Sparks et al. (1990) and Mahood (1990) reinterpreted the data of Halliday et al. (1989) and proposed remelting of recently crystallised granites and the crystallised margins of the magma chamber, respectively, to account for the prolonged magmatism. In both cases remelting takes place episodically and the residence times of these magma bodies as liquids between melting and eruption are short.

The timeframe of magma residence in the Long Valley system is still being debated (eg. Davies and Halliday, 1998; Anderson et al., 2000; Reid and Coath, 2000; Anderson, 2001; Davies and Heumann, 2001; Heumann and Davies, 2001). Data that were previously interpreted as being indicative of a large, long-lived magma chamber have been reinterpreted in favour of smaller, short-lived magma batches. The histories of other silicic magmatic systems have also been interpreted in terms of distinct magma batches. Examples are the Coso Volcanic Field, California (Bacon et al., 1981), the Timber Mountain magmatic system, Nevada (Mills et al., 1997) and the Bandelier magmatic system, New Mexico (Stix and Gorton, 1993). Sutton et al. (2000) note that these examples contrast with the Taupo Volcanic Centre in erupting much less frequently, with major magmatic inputs spaced at intervals of typically hundreds of thousands of years.

Sutton et al. (1995, 2000) have shown that the Taupo Volcanic Centre can be considered as an example of the second model in which magma batches are petrogenetically distinct, relatively smaller and short lived. During Taupo's earlier history (c. 320 - 65 ka) geographically separate groups of lava domes were erupted that possess distinctive geochemical and petrographical traits that cannot be explained by evolution from a single parental magma composition (Sutton et al., 1995; 2000). During the past c. 65 ka Taupo has been particularly frequently and voluminously active (mean eruption rate of c. 0.2 m^3s^{-1} over the past c. 65 ka), and it is the most productive single rhyolitic volcano known (Wilson et al., 1995). Domes and widespread pyroclastics erupted from c. 65 - 28 ka record the growth of an isotopically homogeneous magma chamber that produced the c. 400 km^3 (magma volume) caldera-forming phreatomagmatic Oruanui eruption at 26.5 ka. Development of this large chamber was accompanied by eruption of distinct magma types in other geographic areas of the volcano (Sutton et al., 1995). Twenty-eight eruptions are recognised in the post-Oruanui sequence with ages from 20.5 ka to 1740 years B.P. The four magma types erupted in this sequence, one dacitic (erupted from 20.5 - 17 ka) and three subtly distinct rhyolite compositions (erupted in three discrete periods from 11.8 - 9.95, 7.05 - 2.75 and 2.15 - 1.74 ka), are compositionally distinct from any observed Oruanui magma (Sutton

et al., 1995). The compositional variations between these rhyolite compositions are stepwise, not gradual, and appear to reflect tapping of distinct batches of magma rather than evolution of a single gradually evolving magma chamber (Sutton et al., 1995). Sutton et al. (1995) noted a magma generation time of c. 40 000 years prior to the Oruanui eruption. The maximum times for generation of the three post-Oruanui rhyolite magmas range from 600 - 5 200 years with residence times on the order of 400 - 10 000 years (Sutton et al., 2000).

Hence Taupo is interpreted as a silicic magmatic system where each magma type represents the emplacement of a short-lived magma body into the upper crust. Individual magma bodies apparently erupt distinct magma for only a few thousands to a few tens of thousands of years (Sutton et al., 1995). Sutton et al. (1995) consider that this is in contrast to other rhyolitic systems, (eg. Long Valley) and the lack of significant compositional zonation within Taupo deposits is another unusual characteristic. In addition to the smaller post-Oruanui eruptions, the Taupo and Oruanui caldera-forming eruptions produced moderate to large volume deposits that show little or no compositional zonation (Sutton et al., 1995).

Sutton et al. (2000) attribute this difference in eruptive styles partially to the different tectonic settings of the Taupo Volcanic Centre and the silicic volcanic centres of the western USA. Magmatic systems such as those at Long Valley and Yellowstone occur in a stable continental setting with a relatively thick (~ 30 km; Pakiser, 1963; Priestley et al., 1982), strong cratonic crust. In this setting magma chambers can evolve over extended time intervals allowing significant compositional zonation to develop and extreme fractionation of rhyolitic magmas. Beneath the Taupo Volcanic Zone the crust is younger, thinner (~ 15 km; Stern and Davey, 1987; Beanland and Haines, 1998) and undergoing rapid extension at ~ 2 - 10 mm/year (Villamor and Berryman, 2001). In addition to permitting a considerable flux of mantle-derived magma into the crust, crustal extension allows easy escape of rhyolites, such that magma batches have short residence times in the crust, not long enough for significant zonation or extreme fractionation (Rb/Sr $\approx$ 1 in Taupo Volcanic Centre rhyolites) to develop (Sutton et al., 2000).

7.2.4.2 Implications from the Okataina Volcanic Centre Data

Like Taupo, Okataina is a highly active modern rhyolitic caldera volcano. Post-caldera activity at Okataina contrasts with Taupo in that there have been fewer but generally larger eruptions, with a mean eruption rate of c. 0.08 m^3s^{-1} (c. 2.5×10^{-3} km^3/year) over the past c. 65 ka (Wilson et al., 1995). Many of the observations made by Sutton et al. (2000) with regard to the causes of this frequent eruption style at the Taupo Volcanic Centre can be equally applied to the Okataina Volcanic Centre, namely the young, thin, rapidly extending crust underlying the area.

As at Taupo the eruptive history of the Okataina Volcanic Centre has involved the eruption of multiple, petrogenetically distinct magma batches, many of which are relatively small, and often relatively short lived. This is particularly true for the post-caldera activity in the last c. 25 000 years, with at least nine magma batches erupted. These magma batches each have estimated erupted volumes generally < 15 km^3, although the youngest batch at Haroharo has an estimated erupted volume of ~ 38 km^3 (Table 7.3). Estimated maximum generation times for these magma batches range from 3 800 - 15 500 years, with estimated minimum magma generation rates from 3.1×10^{-4} - 3.2×10^{-3} km^3/year, and residence times up to c. 31 000 years. Estimated minimum magma generation rates are comparable to, or an order of magnitude less than, the mean eruption rate.

The short generation and residence times of magma batches at the Okataina Volcanic Centre during the last c. 25 000 years may have played a role in producing several of the geochemical features of the post-caldera eruptives. Many of the magma batches show very little compositional zonation (eg. Te Rere A, Waiohau and Kaharoa type magmas) suggesting that they did not spend prolonged periods in the crust, or alternatively were vigorously convecting. In addition, Rb/Sr ≈ 0.5 - 2.0 for the eruptives and, as at the Taupo Volcanic Centre, they do not show the extreme fractionation seen in eruptives from longer lived magmas.

The vents for all of the Haroharo, Okareka and Tarawera volcanic complex eruptives lie within the Haroharo and Tarawera linear vent zones. These zones are subparallel to the NE-SW regional tectonic trend throughout the Taupo Volcanic Zone. Bacon (1985) subdivided silicic volcanic fields on the basis of the distribution of vent sites and noted that

linear vent patterns, often controlled by regional tectonics, are commonly associated with the absence of evidence for large, shallow magma bodies. Hence, the distribution of vent locations provide further support for the lack of large shallow magma bodies beneath the Haroharo and Rotoma calderas, and Okareka Embayment, during the last c. 25 000 years. This is comparable to vent sites for post-Oruanui eruptions from the Taupo Volcanic Centre, which Sutton (1995) noted were also consistent with the lack of a large shallow magma body.

Studies on the transport of silicic magmas (eg. Petford et al., 1993) have shown that these magmas can theoretically move rapidly through the crust in dike systems. These dike systems may be controlled by regional tectonics, where fault systems act as conduits by channelling the magma. Petford et al. (1993) calculated a mean ascent velocity of 1 cm/s for magmas with a viscosity of 10^6 Pa·s, equivalent to 30 km in ~ 1 month. The critical (minimum) dike or fault width required for such a magma to ascend without freezing is between ~ 2 and 7 metres. These calculations lend support for the maintenance of a silicic magmatic system at the Okataina Volcanic Centre without the need for a large shallow magma body underlying the area. This is of particular relevance to the post-caldera activity. Given a crustal thickness of ~ 15 km beneath the Taupo Volcanic Zone (Stern and Davey, 1987; Beanland and Haines, 1998), the multiple, relatively small volume magma batches erupted during the post-caldera activity could rise from their lower crustal - upper mantle source regions in relatively short periods of time (~ 15 days), and erupt with only intermittent storage at shallow levels in the crust.

Regional tectonics may not only control silicic dike systems and vent sites, but tectonic activity may also act as an eruption trigger. The eruption of multiple, relatively small volume magma batches from the Okataina Volcanic Centre in the last c. 25 000 years may have been facilitated by an episode of regional extension. Such extension may have not only provided conduits through which the magma could reach the surface, but also allowed intrusion of basaltic magma into the upper crust and the silicic magma bodies residing there. The intrusion of basaltic magma is considered to be an important eruption trigger at the Okataina Volcanic Centre (see below). The accumulation of large volumes of magma, which subsequently erupt as caldera-forming ignimbrites, may not necessarily have resulted from increased magma generation rates. Such an accumulation could be facilitated by an episode of diminished regional extension and hence basaltic magma intrusion.

Regional tectonics may also have an influence on the morphology of storage reservoirs for post-caldera magma batches. Cole et al. (2001) suggest that the magma chamber for the Kaharoa Eruptive Episode from the Tarawera Volcanic Complex was probably elongate parallel to regional faulting. Such elongate magma bodies have been suggested in this study for many of the other post-caldera eruptive episodes (Figures 7.3 and 7.4), primarily a reflection of their eruption from multiple vents along either the Haroharo or Tarawera linear vent zones. This is particularly the case for the magma batch erupted at the Haroharo Volcanic Complex in the Rotoma, Mamaku and Whakatane episodes. This study of rhyolite lavas erupted from different vents along the Haroharo Linear Vent Zone has highlighted lateral compositional variations in the magma erupted from this batch. Such variations are unlikely to have been recognised in a study of pyroclastic compositions.

Of relevance for the Okataina Volcanic Centre, is that small isolated rhyolitic magma batches may be triggered to erupt by the intrusion of mafic magma. Seven eruptions from the Okataina Volcanic Centre in the last c. 65 ka have had a basaltic component (see section 2.2.2.4). The Tarawera (1886 A.D.) and Rotokawau (3 700 years B.P.) eruptions were entirely basaltic with no juvenile rhyolitic material erupted. The Matahi (c. 65 ka), Rotomakariri (c. 26 500 - 31 400 years B.P.), Okareka (22 500 years B.P.), Rotoma (9 500 years B.P.) and Kaharoa (1314 ± 11 A.D.) eruptions involved both basaltic and rhyolitic magmas, and intrusion of basaltic magma into the rhyolitic magma is thought to have initiated rhyolitic eruptions. Cole et al. (2001) suggest that there may have also been a basaltic component in the Waiohau eruption (13 800 years B.P.), although this has yet to be documented. Nairn (1981b) notes that the three most recent eruptions from the Okataina Volcanic Centre have been either basaltic (Rotokawau and Tarawera) or have involved a significant basaltic component (Kaharoa). He suggests that the increasing importance of basaltic events may be due to continuing solidification of rhyolitic magma beneath the Okataina Volcanic Centre, allowing the upward passage of basaltic dikes.

This study provides further evidence to corroborate the observations of Sutton (1995) and Sutton et al. (1995, 2000), that models for the evolution of silicic magmatic systems based on North American examples are not applicable to the Taupo Volcanic Zone. This is likely to be due to the active extensional tectonic setting of the Taupo Volcanic Zone and relatively thin crust. The role of mafic magma intrusion in triggering rhyolitic eruptions at the Okataina Volcanic Centre is of great importance and requires further study.

7.2.5 Implications for the Nature of Future Eruptions

Many studies have discussed the hazards associated with past and future eruptions from the Okataina Volcanic Centre (eg. Nairn, 1981b; Johnston and Nairn, 1993; Scott and Nairn, 1998; Becker, 1999). Stirling and Wilson (2000) have used probabilistic hazard analysis to estimate a 2% probability of a 0.5 - 4.0 km^3 volume eruption in the next 50 years from the Okataina Volcanic Centre. When considering the implications of this study for the nature of future eruptions, of most relevance is the current state of the magmatic system. This is reflected in the post-caldera eruptive activity in the last c. 25 000 years.

An important implication of the present study is that the post-caldera activity has involved the eruption of multiple, relatively small, genetically discrete batches of magma. The data collected in this study for the rhyolite lavas of the Haroharo, Tarawera and Okareka volcanic complexes preclude derivation of these lavas from a single, relatively large magma body residing in the crust beneath the Okataina Volcanic Centre during the last c. 25 000 years. Hence it is likely that a future eruption from the Okataina Volcanic Centre will involve a relatively small magma batch, erupted from multiple vents along either the Haroharo or Tarawera linear vent zones. This observation has implications for volcanic hazard assessment and eruption prediction. The data obtained in this study of rhyolite lavas can be used to place some constraints on the characteristics of the magma involved in future eruptions.

7.2.5.1 Haroharo Volcanic Complex

The last three eruptive episodes at the Haroharo Volcanic Complex (Rotoma, Mamaku and Whakatane) are considered to have tapped a single magma batch that resided in the crust during this c. 4 000 year period. This is the largest body of magma to have been erupted from the Okataina Volcanic Centre during the post-caldera activity, with an estimated 38 km^3 of magma erupted. The repose periods between eruptions of this magma (c. 1 500 and 2 500 years) were significantly shorter than the current repose period of c. 5 500 years.

During the c. 4 000 year period over which this magma batch was erupted, Fe-Ti oxide geothermometry temperatures dropped from ~ 740°C to ~ 680°C (see section 5.10), suggesting an average cooling rate for the magma of ~ 1.5°C every 100 years. Assuming this rate of cooling has persisted for the last c. 5 500 years, the magma temperature may now

be less than 600°C, and a future eruption may be unlikely unless the silicic magma is revived by basaltic intrusion. The existence of a crystallising silicic magma body in the crust beneath the Haroharo Volcanic Complex may account for the lack of basaltic eruptions in this area, compared to the Tarawera Volcanic Complex. Such silicic magmas may not have reached the degree of crystallinity that would allow ascending mafic magmas to reach the surface, but may do so in the future and hence this eruption scenario cannot be ruled out.

On the basis of gravity and magnetic modelling, Rogan (1982) suggested that a partly crystallised silicic magma may reside in the basement beneath the Okataina Volcanic Centre. Wilson et al. (1984) note that the position of this inferred magma body does not accord with vent positions for the post-caldera eruptives. However, if magma erupted from the Haroharo Linear Vent Zone reaches the surface via southeastward dipping faults, this inferred magma body could represent residual magma from the Whakatane eruption.

Rhyolite lavas erupted during the Whakatane episode are among the most geochemically evolved Okataina Volcanic Centre eruptives (~ 75.5 - 77.5 wt. % SiO_2). A future eruption of this magma body would be likely to involve high-silica rhyolite, similar in composition to the most evolved magma erupted during the Whakatane episode, with a ferromagnesian phenocryst assemblage dominated by cummingtonite. However, if basaltic intrusion is involved, as an eruption trigger and/or as a means to revive a crystallising magma, the composition of the erupted magma could differ from that erupted previously.

Vent positions for eruptions during the Rotoma, Mamaku and Whakatane episodes have migrated southwest along the Haroharo Linear Vent Zone over time (Figure 7.3). During the Mamaku and Whakatane episodes, vents to the southwest (vent area 1) produced the greatest volume of lavas and pyroclastics. Hence future eruptions involving this magma body may be more likely from vent area 1, or vents further southwest.

The future eruption of a new, genetically unrelated magma batch can also not be ruled out. Assuming a minimum magma generation rate of ~ 2.0×10^{-3} km^3/year beneath Haroharo (Table 7.3), ~ 11 km^3 of new silicic magma could have been generated since the Whakatane eruption. The repose period between eruptions of genetically unrelated magma at Haroharo during the Te Rere and Rotoma episodes is c. 15 500 years. Insufficient time may have passed since the Whakatane eruption to allow sufficient crystallisation of residual magma, and hence to permit a new rhyolitic magma batch to reach the surface.

The implications of this study for a future eruption from the Haroharo Volcanic Complex are more or less consistent with the scenario proposed by Johnston and Nairn (1993), involving the eruption of ~ 8 km^3 of rhyolite magma from the complex as both explosive pyroclastic eruptions and non-explosive extrusion of lava. They suggest that the first sign of an impending eruption of this kind would involve an increased level of seismicity ~ 12 - 18 months prior to the eruption. Studies such as Petford et al. (1993) have estimated a mean ascent velocity of 1 cm/s for silicic magmas moving through the crust in dike systems (see section 7.2.4.2). Hence, the relatively small volume magma batches erupted from the Okataina Volcanic Centre in the last c. 25 000 years could rise from their lower crustal - upper mantle source regions (~ 15 km deep) in relatively short amounts of time (~ 15 days). Their storage at shallow levels in the crust prior to eruption may be only intermittent. Hence, the first signs of an impending eruption of newly generated magma may occur much closer to the actual eruption than first thought by Johnston and Nairn (1993). Cole et al. (2001) suggest that silicic magma involved in the Kaharoa eruption at Tarawera probably reached the ground surface in less than 4 days after its rise from a high-level chamber was initiated. Hence, a future eruption of residual magma residing in a high-level chamber beneath Haroharo may follow only a short period of precursor activity, such as increased seismicity and ground deformation.

7.2.5.2 Okareka Volcanic Complex

The two eruptive episodes at the Okareka Volcanic Complex (Te Rere and Rotorua) are considered to have tapped a single magma batch that resided in the crust during this c. 9 200 year period. The estimated volume of magma erupted from this batch in the Rotorua episode is 4 km^3. Estimates are not available for the volume of magma erupted in the Okareka Embayment during the Te Rere episode. The repose period between the two eruptions of this magma batch is significantly shorter than the current repose period of c. 15 800 years.

During the c. 9 200 year period over which this magma batch was erupted, Fe-Ti oxide geothermometry temperatures dropped from ~ 830°C to ~ 660°C (see section 5.10), suggesting an average cooling rate for the magma of ~ 1.8°C every 100 years. Assuming this rate of cooling has persisted for the last c. 15 800 years, the magma temperature may now be less than 400°C, and a future eruption would be unlikely. The low predicted present day

temperature for this magma batch suggests that the degree of crystallinity may be such that would allow ascending mafic magmas to reach the surface. Given that basaltic eruptions associated with the Okataina Volcanic Centre have occurred in areas where little or no prior basaltic activity has been detected, the Okareka Embayment is considered a potential location for a future basaltic eruption.

Johnston and Nairn (1993) propose a scenario involving a pyroclastic eruption of 1 - 2 km^3 of basaltic magma from the Okareka Embayment. They suggest that the first sign of an impending eruption of this kind would involve an increased level of seismicity ~ 6 hours prior to the eruption, and may be accompanied by an increase in the outflow of hot springs and geysers at the Whakarewarewa thermal area near Rotorua City. Observations of precursor activity and hazards associated with the 1886 A.D. basaltic Tarawera eruption can be used in developing scenarios for future basaltic eruptions from the Okataina Volcanic Centre.

The future eruption of a new, genetically discrete silicic magma batch at the Okareka Volcanic Complex cannot be ruled out. Assuming a minimum magma generation rate of ~ 6.0×10^{-4} km^3/year beneath Okareka (Table 7.3), ~ 10 km^3 of new silicic magma could have been generated since the Rotorua eruption. Given the estimated cooling rate for residual Rotorua magma, sufficient crystallisation of such magma may have occurred to allow the eruption of this new, genetically discrete magma. The composition of this possible new magma is difficult to constrain, but is likely to have a composition within the range of previous eruptives (~ 74 - 76 wt. % SiO_2).

7.2.5.3 Tarawera Volcanic Complex

The last rhyolitic eruption from the Tarawera Volcanic Complex (Kaharoa episode) tapped a single magma batch that is considered to be genetically discrete from previously erupted magma. This magma batch was relatively small, erupting an estimated equivalent magma volume of 4 km^3. In contrast to the Haroharo Volcanic Complex, there is little evidence for the persistence of magma batches in a liquid state beneath the Tarawera Volcanic Complex during repose periods, and hence for multiple eruptions from the same magma batch.

Repose periods between eruptions of genetically discrete magmas at Tarawera range from c. 4 000 to 13 000 years, with the longest repose period preceding the Kaharoa eruption.

The current repose period for silicic eruptions at Tarawera is only c. 690 years. Assuming a minimum magma generation rate comparable to those for Tarawera in Table 7.3, only very small amounts of new magma could have been generated during this short period. In addition, the eruption of basalt from the Tarawera Linear Vent Zone in 1886 A.D. is cited as evidence to support sufficient crystallisation of residual silicic magma to allow ascending mafic magmas to reach the surface, and may indicate that the generation and/or residence of a new silicic magma body is unlikely.

It is difficult to place constraints on the timeframe and vent locations of future silicic eruptions at Tarawera, and the composition of magma erupted, given that these factors have varied over the past c. 22 500 years. Such a silicic magma is likely to have a composition within the range of previous eruptives (~ 73 - 77 wt. % SiO_2), however there is no basis on which to speculate if it will be a low temperature (650-750°C) biotite-bearing magma, or a relatively higher temperature (750-850°C) biotite-free/poor magma. Given the importance of basaltic magma as an eruption trigger at Tarawera, it is likely that a future silicic eruption will involve a basaltic component.

A future basaltic eruption from the Tarawera Linear Vent Zone, similar to that of 1886 A.D., is viable, and would continue to preclude the existence of silicic magma beneath the area. Such a basaltic eruption would be likely to involve a smaller volume of magma, and be less explosive, than eruption of silicic magma.

7.2.5.4 Caldera-forming Ignimbrite Eruptions

A future large-scale caldera-forming ignimbrite eruption from the Okataina Volcanic Centre cannot be ruled out. It is considered that the current style of post-caldera activity also occurred at the Okataina Volcanic Centre between the caldera-forming ignimbrite eruptions, but little evidence is preserved in the stratigraphic record (Nairn, 1981b). The eruption of multiple, small volume, genetically discrete magmas from the Haroharo and Tarawera linear vent zones in the last c. 25 000 years preclude the coalescence of a large magma body beneath the area. The eruption of these multiple smaller magma batches may be acting as a release valve, preventing the build-up of magma, volatiles and heat beneath the Okataina Volcanic Centre, which would be conducive to a large-scale eruption. In addition, the eruption of these multiple magma batches may have been facilitated by an episode of regional extension. While these relatively small volume eruptions of generally genetically

discrete silicic magmas continue from vents along the Haroharo and Tarawera linear vent zones, and are accompanied by small basaltic eruptions, the build-up of a larger magma body is unlikely.

7.3 SPATIAL AND TEMPORAL EVOLUTION OF THE ROTORUA VOLCANIC CENTRE

The eruptive history of the Rotorua Volcanic Centre can be divided into two main periods separated by the caldera-forming eruption of the Mamaku Ignimbrite at 220 ± 10 ka. The rhyolite lavas erupted from the Rotorua Volcanic Centre have been erupted in one of three time periods:

1) Those erupted adjacent to the caldera margins, pre-dating the widespread Mamaku Ignimbrite (known as the hr_1 rhyolites).

2) Those erupted in the southwestern sector of the caldera, between the Mamaku Ignimbrite and the Rotoiti Ignimbrite eruption from the adjacent Okataina Volcanic Centre at c. 65 ka (known as the hr_2 rhyolites).

3) Those erupted within the caldera, after the Rotoiti Ignimbrite eruption (known as the hr_3 rhyolites).

On the basis of relative age, spatial position, ferromagnesian phenocryst assemblage and geochemistry, the rhyolite lavas of the Rotorua Volcanic Centre have been divided into six magma types. The characteristics of these magma types are summarised in Table 7.5. The history of the Rotorua Volcanic Centre is poorly constrained by age data. In addition, there is a lack of geochemical and particularly isotopic data for many of the eruptives. These factors prevent an in-depth interpretation of the spatial and temporal evolution of the Rotorua Volcanic Centre.

The pre-Mamaku Ignimbrite Endean Road type magma differs from the Hamurana type magma in that it contains significant amounts of biotite and is relatively phenocryst rich. The available whole rock and phenocryst data are insufficient to assess if any genetic relationship exists between these two magma types. Geochemical affinities between the Tokorangi type magma and the hk_1 rhyolite lavas, suggest that this magma type may be related to the Kapenga Volcanic Centre. However, further geochemical and isotopic data

are required to substantiate this. Lynch-Blosse (1998) suggested that at least some of the hr_1 rhyolites represent the eruption of degassed magma following the Waimakariri Ignimbrite eruption. However, until further data becomes available, the Waimakariri type magma cannot be genetically linked to the Hamurana or Endean Road magma types.

Table 7.5: Summary of the petrographic and isotopic characteristics of rhyolite magma types erupted from the Rotorua Volcanic Centre as determined in this study.

Magma Type	Ferromagnesian Mineral Assemblage	Phen. %	Temperature (°C)	$^{87}Sr/^{86}Sr$	ε_{Nd}	Special Features or Extra Notes	Representative Sample (No.)
Post-Rotoiti Ignimbrite (< c. 65 ka)							
Mokoia Island type	Ca-Amph + Opx	29	734	0.70528		Erupted as the Mokoia Island Dome	103
Vaughan Road type	Bio + Ca-Amph + Opx	29-30	661	0.70525	1.79	Erupted as the Vaughan Road and Hinemoa Point domes	104
Mamaku Ignimbrite (220 ± 10 ka)							
Mamaku - Ngongotaha type	Opx ± Ca Amph	4-9		0.70503	1.99	Erupted as the *Mamaku Ignimbrite* and the hr_2 rhyolite lavas.	86 159
Pre-Mamaku Ignimbrite (> 220 ± 10 ka)							
Hamurana type	Opx ± Ca-Amph	14		0.70536		Erupted as the Hamurana and *Fryer Road (?)* lavas	120
Endean Road type	Opx + Ca-Amph + Bio	23	736	0.70541		Erupted as the Endean Road and *Umurua (?)* lavas	87
Tokorangi type **(Kapenga eruptive ?)**	trace Opx	3-5				Erupted as the Tokorangi and Hemo Gorge lavas	84
Waimakariri type	*Opx (trace Bio)*	}	*Lack of data prevents the determination of a genetic relationship between the Waimakariri Ignimbrite and the magma types erupted as rhyolite lavas during this period.*				

Magma type characteristics are based on data obtained in this study for rhyolite lavas and do not specifically include data for associated pyroclastic eruptives from the literature (except where indicated). Age groups are listed in order of increasing age, however within each age group the magma types are listed in no particular order. Units in italics were not sampled in this study. Temperatures are Fe-Ti oxide estimates unless unavailable in which case hornblende-plagioclase estimates were used. Ferromagnesian phenocryst assemblage for the Waimakariri Ignimbrite from Lynch-Blosse (1998).

Mineralogical, geochemical and isotopic similarities suggest a genetic relationship between the Mamaku Ignimbrite magma and the hr_2 rhyolite lavas (Mamaku-Ngongotaha type magma, Table 7.5). Modelling by Milner (2001) also indicated the possibility that these lavas were erupted from the Mamaku Ignimbrite magma chamber. Mineralogical and isotopic differences preclude the evolution of the Mamaku-Ngongotaha type magma from either the Hamurana or Endean Road type magmas by fractional crystallisation or AFC processes. Modelling by Milner (2001) also suggested that the Hamurana rhyolite is not consanguineous with the Mamaku Ignimbrite magma. Hence, it is suggested that magma batches erupted at the Rotorua Volcanic Centre prior to 220 ± 10 ka were exhausted during eruption, or residual magma solidified in the crust prior to 220 ± 10 ka, as it is unlikely that these magmas could have remained in a liquid state and not been incorporated into the caldera-forming Mamaku Ignimbrite eruption.

The post-Rotoiti Mokoia Island type magma differs from the Vaughan Road type magma in that it does not contain biotite. The available whole rock and phenocryst data are insufficient to assess if any genetic relationship exists between these two magma types. Mineralogical, geochemical and isotopic differences preclude the evolution of the Mokoia Island and Vaughan Road type magmas from the Mamaku-Ngongotaha type magma by fractional crystallisation or AFC processes.

The data obtained in this study for rhyolite lavas has contributed to a preliminary framework for the evolution of the Rotorua Volcanic Centre (Table 7.5). With the acquisition of age, geochemical and isotopic data in the future, this framework can be further developed.

7.4 Spatial and Temporal Evolution of the Kapenga Volcanic Centre

The Kapenga Volcanic Centre is considered to be a composite structure that developed during at least three periods of volcanism, two of which were accompanied by inferred caldera-forming ignimbrite eruptions. The rhyolite lavas erupted from the Kapenga Volcanic Centre have been erupted in one of two time periods:

1) Those erupted adjacent to the caldera margins, pre-dating the widespread Mamaku Ignimbrite erupted from the adjacent Rotorua Volcanic Centre at 220 ± 10 ka (known as the hk_1 rhyolites).

2) Those erupted within the Kapenga Volcanic Centre, between the Mamaku Ignimbrite and the Rotoiti Ignimbrite eruption from the adjacent Okataina Volcanic Centre at c. 65 ka (known as the hk_2 rhyolites). Some of the rhyolite lavas erupted in the southwestern Okataina Volcanic Centre during this time (ho_2 rhyolites) are now considered to be eruptives of the Kapenga Volcanic Centre.

On the basis of relative age, spatial position, ferromagnesian phenocryst assemblage and geochemistry, the rhyolite lavas of the Kapenga Volcanic Centre have been divided into several magma types. The characteristics of these magma types are summarised in Table 7.6. The history of the Kapenga Volcanic Centre is poorly constrained by age data. In addition, there is a lack of geochemical and particularly isotopic data for many of the eruptives. These factors prevent an in-depth interpretation of the spatial and temporal evolution of the Kapenga Volcanic Centre.

Lack of age data prevents a determination of the temporal association between magma types erupted as hk_1 rhyolite lavas and caldera-forming ignimbrites. The Tumunui type magma is geochemically indistinguishable from the Horohoro type magma, but contains significant amounts of calcic amphibole and trace biotite. The Tokorangi type magma has been discussed previously (see section 7.3), and is geochemically similar to the Horohoro and Tumunui magma types. The relationship of Upper Atiamuri type magma to the Kapenga Volcanic Centre has yet to be established, and it may be related to a volcanic centre further to the southwest. A small data set for the hk_1 rhyolite lavas, and a lack of isotopic data for both the ignimbrites and the lavas, prevents a detailed comparison of the postulated magma types, and an assessment of possible genetic relationships with the seven caldera-forming ignimbrites.

Mineralogical, geochemical and isotopic similarities suggest that the post-Mamaku Ignimbrite eruptives from the Kapenga Volcanic Centre were derived from a single magma, termed the Blue Lake - Earthquake Flat type magma (Table 7.6). This magma type erupted as the Earthquake Flat Ignimbrite, hk_2 rhyolite lavas occurring within the Kapenga Volcanic Centre, and the biotite-bearing ho_2 rhyolite lavas erupted near the northeastern margin of the Kapenga Volcanic Centre (see section 7.2.2). Mineralogical, geochemical and isotopic differences distinguish the Blue Lake - Earthquake Flat magma type from the spatially adjacent Moerangi magma type, also erupted near the northeastern margin of the Kapenga

Table 7.6: Summary of the petrographic and isotopic characteristics of rhyolite magma types erupted from the Kapenga Volcanic Centre as determined in this study.

Magma Type	Ferromagnesian Mineral Assemblage	Phen. %	Temperature (°C)	$^{87}Sr/^{86}Sr$	ε_{Nd}	Special Features or Extra Notes	Representative Sample (No.)
Post-Mamaku Ignimbrite (< 220 ± 10 ka)							
Blue Lake - *Earthquake Flat* type	Bio + Ca-Amph + Opx	23-32	687-743	0.70529 - 0.70542	0.90 - 1.37	Includes *Earthquake Flat Ignimbrite*, the hk_2 rhyolite lavas and the biotite-bearing ho_2 rhyolite lavas	64 (ho_2) 152 (ho_2) 168 (hk_2) 170 (hk_2)
Moerangi type **(Okataina eruptive ?)**	Opx + Ca-Amph (trace Bio)	17-27	752	0.70516 - 0.70518	1.52	Includes *Te Wairoa Ignimbrites*	72 117 160
Pre-Mamaku Ignimbrite (> 220 ± 10 ka)							
Horohoro type	Opx ± Ca-Amph	5-15	832	0.70553		Erupted as the Horohoro and North Haparangi lavas	126
Tumunui type	Opx + Ca-Amph (trace Bio)	7-10				Erupted as the Tumunui and Waikorapa lavas	165
Tokorangi type **(Rotorua eruptive ?)**	trace Opx	3-5				Erupted as the Tokorangi and Hemo Gorge lavas	84
Upper Atiamuri type ?	Opx + Ca-Amph						
Ohakuri type	*Opx + Ca-Amph + Bio*					*Lack of data prevents the determination of any genetic relationship between these ignimbrites and the rhyolite lavas erupted during this period. Assessing possible genetic relationships between these ignimbrites is beyond the scope of this study.*	
Pokai type	*Opx + Cpx*						
Waihou type	*Opx + Cpx + Ca-Amph*						
Matahana type							
Waiotapu type	*Opx + Cpx ± Ca-Amph*						
Rahopaka type	*Ca-Amph + Opx*						
Tikorangi type	*Opx + Cpx ± Ca-Amph*						

Magma type characteristics are based on data obtained in this study for rhyolite lavas and do not specifically include data for associated pyroclastic eruptives from the literature. Age groups are listed in order of increasing age, however within each age group the magma types are listed in no particular order. Units in italics were not sampled in this study. Temperatures are Fe-Ti oxide estimates unless unavailable in which case hornblende-plagioclase estimates were used. Ferromagnesian phenocryst assemblages for pyroclastics from references cited in section 3.12.

Volcanic Centre. It has not been possible to relate the lavas erupted from the Moerangi magma type to other eruptives from either the Okataina or Kapenga volcanic centres. While they are spatially related to the biotite-bearing lavas erupted from the Blue Lake -

Earthquake Flat magma type, they are not genetically related, and cannot be considered Kapenga Volcanic Centre eruptives based entirely on this spatial relationship.

Similarly to the Rotorua Volcanic Centre, the data obtained in this study for rhyolite lavas has contributed to a preliminary framework for the evolution of the Kapenga Volcanic Centre (Table 7.6). With the acquisition of age, geochemical and isotopic data in the future, this framework can be further developed.

Chapter Eight: Summary and Conclusions

Chapter Eight: Summary and Conclusions

8.1 INTRODUCTION

The primary aim of this thesis was to investigate the evolution of the magmatic system at the Okataina Volcanic Centre, and to obtain supporting data for the adjacent Rotorua and Kapenga volcanic centres, by studying the rhyolite lavas that have been erupted. This chapter presents a summary of the petrography, mineralogy, geochemistry and isotopic composition of rhyolite lavas erupted from the Okataina, Rotorua and Kapenga volcanic centres. Conclusions regarding the implications of this study for the spatial and temporal evolution of the magmatic systems at these volcanic centres are presented. The conclusions of this study for rhyolite petrogenesis in the Taupo Volcanic Zone, general models of continental rhyolite magmatism and the nature of future eruptions from the Okataina Volcanic Centre will also be presented. Recommendations for future areas of study that would facilitate the development of more complete models for the evolution of the Okataina, Rotorua and Kapenga volcanic centres will be outlined.

8.2 SUMMARY

The Okataina, Rotorua and Kapenga volcanic centres lie at the northeastern end of the central Taupo Volcanic Zone, North Island, New Zealand, a region of intense Quaternary silicic volcanism accompanying rapid extension of the continental crust. Caldera-forming ignimbrite eruptions have been responsible for collapse at these centres. In addition, numerous relatively small volume pyroclastic and lava eruptions have occurred between the major caldera-forming events. Rhyolite lavas have been erupted throughout the history of the Okataina, Rotorua and Kapenga volcanic centres, and their study will allow an investigation of the spatial and temporal evolution of these volcanic centres.

The rhyolite lavas erupted at each volcanic centre can be subdivided based on their stratigraphic relationship with two widespread caldera-forming ignimbrites: those predating the Mamaku Ignimbrite (erupted from the Rotorua Volcanic Centre at 220 ± 10 ka), are denoted as ho_1, hr_1 and hk_1 for the Okataina, Rotorua and Kapenga volcanic centres

respectively; those erupted between the Mamaku Ignimbrite and the Rotoiti Ignimbrite eruption from the Okataina Volcanic Centre at c. 65 ka, are denoted as ho_2, hr_2 and hk_2; and thirdly, those lavas erupted at the Okataina and Rotorua volcanic centres that are younger than the Rotoiti Ignimbrite are denoted as ho_3 and hr_3 respectively. The post-Rotoiti Ignimbrite sequence of pyroclastic and lava (ho_3) eruptions at the Okataina Volcanic Centre has been well established by Nairn (1980, 1981a, 1989). Nine rhyolitic eruptive episodes in the last c. 25 000 years have built up the Haroharo, Okareka and Tarawera volcanic complexes, which largely infill the collapse structures of the centre.

The interiors of subaerial silicic lava flows and domes display diverse textures. Three main textural types have been identified in the rhyolite lavas sampled in this study - crystallised rhyolite, obsidian and pumiceous rhyolite, although many samples have intermediate textures. Two samples of an autobreccia were obtained where outcrops of the underlying coherent lava flow were unavailable. The glass groundmass of the rhyolite lavas is commonly flow banded and may contain spherulites, perlitic cracks, quench crystals, and vesicles in varying abundances.

In addition to plagioclase, quartz and Fe-Ti oxide phenocrysts, the rhyolites of the Okataina, Rotorua and Kapenga volcanic centres may contain phenocrysts of the ferromagnesian minerals orthopyroxene, calcic amphibole, biotite and cummingtonite in varying abundances. Apatite and zircon occur as accessory crystals. Nineteen different ferromagnesian phenocryst assemblages are found within the rhyolites obtained in this study, seventeen in Okataina lavas, five in Rotorua lavas and six in Kapenga lavas. Assemblages involving cummingtonite are generally restricted to the Haroharo Volcanic Complex, Okataina Volcanic Centre. The ferromagnesian phenocryst assemblages exhibited by the rhyolite lavas are generally in agreement with spatially and temporally associated pyroclastic eruptives.

Plagioclase is the most common phenocryst type in the rhyolite lavas comprising ~ 3 - 12 % of the total rock and ~ 52 - 84 % of the total phenocrysts. Compositions range from oligoclase (An_{15}) to labradorite (An_{54}). Quartz may be present in only trace amounts, or may comprise up to ~ 9 % of the total rock and ~ 48 % of the total phenocrysts. Orthopyroxene is the most common ferromagnesian phenocryst type, comprising up to ~ 2.5 % of the total rock and ~ 21 % of the total phenocrysts, and may be of enstatite or ferrosilite composition. Amphibole is the second most common ferromagnesian phenocryst type comprising up to

~ 3 % of the total rock and ~ 16 % of the total phenocrysts. Calcic amphibole is most common, but cummingtonite also occurs in Haroharo lavas. Biotite may comprise up to ~ 4 % of the total rock and ~ 16 % of the total phenocrysts. Fe-Ti oxide phenocrysts include both titanomagnetite and ilmenite.

Temperatures determined from Fe-Ti oxide geothermometry range from 650°C - 835°C. Oxygen fugacity (measured as log fo_2) ranges from -18.53 - -12.28. Plots of temperature versus log fo_2 show data for the rhyolite lavas fall onto three curves, which are related to ferromagnesian phenocryst assemblage, that run essentially parallel to the FMQ buffer curve. Temperatures determined by hornblende-plagioclase thermometry range from 677°C - 846°C and are generally in agreement with those obtained by Fe-Ti oxide geothermometry. Average crystallisation pressure estimates using the Al-in-hornblende geobarometer range from 1.6 - 2.3 kbar, depending on the particular technique used, and crystallisation depths could be up to ~ 15 km. The estimated H_2O content of Haroharo rhyolite magmas show some correlation with ferromagnesian phenocryst assemblage, and range from ~ 2.8 - 7.6 wt. %. Given estimated H_2O contents for Haroharo rhyolite lavas of 0.12 and 0.36 wt. % (Stevenson et al., 1994), there must have been significant degassing of the magma between the magma chamber and the surface.

The rhyolite lavas of the Okataina, Rotorua and Kapenga volcanic centres are classified as dominantly peraluminous, medium-K calc-alkaline rhyolites. Chondrite-normalised REE abundance patterns are typical for Taupo Volcanic Zone silicic eruptives, characterised by a strongly enriched LREE pattern with steep slopes, a pronounced negative Eu anomaly, and flat HREE pattern. Chondrite-normalised multi-element (spider) patterns show features typical of arc-related magmas with enrichment in LILE relative to HFSE, and depletion in Nb.

Isotopic compositions for the Okataina, Rotorua and Kapenga volcanic centre rhyolite lavas are within the range of other Taupo Volcanic Zone silicic eruptives, with $^{87}Sr/^{86}Sr = 0.70503 - 0.70583$, $^{143}Nd/^{144}Nd = 0.51264 - 0.51274$ and $\varepsilon_{Nd} = 1.99 - 0.02$. Pb isotopic compositions are also within the range of other Taupo Volcanic Zone silicic eruptives, with the exception of Matawhaura rhyolite (ho_1), which has a unique Sr-Nd-Pb isotopic composition.

Broadly speaking, geochemical and isotopic compositions of rhyolite lavas from the Okataina, Rotorua and Kapenga volcanic centres are similar, and are comparable to compositions for Taupo Volcanic Zone silicic volcanics in general. There is no geochemical basis on which to subdivide these lavas into volcanic centres. These similarities are considered to result from the magmas having similar source compositions, both in terms of the component derived from the mantle beneath the Taupo Volcanic Zone and the crustal basement rock through which the magmas have migrated.

Petrographic, geochemical, mineralogic and isotopic data for the rhyolite lavas have been incorporated to provide a model for the spatial and temporal evolution of the magmatic system at the Okataina Volcanic Centre. Some insights have also been gained of the evolution of the magmatic systems at the adjacent Rotorua and Kapenga volcanic centres. In addition, an attempt has been made, where sufficient data are available, to integrate the pyroclastic eruptives into this model. Subtle differences in lava compositions in time and space have been used to identify individual magma types or batches. These batches may have similar source components to other batches, but have migrated through the crust and evolved independently.

8.3 CONCLUSIONS

Given lava data obtained in this study, and pyroclastic data available in the literature, the following conclusions have been reached regarding the evolution of the Okataina, Rotorua and Kapenga volcanic centres:

- The early period of activity at the Okataina Volcanic Centre (>220 ± 10 ka) involved eruption of multiple rhyolite magma types as caldera-forming ignimbrites, from relatively large magma batches (~ 90 - 150 km^3), and as lavas (ho_1), which at this stage appear to have been erupted from smaller, spatially discrete magma batches confined to particular areas. The exception is the orthopyroxene and calcic amphibole-bearing ho_1 rhyolite lavas erupted in the northern and western Okataina Volcanic Centre, which may represent pre- or post-Matahina Ignimbrite magma.

- The intermediate period of activity at the Okataina Volcanic Centre (220 ± 10 - c. 65 ka) involved eruption of multiple rhyolite magma types. One type of relatively large volume (~ 120 km^3) was erupted as the caldera-forming Rotoiti Ignimbrite. Two smaller volume rhyolite magma types were erupted dominantly as rhyolite lavas (ho_2) in the southwestern Okataina - Kapenga area, and as associated small volume non-caldera forming pyroclastics (the Te Wairoa and Earthquake Flat ignimbrites).

- Data obtained in this study for the ho_2 rhyolite lavas do not facilitate the drawing of a boundary between the Okataina and Kapenga volcanic centres. It is possible that this area is truly an overlap between the Okataina and Kapenga volcanic centres, with the biotite-bearing ho_2 lavas having a strictly Kapenga origin and the biotite-free/poor ho_2 lavas having an Okataina origin.

- The Haroharo, Okareka and Tarawera volcanic complexes have been erupted in the last c. 25 000 years, and largely infill the collapse structures of the Okataina Volcanic Centre. Ferromagnesian phenocryst assemblages, vent locations and temporal constraints suggest that these complexes have not been derived from a single, large magma body evolving beneath the Okataina Volcanic Centre.

- During the post-caldera activity at the Okataina Volcanic Centre in the last c. 25 000 years, at least nine magma batches may have been erupted, with estimated volumes generally < 15 km^3. The youngest batch erupted at Haroharo (during the Rotoma, Mamaku and Whakatane episodes) has an estimated volume of ~ 38 km^3, and is the largest to have been erupted during the post-caldera activity. Estimated maximum generation times for these post-caldera magma batches range from c. 3 800 - 15 500 years, with estimated minimum magma generation rates from 3.1×10^{-4} - 3.2×10^{-3} km^3/year, and residence times ranging from c. 4 000 - 31 000 years.

- The Haroharo Volcanic Complex was built up in four rhyolitic eruptive episodes beginning c. 25 000 years B.P. The lavas and pyroclastics erupted in the Te Rere episode were derived from a single, genetically discrete, relatively volumetrically small magma batch. The lavas and pyroclastics erupted in the Rotoma, Mamaku and Whakatane episodes appear to record the evolution of a relatively larger single magma batch over c. 4 000 years by closed-system fractional crystallisation processes.

- The Okareka Volcanic Complex was built up in two rhyolitic eruptive episodes at c. 25 000 and 15 800 years B.P. Mineralogical, geochemical, thermal and isotopic factors support a genetic relationship between the magma erupted in these two episodes.

- The Tarawera Volcanic Complex was built up in four rhyolitic eruptive episodes beginning c. 22 500 years B.P. During the two earlier episodes (Okareka and Rerewhakaaitu), multiple, relatively volumetrically small magma batches were erupted. The lavas and pyroclastics erupted in each of the two youngest episodes (Waiohau and Kaharoa) were derived from single, genetically discrete, relatively volumetrically small magma batches.

- There is abundant evidence at Okataina that small isolated rhyolitic magma batches may be triggered to erupt by the intrusion of mafic magma. Nairn (1981b) suggests that the increasing importance of basaltic events may be due to continuing solidification of rhyolitic magma beneath the Okataina Volcanic Centre, allowing the upward passage of basaltic dikes. The role of mafic magma intrusion in triggering rhyolitic eruptions at the Okataina Volcanic Centre is of great importance and requires further study.

- An important implication of this study is that the post-caldera eruptive activity has involved the eruption of multiple, relatively small (generally < 15 km^3), genetically discrete batches of magma. Hence it is likely that a future eruption from the Okataina Volcanic Centre will involve a relatively small magma batch, erupted from multiple vents along either the Haroharo or Tarawera linear vent zones. This observation has implications for volcanic hazard assessment and eruption prediction.

- The length of the current repose periods for eruptions from the Haroharo and Okareka volcanic complexes, in addition to estimated magma cooling rates, suggest that the future eruption of residual magma from the Whakatane and Rotorua eruptive episodes may not be viable unless this magma is revived by basaltic intrusion. The eruption of basaltic scoria from the Tarawera Volcanic Complex in 1886 A.D. is cited as evidence that any residual Kaharoa magma must have already crystallised, and no new silicic magma had been generated by this time.

- Future eruptions may involve either residual silicic magmas revived by basaltic intrusion, or basaltic magmas that have reached the surface without interacting with residual silicic magmas because they have crystallised, or new genetically discrete silicic magma. Okareka and Tarawera are potential locations for a future basaltic eruption. The existence of a crystallising silicic magma body in the crust beneath the Haroharo Volcanic Complex may preclude basaltic eruptions in this area.

- Volcanic activity at the Rotorua and Kapenga volcanic centres has also involved eruption of multiple rhyolite magma types. The history of these centres is poorly constrained by age data, and there is a lack of geochemical, and particularly isotopic, data for many of the eruptives. These factors prevent an in-depth interpretation of the spatial and temporal evolution of the Rotorua and Kapenga volcanic centres.

- At the Rotorua Volcanic Centre, pre- and post-Mamaku Ignimbrite rhyolite lavas (hr_1 and hr_3 respectively) appear to record the eruption of multiple, genetically discrete, relatively small volume magma batches that are genetically unrelated to the Mamaku Ignimbrite magma. Mineralogical, geochemical and isotopic similarities suggest a genetic relationship between the Mamaku Ignimbrite magma and the hr_2 rhyolite lavas.

- Lack of age, geochemical and particularly isotopic data prevents an interpretation of the early history of the Kapenga Volcanic Centre. The most recent activity at the Kapenga Volcanic Centre (220 ± 10 - c. 65 ka) involved eruption of a relatively small volume rhyolitic magma batch as lavas in the central and northeastern parts of the centre (hk_2 and biotite-bearing ho_2 lavas), followed by an associated small volume non-caldera forming ignimbrite (Earthquake Flat Ignimbrite) from the northeastern area.

- The Okataina, Rotorua and Kapenga volcanic centre rhyolite lavas collected in this study have compositions that may be consistent with evolution of silicic magmas from basaltic magmas by crustal assimilation and fractional crystallisation processes (AFC). However, closed-system fractional crystallisation processes best model the small variations between spatially and temporally adjacent rhyolite lavas erupted from these centres.

- This study provides further evidence to corroborate the observations of Sutton (1995) and Sutton et al. (1995, 2000), that models for the evolution of silicic magmatic systems

based on North American examples are not applicable to the Taupo Volcanic Zone. This is likely to be due to the active extensional tectonic setting of the Taupo Volcanic Zone and relatively thin crust.

8.4 RECOMMENDATIONS FOR FUTURE AREAS OF STUDY

During the course of this study, several potential areas have been identified that require further attention. Future work in these areas will facilitate the development of more complete models for the evolution of the Okataina, Rotorua and Kapenga volcanic centres.

- The pre-Rotoiti Ignimbrite (> c. 65 ka) activity at the Okataina Volcanic Centre is poorly constrained by age data, particularly for the rhyolite lavas (ho_1 and ho_2). This prevents an integration of the rhyolite lavas into the currently established ignimbrite stratigraphy and a determination of their temporal relationship to the ignimbrites, and status as pre- or post-ignimbrite eruptives. A lack of age data also precludes an integration of hr_1 and hk_1 rhyolite lavas into the ignimbrite stratigraphy for the Rotorua and Kapenga volcanic centres, respectively. Ages for these rhyolite lavas would allow a more accurate interpretation of the temporal evolution of these centres during their early history.

- There is a lack of geochemical and isotopic data for the Quartz Biotite Ignimbrite, Onuku-Pokopoko Pyroclastics and Kawerau Ignimbrite erupted from the Okataina Volcanic Centre. Such data for these pyroclastics, as well as isotopic data for pyroclastics erupted from the Rotorua and Kapenga volcanic centres, would facilitate the determination of possible genetic relationships with the rhyolite lavas.

- Further progress in petrogenetic modelling of silicic magmas in the Taupo Volcanic Zone would be enhanced by an increased knowledge of the composition of the lower crust beneath the area. Such knowledge could be obtained by further in-depth studies of igneous and metamorphic xenoliths.

- The role of mafic magma intrusion in triggering rhyolitic eruptions at the Okataina Volcanic Centre is of great importance and requires further study.

- Preliminary studies of melt inclusions in quartz phenocrysts were undertaken in this study for Haroharo Volcanic Complex rhyolite lavas. Further in-depth studies of melt inclusions in other phenocryst types may be of use in tracing the liquid line of descent of the magmas and possible interaction with more mafic magmas. Melt inclusion compositions may also be used to estimate the pre-eruptive volatile contents of magmas.

- The models proposed in this study for the evolution of the Okataina, Rotorua and Kapenga volcanic centres could be further refined by utilising methods of estimating the residence times of silicic magmas. For example, SHRIMP $^{238}U/^{206}Pb$ dating of zircon crystals from the Whakamaru Ignimbrite, Taupo Volcanic Zone, suggested magma residence times exceeding 250 k.y. for some zircons (Brown and Fletcher, 1999). In addition, magma mixing and/or fractionation events were directly dated. Brown et al. (2000) note that preliminary SHRIMP $^{238}U/^{230}Th$ dating of zircon crystals suggest long-lived and complex magma chamber histories prior to the Rotoiti and Earthquake Flat ignimbrite eruptions. In addition to estimates of residence times for relatively large, caldera-forming ignimbrite magma batches, of interest would be the application of such techniques to the small volume, post-caldera magma batches erupted at the Okataina Volcanic Centre.

Appendices

Appendix I: Sample Catalogue

Table I.1: Sample catalogue listing samples collected, field and University of Waikato rock store numbers, and sample locations.

Field No.	UOW Number	Rhyolite Lava	Grid Reference (NZMS 260)	Location
5	W01 0001	Pokohu Flow	V16/185317	Boulder at the bottom of Tarawera Falls on the Tarawera River
6	W01 0002	Haroharo Dome	V16/160394	Road cut on eastern side of Haroharo Road
7	W01 0003	Hainini Dome	V16/151369	Outcrop on southern side of Makatiti Road
14	W01 0004	Waiti Flow	V15/158410	Road cut on Bennetts Road
15	W01 0005	Waiti Flow	V15/164424	Road cut on Bennetts Road
17	W01 0006	Waiti Flow	V15/172421	Road cut on Bennetts Road
19	W01 0007	Te Horoa Dome	V16/105316	Outcrop on western shore of Humphrey's Bay, Lake Tarawera
20	W01 0008	Rotoroniu Flow	V16/108327	Outcrop on southern shore of Otangimoana Bay, Lake Okataina (Look out for wasps!)
22	W01 0009	Te Koutu Flow	V16/108374	Outcrop on eastern shore of Kaiwaka Bay, Lake Okataina
23	W01 0010	Te Koutu Flow	V16/107378	Outcrop south of Te Koutu Point, Kaiwaka Bay, Lake Okataina
24	W01 0011	Okataina Flow	V16/103368	Outcrop on southern shore of Kaiwaka Bay, Lake Okataina
25	W01 0012	Okataina Flow	U16/096363	Outcrop on southern shore of Waikereru Bay, Lake Okataina
26	W01 0013	Oruaroa Flow	V16/107336	Outcrop on eastern shore of Otangimoana Bay, Lake Okataina
27	W01 0014	Otangimoana Flow	V16/108333	Outcrop on eastern shore of Otangimoana Bay, Lake Okataina
30	W01 0015	Te Horoa Dome	V16/106329	Outcrop on western shore of Otangimoana Bay, Lake Okataina
32	W01 0016	Te Horoa Dome	U16/095305	Outcrop on northern shore of Lake Tarawera
33	W01 0017	Rotoroniu Flow	V16/113316	Outcrop on northern shore of Humphrey's Bay, Lake Tarawera
34	W01 0018	Ruakokopu Flow	V16/125305	Outcrop on northern shore of Lake Tarawera
35	W01 0019	Ruakokopu Flow	V16/134300	Outcrop on northern shore of Lake Tarawera
36	W01 0020	Tapahoro Flow	V16/149297	Outcrop on northern shore of Lake Tarawera
37	W01 0021	Pokohu Flow	V16/166290	Outcrop on eastern shore of Lake Tarawera, south of Tarawera River outlet
38	W01 0022	Waikakareao Flow	V16/163285	Outcrop on eastern shore of Lake Tarawera, south of Tarawera River outlet
40	W01 0023	Te Puha Flow	V16/124266	Outcrop on eastern shore of Lake Tarawera
41	W01 0024	Te Puha Flow	V16/122255	Outcrop on eastern shore of Lake Tarawera
44	W01 0025	Western Dome	V16/125235	Outcrop on eastern shore of Lake Tarawera, north of Rapatu Bay
45	W01 0026	Wahanga Dome	V16/180255	Outcrop on southern side of Wahanga Dome in the 1886 fissure
46	W01 0027	Ruawahia Dome	V16/173245	Outcrop on eastern side of the 1886 fissure, eastern side of Ruawahia Dome
52	W01 0028	Ngongotaha (Quarry)	U15/916402	Mount Ngongotaha Quarry, off State Highway 5, north of Rotorua City
54	W01 0029	Ngongotaha (Quarry)	U15/916402	Mount Ngongotaha Quarry, off State Highway 5, north of Rotorua City
56	W01 0030	Haumingi Flow	V15/123439	Road cut on southern side of State Highway 30, near Gisborne Point
58	W01 0031	Waitangi	V15/214470	Large boulders on eastern shore of Lake Rotoehu
59	W01 0032	Maungawhakamana	V15/237435	Road cut on western side of State Highway 30, near Lake Rotoma
60	W01 0033	Te Pohue Flow	V15/186458	Road cut on southern side of State Highway 30, near Lake Rotoehu
61	W01 0034	Tuarae Flow	V15/142439	Large boulder on beach next to jetty, Tuarae Point, Lake Rotoiti
63	W01 0035	Stancorp Quarry	U16/023313	Stancorp Quarry, Okareka Loop Road
64	W01 0036	Tutaeheka 1	U16/033271	Road cut on southern side of Tarawera Road, near Lake Rotokakahi
65	W01 0037	Eastern Rhyolite	U16/055275	Cutting on road to Punaromia/Kotukutuku Bay jetty, Lake Tarawera

Field No.	UOW Number	Rhyolite Lava	Grid Reference (NZMS 260)	Location
68	W01 0038	Direct Road	U16/989324	Road cut on Red Tank Road, Whakarewarewa Forest
70	W01 0039	Hill Road	U16/991299	Road cut on Hill Road, Whakarewarewa Forest
72	W01 0040	Moerangi Road	U16/002290	Road cut on Moerangi Road, Whakarewarewa Forest
73	W01 0041	Chestnut Road	U16/003287	Road cut on Loop Road, Whakarewarewa Forest
74	W01 0042	Green Lake	U16/004280	Road cut on Bush Road, Whakarewarewa Forest
78	W01 0043	Kakapiko	U16/974276	Road cut on Lookout Road, Whakarewarewa Forest
79	W01 0044	Rotokohu Dome	V16/182398	Road cut on Rata Loop Track, off Haroharo Road
81	W01 0045	Hainini Flow	V16/190345	Old quarry site, Onepu Road, off Pukemaire Road
84	W01 0046	Tokorangi	U16/975328	Old quarry site, Quarry Road, northern edge of Whakarewarewa Forest
85	W01 0047	Hinemoa Point	U16/986369	Excavation for housing, Owhata Road
86	W01 0048	Kawaha Point	U16/943392	Excavation for new subdivision, northern side of Kawaha Point
87	W01 0049	Endean Road	U16/846354	Outcrop on hill above northern side of Endean Road
90	W01 0050	Ridge Flow	V16/236264	Road cut on southern side of Purutai Road
92	W01 0051	Fentons Mill Flow	V16/193365	Outcrop in stream gully at end of track off Fentons Mill Road
95	W01 0052	Waiti Flow	V15/170426	Outcrop on southern side of track which extends east from Bennetts Road
96	W01 0053	Waiti Flow	V15/175425	Outcrop on southern side of track which extends east from Bennetts Road
98	W01 0054	Tikorangi Dome	V15/220421	Road cut on track off Waipiere Road, southern side of Tikorangi Dome
99	W01 0055	Maungawhakamana	V15/222409	Road cut on Waipiere Road
100	W01 0056	Maungawhakamana	V16/227394	Boulders on hill above Kaipara Road
101	W01 0057	Maungawhakamana	V16/224391	Road cut at gate on Kaipara Road
103	W01 0058	Mokoia Island	U15/981412	Outcrop on southern side of Mokoia Island, Lake Rotorua
104	W01 0059	Vaughan Road	U16/979363	Outcrop on hill above eastern shore of Lake Rotorua, southwest of Hinemoa Point
105	W01 0060	Rotoma Flow	V15/240445	Outcrop east of jetty at Pangopangoa Bay, western shore of Lake Rotoma
106	W01 0061	Rotoma Flow	V15/243452	Outcrop on western shore of Lake Rotoma, northwest of Okopua Point
107	W01 0062	North Rotoma	V15/247474	Outcrop on northern shore of Lake Rotoma
108	W01 0063	Maungawhakamana	V15/257440	Outcrop on eastern shore of Lake Rotoma
109	W01 0064	Matawhaura	V15/158464	Outcrop east of Te Papatu Point, Korokitewao Bay, Lake Rotoiti
110	W01 0065	Whakapoungakau	U16/092386	Outcrop at Tahunapo Bay, western shore of Lake Okataina
111	W01 0066	Crater Farm	U16/055314	Outcrop on eastern shore of Lake Okareka
113	W01 0067	Eastern Rhyolite	U16/058306	Outcrop on hill above the southeastern corner of Lake Okareka
114	W01 0068	Eastern Rhyolite	U16/054304	Outcrop on hill above the southern shore of Lake Okareka
117	W01 0069	Tutaeheka 3	U16/067268	Outcrop west of Putauaki Point, Lake Tarawera
118	W01 0070	Tutaeheka 3	U16/073268	Outcrop west of Putauaki Point, Lake Tarawera
119	W01 0071	Wairua	V16/107231	Outcrop on southern shore of Lake Tarawera, near Hot Water Beach, west of Rapatu Bay
120	W01 0072	Hamurana	U15/993465	Road cut on northern side of Hamurana Road, north of Lake Rotorua
121	W01 0073	Upper Atiamuri	U16/775157	Road cut on northern side of Pukerimu Road
123	W01 0074	Upper Atiamuri	U16/803158	Road cut on northwestern side of State Highway 30
126	W01 0075	Horohoro	U16/858235	Outcrop in stream gully at bottom of Horohoro Cliffs
127	W01 0076	Round Hill	U16/916210	Outcrop on farm track, southern side of Round Hill
128	W01 0077	Hapeotoroa	U16/091200	Outcrop south of steaming cliffs, southwestern shore of Lake Rotomahana
129	W01 0078	Waimangu	U16/094196	Outcrop on southern shore of Lake Rotomahana
130	W01 0079	Patiti Island	V16/114203	Outcrop on southwestern edge of Patiti Island, Lake Rotomahana
133	W01 0080	Green Lake Plug	V16/137221	Southwestern edge of Green Lake Plug, northeastern shore of Lake Rotomahana

Field No.	UOW Number	Rhyolite Lava	Grid Reference (NZMS 260)	Location
134	W01 0081	Rotomahana Dome	V16/141225	Outcrop at the most northeastern point of Lake Rotomahana
135	W01 0082	Western Dome	V16/132224	Outcrop on the northwestern shore of Lake Rotomahana, northeast of the jetty
137	W01 0083	Hemo Gorge	U16/945313	Road cut on the northwestern side of State Highway 30
138	W01 0084	Makatiti Dome	V16/147347	Outcrop on walking track off Makatiti Road
141	W01 0085	Makatiti Flow	V16/133346	Road cut on Makatiti Road, side of southern explosion pit
142	W01 0086	Makatiti Flow	V16/138354	Road cut on Makatiti Road, side of northern explosion pit
143	W01 0087	Makatiti Flow	V16/138354	Road cut on Makatiti Road, side of northern explosion pit
144	W01 0088	Te Pohue Flow	V15/186457	Road cut on southern side of State Highway 30, near Lake Rotoehu
145	W01 0089	Kaipara Flow	V15/212415	Outcrop on eastern edge of Kaipara Flow, evidence of geothermal activity
146	W01 0090	Pukepoto	U16/040358	Outcrop on farm track, northwestern edge of Pukepoto
147	W01 0091	Pokohu Flow	V16/209320	Outcrop on hill above southern side of Titoki Road
149	W01 0092	Waikakareao Flow	V16/203269	Outcrop on walking track off Hawea Road
152	W01 0093	Blue Lake	U16/024282	Outcrop on walking track along southern shore of Lake Tikitapu
153	W01 0094	Trig 7693 Dome	U16/028278	Road cut on eastern side of Tarawera Road near Lake Rotokakahi
154	W01 0095	Ngongotaha (Gondola)	U16/906385	Outcrop on hill above southern side of Mountain Road, Mount Ngongotaha
156	W01 0096	Crater Dome	V16/162242	Outcrop in the 1886 fissure
157	W01 0097	Crater Dome	V16/162242	Fallen blocks from outcrop in the 1886 fissure
158	W01 0098	Tarawera Dome	V16/150235	Outcrop on the western side of The Chasm, part of the 1886 fissure
159	W01 0099	Pukehangi (Te Miri)	U16/878365	Road cut on southeastern side of Paradise Valley Road, opposite Relph Road
160	W01 0100	Tutaeheka 2	U16/033240	Road cut on Mead Road
162	W01 0101	Tutaeheka 2	U16/035248	Road cut on Araromoana Road, off Mead Road
164	W01 0102	Tutaeheka 3	U16/038239	Outcrop on southern side above Highlands Road
165	W01 0103	Tumunui	U16/989205	Fallen blocks from outcrop on hill above farm track, off Wilson Road
167	W01 0104	Dome 2	U16/968244	Outcrop on farm track, off Tumunui Road
168	W01 0105	Dome 3	U16/954254	Outcrop on farm track, off Tumunui Road
169	W01 0106	Waikorapa	U16/013176	Outcrop on northwestern side of Earthquake Flat Road
170	W01 0107	Ongahoro	U16/924216	Outcrop on farm track off Rehi Road
171	W01 0108	North Ridge	U16/909255	Outcrop west of track off State Highway 30
172	W01 0109	Haparangi	U16/900247	Cutting on track off State Highway 30
173	W01 0110	Waiti Flow	V15/151411	Cutting on track running west from Bennetts Road
174	W01 0111	Te Rere Dome	U16/034298	Outcrop in stream gully on farmland off Acacia Road
175	W01 0112	Middle Rhyolite	U16/050301	Cutting on farm track off Acacia Road
176	W01 0113	Trig 7693 Dome	U16/043300	Cutting on farm track off Acacia Road
47	W01 0114	Tarawera Basalt	V16/178250	Eastern edge of 1886 Tarawera Fissure
48	W01 0115	Tarawera Basalt	V16/178250	Eastern edge of 1886 Tarawera Fissure
124	W01 0116	Johnson Rd Basalt	U16/821186	Old quarry site near intersection of Johnson and Stag roads
136	W01 0117	Rotomakariri Scoria	V16/121217	Outcrop on the northwestern shore of Lake Rotomahana
148	W01 0118	Okareka Basalt	V16/245316	Cutting on eastern side of Puhipuhi Road
150	W01 0119	Matahi Basalt	V15/260423	Road cut on State Highway 30, near Matahi Lagoon, southern shore of Lake Rotoma
151	W01 0120	Rotokawau Basalt	V15/104423	Outcrop on northwestern side of Lake Okataina Road

Table I.2: Sample catalogue listing analytical procedures performed on each sample and the nature of remaining samples held in the University of Waikato rock store.

Field No.	UOW Number	Rhyolite Lava	HS & TS	PC	VES	XRF	EMP			LA-ICPMS	Isotopes			Stored Sample
							Phen	GM	MI		Sr	Nd	Pb	
5	W01 0001	Pokohu Flow	x	x		x								R P T
6	W01 0002	Haroharo Dome	x	x	x	x	x	x	x	x	x			R P T
7	W01 0003	Hainini Dome	x	x	x	x	x	x	x	x	x	x		R P T
14	W01 0004	Waiti Flow	x	x	x	x								R P T
15	W01 0005	Waiti Flow	x	x	x	x								R P T
17	W01 0006	Waiti Flow	x	x	x	x				x				R P T
19	W01 0007	Te Horoa Dome	x	x	x	x								R P T
20	W01 0008	Rotoroniu Flow	x	x	x	x								R P T
22	W01 0009	Te Koutu Flow	x	x	x	x								R P T
23	W01 0010	Te Koutu Flow	x	x		x								R P T
24	W01 0011	Okataina Flow	x	x	x	x	x	x	x	x	x	x	x	R P T
25	W01 0012	Okataina Flow	x	x		x								R P T
26	W01 0013	Oruaroa Flow	x	x		x								R P T
27	W01 0014	Otangimoana Flow	x	x	x	x								R P T
30	W01 0015	Te Horoa Dome	x	x	x	x								R P T
32	W01 0016	Te Horoa Dome	x	x		x	x			x	x			R P T
33	W01 0017	Rotoroniu Flow	x	x	x	x								R P T
34	W01 0018	Ruakokopu Flow	x	x	x	x								R P T
35	W01 0019	Ruakokopu Flow	x	x	x	x								R P T
36	W01 0020	Tapahoro Flow	x	x	x	x				x				R P T
37	W01 0021	Pokohu Flow	x	x	x	x								R P T
38	W01 0022	Waikakareao Flow	x	x	x	x	x			x	x			R P T
40	W01 0023	Te Puha Flow	x	x		x								R P T
41	W01 0024	Te Puha Flow	x	x	x	x								R P T
44	W01 0025	Western Dome	x	x	x	x	x			x	x			R P T
45	W01 0026	Wahanga Dome	x	x	x	x								R P T
46	W01 0027	Ruawahia Dome	x	x	x	x								R P T
52	W01 0028	Ngongotaha (Quarry)	x	x		x								R P T
54	W01 0029	Ngongotaha (Quarry)	x	x	x	x								R P T
56	W01 0030	Haumingi Flow	x	x	x	x								R P T
58	W01 0031	Waitangi	x	x		x								R P T
59	W01 0032	Maungawhakamana	x	x		x								R P T
60	W01 0033	Te Pohue Flow	x	x	x	x	x	x	x	x	x			R P T
61	W01 0034	Tuarae Flow	x	x		x								R P T
63	W01 0035	Stancorp Quarry	x	x		x	x			x				R P T
64	W01 0036	Tutaeheka 1	x	x	x	x	x			x	x			R P T
65	W01 0037	Eastern Rhyolite	x	x		x								R P T
68	W01 0038	Direct Road	x	x	x	x								R P T
70	W01 0039	Hill Road	x	x	x	x								R P T
72	W01 0040	Moerangi Road	x	x		x	x			x	x	x	x	R P T
73	W01 0041	Chestnut Road	x	x		x								R P T
74	W01 0042	Green Lake	x	x		x								R P T
78	W01 0043	Kakapiko	x	x	x	x								R P T
79	W01 0044	Rotokohu Dome	x	x	x	x				x				R P T
81	W01 0045	Hainini Flow	x	x	x	x								R P T
84	W01 0046	Tokorangi	x	x		x				x				R P T
85	W01 0047	Hinemoa Point	x	x	x	x								R P T
86	W01 0048	Kawaha Point	x	x		x				x	x	x	x	R P T
87	W01 0049	Endean Road	x	x		x	x			x	x			R P T
90	W01 0050	Ridge Flow	x	x		x	x			x	x	x		R P T
92	W01 0051	Fentons Mill Flow	x	x	x	x	x	x		x	x			R P T
95	W01 0052	Waiti Flow	x	x	x	x								R P T
96	W01 0053	Waiti Flow	x	x		x								R P T
98	W01 0054	Tikorangi Dome	x	x	x	x	x	x	x	x	x			R P T
99	W01 0055	Maungawhakamana	x	x		x								R P T
100	W01 0056	Maungawhakamana	x	x		x								R P T
101	W01 0057	Maungawhakamana	x	x		x				x				R P T
103	W01 0058	Mokoia Island	x	x		x	x			x	x			R P T
104	W01 0059	Vaughan Road	x	x	x	x	x			x	x	x		R P T
105	W01 0060	Rotoma Flow	x	x	x	x	x	x	x	x	x			R P T
106	W01 0061	Rotoma Flow	x	x	x	x								R P T
107	W01 0062	North Rotoma	x	x	x	x	x			x	x			R P T
108	W01 0063	Maungawhakamana	x	x		x								R P T
109	W01 0064	Matawhaura	x	x		x	x			x	x	x	x	R P T

Field No.	UOW Number	Rhyolite Lava	HS & TS	PC	VES	XRF	EMP			LA-ICPMS	Isotopes			Stored Sample
							Phen	GM	MI		Sr	Nd	Pb	
110	W01 0065	Whakapoungakau	x	x		x				x	x			R P T
111	W01 0066	Crater Farm	x	x		x								R P T
113	W01 0067	Eastern Rhyolite	x	x	x	x	x			x	x			R P T
114	W01 0068	Eastern Rhyolite	x	x	x	x								R P T
117	W01 0069	Tutaeheka 3	x	x		x	x			x				R P T
118	W01 0070	Tutaeheka 3	x	x	x	x								R P T
119	W01 0071	Wairua	x	x		x	x			x	x	x		R P T
120	W01 0072	Hamurana	x	x		x				x	x			R P T
121	W01 0073	Upper Atiamuri	x			x								R P T
123	W01 0074	Upper Atiamuri	x			x								R P T
126	W01 0075	Horohoro	x	x		x	x			x	x			R P T
127	W01 0076	Round Hill	x	x	x	x								R P T
128	W01 0077	Hapeotoroa	x	x	x	x				x				R P T
129	W01 0078	Waimangu	x	x		x								R P T
130	W01 0079	Patiti Island	x	x	x	x				x	x			R P T
133	W01 0080	Green Lake Plug	x	x	x	x								R P T
134	W01 0081	Rotomahana Dome	x	x		x	x			x	x			R P T
135	W01 0082	Western Dome	x	x	x	x								R P T
137	W01 0083	Hemo Gorge	x	x		x								R P T
138	W01 0084	Makatiti Dome	x	x	x	x								R P T
141	W01 0085	Makatiti Flow	x	x	x	x								R P T
142	W01 0086	Makatiti Flow	x	x		x								R P T
143	W01 0087	Makatiti Flow	x	x	x	x								R P T
144	W01 0088	Te Pohue Flow	x			x								R P T
145	W01 0089	Kaipara Flow	x			x								R P T
146	W01 0090	Pukepoto	x	x		x								R P T
147	W01 0091	Pokohu Flow	x	x	x	x								R P T
149	W01 0092	Waikakareao Flow	x	x		x								R P T
152	W01 0093	Blue Lake	x	x		x	x			x	x	x		R P T
153	W01 0094	Trig 7693 Dome	x	x	x	x								R P T
154	W01 0095	Ngongotaha (Gondola)	x	x		x								R P T
156	W01 0096	Crater Dome	x	x	x	x								R P T
157	W01 0097	Crater Dome	x	x	x	x								R P T
158	W01 0098	Tarawera Dome	x	x	x	x	x			x	x	x	x	R P T
159	W01 0099	Pukehangi (Te Miri)	x	x		x				x				R P T
160	W01 0100	Tutaeheka 2	x	x		x				x	x			R P T
162	W01 0101	Tutaeheka 2	x	x		x								R P T
164	W01 0102	Tutaeheka 3	x	x	x	x								R P T
165	W01 0103	Tumunui	x	x		x				x				R P T
167	W01 0104	Dome 2	x	x		x								R P T
168	W01 0105	Dome 3	x	x		x				x	x			R P T
169	W01 0106	Waikorapa	x	x		x								R P T
170	W01 0107	Ongahoro	x	x	x	x	x			x	x	x	x	R T
171	W01 0108	North Ridge	x	x		x								R P T
172	W01 0109	Haparangi	x	x		x								R P T
173	W01 0110	Waiti Flow	x	x		x	x	x	x	x	x			R T
174	W01 0111	Te Rere Dome	x	x		x								R P T
175	W01 0112	Middle Rhyolite	x	x	x	x								R P T
176	W01 0113	Trig 7693 Dome	x	x	x	x	x			x	x			R T
47	W01 0114	Tarawera Basalt				x								R P T
48	W01 0115	Tarawera Basalt				x								R P T
124	W01 0116	Johnson Rd Basalt				x								R P T
136	W01 0117	Rotomakariri Scoria				x								R P T
148	W01 0118	Okareka Basalt				x								R P T
150	W01 0119	Matahi Basalt				x								P T
151	W01 0120	Rotokawau Basalt				x								R P T

HS & TS: Hand specimen and thin section characteristics have been documented (Appendix IV).
PC: Thin section has been point counted (Appendix III).
VES: Hand specimen vesicularity has been determined (Appendix II).
XRF: Whole rock major and trace elements determined by X-ray fluorescence (XRF) (Appendix V).
EMP: Phenocryst (Appendix VI), glass groundmass (Appendix VIII) and melt inclusion (Appendix VIII) major element compositions have been determined by Electron Microprobe (EMP).
LA-ICPMS: Whole rock trace and rare earth elements determined by laser ablation-inductively coupled plasma mass spectrometry (LA-ICPMS) (Appendix V).
Isotopes: Sr, Nd and Pb isotopes determined by thermal ionisation mass spectrometry (TIMS) (Table 6.1 & 6.2).
Stored Sample: Sample stored in the University of Waikato rock store as rock (R), powder (P) or thin section (T).

Appendix II: Vesicularity Calculations

Table II.1: Vesicularity calculations.

Sample Number	Specific Gravity	Vesicularity	
		%	Classification
6	1.66	31	poorly vesicular
7	2.05	15	incipiently vesicular
14	1.72	29	poorly vesicular
15	0.74	69	highly vesicular
17	1.07	55	moderately vesicular
19	2.12	12	incipiently vesicular
20	2.20	8	incipiently vesicular
22	2.14	11	incipiently vesicular
24	1.71	29	poorly vesicular
27	2.20	8	incipiently vesicular
30	1.95	19	incipiently vesicular
33	1.94	19	incipiently vesicular
34	1.74	28	poorly vesicular
35	2.18	9	incipiently vesicular
36	2.05	15	incipiently vesicular
37	1.42	41	moderately vesicular
38	2.01	16	incipiently vesicular
41	2.21	8	incipiently vesicular
44	2.36	2	non-vesicular
45	1.82	24	poorly vesicular
46	1.01	58	moderately vesicular
54	1.39	42	moderately vesicular
56	1.72	28	poorly vesicular
60	2.01	16	incipiently vesicular
64	1.88	22	poorly vesicular
68	1.64	32	poorly vesicular
70	1.67	30	poorly vesicular
78	1.76	27	poorly vesicular
79	1.66	31	poorly vesicular
81	1.69	29	poorly vesicular
85	1.62	32	poorly vesicular
92	2.14	11	incipiently vesicular
95	1.93	19	incipiently vesicular
98	1.62	32	poorly vesicular
104	1.60	33	poorly vesicular
105	1.71	29	poorly vesicular
106	1.18	51	moderately vesicular
107	1.90	21	poorly vesicular
113	2.15	10	incipiently vesicular
114	1.82	24	poorly vesicular
118	1.97	18	incipiently vesicular
127	1.43	41	moderately vesicular
128	1.77	26	poorly vesicular
130	1.79	25	poorly vesicular
133	1.91	20	poorly vesicular
135	1.77	26	poorly vesicular
138	1.64	32	poorly vesicular
141	1.40	42	moderately vesicular
143	1.53	36	poorly vesicular
147(1)	2.23	7	incipiently vesicular
147(2)	1.57	34	poorly vesicular
153	1.72	28	poorly vesicular
156	1.86	22	poorly vesicular
157	1.63	32	poorly vesicular
158	1.70	29	poorly vesicular
164	1.75	27	poorly vesicular
170	1.68	30	poorly vesicular
175	0.89	63	highly vesicular
176	1.59	34	poorly vesicular

Specific gravity and vesicularity have been determined using the procedure of Houghton and Wilson (1989). Vesicularity calculations assume a dense rock equivalent value of 2.4 g/cm^3.

Appendix III: Point Count Results

Table III.1: Point count results for rhyolite lavas from the Okataina, Rotorua & Kapenga volcanic centres.
(No. of points = 1000. Grid size = 750 microns)

	Ferromagnesian Assemblage	Sample No.	Phenocrysts (percentage of total rock)						Total Phenocrysts	Total Groundmass
			Plagioclase Feldspar	Quartz	Pyroxene	Amphibole	Biotite	Fe-Ti Oxides		
Okataina Volcanic Centre										
ho_1 rhyolites										
Northeastern										
Waitangi	Opx + Ca-Amph	58	10.4	1.8	0.9	0.2	-	0.9	14.2	85.8
Maungawhaka-	Opx ± Ca-Amph	59	6.1	2.4	0.7	tr	-	0.5	9.7	90.3
mana		99	5.9	2.4	1.0	0.6	-	0.7	10.6	89.4
		100	3.4	1.1	0.3	-	-	0.3	5.1	94.9
		101	12.0	0.6	1.4	1.3	-	1.0	16.3	83.7
		108	11.7	0.3	0.9	1.2	-	0.7	14.8	85.2
North Rotoma	Bio+Ca-Amph+Cgt	107	11.5	4.1	-	2.1	2.5	1.3	21.5	78.5
Matawhaura	Opx + Ca-Amph	109	5.1	7.4	0.9	0.6	-	1.3	15.3	84.7
Western										
Stancorp	Opx ± Ca-Amph	63	10.0	2.3	1.1	tr	-	0.6	14.0	86.0
Whakapounga-	Ca-Amph+Bio+Opx	110	10.3	5.3	0.3	1.6	0.6	0.6	18.7	81.3
kau										
Crater Farm	Opx + Ca-Amph	111	13.2	tr	1.8	0.3	-	0.7	16.0	84.0
Pukepoto	Opx+Ca-Amph+Bio	146	7.1	0.3	1.7	0.7	0.2	0.9	10.9	89.1
Southern										
Wairua	Ca-Amph+Bio+Opx	119	20.6	9.6	0.3	2.4	1.8	1.1	35.8	64.2
ho_2 rhyolites										
Moerangi										
Direct Road	Opx + Ca-Amph	68	12.2	1.9	1.8	0.4	-	0.5	16.8	83.2
Hill Road	Opx ± Ca-Amph	70	13.5	1.7	1.1	tr	-	0.4	16.7	83.3
Moerangi Road	Opx + Ca-Amph	72	11.6	5.3	1.4	0.8	-	0.8	19.9	80.1
Chestnut Road	Opx + Ca-Amph	73	13.2	4.9	1.8	0.5	-	0.6	21.0	79.0
Green Lake	Opx+Ca-Amph±Bio	74	19.5	4.2	1.7	0.7	tr	0.9	27.0	73.0
Kakapiko	Bio+Ca-Amph+Opx	78	15.5	6.5	0.6	1.1	2.0	0.7	26.4	73.6
Blue Lake	Ca-Amph+Bio+Opx	152	20.3	3.0	1.6	2.0	1.7	1.1	29.7	70.3
Tutaeheka										
Tutaeheka 1	Bio+Ca-Amph±Opx	64	16.5	5.9	tr	0.8	3.3	0.6	27.1	72.9
Tutaeheka 2	Opx+Ca-Amph±Bio	160	12.9	5.2	1.9	1.4	-	0.7	22.1	77.9
		162	11.6	2.4	1.4	0.6	tr	0.6	16.6	83.4
Tutaeheka 3	Opx+Ca-Amph±Bio	117	17.3	3.8	1.3	1.3	-	0.8	24.5	75.5
		118	20.3	3.1	1.3	1.1	-	0.7	26.5	73.5
		164	14.4	1.9	1.5	1.7	tr	0.6	20.1	79.9
Sth Rotomahana										
Hapeotoroa	Bio+Ca-Amph+Opx	128	17.5	8.4	0.2	0.7	3.4	0.7	30.9	69.1
Waimangu	Bio+Ca-Amph±Opx	129	20.4	7.2	tr	1.1	2.9	0.7	32.3	67.7
ho_3 rhyolites										
Te Rere Episode										
Te Koutu Flow	Opx + Ca-Amph	22	9.3	tr	1.2	0.8	-	0.6	11.9	88.1
		23	6.6	tr	0.5	0.6	-	0.5	8.2	91.8
Haumingi Flow	Opx + Ca-Amph	56	5.9	tr	0.2	0.4	-	0.5	7.0	93.0
Tuarae Flow	Opx + Ca-Amph	61	7.8	0.3	0.7	0.5	-	0.6	9.9	90.1
Fenton's Mill	Opx + Ca-Amph	92	8.1	0.2	0.5	0.4	-	0.6	9.8	90.2
Eastern	Opx+Ca-Amph±Bio	65	11.8	0.2	2.0	1.4	tr	1.4	16.8	83.2
Rhyolite		113	11.9	0.4	2.2	0.9	0.2	0.9	16.5	83.5
		114	9.1	0.2	1.3	0.6	-	0.6	11.8	88.2

	Ferromagnesian Assemblage	Sample No.	Phenocrysts (percentage of total rock)						Total Phenocrysts	Total Groundmass
			Plagioclase Feldspar	Quartz	Pyroxene	Amphibole	Biotite	Fe-Ti Oxides		
ho_3 rhyolites										
Te Rere Episode (continued)										
Te Rere Dome	Opx + Ca-Amph	174	14.3	3.4	2.3	0.6	-	0.7	21.3	78.7
Okareka Episode										
Ridge Flow	Opx+Ca-Amph±Bio	90	12.2	0.2	1.4	0.7	tr	0.7	15.2	84.8
Patiti Island	Ca-Amph + Opx	130	18.0	0.7	1.8	2.7	-	1.0	24.2	75.8
Rerewhakaaitu Episode										
Te Puha Flow	Ca-Amph±Opx±Bio	40	4.8	0.7	0.5	0.2	-	0.4	6.6	93.4
		41	14.4	3.1	tr	0.9	2.7	0.7	21.8	78.2
Western Dome	Opx+Ca-Amph±Bio	44	17.0	0.8	2.1	1.5	-	1.0	22.4	77.6
		135	15.4	1.7	1.2	2.4	0.2	1.2	22.1	77.9
Rotomahana Dome	Bio+Ca-Amph±Opx	134	19.2	5.0	tr	0.9	2.7	0.9	28.7	71.3
Rotorua Episode										
Trig 7693	Bio + Ca-Amph	153	11.4	4.9	-	0.2	3.3	0.6	20.4	79.6
Dome		176	11.6	4.1	-	0.3	3.1	1.0	20.1	79.9
Middle Rhyolite	Bio + Ca-Amph	175	9.0	4.4	-	0.3	2.7	0.4	16.8	83.3
Waiohau Episode										
Pokohu Flows	Opx ± Ca-Amph	5	8.1	0.7	1.3	-	-	0.7	10.8	89.2
		37	3.9	1.1	1.2	tr	-	0.5	6.7	93.3
		147	7.3	1.0	0.6	tr	-	0.7	9.6	90.4
Waikakareao	Opx ± Ca-Amph	38	5.6	0.9	0.7	tr	-	0.5	7.7	92.3
Flows		149	5.0	1.1	0.4	-	-	0.7	7.2	92.8
Rotoma Episode										
Te Pohue Flows	Cgt+Ca-Amph±Opx	60	10.1	1.5	tr	1.5	-	0.7	13.8	86.2
Rotoma Flows	Ca-Amph+Opx±Cgt	105	7.5	0.3	0.5	1.7	-	0.7	10.7	89.3
		106	6.7	0.6	0.7	1.1	-	0.7	9.8	90.2
Mamaku Episode										
Hainini Dome	Opx+Ca-Amph±Cgt	7	10.3	3.4	1.1	0.9	-	0.6	16.3	83.7
Waiti Flow	Opx+Ca-Amph±Cgt	14	10.3	0.3	1.0	1.6	-	0.6	13.8	86.2
		15	5.8	0.7	0.6	1.0	-	0.5	8.6	91.4
		17	6.2	tr	0.4	0.7	-	0.7	8.0	92.0
		95	10.5	0.3	1.9	1.3	-	1.0	15.0	85.0
		96	10.5	0.5	1.6	1.0	-	0.8	14.4	85.6
		173	11.1	0.3	1.2	1.5	-	0.7	14.8	85.2
Te Horoa	Opx+Ca-Amph±Cgt	19	11.3	4.6	1.1	0.8	-	0.7	18.5	81.5
Dome		30	11.3	1.8	1.1	0.4	-	0.9	15.5	84.5
		32	10.0	3.0	1.8	0.7	-	0.7	16.2	83.8
Oruaroa Flow	Opx+Ca-Amph±Cgt	26	11.1	4.0	1.1	0.7	-	0.6	17.5	82.5
Otangimoana Flow	Opx+Ca-Amph±Cgt	27	12.3	2.6	1.4	0.8	-	0.6	17.7	82.3
Ruakokopu	Opx+Ca-Amph±Cgt	34	9.6	2.7	0.5	0.8	-	0.4	14.0	86.0
Flow		35	10.5	2.5	0.8	0.4	-	0.9	15.1	84.9
Hainini Flow	Opx+Ca-Amph±Cgt	81	8.0	1.7	1.3	0.4	-	0.6	12.0	88.0
Whakatane Episode										
Haroharo Dome	Cgt+Opx±Ca-Amph	6	8.9	1.9	0.2	1.3	-	0.8	13.1	86.9
Rotoroniu	Cgt+Opx±Ca-Amph	20	9.8	4.5	0.9	0.7	-	0.8	16.7	83.3
Flows		33	9.4	3.4	0.5	0.9	-	0.6	14.8	85.2

	Ferromagnesian Assemblage	Sample No.	Phenocrysts (percentage of total rock)						Total Phenocrysts	Total Groundmass
			Plagioclase Feldspar	Quartz	Pyroxene	Amphibole	Biotite	Fe-Ti Oxides		
ho_3 rhyolites										
Whakatane Episode (continued)										
Okataina Flow	Cgt+Opx±Ca-Amph	24	8.5	1.9	0.3	0.8	-	0.5	12.0	88.0
		25	7.8	2.5	1.0	1.1	-	0.8	13.2	86.8
Tapahoro Flows	Ca-Amph+Opx±Cgt	36	6.2	2.9	0.4	1.0	-	0.5	11.0	89.0
Rotokohu Dome	Cgt+Opx±Ca-Amph	79	6.9	2.9	0.5	1.6		0.9	12.8	87.2
Tikorangi Dome	Ca-Amph+Opx±Cgt	98	9.7	1.6	0.9	1.4	-	0.7	14.3	85.7
Makatiti Dome	Cgt+Opx±Ca-Amph	138	7.1	2.5	0.4	0.9	-	0.8	11.7	88.3
Makatiti Flows	Cgt+Opx±Ca-Amph	141	8.4	3.4	0.2	0.9	tr	0.7	13.6	86.4
	± Bio	142	10.9	4.2	0.6	0.9	-	0.8	17.4	82.6
		143	10.2	2.4	0.6	0.8	-	0.7	14.7	85.3
Kaharoa Episode										
Wahanga Dome	Bio ± Opx	45	15.0	4.8	tr	-	3.9	1.0	24.7	75.3
Ruawahia Dome	Bio + Ca-Amph	46	14.2	4.9	-	0.2	3.9	0.8	24.0	76.0
Green Lake Plg	Bio+Opx±Ca-Amph	133	8.9	4.0	0.7	tr	1.9	0.5	16.0	84.0
Crater Dome	Bio + Ca-Amph	156	15.6	5.4	-	0.2	3.7	0.9	25.8	74.2
		157	14.1	5.1	-	0.2	3.9	0.8	24.1	75.9
Tarawera Dome	Bio+Ca-Amph±Opx	158	14.1	5.1	tr	0.2	3.4	0.8	23.6	76.4
Rotorua Volcanic Centre										
hr_1 rhyolites										
Tokorangi	Opx	84	3.0	1.0	0.2	-	-	0.3	4.5	95.5
Endean Road	Opx+Ca-Amph+Bio	87	13.2	4.9	1.6	1.3	1.3	0.9	23.2	76.8
Hamurana	Opx ± Ca-Amph	120	11.6	0.3	1.6	tr	-	0.9	14.4	85.6
Hemo Gorge	-	137	2.4	0.8	-	-	-	0.3	3.5	96.5
hr_2 rhyolites										
Ngongotaha (Quarry Dome)	Opx ± Ca-Amph	52	5.8	0.2	1.2	tr	-	0.7	7.9	92.1
		54	3.4	-	0.5	-	-	0.5	4.4	95.6
Kawaha Point	Opx	86	6.8	tr	1.0	-	-	0.8	8.6	91.4
Ngongotaha (Gondola Dome)	Opx	154	4.8	tr	1.5	-	-	0.9	7.2	92.8
Pukehangi (Te Miri Dome)	Opx	159	6.2	tr	0.7	-	-	0.8	7.7	92.3
hr_3 rhyolites										
Hinemoa Point	Bio+Ca-Amph+Opx	85	19.2	4.8	0.6	1.7	2.4	1.1	29.8	70.2
Mokoia Island	Ca-Amph + Opx	103	18.2	6.4	1.5	1.9	-	1.0	29.0	71.0
Vaughan Road	Bio+Ca-Amph+Opx	104	20.4	3.3	0.5	1.7	2.7	0.8	29.4	70.6
Kapenga Volcanic Centre										
hk_1 rhyolites										
Horohoro	Opx ± Ca-Amph	126	10.6	1.8	1.6	tr	-	0.9	14.9	85.1
Tumunui	Opx + Ca-Amph	165	7.8	0.4	0.7	0.5	-	0.7	10.1	89.9
Waikorapa	Opx+Ca-Amph±Bio	169	4.8	1.4	0.5	0.2	tr	0.4	7.3	92.7
Nth Haparangi	Opx	171	4.2	0.2	0.6	-	-	0.5	5.5	94.5
hk_2 rhyolites										
Round Hill	Bio+Ca-Amph+Opx	127	12.3	5.0	0.9	1.5	2.9	0.6	23.2	76.8
Dome 2	Bio+Ca-Amph+Opx	167	13.6	4.6	1.5	1.1	2.5	0.9	24.2	75.8
Dome 3	Bio+Ca-Amph+Opx	168	10.4	8.9	0.7	1.5	2.3	0.6	24.4	75.6
Ongahoro	Ca-Amph+Bio+Opx	170	17.0	5.7	0.7	2.8	1.7	0.8	28.7	71.3
Haparangi	Bio+Ca-Amph+Opx	172	13.3	6.5	0.7	1.0	3.3	0.7	25.5	74.5

Appendix IV: Hand Specimen and Thin Section Descriptions

Table IV.1: Hand specimen and thin section descriptions of ho_1 rhyolite lavas.

Rhyolite	Sample No.	Hand Specimen	Thin Section (Groundmass)
Northeastern			
Waitangi	58	Medium grey rhyolite with some darker grey flow bands.	Crystallised, spherulitic glass. Glass between spherulites is near colourless and contains perlitic cracks and quench crystals.
Maungawhakamana	59	Finely flow banded with black obsidian bands and pink bands of spherulitic material. Individual spherulites can be seen.	Flow banded with two textural types: 1) Non-vesicular glass containing perlitic cracks and quench crystals aligned with flow bands. 2) Crystallised, spherulitic glass.
	99	Blue/grey rhyolite with black obsidian flow bands.	Crystallised, spherulitic glass. Flow banding defined by coalescing spherulites, axiolitic bands, opaque fibre/corroded quench crystal alignment and small lenses of non-vesicular, non-spherulitic glass.
	100	Medium grey rhyolite, with patches of black obsidian. Pink/white spherulites can be seen.	Crystallised, spherulitic glass. Flow banding defined by coalescing spherulites and bands of opaque fibres/corroded quench crystals.
	101	Light brown/grey rhyolite. Black prismatic phenocrysts noticeable.	Crystallised, spherulitic glass. Patches/bands of non-vesicular, near colourless glass contain perlitic cracks and aligned quench crystals/opaque fibres.
	108	Medium brown rhyolite.	Crystallised, spherulitic glass. Flow banding defined by spherulite coalescing, elongation and axiolitic bands.
North Rotoma	107	Pale brown/grey rhyolite with an orange weathering colouration. Black platy and prismatic phenocrysts noticeable.	Poorly vesicular, weakly devitrified glass with a classical perlite texture. Minor small spherulites present. Alignment of quench crystals suggests flow direction as does stretching and elongation of vesicles.
Matawhaura	109	Dark grey rhyolite with white individual spherulites and spherulitic bands. Flow bands vary from coarse to fine.	Flow banded with two textural types: 1) Non-vesicular, near colourless glass containing perlitic cracks and abundant aligned quench crystals. 2) Crystallised, spherulitic glass containing large finger-like spherulites. Dense bands of quench crystals cut across both flow band types.
Western			
Stancorp Quarry	63	Brown-purple rhyolite containing abundant spherulites. Some dark grey glassy patches. Discontinuous flow bands.	Crystallised, spherulitic glass. Discontinuous flow banding defined by variations in spherulite morphology.
Whakapoungakau	110	Medium grey/brown rhyolite. Some alignment of black prismatic phenocrysts noticeable.	Crystallised, spherulitic glass. Mosaic of coalesced spherulitic material.
Crater Farm	111	Discontinuous flow bands of dark grey/black obsidian and pink/white spherulitic material.	Flow banded with two textural types: 1) Non-vesicular, near colourless, cracked glass containing aligned quench crystals. 2) Crystallised, spherulitic glass containing corroded quench crystals/opaque fibres.
Pukepoto	146	Blue/grey and pink rhyolite. Spherulites visible.	Crystallised, spherulitic glass. Mosaic of coalesced spherulitic material. Some alignment of corroded quench crystals/opaque fibres.
Southern			
Wairua	119	Cream/light grey rhyolite. Phenocryst rich with black prismatic and platy phenocrysts noticeable.	Crystallised, spherulitic glass. Mosaic of coalesced spherulitic material. Small patches of non-devitrified glass contain perlitic cracks and quench crystals.

Table IV.2: Hand specimen and thin section descriptions of ho_2 rhyolite lavas.

Rhyolite	Sample No.	Hand Specimen	Thin Section (Groundmass)
Moerangi Rhyolites			
Direct Road	68	Light grey pumiceous rhyolite.	Poorly vesicular glass with vesicles stretched due to flow. Glass contains cracks. Minor spherulites.
Hill Road	70	Light grey pumiceous rhyolite.	Poorly vesicular glass with vesicles stretched due to flow. Glass contains cracks. Minor spherulites.
Moerangi Road	72	Medium brown rhyolite.	Crystallised, spherulitic glass. Mosaic of coalesced spherulitic material.
Chestnut Road	73	Medium brown/grey rhyolite. Slight colour variations highlight flow bands.	Crystallised, spherulitic glass. Mosaic of coalesced spherulitic material. Elongated & axiolitic growths define flow direction.
Green Lake	74	Pink and blue/grey rhyolite. Colour variations highlight fine discontinuous flow bands.	Crystallised, spherulitic glass. Mosaic of coalesced spherulitic material.
Kakapiko	78	Cream pumiceous rhyolite. Phenocryst rich with abundant black platy phenocrysts.	Poorly vesicular glass with tubular subparallel vesicles due to flow. Less vesicular areas of glass contain cracks. Minor spherulites.
Blue Lake	152	Medium grey rhyolite. Spherulites are visible and grey crenulated spherulitic bands occur. Colourless (prismatic) and black (prismatic and platy) phenocrysts noticeable.	Crystallised, spherulitic glass. Mosaic of coalesced spherulitic material. Axiolitic textures and spherulite colour variations suggest flow banding.
Tutaeheka Rhyolites			
Tutaeheka 1	64	Medium grey rhyolite containing discontinuous black obsidian bands. Black platy phenocrysts abundant. Some alignment of phenocrysts. Coarse sugary texture.	Overall poorly vesicular glass, with more and less vesicular flow bands. Glass contains bands of quench crystals and cracks. Minor spherulites.
Tutaeheka 2	160	Medium brown rhyolite. Flow direction suggested by phenocryst alignment.	Crystallised, spherulitic glass. Mosaic of coalesced spherulitic material. Flow direction defined by coalescing spherulites.
	162	Medium grey/brown rhyolite. Flow banding defined by slight colour variations and alignment of phenocrysts.	Crystallised, spherulitic glass. Mosaic of coalesced spherulitic material. Flow banding defined by elongated and coalescing spherulites.
Tutaeheka 3	117	Light grey/brown rhyolite. Some alignment of black prismatic phenocrysts.	Crystallised, spherulitic glass. Mosaic of coalesced spherulitic material. Interstitial areas have an equigranular texture.
	118	Medium grey rhyolite. Phenocryst rich with some alignment of colourless prismatic phenocrysts.	Incipiently vesicular with tubular subparallel vesicles. Minor cracks occur in the glass.
	164	Light grey pumiceous rhyolite. Flow defined by slight colour variation. Some alignment of black prismatic phenocrysts.	Overall poorly vesicular glass, some sections of glass are moderately vesicular with tubular subparallel vesicles, others are incipiently vesicular with noticeable cracks. Minor spherulitic growths.
South Rotomahana Rhyolites			
Hapeotoroa	128	Light grey/brown pumiceous rhyolite. Flow banding defined by colour variation. Phenocryst rich.	Poorly vesicular glass with elongation of vesicles due to flow. Minor cracks. Minor spherulitic material.
Waimangu	129	Pink phenocryst rich rhyolite. Slight colour variations define flow bands.	Crystallised, spherulitic glass. Glass between spherulites is near colourless and contains perlitic cracks and quench crystals.

Table IV.3: Hand specimen and thin section descriptions of ho_3 rhyolite lavas.

Rhyolite	Sample No.	Hand Specimen	Thin Section (Groundmass)
Haroharo Complex			
Te Rere Episode			
Te Koutu Flow	22	Medium grey glassy rhyolite containing crenulated white bands.	Incipiently vesicular cracked glass. Vesicles stretched due to flow. Contains crenulated bands of densely packed quench crystals and minor spherulitic material.
	23	Dark grey/black obsidian with abundant white/pink spherulites.	Highly cracked, non-vesicular glass containing aligned quench crystals which define flow direction. Singular spherulites and coalesced masses abundant.
Haumingi Flow	56	Light and medium grey flow banded rhyolite. Medium grey bands appear less vesicular than light grey bands.	Highly (coarsely) vesicular, poorly vesicular and devitrified glass flow bands. Less vesicular bands contain cracks.
Tuarae Flow	61	Black obsidian with dark grey flow bands. Individual pink spherulites and spherulite clusters are present.	Highly cracked, non-vesicular glass containing aligned quench crystals which define flow direction. Singular spherulites, coalesced masses and axiolitic bands. Minor stretched vesicles.
Fenton's Mill Flow	92	Grey/black obsidian – flow banding defined by slight colour variation.	Incipiently vesicular glass containing aligned quench crystals and stretched vesicles which define flow direction. Cracks occur in the glass. Rare spherulites present.
Rotoma Episode			
Te Pohue Flow	60	Light grey sub-angular rhyolite block from an autobreccia. Block sits in a brown ash matrix. Black prismatic phenocrysts are noticeable in the block.	Rhyolite block consists of incipiently vesicular glass with vesicles stretched due to flow. Glass contains quench crystals and cracks. No spherulites present.
	144	Dark grey/black obsidian lapilli from an autobreccia. Lapilli are aligned and sit in a pinky-brown ash matrix.	Obsidian lapilli consist of cracked glass that varies from non-vesicular to incipiently vesicular, with vesicles stretched due to flow. Glass contains quench crystals. No spherulitic material present.
Rotoma Flow	105	Light grey/brown pumiceous rhyolite. Colour variation defines flow bands. Alignment of black prismatic phenocrysts.	Poorly vesicular glass with stretched, tubular vesicles due to flow. Less vesicular glass contains cracks. No spherulites present.
	106	Light grey pumiceous rhyolite with darker flow bands. Alignment of black prismatic phenocrysts.	Moderately, coarsely vesicular glass with oval and elongate vesicles. Less vesicular glass contains cracks. No spherulites.
Mamaku Episode			
Hainini Dome	7	Light grey rhyolite with pinky coloured patches. Some alignment of black prismatic phenocrysts.	Incipiently vesicular glass with vesicles stretched due to flow. Glass is cracked. Quench crystals present. Spherulites are rare.
Waiti Flow	14	Light grey rhyolite. Fine flow banding defined by slight colour variations. Some alignment of phenocrysts.	Poorly vesicular glass with vesicles stretched due to flow. Cracks present in the glass. No spherulites.
	15	Light grey pumiceous rhyolite.	Highly vesicular glass with round, oval, elongate and tubular vesicles. Vesicles stretched due to flow. Minor cracks in the glass. No spherulites.
	17	Light grey pumiceous rhyolite. Fine flow banding defined by slight colour variations.	Moderately vesicular glass with round, oval, elongate and tubular vesicles. Vesicles stretched due to flow. Minor cracks in the glass. No spherulites.
	95	Light grey rhyolite. Some alignment of black prismatic phenocrysts noticeable.	Incipiently vesicular glass with vesicles stretched due to flow. Cracks occur in the glass. No spherulites.
	96	Dark grey/black obsidian with abundant pink/white spherulites.	Highly cracked, non-vesicular glass. Singular spherulites and coalesced masses common. Quench crystals present.
	173	Dark grey/black obsidian. Some black prismatic phenocrysts noticeable.	Highly cracked, non-vesicular glass with stretching of vesicles due to flow. Glass contains quench crystals. No spherulites.

Rhyolite	Sample No.	Hand Specimen	Thin Section (Groundmass)
Haroharo Complex			
Mamaku Episode			
Te Horoa Dome	19	Medium grey rhyolite.	Highly cracked, incipiently vesicular glass. Vesicles stretched due to flow. Some quench crystals present. No spherulites.
	30	Light/medium grey rhyolite.	Incipiently vesicular glass containing stretched vesicles due to flow. Cracks present in the glass. No spherulites.
	32	Dark grey/black obsidian with some light grey spherulites.	Highly cracked, non-vesicular glass. Singular spherulites and coalesced masses common. Contains bands of aligned, densely packed quench crystals.
Oruaroa Flow	26	Medium grey rhyolite with some patches of black obsidian.	Highly cracked, non-vesicular to incipiently vesicular glass. Bands of quench crystals define flow direction. Some spherulites present.
Otangimoana Flow	27	Medium grey rhyolite.	Incipiently vesicular, highly cracked glass. Vesicles stretched due to flow. Quench crystals and crystallites present, sometimes aligned. Some spherulitic material.
Ruakokopu Flow	34	Light grey rhyolite. Some fine darker grey flow bands. Alignment of black prismatic phenocrysts with flow bands.	Poorly vesicular glass. Stretching of vesicles due to flow. Minor cracks. No spherulitic material.
	35	Light/medium grey rhyolite. Some alignment of black prismatic phenocrysts.	Highly cracked, incipiently vesicular glass. Stretching of vesicles due to flow. Minor spherulitic material.
Hainini Flow	81	Light grey rhyolite. Some darker flow bands. Alignment of black prismatic phenocrysts.	Poorly vesicular glass. Stretching of vesicles due to flow. Cracks occur in the glass. No spherulites.
Kaipara Flow	145	Light grey rhyolite with some darker grey flow bands. Hydrothermally altered.	Glass appears to have originally had a pumiceous texture. Primary minerals have been replaced by green/grey, isotropic secondary minerals.
Whakatane Episode			
Haroharo Dome	6	Light grey/brown pumiceous rhyolite with some darker flow bands. Black prismatic phenocrysts show some alignment with flow bands.	Poorly vesicular with round, oval, elongate and tubular vesicles. Glass contains cracks and quench crystals. No spherulites.
Rotoroniu Flow	20	Medium grey rhyolite. Slight colour variations define flow banding.	Incipiently vesicular, highly cracked glass. Stretching of vesicles due to flow. Rare spherulitic material.
	33	Light grey/brown rhyolite.	Incipiently vesicular glass. Stretching of vesicles due to flow. Cracks occur in the glass. No spherulitic material.
Okataina Flow	24	Light grey pumiceous rhyolite. Black prismatic phenocrysts show some alignment.	Poorly vesicular glass with round, oval, elongate and tubular vesicles. Vesicles stretched due to flow. Glass contains cracks and some quench crystals. No spherulites.
	25	Quite coarsely flow banded with pinky-grey bands and black obsidian bands containing white/pink spherulites.	Flow banded with two textural types: 1) Incipiently vesicular, highly cracked glass with vesicles stretched due to flow. Rare small spherulites. 2) Highly cracked, non-vesicular glass, large individual spherulites and clusters common.
Tapahoro Flow	36	Pinky-grey rhyolite with small patches of black obsidian.	Incipiently vesicular glass. Stretching of vesicles due to flow. Glass contains cracks and quench crystals. Rare spherulitic material.
Rotokohu Dome	79	Light/medium grey pumiceous rhyolite.	Poorly vesicular glass. Stretching of vesicles due to flow. Glass contains cracks. No spherulites.
Tikorangi Dome	98	Medium grey rhyolite with some darker grey flow bands.	Poorly vesicular glass. Stretching of vesicles due to flow. Glass contains cracks and abundant quench crystals. Rare spherulitic material.
Makatiti Dome	138	Light grey pumiceous rhyolite.	Poorly vesicular glass with round, oval, elongate and tubular vesicles. Vesicles stretched due to flow. Cracks occur in the glass. No spherulites.

Rhyolite	Sample No.	Hand Specimen	Thin Section (Groundmass)
Haroharo Complex			
Whakatane Episode			
Makatiti Flow	141	Medium grey pumiceous rhyolite.	Moderately vesicular glass with round, oval, elongate and tubular vesicles. Vesicles stretched due to flow. Quench crystals & cracks present. Minor spherulitic material.
	142	Dark grey/black obsidian.	Highly cracked, non-vesicular glass. Bands of quench crystals define flow direction. Rare bands of devitrified glass.
	143	Cream pumiceous rhyolite with light/medium grey flow bands.	Poorly vesicular glass with round, oval, elongate and tubular vesicles. Vesicles stretched due to flow. Cracks occur in the glass. No spherulitic material.
Okareka Complex			
Te Rere Episode			
Eastern Rhyolite	65	Dark grey rhyolite with abundant light grey spherulites. Some patches of dark grey/black obsidian.	Crystallised, spherulitic glass. Mosaic of coalesced spherulitic material with patches of non-vesicular near colourless glass in between. Bands of quench crystals.
	113	Medium/dark grey rhyolite. Flow bands defined by slight colour variations.	Incipiently vesicular glass. Flow indicated by stretched vesicles and alignment of quench crystals, which are abundant and densely packed. Glass contains cracks and rare spherulites.
	114	Medium grey rhyolite with darker grey flow bands. Some alignment of black prismatic phenocrysts.	Poorly vesicular glass with round, oval and elongated vesicles. Vesicles stretched due to flow. Minor cracks present. No spherulites.
Te Rere Dome	174	Light brown/grey rhyolite with flow banding defined by colour variations.	Crystallised, spherulitic glass. Mosaic of coalesced spherulitic material. Flow defined by spherulite morphology.
Rotorua Episode			
Trig 7693	153	Light grey/brown pumiceous rhyolite. Black (prismatic & platy) and large colourless (rounded) phenocrysts noticeable.	Poorly vesicular glass with round, oval, elongate and tubular vesicles. Vesicles stretched due to flow. Cracks are present in the glass. No spherulites.
	176	Light grey pumiceous rhyolite. Black prismatic and platy phenocrysts noticeable.	Poorly, coarsely vesicular glass with round, oval, elongate and tubular vesicles. Vesicles stretched due to flow. Cracks are present in the glass. No spherulites.
Middle Rhyolite	175	Light grey pumiceous rhyolite. Black prismatic and platy phenocrysts noticeable. Some large vesicles present.	Highly, coarsely vesicular glass with round, oval, elongate and tubular vesicles. Cracks are present in the glass. No spherulites.
Tarawera Complex			
Okareka Episode			
Ridge Flow	90	Dark grey/black obsidian with rare small white spherulites.	Highly cracked, non-vesicular glass. Aligned quench crystals define flow direction. Some spherulites present.
Patiti Island	130	Light grey rhyolite. Alignment of black and colourless prismatic phenocrysts suggests flow direction.	Poorly vesicular glass. Vesicles stretched due to flow. Glass contains cracks. Abundant quench crystals, sometimes aligned. No spherulites.
Rerewhakaaitu Episode			
Te Puha Flow	40	Black obsidian with a "breadcrust" exterior. Contains some white spherulites.	Highly cracked, non-vesicular glass which contains abundant aligned quench crystals which define flow direction. Some singular spherulites.
	41	Medium grey/pink rhyolite. Phenocryst rich. Black prismatic & platy phenocrysts abundant. Large (up to 5mm) colourless phenocryst clots.	Incipiently vesicular glass. Vesicles stretched due to flow. Glass contains cracks. Some spherulites.
Western Dome	44	Dark grey/black obsidian with some pink patches. Large black prismatic phenocrysts noticeable, showing some alignment.	Highly cracked, non-vesicular glass. Bands of quench crystals define flow direction. Some spherulites present.
	135	Grey rhyolite with some pinky flow bands.	Highly cracked, poorly vesicular glass. Some more vesicular patches. Areas of spherulitic material and devitrified glass. Some quench crystals.

Rhyolite	Sample No.	Hand Specimen	Thin Section (Groundmass)
Tarawera Complex			
Rerewhakaaitu Episode			
Rotomahana Dome	134	Medium grey, phenocryst rich rhyolite. Black prismatic and platy phenocrysts noticeable.	Crystallised, spherulitic glass. Mosaic of coalesced spherulitic material. Patches of non-vesicular, near colourless glass between spherulites contain perlitic cracks, quench crystals and opaque fibres.
Waiohau Episode			
Pokohu Flows	5	Medium grey rhyolite. Contains large radiating "star-like" light grey/white spherulites.	Crystallised, spherulitic glass. Mosaic of coalesced spherulitic material. Dominant are the large "star-like" spherulites seen in hand specimen.
	37	Light grey pumiceous rhyolite.	Moderately vesicular glass with round, oval, elongate and tubular vesicles. Cracks occur in the glass. No spherulites.
	147	Light/medium grey rhyolite. Some parts of the sample appear more vesicular. White/pink spherulitic material can be seen.	Glass varies between incipiently and poorly vesicular. Stretching of vesicles and alignment of quench crystals indicates flow direction. Cracks occur in the glass. Singular and coalesced spherulites present.
Waikakareao Flows	38	Dark grey/black obsidian with fine pink flow bands of spherulitic material, along which the rock preferentially splits.	Highly cracked, incipiently vesicular glass containing bands of aligned quench crystals and spherulitic material which define flow direction.
	149	Blue/grey and pink spherulitic rhyolite. Possibly amygdaloidal.	Crystallised, spherulitic glass. Mosaic of coalesced spherulitic material. Orientation suggests flow direction. No amygdales seen in thin section.
Kaharoa Episode			
Wahanga Dome	45	Light brown/grey phenocryst rich rhyolite. Black platy phenocrysts noticeable.	Poorly vesicular glass. Stretching of vesicles due to flow. Cracks present in the glass. No spherulites.
Ruawahia Dome	46	Light grey pumiceous rhyolite. Black platy phenocrysts noticeable.	Moderately vesicular glass with round, oval, elongate and tubular vesicles. Minor cracks present. No spherulites.
Green Lake Plug	133	Medium grey rhyolite with darker grey 'glassy' bands and patches. Whiteish colouration.	Poorly vesicular glass with round, oval, elongate and tubular vesicles. Vesicles stretched due to flow. Quench crystals aligned with flow. Minor cracks present. Rare spherulitic material.
Crater Dome	156	Light brown/cream rhyolite. Black platy phenocrysts abundant.	Poorly vesicular glass with round, oval, elongate and tubular vesicles. Minor cracks present. Some spherulitic material.
	157	Light grey pumiceous rhyolite. Black platy minerals abundant.	Poorly vesicular glass with round, oval, elongate and tubular vesicles. Cracks present in the glass. No spherulitic material.
Tarawera Dome	158	Light grey pumiceous rhyolite. Black platy minerals abundant.	Poorly vesicular glass with round, oval, elongate and tubular vesicles. Minor cracks present in the glass. No spherulitic material.

Table IV.4: Hand specimen and thin section descriptions of Rotorua Volcanic Centre rhyolite lavas.

Rhyolite	Sample No.	Hand Specimen	Thin Section (Groundmass)
hr_1			
Tokorangi	84	Grey-brown flow banded rhyolite with pink spherulitic bands and abundant light grey spherulites.	Crystallised, spherulitic glass. Mosaic of coalesced spherulitic material. Flow banding defined by alignment and morphology of spherulites and bands of quench crystals/opaque fibres.
Endean Road	87	Medium brown rhyolite. Phenocryst rich with large prismatic, black phenocrysts & large colourless phenocryst clots.	Crystallised, spherulitic glass. Mosaic of coalesced spherulitic material.
Hamurana	120	Pinky-brown rhyolite containing light blue-grey spherulites. Some spherulitic bands. Possibly lithophysal.	Crystallised, spherulitic glass. Flow banding defined by varying degrees of devitrification, spherulite morphology and alignment. No lithophysae seen in thin section.
Hemo Gorge	137	Black obsidian with abundant grey-cream spherulites.	Highly cracked, non-vesicular glass containing circular perlitic cracks and aligned quench crystals. Spherulitic material abundant. Flow direction suggested by quench crystal bands and alignment/morphology of spherulitic material.
hr_2			
Ngongotaha Quarry Dome	52	Black obsidian with pink/grey spherulites and spherulitic flow bands along which the rock splits. Pronounced conchoidal fracture.	Highly cracked, non-vesicular glass which is crowded with quench crystals. Alignment of quench crystals and bands of devitrified glass define flow direction. Some spherulite balls and coalesced masses.
	54	Pumiceous, light grey rhyolite with fine darker grey flow bands.	Moderately vesicular glass with oval, elongate and tubular vesicles. Vesicles stretched due to flow. No spherulites.
Ngongotaha Gondola Dome	154	Blue-grey spherulitic rhyolite. Some brown, aphanitic flow bands along which the rock splits.	Crystallised, spherulitic glass. Mosaic of coalesced spherulitic material. Flow banding defined by alignment of spherulites and bands of quench crystals/opaque fibres.
Kawaha Point	86	Medium-dark grey rhyolite with orange-brown (weathered) bands of spherulitic material.	Crystallised, spherulitic glass. Glass between spherulites is non-vesicular, near colourless and contains cracks, abundant aligned quench crystals and opaque fibres.
Pukehangi Te Miri Dome	159	Black obsidian with a pronounced conchoidal fracture. Large pink-grey spherulites occur singularly and in bands.	Highly cracked, non-vesicular glass containing aligned quench crystals. Some spherulite balls and coalesced masses.
hr_3			
Hinemoa Point	85	Cream-light grey pumiceous rhyolite. Phenocryst rich with black prismatic (up to 8mm in length) and platy phenocrysts.	Poorly vesicular glass with round, oval, elongate and tubular vesicles. Vesicles stretched due to flow. Glass contains perlitic cracks. No spherulitic material.
Mokoia Island	103	Pale brown rhyolite with some orange weathering colouration. Phenocryst rich.	Crystallised, spherulitic. Mosaic of coalesced spherulitic material. Interstitial areas have an equigranular texture.
Vaughan Road	104	Cream pumiceous rhyolite with pale grey bands and orange weathering colouration. Phenocryst rich.	Poorly vesicular with round, oval, elongate and tubular vesicles. Vesicles stretched due to flow. Glass contains cracks. No spherulitic material present.

Table IV.5: Hand specimen and thin section descriptions of Kapenga Volcanic Centre rhyolite lavas.

Rhyolite	Sample No.	Hand Specimen	Thin Section (Groundmass)
hk_1			
Horohoro	126	Medium and dark grey discontinuously flow banded rhyolite.	Crystallised, spherulitic glass. Flow banding suggested by alignment and morphology of spherulitic material. Microspherulites abundant. Larger spherulites have an almost equigranular texture.
Tumunui	165	Medium brown rhyolite. Some blue-grey spherulitic material visible. Brown blobs suggest alteration of ferromagnesian phenocrysts.	Crystallised, spherulitic glass. Mosaic of coalesced spherulitic material. Flow banding suggested by alignment and morphology of spherulitic material. Some interstitial areas have an equigranular texture.
Waikorapa	169	Black obsidian with abundant pink/cream spherulites, sometimes clustered into bands.	Highly cracked, non-vesicular glass containing spherulitic material and abundant aligned quench crystals. Spherulite alignment and morphology suggests flow direction.
North Ridge	171	Medium brown rhyolite. Flow banding defined by slight colour variations. Spherulites abundant.	Crystallised, spherulitic glass. Mosaic of coalesced spherulitic material. Flow banding defined by alignment and morphology of spherulitic material.
hk_2			
Round Hill	127	Light brown-grey pumiceous rhyolite. Black prismatic and platy phenocrysts noticeable. Coarse sugary texture.	Moderately vesicular glass with round, oval, elongate and tubular vesicles. Vesicles stretched due to flow. Glass contains cracks. No spherulitic material present.
Dome 2	167	Medium brown rhyolite. Flow bands defined by slight colour variations. Phenocryst rich.	Crystallised, spherulitic glass. Mosaic of coalesced spherulitic material. Flow banding defined by alignment of spherulitic material and bands of corroded quench crystals.
Dome 3	168	Medium grey rhyolite. Phenocryst rich with black prismatic and platy phenocrysts noticeable.	Crystallised, spherulitic glass. Glass between spherulites is non-vesicular, near colourless and contains cracks and vesicles stretched due to flow.
Ongahoro	170	Cream-light grey pumiceous rhyolite. Black prismatic and platy phenocrysts noticeable.	Poorly vesicular glass with round, oval, elongate and tubular vesicles. Vesicles stretched due to flow. Glass contains cracks and some aligned quench crystals. No spherulitic material present.
Haparangi	172	Light brown-grey rhyolite. Some alignment of black prismatic phenocrysts.	Crystallised, spherulitic glass. Mosaic of coalesced spherulitic material. Flow banding suggested by alignment of spherulitic material.

Table IV.6: Hand specimen and thin section descriptions of Upper Atiamuri rhyolite lavas.

Rhyolite	Sample No.	Hand Specimen	Thin Section (Groundmass)
Upper Atiamuri	121	Blue/grey spherulitic rhyolite. Spherulite rims are brown in colour. Brown flow bands.	Crystallised, spherulitic glass. Flow banding defined by coalescing spherulites and bands of opaque fibres/corroded quench crystals.
	123	Light grey-medium brown spherulitic rhyolite. Amygdaloidal.	Crystallised, spherulitic glass. Vesicles infilled with wedge-shaped secondary minerals. Flow banding suggested by variations in the degree of devitrification and elongation of infilled vesicles.

Appendix V: Whole Rock Geochemical Analyses by XRF and LA-ICPMS

Table V.1: Whole rock geochemical analyses of rhyolite lavas from the Okataina, Rotorua and Kapenga volcanic centres.

Okataina Volcanic Centre **ho_1** **Northeastern Rhyolites**								
Rhyolite	Waitangi	Maungawhakamana					North Rotoma	Matawhaura
Field Number	58	59	99	100	101	108	107	109
Major Elements (wt. %)								
SiO_2	75.41	76.89	76.48	77.24	74.47	73.13	75.18	77.23
TiO_2	0.19	0.11	0.21	0.12	0.21	0.30	0.23	0.15
Al_2O_3	13.33	13.09	12.91	12.58	14.11	16.11	13.80	12.55
Fe_2O_3#	1.88	1.30	1.85	1.32	1.76	2.25	1.79	1.59
MnO	0.06	0.05	0.05	0.04	0.05	0.04	0.06	0.05
MgO	0.21	0.10	0.24	0.12	0.31	0.33	0.37	0.18
CaO	1.15	0.99	1.61	0.95	2.07	2.03	1.45	1.35
Na_2O	4.58	4.12	4.09	3.97	3.97	3.73	3.87	3.87
K_2O	3.17	3.33	2.54	3.62	2.99	2.05	3.22	3.00
P_2O_5	0.03	0.02	0.03	0.02	0.05	0.04	0.03	0.03
LOI*	0.75	1.16	0.60	0.21	0.63	1.73	2.60	0.74
Total*	99.95	100.25	100.21	100.10	100.10	99.99	100.04	100.23
Trace Elements (XRF) (ppm)								
V	15	15	18	14	23	27	29	16
Cr	5	3	<3	7	3	13	4	3
Ni	<3	<3	3	3	3	3	3	<3
Zn	44	33	47	29	29	29	32	37
Zr	192	110	185	114	125	182	132	142
Nb	10	8	8	7	7	8	8	7
Ba	787	920	760	906	816	805	1021	789
La	34	27	23	27	25	35	29	25
Ce	57	43	44	49	41	55	48	44
Nd	24	20	21	16	18	28	15	21
Ga	15	13	12	13	14	15	13	12
Pb	16	16	15	17	13	13	12	14
Rb	104	109	82	120	99	37	103	95
Sr	86	84	140	78	156	179	109	120
Th	12	13	10	12	9	11	12	9
Y	34	24	21	23	18	23	24	24
Trace Elements (LA-ICPMS) (ppm)								
Sc					4.6		4.9	6.2
Ti					1249		1252	897
V					34.5		36.9	23.5
Ni					3.2		5.1	4.2
Rb					95		97	89
Y					18.1		22.0	22.4
Zr					144		141	152
Nb					6.58		8.26	7.03
Cs					4.86		4.65	4.32
Ba					778		930	737
La					21.95		23.45	21.08
Ce					41.4		49.5	41.2
Nd					16.06		18.11	17.45
Sm					3.04		3.55	3.60
Eu					0.66		0.59	0.78
Gd					2.75		3.19	3.35
Dy					2.75		3.31	3.52
Er					1.80		2.21	2.28
Yb					2.04		2.54	2.46
Lu					0.33		0.41	0.39
Hf					3.85		4.03	4.32
Ta					0.67		0.74	0.65
Pb					10.7		11.8	12.2
Th					11.28		11.14	9.77
U					2.49		2.50	2.31

Major elements normalised to 100%, volatile free. # All Fe expressed as Fe_2O_3. * Original Values.

Okataina Volcanic Centre								
	ho_1 Western Rhyolites				**ho_1 Southern Rhyolite**	**ho_2 Moerangi Rhyolites**		
Rhyolite	Stancorp Quarry	Whakapou-ngakau	Crater Farm	Pukepoto	Wairua	Direct Road	Hill Road	Moerangi Road
Field Number	63	110	111	146	119	68	70	72
Major Elements (wt. %)								
SiO_2	75.67	75.36	73.25	75.07	74.22	75.08	74.24	75.63
TiO_2	0.19	0.22	0.30	0.22	0.27	0.20	0.21	0.20
Al_2O_3	13.06	13.88	14.82	13.99	14.33	13.58	14.60	13.13
Fe_2O_3#	1.80	1.85	2.43	1.84	1.77	1.92	1.98	1.87
MnO	0.06	0.05	0.08	0.05	0.03	0.07	0.07	0.06
MgO	0.18	0.14	0.27	0.21	0.37	0.21	0.21	0.19
CaO	1.11	1.38	1.49	1.31	1.95	1.16	1.13	1.11
Na_2O	4.62	3.64	4.61	3.87	4.00	4.49	4.34	4.49
K_2O	3.27	3.44	2.72	3.41	3.04	3.25	3.20	3.28
P_2O_5	0.03	0.03	0.03	0.03	0.02	0.02	0.03	0.04
LOI*	0.02	0.68	1.02	0.96	0.64	2.28	2.90	0.30
Total*	99.94	100.05	100.04	100.31	100.14	100.21	100.22	100.18
Trace Elements (XRF) (ppm)								
V	15	23	18	20	34	15	14	16
Cr	5	3	6	4	14	8	5	<3
Ni	3	<3	3	<3	<3	<3	<3	4
Zn	40	32	46	34	31	47	50	41
Zr	185	143	238	177	147	197	202	191
Nb	10	6	10	9	7	10	10	9
Ba	765	779	702	833	783	783	834	760
La	36	35	30	28	26	33	34	35
Ce	57	51	59	42	37	70	67	60
Nd	25	25	34	19	25	17	26	28
Ga	15	13	16	13	13	15	16	15
Pb	19	15	19	14	11	19	19	15
Rb	110	124	85	102	95	106	104	112
Sr	87	121	133	111	157	89	84	89
Th	13	12	11	13	11	11	12	14
Y	34	20	35	19	14	34	38	39
Trace Elements (LA-ICPMS) (ppm)								
Sc	7.1	3.7			5.7			7.1
Ti	1079	1287			1549			1159
V	25.3	32.6			46.5			26.2
Ni	3.8	3.7			7.7			3.6
Rb	104	118			92			105
Y	34.1	18.5			13.0			38.6
Zr	207	152			171			200
Nb	10.15	6.74			6.88			10.03
Cs	3.95	5.57			8.87			3.39
Ba	712	733			736			708
La	27.27	30.80			19.75			29.32
Ce	56.1	40.6			37.5			59.0
Nd	24.72	21.67			12.37			29.54
Sm	5.31	3.86			2.29			6.53
Eu	0.93	0.72			0.60			0.91
Gd	5.04	3.29			1.99			6.40
Dy	5.39	3.14			2.00			6.14
Er	3.41	1.89			1.28			3.79
Yb	3.54	2.00			1.42			3.86
Lu	0.56	0.30			0.23			0.62
Hf	5.59	4.03			4.34			5.42
Ta	0.87	0.69			0.72			0.88
Pb	14.7	12.8			11.4			12.9
Th	11.26	12.29			11.95			11.35
U	2.80	2.88			2.84			3.07

Major elements normalised to 100%, volatile free. # All Fe expressed as Fe_2O_3. * Original Values.

Okataina Volcanic Centre								
	ho_2				**ho_2**			
	Moerangi Rhyolites				**Tutaeheka Rhyolites**			
Rhyolite	Chestnut Road	Green Lake	Kakapiko	Blue Lake	Tutaeheka 1	Tutaeheka 2		Tutaeheka 3
Field Number	73	74	78	152	64	160	162	117
Major Elements (wt. %)								
SiO_2	75.46	75.45	73.97	74.19	74.67	75.08	75.96	75.39
TiO_2	0.21	0.21	0.26	0.27	0.24	0.22	0.19	0.23
Al_2O_3	13.20	13.17	13.91	13.82	13.61	13.46	13.09	13.23
Fe_2O_3#	1.86	1.87	2.07	2.11	1.91	1.96	1.78	1.82
MnO	0.06	0.06	0.07	0.06	0.06	0.06	0.05	0.04
MgO	0.23	0.21	0.42	0.39	0.38	0.20	0.14	0.23
CaO	1.14	1.16	1.87	1.77	1.73	1.25	1.02	1.28
Na_2O	4.57	4.60	4.32	4.30	4.11	4.53	4.43	4.48
K_2O	3.23	3.24	3.06	3.05	3.22	3.22	3.32	3.25
P_2O_5	0.03	0.02	0.05	0.04	0.06	0.02	0.02	0.04
LOI*	0.44	0.59	1.94	0.42	0.81	0.50	0.65	0.15
Total*	100.18	100.48	100.32	100.16	100.15	100.34	100.28	100.05
Trace Elements (XRF) (ppm)								
V	17	17	23	25	21	19	15	18
Cr	<3	5	9	7	8	4	4	<3
Ni	3	4	4	3	<3	<3	<3	3
Zn	36	41	36	35	35	28	32	31
Zr	193	185	163	170	144	186	184	189
Nb	10	10	8	9	8	10	10	9
Ba	771	752	790	773	856	770	780	740
La	33	29	30	31	29	32	31	31
Ce	48	62	60	47	42	47	55	53
Nd	28	22	31	18	15	16	32	27
Ga	14	14	14	14	13	15	14	14
Pb	15	17	15	13	15	13	15	14
Rb	107	107	104	97	110	98	108	109
Sr	95	90	142	136	135	100	81	97
Th	13	12	11	11	12	10	11	12
Y	26	30	26	24	20	26	29	29
Trace Elements (LA-ICPMS) (ppm)								
Sc				5.5	4.4	7.0		7.3
Ti				1536	1379	1270		1313
V				33.4	34.5	29.8		27.6
Ni				4.3	3.1	5.8		4.4
Rb				89	106	94		103
Y				21.8	19.8	25.8		29.4
Zr				174	150	201		216
Nb				8.13	7.34	10.06		9.89
Cs				4.29	4.74	2.86		2.82
Ba				726	780	722		713
La				22.12	22.72	30.15		26.33
Ce				43.4	43.5	50.1		50.8
Nd				17.89	16.34	20.69		24.51
Sm				3.59	3.16	4.11		5.05
Eu				0.76	0.68	0.93		0.96
Gd				3.36	2.84	3.87		4.69
Dy				3.42	2.94	4.04		4.81
Er				2.23	1.95	2.66		2.99
Yb				2.45	2.23	2.82		3.13
Lu				0.38	0.37	0.47		0.48
Hf				4.69	3.99	5.49		5.87
Ta				0.76	0.77	0.90		0.88
Pb				13.4	12.6	11.6		11.5
Th				10.57	11.02	11.31		11.66
U				2.54	2.59	2.60		2.69

Major elements normalised to 100%, volatile free. # All Fe expressed as Fe_2O_3. * Original Values.

Okataina Volcanic Centre								
	ho_2 Tutaeheka Rhyolites		**ho_2 Sth Rotomahana Rhyolites**		**ho_3 Te Rere Episode (Haroharo)**			
Rhyolite	Tutaeheka 3		Hapeotoroa	Waimangu	Te Koutu Flow		Haumingi Flow	Tuarae Flow
Field Number	118	164	128	129	22	23	56	61
Major Elements (wt. %)								
SiO_2	75.10	74.92	74.02	73.96	76.25	76.39	76.22	76.50
TiO_2	0.21	0.21	0.29	0.28	0.20	0.19	0.20	0.19
Al_2O_3	13.28	13.58	13.69	14.06	13.04	13.03	13.17	12.96
Fe_2O_3#	1.92	1.93	2.25	2.14	1.44	1.38	1.42	1.36
MnO	0.06	0.06	0.06	0.06	0.08	0.07	0.08	0.08
MgO	0.28	0.28	0.51	0.47	0.24	0.21	0.21	0.21
CaO	1.35	1.38	1.95	1.95	1.25	1.19	1.23	1.19
Na_2O	4.49	4.39	4.06	4.17	4.51	4.47	4.42	4.47
K_2O	3.27	3.20	3.11	2.87	2.96	3.03	3.01	3.01
P_2O_5	0.05	0.05	0.06	0.04	0.03	0.03	0.03	0.03
LOI*	2.02	2.24	1.88	1.22	0.56	0.29	1.34	0.23
Total*	100.09	100.17	100.04	100.25	100.11	99.88	99.70	100.01
Trace Elements (XRF) (ppm)								
V	16	27	27	24	15	15	15	15
Cr	3	5	6	4	<3	<3	<3	5
Ni	<3	<3	<3	3	<3	3	<3	4
Zn	42	45	36	34	47	46	45	47
Zr	178	181	144	153	166	161	161	158
Nb	9	9	8	8	9	9	9	9
Ba	729	717	812	860	835	814	820	821
La	29	32	22	23	36	28	27	27
Ce	55	56	51	55	58	53	53	56
Nd	24	30	18	17	14	29	25	21
Ga	14	14	13	14	13	13	13	13
Pb	16	16	12	12	16	17	15	15
Rb	110	106	105	94	97	98	96	97
Sr	96	99	142	151	119	118	118	116
Th	11	37	11	13	12	12	10	11
Y	34	37	22	18	32	32	32	33
Trace Elements (LA-ICPMS) (ppm)								
Sc			5.2					
Ti			1601					
V			36.5					
Ni			4.0					
Rb			96					
Y			20.6					
Zr			164					
Nb			7.40					
Cs			5.13					
Ba			737					
La			21.56					
Ce			41.8					
Nd			16.91					
Sm			3.31					
Eu			0.68					
Gd			3.07					
Dy			3.22					
Er			2.12					
Yb			2.36					
Lu			0.38					
Hf			4.38					
Ta			0.72					
Pb			11.5					
Th			10.29					
U			2.47					

Major elements normalised to 100%, volatile free. # All Fe expressed as Fe_2O_3. * Original Values.

Okataina Volcanic Centre								
	ho_3 Te Rere Episode (Haroharo)	**(Okareka)**				**ho_3 Okareka Episode (Tarawera)**		**ho_3 Rerewhakaaitu Episode (Tarawera)**
Rhyolite	Fentons Mill Flow	Eastern Rhyolite			Te Rere Dome	Ridge Flow	Patiti Island	Te Puha Flow
Field Number	92	65	113	114	174	90	130	40
Major Elements (wt. %)								
SiO_2	76.45	73.91	73.74	74.07	75.60	75.37	72.53	77.14
TiO_2	0.19	0.34	0.35	0.33	0.20	0.25	0.35	0.16
Al_2O_3	13.02	13.77	13.74	13.79	13.22	13.18	14.15	12.63
Fe_2O_3#	1.37	2.22	2.31	2.23	1.86	1.82	2.74	1.24
MnO	0.08	0.07	0.08	0.07	0.05	0.07	0.07	0.06
MgO	0.21	0.47	0.51	0.48	0.20	0.36	0.69	0.16
CaO	1.20	2.06	2.09	1.96	1.12	1.58	2.50	1.08
Na_2O	4.47	4.34	4.42	4.33	4.49	4.26	4.05	4.30
K_2O	2.98	2.75	2.68	2.72	3.24	3.06	2.83	3.20
P_2O_5	0.03	0.07	0.08	0.03	0.02	0.05	0.09	0.02
LOI*	0.47	0.20	0.24	1.49	0.45	0.44	1.52	0.39
Total*	100.08	99.97	100.05	100.19	100.18	100.26	100.00	100.12
Trace Elements (XRF) (ppm)								
V	15	25	25	24	18	21	33	13
Cr	7	<3	9	5	<3	5	3	4
Ni	<3	<3	4	3	<3	4	<3	<3
Zn	46	42	43	44	38	38	38	39
Zr	160	228	237	229	195	175	170	126
Nb	9	8	8	8	10	8	8	8
Ba	823	819	789	786	765	807	743	862
La	30	23	24	23	29	27	26	28
Ce	57	46	44	44	56	41	54	47
Nd	17	25	31	19	19	21	20	25
Ga	13	14	13	14	15	13	14	13
Pb	18	13	13	13	14	15	11	15
Rb	99	90	89	90	101	104	94	107
Sr	116	169	169	163	88	131	168	98
Th	8	8	7	9	11	10	11	9
Y	31	26	26	25	22	25	23	27
Trace Elements (LA-ICPMS) (ppm)								
Sc	5.2		7.8			5.8	6.8	
Ti	1126		2065			1576	2034	
V	22.6		35.3			31.3	47.0	
Ni	3.5		3.4			4.9	4.1	
Rb	94		84			103	89	
Y	31.3		25.5			25.7	21.4	
Zr	174		246			201	179	
Nb	9.10		7.88			8.59	7.37	
Cs	3.84		3.56			4.54	4.79	
Ba	769		747			776	701	
La	25.10		21.49			24.14	21.63	
Ce	51.7		43.1			47.5	42.2	
Nd	22.52		19.18			19.13	17.66	
Sm	4.71		4.08			3.94	3.53	
Eu	1.00		1.00			0.83	0.78	
Gd	4.55		3.93			3.71	3.26	
Dy	4.75		4.05			3.89	3.37	
Er	3.10		2.63			2.56	2.19	
Yb	3.34		2.80			2.86	2.37	
Lu	0.55		0.45			0.47	0.38	
Hf	4.72		5.92			5.09	4.62	
Ta	0.76		0.66			0.83	0.75	
Pb	14.7		11.8			13.2	11.9	
Th	9.77		8.66			11.00	9.50	
U	2.32		2.15			2.66	2.30	

Major elements normalised to 100%, volatile free. # All Fe expressed as Fe_2O_3. * Original Values.

Okataina Volcanic Centre								
	ho_3 Rerewhakaaitu Episode (Tarawera)			**ho_3 Rotorua Episode (Okareka)**				**ho_3 Waiohau (Tarawera)**
Rhyolite	Te Puha Flow	Western Dome		Rotomahana Dome	Trig 7693		Middle Rhyolite	Pokohu Flow
Field Number	41	44	135	134	153	176	175	5
Major Elements (wt. %)								
SiO_2	74.99	73.90	73.62	74.97	75.42	75.58	74.76	76.98
TiO_2	0.24	0.31	0.30	0.24	0.21	0.21	0.23	0.17
Al_2O_3	13.36	13.73	13.94	13.36	13.36	13.21	13.63	12.69
Fe_2O_3#	1.91	2.30	2.32	1.90	1.68	1.69	1.85	1.32
MnO	0.06	0.08	0.08	0.06	0.06	0.06	0.06	0.06
MgO	0.37	0.64	0.64	0.38	0.29	0.30	0.35	0.19
CaO	1.70	2.34	2.41	1.72	1.49	1.48	1.71	1.18
Na_2O	4.07	4.17	4.06	4.10	4.14	4.11	4.15	4.33
K_2O	3.22	2.45	2.56	3.20	3.32	3.30	3.20	3.06
P_2O_5	0.06	0.07	0.08	0.06	0.04	0.05	0.05	0.03
LOI*	0.90	0.40	0.85	0.31	1.49	0.96	0.96	-0.02
Total*	100.15	100.24	99.74	100.29	100.38	100.19	100.26	100.06
Trace Elements (XRF) (ppm)								
V	26	32	32	23	19	21	21	15
Cr	9	5	<3	5	4	<3	5	<3
Ni	<3	<3	<3	<3	<3	3	4	<3
Zn	34	33	32	33	33	33	33	38
Zr	140	153	151	136	135	130	135	146
Nb	8	8	7	8	8	8	7	8
Ba	837	812	821	829	845	855	823	857
La	23	25	22	29	28	26	28	27
Ce	41	36	38	52	42	49	46	50
Nd	21	21	23	24	20	19	22	28
Ga	12	12	13	13	12	13	13	13
Pb	12	9	10	14	12	13	12	17
Rb	109	76	78	112	112	113	109	103
Sr	129	173	175	131	117	117	134	106
Th	11	8	9	12	11	12	11	15
Y	20	19	20	20	22	22	20	26
Trace Elements (LA-ICPMS) (ppm)								
Sc		6.3		4.2		4.2		
Ti		1757		1352		1161		
V		49.1		32.0		36.1		
Ni		4.1		3.6		11.4		
Rb		73		105		109		
Y		19.4		19.4		21.8		
Zr		163		153		145		
Nb		7.04		7.23		7.61		
Cs		3.04		5.00		4.95		
Ba		785		773		775		
La		20.78		22.22		23.99		
Ce		40.4		42.8		46.4		
Nd		15.82		16.63		17.37		
Sm		3.05		3.16		3.38		
Eu		0.72		0.65		0.67		
Gd		2.87		2.87		3.05		
Dy		2.90		3.01		3.23		
Er		1.93		1.96		2.13		
Yb		2.15		2.21		2.40		
Lu		0.37		0.37		0.41		
Hf		4.13		4.20		3.98		
Ta		0.66		0.74		0.80		
Pb		9.1		12.8		13.4		
Th		7.63		11.32		11.42		
U		1.81		2.69		2.68		

Major elements normalised to 100%, volatile free. # All Fe expressed as Fe_2O_3. * Original Values.

Okataina Volcanic Centre								
	ho_3 Waiohau Episode (Tarawera)				**ho_3 Rotoma Episode (Haroharo)**			
Rhyolite	Pokohu Flow		Waikakareao Flow		Te Pohue Flow		Rotoma Flow	
Field Number	37	147	38	149	60	144	105	106
Major Elements (wt. %)								
SiO_2	76.75	77.03	76.94	76.93	76.38	77.05	75.14	75.11
TiO_2	0.17	0.18	0.17	0.18	0.19	0.17	0.25	0.25
Al_2O_3	12.90	12.67	12.70	12.70	13.03	12.74	13.44	13.56
Fe_2O_3#	1.34	1.34	1.33	1.34	1.40	1.27	1.82	1.82
MnO	0.06	0.06	0.06	0.06	0.07	0.07	0.08	0.08
MgO	0.20	0.20	0.19	0.20	0.23	0.21	0.34	0.33
CaO	1.17	1.14	1.17	1.19	1.35	1.15	1.61	1.58
Na_2O	4.29	4.26	4.30	4.27	4.35	4.32	4.39	4.35
K_2O	3.09	3.10	3.10	3.10	2.96	2.99	2.88	2.87
P_2O_5	0.02	0.03	0.03	0.03	0.04	0.03	0.05	0.04
LOI*	1.08	0.46	0.42	0.21	1.61	0.80	1.22	1.34
Total*	100.19	99.97	100.12	100.43	100.07	100.15	100.18	100.10
Trace Elements (XRF) (ppm)								
V	14	14	14	14	16	14	18	19
Cr	4	5	3	4	4	<3	5	7
Ni	<3	<3	<3	4	<3	<3	<3	3
Zn	42	38	38	36	38	37	41	41
Zr	139	143	141	141	141	127	174	180
Nb	8	9	8	9	8	8	8	8
Ba	861	864	855	854	810	864	806	795
La	25	25	28	27	27	21	27	29
Ce	44	52	52	42	55	55	46	51
Nd	21	21	25	31	24	20	11	21
Ga	13	13	13	13	13	12	14	14
Pb	15	14	16	13	11	14	14	15
Rb	101	103	101	105	94	95	95	94
Sr	105	103	106	106	122	106	137	138
Th	11	10	10	9	10	11	10	8
Y	27	27	27	27	26	26	26	26
Trace Elements (LA-ICPMS) (ppm)								
Sc			4.6		4.4		5.3	
Ti			1043		1131		1446	
V			25.4		25.8		27.7	
Ni			3.5		3.5		3.5	
Rb			100		92		90	
Y			26.8		25.9		25.1	
Zr			158		160		199	
Nb			8.51		8.22		8.02	
Cs			4.37		3.82		4.02	
Ba			794		784		753	
La			24.39		23.77		22.49	
Ce			49.0		47.8		44.9	
Nd			20.01		19.71		19.16	
Sm			4.11		3.97		3.91	
Eu			0.83		0.87		0.87	
Gd			3.77		3.69		3.72	
Dy			4.04		3.88		3.89	
Er			2.64		2.57		2.57	
Yb			2.87		2.81		2.76	
Lu			0.47		0.46		0.46	
Hf			4.42		4.41		5.13	
Ta			0.79		0.76		0.70	
Pb			13.6		12.6		12.7	
Th			10.41		9.64		9.44	
U			2.48		2.34		2.32	

Major elements normalised to 100%, volatile free. # All Fe expressed as Fe_2O_3. * Original Values.

Okataina Volcanic Centre **ho_3** **Mamaku Episode** **(Haroharo)**								
Rhyolite	Hainini Dome	Waiti Flow						Te Horoa Dome
Field Number	7	14	15	17	95	96	173	19
Major Elements (wt. %)								
SiO_2	76.57	75.18	75.06	75.56	75.23	75.52	75.16	76.43
TiO_2	0.19	0.25	0.26	0.23	0.24	0.25	0.25	0.19
Al_2O_3	12.82	13.45	13.42	13.26	13.38	13.20	13.36	12.91
Fe_2O_3#	1.45	1.82	1.85	1.70	1.79	1.77	1.82	1.45
MnO	0.07	0.07	0.08	0.07	0.07	0.07	0.08	0.06
MgO	0.25	0.34	0.35	0.31	0.33	0.34	0.34	0.23
CaO	1.23	1.57	1.61	1.51	1.60	1.50	1.62	1.27
Na_2O	4.26	4.38	4.42	4.40	4.42	4.38	4.42	4.29
K_2O	3.13	2.89	2.88	2.91	2.89	2.93	2.90	3.13
P_2O_5	0.03	0.05	0.06	0.04	0.05	0.04	0.05	0.04
LOI*	0.52	1.07	0.97	0.94	0.56	0.20	0.38	0.66
Total*	100.12	100.21	100.30	100.20	100.07	100.16	100.06	100.11
Trace Elements (XRF) (ppm)								
V	17	18	19	17	18	18	18	15
Cr	11	5	5	5	3	10	<3	4
Ni	<3	<3	<3	<3	<3	<3	<3	<3
Zn	37	42	41	40	41	41	41	37
Zr	138	177	181	170	174	176	183	142
Nb	8	8	8	8	8	8	8	8
Ba	847	806	806	825	809	823	806	859
La	27	21	24	28	26	24	24	30
Ce	51	47	51	49	48	46	47	52
Nd	28	29	26	21	15	12	<10	18
Ga	13	14	14	14	13	14	14	13
Pb	16	15	15	14	14	16	11	14
Rb	108	99	100	99	97	98	98	104
Sr	108	136	140	132	139	134	141	111
Th	14	13	14	14	9	9	9	11
Y	24	25	25	25	26	25	26	26
Trace Elements (LA-ICPMS) (ppm)								
Sc	4.4			5.2			5.8	
Ti	1067			1332			1496	
V	28.4			30.6			29.6	
Ni	6.0			5.1			5.0	
Rb	101			93			97	
Y	25.1			26.0			28.0	
Zr	159			188			207	
Nb	7.99			8.20			8.91	
Cs	4.37			3.92			4.22	
Ba	792			770			792	
La	23.87			23.56			25.17	
Ce	47.3			46.8			50.3	
Nd	18.66			19.27			20.69	
Sm	3.83			3.97			4.28	
Eu	0.76			0.87			0.99	
Gd	3.54			3.72			4.04	
Dy	3.77			3.93			4.25	
Er	2.51			2.57			2.81	
Yb	2.80			2.81			3.03	
Lu	0.46			0.47			0.50	
Hf	4.30			4.88			5.47	
Ta	0.82			0.78			0.81	
Pb	12.9			12.5			13.2	
Th	10.52			9.64			10.54	
U	2.48			2.29			2.50	

Major elements normalised to 100%, volatile free. # All Fe expressed as Fe_2O_3. * Original Values.

Okataina Volcanic Centre **ho_3** **Mamaku Episode (Haroharo)**								
Rhyolite	Te Horoa Dome		Oruaroa Flow	Otangimoana Flow	Ruakokopu Flow		Hainini Flow	Kaipara Flow
Field Number	30	32	26	27	34	35	81	145
Major Elements (wt. %)								
SiO_2	76.44	76.59	76.63	76.81	76.88	76.56	76.50	79.63
TiO_2	0.19	0.18	0.19	0.19	0.18	0.19	0.20	0.18
Al_2O_3	13.05	12.81	12.79	12.84	12.91	12.90	12.84	11.46
Fe_2O_3#	1.37	1.42	1.45	1.21	1.08	1.34	1.47	0.86
MnO	0.06	0.06	0.06	0.06	0.06	0.07	0.06	0.06
MgO	0.23	0.22	0.24	0.23	0.22	0.23	0.24	0.11
CaO	1.27	1.26	1.22	1.22	1.24	1.25	1.27	0.73
Na_2O	4.22	4.29	4.25	4.26	4.23	4.27	4.22	3.88
K_2O	3.12	3.13	3.14	3.15	3.18	3.14	3.16	3.07
P_2O_5	0.04	0.04	0.03	0.03	0.02	0.04	0.04	0.02
LOI*	1.25	0.29	0.40	0.58	1.72	0.57	1.45	1.54
Total*	99.95	99.87	100.18	100.22	99.94	100.20	100.23	100.31
Trace Elements (XRF) (ppm)								
V	15	15	15	16	14	16	15	14
Cr	6	5	4	4	4	4	5	5
Ni	<3	<3	<3	<3	<3	<3	<3	<3
Zn	41	36	36	37	34	37	35	34
Zr	143	137	141	142	136	140	138	136
Nb	7	8	8	8	8	8	8	8
Ba	763	852	854	844	846	864	846	841
La	24	27	30	29	29	27	29	26
Ce	46	43	46	51	42	43	52	47
Nd	24	22	22	16	21	27	27	22
Ga	12	12	12	12	12	13	13	12
Pb	13	13	14	13	14	14	13	15
Rb	108	105	105	106	104	104	105	98
Sr	113	109	107	108	108	109	109	65
Th	10	10	12	11	9	9	11	11
Y	26	25	26	25	25	25	25	26
Trace Elements (LA-ICPMS) (ppm)								
Sc		4.3						
Ti		1057						
V		27.0						
Ni		3.3						
Rb		100						
Y		24.9						
Zr		147						
Nb		7.87						
Cs		4.36						
Ba		796						
La		23.83						
Ce		47.3						
Nd		18.87						
Sm		3.90						
Eu		0.77						
Gd		3.58						
Dy		3.74						
Er		2.48						
Yb		2.69						
Lu		0.45						
Hf		4.11						
Ta		0.78						
Pb		13.0						
Th		10.51						
U		2.48						

Major elements normalised to 100%, volatile free. # All Fe expressed as Fe_2O_3. * Original Values.

Okataina Volcanic Centre
ho_3
Whakatane Episode
(Haroharo)

Rhyolite	Haroharo Dome	Rotoroniu Flow		Okataina		Tapahoro Flow	Rotokohu Dome	Tikorangi Dome
Field Number	6	20	33	24	25	36	79	98
Major Elements (wt. %)								
SiO_2	76.54	76.95	77.07	77.04	76.94	77.07	76.30	75.71
TiO_2	0.18	0.17	0.16	0.16	0.16	0.17	0.20	0.24
Al_2O_3	12.89	12.68	12.69	12.70	12.72	12.64	12.93	13.19
Fe_2O_3#	1.44	1.31	1.24	1.23	1.28	1.31	1.53	1.65
MnO	0.06	0.06	0.06	0.06	0.06	0.06	0.07	0.07
MgO	0.22	0.20	0.18	0.18	0.19	0.19	0.25	0.31
CaO	1.25	1.11	1.13	1.12	1.14	1.10	1.30	1.49
Na_2O	4.29	4.25	4.20	4.24	4.25	4.16	4.33	4.33
K_2O	3.10	3.24	3.24	3.23	3.22	3.27	3.05	2.97
P_2O_5	0.03	0.03	0.03	0.03	0.03	0.03	0.03	0.03
LOI*	0.41	0.50	0.81	0.61	0.44	0.95	0.87	0.69
Total*	99.95	100.28	99.92	100.21	100.01	100.16	100.12	100.05
Trace Elements (XRF) (ppm)								
V	15	14	15	14	17	15	15	17
Cr	5	3	4	5	3	4	4	4
Ni	<3	<3	<3	<3	<3	<3	4	3
Zn	37	36	34	36	35	34	37	39
Zr	133	124	119	120	121	120	147	168
Nb	8	8	8	8	7	8	8	8
Ba	862	879	852	858	865	868	846	829
La	27	29	28	32	24	27	28	25
Ce	48	46	46	54	46	51	54	44
Nd	22	22	22	25	28	28	26	12
Ga	13	12	12	13	12	12	13	14
Pb	15	15	13	13	14	15	15	15
Rb	106	107	108	108	108	107	102	99
Sr	108	96	96	98	100	94	114	129
Th	14	11	9	11	11	10	10	10
Y	25	26	26	26	26	25	26	25
Trace Elements (LA-ICPMS) (ppm)								
Sc	4.6			4.1		4.1	4.8	5.2
Ti	1108			898		897	1173	1369
V	27.5			24.7		24.6	26.0	27.5
Ni	5.8			5.8		3.9	3.9	3.1
Rb	104			102		101	97	93
Y	26.5			25.0		24.5	25.0	24.3
Zr	160			128		125	165	184
Nb	8.38			7.74		7.59	8.02	7.88
Cs	4.53			4.60		4.71	4.15	4.03
Ba	810			805		793	787	772
La	24.62			23.95		23.41	23.09	22.51
Ce	49.0			47.6		46.4	45.8	44.9
Nd	19.73			18.96		18.55	18.61	18.18
Sm	4.06			3.82		3.72	3.80	3.69
Eu	0.82			0.74		0.72	0.80	0.84
Gd	3.77			3.53		3.46	3.55	3.50
Dy	4.00			3.75		3.66	3.80	3.69
Er	2.63			2.49		2.42	2.51	2.48
Yb	2.88			2.71		2.67	2.72	2.69
Lu	0.48			0.45		0.44	0.45	0.45
Hf	4.49			3.71		3.61	4.38	4.77
Ta	0.89			0.79		0.73	0.73	0.71
Pb	13.5			13.5		12.9	12.8	12.4
Th	10.75			10.75		10.46	9.99	9.73
U	2.56			2.51		2.46	2.42	2.35

Major elements normalised to 100%, volatile free. # All Fe expressed as Fe_2O_3. * Original Values.

Okataina Volcanic Centre								
	ho_3 Whakatane Episode (Haroharo)				**ho_3 Kaharoa Episode (Tarawera)**			
Rhyolite	Makatiti Dome	Makatiti Flow			Wahanga Dome	Ruawahia Dome	Green Lake Plug	Crater Dome
Field Number	138	141	142	143	45	46	133	156
Major Elements (wt. %)								
SiO_2	77.19	77.40	77.02	76.80	76.23	76.29	77.29	76.18
TiO_2	0.16	0.15	0.16	0.17	0.20	0.20	0.10	0.20
Al_2O_3	12.69	12.51	12.67	12.90	12.93	12.95	12.53	12.98
Fe_2O_3#	1.23	1.21	1.30	1.32	1.55	1.50	1.09	1.55
MnO	0.06	0.06	0.06	0.06	0.06	0.06	0.06	0.06
MgO	0.17	0.15	0.18	0.19	0.25	0.25	0.15	0.25
CaO	1.08	1.01	1.12	1.14	1.31	1.32	0.79	1.33
Na_2O	4.13	4.18	4.22	4.15	4.27	4.27	4.20	4.25
K_2O	3.26	3.32	3.24	3.23	3.17	3.14	3.77	3.15
P_2O_5	0.03	0.02	0.03	0.03	0.03	0.03	0.02	0.04
LOI*	1.04	0.19	0.76	1.96	0.77	0.36	1.58	1.30
Total*	100.11	99.65	100.19	99.79	100.37	99.92	100.26	99.71
Trace Elements (XRF) (ppm)								
V	16	14	16	15	18	17	14	18
Cr	5	4	<3	3	7	3	4	5
Ni	<3	3	3	<3	<3	3	3	<3
Zn	34	34	35	35	34	33	31	32
Zr	117	114	123	124	137	137	88	133
Nb	8	8	8	8	8	8	8	8
Ba	879	874	871	870	851	860	923	849
La	29	33	27	29	28	29	28	25
Ce	50	41	48	41	49	46	50	43
Nd	18	20	26	18	28	18	21	27
Ga	13	12	12	12	12	12	13	13
Pb	14	13	14	14	16	13	15	13
Rb	110	111	107	104	106	105	125	104
Sr	92	86	95	98	110	112	54	109
Th	12	11	12	10	11	10	12	12
Y	25	26	26	25	25	25	28	24
Trace Elements (LA-ICPMS) (ppm)								
Sc								
Ti								
V								
Ni								
Rb								
Y								
Zr								
Nb								
Cs								
Ba								
La								
Ce								
Nd								
Sm								
Eu								
Gd								
Dy								
Er								
Yb								
Lu								
Hf								
Ta								
Pb								
Th								
U								

Major elements normalised to 100%, volatile free. # All Fe expressed as Fe_2O_3. * Original Values.

Okataina Volcanic Centre			**Rotorua Volcanic Centre**					
	ho_3		**hr_1**				**hr_2**	
	Kaharoa Episode (Tarawera)							
Rhyolite	Crater Dome	Tarawera Dome	Tokorangi	Endean Road	Hamurana	Hemo Gorge	Ngongotaha Quarry Dome	
Field Number	157	158	84	87	120	137	52	54
Major Elements (wt. %)								
SiO_2	76.25	76.43	77.42	74.40	73.69	77.58	75.76	75.31
TiO_2	0.20	0.19	0.12	0.30	0.34	0.13	0.19	0.20
Al_2O_3	13.04	12.91	12.49	13.72	14.53	12.91	13.02	13.59
Fe_2O_3#	1.66	1.49	1.29	2.39	2.32	0.84	1.73	1.79
MnO	0.06	0.06	0.04	0.04	0.03	0.03	0.06	0.06
MgO	0.25	0.23	0.07	0.42	0.28	0.06	0.18	0.16
CaO	1.31	1.31	0.83	1.72	1.83	0.85	1.10	1.10
Na_2O	3.99	4.26	3.91	3.72	3.88	4.04	4.66	4.44
K_2O	3.18	3.11	3.80	3.26	3.05	3.52	3.28	3.32
P_2O_5	0.04	0.02	0.02	0.02	0.04	0.03	0.03	0.03
LOI*	1.68	0.29	0.37	0.74	0.90	0.73	0.44	3.26
Total*	99.82	99.89	100.09	100.21	100.18	100.24	99.98	100.35
Trace Elements (XRF) (ppm)								
V	18	16	14	27	31	13	15	14
Cr	3	3	<3	6	<3	4	4	3
Ni	<3	<3	3	4	<3	<3	<3	4
Zn	36	34	36	34	34	32	52	50
Zr	131	139	134	153	214	136	214	211
Nb	7	8	8	7	8	9	10	10
Ba	858	853	833	754	742	821	777	792
La	29	30	31	27	27	28	35	32
Ce	50	44	51	31	41	54	56	70
Nd	17	29	23	24	23	20	32	25
Ga	13	13	12	15	14	13	14	14
Pb	13	13	19	13	13	19	22	18
Rb	104	103	133	123	104	114	108	104
Sr	108	111	70	144	152	73	81	81
Th	11	12	13	11	11	15	11	13
Y	24	25	26	13	21	25	36	36
Trace Elements (LA-ICPMS) (ppm)								
Sc		4.5	5.3	5.4	7.2			
Ti		1074	682	1754	2013			
V		24.2	21.5	42.8	41.8			
Ni		8.4	3.4	3.7	3.8			
Rb		97	130	117	97			
Y		23.7	25.2	12.3	20.6			
Zr		148	138	185	238			
Nb		7.73	8.30	7.19	7.46			
Cs		4.19	5.43	5.21	6.67			
Ba		769	761	718	695			
La		23.03	25.94	18.36	23.65			
Ce		44.9	51.8	34.9	43.8			
Nd		16.97	20.66	11.88	21.04			
Sm		3.44	4.20	2.32	4.23			
Eu		0.75	0.63	0.54	0.91			
Gd		3.18	3.83	2.01	3.64			
Dy		3.45	3.96	1.97	3.53			
Er		2.33	2.50	1.21	2.16			
Yb		2.59	2.54	1.31	2.30			
Lu		0.44	0.40	0.21	0.36			
Hf		3.95	4.23	4.69	5.80			
Ta		0.77	0.85	0.70	0.69			
Pb		12.0	16.4	11.6	13.1			
Th		10.28	13.28	11.66	10.79			
U		2.40	3.01	2.72	2.79			

Major elements normalised to 100%, volatile free. # All Fe expressed as Fe_2O_3. * Original Values.

Rotorua Volcanic Centre							**Upper Atiamuri Rhyolites**	
	hr_2			**hr_3**				
Rhyolite	Ngongotaha Gondola Dome	Kawaha Point	Pukehangi Te Miri Dome	Hinemoa Point	Mokoia Island	Vaughan Road	Upper Atiamuri	Upper Atiamuri
Field Number	154	86	159	85	103	104	121	123
Major Elements (wt. %)								
SiO_2	75.76	75.32	75.60	73.46	75.36	73.87	73.74	75.49
TiO_2	0.19	0.20	0.19	0.27	0.24	0.27	0.32	0.22
Al_2O_3	13.34	13.55	13.22	14.50	13.35	13.96	14.27	13.41
Fe_2O_3#	1.78	1.72	1.74	2.06	1.71	2.11	2.22	1.62
MnO	0.06	0.05	0.06	0.06	0.04	0.06	0.06	0.03
MgO	0.13	0.18	0.17	0.42	0.22	0.43	0.38	0.16
CaO	0.94	1.19	1.09	1.96	1.41	1.86	1.69	1.51
Na_2O	4.25	4.50	4.64	4.30	4.42	4.30	4.33	4.32
K_2O	3.53	3.26	3.26	2.96	3.21	3.09	2.97	3.22
P_2O_5	0.02	0.03	0.03	0.02	0.03	0.05	0.03	0.02
LOI*	0.56	0.96	0.47	2.16	0.14	1.50	0.56	0.47
Total*	100.10	100.13	100.11	100.17	99.91	100.17	100.24	100.29
Trace Elements (XRF) (ppm)								
V	13	16	15	25	20	26	23	17
Cr	<3	6	5	5	<3	8	4	<3
Ni	<3	3	<3	5	<3	<3	<3	<3
Zn	47	47	49	36	31	37	43	37
Zr	220	220	216	163	177	164	253	216
Nb	10	11	10	9	9	8	9	9
Ba	853	809	796	776	735	784	782	790
La	30	32	32	28	29	26	27	24
Ce	59	49	59	37	52	44	51	44
Nd	35	32	31	20	26	20	23	18
Ga	15	14	14	14	14	14	15	14
Pb	18	19	16	15	14	14	18	16
Rb	114	98	107	97	109	106	82	111
Sr	76	92	81	153	109	143	142	134
Th	12	12	12	11	10	11	11	11
Y	31	33	35	22	26	22	23	24
Trace Elements (LA-ICPMS) (ppm)								
Sc		6.3	7.0		6.3	5.3		
Ti		1168	1136		1415	1540		
V		23.5	19.7		29.7	34.3		
Ni		4.8	8.9		3.9	4.2		
Rb		93	108		102	100		
Y		31.6	37.4		25.5	21.8		
Zr		221	241		202	185		
Nb		10.28	11.65		9.42	8.00		
Cs		4.12	4.57		4.16	4.87		
Ba		758	737		698	728		
La		26.75	29.18		25.58	22.51		
Ce		53.5	60.1		44.0	43.4		
Nd		23.43	25.51		21.85	17.01		
Sm		4.98	5.52		4.54	3.42		
Eu		0.90	0.94		0.85	0.74		
Gd		4.72	5.31		4.08	3.12		
Dy		4.97	5.66		4.19	3.31		
Er		3.16	3.73		2.57	2.23		
Yb		3.33	3.91		2.68	2.51		
Lu		0.53	0.65		0.42	0.41		
Hf		5.71	6.54		5.34	4.88		
Ta		0.87	1.03		0.83	0.74		
Pb		16.9	17.1		13.1	12.6		
Th		11.26	12.33		11.20	10.70		
U		2.48	2.94		2.65	2.52		

Major elements normalised to 100%, volatile free. # All Fe expressed as Fe_2O_3. * Original Values.

Kapenga Volcanic Centre	**hk_1**				**hk_2**				
Rhyolite	Horohoro	Tumunui	Waikorapa	North Ridge	Round Hill	Dome 2	Dome 3	Ongahoro	Haparangi
Field Number	126	165	169	171	127	167	168	170	172
Major Elements (wt. %)									
SiO_2	76.63	75.80	76.84	76.66	73.06	74.18	72.71	74.08	74.14
TiO_2	0.16	0.19	0.11	0.16	0.28	0.28	0.29	0.26	0.25
Al_2O_3	12.75	13.38	13.16	13.30	14.71	13.93	15.54	14.09	14.01
Fe_2O_3#	1.56	1.88	1.29	1.67	2.24	2.23	2.30	2.05	2.05
MnO	0.04	0.05	0.05	0.06	0.07	0.06	0.07	0.06	0.07
MgO	0.12	0.07	0.09	0.06	0.44	0.32	0.44	0.40	0.32
CaO	0.91	0.93	0.94	0.77	1.94	1.68	1.91	1.78	1.58
Na_2O	4.18	4.41	4.00	3.91	4.41	4.29	4.35	4.27	4.39
K_2O	3.61	3.27	3.50	3.40	2.84	2.98	2.37	2.98	3.15
P_2O_5	0.02	0.02	0.02	0.02	0.02	0.04	0.02	0.03	0.04
LOI*	0.08	0.76	0.98	1.16	1.59	0.71	1.82	1.50	0.69
Total*	99.97	100.27	100.35	100.24	100.29	100.21	100.42	100.03	100.31
Trace Elements (XRF) (ppm)									
V	16	16	15	14	25	23	25	25	24
Cr	<3	<3	4	<3	11	4	5	4	3
Ni	<3	<3	4	<3	<3	<3	<3	<3	<3
Zn	39	35	32	36	38	32	37	35	37
Zr	174	201	108	181	184	190	182	171	172
Nb	9	11	8	10	9	8	9	8	9
Ba	778	743	942	775	776	776	870	765	772
La	30	24	31	27	24	31	29	29	36
Ce	46	52	50	45	55	52	43	43	47
Nd	26	16	12	11	16	23	15	18	25
Ga	14	15	12	14	15	14	15	13	14
Pb	18	14	17	19	15	14	16	14	14
Rb	127	105	112	100	96	94	70	102	105
Sr	74	79	79	69	154	141	151	139	125
Th	14	11	12	11	11	11	10	10	11
Y	28	24	22	19	23	25	21	23	24
Trace Elements (LA-ICPMS) (ppm)									
Sc	8.1	6.1					6.3	5.3	
Ti	984	1053					1675	1399	
V	25.1	24.8					37.8	41.6	
Ni	4.9	8.9					6.3	8.5	
Rb	134	101					69	92	
Y	30.7	23.8					22.0	21.7	
Zr	206	217					214	165	
Nb	10.77	10.90					9.51	7.92	
Cs	2.89	3.11					3.49	4.09	
Ba	729	690					808	708	
La	27.78	24.11					22.04	23.50	
Ce	52.4	48.6					47.6	43.0	
Nd	23.45	17.16					15.98	16.47	
Sm	5.02	3.70					3.32	3.33	
Eu	0.86	0.90					0.85	0.73	
Gd	4.63	3.49					3.10	3.03	
Dy	4.94	3.85					3.37	3.24	
Er	3.18	2.50					2.20	2.16	
Yb	3.36	2.64					2.44	2.41	
Lu	0.55	0.43					0.41	0.41	
Hf	6.06	5.95					5.52	4.28	
Ta	1.06	0.90					0.89	0.76	
Pb	16.7	14.1					15.6	13.9	
Th	14.79	11.34					11.90	10.46	
U	3.54	2.68					2.36	2.48	

Major elements normalised to 100%, volatile free. # All Fe expressed as Fe_2O_3. * Original Values.

Table V.2: Whole rock geochemical analyses of basaltic scoria deposits associated with the Okataina and Kapenga volcanic centres.

Scoria	OVC Tarawera Basalt	OVC Tarawera Basalt (unpicked)	OVC Tarawera Basalt	OVC Rotomaka-riri Scoria	OVC Rotomaka-riri Scoria (unpicked)	OVC Okareka Basalt	OVC Matahi Scoria	OVC Rotokawau Basalt	KVC Johnson Road Basalt
Field Number	47	47-unp	48	136	136-unp	148	150	151	124
Major Elements (wt. %)									
SiO_2	51.27	51.83	51.35	51.04	51.71	51.19	55.70	50.58	51.06
TiO_2	0.79	0.78	0.79	0.79	0.77	0.79	0.97	0.84	1.25
Al_2O_3	17.13	17.04	17.07	17.21	17.12	17.16	17.37	17.29	17.04
Fe_2O_3#	10.15	9.94	10.06	10.04	9.79	10.03	9.03	10.18	10.83
MnO	0.18	0.17	0.17	0.18	0.17	0.18	0.20	0.17	0.18
MgO	6.22	6.10	6.27	6.35	6.20	6.34	4.48	6.36	5.30
CaO	11.35	11.16	11.40	11.53	11.31	11.47	8.32	11.63	10.55
Na_2O	2.21	2.23	2.17	2.18	2.18	2.16	2.72	2.27	2.91
K_2O	0.57	0.62	0.58	0.54	0.61	0.57	0.98	0.57	0.67
P_2O_5	0.13	0.13	0.13	0.13	0.13	0.13	0.22	0.12	0.22
LOI*	-0.43	-0.46	-0.47	-0.76	-0.64	-0.41	1.07	-0.42	-0.13
Total*	100.34	100.38	100.30	100.16	100.23	100.13	100.24	100.21	99.99
Trace Elements (XRF) (ppm)									
V	260	252	256	256	248	257	216	269	279
Cr	26	26	30	34	51	34	30	57	44
Ni	6	6	5	7	6	8	3	24	15
Zn	83	79	81	80	78	81	97	80	87
Zr	61	63	63	61	63	60	128	53	106
Nb	5	5	5	5	5	5	8	4	7
Ba	208	253	222	206	214	213	318	216	212
La	<5	<5	<5	<5	7	6	13	8	6
Ce	22	<5	10	5	8	22	39	20	15
Nd	<10	12	18	21	17	12	22	20	20
Ga	16	16	16	16	15	16	17	16	18
Pb	3	2	1	1	1	2	5	1	<1
Rb	11	13	11	11	13	11	24	9	12
Sr	303	296	297	298	294	295	281	358	353
Th	1	1	<1	<1	<1	1	2	<1	1
Y	19	20	19	19	19	18	26	19	27

Unpicked samples include rhyolite clasts or inclusions within the scoria clasts. Other samples have had any rhyolitic material removed.

Major elements normalised to 100%, volatile free. # All Fe expressed as Fe_2O_3. * Original Values.

Table V.3: Compositional differences between partially devitrified and glassy samples of rhyolite lavas from the Okataina and Rotorua volcanic centres expressed as numbers of standard deviations.

	ho_2	Haroharo (ho_3)			Okareka (ho_3)	Tarawera (ho_3)	hr_2	Mean	Std Dev
Lava	Tuteheka 3	Waiti Flow	Te Horoa Dome	Okataina Flow	Eastern Rhyolite	Pokohu Flow	Ngongotaha Quarry Dome		
Major Elements									
SiO_2	+1.8	+1.3	+0.7	-0.5	0	+0.4	+2.1	+0.9	0.210
TiO_2	+5.0	+1.0	-2.5	0	0	-1.3	-2.5	0	0.004
Al_2O_3	-2.6	-2.2	-2.2	+0.3	+0.1	-1.2	-7.3	-2.2	0.078
Fe_2O_3	-2.9	-0.7	+0.3	+1.4	-1.4	-0.6	-1.7	-0.8	0.036
MnO	-1.1	-0.2	0	0	-0.3	0	0	-0.2	0.018
MgO	-2.5	+0.3	-0.5	+0.5	-1.3	-0.5	+1.0	-0.4	0.020
CaO	-17.0	-16.4	-2.0	+4.0	+7.0	+5.0	0	-2.8	0.005
Na_2O	+0.5	-0.4	+0.5	+0.1	-0.5	+0.7	+3.0	+0.6	0.074
K_2O	+0.5	+1.1	+0.2	-0.3	+1.5	-1.1	-1.2	+0.1	0.033
P_2O_5	-1.4	-1.4	0	0	+2.1	+0.7	0	0	0.007
Trace Elements									
Rb	+0.6	-0.4	-0.6	0	+0.3	+0.6	+2.5	+0.4	1.6
Sr	-1.0	-7.2	-6.0	+4.0	+6.0	+4.0	0	0	0.5
Y	-2.4	-0.1	-0.4	0	+0.2	-0.4	0	-0.4	2.7
Zr	+1.0	-0.1	-0.6	+0.1	-0.5	+0.5	+0.3	+0.1	10
Nb	0	0	+0.5	-1.0	0	-0.5	0	-0.1	1
Ga	0	+0.2	-0.6	-1.1	+0.6	0	0	-0.1	0.9
Zn	-2.7	0	-0.6	-0.2	-0.3	-0.4	+0.4	-0.5	4.7
V	-3.2	0	0	+2.7	+0.5	+0.9	+0.9	+0.3	1.1
La	+0.2	-0.2	0	-3.2	-0.2	+0.8	+1.2	-0.2	2.5

Compositional differences are calculated from data in Table V.1 as an average for each sample of $(X_{devitrified} - X_{glassy})$/ Standard Deviation. Loss of a component upon devitrification is indicated by a negative value and gain of a component by a positive value. The mean is the average compositional change for the seven lavas. All data used in the above calculations are from XRF analyses. Standard deviations are from Weaver et al. (1990) and represent analytical uncertainty for the XRF spectrometer at the University of Canterbury. Major elements in wt. %, trace elements in ppm.

Appendix VI: Electron Microprobe Analyses - Phenocrysts

Table VI.1: Electron microprobe analyses of plagioclase feldspar phenocrysts in rhyolite lavas of the Okataina Volcanic Centre.

Sample No.	63	63	63	63	63	63	109	109	109
Analysis	1	1	2	2	3	3	1	1	2
Location	core	rim	core	rim	core	rim	core	rim	core
SiO_2	60.17	65.58	65.53	65.06	67.75	66.33	63.66	63.13	62.66
TiO_2	0.07	0.03	0.04	0.05	0.05	0.00	0.09	0.02	0.00
Al_2O_3	25.97	23.77	23.37	23.48	23.65	23.89	25.13	24.41	25.05
FeO*	0.21	0.16	0.29	0.20	0.20	0.22	0.17	0.18	0.15
MnO	0.06	0.08	0.05	0.06	0.00	0.00	0.14	0.29	0.00
MgO	0.02	0.04	0.00	0.03	0.01	0.01	0.00	0.05	0.01
CaO	7.04	4.32	4.28	4.44	4.38	4.61	6.24	5.93	6.11
Na_2O	7.37	7.77	8.25	8.50	6.50	8.06	7.84	8.44	7.37
K_2O	0.33	0.65	0.58	0.63	0.55	0.53	0.49	0.45	0.42
Total	101.24	102.40	102.39	102.45	103.09	103.65	103.76	102.90	101.77
Ab	64.2	73.4	75.0	74.8	70.0	73.6	67.5	70.3	66.9
An	33.9	22.5	21.5	21.6	26.1	23.3	29.7	27.3	30.6
Or	1.9	4.1	3.5	3.7	3.9	3.2	2.8	2.5	2.5

Sample No.	109	119	119	119	119	119	119	64	64
Analysis	2	1	1	2	2	3	3	1	1
Location	rim	core	rim	core	rim	core	rim	core	rim
SiO_2	64.99	62.53	63.22	62.85	62.29	62.84	62.61	61.35	60.31
TiO_2	0.08	0.02	0.04	0.00	0.10	0.05	0.02	0.04	0.11
Al_2O_3	24.41	24.50	24.53	23.94	23.80	25.37	24.08	24.01	24.88
FeO*	0.18	0.30	0.23	0.25	0.18	0.19	0.33	0.18	0.13
MnO	0.23	0.00	0.13	0.12	0.00	0.00	0.35	0.09	0.02
MgO	0.00	0.04	0.09	0.01	0.06	0.04	0.05	0.00	0.02
CaO	5.38	6.46	6.34	5.93	5.87	6.66	5.72	5.37	6.08
Na_2O	7.80	7.64	7.05	7.64	7.51	7.24	7.64	7.85	7.65
K_2O	0.50	0.56	0.67	0.68	0.65	0.52	0.58	0.59	0.48
Total	103.57	102.05	102.30	101.42	100.46	102.91	101.38	99.48	99.68
Ab	70.3	66.0	64.1	67.2	67.2	64.3	68.3	70.1	67.6
An	26.8	30.8	31.9	28.8	29.0	32.7	28.3	26.5	29.7
Or	3.0	3.2	4.0	3.9	3.8	3.0	3.4	3.5	2.8

Sample No.	64	64	117	117	117	117	152	152	152
Analysis	2	2	1	1	2	2	1	1	2
Location	core	rim	core	rim	core	rim	core	rim	core
SiO_2	59.54	60.95	65.01	64.67	64.41	65.52	63.71	64.16	61.41
TiO_2	0.10	0.02	0.11	0.10	0.01	0.09	0.09	0.04	0.11
Al_2O_3	25.32	24.6	23.01	23.13	23.09	22.06	23.21	23.21	24.12
FeO*	0.15	0.14	0.15	0.27	0.21	0.20	0.40	0.34	0.38
MnO	0.05	0.09	0.03	0.04	0.07	0.04	1.21	0.81	0.00
MgO	0.03	0.01	0.01	0.07	0.05	0.04	0.00	0.00	0.03
CaO	7.03	5.73	4.33	4.08	4.47	3.27	5.00	5.30	6.04
Na_2O	7.36	7.89	9.07	9.36	9.25	9.58	8.52	8.38	7.65
K_2O	0.41	0.45	0.78	0.84	0.66	1.01	0.64	0.55	0.59
Total	99.99	99.88	102.5	102.56	102.22	101.81	102.78	102.79	100.33
Ab	63.9	69.5	75.7	76.9	76.1	79.5	72.8	71.8	67.2
An	33.7	27.9	20.0	18.5	20.3	15.0	23.6	25.1	29.3
Or	2.3	2.6	4.3	4.6	3.6	5.5	3.6	3.1	3.4

Sample No.	152	6	6	6	6	7	7	7	7
Analysis	2	1	1	2	2	1	1	2	2
Location	rim	core	rim	core	rim	core	rim	core	rim
SiO_2	62.81	54.71	60.35	58.32	62.10	60.65	60.62	59.43	56.60
TiO_2	0.03	0.06	0.05	0.00	0.11	0.10	0.06	0.04	0.01
Al_2O_3	23.00	28.07	24.73	26.22	24.29	23.84	24.08	24.99	26.92
FeO*	0.57	0.24	0.19	0.31	0.10	0.10	0.38	0.47	0.66
MnO	0.41	0.03	0.03	0.05	0.05	0.00	0.28	0.17	0.00
MgO	0.01	0.00	0.01	0.01	0.03	0.03	0.05	0.04	0.05
CaO	5.03	10.63	6.81	8.02	5.89	6.38	6.49	7.40	9.66
Na_2O	8.47	5.28	7.37	6.62	7.76	7.80	7.58	7.22	5.78
K_2O	0.63	0.16	0.37	0.26	0.48	0.37	0.36	0.29	0.25
Total	100.96	99.18	99.91	99.81	100.81	99.27	99.90	100.05	99.93
Ab	72.6	46.9	64.8	59.0	68.5	67.4	66.5	62.8	51.2
An	23.8	52.2	33.1	39.5	28.7	30.5	31.5	35.6	47.3
Or	3.6	0.9	2.1	1.5	2.8	2.1	2.1	1.7	1.4

Analyses in weight percent. All iron expressed as FeO*.

Sample No.	7	7	24	24	24	24	32	32	32
Analysis	3	3	1	1	2	2	1	1	2
Location	core	rim	core	rim	core	rim	core	rim	core
SiO_2	59.24	60.44	59.18	62.94	58.33	62.87	58.99	61.87	59.26
TiO_2	0.06	0.04	0.00	0.06	0.00	0.04	0.07	0.00	0.00
Al_2O_3	25.34	24.35	26.24	24.21	27.24	24.03	25.99	25.07	25.17
FeO*	0.10	0.23	0.26	0.16	0.28	0.25	0.35	0.27	0.19
MnO	0.00	0.00	0.04	0.02	0.01	0.12	0.05	0.15	0.03
MgO	0.09	0.04	0.01	0.01	0.01	0.06	0.03	0.01	0.03
CaO	7.65	6.83	8.36	5.70	9.18	5.42	7.52	6.35	7.17
Na_2O	7.13	7.25	6.65	8.20	6.19	8.02	6.97	7.58	7.31
K_2O	0.30	0.35	0.32	0.54	0.28	0.51	0.29	0.37	0.26
Total	99.91	99.53	101.06	101.84	101.52	101.32	100.26	101.67	99.42
Ab	61.7	64.4	57.9	70.1	54.1	70.7	61.6	66.9	63.9
An	36.6	33.5	40.2	26.9	44.3	26.4	36.7	31.0	34.6
Or	1.7	2.0	1.8	3.0	1.6	3.0	1.7	2.2	1.5

Sample No.	32	38	38	38	38	38	38	44	44
Analysis	2	1	1	2	2	3	3	1	1
Location	rim	core	rim	core	rim	core	rim	core	rim
SiO_2	59.49	58.79	62.67	61.28	62.17	59.53	60.63	56.49	61.31
TiO_2	0.04	0.08	0.05	0.01	0.02	0.07	0.08	0.07	0.05
Al_2O_3	24.78	27.15	25.47	26.31	25.33	27.34	26.42	28.09	25.2
FeO*	0.34	0.23	0.19	0.34	0.21	0.34	0.33	0.22	0.17
MnO	0.01	0.00	0.07	0.02	0.00	0.09	0.05	0.03	0.05
MgO	0.01	0.07	0.03	0.03	0.06	0.03	0.02	0.03	0.07
CaO	6.51	8.49	6.55	7.33	7.06	9.20	7.99	10.17	6.72
Na_2O	7.49	6.47	7.25	7.07	7.39	6.31	6.73	5.49	7.27
K_2O	0.35	0.23	0.30	0.34	0.33	0.26	0.25	0.20	0.43
Total	99.02	101.51	102.58	102.73	102.57	103.17	102.5	100.79	101.27
Ab	66.2	57.2	65.5	62.3	64.2	54.6	59.5	48.8	64.5
An	31.8	41.5	32.7	35.7	33.9	44.0	39.0	50.0	33.0
Or	2.0	1.3	1.8	2.0	1.9	1.5	1.5	1.2	2.5

Sample No.	44	44	60	60	60	60	60	60	90
Analysis	2	2	1	1	2	2	3	3	1
Location	core	rim	core	rim	core	rim	core	rim	core
SiO_2	62.25	60.66	58.94	62.64	63.18	61.21	62.08	63.51	60.19
TiO_2	0.06	0.00	0.06	0.14	0.05	0.08	0.07	0.02	0.06
Al_2O_3	24.62	25.77	27.10	25.24	25.98	26.18	26.23	25.28	25.47
FeO*	0.21	0.32	0.22	0.25	0.23	0.30	0.22	0.24	0.19
MnO	0.07	0.07	0.00	0.07	0.02	0.22	0.15	0.09	0.00
MgO	0.03	0.04	0.06	0.01	0.01	0.00	0.01	0.00	0.01
CaO	6.22	7.19	8.63	6.22	6.99	7.83	7.73	6.34	7.25
Na_2O	7.45	7.24	6.54	7.75	7.28	6.96	7.06	7.62	7.73
K_2O	0.47	0.38	0.24	0.35	0.25	0.26	0.29	0.35	0.32
Total	101.38	101.67	101.79	102.67	103.99	103.04	103.84	103.45	101.22
Ab	66.5	63.2	57.0	67.9	64.4	60.7	61.3	67.1	64.7
An	30.7	34.7	41.6	30.1	34.2	37.7	37.1	30.9	33.5
Or	2.8	2.2	1.4	2.0	1.4	1.5	1.7	2.0	1.8

Sample No.	90	90	90	92	92	98	98	98	98
Analysis	1	2	2	1	1	1	1	2	2
Location	rim	core	rim	core	rim	core	rim	core	rim
SiO_2	60.83	57.45	59.18	61.18	60.77	59.81	61.41	60.68	61.37
TiO_2	0.13	0.03	0.04	0.10	0.07	0.09	0.03	0.09	0.03
Al_2O_3	24.93	27.96	26.35	25.70	26.40	25.28	24.21	25.34	24.57
FeO*	0.25	0.39	0.44	0.30	0.34	0.32	0.20	0.34	0.25
MnO	0.11	0.18	0.06	0.05	0.12	0.09	0.00	0.14	0.00
MgO	0.00	0.05	0.01	0.06	0.03	0.04	0.01	0.03	0.01
CaO	6.63	9.57	7.90	7.20	7.92	7.02	5.91	7.01	6.51
Na_2O	8.06	6.12	7.03	6.96	6.73	7.42	7.85	7.36	7.80
K_2O	0.39	0.19	0.37	0.32	0.26	0.34	0.45	0.30	0.38
Total	101.33	101.94	101.38	101.87	102.64	100.41	100.07	101.29	100.92
Ab	67.3	53.1	60.4	62.4	59.7	64.4	68.8	64.4	67.0
An	30.6	45.8	37.5	35.7	38.8	33.7	28.6	33.9	30.9
Or	2.1	1.1	2.1	1.9	1.5	1.9	2.6	1.7	2.2

Analyses in weight percent. All iron expressed as FeO*.

Sample No.	105	105	105	105	105	105	105	105	113
Analysis	1	1	2	2	3	3	4	4	1
Location	core	rim	core	rim	core	rim	core	rim	core
SiO_2	58.86	59.65	55.11	63.28	61.16	62.09	59.30	60.06	53.88
TiO_2	0.00	0.04	0.03	0.00	0.02	0.00	0.08	0.08	0.03
Al_2O_3	27.42	26.85	28.76	25.63	24.91	24.60	26.62	25.64	28.51
FeO*	0.31	0.26	0.44	0.10	0.15	0.20	0.61	0.31	0.42
MnO	0.05	0.06	0.08	0.02	0.00	0.08	0.86	0.28	0.10
MgO	0.03	0.05	0.04	0.03	0.02	0.00	0.08	0.04	0.06
CaO	9.11	8.63	11.17	6.67	6.95	6.56	8.60	7.82	11.19
Na_2O	6.14	6.46	5.10	7.23	7.97	8.01	7.00	7.59	5.51
K_2O	0.16	0.23	0.15	0.26	0.27	0.31	0.22	0.22	0.13
Total	102.08	102.23	100.88	103.22	101.45	101.85	103.37	102.04	99.83
Ab	54.5	56.8	44.9	65.2	66.5	67.7	58.8	63.0	46.8
An	44.6	41.9	54.3	33.2	32.0	30.6	39.9	35.8	52.5
Or	0.9	1.3	0.9	1.5	1.5	1.7	1.2	1.2	0.7

Sample No.	113	113	113	134	134	134	134	134	158
Analysis	1	2	2	1	1	2	2	3	1
Location	rim	core	rim	core	rim	core	rim	core	core
SiO_2	56.07	56.29	57.42	62.08	61.37	62.88	62.18	62.93	62.38
TiO_2	0.13	0.09	0.01	0.07	0.07	0.03	0.05	0.09	0.06
Al_2O_3	26.81	26.86	26.84	24.07	24.36	23.69	24.24	23.32	24.46
FeO*	0.52	0.44	0.36	0.21	0.23	0.21	0.16	0.28	0.2
MnO	0.11	0.09	0.08	0.00	0.00	0.05	0.08	0.02	0.01
MgO	0.08	0.06	0.05	0.01	0.03	0.03	0.00	0.03	0.03
CaO	9.40	9.45	9.45	5.33	6.12	5.15	5.55	5.04	5.64
Na_2O	6.47	6.66	6.54	8.31	7.56	7.99	8.16	8.13	7.95
K_2O	0.25	0.21	0.23	0.60	0.52	0.74	0.60	0.68	0.45
Total	99.84	100.15	100.98	100.68	100.26	100.77	101.02	100.52	101.18
Ab	54.7	55.4	54.9	71.3	67.0	70.6	70.2	71.6	70.0
An	43.9	43.4	43.8	25.3	30.0	25.1	26.4	24.5	27.4
Or	1.4	1.1	1.3	3.4	3.0	4.3	3.4	3.9	2.6

Sample No.	158	158	158	173	173	173	173	173	173
Analysis	1	2	2	1	1	2	2	3	3
Location	rim	core	rim	core	rim	core	rim	core	rim
SiO_2	64.2	61.23	63.22	59.52	57.95	58.00	61.41	59.25	61.46
TiO_2	0.08	0.02	0.01	0.13	0.09	0.02	0.00	0.00	0.04
Al_2O_3	23.41	25.05	23.67	24.95	26.18	26.65	24.55	27.15	25.25
FeO*	0.16	0.26	0.18	0.81	0.01	0.26	0.23	0.19	0.21
MnO	0.14	0.00	0.00	2.04	0.00	0.04	0.01	0.16	0.11
MgO	0.07	0.01	0.01	0.04	0.03	0.01	0.00	0.04	0.04
CaO	4.65	6.72	4.98	6.96	8.79	8.89	6.36	8.68	6.93
Na_2O	8.71	7.43	8.31	7.78	6.70	6.41	7.62	6.65	7.30
K_2O	0.63	0.36	0.56	0.35	0.21	0.29	0.38	0.23	0.33
Total	102.05	101.08	100.94	102.58	99.96	100.57	100.56	102.35	101.67
Ab	74.5	65.3	72.7	65.6	57.3	55.7	66.9	57.4	64.3
An	22.0	32.6	24.1	32.4	41.5	42.7	30.9	41.4	33.7
Or	3.6	2.1	3.2	1.9	1.2	1.7	2.2	1.3	1.9

Sample No.	176	176	176	176
Analysis	1	1	2	2
Location	core	rim	core	rim
SiO_2	62.36	61.80	59.27	62.08
TiO_2	0.04	0.10	0.07	0.02
Al_2O_3	24.43	24.36	26.29	24.58
FeO*	0.14	0.20	0.20	0.23
MnO	0.05	0.00	0.01	0.04
MgO	0.00	0.00	0.01	0.01
CaO	5.58	5.88	8.05	5.88
Na_2O	7.93	7.85	6.98	8.00
K_2O	0.58	0.58	0.39	0.65
Total	101.11	100.77	101.27	101.49
Ab	69.6	68.4	59.7	68.5
An	27.1	28.3	38.1	27.8
Or	3.3	3.3	2.2	3.7

Analyses in weight percent. All iron expressed as FeO*.

Table VI.2: Electron microprobe analyses of plagioclase feldspar phenocrysts in rhyolite lavas of the Rotorua Volcanic Centre.

Sample No.	87	87	87	87	103	103	104	104	104	104
Analysis	1	1	2	2	1	1	1	1	2	2
Location	core	rim	core	rim	core	rim	core	rim	core	rim
SiO_2	61.23	62.53	61.34	62.06	59.39	65.13	63.52	58.32	61.15	62.86
TiO_2	0.14	0.09	0.17	0.02	0.03	0.03	0.18	0.05	0.10	0.03
Al_2O_3	24.26	23.74	24.51	24.50	26.28	22.96	23.38	23.20	23.67	23.14
FeO*	0.37	0.14	0.27	0.21	0.21	0.17	0.24	0.21	0.18	0.22
MnO	0.29	0.55	0.15	0.72	0.06	0.06	0.10	0.08	0.07	0.07
MgO	0.03	0.04	0.03	0.09	0.01	0.01	0.01	0.01	0.01	0.01
CaO	6.47	5.79	6.76	6.78	8.04	4.47	4.42	5.23	5.44	4.71
Na_2O	7.51	8.00	7.58	7.46	6.71	8.63	8.61	7.50	7.88	8.34
K_2O	0.53	0.64	0.51	0.57	0.32	0.73	0.70	0.61	0.60	0.75
Total	100.83	101.52	101.32	102.41	101.05	102.19	101.16	95.21	99.10	100.13
Ab	65.7	68.8	65.1	64.4	59.1	74.5	74.8	69.5	69.9	72.9
An	31.3	27.5	32.1	32.4	39.1	21.3	21.2	26.8	26.7	22.7
Or	3.1	3.6	2.9	3.2	1.8	4.1	4.0	3.7	3.5	4.3

Table VI.3: Electron microprobe analyses of plagioclase feldspar phenocrysts in rhyolite lavas of the Kapenga Volcanic Centre.

Sample No.	170	170	170	170	170	170
Analysis	1	1	2	2	3	3
Location	core	rim	core	rim	core	rim
SiO_2	60.05	62.49	63.31	62.67	57.54	63.44
TiO_2	0.00	0.01	0.06	0.00	0.13	0.00
Al_2O_3	25.47	24.18	23.65	24.65	27.86	23.58
FeO*	0.18	0.20	0.23	0.3	0.25	0.17
MnO	0.00	0.06	0.00	0.00	0.00	0.04
MgO	0.00	0.05	0.05	0.04	0.01	0.01
CaO	7.64	5.93	5.66	6.36	9.88	4.95
Na_2O	7.05	7.75	8.14	7.86	5.66	8.20
K_2O	0.52	0.51	0.62	0.57	0.23	0.71
Total	100.91	101.18	101.72	102.45	101.56	101.1
Ab	60.7	68.2	69.7	66.9	50.2	71.9
An	36.3	28.8	26.8	29.9	48.4	24.0
Or	3.0	2.9	3.5	3.2	1.3	4.1

Table VI.4: Electron microprobe analyses of pyroxene phenocrysts in rhyolite lavas of the Okataina Volcanic Centre.

Sample No.	63	63	63	63	109	109	109	109	119
Analysis	1	1	2	2	1	1	2	2	2
Location	core	rim	core	rim	core	rim	core	rim	core
SiO_2	51.30	51.78	54.00	52.05	51.99	51.30	51.43	51.36	53.44
TiO_2	0.12	0.13	0.17	0.20	0.11	0.13	0.12	0.14	0.13
Al_2O_3	0.21	0.28	0.63	0.26	0.31	0.34	0.47	0.35	0.50
FeO*	33.97	33.79	26.35	33.39	31.79	32.96	31.99	33.05	26.27
MnO	2.48	2.29	1.41	2.63	1.81	2.04	1.84	1.61	1.40
MgO	13.77	13.88	19.71	13.67	15.80	14.62	15.65	14.65	19.86
CaO	1.05	1.19	1.30	1.10	0.90	0.75	0.77	0.76	1.01
Na_2O	0.00	0.00	0.0i	0.00	0.04	0.05	0.05	0.00	0.00
K_2O	0.04	0.00	0.02	0.03	0.01	0.02	0.02	0.03	0.03
Total	102.94	103.34	103.60	103.33	102.76	102.21	102.34	101.95	102.64
Wo	2.16	2.44	2.58	2.28	1.83	1.55	1.57	1.58	2.01
En	39.35	39.67	54.41	39.41	44.75	42.00	44.47	42.28	54.99
Fs	58.49	57.89	43.02	58.31	53.42	56.45	53.96	56.15	43.00

Analyses in weight percent. All iron expressed as FeO*.

Sample No.	119	117	117	117	117	152	152	6	6
Analysis	2	1	1	2	2	1	1	1	1
Location	rim	core	rim	core	rim	core	rim	core	rim
SiO_2	53.69	51.42	50.39	50.90	51.28	51.55	51.89	52.61	51.99
TiO_2	0.09	0.14	0.15	0.03	0.12	0.17	0.12	0.14	0.11
Al_2O_3	0.32	0.23	0.23	0.26	0.19	1.02	0.30	0.41	0.42
FeO*	28.33	32.73	31.87	31.30	32.88	31.10	32.56	26.16	25.93
MnO	1.72	2.28	2.23	2.09	2.31	2.35	2.42	1.87	2.19
MgO	17.82	14.37	14.74	14.57	13.64	15.72	15.98	18.52	17.94
CaO	0.81	1.02	1.18	1.03	1.11	1.75	1.01	0.76	0.73
Na_2O	0.00	0.00	0.00	0.12	0.01	0.00	0.00	0.00	0.00
K_2O	0.01	0.00	0.03	0.01	0.00	0.01	0.00	0.00	0.06
Total	102.79	102.19	100.82	100.31	101.54	103.67	104.28	100.47	99.37
Wo	1.65	2.11	2.44	2.17	2.33	3.52	2.00	1.57	1.53
En	50.52	41.34	42.44	42.78	39.89	43.96	43.97	53.21	52.37
Fs	47.83	56.55	55.12	55.05	57.78	52.52	54.04	45.22	46.10

Sample No.	7	7	7	7	24	24	24	24	32
Analysis	1	1	2	2	1	1	2	2	1
Location	core	rim	core	rim	core	rim	core	rim	core
SiO_2	53.39	53.55	53.51	53.69	52.60	53.89	53.61	53.43	52.60
TiO_2	0.11	0.13	0.16	0.13	0.18	0.20	0.13	0.04	0.10
Al_2O_3	0.28	0.34	0.27	0.37	0.27	0.44	0.56	0.32	0.46
FeO*	26.61	26.51	25.67	26.30	27.33	25.26	23.59	26.16	22.63
MnO	2.62	2.20	1.91	2.36	1.86	2.28	1.57	2.11	2.10
MgO	19.65	19.73	19.72	19.64	18.24	19.71	20.86	19.32	20.19
CaO	0.75	0.71	0.89	0.79	0.74	0.78	1.14	0.88	0.64
Na_2O	0.00	0.00	0.07	0.00	0.07	0.11	0.06	0.12	0.01
K_2O	0.01	0.03	0.01	0.00	0.07	0.00	0.02	0.00	0.00
Total	103.42	103.20	102.21	103.28	101.36	102.67	101.54	102.38	98.73
Wo	1.47	1.40	1.79	1.56	1.51	1.57	2.29	1.76	1.33
En	53.68	54.26	55.01	54.10	51.88	55.15	58.26	53.93	58.46
Fs	44.85	44.34	43.20	44.34	46.61	43.28	39.45	44.31	40.21

Sample No.	32	32	32	38	38	38	38	44	44
Analysis	1	2	2	1	1	2	2	1	1
Location	rim	core	rim	core	rim	core	rim	core	rim
SiO_2	52.14	52.59	52.24	52.37	53.32	54.12	53.36	54.34	54.44
TiO_2	0.07	0.13	0.10	0.02	0.06	0.08	0.11	0.15	0.14
Al_2O_3	0.35	0.38	0.36	0.42	0.40	0.30	0.25	0.51	0.58
FeO*	25.67	24.98	25.95	27.35	26.62	25.89	26.49	23.20	22.30
MnO	2.18	1.79	2.21	2.58	2.24	2.10	2.20	1.97	1.90
MgO	18.51	19.16	18.88	18.29	18.98	19.13	18.36	21.59	22.03
CaO	0.78	0.79	0.70	0.73	0.66	0.75	0.72	0.60	0.55
Na_2O	0.06	0.01	0.01	0.00	0.09	0.00	0.00	0.01	0.06
K_2O	0.03	0.03	0.05	0.02	0.04	0.05	0.01	0.00	0.07
Total	99.79	99.86	100.50	101.78	102.41	102.42	101.50	102.37	102.07
Wo	1.61	1.64	1.43	1.47	1.33	1.52	1.48	1.19	1.10
En	53.33	55.12	53.64	51.34	53.22	54.06	52.48	59.72	61.17
Fs	45.06	43.24	44.93	47.19	45.45	44.42	46.05	39.09	37.73

Sample No.	44	44	90	90	90	90	90	90	92
Analysis	2	2	1	1	2	2	3	3	1
Location	core	rim	core	rim	core	rim	core	rim	core
SiO_2	54.05	54.38	53.20	54.13	52.74	53.12	53.02	54.33	53.40
TiO_2	0.11	0.07	0.17	0.05	0.07	0.13	0.11	0.12	0.11
Al_2O_3	0.60	0.57	0.41	0.24	0.24	0.38	0.42	0.36	0.57
FeO*	22.71	22.03	28.30	26.47	28.97	28.14	26.53	24.57	22.21
MnO	1.88	1.87	1.53	2.24	2.00	2.02	1.96	1.61	1.94
MgO	21.60	21.95	18.67	19.76	17.25	18.80	19.16	20.29	21.85
CaO	0.60	0.63	0.85	0.71	0.73	0.73	0.99	0.75	0.92
Na_2O	0.00	0.01	0.00	0.11	0.00	0.08	0.05	0.07	0.04
K_2O	0.06	0.03	0.05	0.09	0.03	0.00	0.01	0.04	0.02
Total	101.61	101.54	103.18	103.80	102.03	103.40	102.25	102.14	101.06
Wo	1.20	1.26	1.70	1.40	1.49	1.45	1.98	1.52	1.83
En	60.27	61.27	51.82	54.30	49.06	51.85	53.42	57.11	60.57
Fs	38.53	37.46	46.48	44.30	49.45	46.70	44.60	41.37	37.60

Analyses in weight percent. All iron expressed as FeO*.

Sample No.	92	92	92	92	92	98	98	98	98
Analysis	1	2	2	3	3	1	1	2	2
Location	rim	core	rim	core	rim	core	rim	core	rim
SiO_2	53.44	54.25	54.26	52.84	54.25	51.09	51.53	53.50	53.13
TiO_2	0.13	0.13	0.14	0.17	0.13	0.09	0.06	0.13	0.05
Al_2O_3	0.46	0.20	0.42	0.42	0.46	0.36	0.46	0.41	0.36
FeO*	25.04	26.32	25.05	25.27	24.53	26.59	25.32	26.60	27.00
MnO	2.14	2.61	2.12	2.38	2.10	1.92	1.90	1.72	2.28
MgO	20.25	18.75	20.30	19.66	20.35	18.37	18.88	19.50	18.68
CaO	0.80	0.72	0.80	0.77	0.81	0.90	1.02	1.06	0.74
Na_2O	0.01	0.00	0.00	0.01	0.07	0.00	0.00	0.00	0.00
K_2O	0.01	0.00	0.04	0.00	0.03	0.00	0.00	0.04	0.01
Total	102.28	102.98	103.13	101.52	102.73	99.32	99.17	102.96	102.25
Wo	1.59	1.46	1.59	1.55	1.62	1.85	2.10	2.10	1.49
En	56.11	52.79	56.18	55.00	56.71	52.45	54.10	53.93	52.39
Fs	42.30	45.75	42.23	43.45	41.67	45.70	43.80	43.97	46.12

Sample No.	105	105	105	105	113	113	113	113	173
Analysis	1	1	2	2	1	1	2	2	1
Location	core	rim	core	rim	core	rim	core	rim	core
SiO_2	52.83	52.68	51.80	52.18	53.82	53.61	53.16	52.80	54.31
TiO_2	0.12	0.10	0.15	0.08	0.18	0.15	0.12	0.19	0.15
Al_2O_3	0.49	0.44	0.46	0.44	0.51	0.50	0.89	0.62	0.46
FeO*	25.61	25.38	27.74	26.98	23.66	22.58	20.44	22.80	23.88
MnO	1.53	1.47	1.95	2.10	1.39	1.41	1.25	1.46	1.53
MgO	19.72	19.34	17.91	18.16	21.42	22.19	23.32	21.77	20.60
CaO	0.78	0.83	0.78	0.75	0.93	1.07	0.94	1.03	0.72
Na_2O	0.04	0.09	0.01	0.01	0.06	0.00	0.00	0.19	0.07
K_2O	0.04	0.03	0.01	0.03	0.00	0.00	0.04	0.08	0.01
Total	101.16	100.36	100.81	100.73	101.97	101.51	100.16	100.94	101.73
Wo	1.58	1.70	1.59	1.54	1.85	2.11	1.87	2.05	1.46
En	55.52	55.24	50.97	51.84	59.25	60.92	64.47	60.25	58.22
Fs	42.90	43.06	47.44	46.62	38.90	36.97	33.66	37.70	40.32

Sample No.	173	173	173
Analysis	1	2	2
Location	rim	core	rim
SiO_2	53.71	53.84	53.89
TiO_2	0.13	0.11	0.14
Al_2O_3	0.37	0.39	0.44
FeO*	23.94	25.47	25.52
MnO	2.04	1.57	1.64
MgO	20.62	19.69	19.44
CaO	0.93	0.89	0.93
Na_2O	0.00	0.07	0.00
K_2O	0.03	0.00	0.00
Total	101.77	102.03	102.00
Wo	1.86	1.80	1.89
En	57.47	55.45	54.98
Fs	40.67	42.75	43.13

Table VI.5: Electron microprobe analyses of pyroxene phenocrysts in rhyolite lavas of the Rotorua Volcanic Centre.

Sample No.	87	87	87	87	104	104	104	104
Analysis	1	1	2	2	1	1	2	2
Location	core	rim	core	rim	core	rim	core	rim
SiO_2	52.69	52.71	52.62	53.55	49.91	49.24	52.21	53.42
TiO_2	0.09	0.10	0.20	0.13	0.12	0.14	0.10	0.17
Al_2O_3	0.24	0.32	0.43	0.29	0.26	0.24	0.35	0.57
FeO*	30.08	29.07	28.80	28.75	28.11	27.84	27.79	25.19
MnO	1.16	1.91	1.63	1.56	2.08	2.33	1.93	1.53
MgO	18.43	18.46	18.28	17.88	15.76	15.39	17.27	19.81
CaO	0.71	0.83	0.85	0.75	0.79	0.71	0.77	0.95
Na_2O	0.15	0.06	0.09	0.07	0.01	0.00	0.10	0.01
K_2O	0.01	0.02	0.04	0.00	0.06	0.04	0.08	0.01
Total	103.56	103.48	102.94	102.98	97.10	95.93	100.60	101.66
Wo	1.40	1.64	1.70	1.52	1.71	1.55	1.60	1.92
En	50.53	50.65	50.82	50.46	47.36	46.86	50.04	55.81
Fs	48.07	47.72	47.49	48.02	50.94	51.59	48.35	42.26

Analyses in weight percent. All iron expressed as FeO*.

Table VI.6: Electron microprobe analyses of pyroxene phenocrysts in rhyolite lavas of the Kapenga Volcanic Centre.

Sample No.	170	170	170	170
Analysis	1	1	2	2
Location	core	rim	core	rim
SiO_2	51.89	52.89	53.43	53.20
TiO_2	0.09	0.10	0.15	0.12
Al_2O_3	0.33	0.26	0.37	0.35
FeO*	31.04	30.40	28.91	29.35
MnO	1.85	2.27	1.64	1.86
MgO	15.34	15.18	16.96	16.50
CaO	1.08	0.77	1.37	1.14
Na_2O	0.05	0.01	0.01	0.00
K_2O	0.04	0.04	0.01	0.00
Total	101.71	101.92	102.85	102.52
Wo	2.25	1.62	2.81	2.35
En	44.36	44.55	48.33	47.36
Fs	53.40	53.83	48.87	50.29

Table VI.7: Electron microprobe analyses of amphibole phenocrysts in rhyolite lavas of the Okataina Volcanic Centre.

Sample No.	107	107	107	109	109	109	119	119	64
Analysis	1	2	3	1	2	3	1	2	1
	Cgt	Ca-Amph	Ca-Amph	Ca-Amph	Ca-Amph	Ca-Amph	Ca-Amph	Ca-Amph	Ca-Amph
SiO_2	54.71	50.76	49.26	49.54	44.27	46.72	48.31	47.97	47.16
TiO_2	0.28	1.05	1.27	1.38	2.15	1.93	1.63	1.45	1.45
Al_2O_3	1.46	5.78	6.94	6.95	10.48	7.62	7.01	7.07	6.94
FeO*	20.03	14.00	13.93	19.87	15.96	14.58	17.28	20.05	18.59
MnO	1.55	0.73	0.66	0.65	0.25	0.46	0.79	0.64	0.90
MgO	18.98	15.28	14.03	11.41	12.97	14.5	12.42	11.35	11.81
CaO	1.56	10.06	11.07	10.14	10.39	11.12	10.54	10.77	10.04
Na_2O	0.34	1.18	1.35	1.29	1.98	1.52	1.64	1.49	1.49
K_2O	0.04	0.27	0.20	0.30	0.35	0.33	0.47	0.58	0.41
Total	98.95	99.11	98.71	101.53	98.8	98.78	100.09	101.37	98.79

Sample No.	64	64	64	117	117	152	152	6	6
Analysis	2	3	4	1	2	1	2	1	2
	Ca-Amph	Ca-Amph	Ca-Amph	Ca-Amph	Ca-Amph	Ca-Amph	Ca-Amph	Cgt	Cgt
SiO_2	48.48	47.5	46.13	47.89	46.77	46.73	49.06	53.12	51.89
TiO_2	1.1	1.38	1.35	1.64	1.72	2.13	1.23	0.22	0.39
Al_2O_3	6.00	7.25	7.48	6.58	6.96	8.02	5.76	1.39	1.68
FeO*	16.75	16.61	18.18	17.73	17.56	17.85	19.39	21.49	21.96
MnO	0.58	0.56	0.54	0.74	0.70	1.01	0.65	1.59	1.64
MgO	12.92	12.81	11.63	12.17	11.98	11.99	12.2	17.23	16.8
CaO	10.36	10.29	10.28	10.28	10.24	10.62	10.44	1.69	1.92
Na_2O	1.31	1.59	1.67	1.78	1.98	1.89	1.38	0.33	0.38
K_2O	0.29	0.34	0.39	0.27	0.48	0.33	0.41	0.05	0.01
Total	97.79	98.33	97.65	99.08	98.39	100.57	100.52	97.11	96.67

Sample No.	6	7	7	7	7	24	24	24	24
Analysis	3	1	2	3	4	1	2	3	4
	Cgt	Ca-Amph	Ca-Amph	Ca-Amph	Ca-Amph	Cgt	Cgt	Cgt	Cgt
SiO_2	54.2	48.52	47.77	48.88	49.64	54.56	53.53	54.84	53.61
TiO_2	0.30	1.29	1.98	1.20	1.77	0.37	0.38	0.31	0.31
Al_2O_3	1.52	6.16	7.18	6.13	7.19	1.37	2.03	1.67	1.98
FeO*	21.05	15.34	15.00	15.28	14.57	21.11	20.77	21.02	20.63
MnO	1.59	0.99	0.64	0.73	0.39	1.67	1.52	1.48	1.64
MgO	17.23	14.12	14.01	13.91	14.04	17.76	17.19	17.64	17.53
CaO	1.57	10.53	10.62	10.29	11.29	1.59	2.41	2.47	2.22
Na_2O	0.29	1.39	1.40	1.41	1.64	0.34	0.53	0.43	0.48
K_2O	0.02	0.27	0.29	0.29	0.35	0.03	0.02	0.09	0.04
Total	97.77	98.61	98.89	98.12	100.88	98.8	98.38	99.95	98.44

Analyses in weight percent. All iron expressed as FeO*.

Sample No.	24	32	32	32	32	44	44	44	60
Analysis	5	1	2	3	4	1	2	3	1
	Cgt	Cgt	Ca-Amph	Ca-Amph	Ca-Amph	Ca-Amph	Ca-Amph	Ca-Amph	Cgt
SiO_2	54.54	54.16	49.12	47.79	48.78	50.26	50.55	50.38	54.69
TiO_2	0.29	0.32	1.1	1.44	1.21	0.96	0.84	0.92	0.31
Al_2O_3	1.61	1.70	5.26	6.34	5.77	5.86	5.84	5.74	1.7
FeO*	21.27	21.17	14.48	14.65	14.76	13.64	12.74	14.3	20.19
MnO	1.68	1.69	0.86	0.65	0.99	1.03	0.7	1.12	1.68
MgO	17.62	17.44	14.8	14.16	13.99	15.47	16.11	15.14	18.21
CaO	1.67	2.04	10.00	10.19	10.12	9.95	10.09	10.01	1.75
Na_2O	0.41	0.45	1.24	1.43	1.47	1.02	1.12	1.08	0.35
K_2O	0.02	0.01	0.22	0.32	0.27	0.26	0.23	0.26	0.00
Total	99.11	98.98	97.08	96.97	97.36	98.45	98.22	98.95	98.88

Sample No.	60	60	60	60	90	90	90	92	92
Analysis	2	3	4	5	1	2	3	1	2
	Cgt	Ca-Amph	Cgt	Ca-Amph	Ca-Amph	Ca-Amph	Ca-Amph	Ca-Amph	Ca-Amph
SiO_2	53.66	47.47	55.15	50.74	50.96	50.83	47.79	47.68	48.73
TiO_2	0.33	2.16	0.41	1.04	1.19	1.29	1.86	1.73	1.53
Al_2O_3	1.66	8.62	1.68	5.67	6.18	6.20	6.85	7.47	7.02
FeO*	20.36	13.71	19.68	13.7	15.97	14.7	14.57	14.59	14.25
MnO	1.72	0.59	1.50	0.81	0.76	0.79	0.75	0.70	0.81
MgO	18.6	14.36	18.55	15.46	14.66	14.88	14.67	14.64	14.70
CaO	1.73	10.56	1.78	10.09	10.09	10.43	10.82	10.90	10.91
Na_2O	0.42	1.90	0.44	1.16	1.53	1.50	1.69	1.77	1.60
K_2O	0.01	0.29	0.00	0.19	0.28	0.30	0.34	0.26	0.24
Total	98.49	99.66	99.19	98.86	101.62	100.92	99.34	99.74	99.79

Sample No.	98	98	98	98	105	105	105	105	105
Analysis	1	2	3	4	1	2	3	4	5
	Ca-Amph	Ca-Amph	Ca-Amph	Ca-Amph	Ca-Amph	Ca-Amph	Ca-Amph	Ca-Amph	Ca-Amph
SiO_2	46.86	48.03	48.3	48.14	48.67	48.8	47.88	44.49	47.08
TiO_2	1.74	1.62	1.48	1.47	1.64	1.64	1.41	3.25	2.00
Al_2O_3	7.05	7.21	6.87	6.91	7.05	7.19	6.71	11.43	7.74
FeO*	13.69	14.18	14.4	15.1	14.37	13.9	14.74	13.27	14.97
MnO	0.42	0.77	0.60	0.59	0.66	0.58	0.68	0.26	0.59
MgO	14.29	14.37	14.12	13.87	14.58	14.48	14.4	14.15	13.57
CaO	10.62	10.72	10.6	10.51	10.76	10.62	10.56	10.93	10.95
Na_2O	1.55	1.63	1.48	1.35	1.51	1.48	1.42	2.42	1.96
K_2O	0.30	0.34	0.27	0.28	0.26	0.26	0.23	0.22	0.27
Total	96.52	98.87	98.12	98.22	99.5	98.95	98.03	100.42	99.13

Sample No.	105	105	105	105	113	113	134	134	134
Analysis	6	7	8	9	1	2	1	2	3
	Ca-Amph	Ca-Amph	Ca-Amph	Ca-Amph	Ca-Amph	Ca-Amph	Ca-Amph	Ca-Amph	Ca-Amph
SiO_2	48.8	49.62	49.19	48.6	47.15	47.91	47.9	45.08	48.2
TiO_2	1.20	1.59	1.84	1.76	2.08	1.62	1.34	2.09	1.35
Al_2O_3	6.20	6.45	7.15	7.25	7.85	6.79	6.52	8.72	6.37
FeO*	15.31	14.5	15.19	15.75	13.43	14.08	18.33	17.25	18.75
MnO	0.82	0.52	0.43	0.68	0.55	0.59	1.01	0.50	0.62
MgO	14.08	14.46	14.28	14.06	14.79	14.71	11.83	11.35	12.2
CaO	10.15	10.63	10.85	10.9	10.97	10.66	10.2	10.45	9.97
Na_2O	1.52	1.57	1.72	1.67	1.83	1.87	1.38	1.93	1.39
K_2O	0.26	0.28	0.25	0.28	0.30	0.25	0.39	0.32	0.39
Total	98.34	99.62	100.9	100.95	98.95	98.48	98.9	97.69	99.24

Sample No.	134	173	173	173	173	173	173	176	176
Analysis	4	1	2	3	4	5	6	1	2
	Ca-Amph	Ca-Amph	Ca-Amph	Ca-Amph	Ca-Amph	Ca-Amph	Ca-Amph	Ca-Amph	Ca-Amph
SiO_2	46.22	49.11	47.25	46.17	49.58	48.96	50.57	45.71	47.44
TiO_2	1.91	1.32	1.52	2.05	1.54	1.55	1.20	1.99	1.33
Al_2O_3	8.09	6.36	6.70	8.00	6.78	6.96	5.51	7.99	7.00
FeO*	18.8	13.47	14.12	14.12	13.66	14.78	13.55	21.08	18.12
MnO	0.54	3.74	1.42	0.64	0.71	0.84	0.91	0.38	0.68
MgO	11.11	14.29	13.68	13.81	14.74	14.32	15.77	9.78	11.95
CaO	10.13	10.7	10.33	10.74	10.89	10.54	10.16	10.43	10.47
Na_2O	1.78	1.52	1.57	1.78	1.45	1.50	1.30	1.60	1.53
K_2O	0.45	0.27	0.41	0.29	0.30	0.30	0.25	0.40	0.42
Total	99.03	100.78	97.00	97.6	99.65	99.75	99.22	99.36	98.94

Analyses in weight percent. All iron expressed as FeO*.

Table VI.8: Electron microprobe analyses of amphibole phenocrysts in rhyolite lavas of the Rotorua Volcanic Centre.

Sample No.	87	87	87	103	103	104	104
Analysis	1	2	3	1	2	1	2
	Ca-Amph	Ca-Amph	Ca-Amph	Ca-Amph	Ca-Amph	Ca-Amph	Ca-Amph
SiO_2	47.41	49.02	48.51	48.75	47.92	45.6	47.18
TiO_2	1.37	1.42	1.65	1.34	1.64	1.15	1.24
Al_2O_3	6.73	6.40	6.44	6.09	6.16	5.92	6.36
FeO*	18.56	16.97	16.63	18.14	19.00	17.02	17.85
MnO	0.80	1.02	0.70	0.66	0.86	0.72	0.82
MgO	11.89	13.30	13.38	11.96	11.33	12.07	12.22
CaO	10.30	10.86	11.03	10.39	10.62	9.34	9.79
Na_2O	1.47	1.46	1.54	1.50	1.52	1.21	1.32
K_2O	0.49	0.50	0.29	0.44	0.49	0.28	0.47
Total	99.02	100.95	100.17	99.27	99.54	93.31	97.25

Table VI.9: Electron microprobe analyses of amphibole phenocrysts in rhyolite lavas of the Kapenga Volcanic Centre.

Sample No.	170	170	170	170
Analysis	1	2	3	4
	Ca-Amph	Ca-Amph	Ca-Amph	Ca-Amph
SiO_2	49.17	45.57	48.63	48.32
TiO_2	1.35	2.32	1.70	1.52
Al_2O_3	6.29	8.68	6.44	6.62
FeO*	17.77	19.17	17.65	18.38
MnO	0.75	0.95	0.75	0.85
MgO	12.47	10.65	12.14	11.65
CaO	10.25	10.63	10.83	10.17
Na_2O	1.36	1.94	1.50	1.54
K_2O	0.36	0.51	0.36	0.50
Total	99.77	100.42	100.00	99.55

Table VI.10: Electron microprobe analyses of biotite phenocrysts in rhyolite lavas of the Okataina and Rotorua volcanic centres.

Sample No.	87	87	87	119	134	134
Analysis	1	2	3	1	1	2
SiO_2	36.71	37.00	37.30	37.87	36.18	36.37
TiO_2	5.20	4.89	5.08	5.08	4.92	4.54
Al_2O_3	13.21	13.37	13.65	13.71	13.7	13.89
FeO*	21.00	21.33	19.96	20.17	21.75	22.95
MnO	0.20	0.01	0.08	0.29	0.39	0.48
MgO	11.53	11.8	11.61	11.64	10.03	9.97
CaO	0.00	0.08	0.07	0.09	0.03	0.03
Na_2O	0.67	0.66	0.78	0.73	0.67	0.69
K_2O	7.80	7.66	7.84	8.02	8.31	8.38
Total	96.32	96.80	96.37	97.60	95.98	97.30

Sample No.	152	152	158	158	176	176
Analysis	1	2	1	2	1	2
SiO_2	37.52	36.74	35.07	34.06	35.62	37.12
TiO_2	4.80	4.75	4.69	4.15	5.10	4.97
Al_2O_3	13.52	13.47	13.08	12.88	13.67	13.51
FeO*	22.36	21.98	20.22	19.36	22.06	22.13
MnO	0.93	0.99	0.48	0.39	0.58	0.67
MgO	11.39	11.47	10.84	10.61	9.71	10.16
CaO	0.07	0.00	0.00	0.05	0.00	0.00
Na_2O	0.65	0.74	0.54	0.58	0.50	0.52
K_2O	7.29	7.86	7.79	7.89	8.51	8.38
Total	98.53	98.00	92.71	89.97	95.75	97.46

Analyses in weight percent. All iron expressed as FeO*.

Table VI.11: Electron microprobe analyses of titanomagnetite (TM) and ilmenite (I) phenocrysts in rhyolite lavas of the Okataina Volcanic Centre.

Sample No.	63	63	63	63	63	63	107	107	107
Analysis	1	2	3	4	5	6	1	2	3
	TM	TM	I	TM	I	TM	I	TM	TM
SiO_2	0.09	0.15	0.00	0.01	0.10	0.05	0.12	0.11	0.11
TiO_2	5.86	10.09	41.59	6.73	49.99	12.02	46.34	6.81	6.89
Al_2O_3	1.45	1.26	0.54	2.29	0.11	0.86	0.14	1.43	1.49
FeO*	87.12	82.87	55.25	86.37	46.42	82.79	47.70	83.44	83.74
MnO	0.48	0.96	1.05	0.85	2.83	1.11	1.98	1.13	1.16
MgO	0.19	0.55	0.71	0.36	1.40	0.39	1.94	0.91	0.79
CaO	0.02	0.05	0.02	0.01	0.03	0.00	0.01	0.06	0.01
Na_2O	0.00	0.01	0.00	0.00	0.00	0.06	0.00	0.13	0.06
K_2O	0.04	0.00	0.01	0.05	0.04	0.00	0.04	0.03	0.07
Total	95.25	95.94	99.17	96.67	100.92	97.28	98.27	94.05	94.32
FeO	36.22	39.17	35.01	36.81	39.55	41.05	36.22	34.35	34.91
Fe_2O_3	56.56	48.56	22.49	55.07	7.63	46.38	12.76	54.55	54.26
Total	100.91	100.80	101.42	102.18	101.68	101.92	99.55	99.51	99.75

Sample No.	107	107	107	107	109	109	109	109	119
Analysis	4	5	6	7	1	2	3	4	1
	I	I	I	TM	I	TM	I	TM	TM
SiO_2	0.07	0.08	0.04	0.13	0.07	0.14	0.00	0.07	0.14
TiO_2	47.45	46.76	47.92	6.67	50.18	10.83	48.53	11.01	9.48
Al_2O_3	0.21	0.15	0.12	1.48	0.17	1.71	0.24	1.64	1.54
FeO*	47.52	47.46	47.47	83.01	48.34	80.88	49.96	83.18	84.81
MnO	2.07	1.83	1.78	1.01	1.01	0.75	1.51	0.95	0.88
MgO	1.92	1.89	1.75	0.82	0.70	0.57	0.20	0.41	0.65
CaO	0.03	0.00	0.04	0.02	0.00	0.11	0.05	0.04	0.06
Na_2O	0.01	0.00	0.12	0.01	0.00	0.00	0.11	0.09	0.00
K_2O	0.07	0.03	0.03	0.02	0.00	0.02	0.09	0.00	0.05
Total	99.35	98.20	99.27	93.17	100.47	95.01	100.69	97.39	97.61
FeO	36.94	36.83	37.52	34.81	42.94	39.64	40.91	40.30	39.04
Fe_2O_3	11.76	11.81	11.06	53.56	6.00	45.82	10.06	47.65	50.86
Total	100.53	99.38	100.38	98.53	101.07	99.60	101.70	102.16	102.70

Sample No.	119	119	119	119	119	64	64	64	64
Analysis	2	3	4	5	6	1	2	3	4
	TM	TM	I	I	I	I	TM	TM	TM
SiO_2	0.01	0.11	0.00	0.08	0.08	0.04	0.11	0.13	0.12
TiO_2	9.88	9.50	49.62	48.74	49.94	46.27	8.47	9.20	9.82
Al_2O_3	1.56	1.46	0.19	0.15	0.13	0.19	1.85	1.29	1.27
FeO*	83.88	83.06	48.90	49.50	49.71	51.47	81.29	82.49	83.42
MnO	1.13	1.48	1.98	1.61	2.41	1.04	0.70	1.16	0.96
MgO	0.53	0.62	0.81	1.27	0.94	1.94	1.11	0.40	0.38
CaO	0.04	0.04	0.09	0.12	0.02	0.05	0.03	0.04	0.10
Na_2O	0.17	0.00	0.08	0.00	0.00	0.01	0.01	0.07	0.00
K_2O	0.00	0.04	0.00	0.08	0.03	0.01	0.07	0.00	0.03
Total	97.20	96.31	101.67	101.55	103.26	101.02	93.64	94.78	96.10
FeO	38.47	38.07	40.68	39.63	40.77	37.00	36.26	37.78	39.11
Fe_2O_3	50.46	50.00	9.13	10.97	9.93	16.08	50.03	49.68	49.24
Total	102.25	101.31	102.58	102.65	104.26	102.63	98.65	99.75	101.03

Sample No.	64	72	72	72	72	72	72	72	117
Analysis	5	1	2	3	4	5	6	7	1
	I	TM	I	I	I	TM	TM	TM	I
SiO_2	0.13	0.24	0.01	0.05	0.06	0.58	0.11	0.12	0.05
TiO_2	49.73	12.78	50.98	50.51	49.95	11.52	10.31	10.98	51.92
Al_2O_3	0.08	1.07	0.12	0.06	0.06	0.87	0.96	1.07	0.12
FeO*	47.95	76.15	47.13	47.16	47.32	78.22	80.97	86.31	44.39
MnO	1.93	0.78	1.61	1.65	1.56	0.89	1.04	1.09	1.48
MgO	1.02	0.38	0.91	0.95	1.13	0.32	0.35	0.31	0.44
CaO	0.13	0.02	0.06	0.04	0.02	0.01	0.07	0.04	0.14
Na_2O	0.00	0.12	0.04	0.07	0.00	0.09	0.00	0.00	0.00
K_2O	0.03	0.05	0.04	0.00	0.04	0.03	0.03	0.06	0.04
Total	101.00	91.59	100.90	100.49	100.14	92.53	93.84	99.98	98.58
FeO	40.84	40.01	42.22	41.74	41.25	39.81	38.72	41.34	44.16
Fe_2O_3	7.90	40.16	5.46	6.02	6.75	42.69	46.94	49.97	0.25
Total	101.79	95.61	101.45	101.09	100.82	96.80	98.54	104.98	98.61

Analyses in weight percent. FeO and Fe_2O_3 calculated as in Droop (1987).

Sample No.	117	117	117	117	117	152	152	152	152
Analysis	2	3	4	5	6	1	2	3	4
	TM	TM	I	TM	I	TM	I	I	I
SiO_2	0.11	0.14	0.03	0.06	0.02	0.12	0.01	0.12	0.09
TiO_2	11.55	11.16	50.27	11.63	50.42	10.10	50.46	49.39	50.00
Al_2O_3	1.13	1.17	0.09	1.15	0.09	1.32	0.14	0.12	0.10
FeO*	79.84	80.82	47.41	80.13	48.08	86.47	50.87	50.80	49.80
MnO	0.85	0.85	1.83	0.81	1.38	1.21	1.34	1.43	1.27
MgO	0.44	0.43	0.51	0.40	0.65	0.49	1.07	0.90	1.10
CaO	0.00	0.06	0.07	0.00	0.04	0.08	0.01	0.03	0.03
Na_2O	0.00	0.00	0.00	0.11	0.09	0.00	0.01	0.14	0.07
K_2O	0.05	0.04	0.04	0.00	0.02	0.02	0.04	0.04	0.06
Total	93.97	94.67	100.25	94.29	100.79	99.81	103.95	102.97	102.52
FeO	39.94	39.86	42.27	39.84	42.28	40.23	41.94	40.69	41.28
Fe_2O_3	44.33	45.52	5.72	44.77	6.45	51.39	9.92	11.23	9.47
Total	98.41	99.23	100.82	98.77	101.44	104.95	104.94	104.09	103.47

Sample No.	152	152	152	6	6	6	6	6	7
Analysis	5	6	7	1	2	3	4	5	1
	TM	TM	TM	TM	TM	I	I	TM	I
SiO_2	0.08	0.09	0.13	0.13	0.11	0.00	0.04	0.10	0.12
TiO_2	9.87	9.44	9.88	8.41	8.45	49.34	49.39	8.47	48.77
Al_2O_3	1.39	1.26	1.42	1.40	1.34	0.09	0.07	1.42	0.11
FeO*	85.63	86.50	85.82	82.26	82.13	47.24	46.76	81.69	51.52
MnO	1.47	1.30	1.37	0.89	0.96	1.73	1.80	0.96	2.00
MgO	0.53	0.51	0.55	0.57	0.65	1.59	1.65	0.60	1.61
CaO	0.01	0.07	0.06	0.03	0.07	0.07	0.04	0.04	0.00
Na_2O	0.00	0.00	0.00	0.00	0.00	0.09	0.00	0.00	0.06
K_2O	0.10	0.02	0.01	0.01	0.03	0.00	0.04	0.00	0.01
Total	99.08	99.19	99.24	93.70	93.74	100.15	99.79	93.28	104.20
FeO	39.27	39.29	39.67	37.04	36.76	39.27	39.52	36.82	38.80
Fe_2O_3	51.51	52.46	51.28	50.25	50.42	8.85	8.04	49.86	14.14
Total	104.23	104.44	104.37	98.73	98.79	101.04	100.60	98.27	105.62

Sample No.	7	7	7	7	7	7	7	24	24
Analysis	2	3	4	5	6	7	8	1	2
	I	TM	TM	I	TM	TM	I	I	TM
SiO_2	0.05	0.09	0.03	0.06	0.05	0.07	0.06	0.01	0.12
TiO_2	49.89	4.55	8.26	49.48	0.92	8.04	48.16	51.45	8.36
Al_2O_3	0.12	1.57	1.34	0.15	2.06	1.51	0.09	0.16	1.35
FeO*	48.85	87.24	84.81	47.75	86.14	83.28	47.07	47.54	82.54
MnO	1.79	1.05	1.26	1.68	1.32	0.90	1.82	1.86	1.04
MgO	2.01	0.71	0.71	1.55	0.89	0.70	1.62	1.56	0.71
CaO	0.06	0.04	0.03	0.02	0.03	0.01	0.01	0.01	0.07
Na_2O	0.00	0.05	0.00	0.01	0.01	0.00	0.01	0.00	0.00
K_2O	0.05	0.02	0.03	0.08	0.02	0.01	0.04	0.04	0.04
Total	102.82	95.32	96.47	100.78	91.44	94.52	98.88	102.63	94.23
FeO	39.30	33.59	37.05	39.79	28.80	36.75	38.47	41.48	36.65
Fe_2O_3	10.62	59.62	53.07	8.85	63.72	51.71	9.56	6.74	50.99
Total	103.88	101.29	101.78	101.67	97.82	99.69	99.84	103.30	99.33

Sample No.	24	24	24	32	32	32	32	32	32
Analysis	3	4	5	1	2	3	4	5	6
	I	TM	I	I	TM	TM	I	I	TM
SiO_2	0.03	0.10	0.00	0.07	0.06	0.06	0.05	0.06	0.13
TiO_2	49.08	8.77	50.53	49.61	8.46	8.22	49.01	48.93	8.40
Al_2O_3	0.15	1.42	0.16	0.11	1.40	1.27	0.12	0.11	1.36
FeO*	47.72	84.02	48.10	48.94	82.75	81.02	46.63	48.03	81.26
MnO	1.59	0.83	1.69	1.43	1.07	0.84	1.50	1.52	0.95
MgO	1.51	0.65	1.46	1.53	0.65	0.69	1.57	1.45	0.72
CaO	0.02	0.06	0.02	0.07	0.02	0.03	0.01	0.04	0.04
Na_2O	0.00	0.09	0.00	0.01	0.00	0.00	0.13	0.01	0.00
K_2O	0.03	0.03	0.04	0.01	0.00	0.01	0.02	0.00	0.05
Total	100.13	95.97	102.00	101.78	94.41	92.14	99.04	100.15	92.91
FeO	39.75	37.54	40.98	40.35	36.97	36.12	39.14	39.85	36.35
Fe_2O_3	8.86	51.65	7.92	9.54	50.87	49.90	8.33	9.09	49.91
Total	101.02	101.14	102.79	102.74	99.50	97.13	99.87	101.06	97.90

Analyses in weight percent. FeO and Fe_2O_3 calculated as in Droop (1987).

Sample No.	38	38	38	38	44	44	44	44	44
Analysis	1	2	3	4	1	2	3	4	5
	TM	I	TM	I	I	I	TM	I	TM
SiO_2	0.05	0.00	0.05	0.05	0.00	0.03	0.09	0.00	0.05
TiO_2	8.39	47.08	7.71	47.57	44.70	45.13	6.73	45.69	7.00
Al_2O_3	1.44	0.13	1.47	0.17	0.20	0.21	1.84	0.16	1.77
FeO*	81.61	48.90	82.30	48.27	51.59	52.19	82.10	51.54	82.41
MnO	1.03	1.33	0.83	1.51	1.07	1.12	0.74	1.03	0.65
MgO	0.82	1.82	0.85	1.98	2.11	2.11	1.07	2.02	1.05
CaO	0.00	0.05	0.10	0.03	0.08	0.01	0.11	0.12	0.00
Na_2O	0.13	0.12	0.01	0.00	0.01	0.01	0.01	0.05	0.01
K_2O	0.02	0.09	0.02	0.00	0.05	0.01	0.05	0.01	0.01
Total	93.49	99.52	93.34	99.58	99.81	100.82	92.74	100.62	92.95
FeO	35.80	36.85	35.70	37.74	35.05	35.63	34.41	36.03	35.02
Fe_2O_3	50.91	13.39	51.78	11.70	18.38	18.40	52.99	17.24	52.66
Total	98.58	100.86	98.52	100.75	101.65	102.66	98.04	102.35	98.22

Sample No.	44	44	60	60	60	60	60	60	90
Analysis	6	7	1	2	3	4	5	6	1
	TM	I	TM	I	TM	I	I	I	TM
SiO_2	0.14	0.02	0.14	0.01	0.00	0.00	0.00	0.05	0.16
TiO_2	7.50	44.38	8.01	48.26	8.01	48.06	47.72	47.01	7.77
Al_2O_3	1.76	0.16	1.63	0.20	1.59	0.11	0.08	0.15	1.51
FeO*	84.13	51.41	83.77	49.35	83.04	49.06	48.91	48.89	82.77
MnO	0.85	0.99	0.87	1.60	0.91	1.47	1.43	1.69	0.77
MgO	0.99	2.15	0.72	1.70	0.74	1.62	1.65	1.63	0.83
CaO	0.03	0.03	0.01	0.02	0.06	0.00	0.05	0.07	0.04
Na_2O	0.00	0.10	0.00	0.00	0.10	0.00	0.00	0.01	0.00
K_2O	0.08	0.03	0.06	0.00	0.06	0.01	0.03	0.02	0.12
Total	95.48	99.27	95.21	101.14	94.51	100.33	99.87	99.52	93.97
FeO	36.11	34.50	36.91	38.73	35.95	38.81	38.37	37.52	36.02
Fe_2O_3	53.36	18.79	52.07	11.80	52.33	11.39	11.72	12.64	51.94
Total	100.82	101.15	100.42	102.32	99.75	101.47	101.04	100.79	99.17

Sample No.	90	90	90	92	92	92	92	98	98
Analysis	2	3	4	1	2	3	4	1	2
	TM	I	I	TM	TM	I	I	I	I
SiO_2	0.16	0.10	0.00	0.09	0.04	0.02	0.10	0.02	0.01
TiO_2	8.26	45.47	46.01	8.31	8.37	46.72	46.09	48.97	50.99
Al_2O_3	1.71	0.13	0.20	1.61	1.65	0.18	0.17	0.17	0.12
FeO*	83.83	51.75	52.45	83.05	83.24	48.99	49.37	48.39	48.30
MnO	0.99	1.50	1.44	1.02	0.89	1.68	1.82	1.67	1.65
MgO	0.88	1.92	1.85	0.87	0.93	1.83	2.03	1.55	1.44
CaO	0.06	0.02	0.04	0.03	0.07	0.07	0.03	0.03	0.06
Na_2O	0.00	0.00	0.00	0.13	0.00	0.00	0.00	0.00	0.01
K_2O	0.00	0.03	0.01	0.01	0.02	0.00	0.01	0.00	0.00
Total	95.89	100.92	102.00	95.12	95.21	99.49	99.62	100.80	102.58
FeO	37.14	35.95	36.54	36.27	36.80	36.98	36.03	39.57	41.50
Fe_2O_3	51.88	17.56	17.69	51.98	51.60	13.34	14.82	9.81	7.55
Total	101.08	102.68	103.77	100.32	100.37	100.83	101.10	101.78	103.34

Sample No.	98	98	98	98	105	105	105	105	105
Analysis	3	4	5	6	1	2	3	5	6
	TM	I	I	TM	I	TM	TM	I	I
SiO_2	0.07	0.02	0.01	0.16	0.05	0.11	0.06	0.02	0.06
TiO_2	8.65	49.93	50.40	8.60	47.85	0.84	8.30	48.40	47.11
Al_2O_3	1.42	0.13	0.16	1.47	0.11	1.71	1.63	0.05	0.20
FeO*	84.13	48.28	47.97	81.46	49.00	88.82	83.69	47.06	49.20
MnO	1.02	1.35	1.69	0.88	1.41	1.14	0.88	1.89	1.53
MgO	0.64	1.68	1.68	0.57	1.69	0.89	0.71	2.23	1.54
CaO	0.07	0.08	0.03	0.09	0.09	0.04	0.07	0.00	0.00
Na_2O	0.00	0.06	0.01	0.01	0.29	0.00	0.00	0.00	0.00
K_2O	0.07	0.04	0.03	0.01	0.02	0.03	0.00	0.02	0.00
Total	96.07	101.57	101.98	93.25	100.51	93.58	95.34	99.67	99.64
FeO	37.51	40.06	40.45	37.00	37.13	29.65	37.21	37.60	38.14
Fe_2O_3	51.81	9.14	8.36	49.41	13.19	65.74	51.65	10.52	12.29
Total	101.25	102.49	102.82	98.19	101.83	100.16	100.51	100.72	100.87

Analyses in weight percent. FeO and Fe_2O_3 calculated as in Droop (1987).

Sample No.	113	113	113	113	134	134	134	134	134
Analysis	1	2	3	4	1	2	3	4	5
	I	I	TM	TM	I	TM	TM	TM	I
SiO_2	0.05	0.08	0.11	0.07	0.08	0.04	0.04	0.05	0.03
TiO_2	45.30	45.62	8.67	8.73	49.14	9.45	9.63	9.90	50.77
Al_2O_3	0.25	0.17	1.80	1.79	0.09	1.71	1.45	1.37	0.07
FeO*	50.38	50.25	80.98	82.14	49.33	81.45	82.66	82.36	47.20
MnO	0.86	1.10	0.83	0.55	1.47	1.20	1.09	0.97	2.28
MgO	2.31	2.20	1.31	1.20	0.92	0.34	0.54	0.46	0.98
CaO	0.02	0.07	0.03	0.06	0.02	0.05	0.04	0.01	0.06
Na_2O	0.00	0.00	0.00	0.08	0.09	0.09	0.09	0.00	0.06
K_2O	0.00	0.00	0.00	0.04	0.00	0.01	0.03	0.07	0.02
Total	99.17	99.49	93.73	94.66	101.14	94.34	95.57	95.19	101.47
FeO	35.78	35.99	36.27	36.54	40.71	37.72	38.01	38.66	41.22
Fe_2O_3	16.22	15.84	49.69	50.67	9.58	48.60	49.62	48.56	6.65
Total	100.79	101.08	98.70	99.73	102.10	99.20	100.54	100.05	102.14

Sample No.	158	158	158	158	158	158	173	173	173
Analysis	1	2	3	4	5	6	1	2	3
	TM	TM	TM	TM	I	I	TM	TM	I
SiO_2	0.02	0.07	0.09	0.10	0.08	0.07	0.12	0.08	0.03
TiO_2	9.06	9.27	9.07	9.25	50.15	50.42	8.93	8.63	49.47
Al_2O_3	1.16	1.24	1.20	1.26	0.10	0.09	1.57	1.50	0.08
FeO*	81.59	81.12	82.29	82.90	46.34	45.23	83.08	81.55	48.96
MnO	1.30	1.42	1.26	1.17	2.52	2.56	0.77	0.88	1.42
MgO	0.47	0.44	0.49	0.47	1.20	1.00	0.83	0.71	1.59
CaO	0.07	0.02	0.01	0.03	0.12	0.06	0.03	0.03	0.05
Na_2O	0.07	0.00	0.00	0.01	0.00	0.06	0.05	0.00	0.00
K_2O	0.02	0.00	0.02	0.02	0.03	0.00	0.01	0.01	0.04
Total	93.76	93.58	94.43	95.21	100.54	99.49	95.39	93.39	101.64
FeO	36.82	37.35	37.52	38.01	40.26	40.69	37.58	36.87	40.06
Fe_2O_3	49.75	48.64	49.75	49.88	6.76	5.04	50.56	49.64	9.89
Total	98.74	98.45	99.41	100.20	101.22	99.99	100.45	98.36	102.63

Sample No.	173	173	173	176	176	176	176	176
Analysis	4	5	6	1	3	4	5	6
	TM	I	TM	TM	TM	I	TM	TM
SiO_2	0.11	0.02	0.06	0.04	0.08	0.05	0.08	0.12
TiO_2	9.01	49.46	8.98	8.83	9.09	50.36	9.30	9.70
Al_2O_3	1.51	0.09	1.56	1.16	1.22	0.07	1.22	1.14
FeO*	82.90	48.88	82.09	82.08	82.96	47.48	82.45	83.39
MnO	0.73	1.48	0.84	1.32	1.31	2.54	1.02	1.10
MgO	0.72	1.64	0.75	0.41	0.40	0.92	0.44	0.42
CaO	0.02	0.02	0.03	0.02	0.06	0.00	0.03	0.08
Na_2O	0.13	0.00	0.10	0.01	0.12	0.09	0.00	0.14
K_2O	0.05	0.04	0.01	0.03	0.04	0.06	0.00	0.04
Total	95.18	101.63	94.42	93.90	95.28	101.57	94.54	96.13
FeO	37.33	39.93	37.06	37.05	37.28	40.53	38.10	38.20
Fe_2O_3	50.64	9.95	50.03	50.04	50.76	7.72	49.28	50.21
Total	100.25	102.63	99.43	98.91	100.36	102.34	99.47	101.16

Analyses in weight percent. FeO and Fe_2O_3 calculated as in Droop (1987).

Table VI.12: Electron microprobe analyses of titanomagnetite (TM) and ilmenite (I) phenocrysts in rhyolite lavas of the Rotorua Volcanic Centre.

Sample No.	87	87	87	87	87	87	87	87
Analysis	1	2	3	4	5	6	7	8
	I	TM	TM	I	TM	TM	I	TM
SiO_2	0.03	0.08	0.08	0.08	0.00	0.25	0.08	0.02
TiO_2	49.58	10.08	10.08	49.88	10.16	9.76	48.58	9.54
Al_2O_3	0.16	1.52	1.51	0.15	1.68	1.55	0.09	1.50
FeO*	50.10	83.74	84.29	50.76	83.56	83.58	50.94	83.59
MnO	1.11	0.69	0.00	1.32	0.79	1.53	2.42	0.37
MgO	1.07	0.63	0.51	0.83	0.44	0.46	0.91	0.49
CaO	0.01	0.03	0.01	0.02	0.03	0.08	0.05	0.03
Na_2O	0.00	0.18	0.00	0.01	0.00	0.00	0.07	0.05
K_2O	0.00	0.06	0.04	0.03	0.04	0.08	0.05	0.00
Total	102.06	97.01	96.52	103.08	96.70	97.29	103.19	95.59
FeO	41.58	38.75	40.30	41.97	39.64	38.84	39.17	38.99
Fe_2O_3	9.47	49.99	48.88	9.77	48.80	49.72	13.08	49.56
Total	103.01	102.01	101.41	104.06	101.58	102.27	104.50	100.55

Sample No.	103	104	104	104	104	104
Analysis	1	1	2	3	5	6
	I	TM	I	I	TM	I
SiO_2	0.01	0.14	0.06	0.04	0.14	0.06
TiO_2	50.33	8.93	49.82	48.93	9.91	50.13
Al_2O_3	0.06	1.30	0.08	0.06	1.31	0.10
FeO*	47.53	78.82	45.90	46.01	82.66	47.08
MnO	1.46	0.91	1.66	1.66	0.92	1.80
MgO	1.15	0.49	1.14	1.07	0.48	1.28
CaO	0.01	0.00	0.04	0.01	0.00	0.07
Na_2O	0.01	0.06	0.00	0.04	0.00	0.00
K_2O	0.00	0.04	0.04	0.00	0.06	0.03
Total	100.56	90.69	98.74	97.82	95.48	100.55
FeO	41.68	36.28	40.99	40.26	38.93	40.86
Fe_2O_3	6.50	47.27	5.46	6.39	48.59	6.91
Total	101.21	95.42	99.29	98.46	100.34	101.24

Table VI.13: Electron microprobe analyses of titanomagnetite (TM) and ilmenite (I) phenocrysts in rhyolite lavas of the Kapenga Volcanic Centre.

Sample No.	126	126	126	170	170	170	170	170	170
Analysis	1	2	3	1	2	3	4	5	6
	I	TM	TM	I	TM	I	TM	TM	TM
SiO_2	0.20	0.14	0.09	0.11	0.11	0.10	0.09	0.09	0.08
TiO_2	45.87	12.34	11.83	49.20	10.18	49.09	9.54	9.52	9.70
Al_2O_3	0.11	1.06	0.91	0.07	1.36	0.10	1.36	1.28	1.40
FeO*	47.70	78.42	72.96	47.41	81.56	47.78	81.70	82.59	82.28
MnO	2.25	1.40	1.02	1.71	0.95	1.74	0.77	1.03	0.88
MgO	0.66	0.37	0.17	1.24	0.54	1.25	0.55	0.58	0.51
CaO	0.04	0.04	0.05	0.04	0.04	0.05	0.05	0.08	0.00
Na_2O	0.01	0.01	0.01	0.00	0.01	0.10	0.01	0.00	0.01
K_2O	0.02	0.00	0.02	0.05	0.03	0.06	0.05	0.02	0.01
Total	96.86	93.78	87.06	99.83	94.78	100.27	94.12	95.19	94.87
FeO	37.87	40.20	38.05	40.23	38.77	39.56	38.07	38.19	38.58
Fe_2O_3	10.92	42.47	38.79	7.98	47.54	9.13	48.48	49.34	48.56
Total	97.95	98.03	90.94	100.63	99.54	101.18	98.97	100.13	99.73

Analyses in weight percent. FeO and Fe_2O_3 calculated as in Droop (1987).

Appendix VII: Intensive Parameters

Table VII.1: Temperature and oxygen fugacity calculations for titanomagnetite (spinel) and ilmenite (rhombohedral) pairs in equilibrium.

Sample Number	TM (spinel) Number	Ilmenite (rhomb) Number	Ghiorso and Sack (1991)		Spencer and Lindsley (1981)	
			Temperature (°C)	log fo_2	Temperature (°C)	log fo_2
ho_1						
107	2	1	726	-14.90	768 ± 20	-13.52 ± 0.33
	2	4	705	-15.61	753 ± 22	-14.04 ± 0.37
	2	5	711	-15.39	757 ± 21	-13.90 ± 0.36
	3	1	730	-14.84	769 ± 20	-13.49 ± 0.33
	3	4	708	-15.55	755 ± 22	-14.01 ± 0.37
	3	5	714	-15.34	759 ± 21	-13.87 ± 0.36
	7	1	726	-14.92	767 ± 20	-13.52 ± 0.33
	7	4	705	-15.62	753 ± 22	-14.04 ± 0.37
	7	5	710	-15.41	757 ± 21	-13.90 ± 0.36
119	1	5	748	-15.00	774 ± 25	-14.01 ± 0.41
	3	4	706	-16.42	740 ± 29	-15.21 ± 0.53
ho_2						
64	3	5	682	-17.27	723 ± 31	-15.85 ± 0.60
	4	5	692	-17.06	728 ± 32	-15.75 ± 0.60
152	1	3	744	-15.19	770 ± 26	-14.22 ± 0.44
	7	3	742	-15.23	768 ± 26	-14.26 ± 0.44
ho_3 Tarawera						
38	1	4	752	-14.63	780 ± 22	-13.58 ± 0.36
	3	2	747	-14.55	779 ± 21	-13.44 ± 0.34
	3	4	734	-14.97	770 ± 22	-13.75 ± 0.36
44	3	1	799	-12.66	821 ± 23	-11.93 ± 0.23
	3	2	799	-12.67	820 ± 23	-11.94 ± 0.23
	3	4	783	-13.11	806 ± 23	-12.29 ± 0.25
	3	7	801	-12.62	822 ± 23	-11.90 ± 0.23
	5	1	806	-12.56	828 ± 23	-11.84 ± 0.23
	5	2	806	-12.57	827 ± 23	-11.85 ± 0.23
	5	4	789	-13.01	813 ± 23	-12.20 ± 0.25
	5	7	807	-12.52	829 ± 23	-11.82 ± 0.23
	6	1	818	-12.36	836 ± 23	-11.74 ± 0.23
	6	2	818	-12.37	836 ± 23	-11.75 ± 0.23
	6	4	801	-12.81	821 ± 23	-12.10 ± 0.25
90	1	3	819	-12.50	837 ± 23	-11.84 ± 0.24
	1	4	818	-12.52	837 ± 23	-11.85 ± 0.24
	2	3	830	-12.29	845 ± 23	-11.74 ± 0.24
	2	4	829	-12.31	845 ± 23	-11.75 ± 0.24
134	3	1	720	-15.98	751 ± 29	-14.88 ± 0.50
	4	1	727	-15.86	756 ± 29	-14.80 ± 0.50
158	2	5	654	-18.46	700 ± 35	-16.75 ± 0.71
	4	5	650	-18.53	699 ± 35	-16.77 ± 0.71
ho_3 Haroharo						
6	1	3	684	-16.98	728 ± 29	-15.47 ± 0.54
	1	4	673	-17.40	720 ± 30	-15.80 ± 0.58
	2	3	683	-17.00	728 ± 29	-15.48 ± 0.54
	2	4	672	-17.42	719 ± 30	-15.80 ± 0.58
	5	3	686	-16.95	729 ± 29	-15.54 ± 0.54
	5	4	675	-17.36	721 ± 30	-15.78 ± 0.58
7	4	1	764	-14.13	791 ± 20	-13.10 ± 0.32
	4	8	696	-16.39		
	7	1	766	-14.08	792 ± 20	-13.08 ± 0.32
	7	2	712	-15.83		
	7	8	698	-16.32	742 ± 26	-14.84 ± 0.47
24	2	3	689	-16.74	732 ± 28	-15.27 ± 0.51

Titanomagnetite and ilmenite numbers refer to Tables VI.11 – VI.13.

Sample Number	TM (spinel) Number	Ilmenite (rhomb) Number	Ghiorso and Sack (1991) Temperature (°C)	Ghiorso and Sack (1991) log fo_2	Spencer and Lindsley (1981) Temperature (°C)	Spencer and Lindsley (1981) log fo_2
ho_3 Haroharo						
24	2	5	661	-17.77	711 ± 30	-16.09 ± 0.61
	4	3	695	-16.60	736 ± 28	-15.20 ± 0.51
	4	5	668	-17.62	715 ± 31	-16.03 ± 0.60
32	2	5	696	-16.48	738 ± 27	-15.08 ± 0.50
	3	1	700	-16.32	742 ± 27	-14.92 ± 0.48
	6	1	705	-16.20	744 ± 27	-14.89 ± 0.48
	6	5	699	-16.41	739 ± 27	-15.06 ± 0.50
60	1	2	740	-14.87	773 ± 22	-13.74 ± 0.37
	1	4	734	-15.07	768 ± 23	-13.91 ± 0.38
	1	5	739	-14.89	772 ± 22	-13.77 ± 0.37
	1	6	756	-14.38	784 ± 21	-13.34 ± 0.33
	3	2	738	-14.92	772 ± 22	-13.74 ± 0.37
	3	4	732	-15.12	767 ± 23	-13.91 ± 0.38
	3	5	737	-14.94	771 ± 22	-13.77 ± 0.37
	3	6	754	-14.43	784 ± 21	-13.35 ± 0.33
92	1	3	776	-13.84	798 ± 20	-12.96 ± 0.31
	1	4	800	-13.19	819 ± 24	-12.41 ± 0.28
	2	3	776	-13.84	798 ± 20	-12.95 ± 0.31
	2	4	800	-13.19	819 ± 24	-12.41 ± 0.28
98	3	1	713	-15.94	751 ± 26	-14.62 ± 0.45
	6	1	722	-15.75	755 ± 26	-14.55 ± 0.45
105	3	1	745	-14.80	775 ± 23	-13.71 ± 0.37
	3	5	725	-15.50	761 ± 24	-14.20 ± 0.41
	3	6	757	-14.40	784 ± 22	-13.40 ± 0.34
173	1	3	720	-15.79	754 ± 27	-14.62 ± 0.46
	1	5	721	-15.75	755 ± 26	-14.58 ± 0.46
	2	3	717	-15.87	752 ± 26	-14.65 ± 0.46
	2	5	718	-15.83	753 ± 26	-14.61 ± 0.46
	4	3	723	-15.75	756 ± 27	-14.59 ± 0.46
	4	5	724	-15.71	757 ± 27	-14.55 ± 0.46
	6	3	723	-15.75	756 ± 27	-14.59 ± 0.46
	6	5	724	-15.71	757 ± 27	-14.55 ± 0.46
ho_3 Okareka						
113	3	1	835	-12.28	846 ± 24	-11.85 ± 0.25
	3	2	828	-12.46	841 ± 24	-11.98 ± 0.26
	4	1	834	-12.31	847 ± 24	-11.84 ± 0.25
176	1	4	651	-18.36	702 ± 33	-16.56 ± 0.67
	3	4	656	-18.24	704 ± 33	-16.53 ± 0.67
	6	4	667	-17.99	709 ± 34	-16.43 ± 0.67
hk_1						
126	2	1	832	-13.39	844 ± 30	-12.82 ± 0.38
hk_2						
170	2	1	706	-16.71	736 ± 33	-15.56 ± 0.59
	2	3	721	-16.20	749 ± 31	-15.11 ± 0.54
	4	3	708	-16.46	742 ± 30	-15.23 ± 0.54
	5	3	704	-16.55	739 ± 30	-15.29 ± 0.54
	6	3	710	-16.42	743 ± 30	-15.21 ± 0.54
hr_1						
87	2	1	734	-15.59	761 ± 29	-14.63 ± 0.49
	5	4	738	-15.50	765 ± 29	-14.55 ± 0.48
hr_3						
104	1	6	660	-18.19	703 ± 35	-16.64 ± 0.70
	5	3	655	-18.50	696 ± 37	-17.03 ± 0.76
	5	6	669	-17.97	708 ± 35	-16.55 ± 0.70

Titanomagnetite and ilmenite numbers refer to Tables VI.11 – VI.13.

Table VII.2: Hornblende-plagioclase thermometry calculations.
Thermometer A (edenite-tremolite)

	Sample Number	Plagioclase Composition (Xab)	Calcic Amphibole Number	Temperature (°C) P = 0 kbar	P = 5 kbar	P = 10 kbar	Average Temperature 0-5 kbar (°C)
ho_1	109	0.69	2	872	819	767	846
	109	0.69	3	852	785	719	819
	119	0.66	1	773	723	673	748
	119	0.66	2	795	740	684	768
ho_2	64	0.68	1	787	734	681	761
	64	0.68	2	738	691	644	715
	64	0.68	3	771	724	677	748
	64	0.68	4	802	750	697	776
	117	0.77	1	771	717	663	744
	117	0.77	2	789	730	671	760
	152	0.71	1	833	772	712	803
	152	0.71	2	762	706	650	734
ho_3							
Tarawera	44	0.65	1	697	658	619	678
	44	0.65	2	696	658	619	677
	44	0.65	3	706	664	623	685
	44	0.49	1	729	689	648	709
	44	0.49	2	728	689	649	709
	44	0.49	3	739	696	653	718
	90	0.64	3	838	770	703	804
	134	0.7	1	754	705	656	730
	134	0.7	2	818	769	719	794
	134	0.7	3	758	707	656	733
	134	0.7	4	794	745	696	770
Haroharo	7	0.65	1	791	735	678	763
	7	0.65	2	806	751	697	779
	7	0.65	3	749	702	654	726
	7	0.65	4	755	711	667	733
	32	0.65	2	753	701	648	727
	32	0.65	3	781	728	675	755
	32	0.65	4	752	702	652	727
	60	0.63	3	819	770	721	795
	60	0.63	5	701	661	621	681
	92	0.61	1	853	789	724	821
	92	0.61	2	814	758	703	786

Temperature calculations following Holland and Blundy (1994). Calcic amphibole numbers refer to Tables VI.7-VI.9. Plagioclase Xab composition is an average for each sample excluding outliers.

Sample Number		Plagioclase Composition (Xab)	Calcic Amphibole Number	Temperature (°C) P= 0 kbar	P= 5 kbar	P= 10 kbar	Average Temperature 0-5 kbar (°C)
ho_3							
Haroharo	98	0.66	1	808	753	697	781
	98	0.66	2	800	746	692	773
	98	0.66	3	766	719	671	743
	98	0.66	4	765	718	671	742
	105	0.62	1	799	747	694	773
	105	0.62	2	762	718	675	740
	105	0.62	3	812	756	699	784
	105	0.62	5	846	786	726	816
	105	0.62	6	775	723	672	749
	105	0.62	7	762	713	665	738
	105	0.62	8	805	751	698	778
	105	0.62	9	826	768	709	797
	173	0.61	1	822	759	696	791
	173	0.61	2	802	747	692	775
	173	0.61	4	756	711	666	734
	173	0.61	5	783	733	684	758
	173	0.61	6	745	696	646	721
Okareka	113	0.55	1	875	811	748	843
	113	0.55	2	847	784	720	816
	176	0.69	1	812	759	706	786
	176	0.69	2	777	726	675	752
hk_2	170	0.67	1	727	683	640	705
	170	0.67	3	767	716	664	742
	170	0.67	4	741	696	650	719
hr_1	87	0.66	1	789	734	679	762
	87	0.66	2	789	731	673	760
	87	0.66	3	808	747	686	778
hr_3	103	0.67	1	738	691	643	715
	103	0.67	2	782	725	668	754
	104	0.72	1	755	704	654	730
	104	0.72	2	752	702	652	727

Temperature calculations following Holland and Blundy (1994). Calcic amphibole numbers refer to Tables VI.7-VI.9. Plagioclase Xab composition is an average for each sample excluding outliers.

Table VII.3: Al-in-hornblende geobarometry calculations.

Sample	Amphibole Number	Al_2O_3 (wt %)	Al^T	Johnson and Rutherford (1989) Pressure (kbar)	Anderson and Smith (1995)[1] Pressure (kbar)	Anderson and Smith (1995)[2] Pressure (kbar)
ho_1						
119	1	7.01	1.19	1.6	1.6	2.1
	2	7.07	1.20	1.6	1.6	2.1
ho_2						
64	1	6.94	1.20	1.6	1.8	2.6
	2	6.00	1.03	0.9	1.1	1.8
	3	7.25	1.24	1.8	2.0	2.8
	4	7.48	1.30	2.1	2.2	3.1
152	1	8.02	1.36	2.3	2.1	2.6
	2	5.76	0.98	0.7	0.6	1.0
ho_3						
134	1	6.52	1.12	1.3	1.4	1.8
	2	8.72	1.52	3.0	3.0	3.6
	3	6.37	1.09	1.2	1.2	1.7
	4	8.09	1.39	2.4	2.5	3.0
176	1	7.99	1.39	2.4	2.2	3.7
	2	7.00	1.20	1.6	1.5	2.8
hr_1						
87	1	6.73	1.16	1.4	1.3	1.8
	2	6.40	1.08	1.1	1.0	1.5
	3	6.44	1.09	1.2	1.0	1.5
hr_3						
104	1	5.92	1.08	1.1	1.6	2.2
	2	6.36	1.11	1.2	1.7	2.4
hk_2						
170	1	6.29	1.07	1.1	1.6	1.8
	2	8.68	1.49	2.8	3.5	3.7
	3	6.44	1.09	1.2	1.7	1.9
	4	6.62	1.13	1.3	1.9	2.1

Amphibole numbers from Tables VI.7-VI.9. Al^T = total aluminium content as cations on the basis of 23 oxygens, calculated following Holland and Blundy (1994). Anderson and Smith (1995) pressure estimates use average temperatures following (1) Holland and Blundy (1994) (Table 5.3) and (2) Ghiorso and Sack (1991) (Table 5.1). The errors in pressure estimates are ±0.5 kbar and ±0.6 kbar for Johnson and Rutherford (1989) and Anderson and Smith (1995) respectively. Uncertainty in temperature calculations of ± 50°C leads to an additional average uncertainty of ± 0.8 kbar in the pressure estimates of Anderson and Smith (1995).

Table VII.4: H_2O calculations for rhyolite melts from the Haroharo Volcanic Complex.

Sample Number	Plagioclase Number	Plagioclase Rim An Content	Temperature (°C)	H_2O (Ab) wt %	H_2O (An) wt %
6	1	33	650	11.6	8.1
	1	33	710	8.0	5.6
	2	29	650	11.2	8.7
	2	29	710	**7.6**	**6.1**
24	1	27	650	11.1	8.9
	1	27	710	7.5	6.3
	2	26	650	11.0	9.1
	2	26	710	**7.5**	**6.4**
98	1	29	690	8.7	7.1
	1	29	750	**5.9**	**5.0**
	2	31	690	8.9	6.8
	2	31	750	6.0	4.7
173	1	42	690	9.9	5.9
	1	42	750	6.9	4.0
	2	31	690	9.0	7.2
	2	31	750	**6.1**	**5.0**
	3	34	690	9.2	6.8
	3	34	750	6.3	4.7
7	1	32	700	8.3	6.3
	1	32	760	**5.6**	**4.3**
	2	47	700	9.8	4.8
	2	47	760	6.9	3.1
	3	34	700	8.5	6.0
	3	34	760	5.8	4.1
105	1	42	710	8.8	5.3
	1	42	770	6.1	3.5
	2	33	710	8.0	6.2
	2	33	770	5.4	4.3
	3	31	710	7.8	6.6
	3	31	770	**5.2**	**4.6**
	4	36	710	8.2	5.9
	4	36	770	5.6	4.0
60	1	30	710	7.9	6.4
	1	30	770	**5.3**	**4.5**
	2	38	710	8.5	5.5
	2	38	770	5.9	3.7
	3	31	710	7.9	6.3
	3	31	770	5.4	4.4
92	1	39	760	6.5	4.3
	1	39	820	**4.4**	**2.8**

H_2O calculations following Housh and Luhr (1991). P = 2 kbar. Temperatures from Fe-Ti oxide geothermometry following Ghiorso and Sack (1991) and represent upper and lower limits using averages from Table 5.1 and applying an error of ± 30°C. Plagioclase numbers refer to Table VI.1. Calculations shown in bold font are those that show the closest agreement between H_2O (Ab) and H_2O (An) for each sample.

Appendix VIII: Electron Microprobe Analyses - Glass Groundmass and Inclusions

Table VIII.1: Electron microprobe analyses of the glass groundmass of rhyolite lavas from the Haroharo Volcanic Complex.

Sample	6	6	6	6	6	6	6	6	6
Analysis	GM1	GM2	GM3	GM4	GM5	GM6	GM7	GM8	GM9
SiO_2	77.61	78.05	77.87	78.49	78.31	78.16	77.61	78.43	78.08
TiO_2	0.14	0.27	0.12	0.14	0.16	0.13	0.18	0.14	0.04
Al_2O_3	12.59	12.59	12.51	12.73	12.63	12.62	12.68	12.71	12.56
FeO*	0.82	0.91	0.76	0.91	0.77	0.96	0.86	0.80	0.77
MnO	0.10	0.17	0.04	0.07	0.03	0.04	0.08	0.07	0.12
MgO	0.12	0.10	0.10	0.12	0.09	0.10	0.07	0.10	0.16
CaO	0.76	0.74	0.74	0.68	0.67	0.72	0.72	0.87	0.69
Na_2O	3.49	3.49	3.69	3.69	3.65	3.59	3.62	3.61	3.43
K_2O	3.56	3.64	3.62	3.76	3.66	3.63	3.50	3.44	3.38
Total	99.19	99.96	99.45	100.59	99.97	99.95	99.32	100.17	99.23

Sample	6	6	7	7	7	7	7	7	7
Analysis	GM10	GM11	GM1	GM2	GM3	GM4	GM5	GM6	GM7
SiO_2	77.95	77.68	77.09	77.67	78.03	77.19	77.76	77.90	78.37
TiO_2	0.12	0.27	0.15	0.17	0.06	0.09	0.20	0.14	0.23
Al_2O_3	12.56	12.76	12.68	12.61	12.63	12.71	12.60	12.57	12.41
FeO*	1.07	1.00	0.85	0.95	0.90	0.96	1.02	0.79	0.99
MnO	0.09	0.08	0.19	0.25	0.05	0.19	0.19	0.17	0.08
MgO	0.12	0.14	0.14	0.13	0.13	0.11	0.10	0.10	0.16
CaO	0.70	0.74	0.80	0.78	0.79	0.75	0.71	0.71	0.74
Na_2O	3.52	3.42	3.38	3.54	3.47	3.63	3.48	3.48	3.37
K_2O	3.47	3.79	3.63	3.46	3.63	3.64	3.54	3.56	3.51
Total	99.60	99.88	98.91	99.56	99.69	99.27	99.60	99.42	99.86

Sample	7	7	24	24	24	24	24	24	24
Analysis	GM8	GM9	GM1	GM2	GM3	GM4	GM5	GM6	GM7
SiO_2	77.55	77.15	76.91	77.58	77.11	77.30	77.82	77.90	78.30
TiO_2	0.13	0.08	0.13	0.13	0.24	0.17	0.13	0.13	0.12
Al_2O_3	12.57	12.55	12.75	12.69	12.56	12.68	12.66	12.41	12.68
FeO*	0.92	0.97	0.90	1.04	0.83	0.97	0.88	0.85	0.87
MnO	0.04	0.14	0.11	0.03	0.01	0.18	0.04	0.13	0.07
MgO	0.09	0.11	0.13	0.14	0.13	0.12	0.12	0.11	0.11
CaO	0.86	0.77	0.68	0.73	0.75	0.71	0.57	0.65	0.73
Na_2O	3.52	3.43	3.62	3.60	3.64	3.45	3.89	3.60	3.54
K_2O	3.53	3.54	3.42	3.54	3.44	3.59	3.68	3.72	3.67
Total	99.21	98.74	98.65	99.48	98.71	99.17	99.79	99.50	100.09

Sample	24	24	60	60	60	60	60	60	60
Analysis	GM8	GM9	GM1	GM2	GM3	GM4	GM5	GM6	GM7
SiO_2	78.72	77.89	77.32	75.81	76.42	76.21	76.73	76.96	76.04
TiO_2	0.13	0.17	0.22	0.12	0.21	0.14	0.12	0.23	0.14
Al_2O_3	12.77	12.29	12.69	12.62	12.40	12.79	12.60	12.41	12.52
FeO*	0.71	0.91	1.03	0.84	0.79	0.96	1.02	1.10	0.98
MnO	0.13	0.15	0.06	0.11	0.18	0.11	0.10	0.21	0.06
MgO	0.16	0.07	0.14	0.13	0.13	0.15	0.16	0.13	0.13
CaO	0.67	0.66	0.91	0.81	0.71	0.82	0.94	0.72	0.78
Na_2O	3.43	3.53	3.65	3.56	3.58	3.66	3.46	3.60	3.46
K_2O	3.62	3.61	3.35	2.97	3.24	3.30	3.22	3.15	3.27
Total	100.34	99.28	99.37	96.97	97.66	98.14	98.35	98.51	97.38

Analyses in weight percent. All iron expressed as FeO*.

Sample	60	60	60	92	92	92	92	92	92
Analysis	GM8	GM9	GM10	GM1	GM2	GM3	GM4	GM5	GM6
SiO_2	76.75	76.77	77.75	77.43	77.24	77.01	77.42	76.91	76.77
TiO_2	0.15	0.15	0.15	0.25	0.19	0.27	0.13	0.25	0.22
Al_2O_3	12.66	12.47	12.46	13.04	12.48	12.82	13.02	12.80	12.80
FeO*	0.99	0.89	0.84	1.13	0.99	1.00	1.06	1.04	0.95
MnO	0.07	0.13	0.00	0.12	0.12	0.10	0.21	0.12	0.03
MgO	0.16	0.12	0.13	0.18	0.18	0.20	0.18	0.24	0.16
CaO	0.84	0.77	0.85	0.96	0.90	0.89	1.08	1.06	0.97
Na_2O	3.68	3.65	3.39	3.56	3.68	3.56	3.54	3.58	3.77
K_2O	3.37	3.26	3.16	2.85	2.87	3.06	2.85	2.81	2.96
Total	98.67	98.21	98.73	99.52	98.65	98.91	99.49	98.81	98.63

Sample	92	92	92	92	98	98	98	98	98
Analysis	GM7	GM8	GM9	GM10	GM1	GM2	GM3	GM4	GM5
SiO_2	76.74	77.40	77.78	77.44	76.90	78.06	77.71	78.42	77.63
TiO_2	0.11	0.20	0.21	0.14	0.17	0.11	0.14	0.15	0.13
Al_2O_3	12.83	12.91	12.91	12.84	12.55	12.31	12.40	12.50	12.64
FeO*	0.97	0.99	0.94	1.12	0.92	0.72	0.88	0.88	0.79
MnO	0.17	0.10	0.09	0.09	0.03	0.15	0.16	0.06	0.09
MgO	0.16	0.15	0.19	0.20	0.09	0.05	0.10	0.06	0.09
CaO	0.86	0.98	0.92	0.95	0.85	0.74	0.85	0.76	0.88
Na_2O	3.51	3.59	3.40	3.41	3.54	3.59	3.51	3.68	3.60
K_2O	3.07	3.15	2.95	3.01	3.55	3.43	3.46	3.53	3.43
Total	98.42	99.47	99.39	99.20	98.60	99.16	99.21	100.04	99.28

Sample	98	98	98	98	98	98	98	105	105
Analysis	GM6	GM7	GM8	GM9	GM10	GM11	GM12	GM1	GM2
SiO_2	77.78	77.50	77.84	78.55	76.88	77.87	78.84	77.58	76.75
TiO_2	0.23	0.30	0.14	0.23	0.13	0.08	0.22	0.12	0.15
Al_2O_3	12.53	12.66	12.80	12.81	12.82	12.70	12.42	12.59	12.83
FeO*	1.07	0.93	0.81	0.87	0.92	0.85	0.87	0.90	0.79
MnO	0.20	0.28	0.31	0.08	0.07	0.03	0.00	0.33	0.17
MgO	0.12	0.18	0.09	0.08	0.07	0.09	0.11	0.13	0.16
CaO	0.69	0.86	0.87	0.76	0.73	0.74	0.77	0.96	0.95
Na_2O	3.57	3.39	3.62	3.48	3.46	3.49	3.60	3.45	3.57
K_2O	3.39	3.34	3.50	3.51	3.54	3.58	3.61	3.16	3.28
Total	99.58	99.44	99.98	100.37	98.62	99.43	100.44	99.22	98.65

Sample	105	105	105	105	105	105	105	105	105
Analysis	GM3	GM4	GM5	GM6	GM7	GM8	GM9	GM10	GM11
SiO_2	77.22	77.69	76.67	77.37	77.90	77.96	77.47	77.93	77.78
TiO_2	0.17	0.08	0.25	0.22	0.33	0.26	0.14	0.29	0.19
Al_2O_3	12.59	12.51	12.63	12.51	12.67	12.49	12.71	12.36	12.89
FeO*	1.04	1.07	1.11	1.02	1.02	0.90	1.20	1.10	1.01
MnO	0.17	0.07	0.17	0.23	0.00	0.09	0.17	0.04	0.21
MgO	0.17	0.11	0.12	0.17	0.13	0.18	0.16	0.12	0.19
CaO	0.85	0.88	1.03	0.92	0.94	1.11	0.94	0.90	1.00
Na_2O	3.35	3.47	3.41	3.32	3.52	3.29	3.44	3.59	3.66
K_2O	3.23	3.33	3.17	3.18	3.17	3.32	3.07	3.03	3.29
Total	98.79	99.21	98.56	98.94	99.68	99.60	99.30	99.36	100.22

Analyses in weight percent. All iron expressed as FeO*.

Sample	173	173	173	173	173	173	173	173	173
Analysis	GM1	GM2	GM3	GM4	GM5	GM6	GM7	GM8	GM9
SiO_2	77.64	76.78	77.85	78.45	78.62	78.32	78.13	78.20	77.96
TiO_2	0.11	0.14	0.12	0.15	0.11	0.19	0.20	0.16	0.17
Al_2O_3	12.41	12.61	12.40	12.45	12.72	12.83	12.42	12.62	12.72
FeO*	1.03	1.06	0.89	0.89	1.08	0.77	0.93	0.98	1.00
MnO	0.19	0.12	0.10	0.20	0.06	0.17	0.16	0.25	0.19
MgO	0.14	0.14	0.16	0.15	0.18	0.11	0.10	0.16	0.13
CaO	0.91	0.89	0.91	0.97	0.87	0.98	0.92	0.94	0.87
Na_2O	3.55	3.37	3.53	3.58	3.49	3.58	3.55	3.73	3.54
K_2O	3.18	3.10	3.24	3.05	3.13	3.10	3.38	3.19	3.23
Total	99.16	98.21	99.20	99.89	100.26	100.05	99.79	100.23	99.81

Sample	173	173	173	173
Analysis	GM10	GM11	GM12	GM13
SiO_2	77.13	77.98	78.52	77.66
TiO_2	0.25	0.09	0.22	0.16
Al_2O_3	12.75	12.47	12.86	12.68
FeO*	1.09	1.14	1.02	0.98
MnO	0.01	0.09	0.10	0.08
MgO	0.15	0.17	0.16	0.16
CaO	0.79	0.97	0.89	0.93
Na_2O	3.51	3.45	3.46	3.63
K_2O	3.24	3.25	3.21	3.08
Total	98.92	99.61	100.44	99.36

Table VIII.2: Electron microprobe analyses of melt inclusions in quartz phenocrysts from rhyolite lavas of the Haroharo Volcanic Complex.

Sample	6	6	6	6	6	6	7	7	7
Analysis	MI1	MI2	MI3	MI4	MI5	MI6	MI1	MI2	MI3
SiO_2	77.98	76.40	77.63	77.93	75.62	77.92	77.54	77.37	73.65
TiO_2	0.21	0.21	0.13	0.16	0.18	0.11	0.13	0.20	0.16
Al_2O_3	12.78	13.37	12.88	12.75	13.14	12.49	12.51	12.72	13.88
FeO*	0.93	1.00	0.91	0.79	1.13	1.07	1.12	0.81	0.96
MnO	0.15	0.01	0.00	0.15	0.12	0.07	0.11	0.13	0.17
MgO	0.09	0.14	0.09	0.09	0.15	0.12	0.12	0.10	0.09
CaO	0.82	0.84	0.73	0.76	0.94	0.78	0.77	0.76	0.77
Na_2O	3.70	5.09	3.81	3.84	4.66	3.68	3.55	3.78	5.35
K_2O	3.29	3.65	3.33	3.55	3.93	3.31	3.49	3.54	3.95
Total	99.95	100.71	99.51	100.02	99.87	99.55	99.34	99.41	98.98

Analyses in weight percent. All iron expressed as FeO*.

Sample	7	7	24	24	24	24	60	60	60
Analysis	MI4	MI5	MI1	MI2	MI3	MI4	MI1	MI2	MI3
SiO_2	69.55	74.89	76.34	77.27	76.62	74.32	73.19	73.92	76.03
TiO_2	0.20	0.15	0.19	0.15	0.24	0.33	0.13	0.21	0.15
Al_2O_3	13.93	13.84	12.62	12.59	12.37	14.02	14.12	13.89	12.58
FeO*	0.94	1.00	0.82	0.84	0.68	1.31	0.94	1.19	0.98
MnO	0.16	0.15	0.04	0.00	0.10	0.02	0.20	0.22	0.07
MgO	0.13	0.14	0.11	0.09	0.13	0.15	0.14	0.17	0.12
CaO	0.79	0.79	0.68	0.54	0.60	0.98	0.92	1.07	0.87
Na_2O	4.78	5.44	3.68	3.84	3.57	5.51	4.29	4.44	3.76
K_2O	4.06	3.75	3.85	3.84	3.51	4.06	3.27	3.42	3.01
Total	94.54	100.15	98.33	99.16	97.82	100.70	97.20	98.53	97.57

Sample	98	98	98	98	98	98	98	98	98
Analysis	MI1	MI2	MI3	MI4	MI5	MI6	MI7	MI8	MI9
SiO_2	76.60	77.28	74.50	77.54	71.65	76.46	75.48	73.83	74.23
TiO_2	0.11	0.14	0.14	0.18	0.20	0.17	0.15	0.15	0.21
Al_2O_3	12.89	12.94	12.02	13.11	12.03	12.56	13.45	13.25	11.09
FeO*	0.94	0.94	0.98	1.04	0.79	1.03	1.08	0.73	0.89
MnO	0.10	0.23	0.16	0.00	0.08	0.09	0.12	0.11	0.05
MgO	0.11	0.14	0.18	0.11	0.15	0.17	0.11	0.04	0.11
CaO	0.71	0.73	0.87	0.87	0.78	0.82	1.02	0.48	0.69
Na_2O	4.34	3.26	3.49	3.72	3.25	3.53	4.86	3.78	3.64
K_2O	3.27	3.52	3.05	3.47	3.21	3.37	3.30	3.42	2.88
Total	99.07	99.18	95.39	100.04	92.14	98.20	99.57	95.79	93.79

Sample	98	105	105	173	173	173
Analysis	MI10	MI1	MI2	MI1	MI2	MI3
SiO_2	76.24	78.22	74.80	76.91	76.01	74.75
TiO_2	0.16	0.25	0.23	0.26	0.22	0.13
Al_2O_3	12.95	12.90	14.20	12.61	13.29	13.65
FeO*	0.82	1.01	1.19	0.96	0.94	0.95
MnO	0.01	0.11	0.07	0.00	0.05	0.09
MgO	0.13	0.17	0.20	0.14	0.13	0.14
CaO	0.80	0.90	1.08	0.91	0.96	0.91
Na_2O	3.51	3.59	5.22	3.79	3.84	5.36
K_2O	3.44	3.09	3.53	3.27	3.16	3.46
Total	98.06	100.24	100.52	98.85	98.60	99.44

Analyses in weight percent. All iron expressed as FeO*.

Appendix IX: Mineral-Melt Partition Coefficients

Table IX.1: Mineral-melt partition coefficients used in fractional crystallisation modelling.

	$K_{Orthopyroxene}$	$K_{Amphibole}$	$K_{Biotite}$	$K_{Magnetite}$	$K_{Ilmenite}$	$K_{Plagioclase}$
Rb	**0.003**	**0.014**	3.200			0.105
Sr	**0.009**	**0.022**	0.447			*
Ba	**0.003**	**0.044**	23.533			*
K	0.605	**0.081**				**0.100**
Cs			3.000			0.105
Pb			0.767			0.972
Y	**1.000**	**6.000**	1.233	**2.000**		0.130
Ti	**0.400**	**7.000**		**12.500**		**0.050**
Zr	**0.200**	**4.000**	1.197	**0.800**		0.135
Hf	0.200		0.703		2.492	0.148
Nb	**0.800**	**4.000**	6.367	**2.500**		**0.060**
Ta	0.165		1.567		54.584	0.035
Th	0.130		0.997		3.982	0.048
U	0.145		0.773		1.859	0.093
La	0.780		5.713		4.162	0.380
Ce	0.930	**1.520**	4.357		4.720	0.267
Nd	1.250	**4.260**	2.560		4.934	0.203
Sm	1.600	**7.770**	2.117		4.867	0.165
Eu	0.825	**5.140**	2.020		1.757	5.417
Gd	**0.340**	**10.000**	**0.280**			0.125
Dy	1.800	**13.000**	1.720		3.767	0.112
Er	**0.650**	**12.000**	**0.350**			**0.055**
Yb	2.200	**8.380**	1.473		2.784	0.090
Lu	2.250	**5.500**	1.617		2.402	0.092
Sc	18.000		13.633		8.267	0.053

Mineral-melt partition coefficients are taken from the compilation of Rollinson (1993), based on the work of Arth (1976) (Rb-K and REE, bold font), Pearce and Norry (1979) (Y-Nb, bold font) and Nash and Crecraft (1985) (plain font).

* Partition coefficients for Sr and Ba in plagioclase calculated following Blundy and Wood (1991), and are dependent on plagioclase composition and temperature (Table IX.2).

Table IX.2: Mineral-melt partition coefficients for Sr and Ba in plagioclase.

Sample Number	Sr	Ba
105	7.1	0.6
113	4.9	0.5
173	7.8	0.6
176	11.3	0.9
24	9.6	0.7
32	9.1	0.7
6	8.4	0.6
60	7.9	0.7
7	8.1	0.7
92	6.8	0.6
98	9.3	0.8
109	8.1	0.9
119	9.5	0.9
117	13.1	1.5
152	10.7	1.1
170	9.5	0.8
64	10.8	0.9
134	10.9	1.0
158	13.1	1.0
38	7.3	0.6
44	6.8	0.7
90	6.5	0.7
103	9.8	0.9
104	13.7	1.1
87	9.2	0.8
Average	9.2	0.8

Calculations following Blundy and Wood (1991) using an average An content for each sample and temperatures from Tables 5.1 and 5.3.

Appendix X: Fractional Crystallisation Modelling

Table X.1: Fractional crystallisation modelling for Rotoma Eruptive Episode lavas from the Haroharo Volcanic Complex.

Samples	Rotoma (105) to Te Pohue (60)		Rotoma (105) to Te Pohue (60)	
Composition	(observed)	(calculated)	(observed)	(calculated)
SiO_2	76.41	76.40	76.41	76.40
TiO_2	0.19	0.18	0.19	0.18
Al_2O_3	13.04	13.05	13.04	13.05
Fe_2O_3*	1.40	1.39	1.40	1.39
MnO	0.07	0.06	0.07	0.06
MgO	0.23	0.23	0.23	0.23
CaO	1.35	1.33	1.35	1.33
Na_2O	4.35	4.33	4.35	4.33
K_2O	2.96	3.02	2.96	3.02
Total	100.00	99.99	100.00	99.99
		$\Sigma r^2 = 0.005$		$\Sigma r^2 = 0.005$
Subtracted phases (wt. %)				
Plagioclase		4.15		4.13
Orthopyroxene		0.55		
Calcic Amphibole		0.08		0.05
Cummingtonite				0.57
Titanomagnetite		0.27		0.31
Ilmenite		0.14		0.14
wt % crystallised		5.19		5.20
Trace Element Calculations				
	60			60
	(observed)	(calculated)		(calculated)
Rb	94	100		100
Sr	122	142		142
Ba	810	849		849
Cs	3.82	4.24		4.24
Pb	12.6	13.4		13.4
Y	25.9	26.4		26.4
Zr	141	183		183
Hf	4.41	5.41		5.41
Nb	8.22	8.45		8.44
Ta	0.76	0.74		0.74
Th	9.64	9.95		9.95
U	2.34	2.45		2.45
La	23.77	23.69		23.70
Ce	47.8	47.3		47.3
Nd	19.71	20.18		20.17
Sm	3.97	4.12		4.11
Eu	0.87	0.91		0.91
Gd	3.69	3.92		3.91
Dy	3.88	4.10		4.08
Er	2.57	2.71		2.70
Yb	2.81	2.91		2.90
Lu	0.46	0.48		0.48
Sc	4.4	5.6		5.6

Table X.2: Fractional crystallisation modelling for Mamaku Eruptive Episode lavas from the Haroharo Volcanic Complex.

Samples	Waiti (173) to Hainini (7)		Waiti (173) to Te Horoa (32)	
Composition	(observed)	(calculated)	(observed)	(calculated)
SiO_2	76.59	76.60	76.62	76.63
TiO_2	0.19	0.19	0.18	0.19
Al_2O_3	12.83	12.81	12.82	12.81
Fe_2O_3*	1.45	1.45	1.42	1.43
MnO	0.07	0.05	0.06	0.05
MgO	0.25	0.25	0.22	0.22
CaO	1.24	1.25	1.26	1.27
Na_2O	4.26	4.33	4.29	4.33
K_2O	3.13	3.08	3.13	3.09
Total	100.01	100.01	100.00	100.02
		$\Sigma r^2 = 0.009$		$\Sigma r^2 = 0.004$
Subtracted phases (wt. %)				
Plagioclase		5.21		5.41
Orthopyroxene		0.21		0.60
Calcic Amphibole		0.44		0.10
Cummingtonite				
Titanomagnetite		0.32		0.28
Ilmenite		0.07		0.10
wt % crystallised		6.25		6.49
Trace Element Calculations				
	7		32	
	(observed)	(calculated)	(observed)	(calculated)
Rb	108	104	105	105
Sr	108	147	109	147
Ba	847	858	852	860
Cs	4.37	4.50	4.36	4.51
Pb	12.9	14.0	13.0	14.1
Y	25.1	29.8	24.9	29.9
Zr	138	195	137	196
Hf	4.30	5.83	4.11	5.84
Nb	7.99	9.49	7.87	9.52
Ta	0.82	0.86	0.78	0.86
Th	10.52	11.24	10.51	11.27
U	2.48	2.67	2.48	2.67
La	23.87	26.81	23.83	26.86
Ce	47.30	53.56	47.3	53.7
Nd	18.66	22.02	18.87	22.08
Sm	3.83	4.55	3.90	4.57
Eu	0.76	1.04	0.77	1.04
Gd	3.54	4.30	3.58	4.31
Dy	3.77	4.51	3.74	4.53
Er	2.51	2.99	2.48	3.00
Yb	2.80	3.22	2.69	3.23
Lu	0.46	0.53	0.45	0.53
Sc	4.4	6.2	4.3	6.2

Samples	Waiti (173) to Kaipara*		Waiti (173) to Kaipara*	
Composition	(observed)	(calculated)	(observed)	(calculated)
SiO_2	77.31	77.27	77.31	77.27
TiO_2	0.18	0.15	0.18	0.15
Al_2O_3	12.68	12.64	12.68	12.64
Fe_2O_3*	1.22	1.19	1.22	1.19
MnO	0.06	0.04	0.06	0.04
MgO	0.20	0.20	0.20	0.20
CaO	1.14	1.10	1.14	1.10
Na_2O	4.21	4.30	4.21	4.30
K_2O	3.00	3.13	3.00	3.13
Total	100.00	100.02	100.00	100.02
		$\Sigma r^2 = 0.032$		$\Sigma r^2 = 0.032$
Subtracted phases (wt. %)				
Plagioclase		6.82		6.78
Orthopyroxene		0.11		
Calcic Amphibole		0.89		0.94
Cummingtonite				0.07
Titanomagnetite		0.55		0.56
Ilmenite		0.12		0.11
wt % crystallised		8.49		8.46
Trace Element Calculations				
	Kaipara			Kaipara
	(observed)	(calculated)		(calculated)
Rb	95	107		107
Sr	101	147		147
Ba	786	877		877
Y	26	30		30
Zr	130	199		199
Nb	9	10		10
La	21	27		27
Ce	47	55		55

Major and trace element compositions for the Kaipara Flow are an average of three analyses in Wright (2000).

Table X.3: Fractional crystallisation modelling for Mamaku and Whakatane eruptive episode lavas from the Haroharo Volcanic Complex.

Samples	Waiti (173) to Tikorangi (98)		Waiti (173) to Haroharo (6)		Waiti (173) to Haroharo (6)	
Composition	(observed)	(calculated)	(observed)	(calculated)	(observed)	(calculated)
SiO_2	75.74	75.73	76.57	76.57	76.57	76.57
TiO_2	0.24	0.23	0.18	0.18	0.18	0.18
Al_2O_3	13.20	13.18	12.89	12.87	12.89	12.87
Fe_2O_3*	1.65	1.64	1.44	1.44	1.44	1.44
MnO	0.07	0.07	0.06	0.05	0.06	0.05
MgO	0.31	0.31	0.22	0.22	0.22	0.22
CaO	1.49	1.49	1.25	1.26	1.25	1.26
Na_2O	4.33	4.40	4.29	4.34	4.29	4.34
K_2O	2.97	2.96	3.11	3.07	3.11	3.07
Total	100.00	100.01	100.01	100.00	100.01	100.00
		$\Sigma r^2 = 0.006$		$\Sigma r^2 = 0.005$		$\Sigma r^2 = 0.004$
Subtracted phases						
Plagioclase		1.92		4.82		4.84
Orthopyroxene		0.05		0.20		
Calcic Amphibole		0.20		0.64		0.60
Cummingtonite						0.27
Titanomagnetite		0.18		0.29		0.28
Ilmenite		0.00		0.09		0.09
wt % crystallised		2.35		6.04		6.08
Trace Element Calculations						
	98		6			6
	(observed)	(calculated)	(observed)	(calculated)		(calculated)
Rb	99	100	106	104		104
Sr	129	144	108	147		147
Ba	829	825	862	856		857
Cs	4.03	4.32	4.53	4.49		4.49
Pb	12.4	13.5	13.5	14.0		14.0
Y	24.3	28.7	26.5	29.7		29.7
Zr	168	187	133	194		194
Hf	4.77	5.60	4.49	5.82		5.82
Nb	7.88	9.12	8.38	9.46		9.46
Ta	0.71	0.83	0.89	0.86		0.86
Th	9.73	10.79	10.75	11.21		11.22
U	2.35	2.56	2.56	2.66		2.66
La	22.51	25.77	24.62	26.75		26.76
Ce	44.9	51.5	49.00	53.44		53.46
Nd	18.18	21.18	19.73	21.96		21.96
Sm	3.69	4.38	4.06	4.54		4.53
Eu	0.84	1.01	0.82	1.03		1.03
Gd	3.50	4.13	3.77	4.28		4.28
Dy	3.69	4.35	4.00	4.50		4.49
Er	2.48	2.88	2.63	2.98		2.97
Yb	2.69	3.10	2.88	3.21		3.21
Lu	0.45	0.51	0.48	0.53		0.53
Sc	5.2	5.9	4.6	6.2		6.2

Samples	Hainini (7) to Okataina (24)		Hainini (7) to Okataina (24)		Haroharo (6) to Okataina (24)	
Composition	(observed)	(calculated)	(observed)	(calculated)	(observed)	(calculated)
SiO_2	77.06	77.07	77.06	77.07	77.06	77.08
TiO_2	0.16	0.17	0.16	0.17	0.16	0.17
Al_2O_3	12.70	12.71	12.70	12.71	12.70	12.70
Fe_2O_3*	1.24	1.25	1.24	1.25	1.24	1.25
MnO	0.06	0.06	0.06	0.06	0.06	0.06
MgO	0.18	0.18	0.18	0.18	0.18	0.18
CaO	1.12	1.13	1.12	1.13	1.12	1.13
Na_2O	4.24	4.24	4.24	4.24	4.24	4.26
K_2O	3.23	3.19	3.23	3.19	3.23	3.17
Total	99.99	100.00	99.99	100.00	99.99	100.00
		$\Sigma r^2 = 0.002$		$\Sigma r^2 = 0.002$		$\Sigma r^2 = 0.004$
Subtracted phases (wt. %)						
Plagioclase		1.48		1.50		1.76
Orthopyroxene		0.24				
Calcic Amphibole		0.18		0.11		
Cummingtonite				0.32		0.24
Titanomagnetite		0.12		0.12		0.17
Ilmenite		0.03		0.03		
wt % crystallised		2.05		2.08		2.17
Trace Element Calculations						
	24		24		24	
	(observed)	(calculated)		(calculated)		(calculated)
Rb	108	110		110		108
Sr	98	110		110		110
Ba	858	865		865		881
Cs	4.60	4.46		4.46		4.63
Pb	13.5	13.2		13.2		13.8
Y	25.0	25.6		25.6		27.1
Zr	120	141		141		136
Hf	3.71	4.39		4.39		4.59
Nb	7.74	8.16		8.16		8.56
Ta	0.79	0.84		0.84		0.91
Th	10.75	10.74		10.74		10.99
U	2.51	2.53		2.53		2.62
La	23.95	24.37		24.37		25.16
Ce	47.60	48.28		48.29		50.08
Nd	18.96	19.04		19.05		20.16
Sm	3.82	3.91		3.91		4.15
Eu	0.74	0.77		0.77		0.84
Gd	3.53	3.61		3.61		3.85
Dy	3.75	3.85		3.85		4.09
Er	2.49	2.56		2.56		2.69
Yb	2.71	2.86		2.86		2.94
Lu	0.45	0.47		0.47		0.49
Sc	4.1	4.5		4.5		4.7

Table X.4: Fractional crystallisation modelling for Te Rere and Rotorua eruptive episode lavas from the Okareka Volcanic Complex.

Samples	Eastern (113) to Trig 7693 (176)		Eastern (113) to Trig 7693 (176)	
Composition	(observed)	(calculated)	(observed)	(calculated)
SiO_2	75.62	75.69	75.62	75.66
TiO_2	0.21	0.26	0.21	0.30
Al_2O_3	13.22	13.17	13.22	13.20
Fe_2O_3*	1.69	1.74	1.69	1.95
MnO	0.06	0.07	0.06	0.06
MgO	0.30	0.29	0.30	0.11
CaO	1.48	1.54	1.48	1.43
Na_2O	4.11	4.36	4.11	4.38
K_2O	3.30	2.91	3.30	2.90
Total	99.99	100.03	99.99	99.99
		$\Sigma r^2 = 0.230$		$\Sigma r^2 = 0.346$
Subtracted phases (wt. %)				
Plagioclase		5.37		5.05
Orthopyroxene		0.19		
Calcic Amphibole		1.33		2.68
Biotite				0.27
Titanomagnetite		0.43		
Ilmenite		0.11		
wt % crystallised		7.43		8.00
Trace Element Calculations				
	176			176
	(observed)	(calculated)		(calculated)
Rb	113	96		96
Sr	117	179		179
Ba	855	851		847
Cs	4.95	3.84		3.84
Pb	13.4	12.7		12.7
Y	21.8	27.3		27.2
Zr	130	255		254
Hf	3.98	6.39		6.39
Nb	7.61	8.47		8.43
Ta	0.80	0.71		0.71
Th	11.42	9.35		9.35
U	2.68	2.32		2.32
La	23.99	23.17		23.15
Ce	46.40	46.41		46.32
Nd	17.37	20.60		20.51
Sm	3.38	4.37		4.33
Eu	0.67	1.05		1.05
Gd	3.05	4.20		4.16
Dy	3.23	4.31		4.26
Er	2.13	2.81		2.77
Yb	2.40	3.00		2.97
Lu	0.41	0.48		0.48
Sc	4.2	8.4		8.4

Table X.5: Fractional crystallisation modelling for Tarawera Volcanic Complex lavas.

Samples	Patiti (130) to Western (44)		Rotomahana (134) to Tarawera (158)	
Composition	(observed)	(calculated)	(observed)	(calculated)
SiO_2	73.95	73.85	76.44	76.44
TiO_2	0.31	0.24	0.19	0.17
Al_2O_3	13.74	13.77	12.91	12.96
Fe_2O_3*	2.31	2.24	1.49	1.46
MnO	0.08	0.06	0.06	0.05
MgO	0.64	0.64	0.23	0.15
CaO	2.35	2.26	1.31	1.48
Na_2O	4.17	3.99	4.26	4.02
K_2O	2.46	2.96	3.11	3.26
Total	100.01	100.01	100.00	99.99
		$\Sigma r^2 = 0.310$		$\Sigma r^2 = 0.120$
Subtracted phases (wt. %)				
Plagioclase		4.36		4.17
Orthopyroxene		0.05		
Calcic Amphibole		0.39		0.99
Cummingtonite				1.29
Titanomagnetite		0.49		
Ilmenite		0.21		
wt % crystallised		5.50		6.45
Trace Element Calculations				
	44		158	
	(observed)	(calculated)	(observed)	(calculated)
Rb	76	99	103	119
Sr	173	175	111	136
Ba	812	785	853	866
Cs	3.04	5.07	4.19	5.33
Pb	9.1	12.6	12.0	13.6
Y	19.4	22.6	23.7	20.6
Zr	163	189	139	145
Hf	4.13	4.89	3.95	4.49
Nb	7.04	7.79	7.73	7.66
Ta	0.66	0.79	0.77	0.79
Th	7.63	10.05	10.28	12.09
U	1.81	2.43	2.40	2.87
La	20.78	22.86	23.03	23.61
Ce	40.4	44.59	44.90	45.50
Nd	15.82	18.65	16.97	17.68
Sm	3.05	3.73	3.44	3.35
Eu	0.72	0.81	0.75	0.68
Gd	2.87	3.44	3.18	3.05
Dy	2.9	3.55	3.45	3.18
Er	1.93	2.31	2.33	2.08
Yb	2.15	2.50	2.59	2.35
Lu	0.37	0.40	0.44	0.39
Sc	6.3	7.2	4.5	4.4

Samples	Ridge (90) to Waikakareao (38)		Ridge (90) to Waikakareao (38)	
Composition	(observed)	(calculated)	(observed)	(calculated)
SiO_2	76.96	76.94	76.96	76.94
TiO_2	0.17	0.15	0.17	0.16
Al_2O_3	12.70	12.69	12.70	12.73
Fe_2O_3*	1.33	1.31	1.33	1.32
MnO	0.06	0.05	0.06	0.06
MgO	0.19	0.18	0.19	0.19
CaO	1.17	1.25	1.17	1.17
Na_2O	4.30	4.17	4.30	4.19
K_2O	3.10	3.25	3.10	3.24
Total	99.98	99.99	99.98	100.00
		$\Sigma r^2 = 0.047$		$\Sigma r^2 = 0.032$
Subtracted phases (wt. %)				
Plagioclase		5.19		4.55
Orthopyroxene		1.05		
Calcic Amphibole				1.26
Cummingtonite				
Titanomagnetite		0.18		0.33
Ilmenite		0.21		0.13
wt % crystallised		6.63		6.27
Trace Element Calculations				
	38			38
	(observed)	(calculated)		(calculated)
Rb	101	111		111
Sr	106	137		137
Ba	855	862		859
Cs	4.37	4.86		4.84
Pb	13.6	14.1		14.0
Y	26.8	27.5		27.3
Zr	141	187		186
Hf	4.42	5.45		5.43
Nb	8.51	9.19		9.13
Ta	0.79	0.88		0.88
Th	10.41	11.77		11.73
U	2.48	2.85		2.84
La	24.39	25.79		25.72
Ce	49.00	50.75		50.56
Nd	20.01	20.44		20.32
Sm	4.11	4.21		4.17
Eu	0.83	0.87		0.87
Gd	3.77	3.97		3.92
Dy	4.04	4.16		4.10
Er	2.64	2.74		2.70
Yb	2.87	3.06		3.03
Lu	0.47	0.50		0.50
Sc	4.6	6.1		6.2

References

References

Allen, R.L., 1988: False pyroclastic textures in altered silicic lavas, with implications for volcanic-associated mineralisation. *Economic Geology*, 83. p1424-1446.

Anderson, A.T., 2001: Origins of crystals in silicic magmas. In: Knesel, K., Bergantz, G. and Davidson, J. (convenors): Geological Society of America Penrose Conference. Longevity and Dynamics of Rhyolitic Magma Systems. Abstracts.

Anderson, A.T., Davis, A.M. and Lu, F., 2000: Evolution of Bishop Tuff rhyolitic magma based on melt and magmatic inclusions and zoned phenocrysts. *Journal of Petrology,* 41. p449-473.

Anderson, J.L. and Smith, D.R., 1995: The effects of temperature and fo_2 on the Al-in-hornblende barometer. *American Mineralogist,* 80. p549-559.

Arth, J.G., 1976: Behaviour of trace elements during magmatic processes - a summary of theoretical models and their applications. *Journal of Research of the U.S Geological Survey,* 4. p41-47.

Bacon, C.R., 1985: Implications of silicic vent patterns for the presence of large crustal magma chambers. *Journal of Geophysical Research,* 90. p11243-11252.

Bacon, C.R. and Hirschmann, M.M., 1988: Mg/Mn partitioning as a test for equilibrium between coexisting Fe-Ti oxides. *American Mineralogist,* 73. p57-61.

Bacon, C.R., Macdonald, R., Smith, R.L. and Baedecker, P.A., 1981: Pleistocene high silica rhyolites of the Coso Volcanic Field, Inyo County, California. *Journal of Geophysical Research,* 86. p10223-10241.

Bailey, R.A. and Carr, R.G., 1994: Physical geology and eruptive history of the Matahina Ignimbrite, Taupo Volcanic Zone, North Island, New Zealand. *New Zealand Journal of Geology and Geophysics,* 37. p319-344.

Bea, F., 1996: Residence of REE, Y, Th and U in granites and crustal protoliths; Implications for the chemistry of crustal melts. *Journal of Petrology,* 37. p521-552.

Beanland, S., 1981: The Rotokawau eruption. Unpublished BSc (Hons) Thesis. University of Otago, Dunedin, New Zealand. 169p.

Beanland, S. and Haines, J., 1998: The kinematics of active deformation in the North Island, New Zealand, determined from geological strain rates. *New Zealand Journal of Geology and Geophysics,* 41. p311-323.

Beanland, S. and Houghton, B., 1991: Rotokawau Tephra: Basaltic maars in Okataina Volcanic Centre, Taupo Volcanic Zone. *New Zealand Geological Survey Record,* 43. p37-43.

Becker, J.S., 1999: Volcanic risk mitigation in the Waikato Region, New Zealand. Unpublished MSc Thesis. University of Waikato, Hamilton, New Zealand. 288p.

Bellamy, S., 1991: Some Studies of the Te Wairoa Ignimbrites and the associated volcanic geology of the southwestern Okataina Volcanic Centre. Unpublished MSc Thesis. University of Waikato, Hamilton, New Zealand. 179p.

Beresford, S.W., 1997: Volcanology and geochemistry of the Kaingaroa Ignimbrite, Taupo Volcanic Zone, New Zealand. Unpublished PhD Thesis. University of Canterbury, Christchurch, New Zealand. 346p.

Beresford, S.W. and Cole, J.W., 2000: Kawerau Ignimbrite: a 0.24 Ma ignimbrite erupted from the Okataina caldera complex, Taupo Volcanic Zone, New Zealand. *New Zealand Journal of Geology and Geophysics,* 43. p109-115.

Bibby, H.M., Dawson, G.B., Rayner, H.H., Bennie, S.L. and Bromley, C.J., 1992: Electrical Resistivity and Magnetic Investigations of the Geothermal Systems in the Rotorua Area, New Zealand. *Geothermics,* 21. p43-64.

Blattner, P. and Reid, F.W., 1982: The origin of lavas and ignimbrites of the Taupo Volcanic Zone, New Zealand in the light of oxygen isotope data. *Geochimica et Cosmochimica Acta,* 46. p1417-1429.

Blattner, P., Rui-zhong, H., Graham, I.J. and Houston-Eleftheriadis, C., 1996: Temperatures and isotopic evolution of silicic magmas, Taupo Volcanic Zone and Coromandel, New Zealand. *New Zealand Journal of Geology and Geophysics,* 39. p353-362.

Blundy, J.D. and Wood, B.J., 1991: Crystal-chemical controls on the partitioning of Sr and Ba between plagioclase feldspar, silicate melts and hydrothermal solutions. *Geochimica et Cosmochimica Acta,* 55. p193-209.

Bonnichsen, B. and Kauffman, D.F., 1987: Physical features of rhyolite lava flows in Snake River Plain volcanic province southwestern Idaho. *Geological Society of America Special Paper,* 212. p119-145.

Bowyer, D.A., 1997: Petrology and geochemistry of two andesitic ignimbrites, Ignimbrite C and Tikorangi Ignimbrite, Taupo Volcanic Zone, New Zealand. Unpublished MSc (Tech) Thesis. University of Waikato, Hamilton, New Zealand. 222p.

Boynton, W.V., 1984: Geochemisty of the rare earth elements: meteorite studies. In: Henderson, P. (editor), Rare Earth Element Geochemisty. Elsevier: Amsterdam; New York. p63-114.

Briggs, R.M., Gifford, M.G., Moyle, A.R., Taylor, S.R., Norman, M.D., Houghton, B.F. and Wilson, C.J.N., 1993: Geochemical zoning and eruptive mixing in ignimbrites from Mangakino volcano, Taupo Volcanic Zone, New Zealand. *Journal of Volcanology and Geothermal Research,* 56. p175-203.

Brown, S.J.A., 1994: Geology and geochemistry of the Whakamaru group ignimbrites, and associated rhyolite domes, Taupo Volcanic Zone, New Zealand. Unpublished PhD Thesis. University of Canterbury, Christchurch, New Zealand. 288p.

Brown, S.J.A., Burt, R.M., Cole, J.W., Krippner, S.J.P., Price, R.C. and Cartwright, I., 1998a: Plutonic lithics in ignimbrites of Taupo Volcanic Zone, New Zealand; sources and conditions of crystallisation. *Chemical Geology,* 148. p21-41.

Brown, S.J.A. and Fletcher, I.R., 1999: SHRIMP U-Pb dating of the pre-eruption growth history of zircons from the 340 ka Whakamaru Ignimbrite, New Zealand: Evidence for > 250 k.y. magma residence times. *Geology,* 27. p1035-1038.

Brown, S.J.A., Fletcher, I.R., Smith, R.T. and Cole, J.W., 2000: Timescales in large silicic magma systems in the Taupo Volcanic Zone: ^{238}U-^{206}Pb and ^{238}U-^{230}Th dating of growth zones in magmatic zircons using SHRIMP. In: Smith I.E.M., Davidson, J.P., Gamble, J.A. and Price, R.C. (editors): State of the Arc 2000: Processes and timescales. Extended abstracts. p29-31.

Brown, S.J.A., Wilson, C.J.N., Cole, J.W. and Wooden, J., 1998b: The Whakamaru group ignimbrites, Taupo Volcanic Zone, New Zealand: evidence for reverse tapping of a zoned silicic magmatic system. *Journal of Volcanology and Geothermal Research,* 84. p1-37.

Browne, P.R.L., Graham, I.J., Parker, R.J. and Wood, C.P., 1992: Subsurface andesite lavas and plutonic rocks in the Rotokawa and Ngatamariki geothermal systems, Taupo Volcanic Zone, New Zealand. *Journal of Volcanology and Geothermal Research,* 51. p199-215.

Buddington, A.F. and Lindsley, D.H., 1964: Iron-titanium oxides and synthetic equivalents. *Journal of Petrology,* 5. p310-357.

Burt, R.M., Brown, S.J.A., Cole, J.W., Shelley, D. and Waight, T.E., 1998: Glass-bearing plutonic fragments from ignimbrites of the Okataina caldera complex, Taupo Volcanic Zone, New Zealand: remnants of a partially molten intrusion associated with preceding eruptions. *Journal of Volcanology and Geothermal Research,* 84. p209-237.

Carmichael, I.S.E., 1967: The iron-titanium oxides of salic volcanic rocks and their associated ferromagnesian silicates. *Contributions to Mineralogy and Petrology,* 14. p36-64.

Carr, R.G., 1984: The Matahina ignimbrite, its evolution including its eruption and post depositional changes. Unpublished PhD Thesis. University of Auckland, Auckland, New Zealand. 256p.

Cashman, K.V., 1992: Groundmass crystallization of Mount St. Helens dacite, 1980-1986: a tool for interpreting shallow magmatic processes. *Contributions to Mineralogy and Petrology,* 109. p431-449.

Christensen, J.N. and De Paolo, D.J., 1993: Time scales of large volume silicic magma systems: Sr isotope systematics of phenocrysts and glass from the Bishop Tuff, Long Valley, California. *Contributions to Mineralogy and Petrology,* 113. p100-114.

Christensen, J.N. and Halliday, A.N., 1996: Rb-Sr ages and Nd isotopic compositions of melt inclusions from the Bishop Tuff and the generation of silicic magma. *Earth and Planetary Science Letters,* 144. p547-561.

Cole, J.W., 1966: Tarawera Volcanic Complex. Unpublished PhD Thesis. Victoria University, Wellington, New Zealand. 229p.

Cole, J.W., 1970a: Structure and Eruptive History of the Tarawera Volcanic Complex. *New Zealand Journal of Geology and Geophysics*, 13. p879-902.

Cole, J.W., 1970b: Petrography of the Rhyolite Lavas of the Tarawera Volcanic Complex. *New Zealand Journal of Geology and Geophysics*, 13. p903-924.

Cole, J.W., 1970c: Petrology of the Basic Rocks of the Tarawera Volcanic Complex. *New Zealand Journal of Geology and Geophysics*, 13. p925-936.

Cole, J.W., Leonard, G.S., Nairn, I.A., Shelley, D., Shane, P.R. and Self, S., 2001: Magma chambers beneath Tarawera volcano at the time of the AD1305 Kaharoa rhyolite episode, Taupo Volcanic Zone, New Zealand. In: Knesel, K., Bergantz, G. and Davidson, J. (convenors): Geological Society of America Penrose Conference. Longevity and Dynamics of Rhyolitic Magma Systems. Abstracts.

Conrad, W.K., Nicholls, I.A. and Wall, V.J., 1988: Water-saturated and undersaturated melting of metaluminous and peraluminous crustal composition at 10 kb, evidence for the origin of silicic magmas in the Taupo Volcanic Zone, New Zealand, and other occurrences. *Journal of Petrology,* 29. p765-803.

Crosby, N., 1998: Quaternary geology and tephrostatigraphy of the North-north-eastern Rotorua region. Unpublished MSc Thesis. University of Waikato, Hamilton, New Zealand. 154p.

Davies, G.R. and Halliday, A.N., 1998: Development of the Long Valley rhyolitic magma system: Strontium and neodymium isotope evidence from glasses and individual phenocrysts. *Geochimica et Cosmochimica Acta,* 62. p3561-3574.

Davies, G. and Heumann, A., 2001: Pre-eruption ages from rhyolitic magma chambers: real constraints or artifacts? In: Knesel, K., Bergantz, G. and Davidson, J. (convenors): Geological Society of America Penrose Conference. Longevity and Dynamics of Rhyolitic Magma Systems. Abstracts.

Davis, W.J., 1985: Geochemistry and petrology of the Rotoiti and Earthquake Flat pyroclastic deposits. Unpublished MSc Thesis. University of Auckland, Auckland, New Zealand. 143p.

Deer, W.A., Howie, R.A. and Zussman, J., 1966: An Introduction To The Rock Forming Minerals. Longman : London. 528p.

Deer, W.A., Howie, R.A. and Zussman, J., 1992: An Introduction To The Rock Forming Minerals. Longman Scientific & Technical: Harlow; Wiley: New York. 696p.

DePaolo, D.J., 1981: Trace element and isotopic effects of combined wallrock assimilation and fractional crystallisation. *Earth and Planetary Science Letters,* 53. p189-202.

Doe, B.R., Leeman, W.P., Christiansen, R.L. and Hedge, C.E., 1982: Lead and strontium isotopes and related trace elements as genetic tracers in the upper Cenozoic rhyolite-basalt association of the Yellowstone field. *Journal of Geophysical Research,* 87. p4785-4806.

Dravitzki, D.N.R., 1999: The volcanic history and lake sediment characteristics of Paradise Valley, Rotorua. Unpublished MSc Thesis. University of Waikato, Hamilton, New Zealand. 271p.

Droop, G.T.R., 1987: A general equation for estimating Fe^{3+} concentrations in ferromagnesian silicates and oxides from microprobe analyses, using stoichiometric criteria. *Mineralogical Magazine,* 51. p431-435.

Duffield, W.A. and Ruiz, J., 1992: Compositional gradients in large silicic reservoirs of silicic magma as evidenced by ignimbrite versus Taylor Creek Rhyolite lava domes. *Contributions to Mineralogy and Petrology,* 110. p192-210

Dunbar, N.W., Hervig, R.L. and Kyle, P.R., 1989: Determination of pre-eruptive H_2O, F and Cl contents of silicic magmas using melt inclusions: examples from Taupo Volcanic Centre, New Zealand. *Bulletin of Volcanology,* 51. p177-184.

Dunham, P.B., 1981: Quaternary geology of the Guthrie region – Taupo Volcanic Zone, New Zealand. Unpublished MSc Thesis, University of Waikato, Hamilton. 156p.

Eggins, S.M., Kinsley, L.P.J. and Shelley, J.M.G., 1998a: Deposition and element fractionation processes during atmospheric pressure laser sampling for analysis by ICP-MS. *Applied Surface Science,* 127-129. p278-286.

Eggins, S.M., Rudnick, R.L. and McDonough, W.F., 1998b: The composition of peridotites and their minerals: a laser-ablation ICP-MS study. *Earth and Planetary Science Letters,* 154. p53-71.

Environment Bay Of Plenty, 1999: Rotorua geothermal regional plan. July 1999. Environment BOP: Whakatane, New Zealand. 142p.

Evans, B.W. and Ghiorso, M.S., 1995: Thermodynamics and petrology of cummingtonite. *American Mineralogist,* 80. p649-663.

Ewart, A., 1966: Review of mineralogy and chemistry of the silicic volcanic rocks of Taupo Volcanic Zone, New Zealand. *Bulletin of Volcanology,* 29. p147-172.

Ewart, A., 1967: The petrography of the central North Island rhyolitic lavas. Part 1 - Correlations between the phenocryst assemblages. *New Zealand Journal of Geology and Geophysics,* 10. p182-197.

Ewart, A., 1968: The petrography of the central North Island rhyolitic lavas. Part 2 - Regional petrography including notes on associated ash-flow pumice deposits. *New Zealand Journal of Geology and Geophysics*, 11. p478-545.

Ewart, A., 1971a: Notes on the chemistry of ferromagnesian phenocrysts from selected volcanic rocks, central volcanic region. *New Zealand Journal of Geology and Geophysics,* 14. p323-340.

Ewart, A., 1971b: Chemical changes accompanying spherulitic crystallisation in rhyolite lavas, central volcanic region, New Zealand. *Mineralogical Magazine,* 38. p424-434.

Ewart, A., Bryan, W.B., Chappell, B.W. and Rudnick, R.L., 1994: Regional geochemistry of the Lau-Tonga arc and back-arc systems. In: Hawkins, J., Parson, L. and Allan, J. et al. (editors): Proceedings of the Ocean Drilling Program, Scientific Results 135. College Station, TX: Ocean Drilling Program. p385-425.

Ewart, A., Collerson, K.D., Regelous, M., Wendt, J.I. and Niu, Y., 1998: Geochemical evolution within the Tonga-Kermadec-Lau Arc-Back-arc systems: the role of varying mantle wedge composition in space and time. *Journal of Petrology,* 39. p331-368.

Ewart, A., Green, D.C., Carmichael., I.S.E. and Brown, F.H.,1971: Voluminous low temperature rhyolitic magmas in New Zealand. *Contributions to Mineralogy and Petrology*, 33. p128-44.

Ewart, A. and Hawkesworth, C.J., 1987: The Pleistocene - Recent Tonga - Kermadec Arc lavas: Interpretation of new isotopic and rare earth data in terms of a depleted mantle source model. *Journal of Petrology,* 28. p495-530.

Ewart, A., Hildreth, W. and Carmichael, I.S.E., 1975: Quaternary acid magma in New Zealand. *Contributions to Mineralogy and Petrology*, 51. p1-27.

Ewart, A. and Stipp, J.J., 1968: Petrogenesis of the volcanic rocks of the central North Island, New Zealand as indicated by a study of Sr^{87}/Sr^{86} ratios and Sr, Rb, K, U and Th abundances. *Geochimica et Cosmochimica Acta*, 32. p699-735.

Ewart, A. and Taylor, S.R., 1969: Trace element geochemistry of the rhyolitic volcanic rocks, central North Island, New Zealand. Phenocryst data. *Contributions to Mineralogy and Petrology,* 22. p127-146.

Ewart, A., Taylor, S.R. and Capp, A.C., 1968: Trace and minor element geochemistry of the rhyolitic volcanic rocks, central North Island, New Zealand. Total rock and residual liquid data. *Contributions to Mineralogy and Petrology,* 18. p76-104.

Farmer, G.L., Broxton, D.E., Warren, R.G. and Pickthorn, W., 1991: Nd, Sr, and O isotopic variations in metaluminous ash-flow tuffs and related volcanic rocks at the Timber Mountain/Oasis Valley Caldera Complex, SW Nevada: implications for the origin and evolution of large-volume silicic magma bodies. *Contributions to Mineralogy and Petrology,* 109. p53-68.

Fink, J.H., 1983: Structure and emplacement of a rhyolitic obsidian flow: Little Glass Mountain, Medicine Lake Highland, northern California. *Geological Society of America Bulletin,* 94. p362-380.

Fink, J.H. and Manley, C.R. 1987: Origin of pumiceous and glassy textures in rhyolite flows and domes. *Geological Society of America Special Paper 212.* p77-88.

Froggatt, P.C. and Lowe, D.J., 1990: A review of late Quaternary silicic and some other tephra formations from New Zealand: their stratigraphy, nomenclature, distribution, volume and age. *New Zealand Journal of Geology and Geophysics,* 33. p89-109.

Frost, B.R., 1991: Introduction to oxygen fugacity and its petrologic importance. *Reviews in Mineralogy,* 25. p1-9.

Gamble, J.A., Smith, I.E.M., Graham, I.J., Kokelaar, B.P., Cole, J.W., Houghton, B.F. and Wilson, C.J.N., 1990: The petrology, phase relations and tectonic setting of basalts from the Taupo Volcanic Zone, New Zealand and the Kermadec Island Arc-Harve Trough, SW Pacific. *Journal of Volcanology and Geothermal Research,* 43. p235-270.

Gamble, J.A., Smith, I.E.M., McCulloch, M.T., Graham, I.J. and Kokelaar, B.P., 1993: The geochemistry and petrogenesis of basalts from the Taupo Volcanic Zone and Kermadec Island Arc, S.W. Pacific. *Journal of Volcanology and Geothermal Research,* 54. p265-290.

Gaston, J.P., 1991: The petrology and geochemistry of the Kapenga Caldera rhyolites, Taupo Volcanic Zone. Unpublished BSc (Hons) Thesis. Victoria University, Wellington, New Zealand.

Gerstenberger, H. and Haase, G., 1997: A highly effective emitter substance for mass spectrometric Pb isotope ratio determinations. *Chemical Geology,* 136. p309-312.

Ghiorso, M.S. and Sack, R.O., 1991: Fe-Ti oxide geothermometry: thermodynamic formulation and the estimation of intensive variables in silicic magmas. *Contributions to Mineralogy and Petrology,* 108. p485-510.

Graham, I.J., Blattner, P. and McCulloch, M.T., 1990: Meta-igneous granulite xenoliths from Mount Ruapehu, New Zealand: fragments of altered oceanic crust? *Contributions to Mineralogy and Petrology,* 105. p650-661.

Graham, I.J., Cole, J.W., Briggs, R.M., Gamble, J.A. and Smith, I.E.M., 1995: Petrology and petrogenesis of volcanic rocks from the Taupo Volcanic Zone: A review. *Journal of Volcanology and Geothermal Research,* 68. p59-87.

Graham, I.J., Gulson, B.L., Hedenquist, J.W. and Mizon, K., 1992: Petrogenesis of Late Cenozoic volcanic rocks from the Taupo Volcanic Zone, New Zealand, in the light of new lead isotope data. *Geochimica et Cosmochimica Acta,* 56. p2797-2819.

Grange, L.I., 1937: The Geology of the Rotorua-Taupo Subdivision. *New Zealand Geological Survey Bulletin,* 37. 138p.

Grapes, R., Howard, D. and Thornton, J., 1994: Vug minerals in rhyolite, Henderson's Quarry, Mt. Ngongotaha, Rotorua. *Mineralogical Society of New Zealand Newsletter,* 1. p12-16.

Grindley, G.W., 1959: Sheet N85 - Waiotapu. Geological Map of New Zealand 1:63,360. New Zealand Department of Scientific and Industrial Research, Wellington, New Zealand.

Grindley, G.W., 1960: Sheet 8 - Taupo. Geological Map of New Zealand 1:250,000. New Zealand Department of Scientific and Industrial Research, Wellington, New Zealand.

Grindley, G.W., 1961: Sheet N94 - Taupo. Geological Map of New Zealand 1:63,360. New Zealand Department of Scientific and Industrial Research, Wellington, New Zealand.

Halliday, A.N., Davidson, J.P., Hildreth, W. and Holden, P., 1991: Modelling the petrogenesis of high Rb/Sr silicic magmas. *Chemical Geology,* 92. p107-114.

Halliday, A.N., Mahood, G.A., Holden, P., Metz, J.M., Dempster, T.J. and Davidson, J.P., 1989: Evidence for long residence times of rhyolitic magma in the Long Valley magmatic system: The isotopic record in precaldera lavas of Glass Mountain. *Earth and Planetary Science Letters,* 94. p274-290.

Hawthorn, F., 1981: Crystal chemistry of the amphiboles. *Reviews in Mineralogy,* 9A. p1-102.

Healy, J., 1963: Geology of the Rotorua District. *Proceedings of the New Zealand Ecological Society,* 10. p53-58.

Healy, J., 1964: Volcanic mechanisms in the Taupo Volcanic Zone. *New Zealand Journal of Geology and Geophysics,* 7. p6-23.

Healy, J., Schofield, J.C. and Thompson, B.N., 1964: Sheet 5 - Rotorua. Geological Map of New Zealand 1:250 000. New Zealand Department of Scientific and Industrial Research, Wellington, New Zealand.

Henderson, P., 1984: General geochemical properties and abundances of the rare earth elements. In: Henderson, P. (editor): Rare Earth Element Geochemistry. Elsevier: Amsterdam; New York. p1-32.

Hervig, R.L., Dunbar, N., Westrich, H.R. and Kyle, P.R., 1989: Pre-eruptive water content of rhyolitic magmas as determined by ion microprobe analyses of melt inclusions in phenocrysts. *Journal of Volcanology and Geothermal Research,* 36. p293-302.

Heumann, A. and Davies, G., 2001: Timescales of processes within silicic magma chambers inferred from combined Ar-Ar, U-series and Rb-Sr isotope systematics. In: Knesel, K., Bergantz, G. and Davidson, J. (convenors): Geological Society of America Penrose Conference. Longevity and Dynamics of Rhyolitic Magma Systems. Abstracts.

Hildreth, W., 1981: Gradients in silicic magma chambers: implications for lithospheric magmatism. *Journal of Geophysical Research,* 86. p10153-10192.

Hildreth, W., Halliday, A.N. and Christiansen, R.L., 1991: Isotopic and chemical evidence concerning the genesis and contamination of basaltic and rhyolitic magma beneath the Yellowstone Plateau volcanic field. *Journal of Petrology,* 32. p63-138.

Hildyard, S.C., Cole, J.W. and Weaver, S.D., 2000: Tikorangi Ignimbrite: a 0.89 Ma mixed andesite-rhyolite ignimbrite, Matahana Basin, Taupo Volcanic Zone, New Zealand. *New Zealand Journal of Geology and Geophysics,* 43. p95-107.

Hochstein, M.P., Smith, I.E.M., Regenauer-Lieb, K. and Ehara, S., 1993: Geochemisty and heat transfer processes in Quaternary rhyolitic systems of the Taupo Volcanic Zone, New Zealand. *Tectonophysics,* 223. p213-235.

Hogg, A.G., Higham, T.F.G., Lowe, D.J., Palmer, J.G., Reimer, P.J. and Nairn, I.A., 2000: Precise 'wiggle-match' dating of the Kaharoa Tephra. *Geological Society of New Zealand Miscellaneous Publication 108A.* p74.

Holland, T. and Blundy, J., 1994: Non-ideal interactions in calcic amphiboles and their bearing on amphibole-plagioclase thermometry. *Contributions to Mineralogy and Petrology,* 116. p433-447.

Houghton, B.F. and Wilson, C.J.N., 1989: A vesicularity index for pyroclastic deposits. *Bulletin of Volcanology,* 51. p451-462.

Houghton, B.F., Wilson, C.J.N., Lloyd, E.F., Gamble, J.A. and Kokelaar, B.P., 1987: A catalogue of basaltic deposits within the central Taupo Volcanic Zone. *New Zealand Geological Survey Record,* 18. p95-101.

Houghton, B.F., Wilson, C.J.N., McWilliams, M.O., Lanphere, M.A., Weaver, S.D., Briggs, R.M. and Pringle, M.S., 1995: Chronology and dynamics of a large silicic magmatic system: central Taupo Volcanic Zone, New Zealand. *Geology,* 23. p13-16.

Housh, T.B. and Luhr, J.F., 1991: Plagioclase-melt equilibria in hydrous systems. *American Mineralogist,* 76. p477-492.

Howorth, R., 1975: New formations of late Pleistocene tephras from the Okataina Volcanic Centre, New Zealand. *New Zealand Journal of Geology and Geophysics,* 18. p683-712.

Howorth, R., 1976: Late Pleistocene tephras of the Taupo and Bay of Plenty Regions. Unpublished PhD Thesis. Victoria University, Wellington, New Zealand. 266p.

Huppert, H.E. and Sparks, R.S.J., 1988: The generation of granitic-magmas by intrusion of basalt into continental crust. *Journal of Petrology,* 29. p599-624.

Johnston, D.M. and Nairn, I.A., 1993: Volcanic impacts report: the impact of two eruption scenarios from the Okataina Volcanic Centre on the population and infrastructure of the Bay of Plenty, New Zealand. Environment BOP (Bay of Plenty Regional Council): Whakatane, New Zealand. 153p.

Johnson, M.C. and Rutherford, M.J., 1989: Experimental calibration of the aluminium-in-hornblende geobarometer with application to Long Valley caldera (California) volcanic rocks. *Geology,* 17. p837-841.

Jurado-Chichay, Z. and Walker, G.P.L., 2000: Stratigraphy and dispersal of the Mangaone Subgroup pyroclastic deposits, Okataina Volcanic Centre, New Zealand. *Journal of Volcanology and Geothermal Research,* 104. p319-383.

Kamenetsky, V.S., Everard, J.L., Crawford, A.J., Varne, R., Eggins, S.M. and Lanyon, R., 2000: Enriched end-member of primitive MORB melts: Petrology and geochemistry of glasses from Macquarie Island (SW Pacific). *Journal of Petrology,* 41. p411-430.

Karhunen, R.A., 1993: The Pokai and Chimp Ignimbrites of the northwest Taupo Volcanic Zone. Unpublished PhD Thesis. University of Canterbury, Christchurch, New Zealand. 356p.

Keam, R.J., 1988: Tarawera. The volcanic eruption of 10 June 1886. R.F Keam: Auckland. 472p.

Langridge, R.M., 1990: The geology of the Upper Atiamuri region, Taupo Volcanic Zone: with special reference to the existence of the Kapenga caldera volcano. Unpublished MSc Thesis. University of Waikato, Hamilton, New Zealand. 168p.

Leake, B.E., Woolley, A.R., Arps, C.E.S., Birch, W.D., Gilbert, M.C., Grice, M.C., Hawthorne, F.C., Kato, A., Kisch, H.J., Krivovichev, V.G., Linthout, K., Laird, J., Mandarino, J., Maresch, W.V., Nickel, E.H., Rock, N.M.S., Schumacher, J.C., Smith, D.C., Stephenson, N.C.N., Ungaretti, L., Whittaker, E.J.W. and Youzhi, G., 1997: Nomenclature of amphiboles - Report of the Subcommittee on Amphiboles of the International Mineralogical Association Commission on New Minerals and Mineral Names. *Mineralogical Magazine,* 61. p295-321.

Le Bas, M.J., Le Maitre, R.W., Streckeisen, A. and Zanettin,B., 1986: A chemical classification of volcanic rocks based on the total alkali - silica diagram. *Journal of Petrology,* 27. p745-750.

Le Maitre, R.W. (editor), 1989: A classification of igneous rocks and glossary of terms: recommendations of the International Union of Geological Sciences Subcommission on the Systematics of Igneous Rocks. Blackwell: Oxford; Boston. 193p.

Leonard, G., 1999: Magmatic processes associated with the ~ 650 B.P Kaharoa eruption, Tarawera Volcanic Complex, New Zealand. Unpublished BSc (Hons) Thesis. University of Canterbury, Christchurch, New Zealand.

Lindsley, D.H., Frost, B.R., Andersen, D.J. and Davidson, P.M., 1990: Fe-Ti oxide-silicate equilibria: Assemblages with orthopyroxene. In: Spencer, R.J. and Chou, I-M. (editors): Fluid-mineral interactions: A tribute to H.P. Eugster. *Geochemical Society, Spec* 2. p103-119.

Lipman, P.W., 1965: Chemical Comparison of Glassy and Crystalline Volcanic Rocks. *United States Geological Survey Bulletin,* 1201-D.

Lofgren, G., 1970: Experimental devitrification rate of rhyolite glass. *Geological Society of America Bulletin,* 81. p553-560

Lofgren, G., 1971a: Spherulitic Textures in Glassy and Crystalline Rocks. *Journal of Geophysical Research,* 76. p5635-5648.

Lofgren, G., 1971b: Experimentally produced devitrification textures in natural rhyolitic glass. *Geological Society of America Bulletin,* 82. p111-124.

Lofgren, G., 1974: An experimental study of plagioclase crystal morphology: isothermal crystallization. *American Journal of Science,* 274. p243-273.

Longerich, H.P., Jackson, S.E. and Gunther, D., 1996: Laser ablation inductively coupled plasma mass spectrometric transient signal data acquisition and analyte concentration calculation. *Journal of Analytical Atomic Spectrometry,* 11. p899-904.

Lowe, D.J., 1988: Stratigraphy, age, composition, and correlation of late Quaternary tephras interbedded with organic sediments in Waikato lakes, North Island, New Zealand. *New Zealand Journal of Geology and Geophysics,* 31. p125-165.

Lowe, D.J., Newnham, R.M. and Ward, C.M., 1999: Stratigraphy and chronology of a 15 ka sequence of multi-sourced silicic tephras in a montane peat bog, eastern North Island, New Zealand. *New Zealand Journal of Geology and Geophysics,* 42. p565-579.

Lowenstern, J.B., Clynne, M.A. and Bullen, T.B., 1997: Comagmatic A-type granophyre and rhyolite from the Alid Volcanic Center, Eritrea, Northeast Africa. *Journal of Petrology,* 38. p1707-1721.

Lowther, K.J., 1997: Quaternary geology and tephrostratigraphy of the north-eastern Rotorua region. Unpublished MSc Thesis. University of Waikato, Hamilton, New Zealand. 137p.

Lynch-Blosse, B.R., 1998: Ignimbrite stratigraphy of the Southern Mamaku Plateau Region, North Island, New Zealand. Unpublished MSc Thesis. University of Waikato, Hamilton, New Zealand. 170p.

MacKenzie, W.S., Donaldson, C.H. and Guilford, C., 1982: Atlas of igneous rocks and their textures. Longman: Harlow. 148 p.

Mahood, G.A., 1990: Second reply to comment of R.S.J Sparks, H.E Huppert and C.J.N Wilson on "Evidence for long residence times of rhyolitic magma in the Long Valley magmatic system: The isotopic record in precaldera lavas of Glass Mountain". *Earth and Planetary Science Letters,* 99. p395-399.

Mahood, G. and Hildreth, W., 1983: Large partition coefficients for trace elements in high-silica rhyolites. *Geochimica et Cosmochimica Acta,* 47. p11-30.

Maniar, P.D. and Piccoli, P.M., 1989: Tectonic discrimination of granitoids. *Geological Society of America Bulletin,* 101. p635-643.

Metz, J.M. and Mahood, G.A., 1991: Development of the Long Valley, California, magma chamber recorded in precaldera rhyolite lavas of Glass Mountain. *Contributions to Mineralogy and Petrology,* 106. p379-397.

McCulloch, M.T. and Gamble, J.A., 1991: Geochemical and geodynamical constraints on subduction zone magmatism. *Earth and Planetary Science Letters,* 102. p358-374.

McCulloch, M.T., Keyser, T.K., Woodhead, J. and Kinsley, L., 1994: Pb-Sr-Nd-O isotopic constraints on the origin of rhyolites from the Taupo Volcanic Zone of New Zealand: evidence for assimilation followed by fractionation from a basalt. *Contributions to Mineralogy and Petrology,* 115. p303-312.

McPhie, J., Doyle, M. and Allen, R., 1993: Volcanic Textures: A guide to the interpretation of textures in volcanic rocks. Centre for Ore Deposit and Exploration Studies (CODES): University of Tasmania, Australia. 198p.

Mills, J.G., Saltoun, B.W. and Vogel, T.A., 1997: Magma batches in the Timber Mountain Magmatic System, southwestern Nevada Volcanic Field, Nevada, USA. *Journal of Volcanology and Geothermal Research,* 78. p185-208.

Milner, D., 2001: The structure and eruptive history of the Rotorua Caldera, Taupo Volcanic Zone, New Zealand. Unpublished PhD Thesis. University of Canterbury, Christchurch, New Zealand.

Morimoto, N., Fabries, J., Ferguson, A.K., Ginzburg, I.V., Ross, M., Seifert, F.A., Zussman, J., Aoki, K. and Gotlardi, G., 1988: Nomenclature of pyroxenes. *Mineralogical Magazine,* 52. p535-550.

Murphy, R.P. and Seward, D., 1981: Stratigraphy, lithology, paleomagnetism and fission track ages of some ignimbrite formations in the Matahana Basin, New Zealand. *New Zealand Journal of Geology and Geophysics,* 24. p325-331.

Nagasawa, H., 1970: Rare earth concentrations in zircons and apatites and their host dacites and granites. *Earth and Planetary Science Letters,* 9. p359-364.

Nairn, I.A., 1972: Rotoehu Ash and the Rotoiti Breccia Formation, Taupo Volcanic Zone, New Zealand. *New Zealand Journal of Geology and Geophysics*, 15. p251-261.

Nairn, I.A., 1980: Source, age and eruptive mechanisms of Rotorua Ash. *New Zealand Journal of Geology and Geophysics,* 23. p193-207.

Nairn, I.A., 1981a: Some studies of the geology, volcanic history and geothermal resources of the Okataina Volcanic Centre, Taupo Volcanic Zone, New Zealand. Unpublished PhD Thesis. Victoria University, Wellington, New Zealand. 371p.

Nairn, I.A., 1981b: Potential Eruption Hazards at Okataina Volcanic Centre. Unpublished report submitted to the National Civil Defence Committee on Volcanic Hazards. New Zealand Geological Survey: Rotorua, New Zealand. 126p.

Nairn, I.A., 1989: Sheet V16 AC - Mount Tarawera. Geological Map of New Zealand 1:50 000. Map and notes. New Zealand Department of Scientific and Industrial Research, Wellington, New Zealand.

Nairn, I.A., 1992: The Te Rere and Okareka eruptive episodes - Okataina Volcanic Centre, Taupo Volcanic Zone, New Zealand. *New Zealand Journal of Geology and Geophysics,* 35. p93-108.

Nairn, I.A., 2000: Geology of the Okataina Volcanic Centre. Scale 1:50 000. Institute of Geological and Nuclear Sciences geological map 25. 1 sheet and text. Institute of Geological and Nuclear Sciences Limited: Lower Hutt, New Zealand.

Nairn, I.A. and Cole, J.W., 1981: Basalt dikes in the 1886 Tarawera Rift. *New Zealand Journal of Geology and Geophysics,* 24. p585-592.

Nairn, I.A. and Kohn, B.P., 1973: Relation of the Earthquake Flat Breccia to the Rotoiti Breccia, central North Island, New Zealand. *New Zealand Journal of Geology and Geophysics*, 16. p269-279.

Nairn, I.A. and Wood, C.P., 1987: Active volcanoes of the Taupo Volcanic Zone. In: International Volcanic Congress 1987: Active volcanoes and geothermal systems, Taupo Volcanic Zone, New Zealand. *New Zealand Geological Survey Record 22.* p5-84.

Naney, M.T., 1983: Phase equilibria of rock-forming ferromagnesian silicates in granitic systems. *American Journal of Science,* 283. p993-1033.

Nash, W.P. and Crecraft, H.R., 1985: Partition coefficients for trace elements in silicic magmas. *Geochimica et Cosmochimica Acta,* 49. p2309-2322.

Nicholls, I.A., Oba, T. and Conrad, W.K., 1992: The nature of primary rhyolitic magmas involved in crustal evolution: Evidence from an experimental study of cummingtonite-bearing rhyolites, Taupo Volcanic Zone, New Zealand. *Geochimica et Cosmochimica Acta,* 56. p955-962.

Noble, D.C., 1967: Sodium, potassium and ferrous iron contents of some secondarily hydrated natural silicic glasses. *American Mineralogist,* 52. p280-285.

Norrish, K. and Hutton, J.T., 1969: An accurate X-ray spectrographic method for the analysis of a wide range of geological samples. *Geochimica et Cosmochimica Acta,* 33. p431-453.

Pakiser, L.C., 1963: Structure of the crust and upper mantle in the western United States. *Journal of Geophysical Research,* 68. p5747-5756.

Pearce, J.A., 1983: Role of sub-continental lithosphere in magma genesis at active continental margins. In: Hawkesworth, C.J. and Norry, M.J. (editors): Continental Basalts and Mantle Xenoliths. Shiva, Nantwich. p230-249.

Pearce, J.A. and Norry, M.J., 1979: Petrogenetic implications of Ti, Zr, Y and Nb variations in volcanic rocks. *Contributions to Mineralogy and Petrology,* 69. p33-47.

Pearce, J.A. and Peate, D.W., 1995: Tectonic implications of the composition of volcanic arc magmas. *Annual Review of Earth and Planetary Sciences,* 23. p251-285.

Petford, N., Kerr, R.C. and Lister, J.R., 1993: Dike transport of granitoid magmas. *Geology,* 21. p845-848.

Pin, C., Briot, D., Bassin, C. and Poitrasson, F., 1994: Concomitant separation of strontium and samarium-neodymium for isotopic analysis in silicate samples, based on specific extraction chromatography. *Analytica Chimica Acta,* 298. p209-217.

Priestley, K.F., Ryall, A.S. and Fezie, G.S., 1982: Crust and upper mantle structure in the northwest Basin and Range Province. *Bulletin of the Seismological Society of America,* 72. p911-923.

Pullar, W.A. and Nairn, I.A., 1972: Matahi basaltic tephra member, Rotoiti Breccia Formation. *New Zealand Journal of Geology and Geophysics,* 15. p446-450.

Reid, F.W., 1983: Origin of the rhyolitic rocks of the Taupo Volcanic Zone. *Journal of Volcanology and Geothermal Research,* 15. p315-338.

Reid, M.R. and Coath, C.D., 2000: In situ U-Pb ages of zircons from the Bishop Tuff: No evidence for long crystal residence times. *Geology,* 28. p443-446.

Reid, M.R., Coath, C.D., Harrison, T.M. and McKeegan, K.D., 1997: Prolonged residence times for the youngest rhyolites associated with Long Valley Caldera: $^{230}Th - ^{238}U$ ion microprobe dating of young zircons. *Earth and Planetary Science Letters,* 150. p27-39.

Richard, P., Shimizu, N. and Allegre, C.J., 1976: $^{143}Nd/^{146}Nd$, a natural tracer: an application to oceanic basalts. *Earth and Planetary Science Letters,* 31. p269-278.

Richnow, J., 1999: Eruptional and post-eruptional processes in rhyolite domes. Unpublished PhD Thesis. University of Canterbury, Christchurch, New Zealand. 545p.

Rickwood, P.C., 1989: Boundary lines within petrologic diagrams which use oxides of major and minor elements. *Lithos,* 22. p247-263.

Ritchie, A.B.H., 1996: Volcanic geology and geochemistry of Waiotapu Ignimbrite, Taupo Volcanic Zone, New Zealand. Unpublished MSc Thesis. University of Canterbury, Christchurch, New Zealand. 153p.

Robinson, R., Smith, E.G.C. and Latter, J.H., 1981: Seismic studies of the crust under the hydrothermal areas of the Taupo Volcanic Zone, New Zealand. *Journal of Volcanology and Geothermal Research,* 9. p253-267.

Roedder, E., 1984: Fluid Inclusions. *Reviews in Mineralogy,* 12. 644p.

Rogan, A.M., 1980: Geophysical studies of the Okataina Volcanic Center. Unpublished PhD Thesis, Auckland University, Auckland, New Zealand.

Rogan, A.M., 1982: A geophysical study of the Taupo Volcanic Zone, New Zealand. *Journal of Geophysical Research,* 87. p4073-4088.

Rollinson, H.R., 1993: Using geochemical data: Evaluation, presentation, interpretation. Longman Group, London. 352p.

Ross, C.S., 1962: Microlites in glassy volcanic rocks. *The American Mineralogist,* 47. p723-740.

Ruiz, J., Patchett, P.J. and Arculus, R.J., 1988: Nd-Sr isotope composition of lower crustal xenoliths - evidence for the origin of mid-Tertiary felsic volcanics in Mexico. *Contributions to Mineralogy and Petrology,* 99. p36-43.

Schmitz, M.D., 1995: Geochemical studies of the Rotoiti Pyroclastics eruption, Okataina Volcanic Centre, Taupo Volcanic Zone, North Island, New Zealand. Unpublished MSc Thesis. University of Auckland, Auckland, New Zealand. 98p.

Scott, B.J. and Nairn, I.A., 1998: Volcanic hazard map of Okataina Volcanic Centre. Environment Bay of Plenty resource planning publication 97/4.

Shane, P., 1998: Correlation of rhyolitic pyroclastic eruptive units from the Taupo Volcanic Zone by Fe-Ti oxide compositional data. *Bulletin of Volcanology,* 60. p224-238.

Shane, P., 2000: Tephrochronology: a New Zealand case study. *Earth-Science Reviews,* 49. p223-259.

Shane, P., Black, T. and Westgate, J., 1994: Isothermal plateau fission-track age for a paleomagnetic excursion in the Mamaku Ignimbrite, New Zealand, and implications for late Quaternary stratigraphy. *Geophysical Research Letters,* 21. p1695-1698.

Sharp, T.G., Stevenson, R.J. and Dingwell, D.B., 1996: Microlites and "nanolites" in rhyolitic glass: microstructural and chemical characterization. *Bulletin of Volcanology,* 57. p631-640.

Shelley, D. 1993: Igneous and metamorphic rocks under the microscope: classification, textures, microstructures, and mineral preferred-orientations. Chapman & Hall: London; New York. 445p.

Shepherd, A.D., 1991: Volcanology and petrology of the post-caldera rhyolitic domes, Rotorua Volcanic Centre, New Zealand. Unpublished BSc (Hons) Thesis. Victoria University, Wellington, New Zealand.

Smith, V.C., 2001: The stratigraphy and geochemistry of the Mangaone Subgroup tephra beds, Okataina Volcanic Centre, New Zealand. Unpublished MSc Thesis. University of Auckland, Auckland, New Zealand. 111p.

Sparks, R.S.J., Huppert, H.E. and Wilson, C.J.N., 1990: Comment on "Evidence for long residence times of rhyolitic magma in the Long Valley magmatic system: The isotopic record in precaldera lavas of Glass Mountain" by A.N. Halliday, G.A. Mahood, P. Holden, J.M. Metz, T.J. Dempster and J.P. Davidson. *Earth and Planetary Science Letters,* 99. p387-389.

Speed, J.A., 2001: The 11.9 ka Waiohau eruptive episode, Okataina Volcanic Centre. Unpublished MSc Thesis. University of Auckland, Auckland, New Zealand.

Spell, T.L., Kyle, P.R., Thirlwall, M.F. and Campbell, A.R., 1993: Isotopic and geochemical constraints on the origin and evolution of postcollapse rhyolites in the Valles Caldera, New Mexico. *Journal of Geophysical Research,* 98. p19723-19739.

Spencer, K.J. and Lindsley, D.H., 1981: A solution model for co-existing iron-titanium oxides. *American Mineralogist,* 66. p1189-1201.

Spinks, K.D., 1998: The Rahopaka Ignimbrite and associated volcaniclastics, Taupo Volcanic Zone, New Zealand. Unpublished BSc (Hons) Thesis. University of Canterbury, Christchurch, New Zealand. 89p.

Stern, T.A., 1986: Geophysical studies of the upper crust within the Central Volcanic Region, New Zealand. In: I.E.M Smith (editor): Late Cenozoic Volcanism in New Zealand. *Royal Society of New Zealand Bulletin,* 23. p92-111.

Stern, T.A. and Davey, F.J., 1987: A seismic investigation of the crustal and upper mantle structure within the Central Volcanic Region of New Zealand. *New Zealand Journal of Geology and Geophysics,* 30. p217-231.

Stevenson, R.J., Briggs, R.M. and Hodder, A.P.W., 1993: Emplacement history of a low-viscosity, fountain-fed pantelleritic lava flow. *Journal of Volcanology and Geothermal Research,* 57. p39-56.

Stevenson, R.J., Hodder, A.P.W. and Briggs, R.M., 1994: Rheological estimates of rhyolite lava flows from the Okataina Volcanic Centre, New Zealand. *New Zealand Journal of Geology and Geophysics,* 37. p211-221.

Stirling, M.W. and Wilson, C.J.N., 2000: Eruption size - frequency relationships for Taupo and Okataina volcanoes: Towards a probabilistic volcanic hazard model. *Geological Society of New Zealand Miscellaneous Publication 108A (GSNZ/NZGS Joint Meeting, 2000, Wellington).* p150.

Stix, J. and Gorton, M.P., 1993: Replenishment and crystallization in epicontinental silicic magma chambers: evidence from the Bandelier magmatic system. *Journal of Volcanology and Geothermal Research,* 55. p201-215.

Stormer, J.C., 1982: The recalculation of multicomponent Fe-Ti oxide analyses for geothermometry: a quasi-thermodynamic model. *EOS,* 63. p471.

Stormer, J.C. and Nicholls, J., 1978: XLFRAC: A program for the interactive testing of magmatic differentiation models. *Computers and Geosciences,* 4. p143-159.

Stuiver, M., Reimer, P.J., Bard, E., Beck, J.W., Burr, G.S., Hughen, K.A., Kromer, B., McCormac, G., van der Plicht, J., Spurk, M., 1998: INTCAL98 radiocarbon age calibration, 24,000 - 0 cal BP. *Radiocarbon,* 40. p1041-1083.

Sutton, A.N., 1995: Evolution of a large silicic magma system: Taupo Volcanic Centre, New Zealand. Unpublished PhD Thesis. The Open University, Milton Keynes, United Kingdom.

Sutton, A.N., Blake, S. and Wilson, C.J.N., 1995: An outline geochemistry of rhyolite eruptives from Taupo Volcanic Centre, New Zealand. *Journal of Volcanology and Geothermal Research,* 68. p153-175.

Sutton, A.N., Blake, S., Wilson, C.J.N. and Charlier, B.L.A., 2000: Late Quaternary evolution of a hyperactive rhyolite magmatic system: Taupo volcanic centre, New Zealand. *Journal of the Geological Society, London,* 157. p537-552.

Swanson, S.E., Naney, M.T., Westrich, H.R. and Eichelberger, J.C., 1989: Crystallisation history of Obsidian Dome, Inyo Domes, California. *Bulletin of Volcanology,* 51. p161-176

Taylor, B.E., Eichelberger, J.C. and Westrich,H.R., 1983: Hydrogen isotopic evidence of rhyolite magma degassing during shallow intrusion and eruption. *Nature,* 306. p541-545.

Thompson, B.N., 1974: Geology of the Rotorua Geothermal District. In: Geothermal Resources Survey, Rotorua Geothermal District. *New Zealand Department of Scientific and Industrial Research geothermal report No. 6.* p10-36.

Thompson, R.N., Morrison, M.A., Hendry, G.L. and Parry, S.J., 1984: An assessment of the relative roles of crust and mantle in magma genesis: an elemental approach. *Philosophical Transactions of the Royal Society, London,* A310. p549-590.

van den Bogaard, P. and Schirnick, C., 1995: $^{40}Ar/^{39}Ar$ laser probe ages of Bishop Tuff quartz phenocrysts substantiate long-lived silicic magma chamber at Long Valley, United States. *Geology,* 23. p759-762.

Villamor, P. and Berryman, K., 2001: A late Quaternary extension rate in the Taupo Volcanic Zone, New Zealand, derived from fault slip data. *New Zealand Journal of Geology and Geophysics,* 44. p243-269.

Vucetich, C.G. and Pullar, W.A., 1969: Stratigraphy and chronology of Late Pleistocene volcanic ash beds in central North Island, New Zealand. *New Zealand Journal of Geology and Geophysics,* 12. p784-837.

Walker, G. P.L., Self, S. and Wilson, L., 1984: Tarawera 1886, New Zealand - A basaltic plinian fissure eruption. *Journal of Volcanology and Geothermal Research,* 21. p61-78.

Watson, E.B. and Green, T.H., 1981: Apatite/liquid partition coefficients for the rare earth elements and strontium. *Earth and Planetary Science Letters,* 56. p405-421.

Weaver, S.D., Gibson, I.L., Houghton, B.F. and Wilson, C.J.N., 1990: Mobility of rare earth and other elements during crystallisation of peralkaline silicic lavas. *Journal of Volcanology and Geothermal Research,* 43. p57-70.

Wilson, C.J.N., 1993: Stratigraphy, chronology, styles and dynamics of late Quaternary eruptions from Taupo volcano, New Zealand. *Philosophical Transactions of the Royal Society of London,* A 343. p205-306.

Wilson, C.J.N., Houghton, B.F., McWilliams, M.O., Lanphere, M.A., Weaver, S.D. and Briggs, R.M., 1995: Volcanic and structural evolution of the Taupo Volcanic Zone, New Zealand: A review. *Journal of Volcanology and Geothermal Research,* 68. p1-28.

Wilson, C.J.N., Rogan, A.M., Smith, I.E.M., Northey, D.J., Nairn, I.A. and Houghton, B.F., 1984: Caldera volcanoes of the Taupo Volcanic Zone, New Zealand. *Journal of Geophysical Research,* 89. p8463-8484.

Wilson, M., 1989: Igneous Petrogenesis. Unwin Hyman Academic, London. 466p.

Wones, D.R. and Gilbert, M.C., 1969: The Fayalite-magnetite-quartz assemblage between 600 and 800°C. *American Journal of Science,* 267-A. p480-488.

Wood, C.P., 1992: Geology of the Rotorua Geothermal System. *Geothermics,* 21. p25-41.

Woodhead, J.D., Volker, F. and McCulloch, M.T., 1995: Routine lead isotope determinations using a ^{207}Pb-^{204}Pb double spike: a long-term assessment of analytical precision and accuracy. *The Analyst*, 120. p35-39.

Wright, C.M., 2000: Stratigraphy, volcanology, petrology and geochemistry of the 7.5ka Mamaku Eruptive Episode, Okataina Volcanic Centre, North Island, New Zealand. Unpublished MSc Thesis, University of Auckland, Auckland, New Zealand. 119p.